



University of HUDDERSFIELD

University of Huddersfield Repository

Ghori, Muhammad U.

Release kinetics, compaction and electrostatic properties of hydrophilic matrices

Original Citation

Ghori, Muhammad U. (2014) Release kinetics, compaction and electrostatic properties of hydrophilic matrices. Doctoral thesis, University of Huddersfield.

This version is available at <http://eprints.hud.ac.uk/id/eprint/24269/>

The University Repository is a digital collection of the research output of the University, available on Open Access. Copyright and Moral Rights for the items on this site are retained by the individual author and/or other copyright owners. Users may access full items free of charge; copies of full text items generally can be reproduced, displayed or performed and given to third parties in any format or medium for personal research or study, educational or not-for-profit purposes without prior permission or charge, provided:

- The authors, title and full bibliographic details is credited in any copy;
- A hyperlink and/or URL is included for the original metadata page; and
- The content is not changed in any way.

For more information, including our policy and submission procedure, please contact the Repository Team at: E.mailbox@hud.ac.uk.

<http://eprints.hud.ac.uk/>

Release kinetics, compaction and
electrostatic properties of
hydrophilic matrices

Muhammad Usman Ghori Pharm.D

A thesis submitted in partial fulfilment of the requirements for the degree of
Doctor of Philosophy

The University of Huddersfield
2014

***“He who leaveth home in search of knowledge, walk
in the path of God”***

Prophet Muhammad (PBUH)

Abstract

This thesis illustrates the behaviour of cellulose ethers during powder processing, compaction and drug release, as these are frequently employed in the fabrication of compressed hydrophilic matrices. The handling operations can give rise to the electrification of powder particles, which can affect the end product's quality. Controlling the parameters which can dictate the quality of compressed matrices is an ambition inherent in the development of pharmaceutical formulations. Thus, the aims and objectives of this thesis were to firstly study the electrostatic, surface adhesion, dissolution and compaction properties of plain polymers and model drugs. Secondly, binary mixtures of fixed drug to polymer ratios were made in order to investigate the effect of polymer concentration and physico-chemical attributes (particle size, chemistry and viscosity) on the tribo-electric charging, surface adhesion (SA), swelling, erosion, drug release kinetics and compaction properties of model drugs.

It can be discerned that the both drugs charged negatively, whereas the methylcellulose (MC) and hydroxypropyl methylcellulose (HPMC) particles charged positively. The physico-chemical properties associated with MC and HPMC, such as particle size, chemical heterogeneity and molecular size of cellulose ethers all have a significant effect on charging and adhesion behaviour of plain MC and HPMC particles. Moreover, the concentration, particle size, chemical heterogeneity and molecular size of MC/HPMC all significantly affect the charging and SA propensity of the model drugs studied.

The swelling and dissolution results confirm that the extent and rate of swelling, swelling exponent, dissolution rate and drug release kinetic parameters were affected by physico-chemical attributes (concentration, particle size, substitution and viscosity) of MC/HPMC and drug solubility. The mechanism of swelling and drug release was found to be anomalous. However, it inclined towards more diffusion-oriented swelling/drug release with higher MC/HPMC levels, viscosity, Hpo/Meo substitution ratios, drug solubility but smaller MC/HPMC particle size.

The matrix erosion results obtained from newly developed phenol-sulphuric acid assay (PSA) method confirmed that the solubility of the drug, and levels of HPMC in a particular matrix tablet, significantly affect the matrix erosion rate and the results were similar to those determined using the much more labour-intensive gravimetric method. Moreover, the combination of conventional UV drug analysis technique and PSA assay can be used to simultaneously quantify the matrix erosion, polymer dissolution and drug release kinetics in a single set of experiments avoiding the need for separate studies.

The compaction results confirmed that the FBP has poor compaction as compare to THP. The particle size, substitution ratios and molecular size of MC/HPMC affect the compaction and consolidation behaviour of plain MC/HPMC compacts. Furthermore, it can be noticed that the concentration and physico-chemical attributes (particle size, chemistry and molecular size) of MC/HPMC have a significant influence on the densification and consolidation process of hydrophilic matrices.

In summary, the information obtained can be used in the future to develop and adopt strategies for development and further optimization of compressed hydrophilic matrices.

Dedication

This thesis is dedicated to my family, especially in the memory of my father, without their love, support and encouragement, this would not have been possible.

Acknowledgments

I would like to express my sincere appreciation to my research supervisor, Prof. Barbara Conway, for her supervision, guidance, support and freedom in the development of this project. You have been my mentor, my colleague, friend and a never-ending fount of moral support. If I do take the academic path, I only hope that I can be half the advisor that you have been to me. Whatever path I do take, I will be prepared because of you. I sincerely thank you for making my doctoral degree a wonderful learning experience with not only the technical content but also the philosophical aspects.

I must also extend my thanks to Dr. Alan Smith, Dr. Enes Šupuk, Dr. Kofi Asare-Addo and Miss Hayley Markham for their friendship, support and help.

Further my thanks are due towards Dr. Peter Laity (University of Sheffield) who provided me much needed training on Testometric[®] and Prof. Liam Grover (University of Birmingham) for his help using the helium pycnometer.

I would also like to thank all my colleagues who work in W1/28 and XG/11 for creating a friendly working environment, as well as to the technical staff of the School of Applied Sciences for their laboratory assistance.

I would also like to thank the University of Huddersfield for providing me a fee-waiver scholarship to pursue doctoral degree at the School of Applied Sciences. I would also like to thank the University of Huddersfield Graduate Centre for providing me with the much needed conference presentation funds throughout the duration of my PhD.

To my mother, I thank you for everything you taught me growing up, and for instilling in me a desire to learn and the belief that hard work pays off no matter how long it takes.

Finally, I would like to thank my brother and sister for their tremendous support and encouragement throughout this project.

Table of Contents

| | |
|--|-------|
| Abstract | iii |
| Dedication | iv |
| Acknowledgments | v |
| Table of Contents | vi |
| List of Figures | xvii |
| List of Tables | xxvii |
| List of abbreviations | xxxii |
| Chapter 1: Introduction | 1 |
| 1.1. Cellulose ethers | 2 |
| 1.2. Manufacturing of cellulose ethers | 4 |
| 1.3. Derivatives of cellulose ethers | 6 |
| 1.4.1. Methylcellulose (MC)..... | 8 |
| 1.4.2. Hypromellose (Hydroxypropyl methylcellulose, HPMC)..... | 9 |
| 1.4. Pharmaceutical applications of MC and HPMC | 10 |
| 1.5. Profiles of model drugs | 13 |
| 1.5.1. Flurbiprofen | 13 |
| 1.5.2. Theophylline | 15 |
| 1.6. Aims and objectives | 16 |
| Chapter 2: General experimental | 19 |
| 2.1. Materials..... | 20 |

| | | |
|-------------------|---|-----------|
| 2.2. | Methods..... | 21 |
| 2.2.1. | Preparation of sodium phosphate buffer, pH 7.2 | 21 |
| 2.2.2. | Saturated solubility determination of model drugs | 21 |
| 2.2.3. | Particle size fractionation and storage of powders..... | 22 |
| 2.2.4. | Characterisation of powders..... | 22 |
| 2.2.5. | Tribo-electrification and powder SA studies | 24 |
| 2.2.6. | Swelling and erosion studies..... | 27 |
| 2.2.7. | Dissolution studies | 31 |
| 2.2.8. | Development and validation of PSA assay for erosion analysis..... | 35 |
| 2.2.9. | Compaction studies | 40 |
| Chapter 3: | Tribo-electrification and adhesion studies | 45 |
| 3.1. | Introduction..... | 46 |
| 3.2. | Tribo-electrification | 47 |
| 3.2.1. | Metal-metal contacts..... | 47 |
| 3.2.2. | Metal-insulator contacts | 48 |
| 3.2.2.1. | Electron transfer in metal-insulator contacts | 49 |
| 3.2.2.2. | Ion transfer in metal-insulator contacts..... | 51 |
| 3.2.2.3. | Material transfer in metal-insulator contacts | 53 |
| 3.2.3. | Insulator-insulator contacts | 55 |
| 3.3. | Powder processing | 57 |
| 3.4. | Factors affecting tribo-electrification..... | 58 |

| | | |
|----------|--|----|
| 3.4.1. | Nature and work function of contacting surfaces | 58 |
| 3.4.2. | Contact surface roughness | 60 |
| 3.4.3. | Contact surface contamination | 62 |
| 3.4.4. | Particle size..... | 62 |
| 3.4.5. | Particle shape and roughness | 65 |
| 3.4.6. | Material chemistry | 66 |
| 3.4.7. | Crystallinity and amorphicity..... | 66 |
| 3.4.8. | Mixing ratios..... | 67 |
| 3.4.9. | Mixing speed/frequency of contact | 68 |
| 3.4.10. | Atmospheric conditions..... | 69 |
| 3.5. | Applications and hazards of tribo-electric charging | 71 |
| 3.6. | Powder mixing | 73 |
| 3.6.1. | Random powder mixtures | 74 |
| 3.6.2. | Ordered powder mixtures..... | 75 |
| 3.7. | Section A, Tribo-electrification and adhesion studies of model drugs. | 75 |
| 3.7.1. | Introduction..... | 75 |
| 3.7.2. | Experimental | 76 |
| 3.7.2.1. | Materials..... | 76 |
| 3.7.2.2. | Methods..... | 76 |
| 3.7.3. | Results and discussion | 77 |
| 3.7.3.1. | Surface morphology of model drugs..... | 77 |

| | |
|---|-----|
| 3.7.3.2. Tribo-electrification and adhesion properties of model drugs | 78 |
| 3.8. Section B, Tribo-electrification and adhesion studies of cellulose ethers | 81 |
| 3.8.1. Introduction | 82 |
| 3.8.2. Experimental | 82 |
| 3.8.2.1. Materials..... | 82 |
| 3.8.2.2. Methods..... | 82 |
| 3.8.3. Results and discussion | 83 |
| 3.8.3.1. Surface morphology of MC and HPMC powder particles..... | 83 |
| 3.8.3.2. Tribo-electrification and adhesion properties of MC and HPMC..... | 85 |
| 3.8.3.2.1. Effect of Methocel [®] particle size | 86 |
| 3.8.3.2.2. Effect of Methocel [®] substitution..... | 87 |
| 3.8.3.2.3. Effect of Methocel [®] molecular size (viscosity) | 88 |
| 3.9. Section C, Tribo-electrification and adhesion studies of MC and HPMC based binary mixtures..... | 90 |
| 3.9.1. Introduction..... | 90 |
| 3.9.2. Experimental | 92 |
| 3.9.2.1. Materials..... | 92 |
| 3.9.2.2. Methods..... | 92 |
| 3.9.3. Results and discussion | 93 |
| 3.9.3.1. Formation of ordered mixtures | 93 |
| 3.9.3.2. Tribo-electrification and adhesion properties of binary mixtures.... | 106 |
| 3.9.3.2.1. Effect of Methocel [®] concentration..... | 106 |

| | |
|---|------------|
| 3.9.3.2.2. Effect of Methocel [®] particle size | 110 |
| 3.9.3.2.3. Effect of Methocel [®] substitution..... | 113 |
| 3.9.3.2.4. Effect of Methocel [®] molecular size (viscosity) | 113 |
| 3.9.4. Relationship between tribo-electric charging and surface adhesion | 117 |
| 3.10. Summary | 121 |
| Chapter 4: Swelling, erosion and dissolution studies of hydrophilic matrices | 122 |
| 4.1. Introduction..... | 123 |
| 4.2. Hydrophilic matrices..... | 123 |
| 4.3. Cellulose ether based hydrophilic matrices | 124 |
| 4.4. Mechanism of swelling, drug release and matrix erosion..... | 125 |
| 4.5. Factors affecting swelling, erosion and drug release | 131 |
| 4.5.1. Effect of Methocel [®] concentration..... | 131 |
| 4.5.2. Effect of Methocel [®] particle size | 133 |
| 4.5.3. Effect of Methocel [®] substitution..... | 134 |
| 4.5.4. Effect of Methocel [®] molecular size (viscosity) | 135 |
| 4.5.5. Effect of drug solubility | 136 |
| 4.6. Section A, Compaction of model drugs | 139 |
| 4.6.1. Introduction..... | 139 |
| 4.6.2. Experimental | 139 |
| 4.6.2.1. Materials..... | 139 |
| 4.6.2.2. Methods..... | 140 |

| | |
|---|-----|
| 4.6.3. Results and discussion | 140 |
| 4.7. Section B, Swelling, erosion and dissolution properties of hydrophilic matrices. . | 143 |
| 4.7.1. Introduction | 143 |
| 4.7.2. Experimental | 144 |
| 4.7.2.1. Materials..... | 144 |
| 4.7.2.2. Methods..... | 145 |
| 4.7.3. Results and discussion | 146 |
| 4.7.3.1. Swelling and erosion properties of plain Methocel [®] matrices... | 146 |
| 4.7.3.1.1. Effect of Methocel [®] particle size | 147 |
| 4.7.3.1.2. Effect of Methocel [®] substitution..... | 147 |
| 4.7.3.1.3. Effect of Methocel [®] molecular size (viscosity) | 148 |
| 4.7.3.2. Mixing efficiency of Methocel [®] : FBP/THP powders | 151 |
| 4.7.3.3. Swelling, erosion and dissolution studies of FBP/THP matrices..... | 152 |
| 4.7.3.3.1. Effect of Methocel [®] concentration..... | 152 |
| 4.7.3.3.2. Effect of Methocel [®] particle size | 160 |
| 4.7.3.3.3. Effect of Methocel [®] substitution..... | 167 |
| 4.7.3.3.4. Effect of Methocel [®] molecular size (viscosity) | 174 |
| 4.7.3.3.5. Effect of drug solubility | 191 |
| 4.7.3.4. Inter-relationship between swelling and dissolution rates | 193 |
| 4.8. Summary | 197 |

| | |
|--|------------|
| Chapter 5: Development and validation of PSA assay for erosion analysis | 198 |
| 5.1. Introduction | 199 |
| 5.2. Experimental | 201 |
| 5.2.1. Materials..... | 201 |
| 5.2.2. Methods..... | 201 |
| 5.3. Results and discussion | 202 |
| 5.3.1. Erosion study of plain MC/HPMC compacts | 202 |
| 5.3.1.1. Effect of Methocel [®] particle size | 203 |
| 5.3.1.2. Effect of Methocel [®] substitution..... | 205 |
| 5.3.1.3. Effect of Methocel [®] molecular size (viscosity) | 206 |
| 5.3.2. Drug release studies from K4M : FBP/THP matrices..... | 207 |
| 5.3.3. HPMC dissolution studies..... | 210 |
| 5.3.4. Matrix tablet erosion studies | 213 |
| 5.3.5. Quantitative relationship between GM and PSA | 217 |
| 5.3.6. Inter-relationship between HPMC erosion and drug release kinetics... | 223 |
| 5.4. Summary | 224 |
| | |
| Chapter 6: Compaction studies of hydrophilic matrices | 226 |
| 6.1. Introduction | 227 |
| 6.2. Powder compaction..... | 228 |
| 6.3. Mechanism of powder compaction | 229 |
| 6.4. Bonding during powder compaction..... | 233 |

| | |
|---|-----|
| 6.4.1. Distance attraction forces | 233 |
| 6.4.2. Solid bridges | 234 |
| 6.4.3. Non- freely movable bridges..... | 234 |
| 6.4.4. Bonding due to movable bridges | 234 |
| 6.4.5 Mechanical interlocking..... | 235 |
| 6.5. Compaction properties of Methocel [®] | 235 |
| 6.6. Factors affecting compaction properties of Methocel [®] | 236 |
| 6.6.1. Effect of particle size | 236 |
| 6.6.2. Effect of substitution..... | 237 |
| 6.6.3. Effect of molecular size (viscosity) | 238 |
| 6.6.4. Effect of humidity | 238 |
| 6.7. Mathematical models of powder compression..... | 241 |
| 6.7.1. The Heckel mathematical equation..... | 241 |
| 6.7.2. The Kawakita mathematical equation..... | 244 |
| 6.8. Section A, Compaction of model drugs | 246 |
| 6.8.1. Introduction | 246 |
| 6.8.2. Experimental | 246 |
| 6.8.2.1. Materials..... | 246 |
| 6.8.2.2. Methods..... | 246 |
| 6.8.3. Results and discussion | 246 |
| 6.9. Section B, Compaction properties of hydrophilic matrices | 254 |

| | |
|---|------------|
| 6.9.1. Introduction | 254 |
| 6.9.2. Experimental | 255 |
| 6.9.2.1. Materials..... | 255 |
| 6.9.2.2. Methods..... | 256 |
| 6.9.3. Results and discussion | 256 |
| 6.9.3.1. Compaction properties of plain Methocel [®] compacts..... | 256 |
| 6.9.3.1.1. Effect of Methocel [®] particle size | 258 |
| 6.9.3.1.2. Effect of Methocel [®] substitution..... | 259 |
| 6.9.3.1.3. Effect of Methocel [®] molecular size (viscosity) .. | 267 |
| 6.9.3.2. Mixing efficiency of Methocel [®] : FBP/THP powders | 268 |
| 6.9.3.3. Compaction properties of FBP/THP matrices | 268 |
| 6.9.3.3.1. Effect of Methocel [®] concentration..... | 269 |
| 6.9.3.3.2. Effect of Methocel [®] particle size | 280 |
| 6.9.3.3.3. Effect of Methocel [®] substitution..... | 288 |
| 6.9.3.3.4. Effect of Methocel [®] molecular size (viscosity) | 296 |
| 6.9.3.4. Inter-relationship between P_y and b^{-1} | 316 |
| 6.10. Summary | 319 |
| Chapter 7: Conclusions and future work..... | 320 |
| 7.1. Conclusions..... | 321 |
| 7.2. Future work..... | 324 |

| | |
|------------------------------------|-----|
| Chapter 8: References | 326 |
| Appendix A | 351 |

List of Figures

Chapter 1

| | |
|---|----|
| Figure 1.1: Structure of cellulose..... | 3 |
| Figure 1.2: Schematic outline of cellulose ether manufacturing process | 6 |
| Figure 1.3: Structure of cellulose ethers | 7 |
| Figure 1.4: Structure of FBP | 14 |
| Figure 1.5: Structure of THP | 15 |
| Figure 1.6: Outline of aims and objectives of thesis..... | 18 |

Chapter 2

| | |
|--|----|
| Figure 2.1: Helium pycnometer | 23 |
| Figure 2.2: Tribo-electric charging measurement set up | 26 |
| Figure 2.3: (a) Specac [®] 13.00 mm evacuable die set and (b) Specac [®] manual hydraulic press. | 28 |
| Figure 2.4: Swelling experimental set up (a) wire mesh (b) glass petri dish (17 mm × 45 mm)..... | 30 |
| Figure 2.5: Dissolution apparatus used for IDR determination | 32 |
| Figure 2.6: Tubular shaker-mixer | 36 |
| Figure 2.7: Dissolution apparatus I (basket assembly) | 38 |
| Figure 2.8: (a) Testometric [™] material testing machine equipped with, (b) Specac [®] 13.00 mm evacuable die set | 42 |

Chapter 3

| | |
|--|-----|
| Figure 3.1: Schematic illustration of charge generation during metal-metal contact..... | 48 |
| Figure 3.2: Schematic illustration of electron transfer theory of tribo-electric charge generation..... | 50 |
| Figure 3.3: Schematic illustration of ion transfer theory of tribo-electric charge generation..... | 52 |
| Figure 3.4: Schematic illustration of material transfer theory of tribo-electric charge generation..... | 54 |
| Figure 3.5: SEM micrographs of (a) FBP and (b) THP powder particles..... | 77 |
| Figure 3.6: Tribo-electrification charging profiles of (a) FBP and (b) THP powder particles (n = 3)..... | 78 |
| Figure 3.7: Schematic illustration of tribo-electrific charging of FBP and THP powder particles..... | 79 |
| Figure 3.8: SEM micrographs of MC and HPMC, (a) A4M (b) F4M (c) E4M (d) K4M (e) K15M (f) K100M..... | 84 |
| Figure 3.9: Schematic illustration of tribo-electrification charging of MC and HPMC powder particles..... | 86 |
| Figure 3.10: Schematic illustration of tribo-electric charge generation of powder mixtures..... | 95 |
| Figure 3.11: Figure 3.11, SEM micrographs of FBP powder mixtures, (a) A4M/THP (b)F4M/THP (c) E4M/THP (d) K4M/THP (e) K15M/THP and (d) K100M/THP | 98 |
| Figure 3.12: SEM micrographs of THP powder mixtures, (a) A4M/THP (b) F4M/THP (c) E4M/THP (d) K4M/THP (e) K15M/THP and (d) K100M/THP..... | 99 |
| Figure 3.13: DSC profiles of (a) MC/HPMC and (b) FBP/THP | 101 |
| Figure 3.14: DSC profiles of (a) FBP and (b) THP powder mixtures..... | 102 |

| | |
|---|-----|
| Figure 3.15: PXRD patterns of (a) MC/HPMC and (b) FBP/THP..... | 104 |
| Figure 3.16: PXRD patterns of (a) THP and (b) FBP powder mixtures..... | 105 |
| Figure 3.17: Effect of polymer concentration on the tribo-electric charging of cellulose ether : FBP powder mixtures; polymer particle size (a) 150 - 250 μm and (b) 90 - 150 μm (n=3) | 108 |
| Figure 3.18: Effect of polymer concentration on the tribo-electric charging of cellulose ether : THP powder mixtures; polymer particle size (a) 150 - 250 μm and (b) 90 - 150 μm (n=3) | 109 |
| Figure 3.19: Effect of polymer molecular size (viscosity) on the tribo-electric charging of MC/HPMC : FBP powder mixtures; polymer particle size (a) 150 - 250 μm and (b) 90 - 150 μm , n=3, (viscosity (cp) in parentheses on x-axis)..... | 115 |
| Figure 3.20: Effect of polymer molecular size (viscosity) on the tribo-electric charging of MC/HPMC : THP powder mixtures; polymer particle size (a) 150 - 250 μm and (b) 90 - 150 μm , n=3, (viscosity (cp) in parentheses on x-axis)..... | 116 |
| Figure 3.21: Effect of tribo-electric charging (nC/g) of FBP powder mixtures on SA(%), (a) A4M (b) F4M (c) E4M (d) K4M (e) K15M (f) K100M having polymer particle size 90-150 μm and 150-250 μm | 119 |
| Figure 3.22: Effect of tribo-electric charging (nC/g) of THP powder mixtures on SA(%), (a) A4M (b) F4M (c) E4M (d) K4M (e) K15M (f) K100M having polymer particle size 90-150 μm and 150-250 μm | 120 |

Chapter 4

| | |
|---|-----|
| Figure 4.1: Cross-sectional view of a typical hydrophilic matrix tablet..... | 124 |
| Figure 4.2: Mechanism of drug release from hydrophilic matrix tablets | 128 |
| Figure 4.3: Drug release mechanism of water soluble and poorly water soluble drugs from hydrophilic matrix tablets | 130 |

| | |
|---|-----|
| Figure 4.4: Dissolution profiles of FBP and THP compacts | 142 |
| Figure 4.5: Swelling profiles of cellulose ethers based matrix tablets of particle prize (a) 90-150 (b) 150-250 μm (n = 3) | 149 |
| Figure 4.6: Comparative erosion of plain MC/HPMC compacts (n = 3). | 150 |
| Figure 4.7: Swelling profiles of A4M/FBP, (a) 90-150 μm and (b) 150-250 μm and A4M/THP (c) 90-150 μm and (d) 150-250 μm hydrophilic matrices (n=3) | 155 |
| Figure 4.8: Comparative erosion of (a) A4M/FBP and (b) A4M/THP hydrophilic matrices (n=3)..... | 156 |
| Figure 4.9: Dissolution profiles of A4M/FBP hydrophilic matrices having A4M particle size (a) 90-150 μm and (b) 150-250 μm (n=3) | 157 |
| Figure 4.10: Dissolution profiles of A4M/THP hydrophilic matrices having A4M particle size (a) 90-150 μm and (b) 150-250 μm (n=3) | 158 |
| Figure 4.11: Swelling profiles of F4M/FBP, (a) 90-150 μm and (b) 150-250 μm and F4M/THP (c) 90-150 μm and (d) 150-250 hydrophilic matrices (n=3) | 162 |
| Figure 4.12: Comparative erosion of (a) F4M/FBP and (b) F4M/THP hydrophilic matrices (n=3)..... | 163 |
| Figure 4.13: Dissolution profiles of F4M/FBP hydrophilic matrices having F4M particle size (a) 90-150 μm and (b) 150-250 μm (n=3).... | 164 |
| Figure 4.14: Dissolution profiles of F4M/THP hydrophilic matrices having F4M particle size (a) 90-150 μm and (b) 150-250 μm (n = 3) | 165 |
| Figure 4.15: Swelling profiles of E4M/FBP, (a) 90-150 μm and (b) 150-250 μm and E4M/THP (c) 90-150 μm and (d) 150-250 μm hydrophilic matrices (n = 3)..... | 169 |
| Figure 4.16: Comparative erosion of (a) E4M/FBP and (b) E4M/THP hydrophilic matrices (n = 3)..... | 170 |

| | |
|--|-----|
| Figure 4.17: Dissolution profiles of E4M/FBP hydrophilic matrices having E4M particle size (a) 90-150 μm and (b) 150-250 μm (n = 3) | 171 |
| Figure 4.18: Dissolution profiles of E4M/THP hydrophilic matrices having E4M particle size (a) 90-150 μm and (b) 150-250 μm (n = 3) | 172 |
| Figure 4.19: Swelling profiles of K4M/FBP, (a) 90-150 μm and (b) 150-250 μm and K4M/THP (c) 90-150 μm and (d) 150-250 μm hydrophilic matrices (n = 3) | 176 |
| Figure 4.20: Comparative erosion profiles of (a) K4M/FBP and (b) K4M/THP hydrophilic matrices (n = 3) | 177 |
| Figure 4.21: Dissolution profiles of K4M/FBP hydrophilic matrices having K4M particle size (a) 90-150 μm and (b) 150-250 μm (n = 3) | 178 |
| Figure 4.22: Dissolution profiles of K4M/THP hydrophilic matrices having K4M particle size (a) 90-150 μm and (b) 150-250 μm (n = 3) | 179 |
| Figure 4.23: Swelling profiles of K15M/FBP, (a) 90-150 μm and (b) 150-250 μm and K15M/THP (c) 90-150 μm and (d) 150-250 μm hydrophilic matrices (n = 3) | 181 |
| Figure 4.24: Comparative erosion of (a) K15M/FBP and (b) K15M/THP hydrophilic matrices (n = 3) | 182 |
| Figure 4.25: Dissolution profiles of K15M/FBP hydrophilic matrices having K15M particle size (a) 90-150 μm and (b) 150-250 μm (n = 3) | 183 |
| Figure 4.26: Dissolution profiles of K15M/THP hydrophilic matrices having K15M particle size (a) 90-150 μm and (b) 150-250 μm (n = 3) | 184 |
| Figure 4.27: Swelling profiles of K100M/FBP, (a) 90-150 μm and (b) 150-250 μm and E4M/THP (c) 90-150 μm and (d) 150-250 μm hydrophilic matrices (n = 3) | 186 |
| Figure 4.28: Comparative erosion of (a) K100M/FBP and (b) K100M/THP hydrophilic matrices (n = 3) | 187 |

| | |
|---|-----|
| Figure 4.29: Dissolution profiles of K100M/FBP hydrophilic matrices having K100M particle size (a) 90-150 μm and (b) 150-250 μm (n = 3) | 188 |
| Figure 4.30: Dissolution profiles of K100M/THP hydrophilic matrices having K100M particle size (a) 90-150 μm and (b) 150-250 μm (n = 3) | 189 |
| Figure 4.31: Effect of swelling on IDR of FBP based matrix tablets, (a) A4M (b) F4M (c) E4M (d) K4M (e) K15M (f) K100M having polymer particle size 90-150 μm and 150-250 μm (n = 3) | 195 |
| Figure 4.32: Effect of swelling on IDR of THP based matrix tablets, (a) A4M (b) F4M (c) E4M (d) K4M (e) K15M (f) K100M having polymer particle size 90-150 μm and 150-250 μm (n = 3) | 196 |
| Chapter 5 | |
| Figure 5.1: Dissolution/erosion profiles of cellulose ethers based matrix tablets of particle size (a) 90-150 (b) 150-250 μm (n = 3) | 204 |
| Figure 5.2: Effect of HPMC (K4M) concentration on the (a) FBP and (b) THP release from matrix tablets..... | 209 |
| Figure 5.3: Effect of HPMC concentration on the HPMC release from (a) FBP and (b) THP containing matrix tablets..... | 211 |
| Figure 5.4: Erosion profiles of HPMC/FBP matrix tablets, (a) gravimetric technique and (b) phenol-sulphuric acid assay method. | 214 |
| Figure 5.5: Erosion profiles of HPMC/THP matrix tablets, (a) gravimetric technique and (b) phenol-sulphuric acid assay method | 215 |
| Figure 5.6: Comparative analysis of erosion rates calculated from both techniques..... | 218 |
| Figure 5.7: Comparative analysis of degree of erosion calculated from both techniques, (a) FBP and (b) THP based hydrophilic matrices | 219 |

| | |
|---|-----|
| Figure 5.8: Residual plot of erosion rate, a comparison between GM and PSA techniques... | 220 |
| Figure 5.9: Residual plot of comparative degree of erosion between GM and PSA assay, (a) FBP and (b) THP matrices..... | 222 |
| Figure 5.10: Comparative analysis between HPMC erosion rate (k) and drug release diffusional exponent (n)..... | 224 |
| Chapter 6 | |
| Figure 6.1: Schematic illustration of different phases of powder compaction | 232 |
| Figure 6.2: Schematic illustration of a typical Heckel plot, representing three different powder compression regions..... | 243 |
| Figure 6.3: Schematic illustration of a typical engineering strain (C) and compressional pressure (MPa) and interpretation of Kawakita parameters | 245 |
| Figure 6.4: A typical force-displacement curve for FBP and THP | 248 |
| Figure 6.5: In-die relative density profile of model drugs | 250 |
| Figure 6.6: In-die porosity profile of model drugs. | 250 |
| Figure 6.7: Heckel plots of FBP and THPwith respect to compression pressure..... | 251 |
| Figure 6.8: Kawakita plots of model drugs with respect to compression pressure | 251 |
| Figure 6.9: Schematic illustrating the compaction mechanisms of FBP and THP..... | 253 |
| Figure 6.10: In-die relative density profiles of Methocel [®] with respect to compression pressure (a) 90-150 μm and (b) 150-250 μm | 261 |
| Figure 6.11: In-die porosity profiles of Methocel [®] with respect to compression pressure (a) 90-150 μm and (b) 150-250 μm | 262 |
| Figure 6.12: Heckel plots of Methocel [®] with respect to compression pressure (a) 90-150 μm and (b) 150-250 μm (n = 3) | 264 |

| | |
|---|-----|
| Figure 6.13: Kawakita plots of Methocel [®] with respect to compression pressure (a) 90-150 μm and (b) 150-250 μm | 265 |
| Figure 6.14: Compaction mechanism of MC/HPMC : FBP/THP matrices..... | 273 |
| Figure 6.15: In-die relative density profiles of matrices with respect to compression pressure (a) A4M: FBP and (b) A4M : THP (n = 3)..... | 274 |
| Figure 6.16: In-die porosity profiles of matrices with respect to compression pressure (a) A4M : FBP and (b) A4M : THP (n = 3) | 275 |
| Figure 6.17: Heckel plots of matrices with respect to compression pressure (a) A4M : FBP and (b) A4M : THP (n = 3)..... | 277 |
| Figure 6.18: Kawakita plots of matrices with respect to compression pressure (a) A4M : FBP and (b) A4M : THP (n = 3)..... | 278 |
| Figure 6.19: In-die relative density profiles of matrices with respect to compression pressure (a) F4M : FBP and (b) F4M : THP (n = 3) | 282 |
| Figure 6.20: In-die porosity profiles of matrices with respect to compression pressure (a) F4M : FBP and (b) F4M : THP (n = 3)..... | 283 |
| Figure 6.21: Heckel plots of matrices with respect to compression pressure (a) F4M : FBP and (b) F4M : THP (n = 3)..... | 285 |
| Figure 6.22: Kawakita plots of matrices with respect to compression pressure (a) F4M : FBP and (b) F4M : THP (n = 3)..... | 286 |
| Figure 6.23: In-die relative density profiles of matrices with respect to compression pressure (a) E4M : FBP and (b) E4M : THP (n = 3)..... | 290 |
| Figure 6.24: In-die porosity profiles of matrices with respect to compression pressure (a) E4M : FBP and (b) E4M : THP (n = 3). | 291 |
| Figure 6.25: Heckel plots of matrices with respect to compression pressure (a) E4M : FBP and (b) E4M : THP (n = 3)..... | 293 |

| | |
|--|-----|
| Figure 6.26: Kawakita plots of matrices with respect to compression pressure (a) E4M : FBP and (b) E4M : THP (n = 3)..... | 294 |
| Figure 6.27: In-die relative density profiles of matrices with respect to compression pressure (a) K4M : FBP and (b) K4M : THP (n = 3)..... | 298 |
| Figure 6.28: In-die porosity profiles of matrices with respect to compression pressure (a) K4M : FBP and (b) K4M : THP (n = 3) | 299 |
| Figure 6.29: Heckel plots of matrices with respect to compression pressure (a) K4M : FBP and (b) K4M : THP (n = 3)..... | 301 |
| Figure 6.30: Kawakita plots of matrices with respect to compression pressure (a) K4M : FBP and (b) K4M : THP (n = 3)..... | 302 |
| Figure 6.31: In-die relative density profiles of matrices with respect to compression pressure (a) K15M : FBP and (b) K15M : THP (n = 3)..... | 304 |
| Figure 6.32: In-die porosity profiles of matrices with respect to compression pressure (a) K15M : FBP and (b) K15M : THP (n = 3) | 305 |
| Figure 6.33: Heckel plots of matrices with respect to compression pressure (a) K15M : FBP and (b) K15M : THP (n = 3)..... | 307 |
| Figure 6.34: Kawakita plots of matrices with respect to compression pressure (a) K15M: FBP and (b) K15M : THP (n = 3)..... | 308 |
| Figure 6.35: In-die relative density plots of matrices with respect to compression pressure (a) K100M : FBP and (b) K100M : THP (n = 3) | 310 |
| Figure 6.36: In-die porosity plots of matrices with respect to compression pressure (a) K100M : FBP and (b) K100M : THP (n = 3) | 311 |
| Figure 6.37: Heckel plots of matrices with respect to compression pressure (a) K100M : FBP and (b) K100M : THP (n = 3)..... | 313 |

Figure 6.38: Kawakita plots of matrices with respect to compression pressure (a) K100M : FBP and (b) K100M : THP ($n = 3$)314

Figure 6.39: Relationship between P_y and b^{-1} of FBP based matrices, (a) A4M, (b) F4M, (c) E4M, (d) K4M, (e) K15M AND (f) K100M317

Figure 6.40: Relationship between P_y and b^{-1} of THP based matrices, (a) A4M, (b) F4M, (c) E4M, (d) K4M, (e) K15M AND (f) K100M318

List of Tables

Chapter 2

Table 2.1: Specifications of methylcellulose (MC) and hypromellose (HPMC).....21

Table 2.2: Equations derived from standard calibration curves of model drugs.22

Table 2.3: Equations derived from standard calibration curves of different Methocel[®] grades.
.....37

Chapter 3

Table 3.1: Summary of insulator-metal tribo-electric charging theories56

Table 3.2: Summary of factors affecting tribo-electric charging61

Table 3.3: Tribo-electric charging and surface adhesion results for theophylline and flurbiprofen (standard deviations in parentheses).....80

Table 3.4: Charge-to-mass ratio and percentage particle adhesion of MC/HPMC (standard deviation is shown in parentheses, n=3)89

Table 3.5: Content uniformity of powder mixture containing (a) FBP and (b) THP (n=3)....96

Table 3.6: Adhesion (%) of polymer/ FBP powder mixtures (standard deviation in parentheses, n=3)111

Table 3.7: Adhesion (%) of polymer/ THP powder mixtures (standard deviation in parentheses, n=3)112

Table 3.8: Inter-relationship between tribo-electric charge and surface adhesion (n = 3)....118

Chapter 4

Table 4.1: Summary of factors affecting drug release from Methocel[®] based hydrophilic matrices138

| | |
|--|-----|
| Table 4.2: Solubility and dissolution parameters of FBP and THP (n = 3, standard deviation given in parenthesis) | 142 |
| Table 4.3: Swelling kinetics and erosion parameters of plain Methocel® compacts (n = 3, standard deviation given in parenthesis) | 150 |
| Table 4.4: Content uniformity of powder mixture containing FBP and THP (n=3)..... | 151 |
| Table 4.5: Swelling kinetics and matrix erosion of A4M based hydrophilic matrices (n = 3, standard deviation given in parenthesis) | 156 |
| Table 4.6: Summary of dissolution parameters of A4M based hydrophilic matrices (n = 3, standard deviation given in parenthesis) | 159 |
| Table 4.7: Summary of drug release kinetics parameters from A4M based hydrophilic matrices (n=3) | 159 |
| Table 4.8: Swelling kinetics and matrix erosion of F4M based hydrophilic matrices (n = 3, standard deviation given in parenthesis) | 163 |
| Table 4.9: Summary of dissolution parameters of F4M based hydrophilic matrices (n = 3, standard deviation given in parenthesis) | 166 |
| Table 4.10: Summary of drug release kinetics parameters of F4M based hydrophilic matrices (n = 3) | 166 |
| Table 4.11: Swelling kinetics and matrix erosion of E4M based hydrophilic matrices (n = 3, standard deviation given in parenthesis) | 170 |
| Table 4.12: Summary of dissolution rate parameters of E4M based hydrophilic matrices (n = 3, standard deviation given in parenthesis) | 173 |
| Table 4.13: Summary of drug release kinetics parameters of E4M based hydrophilic matrices (n = 3) | 173 |
| Table 4.14: Swelling kinetics and matrix erosion of K4M based hydrophilic matrices (n = 3, standard deviation given in parenthesis) | 177 |

| | |
|--|-----|
| Table 4.15: Summary of dissolution parameters of K4M based hydrophilic matrices (n = 3, standard deviation given in parenthesis)..... | 180 |
| Table 4.16: Summary of drug release kinetic parameters of K4M based hydrophilic matrices (n = 3)..... | 180 |
| Table 4.17: Swelling kinetics and matrix erosion of K15M based hydrophilic matrices (n = 3, standard deviation given in parenthesis)..... | 182 |
| Table 4.18: Summary of dissolution parameters of K15M based hydrophilic matrices (n = 3, standard deviation given in parenthesis)..... | 185 |
| Table 4.19: Summary of drug release kinetic parameters of K15M based hydrophilic matrices (n = 3)..... | 185 |
| Table 4.20: Swelling kinetics and matrix erosion of K100M based hydrophilic matrices (n = 3)..... | 187 |
| Table 4.21: Summary of dissolution parameters of K100M based hydrophilic matrices (n = 3, standard deviation given in parenthesis)..... | 190 |
| Table 4.22: Summary of drug release kinetics parameters of K100 based hydrophilic matrices (n = 3)..... | 190 |
| Table 4.23: Correlation co-efficient of swelling and IDR inter-relationship (n = 3)..... | 194 |

Chapter 5

| | |
|---|-----|
| Table 5.1: Summary of MC/HPMC erosion kinetics parameters (n = 3). | 205 |
| Table 5.2: HPMC (K4M) and drug release kinetics parameters of THP and FBP matrix tablets (n = 3, standard deviation are in parenthesis)..... | 212 |
| Table 5.3: Erosion kinetic parameters for THP and FBP matrix tablets..... | 216 |
| Table 5.4: Comparison of erosion rates of matrix tablets from gravimetric and PSA assay from residual plots | 220 |

| | |
|--|-----|
| Table 5.5: Comparison of degree of erosion (%) of matrix tablets from gravimetric and PSA assay from residual plots (n = 3, standard error is in parenthesis) | 221 |
|--|-----|

Chapter 6

| | |
|--|-----|
| Table 6.1: Summary of factors affecting compaction properties of Methocel® matrices.... | 240 |
|--|-----|

| | |
|--|-----|
| Table 6.2: Relative density, porosity (in-die and out-of-die), tensile strength and elastic recovery of FBP and THP compacts (n = 3, standard deviation given in parenthesis) | 252 |
|--|-----|

| | |
|---|-----|
| Table 6.3: Heckle and Kawakita compression parameters for FBP and THP compacts (n = 3) | 252 |
|---|-----|

| | |
|---|-----|
| Table 6.4: Relative density, porosity (in-die and out of die), tensile strength and elastic recovery of Methocel® compacts (n = 3, standard deviation given in parenthesis)..... | 263 |
|---|-----|

| | |
|---|-----|
| Table 6.5: Heckel and Kawakita compression parameters of Methocel® compacts (n = 3). | 266 |
|---|-----|

| | |
|---|-----|
| Table 6.6: Summary of In-die and out of die relative density values of A4M : FBP/THP matrices (n = 3)..... | 276 |
|---|-----|

| | |
|---|-----|
| Table 6.7: Summary of In-die and out of die porosity values of A4M : FBP/THP matrices (n = 3)..... | 276 |
|---|-----|

| | |
|--|-----|
| Table 6.8: Summary of tensile strength and elastic recovery of A4M : FBP/THP matrices (n = 3, standard deviation given in parenthesis)..... | 279 |
|--|-----|

| | |
|--|-----|
| Table 6.9: Summary of Heckel and Kawakita compressional parameters of A4M : FBP/THP matrices (n = 3). | 279 |
|--|-----|

| | |
|--|-----|
| Table 6.10: Summary of In-die and out of die relative density values of F4M : FBP/THP matrices (n = 3). | 284 |
|--|-----|

| | |
|---|-----|
| Table 6.11: Summary of In-die and out of die porosity values of F4M : FBP/THP matrices (n = 3)..... | 284 |
| Table 6.12: Summary of tensile strength and elastic recovery of F4M : FBP/THP matrices (n = 3)..... | 287 |
| Table 6.13: Summary of Heckel and Kawakita compressional parameters of F4M : FBP/THP matrices (n = 3)..... | 287 |
| Table 6.14: Summary of In-die and out of die relative density values of E4M : FBP/THP matrices (n = 3)..... | 292 |
| Table 6.15: Summary of In-die and out of die porosity values of E4M : FBP/THP matrices (n = 3)..... | 292 |
| Table 6.16: Summary of tensile strength and elastic recovery of E4M : FBP/THP matrices (n = 3, standard deviation given in parenthesis)..... | 295 |
| Table 6.17: Summary of Heckel and Kawakita compressional parameters of E4M : FBP/THP matrices (n = 3)..... | 295 |
| Table 6.18: Summary of In-die and out of die relative density values of K4M : FBP/THP matrices (n = 3)..... | 300 |
| Table 6.19: Summary of In-die and out of die porosity values of K4M : FBP/THP matrices (n = 3)..... | 300 |
| Table 6.20: Summary of tensile strength and elastic recovery of K4M : FBP/THP matrices (n = 3, standard deviation given in parenthesis)..... | 303 |
| Table 6.21: Summary of Heckel and Kawakita compressional parameters of K4M : FBP/THP matrices (n = 3)..... | 303 |
| Table 6.22: Summary of In-die and out of die relative density values of K15M : FBP/THP matrices (n = 3)..... | 306 |

| | |
|--|-----|
| Table 6.23: Summary of In-die and out of die porosity (%) values of K15M : FBP/THP matrices (n = 3). | 306 |
| Table 6.24: Summary of tensile strength and elastic recovery of K15M : FBP/THP matrices (n = 3, standard deviation given in parenthesis) | 309 |
| Table 6.25: Summary of Heckel and Kawakita compressional parameters of K15M : FBP/THP matrices (n = 3). | 309 |
| Table 6.26: Summary of In-die and out of die relative density values of K100M : FBP/THP matrices (n = 3). | 312 |
| Table 6.27: Summary of in-die and out of die porosity (%) values of K100M : FBP/THP matrices (n = 3). | 312 |
| Table 6.28: Summary of tensile strength and elastic recovery of K100M : FBP/THP matrices (n = 3, standard deviation given in parenthesis) | 315 |
| Table 6.29: Summary of Heckel and Kawakita compressional parameters K100M : FBP/THP matrices (n = 3). | 315 |
| Table 6.30: Correlation co-efficients of P_y and b^{-1} inter-relationship (n = 3) | 316 |

List of abbreviations

| | |
|-------|-----------------------------------|
| AGU | Anhydroglucose unit |
| ANOVA | Analysis of variance |
| API | Active pharmaceutical ingredient |
| CMC | Carboxymethyl cellulose |
| CPD | Contact potential difference |
| Cp | Centipoise |
| CR | Controlled release |
| CI | Compressibility index |
| DC | Direct compression |
| DSC | Differential scanning calorimetry |
| EC | Ethyl cellulose |
| ER | Extended release |
| FBP | FBP |
| FG | Food grade |
| GIT | Gastrointestinal tract |
| GM | Gravimetric method |
| HCO | Hydrogenated castor oil |
| HEC | Hydroxyethyl cellulose |
| HPMC | Hydroxypropyl methylcellulose |

| | |
|----------------|---------------------------------------|
| Hpo | Hydroxypropyl |
| IDR | Intrinsic dissolution rate |
| kN | Kilonewtons |
| LV | Low viscosity |
| MC | Methylcellulose |
| Meo | Methoxy |
| MPa | Megapascals |
| NSAIDs | Non-steroidal anti-inflammatory drugs |
| PS | Polystyrene |
| PET | Polyethylene terephthalate |
| PI | Plasticity index |
| PSA | Phenol-sulphuric acid assay |
| PTFE | Polytetrafluoroethylene |
| PVC | Polyvinyl chloride |
| PXRD | Powder x-ray diffraction |
| P_y | Yield pressure |
| R ² | Correlation co-efficient |
| RH | Relative humidity |

UV

Ultraviolet

W

Work function

1-Introduction

1- Introduction

1.1- Cellulose ethers

Over the past few decades, the application of polymers in the science of drug delivery has led to the development of numerous polymer-based drug delivery systems (Wen *et al.*, 2010). Among them, hydrophilic cellulose ethers are unarguably the most frequent and widely used polymers, and are usually manufactured through etherification of cellulose (Maderuelo *et al.*, 2011). Cellulose is an abundantly occurring biopolymer and there are many sources considered suitable for cellulose ether manufacturing. These include seed fibres (cotton), wood fibres, bast fibres, grasses, algae and bacteria, however, cotton seed and wood fibres are considered to be the prime and more reliable sources (Craver and Carraher, 2000). Cellulose is a polysaccharide made up of glucose units with an empirical formula $C_6H_{12}O_6$ and sometimes designated as a beta-D-glucopyranose or anhydroglucose unit (AGU). These units usually hooked together through a condensation reaction to form a cellulose molecule (Figure 1.1). It is insoluble in water and its poor solubility is considered to be linked primarily with the strong inter- and intra-molecular hydrogen bonding between the individual polymer chains. Despite its poor solubility, it is used in range of applications including netting, composites, upholstery, coatings and paper. Moreover, chemical modification can be performed to produce different derivatives suited for specific pharmaceutical applications (Feller and Wilt, 1991; Wertz *et al.*, 2010).

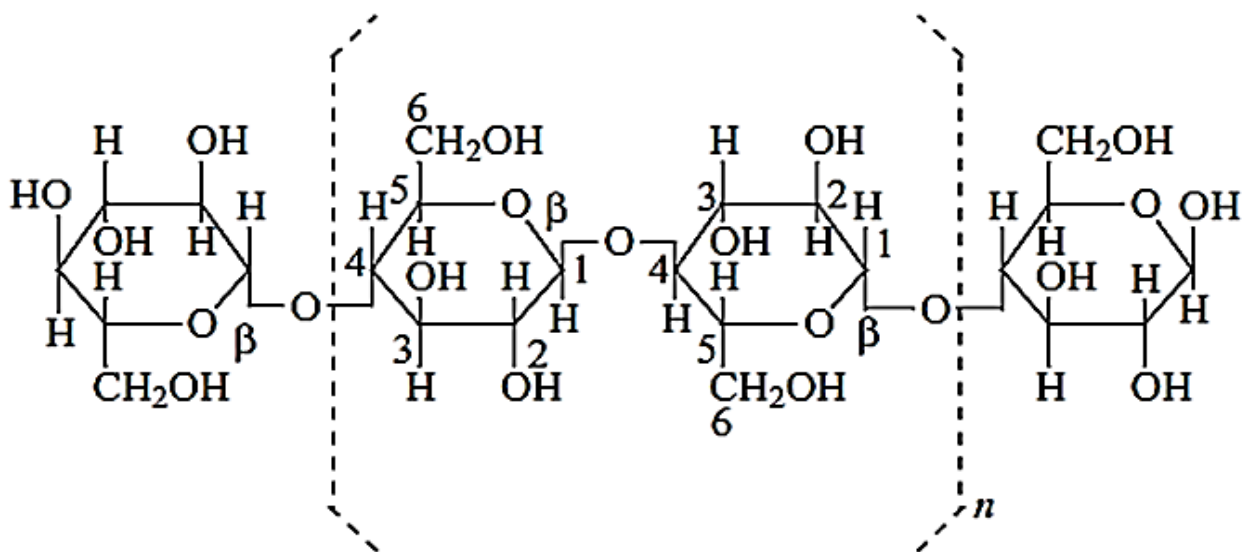


Figure 1.1, Structure of cellulose

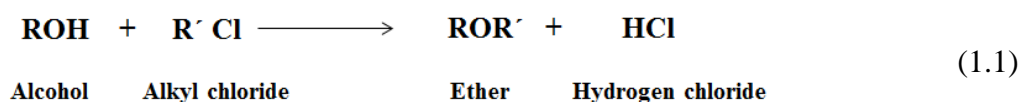
In 2000, the net global consumption of cellulose ethers was estimated to be 371,000 tonnes, with a total world market of nearly \$2.0 billion. An overall average growth rate of 3.5 % per year is expected for all cellulose ether products in 2012–2018. In Asia, the lowest growth is expected in Japan, while China will lead global growth. The regions with the largest current consumption are Europe and China with an annual growth rate of 2.0 % and 4.6 %, respectively (SRI, 2013). Their popularity can be attributed to their non-toxic and biocompatible properties, with some even being approved as direct food additives (Alderman, 1984).

The only considerable recognised risk related to cellulose ethers utilization is that they may form flammable dusts when finely divided powder particles are suspended in air. An explosion may result if suspended dust contacts an ignition source. Cloud and layer ignition temperatures generally vary between 290 and 410 °C and critical airborne concentrations vary depending on particle size. This hazard can be minimized largely through good housekeeping

and proper design and operation of handling equipment (NFPA, 1986). Another minor hazard is associated with water-soluble cellulose ether powders as they have a tendency to form a slippery surface when wet; therefore spills should be cleaned immediately in the working area to avoid slipping mishaps.

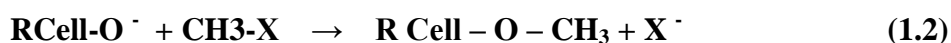
1.2- Manufacturing of cellulose ethers

In 1912 the first experimental work was conducted to produce useful derivatives of cellulose. Firstly, methyl and ethyl derivatives were manufactured but soon after that carboxymethylcellulose (CMC) and hydroxyethylcellulose (HEC) were produced (Worden, 2011). In 1920s, Germany started to produce these cellulose ethers on a commercial scale, however, in United States commercial production was started in 1930s. The presence of hydroxyl groups in cellulose structure gave a hope to organic chemists that it could be converted to useful derivatives and since then, there have been much advancement in the preparation methodologies (Kroschwitz and Seidel, 2007; Mark, 2014; Worden, 2011). The building blocks of cellulose are AGUs bound through β -1,4-glycosidic linkages (Figure 1.1). The AGU rings contain three hydroxyl groups, a primary hydroxyl at the C- 6 position and two secondary groups at the C- 2 and C- 3 positions. In the native state the chains are linked together by strong inter- and intra-molecular bonds and as a result cellulose is not water soluble (Wertz *et al.*, 2010). For manufacturing of cellulose ethers, the irreversible nucleophilic substitution reaction is commonly employed and its simplified form can be expressed as shown in scheme 1.1 (Trimm, 2011).



Where other organic radicals are represented by R, such as methyl (- CH₃), ethyl (- C₂H₅), hydroxypropyl (- CH₂CH(OH)CH₃) or any other complex moiety.

Cellulose ethers are commonly manufactured on a commercial scale by reaction of purified cellulose with alkylating reagents, usually in the presence of a base (sodium hydroxide) and an inert diluent (acetone or propanol) (Salamone, 1996). The combination of water and base activates the cellulose matrix by disrupting hydrogen-bonded crystalline regions, thereby increasing accessibility to the alkylating reagent and this activated matrix is termed ‘alkali cellulose’ (Mark, 2014). Methylcellulose (MC) is usually produced by methylation of alkali cellulose through methyl halide, as shown in scheme 1.2:



Where, RCell-O⁻ is ‘alkali cellulose’ and RCell-O-CH₃ is methylcellulose.

Hydroxypropyl methylcellulose (HPMC), a mixed cellulose ether, is prepared by reaction of mixtures of methyl chloride and propylene oxide with alkali cellulose (CH₃ CH CH₂O) as shown in scheme 1.3;



Where, Rcell-O-CH₂CH(OH)CH₃ is hydroxypropyl methylcellulose.

The ratios of methyl and hydroxypropyl groups can be controlled by changing the concentration of the reactants (România, 1995). To make this complex manufacturing process more commercially reliable and robust, different types of reagents can be added. Likewise inert diluents are frequently used in these processes which firstly suspend/disperse the cellulose, provide heat transfer, moderate reaction kinetics, and facilitate recovery of the

product. Secondly, the diluent can facilitate the reagents' distribution which might lead to uniform reaction (Yokota, 1985). Moreover, these reactions are typically conducted at elevated temperatures ($\sim 50\text{--}140^\circ\text{C}$), under nitrogen, to inhibit oxidative molecular weight degradation of the polymer (Kroschwitz and Seidel, 2007). After reaction, crude grades are simply dried, ground, and packed; however, purified grades require eradication of by-products before drying. Low concentrations of colloidal silica can be added to some products prior to drying or before packaging to improve handling operations (Mark, 2014; Worden, 2011). A schematic outline of the manufacturing process is illustrated in Figure 1.2.

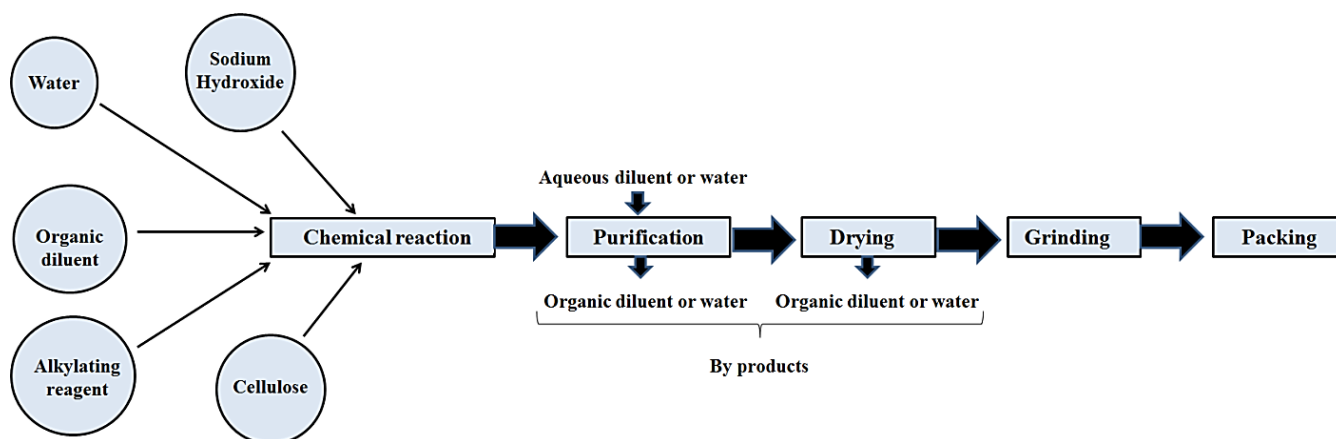
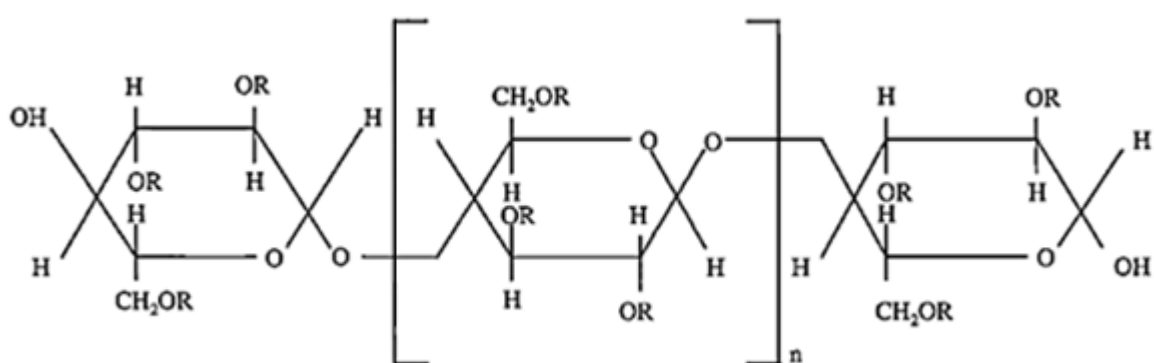


Figure 1.2, Schematic outline of cellulose ether manufacturing process (Mark, 2014)

1.3- Derivatives of cellulose ethers

Cellulose ethers are a commercially important class of polymers and their properties are generally determined by their molecular weights, distribution of the substitution groups and degree of substitution. Moreover, their important intrinsic properties usually include solubility, viscosity and stability against biodegradation, hydrolysis and oxidation. Examples

of mostly used cellulose ethers are: methylcellulose (MC), hydroxypropyl methylcellulose (HPMC), hydroxyethylcellulose (HEC), hydroxypropyl cellulose (HPC), ethylcellulose (EC) and sodium carboxymethylcellulose (NaCMC). However, MC and HPMC are most frequently employed candidates in pharmaceutical controlled release matrix systems (Wen *et al.*, 2010). A general chemical structure of cellulose ethers with their respective substituents (R) is shown in Figure 1.3.



| Cellulose ether | Substituents (R) |
|-----------------|---|
| MC | -H, -CH ₃ |
| HPMC | -H, -CH ₃ , -CH ₂ CH(OH)CH ₃ |
| HPC | -H, -CH ₂ CH(OH)CH ₃ |
| EC | -H, -C ₂ H ₅ |
| HEC | -H, -CH ₂ CH ₂ OH |
| NaCMC | -H, -CH ₂ COONa |

Figure 1.3, Structure of cellulose ethers

1.3.1- Methylcellulose

Methylcellulose is a long chain, linear, non-ionic and substituted cellulose in which almost 27–32 % of parent hydroxyl groups are in the form of the methyl ether (Mark, 2014). Methylcellulose is an odourless, tasteless, white, fibrous granular powder which is practically insoluble in acetone, chloroform, methanol, ethanol (95%), ether, saturated salt solutions, toluene, and hot water. In cold water, methylcellulose swells and disperses slowly to form a clear to opalescent, viscous and colloidal dispersion (Rowe *et al.*, 2012).

The various grades of methylcellulose have degrees of polymerization in the range 50–1000, with molecular weights (average number) in the range of 10 000 – 220 000 Da. The degree of methylcellulose substitution is defined as the average number of methoxyl (- OCH₃) groups attached to each of the AGUs along the chain. The degree and levels of substitution affect the physical properties of methylcellulose, including its solubility. MC contains a two-fold helix conformation similar to cellulose, however, the integration of - OCH₃ groups on glucose monomer induce steric hindrance which in turn opens up the cellulose backbone (Embuscado, 2014) resulting in an ability to dissolve in cold water (Sarkar and Walker, 1995).

MC is available commercially from a number of sources; grades in this thesis were from Dow Chemical Company. The first part of the trade name (A) is indicative of its chemistry which is followed by an indication of the viscosity of an aqueous 2% w/w solutions (cps) at 20 °C, with a multiplier of 100 (denoted by the letter C) or 1000 (denoted by the letter M). A final suffix identifies the grade of the material, such as premium (P), low viscosity (LV), controlled release (CR), granular (G), surface treated (S) or food grade (FG) (Dow, 2006).

1.3.2- Hypromellose (Hydroxypropyl methylcellulose, HPMC)

Hydroxypropyl methylcellulose (HPMC) is a semisynthetic, inert, viscoelastic polymer used as an excipient in pharmaceutical formulations and a controlled-delivery component in oral medicaments (Wertz *et al.*, 2010). It is a non-ionic, odourless, tasteless, white or creamy-white fibrous or granular powder. It is soluble in cold water, forming a viscous colloidal solution; practically insoluble in hot water, chloroform, ethanol (95%), and ether, but soluble in mixtures of ethanol and dichloromethane, mixtures of methanol and dichloromethane, and mixtures of water and alcohol. It is available in several grades that vary in viscosity and extent of substitution (Rowe *et al.*, 2012).

HPMC also contains a two-fold helix conformation similar to MC and cellulose but the presence of -OCH₃ and hydroxypropoxy groups (-CH₂CH(OH)CH₃) on AGUs induce steric hindrance which opens up the cellulose backbone in a similar manner to MC. This modification in chemical structure of HPMC also confers the ability to dissolve in cold water same (like MC, as described earlier in section 1.3.1) (Embuscado, 2014). However, the presence of different levels of -CH₂CH(OH)CH₃ groups in various HPMC grades affects their gelation behaviour (Sarkar and Walker, 1995). HPMC produces strong films but these are not as strong as those produced using MC because MC has a linear structure and non-ionic nature, ideal for inter-polymer association which is necessary for films development. However, in case of HPMC the -CH₂CH(OH)CH₃ groups result in a greater level of steric hindrance which keeps these HPMC polymeric chains further apart compared to MC (Embuscado, 2014).

Many commercial hypromelloses are identified by codes. For instance, for those manufactured by the Dow Chemical Company, the first part of the nomenclature is a letter (E, F or K) that relates to the degree of substitution. The K grades (hypromellose 2208) have a methoxy substitution of 19–24% and a hydroxypropyl substitution of 7–12%. F grades

(hypromellose 2906) have a methoxy substitution of 27–30% and a hydroxypropyl substitution of 4.0– 7.5%. E grades (hypromellose 2910) have a methoxy substitution of 28–30% and a hydroxypropyl substitution of 7–12% (Dow Commercial Information 2002). This first letter is followed by an indication of the viscosity of their aqueous 2% w/w gels (in centipoises) at 20 °C, with a multiplier of 100 (denoted by the letter C) or 1000 (denoted by the letter M). A final suffix identifies the grade of the material, such as premium (P), low viscosity (LV), controlled release (CR), granular (G), surface treated (S) or food grade (FG). Controlled-release dosage forms mainly use the K or E grades of hypromellose (Dow, 2006).

1.4- Pharmaceutical applications of MC and HPMC

Methylcellulose (MC) and hypromellose (HPMC) are used extensively in the pharmaceutical industry for a wide range of purposes.

(i) Applications in pharmaceutical coating

Pharmaceutical solid dosage forms like tablets, pellets, pills, beads, granules and microcapsules are often coated for various reasons such as protection of sensitive drugs from humidity and inappropriate environmental conditions, taste masking or enabling site or time specific release characteristics (Wen *et al.*, 2010). MC and HPMC are generally hydrophilic, having excellent film-forming characteristics and are widely used for coating solid dosage forms (Banker *et al.*, 1981; Entwistle and Rowe, 1979). Lower molecular weight grades of MC and HPMC tend to be employed for coating tablets and granules. Film properties have been shown to be affected by the molecular weight of the polymer with higher molecular weight polymers producing harder and less elastic films (Fukui *et al.*, 2000; Macleod *et al.*, 1999; Pradhan *et al.*, 2014).

(ii) Ophthalmic applications

MC and HPMC are used as stabilizers and thickeners for ophthalmic solutions (eye drops and contact lens solutions) and ointments (Jansook *et al.*, 2014). The MC and HPMC reduce

surface tension which improves wetting and spreading of the solution over the surface of the eye (Kaur *et al.*, 2000; Liu *et al.*, 2006).

(iii) Applications as tablet binders

Wet granulation is an important tableting process in which drug substance is combined with other excipients and processed using solvent (aqueous or organic) with subsequent drying and sieving to produce uniform granules (Chowhan, 1980). The strong binding properties exhibited by MC and HPMC enable their utilization in granule preparation in moist and dry granulation formulations, to produce harder tablets upon compression (Itiola, 1991).

(iv) Applications as suspending agents

MC and HPMC can be used as suspending agents because of their viscosity enhancing properties. Choice of the optimum concentration and viscosity grade is vital, as too high a polymer concentration can cause gelling and failure of the sedimented particles to redisperse (Raghavan *et al.*, 2003).

(v) Applications as emulsifying agents

Cellulose ethers, especially MC and HPMC, act to stabilize an emulsion by forming a multimolecular film around the dispersed globules at the oil/water interface. They can also increase the viscosity of the continuous phase of an o/w emulsion. Lower molecular weight MC and HPMC were found to be better emulsifying agents than higher molecular weight grades because of their polymer chain flexibility (Schulz and Daniels, 2000; Wollenweber *et al.*, 2000).

(vi) Applications as extended release (ER) solid dosage form excipients

Matrices are very simple and efficient systems for controlling drug release from dosage forms. Cellulose ethers, in particular MC and HPMC, are widely used to develop ER hydrophilic matrices due to their good compression properties (Maderuelo *et al.*, 2011; Wen

et al., 2010). Varying concentration of MC and HPMC can be used to delay or control the drug release profiles regardless of their solubility characteristics, however, the relative solubility of the drug can affect the release mechanism; water soluble drugs are released mainly by diffusion but poorly water soluble drugs are released predominantly by erosion (Ghori *et al.*, 2014b; Li *et al.*, 2005).

(ix) Applications as compressibility enhancers

Almost 80 % of pharmaceutical products are administered in the form of tablets. There are different ways of tablet manufacturing but direct compression is a straight forward, simple and fast tablet compression technique. This method commonly used for tableting of medium to high potency drugs where the drug contents are less than 30 % of the formulation (Jivraj *et al.*, 2000). One of the common difficulties in direct compression and dry granulation is poor compaction properties of drugs, especially when the amount of drug in tablet formulation is more than 30 %. So, in these scenarios an efficient compressibility enhancer can help in the development of tablets having acceptable pharmaceutical characteristics. All of the cellulose ethers have good compaction properties and these can significantly improve compressibility of poorly compactable powder mixtures (Shokri and Adibkia, 2013).

(x) Applications as tablet fillers

MC and HPMC can be used as fillers in pharmaceuticals solid dosage forms because of their compatibility with the most of the other pharmaceutical excipients and drugs. Furthermore, neither of these polymers cause any irritancy to any part of gastrointestinal tract (GIT) (Shokri and Adibkia, 2013).

(xi) Applications as disintegrants

Solid oral dosage forms, specifically tablets, go through several steps before the drug reaches the systemic circulation. Among these, disintegration is the key initial step which starts immediately after administration and breaks up the dosage forms into smaller fragments in an

aqueous environment (Esezobo, 1989). MC and HPMC, in low concentrations, can be used as disintegration agents (Rowe *et al.*, 2012).

(xii) Miscellaneous pharmaceutical applications

Other pharmaceutical applications of MC include use as a bulk laxative and HPMC can be an alternative to gelatin in the manufacturing of hard-shell medicinal capsules (Sarkar, 1979). MC and HPMC have also been reported to have applications as a contraceptive as they have the ability to immobilize human sperm (Hofmann and Steiner, 1980; Loewit, 1977; Oyelola *et al.*, 1987).

1.5- Profiles of model drugs

1.5.1- Flurbiprofen

Flurbiprofen (FBP) is a propionic acid derivative, first synthesized in 1974 during the pharmacological testing of substituted phenylalkanoic acid and the most potent was substituted 2- (4-biophenyl) propionic acid (Lemke and Williams, 2012). It was initially marketed as a sodium salt for topical ophthalmic use in 1987 in United States. However, the first oral form of FBP (Ansaid[®]) was introduced in 1988. It is a white crystalline powder, practically insoluble in water, (variously reported as 0.034 mg/ml (Tavornvipas *et al.*, 2002), 0.008 mg/ml (Yalkowsky *et al.*, 2010) and 0.024 mg/ml (Maitre *et al.*, 2007)), however, it is freely soluble in alcohol (Sweetman, 2009). It has a high propensity to electrostatic charging, poor compaction and SA properties in comparison to other drugs and pharmaceutical excipients (Šupuk *et al.*, 2012; Šupuk *et al.*, 2013). It is a weak acid ($pK_a = 4.22$) (Xu and Madden, 2011) and contains a biphenyl group with a fluorine atom in the ortho position (Fig 1.4).

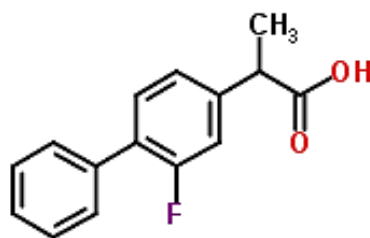


Figure 1.4, Structure of FBP.

FBP is a non-steroidal anti-inflammatory drug (NSAID), a group of drugs that have analgesic, anti-inflammatory, and antipyretic effects. NSAIDs inhibit cyclooxygenase (COX) and which is in turn responsible for the inhibition of biosynthesis of prostaglandins (PG) and thromboxanes from arachidonic acid (Katzung, 2007). It undergoes entero-hepatic circulation and extensively metabolised by phase-I and phase-II biotransformation reaction. It is recanted as a non-selective cox inhibitor as it inhibits both types of COX (COX-1 and COX-2) enzymes. Its anti-inflammatory action is more effective than ibuprofen as it inhibits both PGE₂ and PGF₂. However, inhibition of COX-1 is related to the toxic effects associated with GIT (August *et al.*, 1996). It is available in 50 and 100 mg tablets and indicated for acute or chronic osteoarthritis, and rheumatoid arthritis (BNF, 2014). The most prominent adverse effect related to NSAIDs is their toxicity prevailing in long term GIT intolerance and ulceration. The commonest adverse effects of FBP are generally GIT disturbances, such as GIT discomfort, nausea, and diarrhoea; these are usually mild and reversible but in some patients, peptic ulceration and severe GIT bleeding may occur. However, FBP is generally better tolerated compared to aspirin with low incidence of hepatic toxicity. Like other NSAIDs it is contraindicated for patients suffering from nasal polyps, rhinitis, angioedema, asthma, bronchospasm and allergy to FBP (Atkinson *et al.*, 2012; Bennett *et al.*, 2012) .

1.5.2- Theophylline

Theophylline (THP) is a methyl xanthine belonging to xanthine family. It was extracted from tea plant leaves and its chemical identification was carried out in 1888, moreover its commercial synthesis was started in 1895. THP was firstly marketed as a diuretic drug but later its anti-asthmatic action was established. In 1970s it was introduced to the market as a liquid syrup (Rheostat[®] 20 and Rheostat[®] 80) but in 1980s the first oral tablet (Quiroz[®]) was introduced in United States (Lemke and Williams, 2012). It is a white, odourless, crystalline powder which is slightly soluble in water, 8.3 g/L, (Yalkowsky *et al.*, 2010), sparingly soluble in alcohol, chloroform, and ether but freely soluble in solutions of alkali hydroxides and in ammonia (Sweetman, 2009). Chemically, it is 1,3-dimethylxanthine and contains an acidic and basic nitrogen at N-7 and N-9, respectively (Fig. 1.5). It has good compaction and electrostatic properties in comparison to FBP (Asare-Addo *et al.*, 2013b; Šupuk *et al.*, 2012; Šupuk *et al.*, 2013).

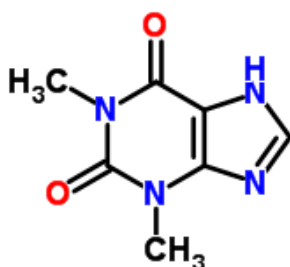


Figure 1.5, Structure of THP.

Although THP is considered among the pioneering drugs developed for the treatment of asthma and chronic obstructive pulmonary disease (COPD), its precise mode of action is still ambiguous. The main possibilities include non-selective phosphodiesterase inhibition and antagonistic effects of adenosine. It undergoes n-methylation due to cytochrome P450 1A2 and is extensively metabolised in liver (Atkinson *et al.*, 2012; Katzung, 2007). It is indicated

in reversible airways obstruction, severe acute and chronic asthma. However, it should be avoided in peptic ulcer, hypertension and cardiac diseases. Nausea, vomiting, insomnia, gastric irritation, tachycardia and palpitation are the typical adverse effects associated with THP (Craig and Stitzel, 2004).

1.6- Aims and objectives

The aims of this thesis were to understand the tribo-electrification, swelling, erosion, dissolution and compaction properties of MC and HPMC matrices containing model poorly soluble and soluble drugs, as summarised below (Figure, 1.6).

1.6.1- Tribo-electrification and adhesion studies

1. To investigate the tribo-electrification and adhesion properties of MC and HPMC powders.
2. To study the impact of polymeric attributes such as particle size fractions, substitution levels and molecular size (viscosity) on tribo-electric and adhesion properties.
3. To study the tribo-electrification and adhesion properties of model drugs.
4. To study the impact of varying proportions and physical attributes of MC and HPMC on tribo-electric and adhesion properties of model drugs.

1.6.2- Swelling, erosion and dissolution studies

1. To study the swelling and erosion properties of MC and HPMC matrices.
2. To study the impact of polymeric attributes such as particle size fractions, substitution levels and molecular size (viscosity) on the swelling and erosion properties.
3. Determination of intrinsic dissolution rate (IDR) for model drugs.

4. To study the impact of varying proportions and physical attributes of MC and HPMC on swelling, erosion and dissolution properties of hydrophilic matrices.
5. Development, characterisation and validation of phenol-sulphuric acid assay (PSA) based erosion determination technique for hydrophilic matrices.

1.6.3- Compaction studies

1. To study the compaction, compression and relaxation properties of MC and HPMC matrices.
2. To study the impact of polymeric attributes such as particle size fractions, substitution levels and molecular size (viscosity) on compaction, compression and relaxation properties of MC and HPMC.
3. To study the compaction, compression and relaxation properties of model drugs.
4. To study the impact of varying proportions and physical attributes of MC and HPMC on compaction, compression and relaxation properties of model drugs.

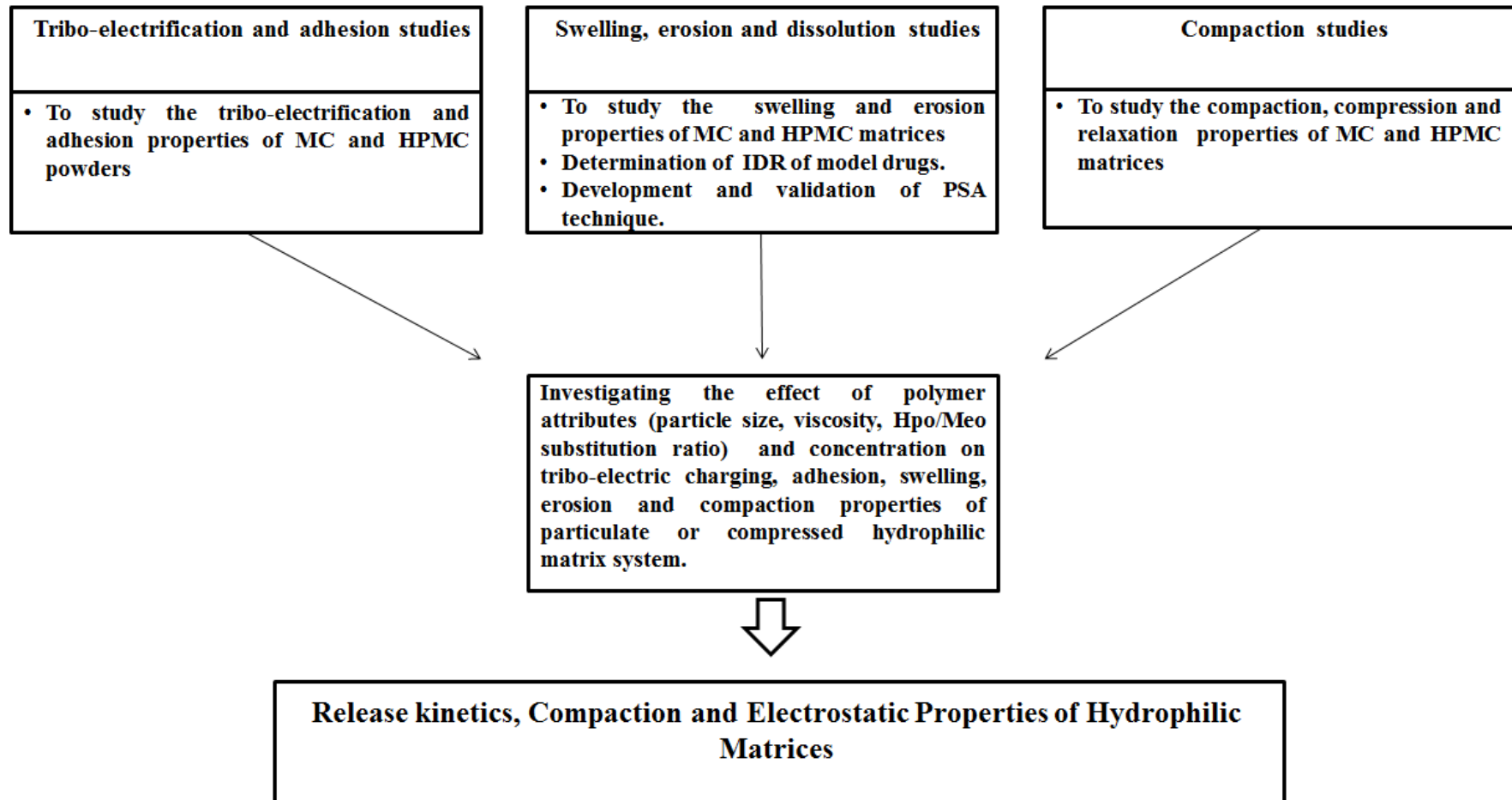


Figure 1.6, Outline of aims and objectives of thesis.

2-General experimental

2- General experimental

2.1-Materials

2.1.1- Cellulose ethers

Methylcellulose, MC, (Methocel[®] A4M) and hydroxypropyl methylcellulose, HPMC, (Methocel[®] F4M E4M, K4M, K15M and K100M) were donated by Colorcon Ltd. (Dartford, UK) and their specifications are listed in Table 2.1.

2.1.2- Model drugs

Flurbiprofen (FBP) and theophylline (THP) were purchased from Aesica Pharmaceutical Ltd, Cramlington, UK and Tokyo Chemical Industry Ltd, UK, respectively. A detailed description of both the drugs is given in section 1.5.

2.1.3- Buffering agents

Disodium hydrogen orthophosphate (Na_2HPO_4) and sodium dihydrogen orthophosphate (NaH_2PO_4) salts were purchased from Fisher Scientific, UK for the preparation of pH 7.2 sodium phosphate buffer.

Table 2.1, Specifications of methylcellulose (MC) and hypromellose (HPMC)

| Methocel[®] grade | Methoxy (Meo) (% w/w)^a | Hydroxypropyl (Hpo) (% w/w)^a | Hpo/Meo ratio | Total substitution (% w/w) | Viscosity (cps)^a | molecular weight g/mol^a |
|---------------------------------------|--|--|--------------------------|---|--|---|
| A4M | 30 | 0 | 0 | 30 | 4878 | ~86000 |
| F4M | 28.1 | 6.7 | 0.238 | 34.8 | 4031 | ~90000 |
| E4M | 29.0 | 8.3 | 0.286 | 37.3 | 3919 | ~92000 |
| K4M | 22.3 | 8.5 | 0.381 | 30.8 | 4351 | ~88000 |
| K15M | 22.3 | 9.0 | 0.403 | 31.3 | 17129 | ~125000 |
| K100M | 22.5 | 8.9 | 0.395 | 31.4 | 79279 | ~215000 |

^a Data obtained from the manufacturer.

2.2-Methods

2.2.1- Preparation of sodium phosphate buffer, pH 7.2

De-ionized (DI) water was used to prepare pH 7.2 (0.2 M) sodium phosphate buffer solutions using disodium hydrogen orthophosphate (Na_2HPO_4), and sodium dihydrogen orthophosphate (NaH_2PO_4) salts.

2.2.2- Saturated solubility determination of model drugs

Saturated solubility of FBP and THP was determined at ambient temperature (22-24 °C) using sodium phosphate buffer pH 7.2. An excess amount of the drug was added to 100 ml of medium and stirred for 48 hours before extracting a 5 ml aliquot with a plastic syringe fitted with 0.45 μm PTFE syringe filter. The concentrations of FBP and THP were determined using UV spectrometry at maximum wavelength (λ_{max}) 247 and 272 nm for FBP and THP, respectively. The equations derived from the standard calibration curves (Table 2.2) for both the model drugs were subsequently used to determine drug concentration.

Table 2.2, Equations derived from standard calibration curves of model drugs.

| Model drug | Wavelength (nm) | Equation ^a | Co-efficient of determination (R ²) |
|------------|-----------------|------------------------|---|
| FBP | 247 | $y = 0.0829 x - 0.012$ | 0.9991 |
| THP | 272 | $y = 0.0559 x + 0.016$ | 0.9995 |

^a *y and x represent the absorbance and concentration of FBP or THP (mg/ml), respectively.*

2.2.3- Particle size fractionation and storage of powders

Particle size fractions of each polymer (90-150 μm and 150-250 μm) and drug (38-63 μm) were obtained by mechanical sieving. Powder sample of 25 g was used and sieves were assembled in decreasing aperture size and agitated for 30 minutes using Endecotts Test Sieve Ltd. Moreover, all the powders were stored at ambient temperature (18-24 °C) and humidity (RH 36-44 %) before any further investigation.

2.2.4- Characterisation of powders

2.2.4.1- Surface morphology of powder particles

The surface morphology of all the Methocel[®] grades (MC/HPMC), model drugs and their respective binary powder mixtures was imaged using scanning electron microscopy (SEM). Dry samples were mounted onto stubs using double sided adhesive tape and were sputter-coated with gold/palladium (80:20) for 60 seconds by using Quorum SC7620 Sputter Coater. The coated samples were individually placed on the specimen holder of the SEM (Jeol JSM-6060CV) under vacuum and image formed was viewed directly on attached computer and recorded photographically.

2.2.4.2- Determination of true density

The true density of solids is an intrinsic property and expressed as mass per unit volume (g cm^{-3}), exclusive to all the inter-particulate voids which are not a fundamental part of the molecular packing arrangement. The true density of all the Methocel[®] grade polymers, model

drugs and their respective binary powder mixtures was determined ($n = 10$), using AccuPyc 1340 II Pycnometer (Micromeritics, UK) employing helium as an inert gas. The helium pycnometer determined the volume occupied by the known mass of powder sample by measuring the volume of displaced helium gas by the particular mass of powder sample.



Figure 2.1, Helium pycnometer

2.2.4.3- Differential scanning calorimetry (DSC)

Differential scanning calorimetry (DSC) has been the most frequently used thermal analysis technique, mainly because of its promptness, simplicity and wide range of applications. In this study DSC (Mettler Toledo SC 821) analysis for all the powder samples (plain drugs, polymers and their respective powder mixtures) was performed using 5 – 10 mg of powder samples in an atmosphere of flowing nitrogen at 50 mL per minute and temperature program of 10 °C/min from 20 °C to 300 °C.

2.2.4.4- Powder X-ray diffraction (PXRD)

In this study the powder X-ray diffraction study of all the powder samples (plain drugs, polymers and their respective powder mixtures) was carried out by using D2-Phase (Bruker) X-

ray diffractometer, equipped with a Cu K α radiation source at 30 KV voltage and 10 mA current. Diffraction patterns were obtained in the 2 θ range of 5-100° using 0.02 step sizes.

2.2.5-Tribo-electrification and powder surface adhesion studies

2.2.5.1- Preparation and storage of powder mixtures

Binary powder mixtures were fabricated by using model drugs (THP and FBP) and different Methocel[®] grades (90 - 150 μ m and 150-250 μ m), at a fixed polymer to drug ratios of 0.5 , 1 , 2.5 , 5, 10 and 15 % w/w. The powder samples were blended in bespoke tumble mixer for 20 minutes (50 rpm) and to ensure a homogeneous powder mix and random samples of 10 mg were taken from each batch (n=3) and dissolved in 100 ml of 7.2 pH phosphate buffer. The drug content was determined using UV-Vis Spectrophotometry (Jenway 6305, UV-VIS spectrophotometer). The equations listed in Table 2.2 were used and an acceptance limit of 95-105 % was set (BP, 2012).

2.2.5.2-Tribo-electrification

Tribo-electric charge to mass ratio (Q/M) was determined using an electrostatic charge measurement apparatus, based on a shaking concept, Figure 2.2, (Šupuk *et al.*, 2009). Powder sample (~ 0.1 g) was placed inside a stainless steel cylindrical container (10 ml) and shaken in a horizontal direction (Retsch MW 4000) for 0.5, 2, 5 and 10 minutes at a vibration frequency of 20 Hz. The charged powder particles were then poured into a Faraday cup, connected to an electrometer (Keithley Model 6514). A Faraday cup comprises two concentric cups made up of a conducting material. The outer cup is slightly larger and acts as an electrical shield and it is covered by a lid. Both are very important to prevent the effect of any extraneous electric fields. The inner cup is directly attached to an electrometer for charge measurement and can be removed to measure the weight of the sample retrieved. The two cups are separated by a polytetrafluoroethylene (PTFE) insulator. As charged samples are loaded into the inner Faraday cup, this induces an equal but opposite charge on the wall of inner Faraday cup,

providing the net charge on the object (Šupuk *et al.*, 2013). The resolution of the charge measurement was in nano-coulombs (nC). The charge to mass ratio (Q/M) was calculated by dividing the final charge by the final mass of the respective powder. Each tribo-electric charging test was repeated three times and the shaking container was cleaned between each test by washing with isopropyl alcohol to remove any residual deposits, impurities and surface charges. Studies were carried out at an ambient temperature (18-24 °C) and humidity (RH 36-44 %). Maximum charge acquisition data were presented as a charge to mass ratio (Q/M) at the end of each tribo-electrification experiment (n= 3).

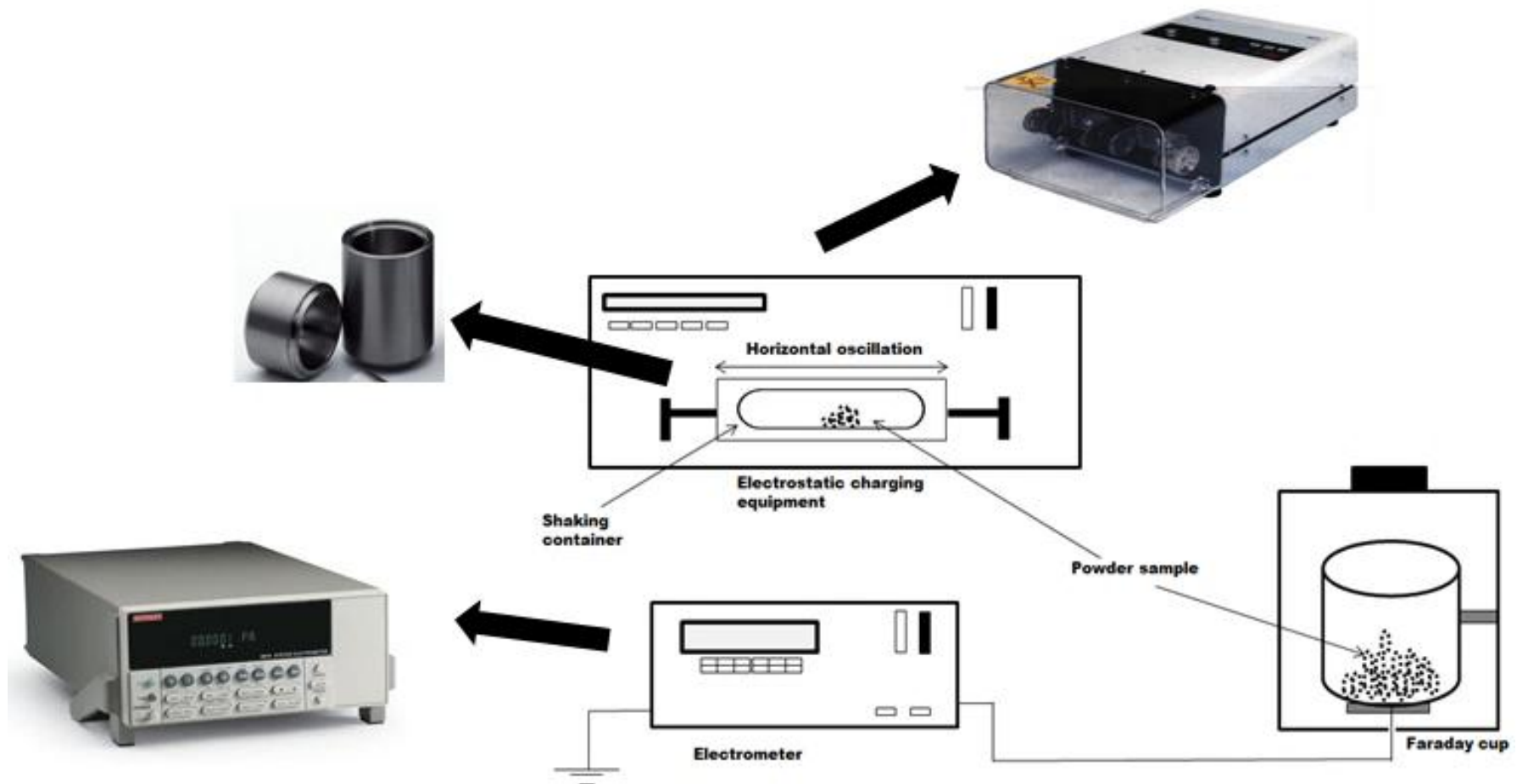


Figure 2.2, Tribo-electric charging measurement set up (Šupuk *et al.*, 2009)

2.2.5.3- Surface adhesion (SA) of powder particles

During powder processing, powder particles can adhere to equipment surfaces, resulting in losses through deposition but it may also cause changes in their proportionalities. Particle adherence to the surface of the stainless steel container used in the tribo-electrification studies was calculated from mass difference by deducting the final amount recovered (post shaking and tapping) from the initial amount of sample loaded into the shaking vessel (Šupuk *et al.*, 2012) and powder mass loss was reported as a percentage (%) powder adhesion.

2.2.5.4- Statistical analysis

One way analysis of variance (ANOVA) (confidence limit of $P < 0.05$) was used to investigate the statistical significance of different underlying factors on tribo-electrification and adhesion properties of polymers and their blends with FBP.

2.2.6- Swelling and erosion studies

2.2.6.1- Preparation and storage of powder mixtures

Binary powder mixtures of Methocel[®] polymers and model drugs for swelling, erosion and dissolution studies were prepared at a fixed polymer to drug ratio of 5, 10 and 15 % w/w. The powder samples were mixed and furthermore the respective drug contents were quantified by using the method described in section 2.2.5.1. For drug content uniformity an acceptance limit of 95-105 % was set (BP, 2012), as described earlier. Furthermore, all the powder blends were stored at ambient temperature (18-24 °C) and humidity (RH 36-44 %) before any further investigations.

2.2.6.2- Tableting of Methocel[®] polymers

Tablet matrices of all the Methocel[®] grades (MC/HPMC) were prepared using a Specac[®] manual hydraulic press GS25011 (Specac[®] Ltd, UK) equipped with 13.00 mm evacuable die set (Specac[®] Ltd, UK), Figure 2.3. The matrix tablet weight was adjusted to 300 (\pm 2) mg which was constantly maintained and a compression pressure of 20 kiloNewtons (kN) with a 20 second dwell time was used. All the matrices were stored in an airtight container over silica gel for 24 h before any further investigation.

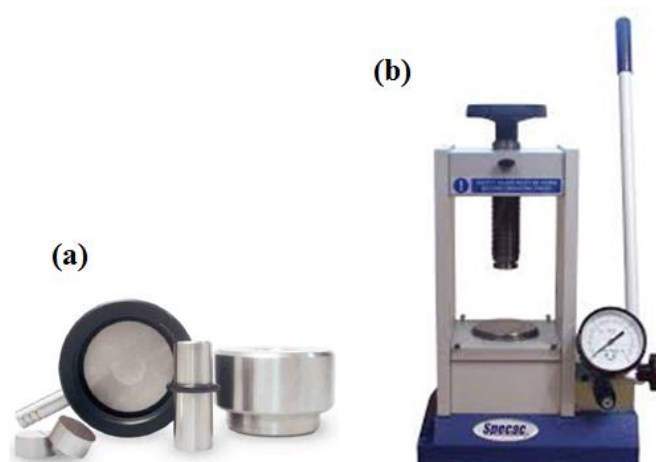


Figure 2.3, (a) Specac[®] 13.00 mm evacuable die set and (b) Specac[®] manual hydraulic press.

2.2.6.3- Tableting of powder mixtures

The matrices of all the Methocel[®] / drug powder mixtures (Table 2.5) were prepared using Specac[®] manual hydraulic press GS25011 (Specac[®] Ltd, UK) equipped with 13.00 mm evacuable die set (Specac[®] Ltd, UK), Figure 2.3. The FBP and THP powder mixtures were compacted at 2 tonnes for 3 minutes and 2 tonnes for 1 minute, respectively. Moreover, a constant weight of 300 mg (\pm 2) was constantly maintained and the tablets were stored in an airtight container over silica gel for 24 h before any further investigation.

2.2.6.4- Swelling and erosion studies

The swelling studies were carried out for all the matrices using the swelling experimental setup shown in Figure 2.4. Initially the matrices were placed on a wire mesh and weighed (W_i). Subsequently, these pre-weighed dry matrix tablets were placed in glass petri dishes (17 mm × 45 mm) containing 20 ml of sodium phosphate buffer (pH 7.2) at ambient temperature 22 - 25 °C. At 5, 10,15, 30, 60, 120, 240 and 360 minute intervals, the previously weighed wire mesh containing the tablet were removed, lightly blotted with 125 mm filter paper (Whatman[®], UK) to remove excess water, reweighed (W_s) and were rapidly replaced into the glass petri dishes . The mean weight was determined for each formulation and degree of swelling (S) was calculated using Eq. (2.1) (Ghori *et al.*, 2014a):

$$S = \frac{W_s - W_i}{W_i} \times 100 \quad (2.1)$$

Where W_i and W_s are initial dry or swollen matrix tablet weight, respectively, at immersion time (t) in the phosphate buffer. The degree of swelling was determined from the mean of three replicates and presented as degree of swelling (S, %) against time (t).

After a swelling period of 360 min these matrices were subsequently dried in a convection oven at 50 °C. After 24 hours, the tablets were cooled to ambient temperature and then weighed until a constant weight had been achieved and this was termed the dried weight. All studies were conducted in triplicate (n = 3) and the degree of erosion (E) was calculated using Eq. 2.2.

$$E = \frac{W_i - W_f}{W_i} \times 100 \quad (2.2)$$

Where, W_i is the initial weight of the matrix tablets and W_f is the weight of the dried matrices.

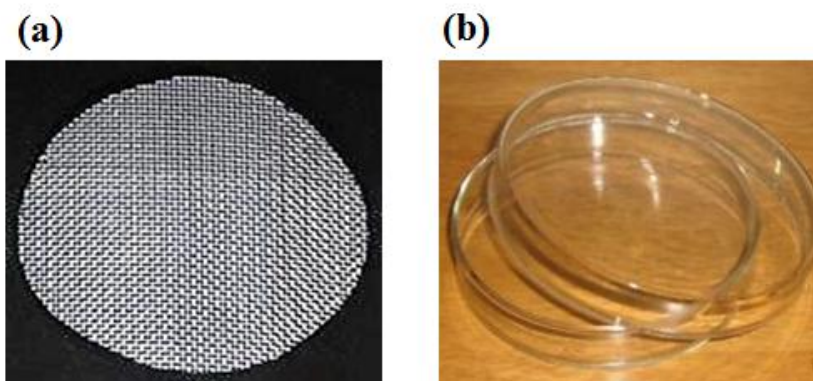


Figure 2.4, Swelling experimental set up (a) wire mesh (b) glass petri dish (17 mm × 45 mm)

2.2.6.5- Swelling kinetics

The mathematical model described by Vergnaud (1993) was applied to the swelling data to determine the rate of water uptake. This Vergnaud model has been frequently adopted by different authors to evaluate the mechanism of hydrophilic matrix tablet swelling. The generalized form of the Vergnaud model is shown in Eq. 2.3 (Ebube *et al.*, 1997; Vergnaud, 1993):

$$M = kt^n \quad (2.3)$$

Where,

M = the amount of liquid transferred

t = time

k = the swelling constant,

n = the mechanism of water uptake,

Ebube *et al.* (1997) reported that a value of $n < 0.5$ is indicative of a diffusion-controlled mechanism in which the rate of diffusion is much less compared to the rate of polymer relaxation in a matrix tablet. However, when $n = 1$, water diffuses through the matrix at a

constant velocity showing an advancing liquid front marking the limit of liquid penetration into the matrix. A value of $0.45 < n < 1$ indicates an anomalous behaviour in which diffusion of liquid and polymer relaxation are of the same magnitude.

2.2.7- Dissolution studies

2.2.7.1- Tableting of model drugs

Compacts containing only FBP and THP were compacted at 2 tonnes for 3 minutes and 2 tonnes for 1 minute, respectively. The Specac[®] manual hydraulic press GS25011 (Specac[®] Ltd, UK) equipped with 13.00 mm evacuable die set (Specac[®] Ltd, UK, Figure 2.3) was used. Moreover, a constant weight of 300 mg (± 2) was constantly maintained and the tablets were stored in an airtight container over silica gel for 24 h before any further investigation.

2.2.7.2- Preparation of powder mixtures

The powder mixtures were prepared essentially using the same Methocel[®] concentration and mixing parameters described in section 2.2.6.1.

2.2.7.3- Tableting of powder mixtures

The tablets of resultant powder mixtures were prepared by adopting a method described in section 2.2.6.2.

2.2.7.4- Determination of intrinsic dissolution rate (IDR)

The IDRs of all the compacts were fabricated by the methods described in sections 2.2.5.2 and 2.2.5.3 were determined by using stationary disk method. To determine IDR, the 13 mm compacts were fixed in PTFE holders (Figure 2.4) and the edges of the disk were sealed using the paraffin wax which was previously melted at 70 °C. The fixed tablets were introduced into USP apparatus II which was a fully automated assembly, comprising a dissolution bath (Pharmatest DT 70), peristaltic pump and UV visible spectrophotometer (Cecil 3201, series

3000). The temperature of the dissolution bath was maintained at 37 °C and paddle stirring speed of 75 rpm. Sodium phosphate buffer pH 7.2 was used as the dissolution medium and the volume was 900 ml. In this way, only one face of the compact was exposed to the liquid medium and samples were taken after every predetermined time interval using an auto-sampling system equipped with PTFE filters. UV measurements were carried out at 252 and 276 nm for FBP and THP, respectively. All the experiments were conducted in triplicate with mass (mg) or percentage (%) of dissolved drug calculated based on a series of standard solutions at known concentrations. A relationship between dissolved drug mass (mg) and time was plotted, and IDR ($\text{mg min}^{-1} \text{cm}^2$) was determined by dividing the gradient (m) obtained from each linear profile by the surface area ($A = 1.33 \text{ cm}^2$) of the exposed drug, Eq. 2.4; (Shaw *et al.*, 2005)

$$IDR = \frac{m}{A} \quad (2.4)$$



Figure 2.5, Dissolution apparatus used for IDR determination.

2.2.7.5- Drug release kinetics

Over the years, a number of mathematical models have been developed to explain the mechanism of drug release from polymeric matrices. Mathematical modelling of drug release data can be used to elucidate the mass transport mechanisms and predict the effect of matrix tablet physical characteristics, especially those related to its design (shape, size and composition of matrix tablets), on the rate of particular drug release (Siepmann and Peppas, 2001). In this study, drug release profiles were curve-fitted to commonly used models to characterize and derive drug release parameters for comparative purposes. These include the zero order, first order, Higuchi and Korsmeyer-Peppas mathematical models.

2.2.7.5.1- Zero-order equation

Equation 2.5 describes a constant rate of drug release with time:

$$Q = Q_0 + K_0 t \quad (2.5)$$

where Q is the amount of drug released at time t , Q_0 is the initial amount of drug and K_0 is the zero order release constant (Costa and Sousa Lobo, 2001). In swellable-erodible polymer matrices, a constant drug delivery rate can be achieved when a constant gel layer thickness is attained by synchronization of the swelling and eroding fronts (Baveja *et al.*, 1987; Costa and Sousa Lobo, 2001).

2.2.7.5.2- First-order equation

The first order kinetic model can be applied to drug release data by using Eq. 2.6

$$\ln Q = \ln Q_0 - K_1 t \quad (2.6)$$

Where Q is the amount of drug released in time t , Q_0 is the initial amount of drug in the solution and K_1 is the first order release constant. This relationship can be used to describe the drug dissolution from pharmaceutical dosage forms such as those containing water-soluble drugs in porous matrices (Costa and Sousa Lobo, 2001).

2.2.7.5.3- Higuchi square root equation

The Higuchi model (Higuchi, 1961; Higuchi, 1963) is commonly used to describe drug release from matrix systems. It describes a linear relationship between the cumulative amount of drug released and the square root of time, which is an indicator of diffusion controlled release. Higuchi (1961) proposed the mathematical model to describe the drug release from a planar system consisting of a homogeneous matrix in the form of an ointment base containing finely dispersed drug. The mathematical equation of the Higuchi model can be simplified and expressed as Eq. 2.7.

$$M_t = K_H t^{0.5} \quad (2.7)$$

where M_t amount of drug released at time t and K_H is the Higuchi rate constant.

2.2.7.5.4- Korsmeyer-Peppas equation

The mechanism and kinetics of drug release were further evaluated by fitting drug release data to the Korsmeyer–Peppas mathematical model, Eq. 2.8 (Korsmeyer *et al.*, 1983).

$$\frac{M_t}{M_\infty} = K t^n \quad (2.8)$$

Where $\frac{M_t}{M_\infty}$ is the fraction of drug released at time t while K is a drug release constant incorporating the geometrical characteristics of matrix tablet, and n is the diffusional exponent

of drug release and used to elucidate the drug release mechanism (Siepmann and Peppas, 2001). The goodness of fit was established using the adjusted coefficient of determination where the closer the value is to unity, the better the data fit to the model. The value of n is dependent on the mechanism of drug release and geometrical shape of the matrix that is being assessed and was further used to describe drug release patterns. This drug release model is also known as the power law and subsequently showed that the equation can be used to describe the general drug release behaviour of non-swelling and swelling polymeric matrices in the form of slabs, spheres and cylinders. Solute or solvent transport process can be Fickian or non-Fickian, depending on the relative rate of diffusion and polymer swelling (Ritger and Peppas, 1987a; Ritger and Peppas, 1987b). When solvent transport is slower than polymer relaxation, Fickian diffusion is observed. In contrast, when polymer relaxation is rate-limiting to solvent transport, case II transport, or time-independent diffusion, is observed. For cylindrical matrix tablets when the value of n is 0.45, Fickian diffusion is the predominant mechanism of drug release. However, when its value is equal to 0.89, drug release occurs via case II transport. Moreover, when the value of n falls between 0.45 and 0.89, the mechanism of drug release is considered anomalous. This is attributed to the concurrent occurrence of diffusion and swelling controlled mechanisms (Ritger and Peppas, 1987b; Siepmann and Peppas, 2001).

2.2.8- Development and validation of PSA assay for erosion analysis

2.2.8.1- Preparation of powder mixtures

All the powder mixtures comprising different HPMC to drug ratios (FBP/THP, 20-80%) were blended for 15 minutes (Turbula mixer, Figure 2.5). To evaluate the mixing efficiency, samples were taken from each powder mixture and FBP and THP content were determined using their respective UV-VIS standard calibration curves as described in the sections 2.2.5.1 and 2.2.6.1.



Figure 2.6, Turbula shaker-mixer

2.2.8.2- Preparation of matrix tablets

The matrices comprising Methocel[®] polymers without drug (Table, 2.1) having different particle size fractions (90-150 and 150-250 μm) and their respective powder mixtures enlisted in Table 2.6, were compacted using a Specac[®] manual hydraulic press GS25011 equipped with 13.00 mm die set (Specac[®] Ltd, UK), Figure 2.3. The compact weight was maintained to 500 ± 2.5 mg each and was compressed at 20 kN with a 20 second dwell time. All the matrix tablets were stored in an airtight container over silica gel for 24 hours before any further investigation.

2.2.8.3- *In vitro* release studies

2.2.8.3.1- Drug release studies

In vitro drug release studies were performed on all the drugs based hydrophilic matrices, except those containing 100 % Methocel[®], using USP dissolution apparatus I, SR II 6-flask, basket apparatus (Hanson Research, USA, Figure, 2.7) at 100 rpm. pH 7.2 sodium phosphate buffer (900 ml) was used as the release medium and was maintained at 37.5 ± 0.5 °C. Aliquots of dissolution media (5 ml) were withdrawn manually after 30, 60, 120, 360, 740 and 1440 minutes and replaced with an equal amount of fresh dissolution medium. The dissolution

samples were then analysed for drug content using the standard calibration curves of respective drugs as described in section 2.2.2.

2.2.8.3.2- Methocel[®] (MC/HPMC) dissolution studies

The Methocel[®] polymer dissolution of all the matrices, alone or in combination with drugs, was studied. Dissolved Methocel[®] was quantified using a phenol-sulphuric acid assay (Ghori *et al.*, 2014b) alone or alongside drug analysis using the removed samples described in section 2.2.5.2.1. Filtered samples (1 ml) were added to 1 ml of 5% phenol in 0.1 M hydrochloric acid, followed by 5 ml of concentrated sulphuric acid. The resultant solution was mixed vigorously for 10 minutes and placed in a water bath at 25-30 °C for 20 minutes. Absorbance was measured at maximum wavelength (λ_{max}) 490 nm and dissolved polymeric content was calculated by using the equation derived from the standard calibration curves of respective grades of Methocel[®] enlisted in Table 2.7 (Brummer and Cui, 2005; Dubois *et al.*, 1956).

Table 2.3, Equations derived from standard calibration curves of different Methocel[®] grades.

| Methocel [®] | Wavelength (nm) | Equation ^a | R ² |
|-----------------------|-----------------|-------------------------|----------------|
| A4M | 490 | $y = 0.0089 X - 0.0139$ | 0.999 |
| F4M | 490 | $y = 0.0098 X + 0.0295$ | 0.997 |
| E4M | 490 | $y = 0.0095 X + 0.0250$ | 0.998 |
| K4M | 490 | $y = 0.0088 X + 0.0172$ | 0.999 |
| K15M | 490 | $y = 0.0090 X + 0.0273$ | 0.997 |
| K100M | 490 | $y = 0.0097 X + 0.0292$ | 0.997 |

^a *y* and *x* represent the absorbance and concentration of Methocel[®] (mg/ml), respectively.

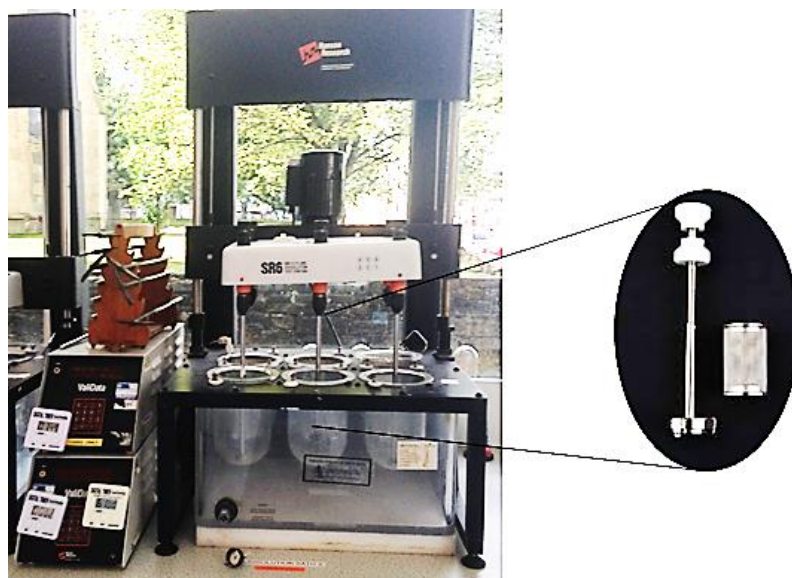


Figure 2.7, Dissolution apparatus I (basket assembly)

2.2.8.4- Matrix erosion studies

2.2.8.4.1- Gravimetric method

Erosion of matrix tablets was determined using a gravimetric technique (Chaibva *et al.*, 2010; Dhopeswarker and Zatz, 1993; Ebube *et al.*, 1997; Ranga Rao *et al.*, 1988, Sinha Roy and Rohera, 2002). The study was conducted using USP apparatus I, SR II 6-flask (Hanson Research, USA, Figure, 2.8) at 100 rpm. The dry hydrophilic matrix tablets were accurately weighed and placed in baskets prior to immersion in dissolution medium (pH 7.2 sodium phosphate buffer) which was maintained at 37 ± 0.5 °C. Tablets were removed at 30, 60, 120, 360, 720 and 1440 minutes and lightly blotted dry with 125 mm filter paper (Whatman[®]) to remove excess water. They were subsequently dried in a convection oven at 50°C. After 24 hours, the tablets were cooled to ambient temperature and then weighed until a constant weight had been achieved. All studies were conducted in triplicate and the degree of erosion (E) was calculated using the method described in section 2.2.4.2.

2.2.8.4.2- Combined dissolution method of matrix erosion

Matrix tablet erosion was also determined by using the collective amount of drug and polymer dissolved during dissolution and the percentage erosion was calculated at each sampling time using Eq. 2.9.

$$\text{Matrix Erosion (E)} = \frac{W_d + W_p}{W_i} \times 100 \quad (2.9)$$

where, W_d is amount of drug released (mg) and W_p is amount of HPMC released (mg), determined using the phenol-sulphuric assay method in the dissolution medium at specific sampling times while W_i is the initial weight of matrix tablet. Moreover, the HPMC degree of erosion (H_e) was also calculated by using the equation 3.

$$\text{HPMC Erosion (H}_e\text{)} = \frac{W_p}{W_{pi}} \times 100 \quad (2.10)$$

where, W_p is amount of dissolved HPMC (mg) and W_{pi} is the initial amount of HPMC in the matrix tablet. Percentage matrix or HPMC erosion (E or H_e) was plotted against time up to 720 minutes for all the matrix tablets with an aim to get a linear profile. Then simple linear regression was applied representing slope as an erosion rate (k , % min^{-1}).

2.2.8.4.3- Modelling of drug release profiles

The mechanism and kinetics of drug release were deduced by fitting respective dissolution data to the Korsmeyer– Peppas model (Korsmeyer *et al.*, 1983) as described in section 2.2.4.5.2.

2.2.9- Compaction studies

2.2.9.1- Powder compression and data acquisition

All the powder samples of Methocel[®] (MC and HPMC), having different particle size fractions (90-150 and 150-250 μm), were compressed using a Testometric[™] M500 - 50 CT, 50 KN (Testometric[™] Company Ltd., United Kingdom) materials testing machine equipped with 13.00 mm Atlas Evacuable Pellet Die (Specac[®] Limited, United Kingdom) and directly connected to a computer. The powder samples were accurately weighed (300 ± 1.5 mg) on an analytical balance and manually poured into the die. The initial height (h) of the powder bed was determined from the starting cross-head position. The compaction rate was determined by the movement of the cross-head, which was set at 10 mm min^{-1} during the compression phase. The force (F) was transmitted through a pushrod to the upper punch, while the lower punch remained stationary during the experiment. The upper punch displacement was measured using a linear variable differential transformer (LVDT) position gauge attached to the compression platens. As soon as the required maximum force (150.77 MPa) had been achieved, the force was gradually reduced by allowing the upper punch to retract at 1 mm min^{-1} . When the force was completely removed, the specimen was immediately ejected from the die in the same direction as the initial compaction and force-displacement data was recorded automatically during the experiment. The height of the powder bed (X) during compression with respect to time and progressing pressure was calculated from the initial height (h), using force-displacement data. Thus, the average relative density (ρ_{rel}) of the powder bed could be calculated throughout the experiment, using Eq. 2.11:

$$\rho_{\text{rel}} = \frac{4W}{\rho \pi d^2 (h-X)} \quad (2.11)$$

The porosity (ϵ ,%) of the powder bed during the compression phase was subsequently determined using the Eq. 2.12:

$$\epsilon (\%) = \left(1 - \frac{4W}{\rho \pi d^2 (h-X)} \right) \times 100 \quad (2.12)$$

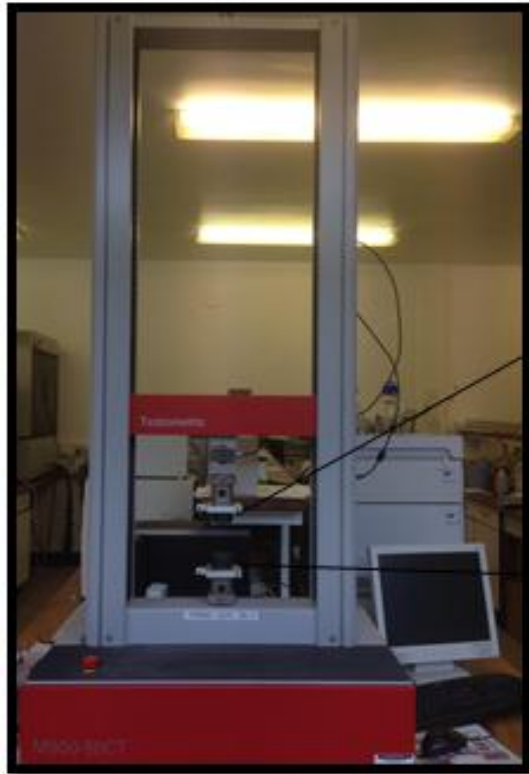
Where W , ρ , d , h and X represents the weight of the poured powder sample, true density, tablet diameter, initial height and height of the powder bed with respect to time and pressure, respectively. As the compression cycle completed, the thickness (T) and diameter (d) of the ejected compacts were measured, using a digital calliper, within ~1 min and after 24 h of releasing the compaction force. The weight (W) was also determined by using the analytical weight balance. The out-of-die relative density and porosity at zero h and 24 h was calculated using the Eq. 2.13 and 2.14, respectively.

$$\rho_{\text{rel}} = \frac{W}{\rho (d/2)^2 \pi T} \quad (2.13)$$

$$\epsilon (\%) = \left(1 - \frac{W}{\rho (d/2)^2 \pi T} \right) \times 100 \quad (2.14)$$

After ejection, the tablets were stored over silica gel for 24 h for elastic recovery. Relative humidity (RH) and temperature during compaction work were in the range of 25-45 % and 22-25 °C, respectively.

(a)



Upper compression
platens

Lower compression
platens

(b)



Figure 2.8, (a) Testometric™ material testing machine equipped with, (b) Specac® 13.00 mm evacuable die set

2.2.9.2- Compressional analysis

The tablet compression characteristics were studied firstly by using the Heckel compression mathematical model, relating powder porosity (ϵ) during compression to the applied pressure (P). The equation is written as follows, Eq. (2.15) (Heckel, 1961a; Heckel, 1961b):

$$\ln\left(\frac{1}{\epsilon}\right) = KP + A \quad (2.15)$$

Where A and K are constants representing particle rearrangement and the slope of the linear region, respectively. The slope of the straight line portion (K) is inversely related to the material's mean yield pressure (P_y) which gives an indication regarding the plasticity and pressure required for deformation of materials. This can be determined from Eq. (2.16):

$$\frac{1}{K} = P_y \quad (2.16)$$

The compression data profiles were further fitted to the linear form of Kawakita's equation, (Kawakita and Ludde, 1971) given by Eq. (2.17):

$$\frac{P}{C} = \frac{1}{ab} + \frac{p}{a} \quad (2.17)$$

Where, P is the applied axial pressure, and "a" is the value of initial porosity which corresponds to the total portion of reducible volume at maximum pressure. Mathematically, $1/b$ is simply the pressure needed to compress the powder to one half of the total volume. Moreover, it was proposed that it is related to the plasticity of powder particles during compression. C is the degree of volume reduction (engineering strain) and can be calculated using Eq. (2.18),

$$C = V_0 - \frac{V}{V_0} \quad (2.18)$$

Where V_0 is the initial powder volume and V is the volume of the powder at pressure P . The Kawakita parameters a and b were calculated from the linear regression of the profiles.

2.2.9.3- Tensile strength and elastic recovery determination

After a relaxation phase (24 h.) the matrix tablets were fractured diametrically using a Tablet Hardness Tester (PharmaTest PTB 311E). The diameter (D) and thickness (H) of compacts calculated after 24 h. and maximum breaking force (F), were used to calculate tensile strength T according to Eq. (2.19), (Fell and Newton, 1970):

$$T = \frac{2F}{\pi DH} \quad (2.19)$$

Moreover, the percentage of elastic recovery of each matrix tablet was determined using Eq. (2.20): (Armstrong and Haines-Nutt, 1972)

$$ER = \left(\frac{H_i - H_e}{H_e} \right) \times 100 \quad (2.20)$$

Where H_e is the height of the tablet at maximum pressure and H_i is the tablet height after 24 h. of ejection.

3- Tribo-electrification and adhesion studies

3- Tribo-electrification and adhesion studies

3.1- Introduction

Electrostatic charging on solids arising from the contact between two surfaces is a phenomenon considered as one of the oldest manifestations of electricity. The concept of electrostatic charging has been known for centuries, as the ancient Greeks in the sixth century B.C. observed that amber attracts small objects after rubbing. The earliest experiments of Thales of Miletus, around 500 B.C., describe the mineral amber attracted light bodies such as feathers and pieces of straw after rubbing with fur or wool (Arfken, 1984). In 1600, William Gilbert used the word 'electric' for the first time, originating from the Greek word *elektron* and differentiates the electrical and magnetic phenomena. Gilbert also explains the electrical mechanism of a range of different materials and concluded that many materials other than amber can also be electrified. In 1733, Charles du Fay discussed the polarity of charge on glass and amber respectively, after rubbing with silk and introduced the terms 'vitreous' and 'resinous'. Subsequently, in 1750, Benjamin Franklin named these charges as positive and negative, respectively. Around the same time Stephen Gray classified substances into two major groups, firstly, 'conductors' for materials such as metals and water, which allowed the charge to flow freely whereas 'insulators' a group including wood, rubber and glass, do not allow charge to flow (Smith *et al.*, 1966). However, a quantitative investigation of electrical interaction between two charged particles was begun in 1785 when the French scientist Charles Augustin de Coulomb was able to establish an electrostatic force law or Coulomb's Law by using a torsion balance (Arfken, 1984). According to this law, it was established that the force between two small electrically charged spheres, at rest, was inversely proportional to the square of the distance of separation. Furthermore, in 1843, Faraday conducted experiments on electrostatic induction using an ice-pail (Faraday well) connected to a gold-leaf electroscope and placed on an insulator. It was concluded that as a charged body was

enclosed in a hollow conductor, it induced, on the inside of that conductor, a charge equal in magnitude but opposite in polarity to its own. He also suggested that equal and opposite charges are produced when a body is electrified by rubbing (Chang *et al.*, 1995).

3.2- Tribo-electrification

Tribo-electrification is intrinsically a dynamic, strenuous and dissipative phenomenon, arising due to the difference in electrical potential when two materials come into contact with each other (either by impact, friction or shear) and then separated (Harper, 1967). There are two broad categories that are considered under tribo-electrification; firstly, contact charging, which involves the direct contact and subsequent separation of two surfaces without rubbing. Secondly, frictional charging involves relatively adjacent movement of two contacting surfaces. However, with regard to a mechanistic point of view, these two modes of charging are difficult to discern and the term tribo-electrification is conventionally used to describe the overall process, even though the prefix “tribo” literally means rubbing (Swarbrick, 2007; Cross, 1987). Mostly, pharmaceutical powders are insulators and composed of fine powder particles, which are in contact with each other or with the surfaces of different processing equipment surrounding the powder leading to tribo-electric charging. This charge generation arises due to the contact potential differences (CPD) between the bodies caused by the type of different materials but may also be influenced by particle size, surface roughness, environmental factors, contamination and type of contacting surfaces (Karner and Anne Urbanetz, 2011). The tribo-electrification phenomenon can be classified into metal-metal, metal-insulator, and insulator-insulator contacts.

3.2.1- Metal-metal contacts

The rationale for charge generation and transfer between two contacting metals is well known, however, quantification of tribo-electric charging of metallic material is usually difficult, as the charge migrates from the contact point quickly. The charging process can be

explained in terms of the work functions of the materials; when two dissimilar metal objects make contact, electrons will flow from the metal with the lower work function (W_{low}) to the metal having a higher work function (W_{high}), as illustrated in Figure 3.1. This is due to the CPD generated on the contact of two surfaces having different energy levels (Matsusaka and Masuda, 2003).

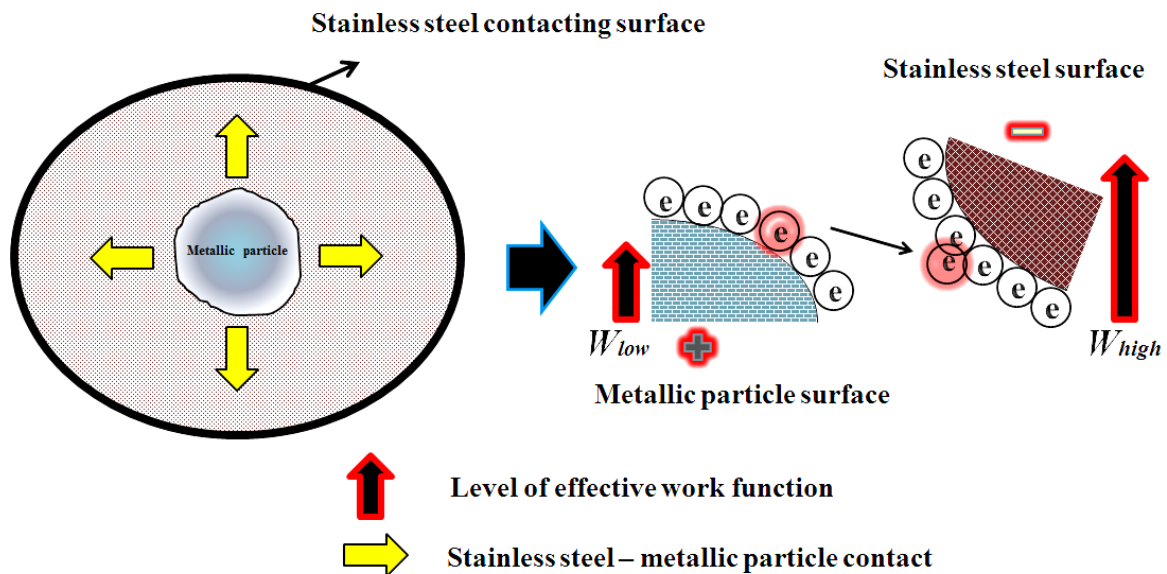


Figure 3.1, Schematic illustration of charge generation during metal-metal contact.

3.2.2- Metal-insulator contacts

The theory of contact electrification between metals can be extended to metal-insulator contacts, as various authors have used the same concept to describe the metal-insulator charge generation mechanism (Matsusaka *et al.*, 2010). However, this type of contact charging is less well understood, despite a considerable amount of research carried out in this area. For instance, none of the literature on this subject discusses the exact mechanism of charge transfer, however, several charge transfer mechanisms have been proposed (Lowell and Rose-Innes, 1980), as described in the following sub-sections. Moreover, a summary of all the theories is summarised in Table 3.1.

3.2.2.1- Electron transfer in metal-insulator contacts

Early experiments conducted using insulators and metallic surfaces have shown a direct relationship between the charging propensity and the level of work function. Davies (1969) determined the charge density on the insulator, dielectric polymer surfaces, due to contact with metallic surfaces of a known work function. The charge density produced by each metal was plotted against the CPD of that metal with respect to gold as a reference. Results showed the dependence of charge density on the metal work function, and are therefore described by way of electron transfer for all the materials tested. Murata and Kittaka (1979) presented evidence for electron transfer as the mechanism for contact electrification of polymers and metals by measuring photoelectric emission. According to Lowell and Rose-Innes (1980), charges acquired by an insulator, when in contact with a metal, are usually attributed to electron transfer. During the contact charging process, the valence electron energy state of powder particles on an atomic scale is designated as the Fermi level whilst the vacuum energy level is a thermodynamic state of electrons far from the atom and can be considered as a reference point. The difference between the Fermi level and vacuum energy level equates to the work function (W), which is a unique surface property of materials and refers to the minimum energy difference required for the liberation of loosely bonded electrons present in the outer electron shells of an atom (Lowell, 1979). When inter- or intra-particulate contacts of powder particles are established, electrons flow from the lower work function (W_{low}) towards the higher (W_{high}), consequently a CPD ($W_{high} - W_{low}$) is generated across the particle surface (Lang and Kohn, 1971). Moreover, this leads to the generation of electrostatic charge, which is exclusively a surface phenomenon (Lowell and Rose-Innes, 1980). A schematic illustration of electron transfer theory is described in Figure 3.2.

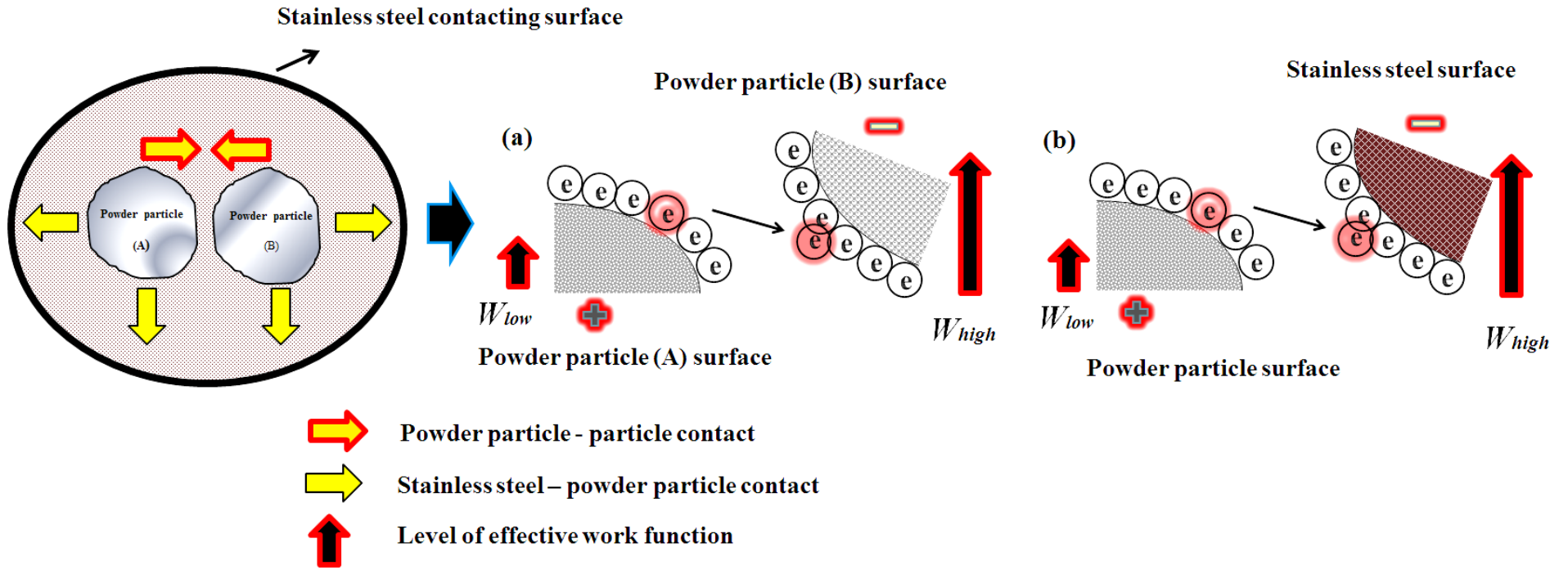


Figure 3.2, Schematic illustration of electron transfer theory of tribo-electric charge generation.

3.2.2.2- Ion transfer in metal-insulator contacts

Ion transfer has been suggested by various researchers as a mechanism of charge transfer during insulator and metal contact (Harper, 1967; Robins *et al.*, 1980). The fundamental principles of this theory are based on the fact that insulating materials contain free, movable ions in their body or on their surface. These ions can be transferred by diffusion; relative affinities and the kinetic effect based on shearing and cause one member of a pair of positive and negative ions to relocate to the other surface, which can be a polymer or a metal. This will then determine the magnitude and polarity of tribo-electric charge on the contacting material surfaces (Matsusaka *et al.*, 2002). A schematic illustration of ion transfer theory is described in Figure 3.3.

Furthermore, it was assumed that the insulators contain an internal electric field. The charged defects present in their lattice structure and the ions present in the atmosphere compensate for this field which leads to the formation of a surface layer. The friction between the two materials mixes their respective surface layers. Finally, the compensation of the intrinsic field of the two bodies is disturbed and the insulator gains a tribo-electric charge (Kornfeld, 1976). However, ion transfer is commonly not regarded as a dominant cause of tribo-electrification (Harper, 1967).

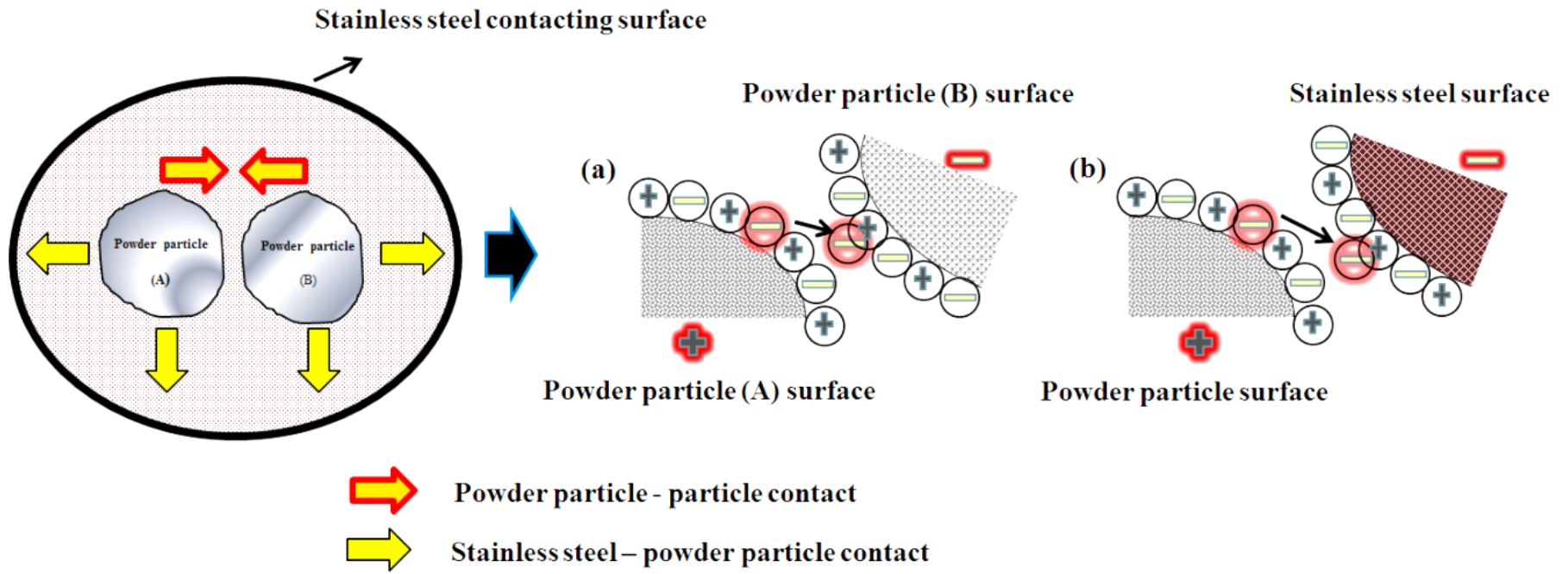


Figure 3.3, Schematic illustration of ion transfer theory of tribo-electric charge generation.

3.2.2.3- Material transfer in metal-insulator contacts

According to this theory, the material in the nanometer to the micrometer range can be transferred during contact and that dislodged material is expected to bear the charge. The impact or friction between two surfaces can break the bonds and this is particularly true for brittle and friable particles, such as pharmaceutical powders, and this eventually determines the net overall charge of the resultant material bearing the detached material (Matsusaka *et al.*, 2010). Jain and Bahadur (1978) probed the impact of material transfer in polymer-polymer sliding as a function of time, speed and load. It was concluded that material transfer occurred under all conditions of rubbing. Material transfer may also contribute to the charge transfer between a metal and an insulator (Tanoue *et al.*, 1999). Electrons in insulators do not possess single energy levels like conductive materials. Electron energy can be explained as a function of its physical position, surface impurities, and the material's chemical and atomic structure (Hogue *et al.*, 2004). Research investigating the impact of surface impurities has shown that cleaning the container surface with acetone to remove surface impurities during the experiments has a significant effect on the tribo-electric charging of particles. This study suggested that charge transfer is not solely an intrinsic feature of the material (Eilbeck *et al.*, 2000). However, recently there are experimental data using X-ray photoelectron spectroscopy and Raman spectroscopy that support and that material transfer model mechanism of charge generation (Baytekin *et al.*, 2013; Piperno *et al.*, 2011). A schematic illustration of material transfer theory is described in Figure 3.4. A physical clump of material rubs onto the opposing surface of material bearing either positive or negative charges.

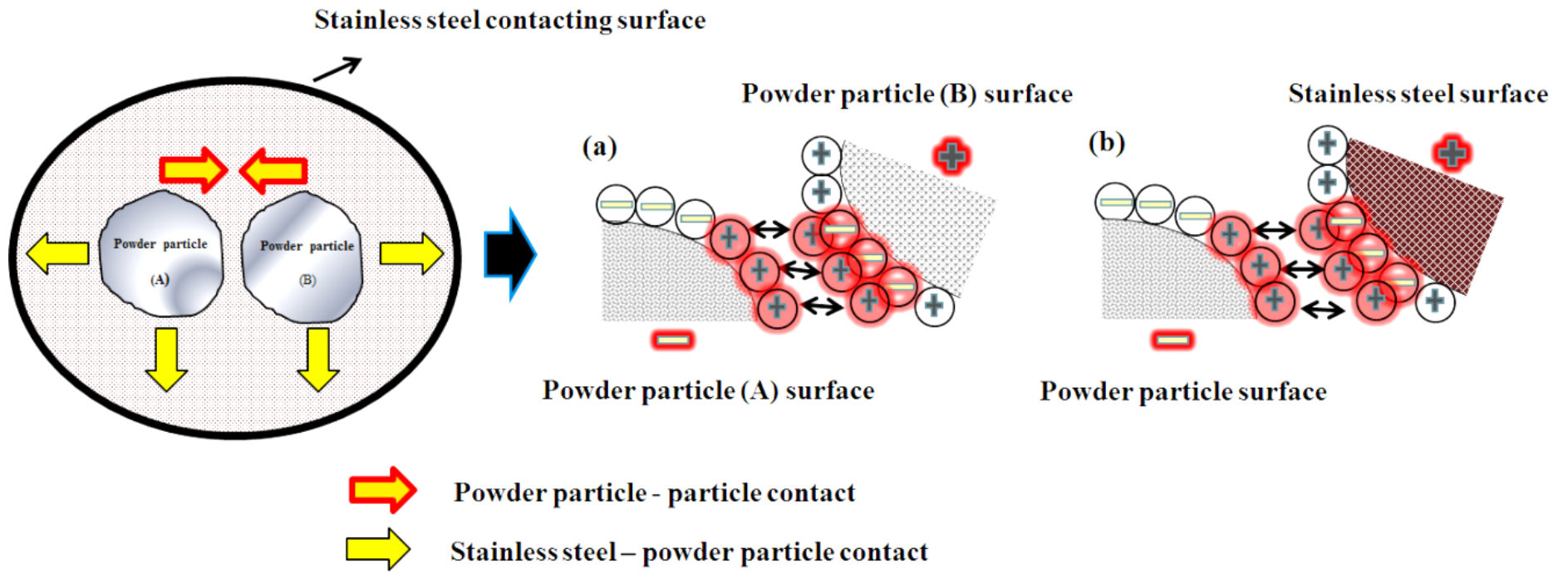


Figure 3.4, Schematic illustration of material transfer theory of tribo-electric charge generation.

3.2.3- Insulator-insulator contacts

The experimental and theoretical principles of charging generation during insulator-insulator contact have been applied mostly to toner charging (Lowell and Rose-Innes, 1980; Yoshida *et al.*, 2003; Yoshida *et al.*, 2006) . The mechanism of charge generation is similar to that for metal-insulator contacts, but in this particular scenario, movement of electrons and ions is more restricted (Matsusaka *et al.*, 2010). According to Castle, (1997), all three aforementioned mechanisms (electron transfer, ion transfer and material transfer) may occur during insulator-insulator contacts. Moreover, another theory associated with insulator charging may also be involved. According to that theory, to generate charging between two insulating surfaces, there must be donor and acceptor sites near the surface of the non-conductive particles (Bailey, 1984). In order for insulators to charge, surface impurities must be present if the particles are to charge when in contact with each other. According to Bailey (1984), tests carried out using perfect insulators showed that no charging occurred and when slight impurities were added charging became detectable. Hogue *et al.*, (2004) states that many materials are hydrophilic and have a thin layer of water molecules on their surfaces; this is where ions can exist which play a role in charge exchange.

Table 3.1, Summary of insulator-metal tribo-electric charging theories.

| Electrostatic theory | Description | Reference |
|---------------------------------|---|---|
| Electron transfer theory | Electrons move from material having a low work function to a higher work function which generates a charge. | Davies, 1969 ; Murata <i>et al.</i> , 1979 ; Lowell and Rose-Innes, 1980 ; Lowell, 1979 ; Lang and Kohn, 1971 |
| Ion transfer theory | On contact, the free movable ion (positively or negatively) relocates to another surface. | Harper, 1967 ; Kornfeld, 1976 ; Matsusaka <i>et al.</i> , 2010 ; Robins <i>et al.</i> , 1980 |
| Material transfer theory | A physical clump of material rubs onto an opposing surface of material bearing either positive or negative charges. This eventually decides the net overall charge of the resultant material bearing the detached material. | Jain and Bahadur, 1978 ; Tanoue <i>et al.</i> , 1999 ; Hogue <i>et al.</i> , 2004 ; Eilbeck <i>et al.</i> , 2000 ; Baytekin <i>et al.</i> , 2013 ; Piperno <i>et al.</i> , 2011 |

3.3- Powder processing

Pharmaceutical solids are mainly organic materials that have high resistivities ($> 10^{13} \Omega \text{ m}$) and charge relaxation times of minutes to hours (Bailey, 1993). The processing of pharmaceutical powders during manufacturing inevitably involves relative movement of particles against each other and alongside solid surfaces of processing equipment, hence providing ample opportunities for tribo-electrification (Glor, 1985, Harper, 1967). Powder processing operations, including micronisation, fluidisation, sieving, conveying of powders through pipes, bags, and hoppers and spray drying, invariably generate tribo-electric charges (Glor, 1985 ; Matsusaka *et al.*, 2010 ; Matsusaka and Masuda, 2003). Commonly, the higher the energy involved in a procedure, the greater tribo-electric charging. This can instigate problems such as dust explosions, particle adhesion during manufacturing, alteration in the dose uniformity of dosage form, particle accumulation on the surface and segregation (Šupuk *et al.*, 2011 ; Staniforth and Rees ; 1982, Glor, 2005 ; Glor, 1985). Surface adhesion (SA) of powder, is the propensity of dissimilar powder particles or contacting surfaces to cling together. SA during processing seems to be the root cause of other problems, having a direct relationship with the aforementioned problems related to binary powder mixtures. The inter-molecular forces considered responsible for SA include van der Waals forces, electrostatic charges and bridging forces, mainly surface liquid capillary attractions (Cross, 1987). However, it was proposed that the main particle/substrate forces are van der Waals forces and electrostatic forces. These forces are strongly affected by surface properties such as morphology, surface chemistry and contact area. For larger particles, gravity and inertia are generally greater than the adhesion force, hence they normally flow easily. For fine particles, the inter-particle adhesion force is appreciable relative to gravity, therefore, they tend to adhere to one another and are difficult to handle (Lam and Newton, 1991 ; Podczeck, 1998).

3.4- Factors affecting tribo-electrification

The electrostatic charging of powder particles in relation to the manufacturing and use of pharmaceutical products is usually considered due to a tribo-electrification phenomenon. Tribo-electrification and its associated adhesion of powder particles are complex processes affected by different factors. In this section, the principal factors that can affect electrostatic charge transfer and powder SA will be discussed; however, a summary of all the major contributing factors has been given in Table 3.2.

3.4.1 - Nature and work function of contacting surfaces

The work function of a material can be defined as, the minimum energy required to remove the weakest bonded electron from the surface to infinity. The earliest research work demonstrated conflicting evidence regarding the relationship between work function and electrostatic charging (Elsdon and Mitchell, 1976) but with progress in the area, now there is better established evidence to show that there is a relationship between work function and electrostatic charge generation and transfer. Davies (1969) studied the charge densities generated on dielectric surfaces, polycarbonate, PTFE, polyvinyl chloride (PVC), polyimide, polyethylene terephthalate (PET) , polystyrene (PS) and nylon, and studies revealed that the dielectric surfaces were directly related to the work function of the respective contacting surface, as described earlier. Lowell (1976) performed electrostatic experiments to explain the mechanism of charge generation and transfer between platinum, gold, nickel, rhodium, and aluminium and three kinds of polymers (polyethylene, PTFE and PET), using a single non-sliding contact, repeated non-sliding contacts and a sliding contact. The results demonstrated that in a single non-sliding contact, the charge did not depend on the work function. However, on repeated contact, or if the metal slides on the polymer, then the resultant charge density has a linear relationship with the work function of contacting

surfaces. The electrostatic charging of aluminium, copper, gold, magnesium and platinum electrodes was investigated by Nordhage and Bäckström (1977) against sodium chloride. It was found that the charge density transferred to the metals was enhanced with increasing work function of each respective metal. A study using lactose of different surface type and distinct different levels of work function revealed that it charged differently as the contacting surface changed. The tribo-electric charge was -13.23, -18.76 and $+ 76.90 \times 10^{-9}$ C/g, when the contacting surfaces were brass, steel and cellulose, respectively (Carter *et al.*, 1992). The authors explained that the metals generally donate electrons due to higher work function, whereas insulators accept electrons because of lower work function. So in this particular study, the difference in tribo-electric charge generation is entirely due to a difference in work function (Carter *et al.*, 1992). Bennett (1998) investigated the electrostatic properties of salbutamol sulphate which acquired negative and positive charges following agitation in stainless steel and polypropylene, respectively. The polarity of charge was found to depend on the level of the work function of the contacting surface (Bennett 1998). Furthermore, the tribo-electrical properties of α -lactose monohydrate powder particles were investigated by Eilbeck *et al.* (1999) using a cyclone separator at < 10 % RH. It was found that the α -lactose monohydrate gained a higher magnitude of negative charge following contact with stainless steel than with acetal, and a higher positive charge following contact with polyvinylchloride (PVC) than with polypropylene, thus again demonstrating that the charge generation and transfer have a linear relationship with the level of work function. Li *et al.*, (1999) also concluded that the charge transferred for synthetic mineral against a copper surface had a linear relationship with work function. Similar conclusions have been drawn by Akande and Adedoyin (2001), Elajnaf *et al.* (2006), Engers *et al.* (2006), Greason (2000) and Zhu *et al.* (2007).

Furthermore, Šupuk *et al.* (2012) studied the tribo-electric charging of numerous pharmaceutical materials, including lactose and hydroxypropylcellulose (HPC), using glass, PTFE and stainless steel surfaces. This study again demonstrated that the work function plays an important role in determining the magnitude and polarity of tribo-electric charging of powder particles and the powders, themselves and a 50:50 binary mixture was found to charge positively against PTFE, but negatively against glass and stainless steel.

3.4.2- Contact surface roughness

Coste and Pechery (1981) investigated the effect of contact surface roughness of polyethylene terephthalate (PET) on the electrostatic charge density acquired through contact with metal. This study demonstrated that the charge density was increased as the PET powder particles collided with the smooth metal surface. Additionally, the experiments conducted by Eilbeck *et al.*, (1999) investigated the effects of contact surface roughness on tribo-electrification using α -lactose monohydrate charged against a rough and smooth stainless steel cyclone separator at < 10% RH. The results showed that the α -lactose monohydrate acquired a highly negative charge against the smoother stainless steel surface.

Table 3.2, Summary of factors affecting tribo-electric charging

| Factor | Effect | Reference |
|---|---|--|
| Nature and work function of contacting surface | Work function is considered the principal driving force for the generation of tribo-electric charge. | Akande and Adedoyin, 2001 ; Bennett, 1998 ; Carter <i>et al.</i> , 1992 ; Davies, 1969 ; Eilbeck <i>et al.</i> , 1999 ; Elajnaf <i>et al.</i> , 2006 ; Elsdon and Mitchell, 1976 ; Engers <i>et al.</i> , 2006 ; Greason, 2000 ; Li <i>et al.</i> , 1999 ; Lowell, 1976 ; Šupuk <i>et al.</i> , 2012 ; Zhu <i>et al.</i> , 2008 |
| Contact surface roughness | The smooth contact surface leads to higher magnitude of tribo-electric charge. | Coste and Pechery, 1981, Eilbeck <i>et al.</i> , 1999 |
| Contact surface contamination | Surface contamination of contacting surface impacts the polarity and magnitude of tribo-electric charge | Eilbeck <i>et al.</i> , 2000 ; Harper, 1953 ; Murtomaa <i>et al.</i> , 2002a ; Murtomaa <i>et al.</i> , 2002c |
| Particle size | A decrease in particle size enhances the magnitude of tribo-electric charge. | Bailey, 1984 ; Carter <i>et al.</i> , 1992 ; Duff and Lacks, 2008 ; Eilbeck <i>et al.</i> , 1999a ; Engers <i>et al.</i> , 2006 ; Gallo and Lama, 1976 ; Karner and Urbanetz, 2012 ; Karner and Urbanetz, 2013 ; Kwek <i>et al.</i> , 2013 ; Lacks <i>et al.</i> , 2008 ; Lacks and Levandovsky, 2007 ; Lacks and Sankaran, 2011 ; Rowley, 2001b ; Smeltzer <i>et al.</i> , 1982 ; Staniforth and Rees, 1982 ; Zhao <i>et al.</i> , 2003 |
| | An increased particle size enhances the magnitude of tribo-electric charge. | Carter <i>et al.</i> , 1998 ; Fasso <i>et al.</i> , 1982 ; Nieh and Nguyen, 1988 |
| Particle shape and roughness | A rougher particle surface lead to higher magnitude of tribo-electric charge. | Kwek <i>et al.</i> , 2013 ; Matsusaka <i>et al.</i> , 2000 ; Murtomaa <i>et al.</i> , 2004 ; Trigwell <i>et al.</i> , 2008 |
| Material chemistry | The chemical structure, functional groups and surface chemistry can significantly affect the tribo-electrification | Kamiyama <i>et al.</i> , 1994 ; Mazumder <i>et al.</i> , 2006a ; Sharma <i>et al.</i> , 2007 ; Sharma <i>et al.</i> , 2003 ; Shinohara <i>et al.</i> , 1976 ; Trigwell <i>et al.</i> , 2003 |
| Crystallinity and amorphicity | Higher crystallinity leads to higher propensity of tribo-electric charge. | Carter <i>et al.</i> , 1998 ; Cassidy <i>et al.</i> , 2000 ; Kwok and Chan, 2009 ; Murtomaa <i>et al.</i> , 2002a ; Shekunov <i>et al.</i> , 2002 ; Wong <i>et al.</i> , 2014b |
| Mixing ratio | Increasing fraction of excipients in powder mixtures with APIs tends to decrease the final tribo-electric charging. | Asare-Addo <i>et al.</i> , 2013b ; Engers <i>et al.</i> , 2006 ; Ghori <i>et al.</i> 2014c ; Murtomaa and Laine, 2000 ; Pingali <i>et al.</i> , 2009 ; Rowley, 2001 ; Sarkar <i>et al.</i> , 2012 ; Zhu <i>et al.</i> , 2007 |
| Frequency of contacts | The increased and repeated powder particle contacts increase the magnitude tribo-electric charge | Cunningham and Goodings, 1986 ; Engers <i>et al.</i> , 2006 ; Harper, 1953 ; Lowell, 1976 ; Lowell and Akande, 1988 ; Matsusaka <i>et al.</i> , 2000 ; Watanabe <i>et al.</i> , 2007 ; Zhu <i>et al.</i> , 2007 |
| Atmospheric conditions | As the RH decreases, the charge on a powder sample increases. | Eilbeck <i>et al.</i> , 2000 ; Greason, 2000 ; Nguyen and Nieh, 1989 ; Nieh and Nguyen, 1988 ; Nomura <i>et al.</i> , 2003 ; Rowley and Mackin, 2003 ; Smeltzer <i>et al.</i> , 1982 ; Turner and Balasubramanian, 1976 |
| | However, some studies report increased propensity of charging with increased RH | Boschung and Glor, 1980 ; Wiles <i>et al.</i> , 2004 |

3.4.3- Contact surface contamination

Contact surface contamination and the procedure for cleaning surfaces can affect the tribo-electrification process and hence the charge acquired by contacting powders. Early work by Harper (1953) showed the electrification of powders was affected by the cleaning procedure and surface contamination. Eilbeck *et al.*, (2000) investigated the effect of contamination of pharmaceutical equipment on powder tribo-electrification following contact with a stainless steel cyclone separator. Charging of α -lactose monohydrate was undertaken without cleaning between experimental runs and the results showed a decrease in the net negative charge acquired by the lactose with replicated experiments, due to an increase in the extent of powder adhesion to the cyclone surface. Murtomaa *et al.*, (2002) studied the tribo-electrification of glucose powder in a glass pipe, and the effect of adding smaller particles of lactose, magnesium stearate, dicalcium phosphate, or starch 1500 of different size fractions to the glucose. Mixtures of different ratios were charged by sliding them down a glass pipe into a Faraday well and differences were obtained in the polarity and magnitude of transferred charge after mixing. For example, when the glucose was mixed with lactose, the particle charge changed from positive to negative due to contact between glucose particles and adhered lactose particles. Also Murtomaa *et al.*, (2000) investigated the tribo-electrification of microcrystalline cellulose and PS spheres in contact with stainless steel pipes washed with several different detergents. The results clearly indicated that some detergents left contamination on the pipe surface that had a significant effect on the polarity and the magnitude of the transferred charge.

3.4.4- Particle size

The effect of particle size on the magnitude and charge of powder particles has been studied extensively for many years. In general, particle size affects many industrial processes; a small

size improves drug absorption, but may lead to flow problems and segregation. In the literature, there are contradictory findings on the effect of particle size on tribo-electrification. Gallo and Lama (1976) proposed that the work function decreases with an increase in particle size, suggesting that, under some experimental conditions, the difference in work function between small and large particles of the same material will result in charge generation and transfer. The tendency for such charge exchange is greatest when one of the particles is very small and the other is comparatively large (Gallo and Lama, 1976). It was also suggested that electrons should transfer from larger particles, due to their lower work function, to smaller particles when they contact each other and therefore, the smaller particles should charge negatively and the large particles positively. The studies conducted by Duff and Lacks, (2008); Engers *et al.* (2006); Lacks *et al.* (2008); Lacks and Levandovsky (2007); Rowley (2001) and Lacks and Sankaran (2011) discussed the theoretical mechanisms for particle size dependent charging. In most cases, smaller particles charged negatively whereas larger particles charged positively and these findings are in complete accordance with the theory of Gallo and Lama (1976). However, this theory is contradicted by Ali *et al.* (1998) who reported that for a specific polymer powder tested, the small particles charged positively and the larger ones charged negatively. It could be argued that if the charging is the result of ion transfer rather than electron transfer, the Gallo and Lama theory may still be valid (Bailey, 1984).

Many studies have shown an inverse relationship between particle size and charge, i.e., as particle size is decreased, the charge on a powder particle increased (Carter *et al.*, 1992; Eilbeck *et al.*, 1999; Engers *et al.*, 2006; Ghori *et al.* 2014c; Smeltzer *et al.*, 1982; Staniforth and Rees, 1982 ; Rowley, 2001; Zhao *et al.*, 2003).

The study conducted by Staniforth and Rees (1982) showed that recrystallised lactose acquired negative charges, which increased with decreasing sieve fraction from 710-1000 μm

to 500-710 μm . The studies carried out by Smeltzer *et al.* (1982) investigated the effect of particle size on the charging of glass beads during pneumatic transport along a pipe, with an increase in charge transfer, as the particle size decreased from 150 to 75 μm . This was thought to be due to a higher number density, giving an increased number of collisions for smaller particles. Carter *et al.* (1992) investigated the tribo-electrification properties of α -lactose monohydrate against a stainless steel and brass cyclone separator. The specific charge values were inversely related to particle size. Eilbeck *et al.* (1999) investigated the tribo-electrification of lactose after contact with a stainless steel and PVC cyclone separator at < 10% RH. The mean specific charge for the α -lactose monohydrate sieve fraction samples increased with decreasing particle size, over the range 90-1000 μm . Rowley (2001) proposed that as the lactose sieve fraction size decreased from 355-500 μm to 90-125 μm , there was an increase in the specific charge following contact with a stainless steel surface and likewise for fractions 355-500 μm to 125-150 μm in contact with a PVC surface.

Zhao *et al.* (2003) investigated the effect of particle size on charge-to-mass ratio of polymer powders using fluidized beds. It was observed that smaller particles charged negatively and possessed a high charge-to-mass ratio, whilst the larger particles charged positively and possessed lower charge-to-mass ratios. Engers *et al.* (2006) investigated the effect of particle size of dicalcium phosphate dihydrate on the specific charge of powder samples. The study revealed that the specific charge was significantly higher for the sample containing a higher proportion of fines than that observed for particles in the size range of 425 – 800 μm . Ghori *et al.* (2014c) reported that when the particle size of MC/HPMC has decreased from 150-250 μm to 90-150 μm the charge was increased. The studies carried out by Karner and Urbanetz (2012, 2013) and Kwek *et al.* (2013) reach the same conclusions, the fine powder particles acquired a higher magnitude of the charge.

Conversely, other studies have shown a direct relationship between increasing particle size, and the specific charge (Carter *et al.*, 1998a; Fasso *et al.*, 1982; Nieh and Nguyen, 1988). In a study by Fasso *et al.* (1982), the electrostatic charge and charge distribution of glass beads was measured in a freeboard and the main charge for glass beads (30 to 55 μm) at various flow velocities was found to be enhanced with the increase in particle size. Nieh and Nguyen (1988) studied the electrostatic charging of flowing glass beads (137 to 550 μm). The results showed that large particles acquired a higher charge, but lower specific charge and the mean surface charge density of the particle remained almost constant over a wide particle size range. Carter *et al.* (1998a) investigated the tribo-electrification for both fractionated crystalline and spray-dried lactose samples. The results showed that the magnitude of charge on the lactose samples increased with increasing particle size, over the range 45-125 μm and 63-180 μm for crystalline and spray dried lactose, respectively. This was due to particle adhesion to the contact surface which causes increased particle-particle interactions and reduced particle-contact surface collisions.

3.4.5- Particle shape and roughness

The transfer of charge takes place between surfaces in contact and the shape and surface morphology of powder particles play an important role in the exchange of tribo-electric charges. Transferred charge is proportional to the maximum contact area in an impact process; consequently the particle shape is extremely important (Matsusaka *et al.*, 2000; Trigwell *et al.*, 2008). The rougher the surface of the particle, the smaller the area of contact and surface-charge density, which is transferred between the materials in contact. In reality, most pharmaceutical materials have rough surfaces, containing many asperities. When such surfaces are in contact, there will be a small distance between the materials in contact, known as the effective distance. The flatter the contact surfaces of the powders, the smaller the

effective distance will be (Trigwell *et al.*, 2008). Murtomaa *et al.* (2004) investigated tribo-electric charging of lactose with different particle morphology, finding that the overall reproducibility was improved with homogeneous particle morphology. However, the study could not clearly explain the effect of shape and morphology of lactose on the tribo-electric charging. Recently, Kwek *et al.* (2013) studied the tribo-electrification properties of mannitol, comparing smooth and rough surfaces using shaking and aerosolisation techniques. This study revealed that the mannitol powder particles with a rougher surface had a higher magnitude of surface charged than those with a smoother surface.

3.4.6- Material chemistry

The chemical structure, functional groups and surface chemistry (Kamiyama *et al.*, 1994; Mazumder *et al.*, 2006; Shinohara *et al.*, 1976) can significantly affect the tribo-electrification and subsequent particle SA processes. Kamiyama *et al.* (1994) investigated the tribo-electrical properties of polymeric materials by introducing different ions on their surface, demonstrating that the change in surface chemistry can significantly impact the materials' tribo-electrification properties. Furthermore, Sharma *et al.* (2003 and 2004) and Trigwell (2003) determined that the magnitude and polarity of charge exchange between two dissimilar materials are directly related to the chemical nature of the polymer powders. Recently, Ghori *et al.* (2014c) reported that the substitution groups of MC/HPMC have significant impact on the tribo-electrification properties.

3.4.7- Crystallinity and amorphicity

Theoretically, amorphous and crystalline materials have different crystal packing which would lead to varied surface energies that may influence charge transfer behaviours. Cassidy *et al.* (2000) investigated the tribo-electrification of spray-dried lactose prepared from different feedstock concentrations (10 - 50%), following contact with a stainless steel surface,

using either a mixing vessel or cyclone separator. Increasing the feedstock concentrations from 10 to 50% decreased the mean specific charge on lactose from -20.8 to -1.3 nC g and 54.9 to -4.1 nC g for the mixing vessel and cyclone separator, respectively. This was attributed to differences in crystal form of the spray dried lactose powder samples. Carter *et al.* (1998a) investigated tribo-electric charging of spray-dried amorphous and fractionised crystalline lactose. Both the materials showed significantly different charging tendencies with crystalline lactose charging gaining a higher tribo-electric charge than spray-dried amorphous lactose. Shekunov *et al.* (2002) compared micronized and supercritical fluid-conditioned salmeterol xinafoate, Murtomaa (2002a) studied the tribo-electrification properties of lactose and Kwok and Chen (2008) studied amorphous spray-dried salbutamol sulphate (spherical shape) and crystalline jet-milled salbutamol sulphate (plate-like). In all studies, the tribo-electric charge decreased as the crystalline component of respective powder samples was increased. The particle surface morphology was not experimentally controlled and this is an area that may need further investigation. However, a recent study carried out by Wong *et al.* (2014b) has, for the first time, attempted to resolve this ambiguity. Electrostatic charging was characterised in two ways, firstly, through aerosolisation from an inhaler and secondly, by tumbling in containers made of different materials. Following aerosolisation, crystalline salbutamol sulphate showed more consistent charging and mass deposition than the amorphous formulation. Alternatively, the tumbling experiments found, the net charge of crystalline salbutamol sulphate correlated linearly with work function. This correlation was absent in amorphous salbutamol sulphate. It is possible that the long-range crystal packing in crystalline salbutamol sulphate caused more predictable charging.

3.4.8- Mixing ratios

The quantification of tribo-electric charge of different powder blends is a difficult task as due to different mixing ratios; the component powder particles of a powder blend have complex charging kinetics. Additionally, the tendency of one material to coat either the equipment surface or other particles leads to unpredictable behaviour, and the volume of powder used determines the nature of the contact. If the volume is small compared to the surface of the container, particle-particle contacts may be negligible (Zhu *et al.*, 2007). Pingali *et al.* (2009) concluded that the composition of powder blends can significantly impact the tribo-electric charging properties.

Rowley (2001) investigated the effect of different salbutamol sulphate concentrations (0.5, 1.0 and 5.0% w/w) in a binary mixture with α -lactose monohydrate carriers charging against steel and polyamide contacting surfaces. The magnitude of tribo-electric charge decreased as salbutamol sulphate concentration increased from 0.5 to 5% w/w, and the values were -38 to -91 nC/g for steel and -10 to -42 nC/g for polyamide. Among different pharmaceutical excipients, lactose and glucose are widely used excipients in the pharmaceutical industry. It was reported that pure glucose became positively charged, but as soon as lactose was introduced, the accumulated net charge on the powder mixture became negative. The mixture charged negatively if the amount of lactose was between 20 and 40 % w/w, but became positively charged again when the amount of lactose was increased further (Murtomaa and Laine, 2000). Engers *et al.* (2006) reported that specific tribo-electric charges of powder mixtures can be controlled by using compatible excipients. Sarkar *et al.* (2012) observed reduction of tribo-electric charge on incorporation of additives (L-ascorbic acid, Magnesium stearate, and stearic acid). Moreover, Sarkar *et al.* (2012) also proposed that the extent of charge reduction appeared to relate to moisture content and levels of effective work function.

Šupuk *et al.* (2010) concluded that binary mixtures of α -lactose monohydrate and hydroxypropyl cellulose charged to significantly higher magnitudes with increasing concentrations of α -lactose monohydrate in a binary mix. Asare-Addo *et al.* (2013b) and Ghori *et al.* (2014c) confirm that the HPMC has antistatic properties as with higher polymer concentration it has the ability to dissipate the charge of drug particles.

3.4.9- Mixing speed/frequency of contact

Cunningham and Goodings (1986); Harper (1953) and Lowell (1976) have shown that an increase in the number of contacts may increase the propensity of tribo-electric charge on the surface of powder particles. Cunningham and Goodings (1986) demonstrated that repeated contacts increased the quantity of net charge transferred between a gold probe and a polymer. Moreover, Lowell and Arkande (1988) also found that repeated contacts increased the extent of tribo-electric charging. Watanabe *et al.* (2006, 2007) found that the amount of tribo-electric charge generated during single particle impacts under different impact velocities and angles relates to the normal component of the impact velocity. Furthermore, an equilibrium initial charge was quantified, where no charge transfer took place on impact of the particle due to the surface potential of the contacting bodies. Similar results were reported by Matsusaka *et al.* (2000) using 30 mm rubber balls. Zhu *et al.* (2007) investigated the contact energy as a function of the rotation speed of a mixer, finding that was not influenced by the rotation speed. This is because the rotation speed of the mixer only influences the frequency of particle contacts. Thus the time required to reach saturation increases with decrease in rotation speed, but the total amount of saturated charge is defined by the surface potential difference of the contacting bodies and therefore cannot be influenced by the rotation speed. These results are in agreement with the blender studies performed by Engers *et al.* (2006).

3.4.10- Atmospheric conditions

Most authors have shown an inverse relationship between RH and charge. (e.g. Eilbeck *et al.*, 2000; Greason,2000; Smeltzer *et al.*, 1982; Nguyen and Nieh (1989); Nieh and Nguyen, 1988; Nomura *et al.*, 2003; Mackin *et al.*, 1993, 1994; Rowley and Mackin, 2003; Turner and Balasubramanian,1976).

Conversely, Boschung and Glor (1980) and Wiles *et al.* (2004) showed that charge increased linearly with RH. In the study carried out by Turner and Balasubramanian (1976), a lower electrostatic charge on glass spheres was found at higher levels of relative humidity. Similarly, Smeltzer *et al.* (1982) investigated the effect of RH (25 to 65%) on the charging of glass beads (75-150 μm) during pneumatic transport along a pipe and showed a greater charge was generated at the lower RH. Nieh and Nguyen (1988) found that the mean particle charge on 550 μm glass beads flowing in a copper pipe fell with an increase in RH from 4 to 76 %. This may be due to the moisture around the dielectric particles, increasing their surface conductivity, and thereby enhancing the transfer of electrons upon contact with an earthed pipe wall. Nguyen and Nieh (1989) investigated the effect of carrier gas RH on the electrostatic charges of glass beads flowing in a continuous copper pipe loop. As RH increased from 0 to 65%, electrostatic charges decreased; this was attributed to sorbed moisture on the glass particle surface, providing an earthing path to the metal walls during particle/metal collisions and it was proposed that hydrated ions and water vapour would act as charge carriers to redistribute the surface charge into free space. Eilbeck *et al.* (2000) investigated the effect of moisture contamination of the contact surface on the charge of α -lactose monohydrate (180-212 μm) following tribo-electrification with a stainless steel cyclone separator at 2 and 100% RH. The results showed a decrease in the net negative charge on the lactose at the higher RH. There was a decrease in net charge as the RH % and

the temperature increased after rolling a stainless steel sphere (1.27 cm diameter) in tubes constructed from glass, quartz, PTFE, acrylic, polycarbonate, and nylon at range of 10-30°C and RH range from 10 to 70% (Greason, 2000). The results showed a decrease in the tribo-electric charge which can be attributed to a decrease in the volume and surface resistivities of the insulators caused by an increase in temperature and RH. Nomura *et al.* (2003) studied the effect of environment humidity on the tribo-electrification of a ferrite powder coated with silicone resin following rotating samples in cylindrical nickel vessels and showed a decrease in the specific charge on the powder with increasing humidity. With a variety of contact surfaces, Rowley and Mackin (2003) showed that for relatively non-hygroscopic excipients α -lactose monohydrate and dextrose monohydrate there was a negligible change in charge values in RH range 0-80 %, however a hygroscopic excipient, sodium starch glycolate, showed a decrease in electrostatic charge from RH 0 to 80 %. There was no relationship between moisture sorption and charge for the intermediately hygroscopic material, spray-dried sorbitol. Care must be taken when considering total sorption data for predicting electrostatic charge behaviour, where significant proportions of total moisture are present as absorbed moisture, as may be the case with porous spray-dried sorbitol. When nylon, Teflon and polyacetal pellets were fired at a metal target at temperatures ranging between ambient temperature conditions and 230 °C, Bailey and Smedley (1991) found there was little effect of temperature on tribo-electrification between metal and insulator contacts.

3.5 – Applications and hazards of tribo-electric charging

In pharmaceutical manufacturing, processing operations such as mixing, spray-drying, coating and pneumatic conveying, have a tendency to induce an electrostatic charge on powder particles due to inter and intra-particulate collisions (Carter *et al.*, 1992). Fine powder particles, such as those used in inhalation, typically experience problems in flow and

dispersion because of the small particle size. Moreover, electrostatic, capillary and Van der Waals forces play a critical role contributing to adhesion and cohesion (Bailey, 1993) with implications on transporting, filling, blending, drying, milling, and mixing; and subsequently, non-uniform dosages in the final product (Bennett *et al.*, 1999; Elajnaf *et al.*, 2007; Elajnaf *et al.*, 2006; Rowley, 2001; Staniforth and Rees, 1982). Due to the potent nature of many APIs, there are strict quality control processes governing pharmaceutical production for acceptance of finished pharmaceutical product. A single batch of powder worth hundreds of thousands of pounds is sometime discarded, if the amount of APIs dose not meet the pharmacopoeial standards. Therefore, the control of electrostatic charge is important to ensure the final product is safe and effective to use. Aside from the mechanical behaviour of charged particles, electrostatic discharges are also an area of concern as large quantities of powders being handled with high transfer rates in filling and emptying during tableting process. This can rapidly build up a charge and increases the probability of an electrical discharge. Additionally, fine pharmaceutical powder particles have a larger surface area that enhances surface contact, which leads to charge accumulation and their distribution in the air provides the oxygen for combustion. The combination of these elements is considered highly dangerous as it has the potential to ignite fires and explosions (Ohsawa, 2011). In 2012, an electrostatic spark discharge ignited a fire during a pharmaceutical powder transfer operation. Following investigation, the source was found to be a 15 year old filter which was not appropriate for handling low minimum ignition energy powders (Kong, 2006). A statistical study about industrial dust explosions revealed that one dust explosion happens every day and every tenth explosion is caused by static electricity discharge (Glor, 2003). Similar statistics in Japan found 70 % of 153 industrial accidents that occurred over the past 50 years were attributable to static electricity (Ohsawa, 2011). A noteworthy finding was that these

incidents were caused by isolating conductors, including workers, which led to spark discharges and could have been easily been prevented with earthing (Wong *et al.*, 2014a).

Despite the issues discussed in the previous section, there have also been several useful applications of electrostatics in the pharmaceutical industry. Blend homogeneity of powder mixes can be promoted by APIs and excipients with opposite charges as they tend to attract each other and segregation becomes unlikely (Pu *et al.*, 2009; Staniforth and Rees, 1981, 1982). While the physicochemical properties determine the inherent polarity of charge gained, the magnitude of charge can be enhanced by charging processes. Conversely, homogeneity could be compromised if an opposite polarity is induced. Other critical parameters that should be considered, in particular for potent low-dose formulations, include the choice of an appropriate mixer, mixing time, and content uniformity (Venables and Wells, 2001). Pu *et al.* (2009) evaluated three different API blending procedures: (I) conventional blending without any charge control, (II) blending with simultaneous charge neutralisation, and (III) blending combined with a corona charging process. Variation in API content increased with specific charges, which suggested that uncontrolled electrostatic charging had an adverse effect. The elimination or minimisation of electrostatic charge did not resolve the problem, rather the mixing of oppositely charged components remained the only controlled charging that improved blend uniformity (Staniforth and Rees, 1982). Interestingly, there is a relationship between electrostatic charging and blend homogeneity and selection of the time points with the least charge variation were expected to correlate with relatively more uniform content, and the authors proposed this as a useful monitoring tool in mixing processes (Chang *et al.*, 1995).

3.6 – Powder mixing

Mixing may be defined as the merger of two or more dissimilar portions of material resulting in the attainment of a required level of uniformity in the final product (Swarbrick, 2007).

There are three types of mixtures namely, positive, negative and neutral mixes. The first occurs spontaneously by diffusion, for example, in miscible liquids and gases where no energy is needed, whereas with negative mixing, such as the dispersion of insoluble solid particles with a liquid, work is required by stirring to maintain the dispersion. In the neutral mix, work must be done initially to mix the components as in a mixture of powders. Powder mixing is a fundamental, important and often the very first processing step, for many industrial processes and is one of the most common unit operations utilised in many industries such as pharmaceutical, chemical, food, cosmetic, cement, glass, and detergent. Mixing performance assessment, which has been a main issue for about a decade, is likely to become even more important as dosages become smaller. Specifically, the pharmaceutical industry uses powder mixing operations to incorporate highly active pharmaceutical ingredients in many pharmaceutical formulations, such as powders, granules, capsules and tablets. Powder mixing can be classified either as randomised or ordered mixing (Hersey, 1975).

3.6.1 – Random powder mixtures

In random mixtures, the component particles should be free flowing and of similar size, density and shape. However, in practice, the components of particulate solids often consist of materials with different morphologies and sizes. These powder mixtures can be produced by random or ordered methods. Random mixing is the process of repeatedly splitting and recombining a bed of particles until there is an equal chance of any individual particle being at any given point in the mix at any one time (Venables and Wells, 2001). Random mixing is based on the statistical randomization of non-cohesive particles (Hersey, 1975). It is a rough estimate of disorder and does not result in an “ideal” mixture.

3.6.2 – Ordered powder mixtures

When inter-particulate forces, either attraction or repulsion, are introduced in mixtures, the randomized distribution of component particles will be disturbed; this type of mixing is described by ordered mixing. Tribo-electrification can be used to help with such mixing operations in industry (Swaminathan and Kildsig, 2000; Venables and Wells, 2001). Fine particles charge opposite to coarse particles during particle collisions with material surfaces, (see section 3.4.4 for more detail). This results in fine particles adhering to larger carrier particles, known as ordered mixing. Ordered mixing is believed to result in a more homogeneous and stable system compared to that of a random mixture (Hersey, 1975). Both gravitational and electrostatic forces are presented in random and ordered mixes. In an ordered mix, the gravitational force is weak compared to the electrostatic forces, whilst the opposite is true of a random mix. A mixture is likely to retain its integrity if the bonds between the carrier and the fine particle are strong enough; in this case, handling problems are greatly reduced (Mäki *et al.*, 2007; Hersey, 1975)

3.7- Section A, Tribo-electrification and adhesion studies of model drugs

3.7.1- Introduction

The conversion of active pharmaceutical ingredient (API) into pharmaceutical formulations encompasses an array of processes that are involved in powder processing and handling, such as powder transport, milling and mixing. In recent years, formulation development has become more challenging because new drug molecules often display poor physico-chemical properties (Swarbrick, 2007). These include a high propensity to electrostatic charging and occurrence of associated problems. In powder handling operations, particles frequently come in contact with each other and with the walls of the processing equipment causing tribo-electrification of the particles (Cross, 1987). The irregular surface morphology, fine particle

size distribution and low bulk density of APIs makes them highly susceptible to electrostatic charging. Moreover, the APIs have high electrical resistance which prevents charge dissipation. The charge duration on a powder particle surface depends on relaxation time, which is the product of permittivity and surface resistivity of drug particles. As the majority of APIs are insulators, so this process is extended, perhaps over minutes to hours, in comparison to conductive materials (Bailey, 1984). The accumulation of charge for extended durations can generate inter-particulate bonding forces which lead to SA and deposition of the powder particles on the walls of the processing equipment (Harper, 1967). Therefore, characterisation and optimization of tribo-electrification and adhesion properties of APIs can be considered as a key task during pharmaceutical formulation development. The aim of this particular study was to investigate the tribo-electrification and adhesion properties of poorly soluble (FBP) and freely soluble (THP) model drugs with a mechanistic perspective.

3.7.2- Experimental

3.7.2.1- Materials

The model drugs were obtained as detailed in section 2.1.2.

3.7.2.2- Methods

3.7.2.2.1- Surface morphology of drug particles

The surface morphology of the powder particles of model drugs was examined by following the method as described in section 2.2.4.1.

3.7.2.2.2 - Tribo-electrification

Tribo-electric charging of drug powder particles was studied by adopting a method based on a shaking concept as described in section 2.2.5.2.

3.7.2.2.3- Surface adhesion (SA) of powders

The SA of the powder particles of model drugs was examined following the method described in section 2.2.5.3.

3.7.3- Results and discussion

3.7.3.1- Surface morphology of model drugs

SEM micrographs were used to study the surface morphology of pure model drugs. Figure 3.5 illustrates SEM micrographs of (a) FBP and (b) THP which were imaged at a magnification of $\times 800$ and $\times 750$, respectively. FBP has rectangular shaped crystals, whereas THP has elongated crystals with a columnar habit. Moreover, from both the SEM micrographs, it can be concluded that both the drug crystals have rough surfaces, however, THP crystals have more irregularity than FBP crystals.

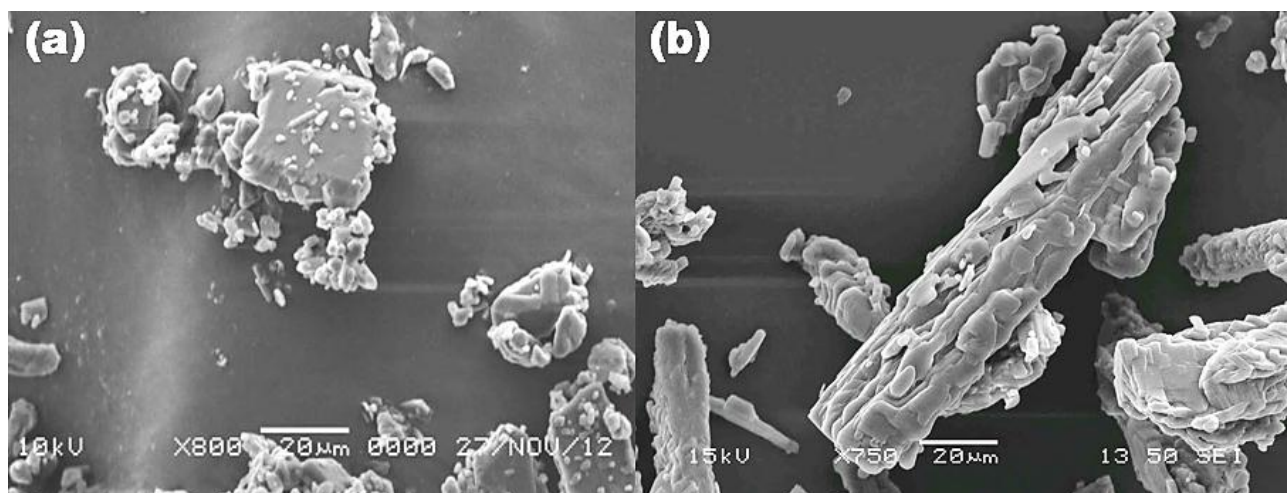


Figure 3.5, SEM micrographs of (a) FBP and (b) THP powder particles

3.7.3.2- Tribo-electrification and adhesion properties of model drugs

In the present study, maximum charge acquisition data (Q_{max}) are presented as a charge to mass ratio (Q/M) at the end of each tribo-electrification experiment (n=3), as exemplified in Figure 3.6. Moreover, the SA of powders related to Q_{max} was determined, (n=3).

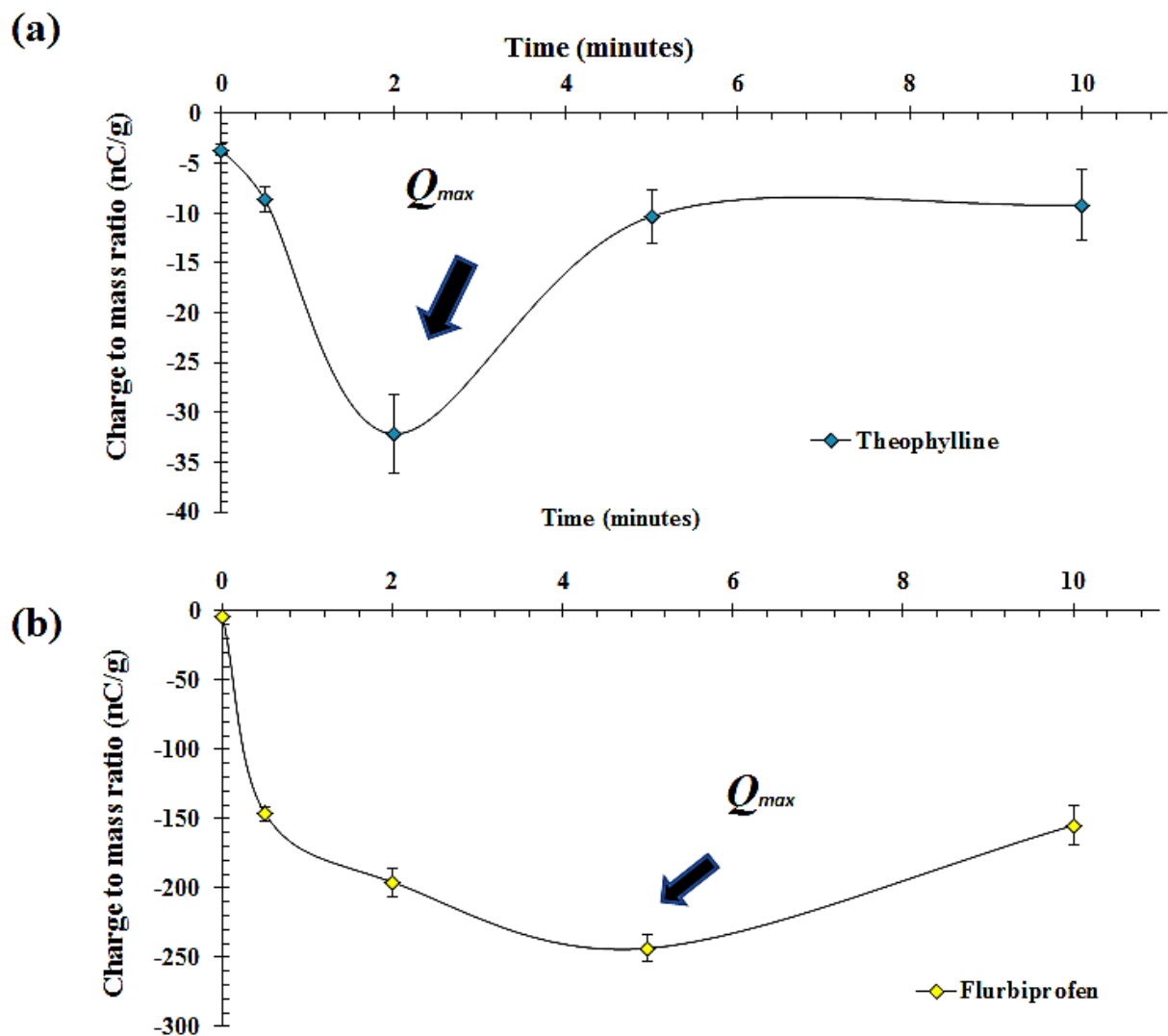


Figure 3.6, Tribo-electrification charging profiles of (a) FBP and (b) THP powder particles (n = 3).

The model drugs (FBP and THP), like many other APIs, possess a high degree of crystallinity and were presumed to have a higher electrical resistance. FBP and THP attained Q_{max} in 5 and 2 minutes respectively, when shaken against a stainless steel container (Figure 3.6). The tribo-electrification phenomenon is considered to be ambiguous, but the electron transfer theory is widely accepted to explain the mechanism of charge generation of pharmaceutical materials. In the present study it can be assumed that the effective work function of FBP (W_f) and THP (W_t) is higher than the work function of stainless steel contacting surface (W_s). This might be due to the greater electrical resistivity of drug crystals.

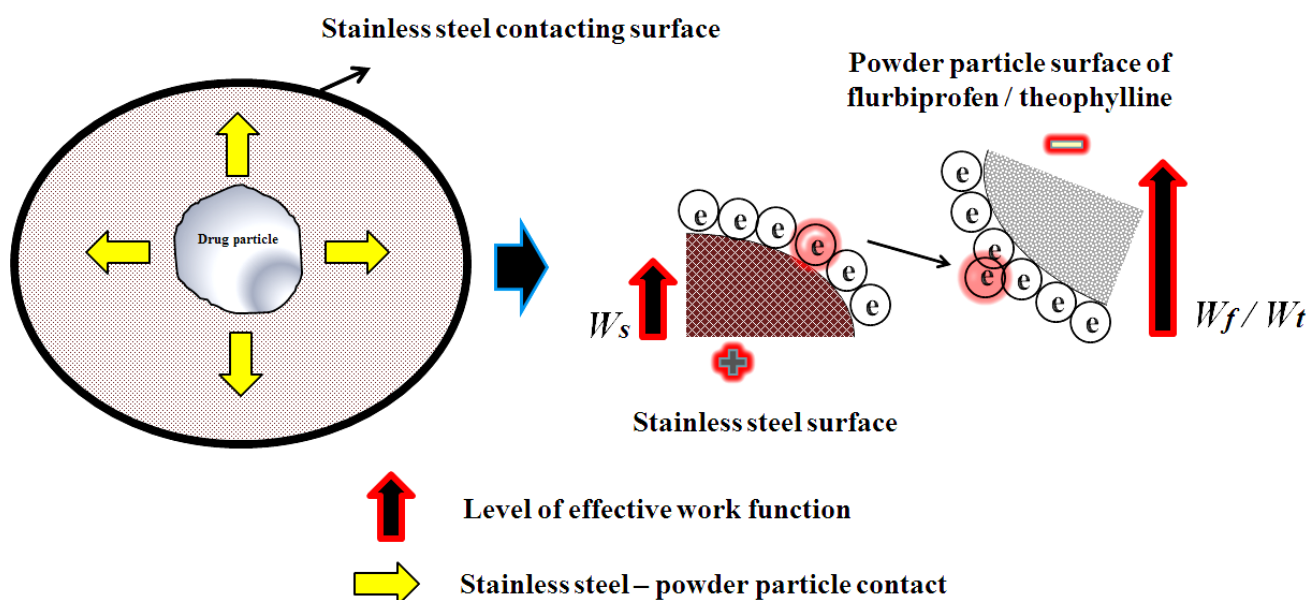


Figure 3.7, Schematic illustration of tribo-electric charging of FBP and THP powder particles.

Therefore, when the powder particles of both the drugs were introduced into the stainless steel container, the electrons from the stainless steel surface, presumably moved to the interface of the contacting drug powder particles, thus inducing a positive surface charge on the donor,

with a negative charge (acceptor) on the FBP and THP powder particles (as illustrated in Figure 3.7).

Table 3.3, Tribo-electric charging and SA results for THP and FBP (n = 3, standard deviations in parentheses).

| Drug | Particle size | Charge to mass ratio (nC/g) | Adhesion (%) |
|-------------|----------------------|------------------------------------|---------------------|
| THP | 38 – 63 µm | -32.01 (3.8) | 38.42 (5.11) |
| FBP | 38 – 63 µm | -243.13 (13.25) | 74.23 (4.32) |

Both FBP and THP attained a negative net charge across their particle surface, gaining maximum tribo-electric charge of -243 nC/g and -32 nC/g, respectively. The higher charging tendency associated with FBP resulted in more SA (74 %) due to higher dispersive, chemical and electrostatic forces. THP tended to have lower SA which might be due to the fact that lower levels of tribo-electric charging tend to generate strong inter- or intra-particulate dispersive forces. The electrostatic behaviour of FBP can be categorised as highly charging when compared to other APIs and pharmaceutical excipients and is likely to cause problems during powder processing.

3.8- Section B, tribo-electrification and adhesion studies of cellulose ethers

3.8.1- Introduction

The pervasiveness of tribo-electric charge during pharmaceutical processing can lead to the exacerbation of a range of problems, including segregation, content heterogeneity and particle SA (Harper, 1967). During pharmaceutical powder processing (e.g., milling, transporting, mixing, coating, spray drying, pneumatic conveying and sieving), particles develop tribo-electric charges due to the frequent abrasion and collision between the powder particles and the contacting surface of the processing equipment (Cross, 1987; Cross *et al.*, 1981; Lowell and Rose-Innes, 1980). This can instigate problems such as dust explosions, particle adhesion during manufacturing, alteration in the dose uniformity of dosage form, particle accumulation on the surface and segregation (Hussain *et al.*, 2013; Pu *et al.*, 2009; Staniforth and Rees, 1981; Staniforth and Rees, 1982; Šupuk *et al.*, 2011b). The chemical structure, functional groups, surface chemistry (Kamiyama *et al.*, 1994; Mazumder *et al.*, 2006b; Shinohara *et al.*, 1976), particle size, shape, surface roughness (Carter *et al.*, 1998a; Eilbeck *et al.*, 1999b; Traini *et al.*, 2012) and electrical properties of powders and contacting surfaces (Bailey and Smedley, 1991; Rowley, 2001) can all affect the tribo-electrification process and subsequent particle surface adhesion. Moreover, the charge transfer process is further complicated due to external factors that may influence the charging, process including relative humidity, temperature, nature of contacting material and the velocity of particles (Matsusaka *et al.*, 2010).

Numerous varieties of pharmaceutical excipients are employed to improve or modulate tablet characteristics, among them methylcellulose MC and HPMC are frequently used for controlling drug release from hydrophilic matrix systems (Ghori *et al.*, 2014b; Li *et al.*, 2005; Maderuelo *et al.*, 2011). These polymers are available in different grades varying in viscosity

(molecular size), substitution ratios and particle size. Asare-Addo *et al.* (2013b) recently described the tribo-electric charging behaviour of Methocel[®] E4M, K4M and their powder mixtures with the negatively charging API, THP. The polarity of the singular polymers was positive and was generally higher in magnitude than other common pharmaceutical excipients (Šupuk *et al.*, 2012). It was shown that when THP came into contact with HPMC, it attached to its surface due to opposite polarities and the tribo-electric charge of the final powder mixture was decreased (Asare-Addo *et al.*, 2013b). Surprisingly, despite being so widely used, the tribo-electrification and adhesion characteristics of MC and HPMC are still poorly understood. The aim of this study was to investigate the tribo-electrification and adhesion properties of different cellulose ethers. The impact of polymer attributes (concentration, particle size, hydroxypropyl (Hpo) / methoxyl (Meo) substitution ratio and molecular size) on tribo-electric charging and SA of cellulose ethers was studied.

3.8.2- Experimental

3.8.2.1- Materials

MC and HPMC were obtained as detailed in section 2.1.1.

3.8.2.2- Methods

3.8.2.2.1- Surface morphology of drug particles

The surface morphology of the powder particles of MC and HPMC was examined by following the method as described in section 2.2.4.1.

3.8.2.2.2 - Tribo-electrification

Tribo-electric charging of drug powder particles were studied by adopting a method based on shaking concept as described in section 2.2.5.2.

3.8.2.2.3- Powder surface adhesion (SA)

The SA of the powder particles of model drugs was examined by following the method as described in section 2.2.5.3.

3.8.2.2.4- Statistical analysis

One way analysis of variance (ANOVA) (confidence limit of $P < 0.05$) was used to investigate the statistical significance of different underlying factors on tribo-electrification and adhesion properties of MC/HPMC.

3.8.4- Results and discussion

3.8.4.1- Surface morphology of MC and HPMC powder particles

The surface morphology is considered an important attribute which can impact the tribo-electrification and SA properties of powder particles. Figure 3.8 is a group of six SEM micrographs where the images of (a) A4M (b) F4M (c) E4M (d) K4M (e) K15M and K100 M are merged. All the grades of HPMC and MC contained mixtures of irregular-shaped flat and fibrous particles. Generally, the proportion of fibrous material is higher in MC (a) than HPMC (b-f). It was also noticed that the K-chemistry grades of HPMC and, in particular, K100M have more irregularly shaped particles with rough surfaces than any of the other grades of cellulose ethers. This is attributed to the higher Hpo/Meo substitution ratio and molecular size, which result in more complex surfaces (Gustafsson *et al.*, 1999; Okimoto *et al.*, 1997).

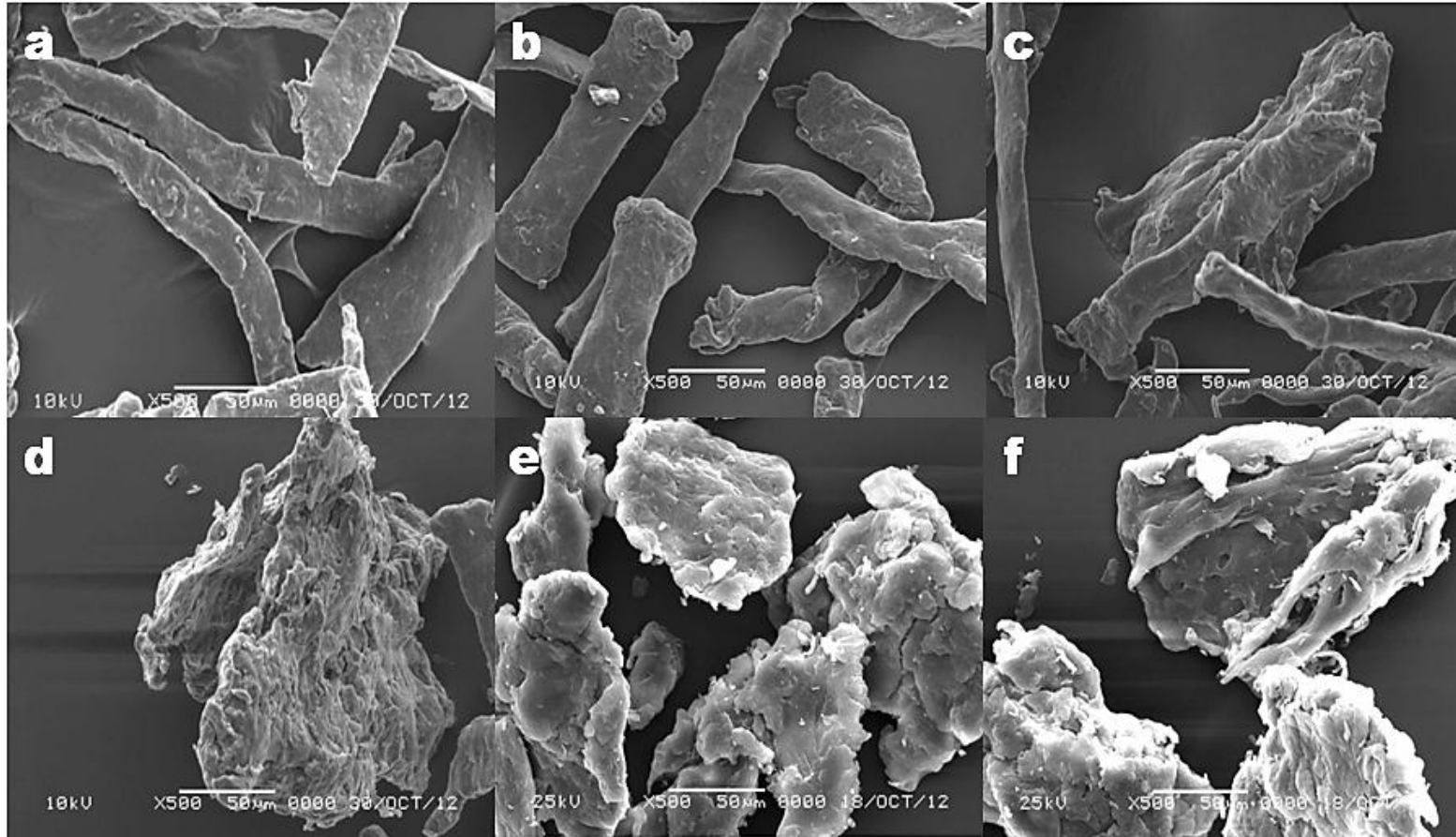


Figure 3.8, SEM micrographs of MC and HPMC, (a) A4M (b) F4M (c) E4M (d) K4M (e) K15M (f) K100M.

3.8.4.2 - Tribo-electrification and adhesion properties of MC and HPMC

In the present study, maximum charge acquisition data (Q_{max}) are presented as a charge to mass ratio (Q/M) at the end of each tribo-electrification experiment ($n=3$), as exemplified in Figure 3.6. Moreover, the SA of powders related to Q_{max} was reported, ($n=3$). All grades of cellulose ethers charged positively against the stainless steel container and gained Q_{max} after 0.5 minutes of shaking. The charge and SA of MC and HPMC powder particles ranged between 4 - 57 nC/g and 6 - 33 %. The order of charging and particle SA was A4M > F4M > E4M > K4M > K15M > K100M, with the amount of charge transferred assumed to be due to differences in the effective work function between the contacting surfaces. The MC and HPMC have a lower effective work function (W_h) than the steel surface (W_s), therefore it is assumed that electrons from the surface of polymer particle move to the interface of the contacting surface inducing a positive surface charge on the surface of polymer particle (donor), with a negative charge (acceptor) on the steel surface. An equilibrium state is reached when both the potential difference and charged layers become equal in magnitude. As the particle moves away from a contact point, the initial high magnitude of capacitance is reduced (Matsusaka *et al.*, 2010). A schematic illustration of MC and HPMC charge generation phenomena is described in Figure 3.9. Furthermore, the potential difference between the materials initiates cohesive and adhesive interactions, with the latter apparently having a dominant role in particle adherence to the contacting surface (Cross, 1987).

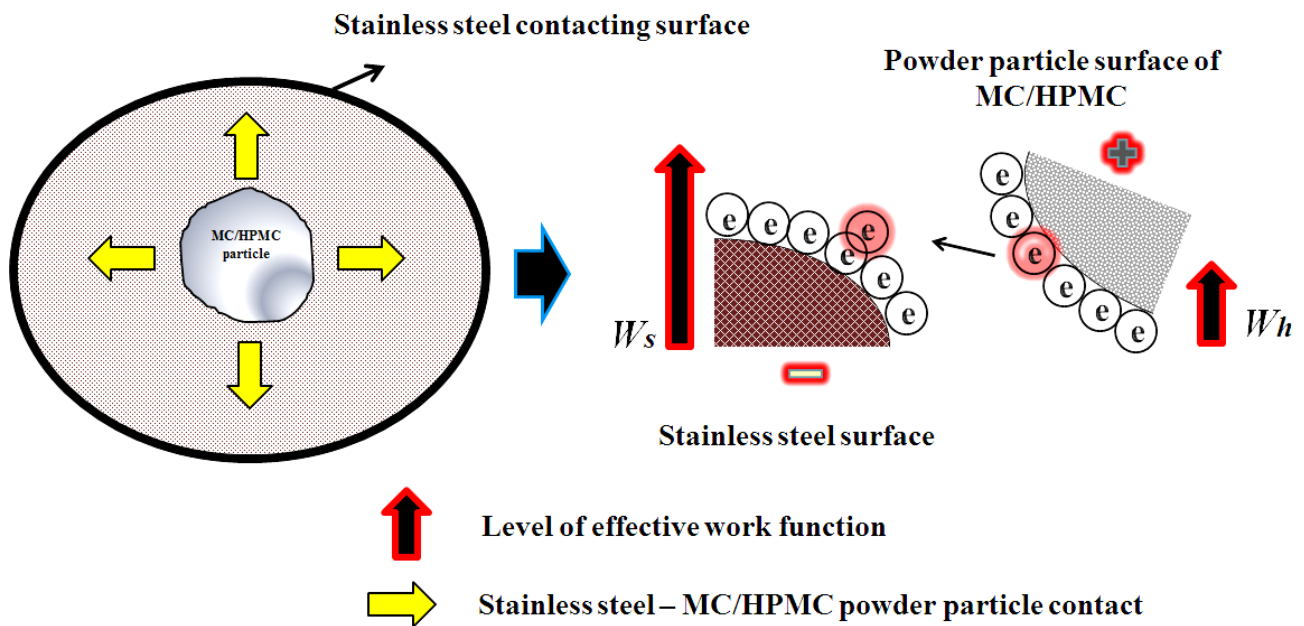


Figure 3.9, Schematic illustration of tribo-electrification charging of MC and HPMC powder particles.

3.8.4.2.1- Effect of particle size

The propensity and magnitude of inter-particulate forces within pharmaceutical powders often seem to be directly related to the powder particle size (Rowley, 2001). In this study, the charge and adhesion of A4M were increased by 3.1 nC/g and 3.3 % respectively when particle size was reduced from 150 – 250 to 90 - 150 μm . This trend is exhibited by all HPMC grades except the very low charging K100M (Table 2). The tribo-electric charge and adhesion of polymer are inversely related to particle size ($P < 0.05$, Table 3.4); presumably, fine particle fractions have a large specific surface area thereby increasing the number of particle and surface contacts (Cross, 1987; Rowley, 2001). Moreover, particle size can also influence the effective work function of the materials, as larger particles might lose their electrons easily,

decreasing the effective work function, which was assumed to be linked with their charge density (Gallo and Lama, 1976).

3.8.4.2.2- Effect of substitution ratios

When two dissimilar materials such as metals and polymers contact, the magnitude and polarity of tribo-electric charging is determined by functional groups, structural and surface chemistries (Kamiyama *et al.*, 1994; Mazumder *et al.*, 2006b; Sharma, 2004; Shinohara *et al.*, 1976; Trigwell *et al.*, 2003). It can be hypothesised that the substitution ratio on the anhydrous glucose ring of cellulose ethers and their molecular size will alter the charging and adhesion behaviour due to variations in electrical resistivity and effective work function and this was borne out in this study ($P < 0.05$). These materials are manufactured commercially from the parent cellulose which is highly crystalline and insoluble in water. However, various substitution groups (methyl chloride and/or propylene oxide) can be integrated along the anhydrous glucose backbone which helps to reduce crystallinity and impart solubility (Sarkar and Walker, 1995). Additionally, the integration of methoxy (- OCH₃) or hydroxypropyl groups (- CH₂CH(OH)CH₃) on AGUs induce steric hindrance which opens up the cellulose backbone. Previous studies have reported that degree of crystallinity and modifications to surface composition can alter the effective work function of pharmaceutical powders (Kamiyama *et al.*, 1994; Murtomaa *et al.*, 2002b; Mazumder *et al.*, 2006b; Wong *et al.*, 2014a). As the ratio of the hydrophilic substitution group, hydroxypropyl, increased (with respect to methoxy groups), the charge and SA decreased (Table 3.4). Therefore, methylcellulose, A4M (i.e. 0 % hydroxypropyl substitution) has the highest tribo-electric charge and surface adhesion. K4M, which has a higher Hpo/Meo substitution ratio (0.382), but similar molecular weight as Methocel[®] F4M and E4M, shows lower propensity of charge and SA (Table 3.4). So, the tribo-electric charging and SA behaviour of HPMC and MC can be assumed to be related to work function variations induced during the substitution process.

3.8.4.2.3- Effect of molecular size (viscosity)

Cellulose ethers are polydisperse molecules with longer chain length impacting viscosity grades (Sarkar and Walker, 1995). Polymeric chains in K100M are longer than those in K15M and K4M and show the lowest tribo-electric charge and surface adhesion. The magnitude of charge and SA decreased with increasing polymer chain length within the HMPC series (i.e. K4M >K15M >K100M (Table 3.4). The arrangement and length of the polymeric chains affect the surface roughness, physical, rheological and mechanical properties of the particles (Keary, 2001). Therefore, it can be anticipated that the molecular size and arrangement of polymeric chains within HPMC particles modifies the polymeric architecture and localises change in the atomic structure, resulting in alteration of electrical resistivity and effective work function. These characteristics dictate the charge transfer process and generation of operational forces (van der Waal forces, ionic bonding and electrostatic forces) thus impacting phenomena (Harper 1967).

Table 3.4, Charge-to-mass ratio and percentage particle adhesion of MC/HPMC (standard deviation is shown in parentheses, n=3)

| Methocel® | Particle size (μm) | Charge to mass ratio (<i>Q/M</i>) | Adhesion (%) |
|------------------|--------------------------------|--|-------------------------|
| A4M | 90 – 150 | 57.44 (2.81) | 32.98 (2.12) |
| | 150 – 250 | 54.33 (2.21) | 29.69 (1.89) |
| F4M | 90 – 150 | 44.02 (1.32) | 25.08 (2.23) |
| | 150 – 250 | 39.67 (3.14) | 20.64 (0.99) |
| E4M | 90 – 150 | 26.90 (2.64) | 20.11 (1.55) |
| | 150 – 250 | 19.86 (1.15) | 17.87 (1.23) |
| K4M | 90 – 150 | 12.33 (2.23) | 11.37 (1.11) |
| | 150 – 250 | 9.78 (3.69) | 11.82 (2.55) |
| K15M | 90 – 150 | 10.36 (2.15) | 12.09 (1.12) |
| | 150 – 250 | 7.06 (1.68) | 10.51(0.88) |
| K100M | 90 – 150 | 4.23 (0.85) | 5.59 (1.15) |
| | 150 – 250 | 3.94 (0.66) | 7.93 (0.91) |

3.9- Section C, Tribo-electrification and adhesion studies of MC and HPMC based binary mixtures with model drugs

3.9.1- Introduction

The pharmaceutical industry relies heavily on powder processing since more than 80 % of its products are provided in tablet form (Jivraj *et al.*, 2000). In order to manufacture a tablet, the excipients and API need to be mixed together thoroughly to form a homogenous powder mixture. Pharmaceutical products have special quality control requirements with regard to uniformity of active contents, consistency in appearance, longevity for storage, transportation and shelf life, demanding an exceptional degree of control and precision (Swarbrick, 2007). However, during powder processing, powder particles frequently come into contact with each other and with the walls of the processing equipment lead to the generation of tribo-electric charging on the surface of powder particles (Harper, 1967). Such phenomena become more prominent when excipients are introduced to a powder mixture alongside the APIs with inter- and intra-particulate interactions giving rise to electrification and SA of powder particles. The study and characterisation of electrostatic and SA properties of powders are vitally important in pharmaceutical dosage form development. Electrostatic charging and SA of powders is influenced by particle size, shape, surface morphology, surface energy, chemical composition, moisture content, processing vessel geometry, and other experimental factors, as explained in the detail in the previous section 3.6. In response to this complexity, numerous methods for measuring electrostatic charge and SA have been developed, largely based on empirical understanding.

The electrostatic particle charging is a common nuisance as it can cause segregation, dust explosions, adhesion and deposition or blockage of pipelines, leading to loss of powder and difficulties controlling the powder flow, as this have been discussed in detail in the

aforementioned section 3.4. The ability to control the charging of pharmaceutical powders is essential in improving the quality of the end product and minimising deposition and powder loss. So powder processing techniques need an in depth evaluation and further improvement to meet these challenges. Despite the negative influences described above, electrostatic charging phenomena can be beneficial under certain conditions, for example, exploiting the opposite polarity of charged powder particles to fabricate ordered mixtures. Electrostatic assisted ordered mixtures are considered stable and further have a potential to improve content homogeneity, stability and powder processing problems (Wong *et al.*, 2014b)

Various excipients are added to tablet formulations, acting as binders, lubricants and disintegrants in order to improve the processability and bioavailability of the tablet product. MC and HPMC are considered to be the main excipients of choice in the development of extended release hydrophilic matrix tablets. Recently, tribo-electric charging behaviour of Methocel[®] E4M, K4M based powder mixtures with the negatively charging API, THP have been studied. It was shown that when THP came into contact with HPMC, it attached to its surface due to opposite polarities and the tribo-electric charge of the final powder mixture was decreased (Asare-Addo *et al.*, 2013b). However, the impact of diverse physico-chemical attributes related to MC and HPMC on API in a binary system still needs further investigation. Therefore, the aim of this study was to investigate the tribo-electrification and adhesion properties of different MC and HPMC based powder mixtures, using THP and FBP as model drugs. The impact of polymer attributes (concentration, particle size, hydroxypropyl (Hpo) / methoxyl (Meo) substitution ratio and molecular size) on tribo-electric charging and SA of powder mixtures were studied. Furthermore, a relationship between tribo-electric charging and SA was also studied.

3.9.2- Experimental

3.9.2.1- Materials

MC, HPMC and model drugs were obtained as detailed in section 2.1.1 and 2.1.2, respectively.

3.9.2.2- Methods

3.9.2.2.1- Efficiency of powder mixing

3.9.2.2.2- Surface morphology of powder mixtures

SEM was used to analyse the surface attachment of drug particles on the surface of MC or HPMC powder particles as described in section 2.2.4.1.

3.9.2.2.3- Drug content uniformity of powder mixtures

The contents of FBP and THP were quantified using the method described in section 2.2.4.2

3.9.2.2.4- Differential scanning calorimetry (DSC) of powders

Differential scanning calorimetry (DSC) study of MC/HPMC, model drugs (FBP/THP) and their respective powder mixtures were carried out using the method described in section 2.2.4.3.

3.9.2.2.5- Powder X-ray diffraction (PXRD)

PXRD of MC/HPMC, model drugs (FBP/THP) and their respective powder mixtures were carried out using the method described in section 2.2.4.4.

3.9.2.2.6 - Tribo-electrification

Tribo-electric charging of drug powder particles was studied using the method based on the shaking concept as described in section 2.2.5.2.

3.9.2.2.7- Surface adhesion (SA) of powders

The SA of model drugs was examined by following the method as described in section 2.2.5.3.

3.9.2.2.8- Statistical analysis

One way analysis of variance (ANOVA) (confidence limit of $P < 0.05$) was used to investigate the statistical significance of different underlying factors on tribo-electrification and adhesion properties of MC/HPMC on the tribo-electric charging and SA properties of model drugs.

3.9.3- Results and discussion

3.9.3.1- Formation of ordered mixtures

Among different mixing methods, ordered mixing results in more homogeneous and stable particulate powder mixtures. Ordered mixing can be achieved using powder particles having electrostatic charges of opposite polarity (Mäki *et al.*, 2007; Swaminathan and Kildsig, 2000; Venables and Wells, 2001). Drugs are usually negatively charged while the excipients or polymers are positively charged. This can be used to maintain the homogeneity of a mix through different processing conditions (Saharan *et al.*, 2008). In the present study, an ordered binary mix was formed by mixing a polymer (positively charged) and FBP/THP (negatively charged) powders. The powder particles of polymers and drugs gained positive and negative tribo-electric charge, respectively, due to the difference in the effective work

functions between the powder particles and contacting surfaces. In the present study, when FBP and THP charged negatively and polymers charged positively, it was observed that the negatively charged FBP and THP powder particles were attracted towards the positively charged polymeric powder particles and adhered to their surfaces. A schematic illustration of powder charging and further the attachment of fine drug particles to the polymer surface are shown in Figure 3.10.

Pharmaceutical products have strict quality control requirements with regard to drug content uniformity. So, all binary mixtures were analysed and contained between 95 - 105% of the expected drug (FBP/THP) content. The results of content uniformity are detailed in Table 3.5.

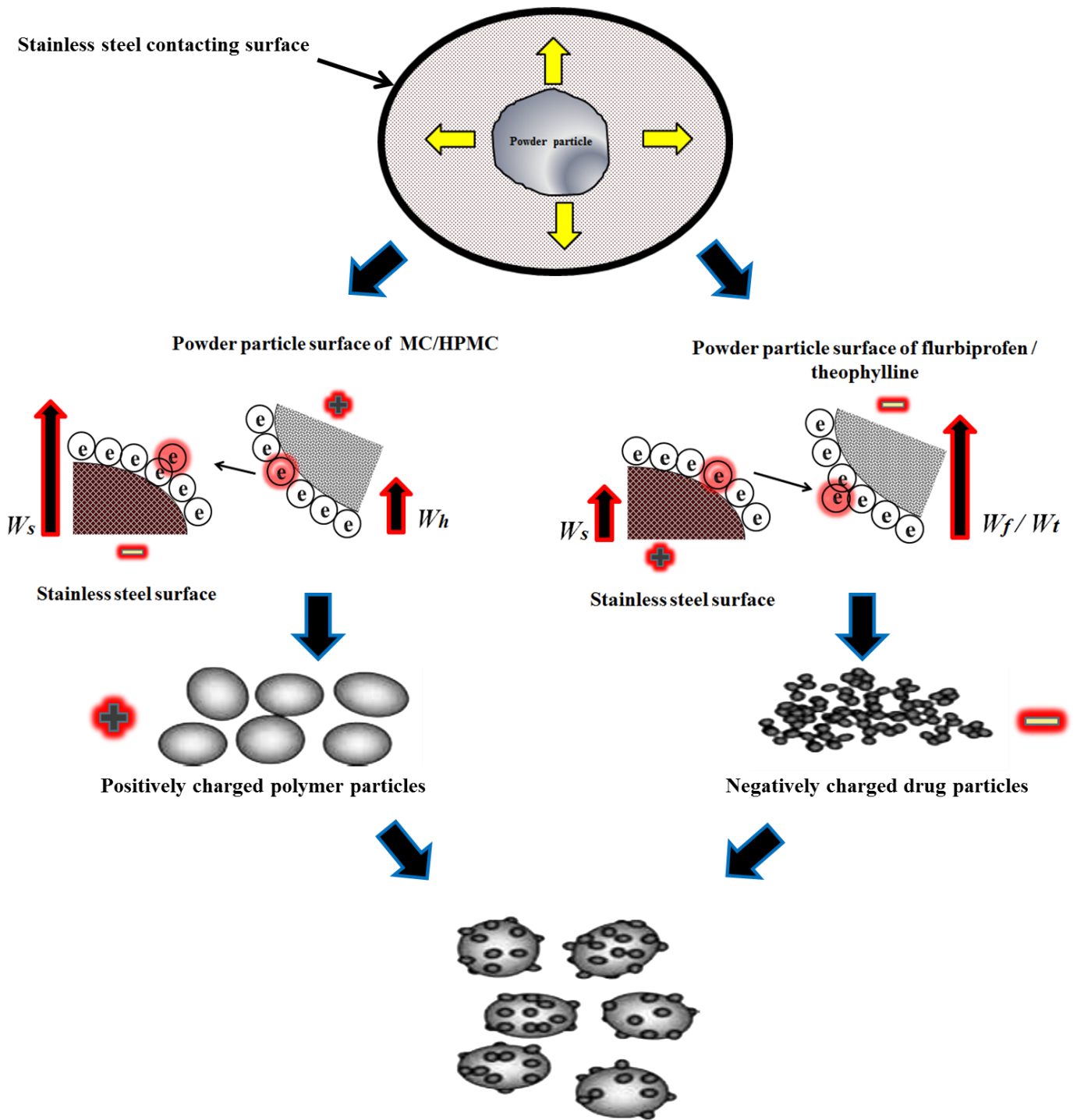


Figure 3.10, Schematic illustration of tribo-electric charge generation of powder mixtures.

Table 3.5, Content uniformity of powder mixture containing (a) FBP and (b) THP (n=3).

(a)

| Methocel® | Particle Size (μm) | FBP content (%) | | | | | |
|-----------|------------------------------------|---------------------------|-------------|-------------|-------------|-------------|-------------|
| | | Polymer concentration (%) | | | | | |
| | | 0.5 | 1 | 2.5 | 5 | 10 | 15 |
| A4M | 90 – 150 | 98.3 (1.1) | 96.2 (0.5) | 98.6 (1.2) | 98.2 (1.8) | 99.6 (2.5) | 98.6 (2.3) |
| | 150 – 250 | 97.2 (0.5) | 99.2 (1.7) | 99.5 (1.5) | 96.3 (1.2) | 98.5 (2.1) | 99.2 (1.8) |
| F4M | 90 – 150 | 99.3 (1.7) | 98.1 (2.0) | 97.4 (1.3) | 98.5 (2.1) | 96.5 (1.0) | 101.3 (2.1) |
| | 150 – 250 | 103.2 (1.9) | 97.5 (1.1) | 104.3 (1.8) | 99.4 (1.3) | 98.3 (2.3) | 103.6 (1.5) |
| E4M | 90 – 150 | 98.3 (0.8) | 96.7 (1.2) | 100.5 (1.7) | 97.6 (1.4) | 100.5 (2.1) | 99.6 (2.5) |
| | 150 – 250 | 97.2 (1.2) | 99.2 (1.7) | 99.1 (2.1) | 97.4 (2.1) | 101.2 (1.5) | 98.2 (1.1) |
| K4M | 90 – 150 | 96.1 (0.3) | 100.5 (0.8) | 98.6 (1.0) | 99.32 (1.8) | 98.3 (2.5) | 96.3 (1.0) |
| | 150 – 250 | 100.2 (2.5) | 97.1 (0.8) | 97.8 (2.1) | 99.87 (1.3) | 102.5 (1.3) | 98.3 (2.0) |
| K15M | 90 – 150 | 98.3 (0.9) | 97.5 (1.1) | 99.2 (2.7) | 100.5 (1.7) | 99.3 (2.8) | 99.3 (1.8) |
| | 150 – 250 | 98.6 (1.7) | 99.6 (1.8) | 97.6 (1.3) | 98.63 (2.0) | 100.5 (1.9) | 98.3 (2.1) |
| K100M | 90 – 150 | 99.2 (2.8) | 97.8 (1.0) | 98.2 (0.8) | 99.57 (2.8) | 97.3 (1.8) | 100.5 (1.3) |
| | 150 – 250 | 99.1 (1.1) | 98.4 (2.1) | 99.5 (3.1) | 97.82 (1.0) | 98.3 (2.5) | 101.9 (2.8) |

(b)

| Methocel® | Particle Size (μm) | THP content (%) | | | | | |
|-----------|------------------------------------|---------------------------|-------------|------------|-------------|-------------|-------------|
| | | Polymer concentration (%) | | | | | |
| | | 0.5 | 1 | 2.5 | 5 | 10 | 15 |
| A4M | 90 – 150 | 99.3 (1.8) | 98.2 (2.1) | 99.3 (3.2) | 101.2(2.8) | 99.6 (3.1) | 100.5 (2.4) |
| | 150 – 250 | 99.2 (2.1) | 98.2 (1.8) | 98.5 (3.0) | 97.3 (0.5) | 99.3 (2.1) | 98.6 (1.6) |
| F4M | 90 – 150 | 98.5 (1.5) | 99.7 (1.9) | 97.7 (1.8) | 99.3 (1.9) | 98.3 (1.0) | 99.2 (2.1) |
| | 150 – 250 | 99.5 (2.1) | 99.8 (1.8) | 99.1 (1.0) | 100.5 (0.9) | 97.2 (2.2) | 96.3 (1.1) |
| E4M | 90 – 150 | 100.1 (1.7) | 103.6 (2.2) | 96.8 (1.2) | 98.3 (1.2) | 99.8 (2.5) | 99.3 (1.5) |
| | 150 – 250 | 98.1 (2.5) | 99.2 (1.7) | 96.9 (1.1) | 99.6 (1.5) | 100.8 (0.9) | 97.1 (1.3) |
| K4M | 90 – 150 | 99.5 (2.3) | 100.5 (0.8) | 99.5 (1.7) | 97.8 (2.0) | 101.0 (1.5) | 102.8 (2.5) |
| | 150 – 250 | 99.8 (2.5) | 99.6 (1.8) | 97.9 (2.8) | 101.5 (2.8) | 100.5 (2.3) | 101.2 (1.8) |
| K15M | 90 – 150 | 101.8 (2.9) | 97.5 (1.8) | 99.8 (2.4) | 100.5 (1.9) | 97.3 (0.2) | 98.3 (1.7) |
| | 150 – 250 | 99.3 (0.1) | 96.3(1.0) | 97.7 (1.7) | 99.3 (1.3) | 99.8 (1.8) | 97.6 (0.7) |
| K100M | 90 – 150 | 97.3 (1.8) | 102.5 (2.0) | 98.8 (2.8) | 97.5 (2.4) | 97.5 (2.2) | 99.7 (1.5) |
| | 150 – 250 | 99.6 (1.7) | 99.5 (3.1) | 97.5 (1.1) | 98.6 (1.5) | 100.1 (1.3) | 100.8 (2.3) |

To validate the attachment of negatively charged drug particles on the positively charged polymer particle and further confirm the formation of electrostatic ordered powder mixtures, SEM was used. The general findings of this work are exemplified in Figures 3.11 and 3.12.

Figure 3.11 illustrates six SEM micrographs of FBP powder mixtures with different grades of MC and HPMC and the negatively charged FBP powder particles are attached to the positively charged polymer surface, regardless of grade. Furthermore, it is clearly evident from the micrographs that the FBP has retained its crystalline habit.

Figure 3.12 also illustrates six SEM micrographs of THP powder mixtures with different grades of MC and HPMC. Like FBP, mixtures of THP powder particles also attached to the positively charged MC or HPMC powder particles. The crystalline nature of the drug is also evident with irregular-shaped HPMC or MC powder particles.

Overall, it can be concluded from the SEM work that the negatively charged (FBP and THP) powder particles are attached to the positively charged MC or HPMC powder particles and this lead to the successful formation of homogeneous, electrostatic-assisted, ordered mixtures.

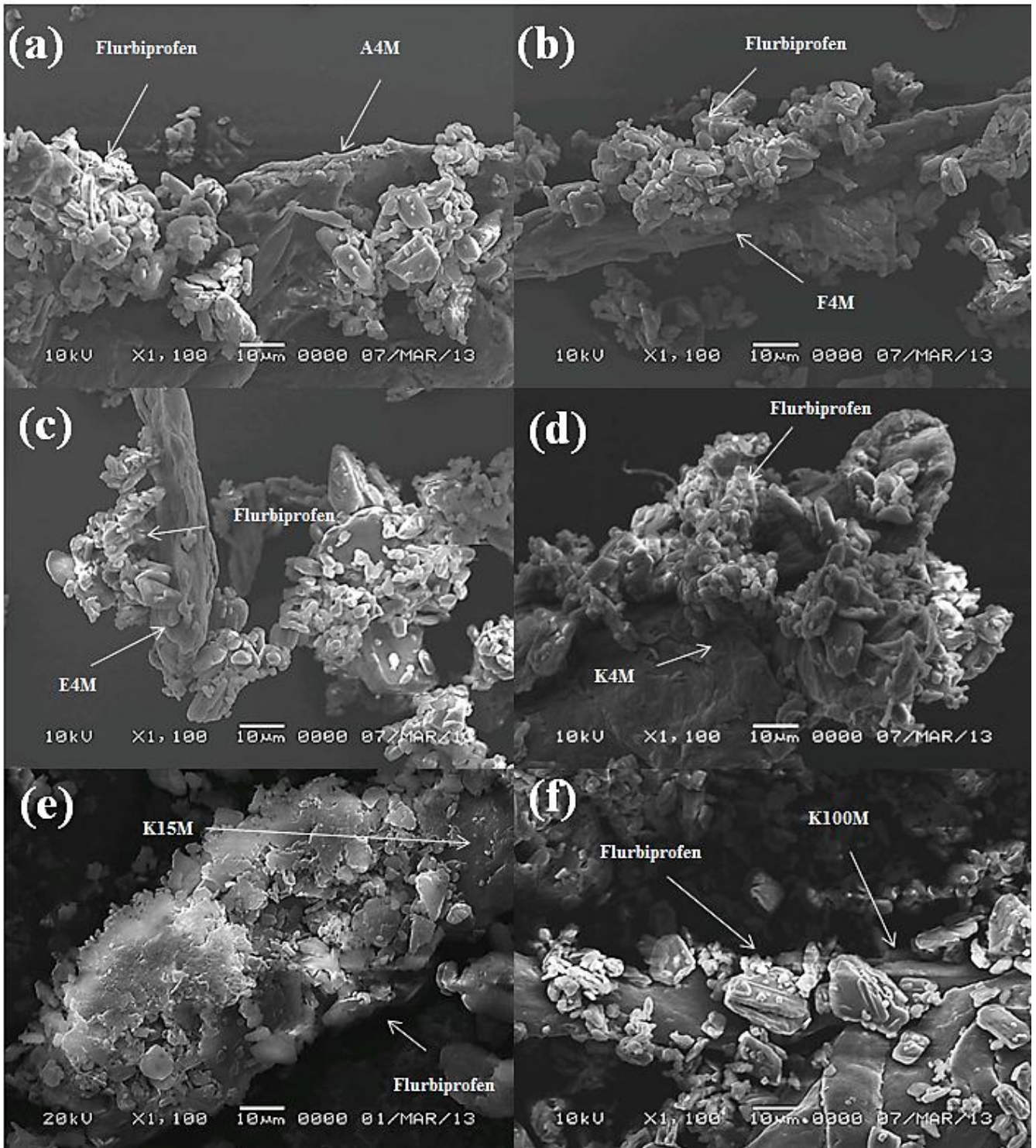


Figure 3.11, SEM micrographs of FBP powder mixtures, (a) A4M/FBP (b)F4M/FBP (c) E4M/FBP (d) K4M/FBP (e) K15M/FBP and (d) K100M/FBP.

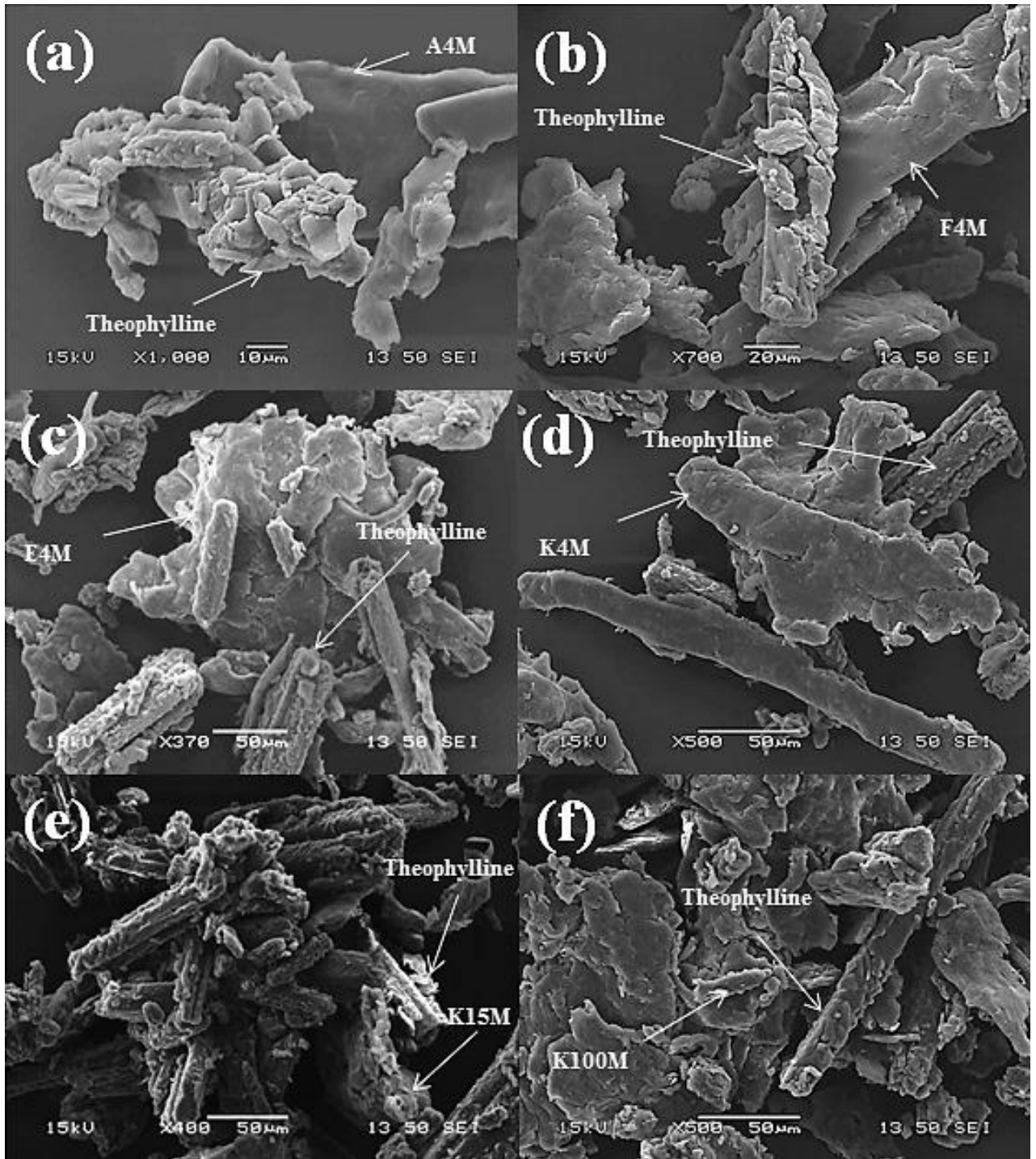


Figure 3.12, SEM micrographs of THP powder mixtures, (a) A4M/THP (b) F4M/THP (c) E4M/THP (d) K4M/THP (e) K15M/THP and (f) K100M/THP.

DSC was employed to investigate any possible solid-solid interaction between the FBP and THP with MC/HPMC powders. Figure 3.12 (a) depicts the DSC thermograms of MC and HPMC showing no melting peak, suggesting they are amorphous. Figure 3.12 (b) demonstrated sharp endothermic melting peaks at 115.45 °C and 272.02 °C for FBP and THP, respectively.

Moreover, Figure 3.13 (a and b) showed DSC thermograms of MC/HPMC : FBP/THP powder mixtures containing 15 % w/w of polymer content to exemplify and indicate any possible drug-polymer interaction. There was a negligible depression in the melting peaks and it can be concluded that the drugs retained their crystalline structure and no drug-polymer interaction was discerned.

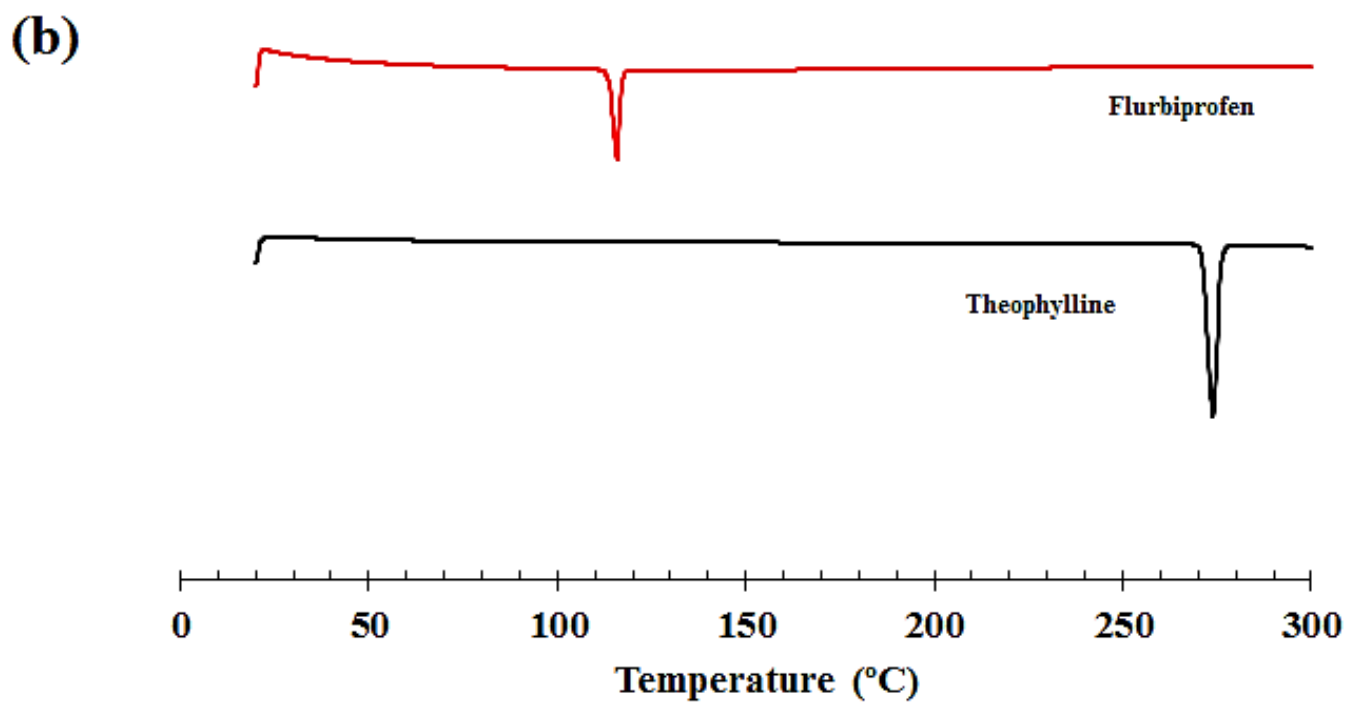
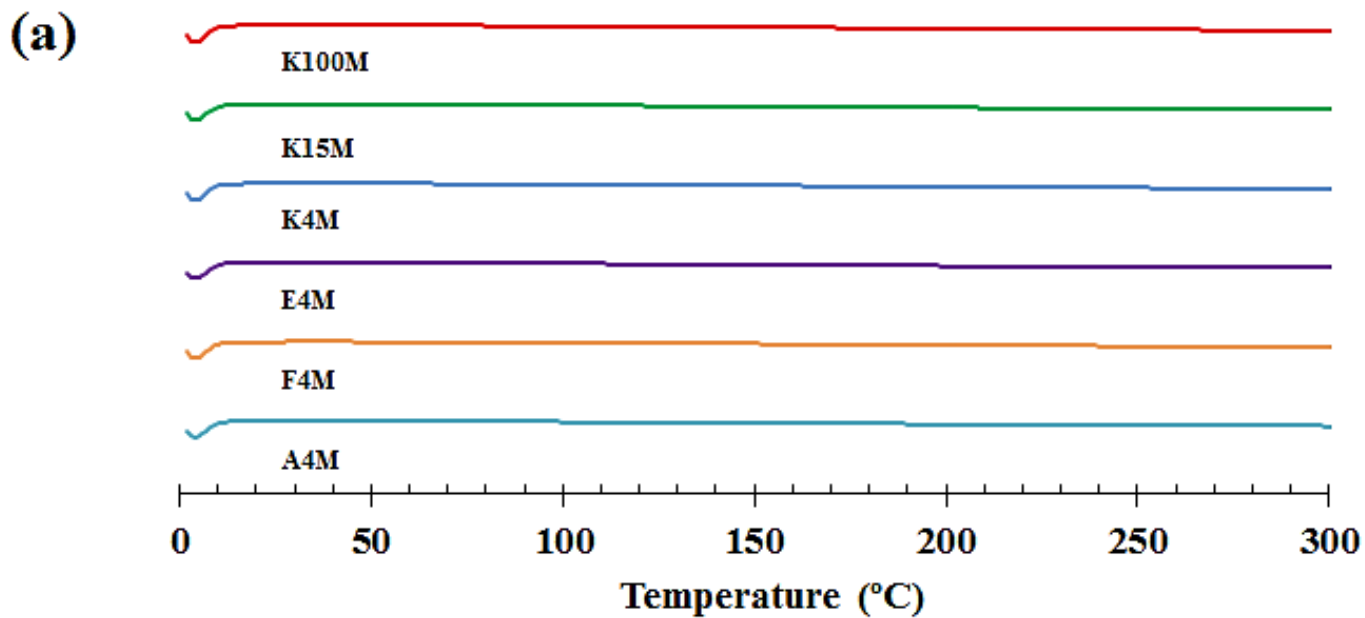


Figure 3.13, DSC profiles of (a) MC/HPMC and (b) FBP/THP.

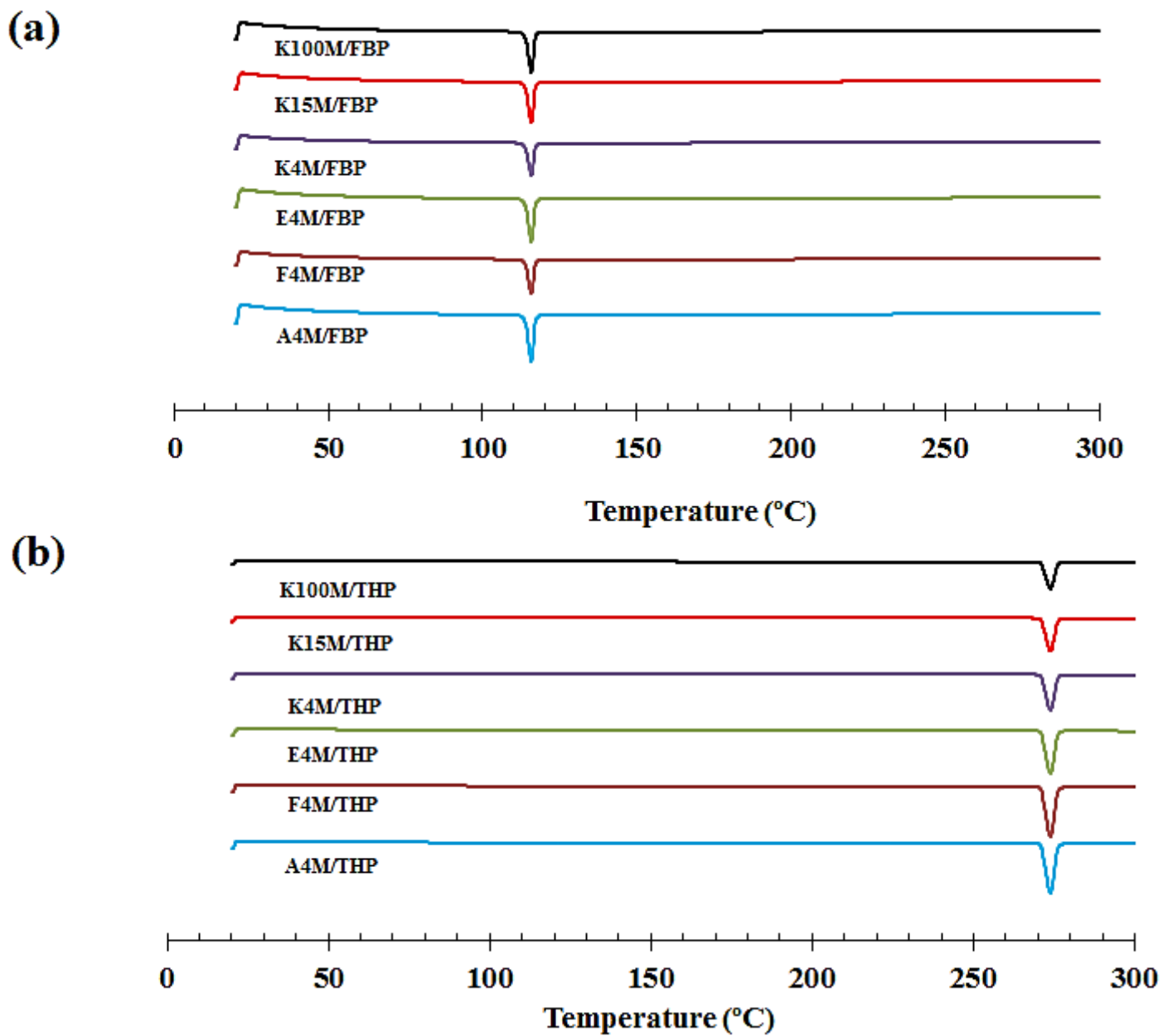


Figure 3.14, DSC profiles of (a) FBP and (b) THP powder mixtures.

Figure 3.14 (a) demonstrates the PXRD patterns of MC and HPMC powders. The absence of any sharp diffraction peaks confirms their amorphous nature. Figure 3.14 (b) shows characteristic diffraction peaks at 15.76° and 20.49° for FBP, however, THP showed characteristic diffraction peaks at 12.30° and 25.22° . The sharp and intense diffraction peaks of model drugs represent their crystalline structure.

Figure 3.15 (a and b) shows PXRD patterns of MC/HPMC : FBP/THP powder mixtures containing 15 % w/w of polymer contents to exemplify and indicate any possible drug-polymer interaction. It is evident from the Figure 3.15 (a and b) that the model drugs retained their diffraction peaks, which confirms that after powder mixing, the drugs retained their crystalline structure. Furthermore, it can be concluded that no drug-polymer interaction was evident.

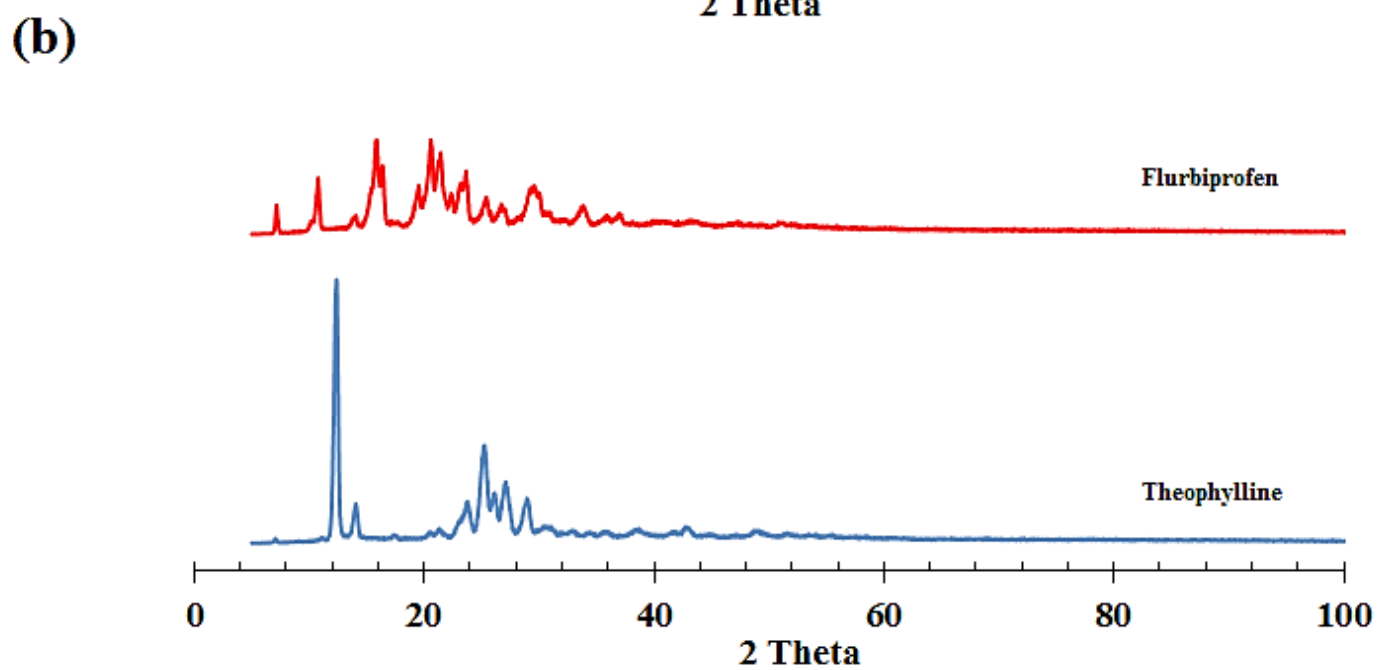
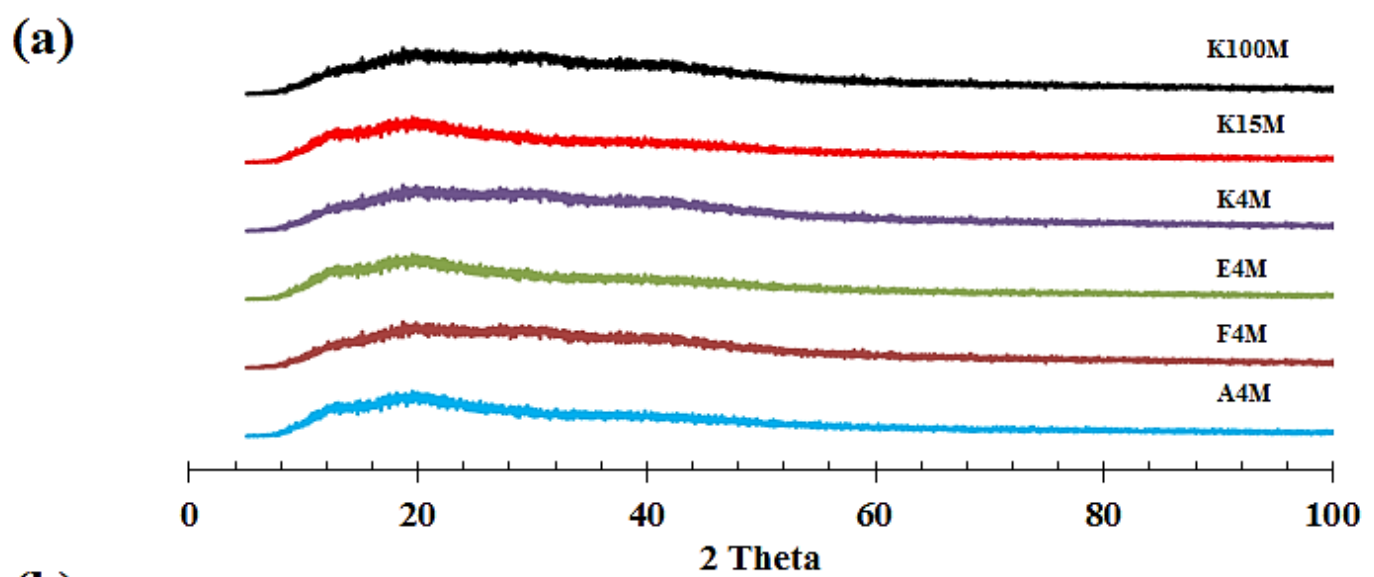


Figure 3.15, PXR D patterns of (a) MC/HPMC and (b) FBP/THP.

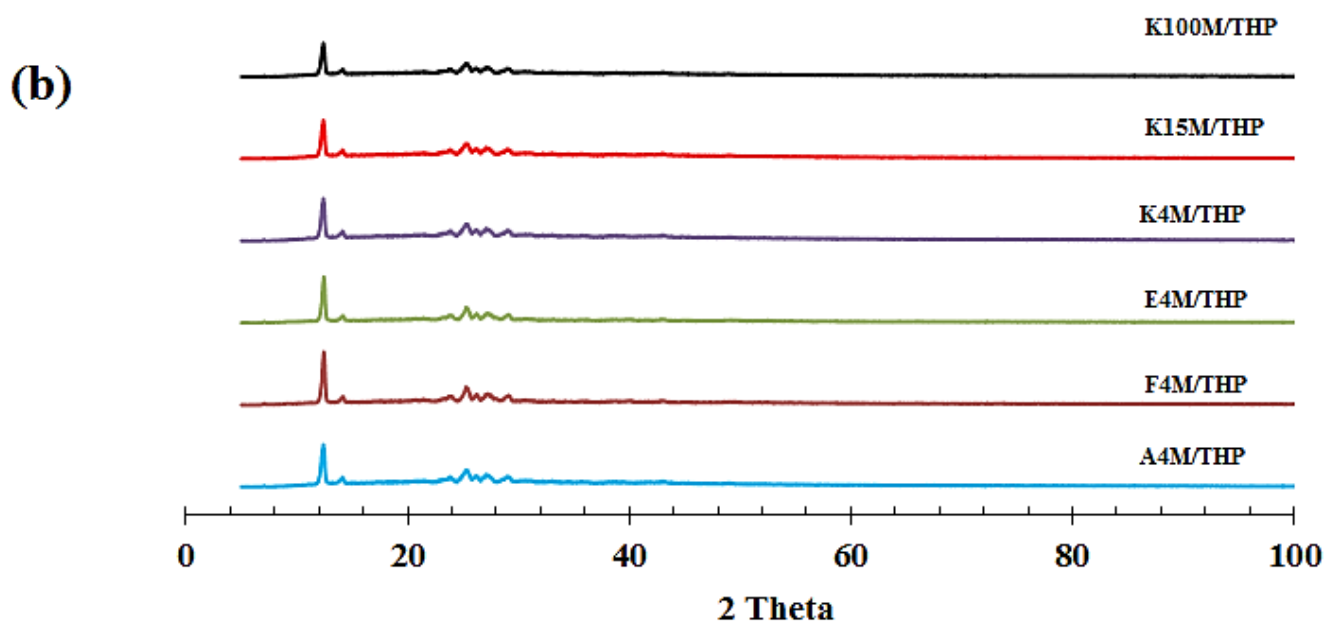
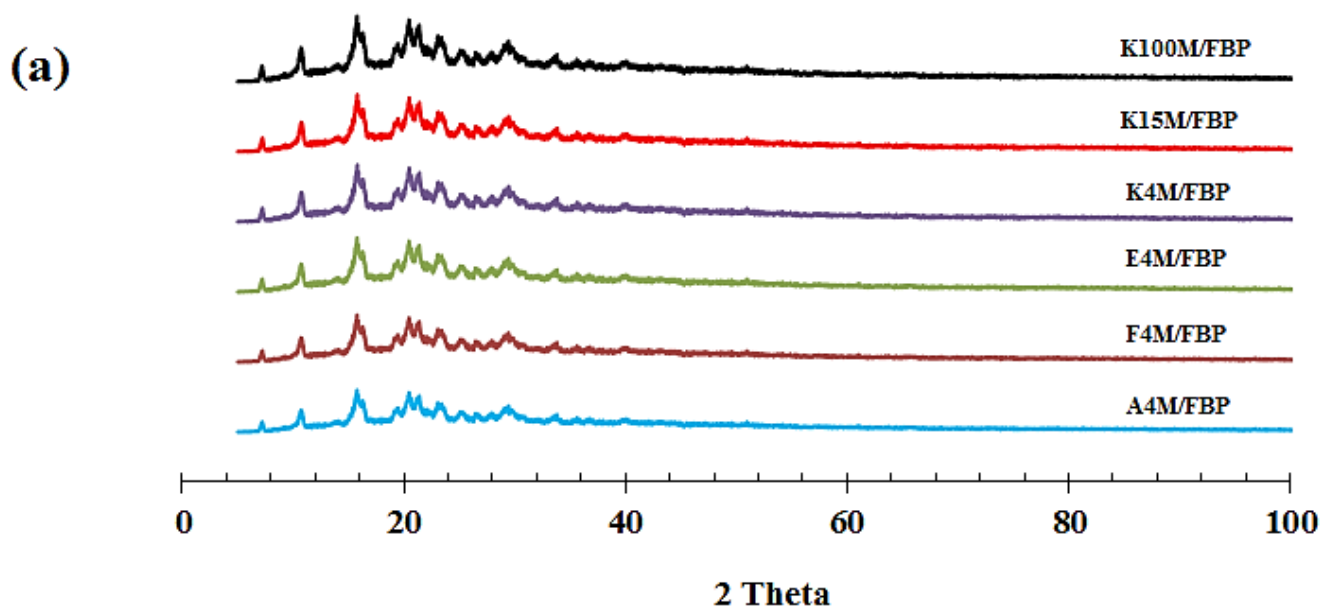


Figure 3.16, PXRD patterns of (a) THP and (b) FBP powder mixtures.

3.9.3.2- Tribo-electrification and adhesion properties of binary mixtures

In the present study, maximum charge acquisition data (Q_{max}) are presented as charge to mass ratio (Q/M) at the end of each tribo-electrification experiment ($n=3$), as exemplified in Figure 3.6. Moreover, the SA of powders related to Q_{max} was reported, ($n=3$).

3.9.3.2.1- Effect of polymer concentration

The acquisition of tribo-electric charge and SA of powder formulations can be affected by the component ratios in a binary powder mixture as explained in section 3.5.2 (Engers *et al.*, 2007; Murtomaa and Laine, 2000). Tribo-electric charging and adhesion experiments were carried out on MC/HPMC : FBP and MC/HPMC : THP powder mixtures with fixed polymer to drug loading ratios of 0.5, 1, 2.5, 5, 10 and 15 w/w %. The charging and adhesion results show that the addition of increasing proportions of MC/HPMC has a significant impact ($P < 0.05$) on these properties; as the level of MC/HPMC increased from 0.5 to 15 %, the charge and PSA was decreased (Tables 3.6 and 3.7).

In case of MC/HPMC : FBP or MC/HPMC : THP powder mixtures, at 0.5 % polymer content, there is a slight decrease in the charge and SA of FBP with the addition of A4M, F4M and E4M. With further increases in polymer concentration, the charge dissipation increases significantly due to the influence of polymer-to-drug ratio on the overall effective work function and surface resistivity of a bulk powder sample (Figures 3.17-3.18 and Tables 3.6-3.7). The charge reduction reached a plateau level at 5 and 10 % and so further increases in polymer concentration only had a small impact on charge, however, the SA was further reduced, especially in the case of MC/HPMC : THP powder mixtures (Table 3.6-3.7). The powder mixtures of FBP or THP formed using polymers K4M, K15M and K100M were the lowest charging blends as compared to A4M, F4M and E4M. The addition of 0.5% w/w of polymer halved the overall net charge on FBP. Moreover, at 15% polymer, the charge was

neutralised completely and particle adhesion was also very low. In the case of THP powder mixtures, at 0.5 %, significant dissipation of the tribo-electric charge was noticed and this phenomenon was previously discussed by Asare-Addo *et al.*, (2013b), however in that study 20 % w/w of E4M and K4M with THP was used. The charge reduction is likely due to ordering of particles as particles of opposite charges adhered to each other as electrovalent bonds developed between drug and excipient powder particles due to an exchange of electrons.

Additionally, in the present study a shift in polarity of charge from negative to positive was also noticed for FBP powders containing 15% w/w K15M and K100M (Figure 3.17). Likewise THP powder mixtures also showed a similar trend at 15 % w/w concentrations of K15M and K100M, Additionally, K100M also showed a shift in polarity at 10 % w/w concentration (Figure 3.18). This phenomenon was previously encountered for glucose/lactose mixtures by Murtooma and Laine, (2000). In the present scenario, it can be assumed that the K15M and K100M have a lower work function and surface resistivity than FBP/THP and the contacting surface (stainless steel). Thus, when the percentage of polymer is increased, the net surface resistivity and effective work function of powders is altered, leading to a reduction and shift in polarity of electrostatic charge. As expected, such a significant charge reduction changes the classification from a high charging to a lower charging category, and the impact of charge during powder handling will be reduced.

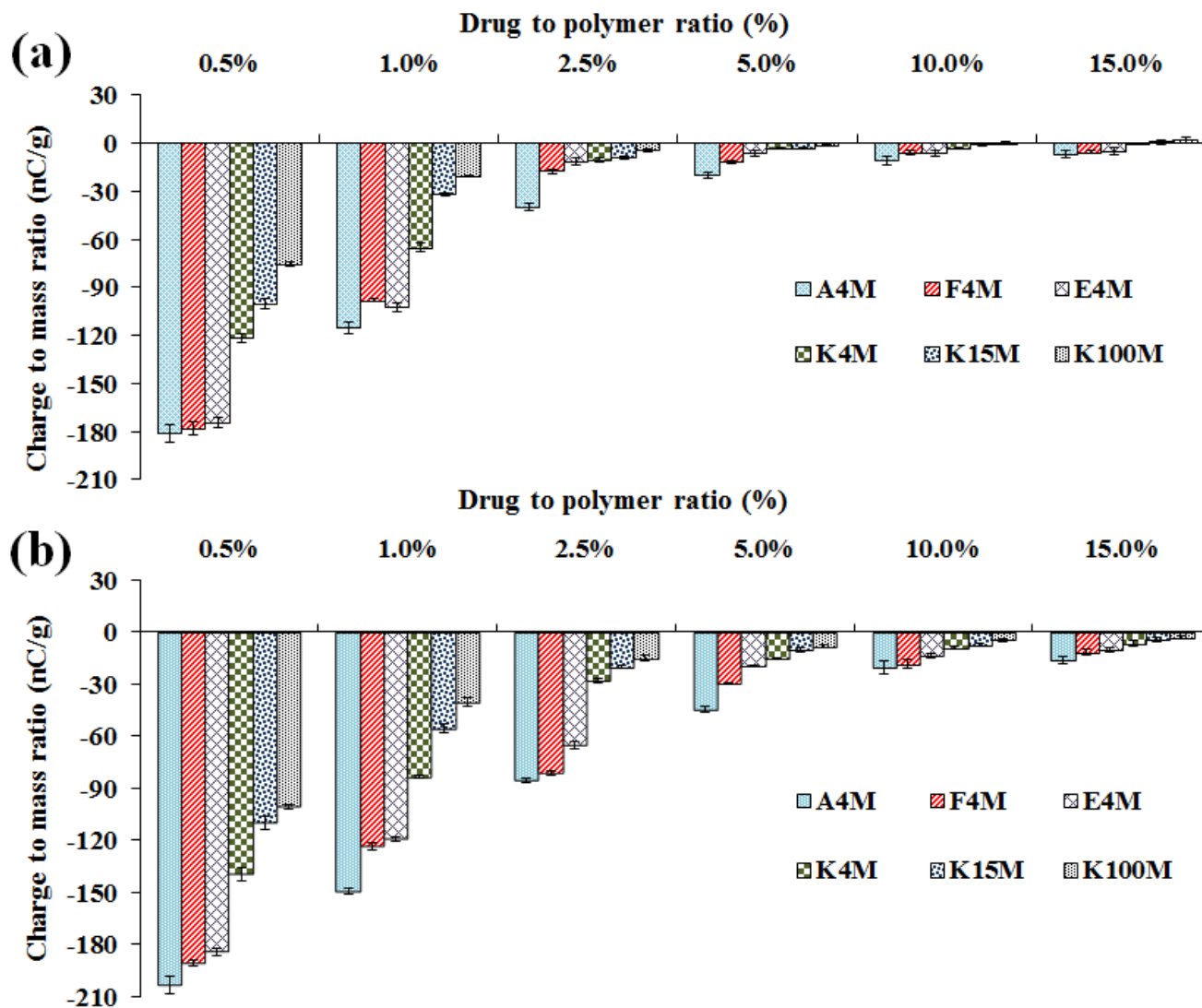


Figure 3.17, Effect of polymer concentration on the tribo-electric charging of cellulose ether : FBP powder mixtures; polymer particle size (a) 150 - 250 μm and (b) 90 - 150 μm (n=3).

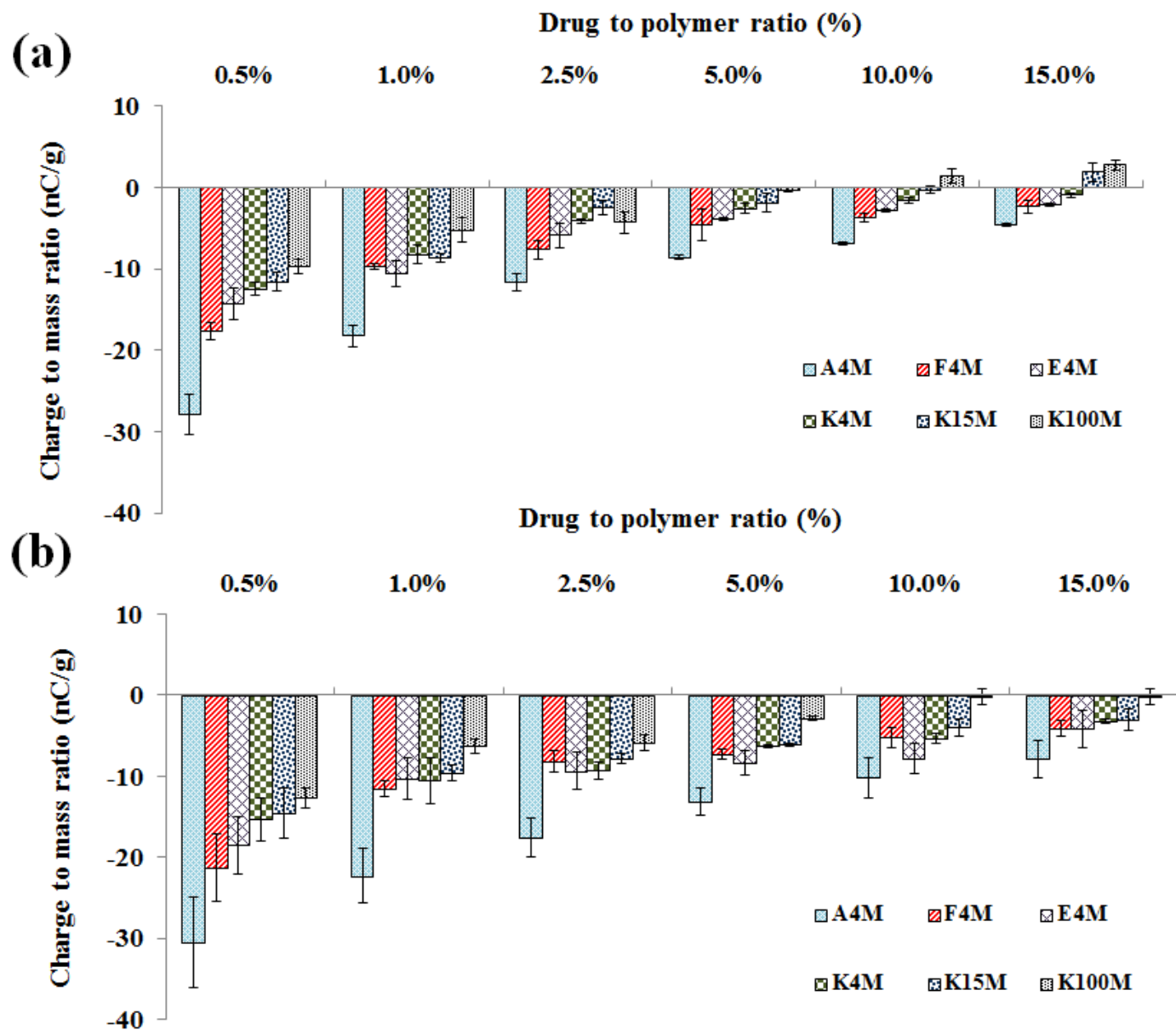


Figure 3.18, Effect of polymer concentration on the tribo-electric charging of cellulose ether : THP powder mixtures; polymer particle size (a) 150 - 250 μm and (b) 90 - 150 μm (n=3).

3.9.3.2.2- Effect of particle size

The effect of polymer particle size on the propensity of charge and SA of FBP and THP powder mixtures during the contact electrification process against a the stainless steel surface, is shown in Figures 3.17- 3.18 and Tables 3.6 - 3.7, respectively. Charge and SA of all the powder mixtures were increased as the particle size of MC/HPMC was reduced from 150-250 to 90-150 μm , regardless of concentration and MC/HPMC grade. With an increase in particle size, the positively charging polymer powder particles provide more active sites on a single carrier particle for negatively charged FBP/THP to attach, leading to an ordered mixing, as described in Figure 3.10 and section 3.5.8. This particle size alteration and ordering of oppositely charged powder particles reduces the electrostatic charge and SA of powder particles. Furthermore, the particle size variation might also change the effective work function of powder blends as previously explained by various authors (Duff and Lacks, 2008; Engers *et al.*, 2006; Gallo and Lama 1976;, Lacks *et al.*, 2008; Lacks and Levandovsky, 2007; Lacks and Sankaran, 2011; Rowley, 2001). So, the findings of current study imply that the manipulation of polymer particle size may aid reduction of electrostatic properties and adhesion of pharmaceutical powder mixtures.

Table 3.6, Adhesion (%) of polymer/ FBP powder mixtures (standard deviation in parentheses, n=3).

| Methocel [®] | Particle Size (μm) | Adhesion (%) | | | | | |
|-----------------------|------------------------------------|---|-------------|-------------|-------------|-------------|-------------|
| | | Methocel [®] concentration (%) | | | | | |
| | | 0.5 | 1 | 2.5 | 5 | 10 | 15 |
| A4M | 90 – 150 | 71.5 (3.81) | 67.1 (3.51) | 48.5 (2.77) | 28.9 (1.82) | 24.1 (1.59) | 21.4 (1.54) |
| | 150 – 250 | 69.7 (3.77) | 58.1 (1.89) | 29.2 (2.38) | 22.4 (2.54) | 18.2 (0.88) | 16.3 (1.05) |
| F4M | 90 – 150 | 70.8 (2.74) | 63.4 (3.14) | 42.3 (1.25) | 21.9 (2.47) | 20.2 (1.58) | 19.4 (0.92) |
| | 150 – 250 | 66.3(3.55) | 45.2 (2.02) | 26.5 (2.34) | 18.4 (3.25) | 15.2 (2.21) | 12.9 (1.09) |
| E4M | 90 – 150 | 68.2 (3.88) | 47.2 (1.46) | 37.5 (1.4) | 27.2 (2.21) | 17.6 (2.17) | 18.6 (1.06) |
| | 150 – 250 | 61.3 (3.24) | 36.5 (1.69) | 22.2 (2.54) | 14.5 (1.37) | 12.9 (1.54) | 10.5 (1.15) |
| K4M | 90 – 150 | 57.3 (1.85) | 44.5 (0.88) | 34.5 (1.27) | 23.5 (2.88) | 17.2 (0.56) | 14.3(1.54) |
| | 150 – 250 | 48.1 (2.12) | 34.5 (2.25) | 19.2 (1.25) | 12.3 (1.25) | 11.1 (1.12) | 8.0 (0.23) |
| K15M | 90 – 150 | 47.3 (2.33) | 41.2 (1.48) | 30.5 (1.15) | 24.3 (2.41) | 15.1 (2.25) | 12.6 (0.58) |
| | 150 – 250 | 50.2 (2.51) | 31.5 (1.55) | 16.5 (0.88) | 10.2 (0.88) | 9.5 (1.47) | 6.5 (2.10) |
| K100M | 90 – 150 | 48.5 (1.89) | 38.3 (1.21) | 24.5 (0.78) | 19.3 (1.10) | 11.5 (1.09) | 9.8 (0.48) |
| | 150 – 250 | 44.2 (2.20) | 29.3 (1.25) | 14.1 (0.98) | 9.2 (0.55) | 7.3 (0.88) | 4.2 (0.51) |

Table 3.7, Adhesion (%) of polymer/ THP powder mixtures (standard deviation in parentheses, n=3).

| Methocel [®] | Particle Size (μm) | Adhesion (%) | | | | | |
|-----------------------|------------------------------------|---|-------------|-------------|-------------|-------------|-------------|
| | | Methocel [®] concentration (%) | | | | | |
| | | 0.5 | 1 | 2.5 | 5 | 10 | 15 |
| A4M | 90 – 150 | 35.1 (5.27) | 30.2 (4.53) | 28.1 (5.63) | 22.2 (4.89) | 20.3 (4.69) | 18.5 (4.64) |
| | 150 – 250 | 34.6 (5.20) | 28.3 (4.25) | 20.5 (4.12) | 18.6 (4.11) | 15.1 (3.47) | 12.6 (3.17) |
| F4M | 90 – 150 | 33.8 (5.08) | 27.5 (4.14) | 22.5 (4.51) | 15.5 (3.43) | 17.3 (3.99) | 14.2 (3.57) |
| | 150 – 250 | 32.2 (4.84) | 21.5 (3.24) | 16.2 (3.25) | 11.4 (2.52) | 10.7 (2.46) | 8.8 (2.22) |
| E4M | 90 – 150 | 30.8 (4.62) | 21.3 (3.20) | 16.3 (3.27) | 13.9 (3.08) | 10.5 (2.43) | 9.5 (2.40) |
| | 150 – 250 | 27.3 (4.11) | 18.2 (3.29) | 14.3 (2.87) | 11.4 (2.51) | 8.5 (1.97) | 7.5 (1.89) |
| K4M | 90 – 150 | 27.3 (5.47) | 17.5 (3.15) | 14.3 (2.88) | 9.6 (2.13) | 8.9 (2.06) | 6.2 (1.55) |
| | 150 – 250 | 20.7 (4.16) | 11.5 (2.07) | 9.7 (1.95) | 7.6 (1.69) | 7.1 (1.64) | 5.5 (1.40) |
| K15M | 90 – 150 | 24.3 (4.88) | 18.6 (3.36) | 11.3 (2.26) | 8.8 (1.95) | 7.5 (1.74) | 5.8 (1.47) |
| | 150 – 250 | 14.3 (2.88) | 9.6 (1.74) | 7.3 (1.46) | 6.8 (1.71) | 4.5 (1.05) | 3.8 (0.97) |
| K100M | 90 – 150 | 18.3 (3.66) | 9.5 (1.71) | 7.2 (1.44) | 6.2 (1.56) | 5.8 (1.35) | 4.1 (1.05) |
| | 150 – 250 | 8.3 (1.66) | 6.5 (1.17) | 5.2 (1.04) | 3.9 (1.00) | 3.8 (0.89) | 2.90 (0.75) |

3.9.3.2.3- Effect of substitution ratios

The chemistry of polymers can affect the tribo-electric charging and SA properties of powders as it instigates variations in particle dynamics during the tribo-charging process. The major difference between MC (A4M) and other various grades of HPMC (F4M, E4M and K4M) is the level of Meo and Hpo groups attached to the parent glucose ring. The variation in the Hpo/Meo substitution ratios had a significant impact on the tribo-electric charge and SA properties of plain MC and HPMC powders, as explained in section 3.5 and Table 3.4.

In the present study of MC/HPMC : FBP/THP powder mixtures, the Hpo to Meo substitution ratio showed a significant impact. The overall net charge and SA were decreased with an increase in Hpo/Meo substitution ratios (i.e. $A > F > E > K$) and this was the case for both particle size fractions (Figures 3.17 - 3.18 and Tables 3.6 – 3.7)

It is notable that as the substitution ratio increases, the surface irregularities were increased, resulting in a more complex surface morphology of powder particles. Moreover, it induced steric hindrance due to the difference in local atomic number as described earlier in section 3.7.4.2.2. These changes can modify surface resistivity, work function and steric hindrance, thus enabling MC/HPMC to show anti-static and anti-adhesive properties.

3.9.3.2.4- Effect of molecular size (viscosity)

The molecular size of MC/HPMC can affect charging and SA due to its impact on the polymer chain lengths and their subsequent packing in a powder particle. The molecular size of MC/HPMC has a significant effect on the tribo-electric charging and SA properties of powder mixtures either containing FBP/THP (Figures 3.19-3.20 and Tables 3.5-3.6). The net tribo-electric charge and SA were decreased with an increase in the molecular size (for K series); both the particle size fraction showed similar behaviour. It is evident that as

molecular size increases, it affects the packing of the polymeric chains which leads to surface irregularities of powder particle, as described earlier (section 3.5.6). Moreover, these changes can modify surface resistivity and the effective work function of powder particles in a blend. Moreover, these characteristics dictate the charge transfer process and generation of operational forces (van der Waals forces, ionic bonding and electrostatic forces) thus impacting phenomena. Additionally, the agglomeration and stability of these powder mixtures are improved with more complex surface carrier particles compared with particles having a smooth surface (Saharan *et al.*, 2008; Swaminathan and Kildsig, 2000).

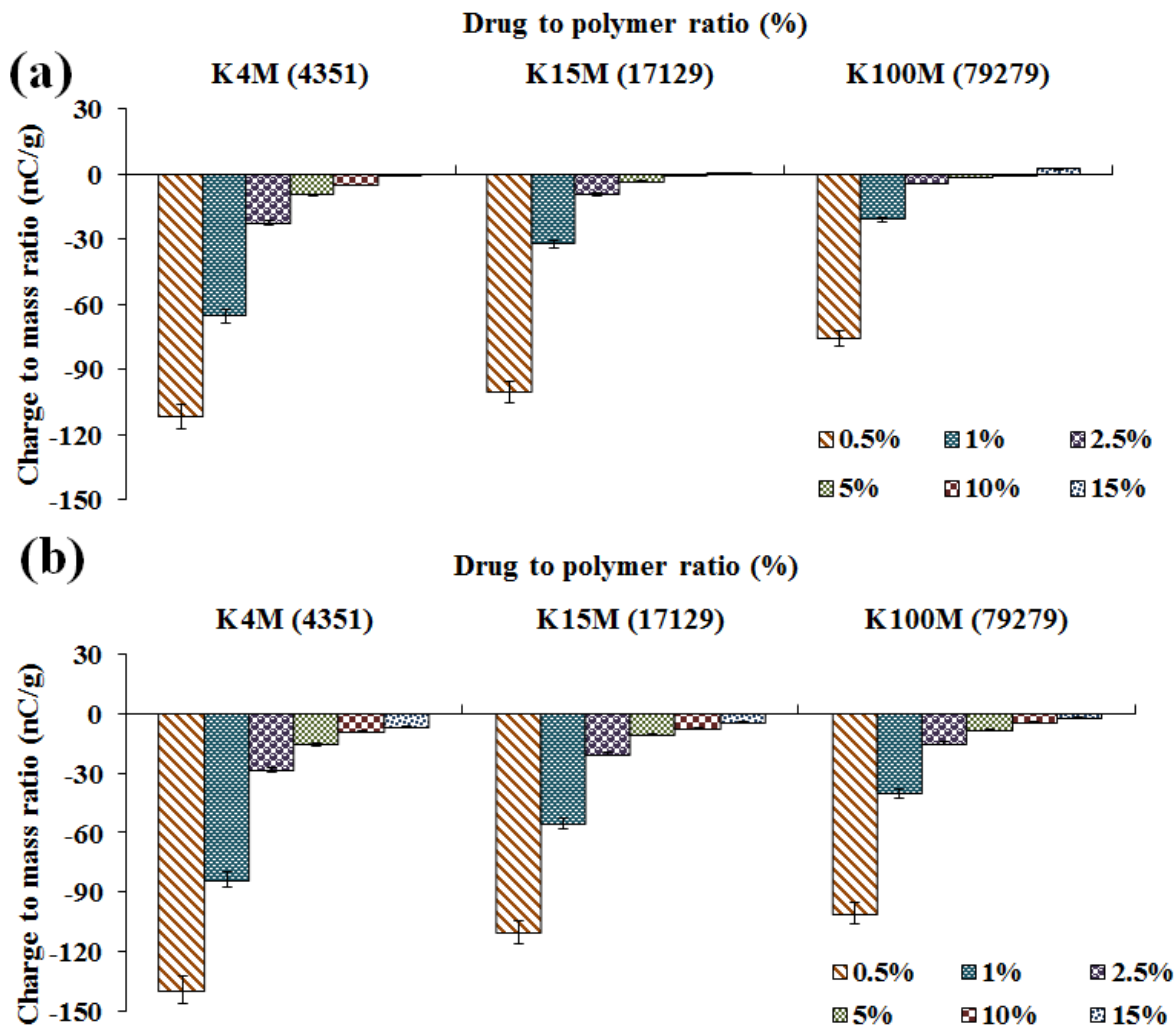


Figure 3.19, Effect of polymer molecular size (viscosity) on the tribo-electric charging of MC/HPMC : FBP powder mixtures; polymer particle size (a) 150 - 250 μm and (b) 90 - 150 μm , $n=3$, (viscosity (cps) in parentheses on x-axis)

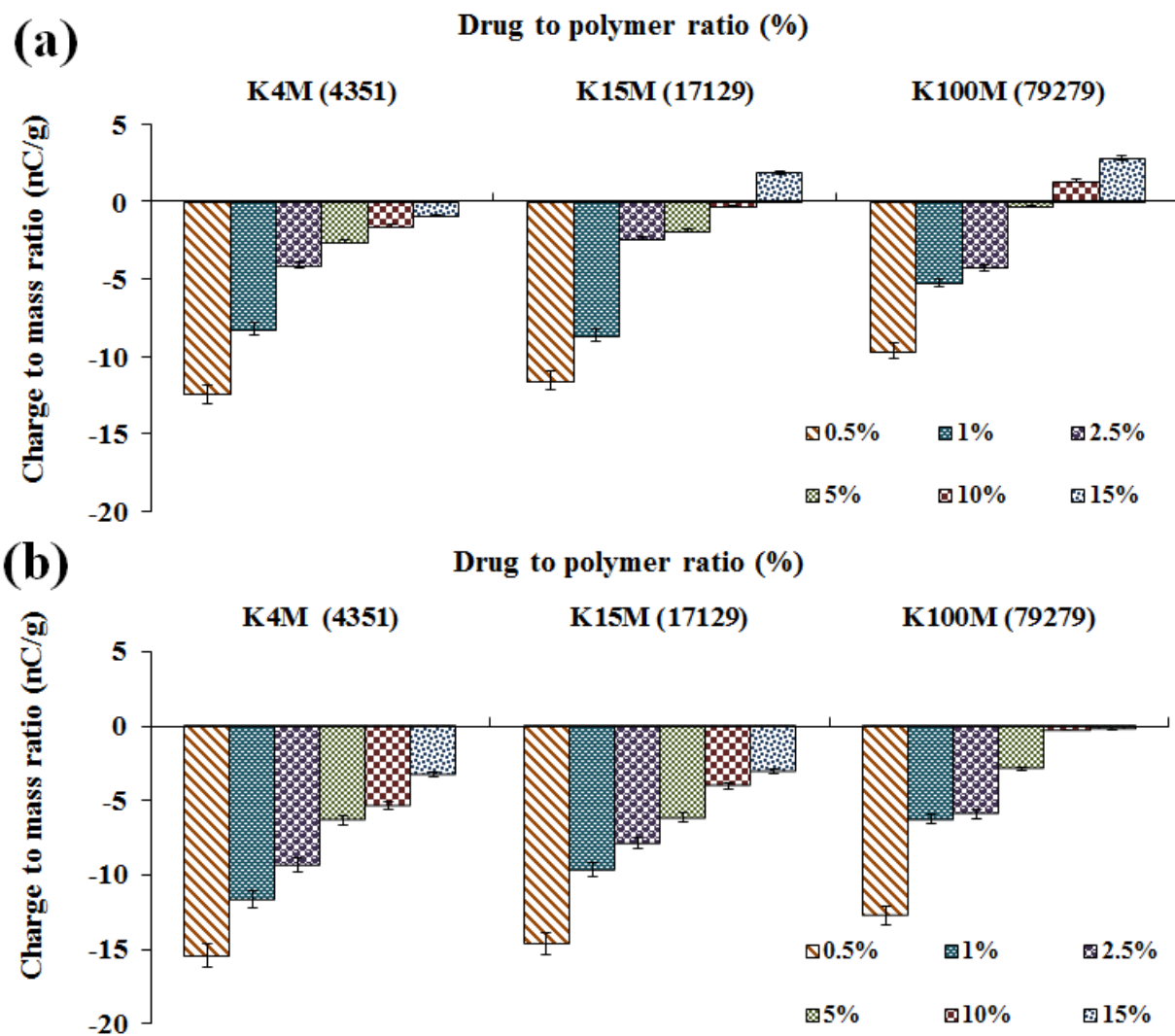


Figure 3.20, Effect of polymer molecular size (viscosity) on the tribo-electric charging of MC/HPMC : THP powder mixtures; polymer particle size (a) 150 - 250 μm and (b) 90 - 150 μm , $n=3$, (viscosity (cps) in parentheses on x-axis).

3.9.4- Relationship between tribo-electric charging and surface adhesion

Table 3.7 shows the adhesion of polymer particles to the steel surface calculated as a ratio between the initial feed and the mass loss due to powder sticking. A reduction in adhesion is observed with a decrease in electrostatic charge on the particles. Figures 3.21 and 3.22 show the relationship between charge and SA for all binary mixtures having varying polymer particle size (90 -150 μm and 150 - 250 μm) and concentration (0.5 - 15 % w/w). The electrostatic charge was spawned due to electron transfer from the polymer to FBP/THP powder particles, as described earlier. A reduction in susceptibility towards tribo-electric charging is directly related to surface adhesion, with correlation coefficients ranging between 0.81-0.98 and (Table 3.8). As in the case of FBP powder mixtures, the A4M blends show a higher degree of correlation (R^2) than others, while K100M blends were at the lower end of this series. Conversely, F4M: THP blends showed a good correlation coefficient, but A4M powder mixtures had lower values. The particle size distribution also has a significant impact on the R^2 which tends to decrease with decreasing particle size and it is more eminent in the THP powder blends study. This might be due to the fact that the reduction in particle size has generated molecular and Van der Waals forces, as both depend on the distance between the contacting powder particles (Cross, 1987). The large surface area associated with a reduction in particle size reduced the distance between the powder particles, thus giving rise to a higher intensity of operational forces during the experiments. The current study shows that electrostatic forces generated during the tribo-electrification process played a significant role during the SA phenomena of pharmaceutical powders. However, it is appreciated that the mechanism of particle adhesion is a complex process and other mechanisms may also be involved (Cowell, 2003; Donald, 1969).

Table 3.8, Inter-relationship between tribo-electric charge and SA (n = 3).

| Powder mixtures | Correlation co-efficient (R^2) | |
|-----------------|--|---|
| | Particle size (90-150 μm) | Particle size (150-250 μm) |
| A4M/FBP | 0.959 | 0.980 |
| F4M/FBP | 0.956 | 0.973 |
| E4M/FBP | 0.974 | 0.961 |
| K4M/FBP | 0.913 | 0.955 |
| K15M/FBP | 0.815 | 0.940 |
| K100MFBP | 0.857 | 0.894 |
| A4M/THP | 0.750 | 0.947 |
| F4M/THP | 0.880 | 0.992 |
| E4M/THP | 0.917 | 0.967 |
| K4M/THP | 0.982 | 0.930 |
| K15M/THP | 0.975 | 0.938 |
| K100M/THP | 0.899 | 0.963 |

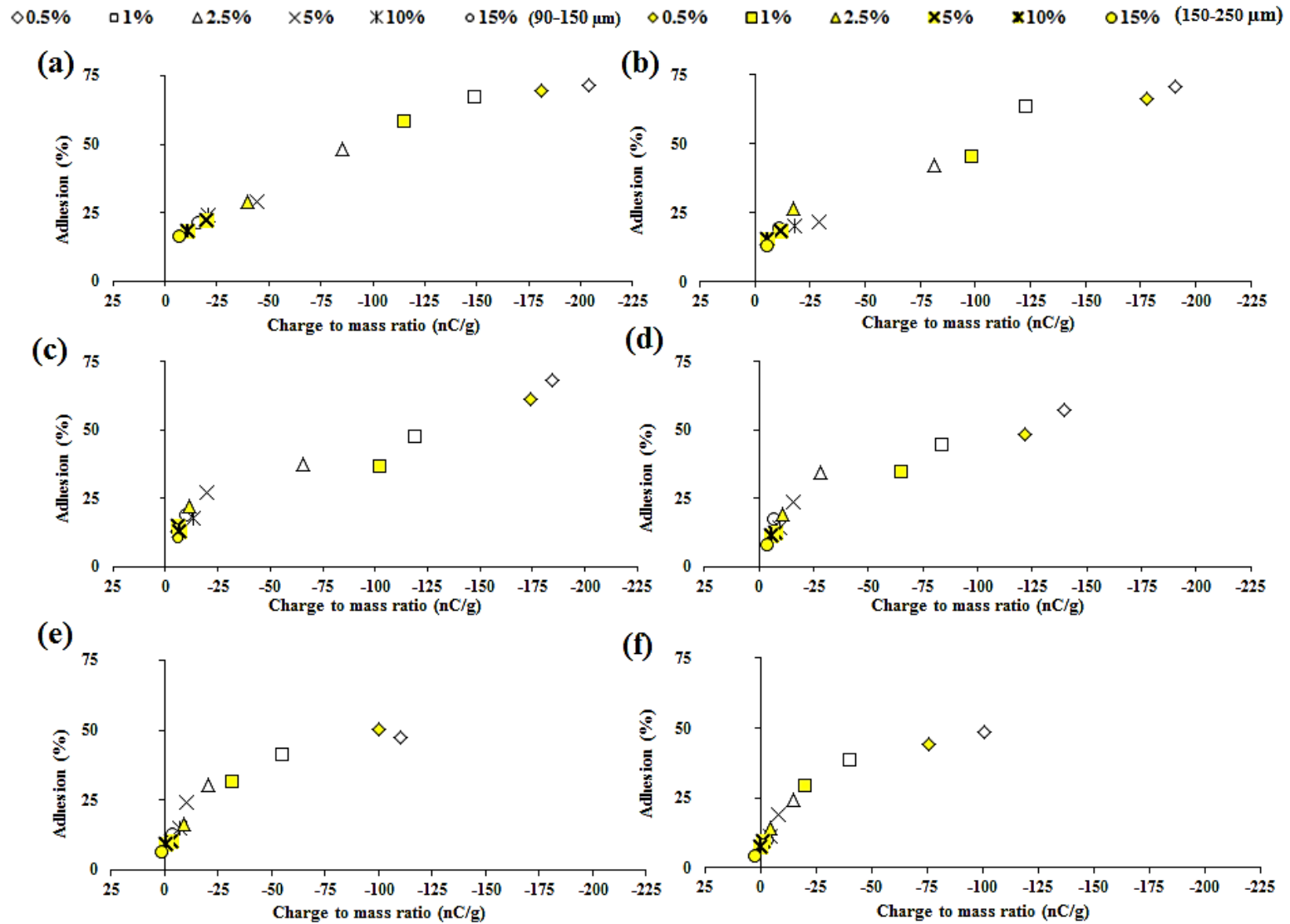


Figure 3.21, Effect of tribo-electric charging (nC/g) of FBP powder mixtures on SA (%), (a) A4M (b) F4M (c) E4M (d) K4M (e) K15M (f) K100M having polymer particle size 90-150 μm and 150-250 μm.

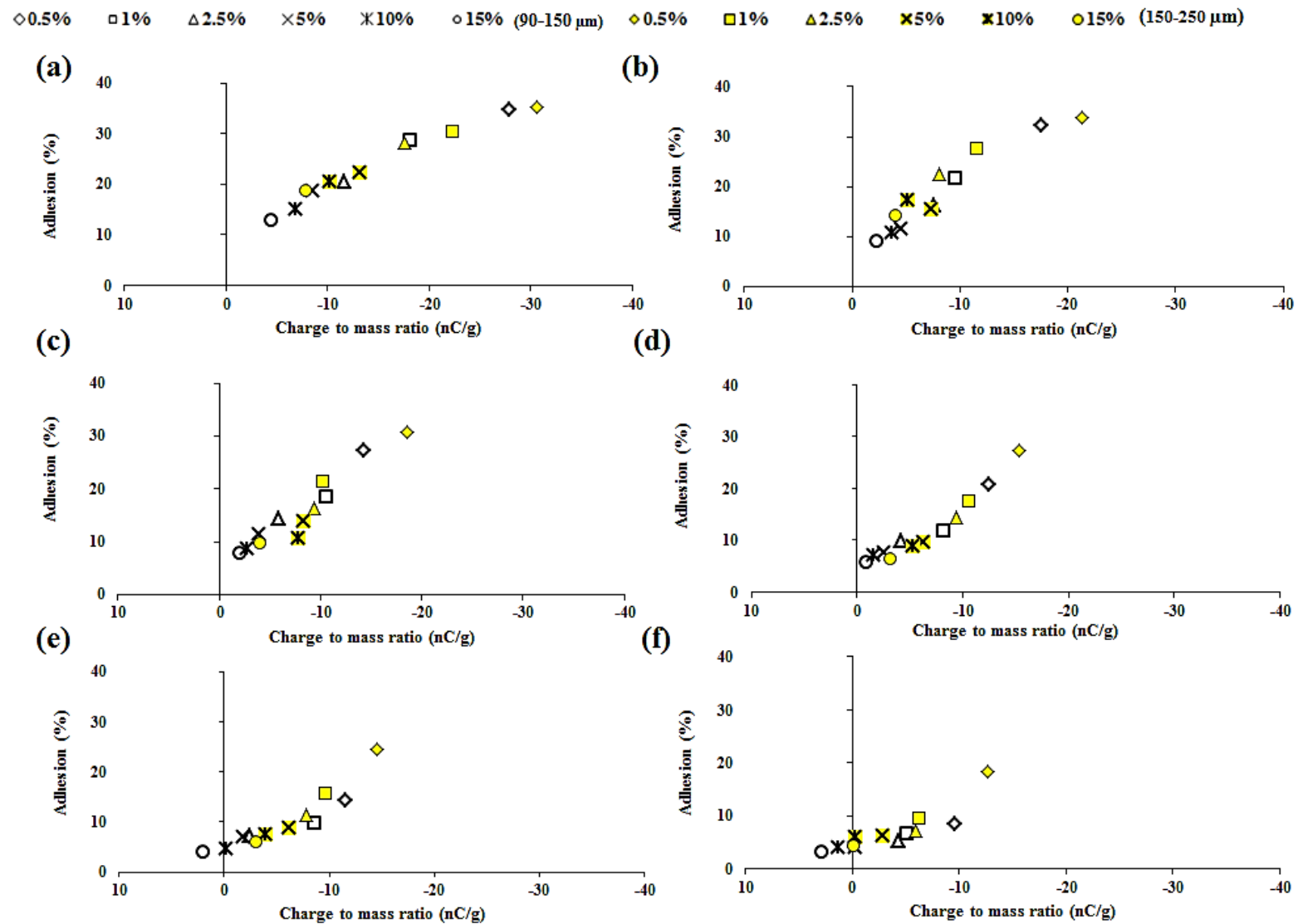


Figure 3.22, Effect of tribo-electric charging (nC/g) of THP powder mixtures on SA (%), (a) A4M (b) F4M (c) E4M (d) K4M (e) K15M (f) K100M having polymer particle size 90-150 μm and 150-250 μm .

3.10- Summary

In summary, it can be concluded that both the drugs charged negatively, with the electrostatic behaviour of FBP and THP categorised as highly charging and low charging materials, respectively, when compared to other APIs and pharmaceutical excipients. The high charging of FBP is likely to result in processing problems during powder processing. Moreover, the study revealed that the MC and HPMC powder particles charged positively and have lower work function in comparison to steel surface. The physico-chemical properties associated with MC and HPMC, such as particle size, chemical heterogeneity and molecular size of cellulose ethers all have significant impact on their charging and adhesion properties.

The study further revealed that the particle size, substitution and molecular size of cellulose ethers all can significantly affect the charging and adhesion behaviour. An electrostatic charge-assisted ordering has been showed to be an efficient tool for the dissipation of charge on the API. The charge and adhesion were highly dependent on the concentration ($P < 0.05$), particle size, substitution ratios and molecular size of the cellulose ethers. The decrease in PSA and charge dissipation of FBP powder mixtures is intuitively expected to improve its flowability and compaction which is expected to have a positive effect on the finished pharmaceutical dosage forms.

4- Swelling, erosion and dissolution studies of hydrophilic matrices

4- Swelling, erosion and dissolution studies of hydrophilic matrices

4.1- Introduction

The goal of any drug delivery system is to provide a therapeutic amount of drug to its proper site in the body, so that a desired drug concentration at the site of action is achieved promptly and then maintained over a specified period of time. Thus, an ideal drug delivery system should have the capacity to deliver drugs at a particular rate as required by the patient. However, most of the traditional oral dosage forms require frequent and repeated doses to achieve these objectives (Wise, 2000; Yihong, 2009). Thus, it is far from an ideal therapeutic environment as fluctuation of plasma drug concentrations over successive administrations may lead to overdosing or underdosing of the patient. Moreover, drugs with short biological half-lives require frequent doses to maintain therapeutic concentrations in the body. Additionally, the lack of compliance due to a forgotten dose or overnight can significantly deteriorate the treatment plan (Remington and Allen, 2013).

Owing to these problems, controlled drug release approaches have become popular over the years. The use of hydrophilic polymers to develop hydrophilic matrices became eminent as they enable the drugs to be released continuously over long periods of time, which ultimately improves patient compliance and decreases patient to patient variations in drug administration patterns. Furthermore, it reduces the total amount of administered drug and possible side-effects related to high peak plasma drug levels (Wen and Park, 2011).

4.2- Hydrophilic matrices

Hydrophilic matrix tablets are the most frequently used controlled release oral dosage forms intended for oral administration (Alderman, 1984; Maderuelo *et al.*, 2011). Commonly, hydrophilic matrices are compressed matrix tablets and can easily be prepared by direct

compression of a powder mixture of drug with a release retardant swellable-polymer and other additives to aid processing. Such matrices are commonly employed because of the advantages associated with their manufacturing, including simple formulation, the use of existing tableting technologies and the low cost of polymers, which are generally regarded as safe excipients (Wen *et al.*, 2010). These hydrophilic matrices have the ability to release the drug over a defined period of time, as they do not undergo disintegration when delivered to patients, as the drug is entrapped in the polymeric network at the particulate level (Figure 4.1). Numerous swellable, carbohydrate-based polymers are available, allowing flexibility for the needs of an individual formulation to achieve specific goals in drug therapy (Siepmann *et al.*, 2011).

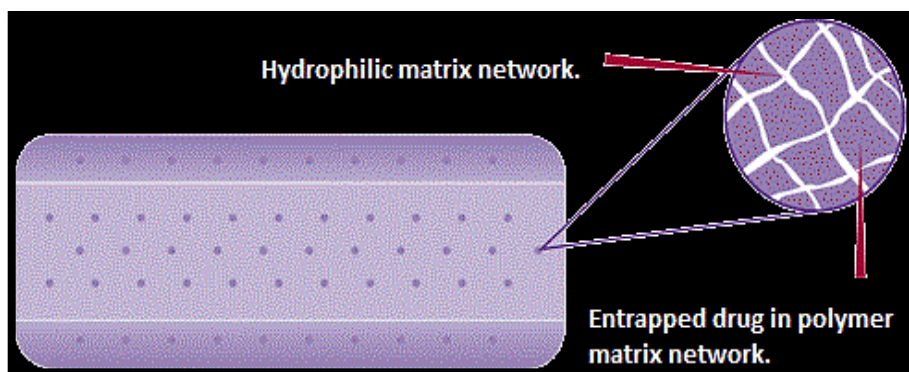


Figure 4.1, Cross-sectional view of a typical hydrophilic matrix tablet.

4.3- Cellulose ether based hydrophilic matrices

Among the swellable polymers usually used to develop these hydrophilic matrices, cellulose ethers, specifically methylcellulose (MC) and hypromellose (hydroxypropyl methylcellulose, HPMC), have provoked extensive interest (Maderuelo *et al.*, 2011). Their widespread acceptance can be attributed to good compression properties, adequate swelling

characteristics which allow the matrix tablet to develop an external gel layer on the surface of matrix tablet, non-toxic nature, availability in different grades, ability to give pH independent drug release profiles and amenability to high levels of drug loading, (see chapter 1, sections 1.1-1.4 for more detail).

4.4- Mechanism of swelling, drug release and matrix erosion

Polymer swelling, drug dissolution and matrix erosion are the phenomena that determine the mechanism of drug release from hydrophilic matrix tablets, either on a macroscopic or molecular level (Chaibva *et al.*, 2010). When drug loaded swellable Methocel[®] based hydrophilic matrices are exposed to dissolution fluid, steep water concentration gradients are formed between the dissolution fluid and the outermost surface of matrix tablet. This results in water imbibition into the polymer matrix network. To describe this process adequately, it is important to consider the exact geometry of the matrix tablet, as in the case of cylinders, both, axial and radial directions of mass transport can be manifested which have a significant dependence of the water diffusion coefficient and the matrix swelling (Ford *et al.*, 1987; Siepmann and Peppas, 2001). When dry matrix tablets are introduced into the liquid system, the diffusion coefficient tends to be very low, whereas in highly swollen gels, it is of the same magnitude as pure water. So, the liquid acts as a plasticizer and the glass transition temperature (T_g) reduces from somewhere between 154 – 184 °C to around the system temperature, 37 °C (Conti *et al.*, 2007). Once the T_g equals the temperature of the system, the polymer chains start to relax and eventually disentangle enhancing the molecular surface area (Maderuelo *et al.*, 2011). This phenomenon of polymer chains relaxation is termed ‘swelling’ and the continuous inward ingression of liquid breaks the hydrogen bonds formed during tablet compaction and can lead to the development of new hydrogen bonds accommodating water molecules (Li *et al.*, 2005). Therefore, the reduction in T_g and

formation of new hydrogen bonds results in the swelling of polymer chains. As a consequence, a thick gelatinous layer appears on the surface of matrix tablets, commonly known as a gel layer, as MC/HPMC pass from the amorphous glassy state to the rubbery state (Colombo *et al.*, 1999; Colombo *et al.*, 2000; Siepmann and Peppas, 2001). The development of the gel layer actually divides the matrix tablet into three different distinguishable regions. The highly swollen outer region (erosion front) has the highest amount of water molecules but it is mechanically weak. However, it acts as a diffusion barrier preventing water penetration into the other two regions. The middle region (dissolution front) is moderately swollen and is relatively stronger than the outer one. The core of the matrix tablet which actually forms the innermost region (swelling front), remains essentially dry and holds its glassy state for a longer period of time (Omidian and Park, 2008; Maderuelo *et al.*, 2011). Moreover, there is evidence that a fourth front (penetration front) is also present, between the swelling and dissolution fronts, adding further complexity to the system (Ferrero *et al.*, 2010). A schematic illustration of the different fronts which develop due to liquid penetration is shown in Figure 4.2.

The gel layer grows over time as more water penetrates into the matrix tablet. The polymer chains present on the surface of matrix tablet hydrate quickly compared to those located inside the core and contact with the liquid causes chain relaxation (swelling) which initiates erosion of the matrix. Instantaneously, the outermost layer becomes fully hydrated and starts to relax, leading to the disentanglement of polymeric chains (Vueba *et al.*, 2005). Consequently, matrices start to dissolve from their surface, as water continuously permeates towards the core (Tiwari and Rajabi-Siahboomi, 2008). The relative rates of liquid uptake and erosion of a polymer matrix play a critical role in controlling the rate of drug release. The swelling, matrix erosion, drug release mechanism and rate are dependent on the concentration and viscosity of HPMC being used in the hydrophilic matrices (Mitchell *et al.*, 1993; Wan *et*

al., 1991). HPMC has the potential to hydrate quickly enough to form a gel layer before the drug entrapped in the tablet matrix can dissolve.

There are two processes involved during the dissolution of hydrophilic matrix tablets, by which polymer erosion from the hydrophilic matrices takes place. Firstly, the disentanglement of individual polymer chains at the surface of matrix tablets and secondly their subsequent transport to the surrounding bulk solution. The physical entanglement of the polymer chains precludes polymer dissolution, but polymer present at the outermost surface is diluted by the bulk dissolution medium over time to a point when the polymeric network no longer has structural integrity. This eventually leads to polymer disentanglement and the matrix tablet starts to disappear (Colombo *et al.*, 2000; Maderuelo *et al.*, 2011; Miller-Chou and Koenig, 2003; Siepmann and Peppas, 2001; Wen *et al.*, 2010). Both MC and HPMC are water soluble and, as the water penetrates into the hydrophilic matrix, the polymer chains become hydrated and these eventually start to disentangle from the matrix because MC and HPMC contain linear hydrophilic polymeric chains which do not cross-link but instead form a gelatinous layer on the surface of the tablets that is vulnerable to matrix erosion. At high polymer concentrations, the linear polymer chains entangle to form what may be considered a physically cross-linked structure, which eventually erodes, resulting in the liberation of polymer and drug molecules (Mitchell *et al.*, 1993). However, the rate of polymer erosion is dependent on the viscosity of the MC/HPMC grade being used in the formulation. Tablets were produced using a high molecular weight and viscosity grade MC/HPMC shows more resistance to polymer erosion than the low molecular weight and low viscosity grades (Wen *et al.*, 2010).

Figure 4.3 illustrates a general drug release mechanism on the basis of solubility of incorporated drugs. Release is controlled by diffusion through, and erosion of, the

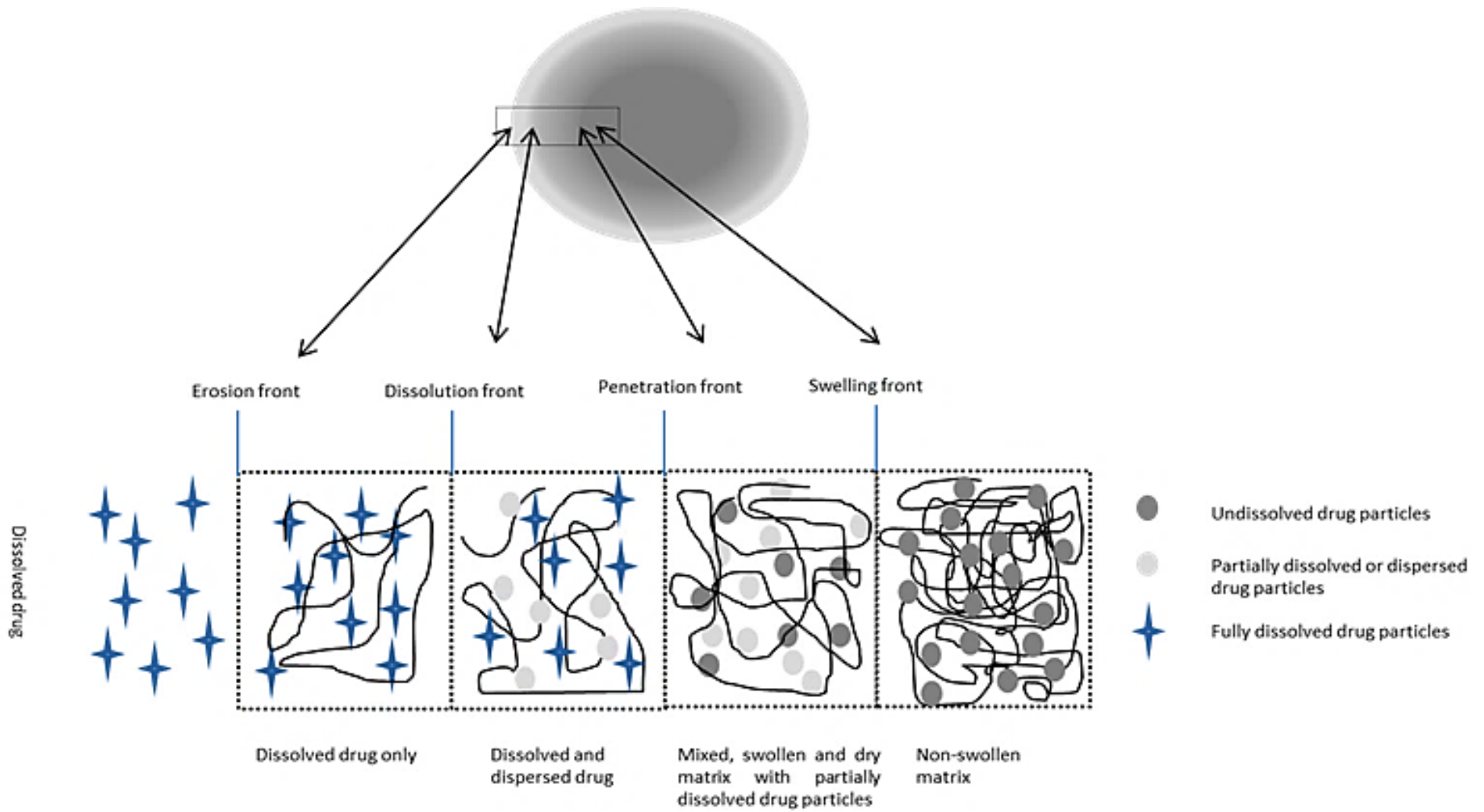


Figure 4.2, Mechanism of drug release from hydrophilic matrix tablets.

gel layer and any drug present on the surface of the matrix tablet are quickly released. This is followed by expansion of the gel layer as water permeates into the tablet, increasing the thickness of the gel layer (Ford *et al.*, 1985a; Talukdar *et al.*, 1996). If a well-defined gel layer is formed, the rate of drug release is reduced and becomes dependent on the rate at which the drug molecules diffuse through the gel, as well as the rate at which the barrier layer is mechanically removed by attrition and disentanglement of the matrix. In most cases, both diffusion and erosion occur simultaneously (Gao *et al.*, 1996; Ju *et al.*, 1995; Kim and Fassihi, 1997). Highly water soluble drugs diffuse through the gel layer before the matrix erodes, but it is suggested that the presence of poorly soluble drugs can increase matrix erosion by imperilling the integrity of the gel layer (Bettini *et al.*, 2001; Ghori *et al.*, 2014b; Yang and Fassihi, 1997). So, the solubility of entrapped drugs is another key factor in determining the drug release behaviour from hydrophilic matrices. Mechanistically, both diffusion and erosion will be contributing factors in controlling drug release from a hydrophilic matrix tablet. In practical terms, however, one process will often play a predominant role over the other depending on the HPMC level and solubility of other matrix tablet contents (Sinha Roy and Rohera, 2002).

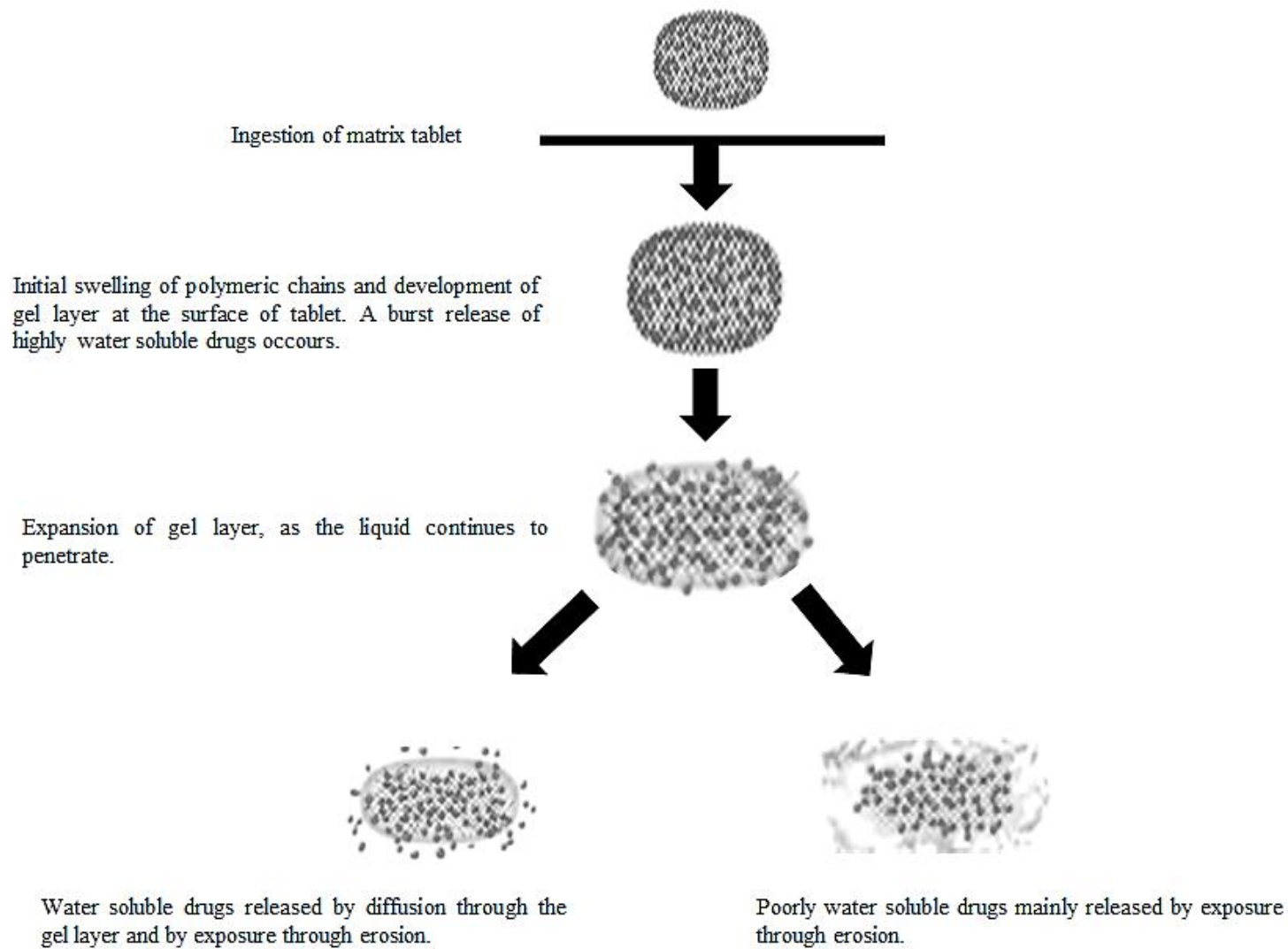


Figure 4.3, Drug release mechanism of water soluble and poorly water soluble drugs from hydrophilic matrix tablets.

4.5- Factors affecting swelling, erosion and drug release

Although the fabrication of compressed hydrophilic matrices may be simple, it becomes very complex and challenging when it comes to explaining the mechanism of drug release from these polymeric devices. The physicochemical properties of MC/HPMC and incorporated drug significantly impact the swelling, erosion and drug release. In this section, the principal factors that can affect swelling, erosion and drug release will be discussed; however, a summary of all the major contributing factors has been given in Table 4.1.

4.5.1- Effect of Methocel[®] concentration

Commonly, it is noticed that regardless of the physicochemical properties of hydrophilic polymer, the drug release rate decreases with an increase in the levels of polymer in a hydrophilic matrix tablet. Reza *et al.* (2003) reported that higher levels of polymer correspond to a lower porosity of the matrix tablet and slower drug release rates can be achieved. Moreover, Ebube *et al.* (2004) investigated the effect of polymer levels on the release of acetaminophen and found an increase in the percentage of polymer (3.5% to 19.2%) in the matrix tablet lead to a decrease in the drug release rate. The results of these experiments are in complete agreement with the findings of Mitchell *et al.* (1993), who concluded that a greater degree of physical cross-linking of polymer chains is evident when the amount of HPMC has been increased. This in turn increases the tortuosity of the matrix tablets and essentially corresponds to slower drug release. The studies of Campos-Aldrete and Villafuerte-Robles (1997), Kim and Fassihi (1997), Nellore *et al.* (1998) concluded that the first 5 min contact between the matrix tablet and aqueous fluids is a very important time for the development of the gel layer on the surface of matrix tablet. After such times, if the structure has not formed, the matrix may erode too quickly and lead to premature drug release. Higher polymer content in a matrix tablet results in the formation of a stronger gel; at

low polymer levels the gel does not form quickly. As hypromellose content is increased, the resulting gelatinous diffusion layer becomes stronger and more resistant to diffusion and erosion (Xu and Sunada, 1995). Recently, Jain *et al.* (2014) concluded that the higher levels of HPMC in a matrix tablet exhibit slower erosion and drug release rate. These conclusions are in complete accordance with the findings of Ghori *et al.* (2014), who reported that the increase in the HPMC concentration (20% to 80 %) in a matrix tablet tends to decrease the rate drug release, regardless of drug solubility.

However, there is a difference of opinion, as some authors do not agree with this notion, as in the case of Tiwari *et al.* (2003). In their studies, these authors prepared the hydrophilic matrices by using a highly water soluble drug, tramadol, and failed to observe significant changes in the release profile with changes in the polymer concentration. In formulations of drugs that are highly soluble in water, it is usual to find that, above a certain percentage of polymers, the release rate does not decrease.

It was reported that once a particular polymer level is reached, the effects from characteristics such as viscosity, burst effect and particle size are less evident. A polymer content of 30% – 40% appears to be the level at which similar drug-release profiles are obtained from differing grades of hypromellose (2208, 2906, and 2910) (Ford *et al.*, 1985a; Nellore *et al.*, 1998). However, Campos-Aldrete and Villafuerte-Robles (1997) reported that the HPMC concentrations higher than 20% can become the overriding factor and the effect of viscosity and particle size do not cause any significant changes in the drug release profiles. Moreover, the conclusions of Heng *et al.* (2001) are in complete accordance with aforementioned studies, that the increase in HPMC concentration can significantly suppress the impact of particle size.

4.5.2- Effect of Methocel[®] particle size

Over the years, the effect of the particle size of the polymer on drug release has been studied in depth by different authors (Campos-Aldrete and Villafuerte-Robles, 1997; Caraballo, 2010; Dabbagh *et al.*, 1996; Reza *et al.*, 2003; Velasco *et al.*, 1999; Zuleger and Lippold, 2001). A general observation can be drawn from these studies that the particle size of the polymer is not as decisive as expected. However, narrower particle size distribution of polymer in a matrix system initiates the prompt development of the gel layer on the surface of matrix tablet.

The hydrophilic matrices formulated with polymer particles sizes larger than 200 μm disintegrate before the development of the so-called surface gel layer, while those formulated with particle sizes smaller than 150 μm can form the gel layer rapidly, preventing the disintegration of the system and lead to prolonged drug release profiles (Dow, 2006). Mitchell *et al.* (1993) reported that the polymer particles tend to dissolve slowly and failed to provide adequate controlled drug release. The use of larger sized hypromellose K15M particles ($> 355 \mu\text{m}$) left much larger pores on the surface of matrices that essentially make the gel layer structure unstable and lead to rapid drug release.

Some authors have proposed that the effect of MC/HPMC particle size can be minimised with high concentrations of polymers, as described in the earlier section, 4.5.1. Heng *et al.* (2001) carried out the experiments to elucidate the effect of particle size on drug release profiles. It was revealed that the HPMC K15M matrices, with a mean particle size smaller than 113 μm , release drug through a combination of erosion and diffusion mechanisms. However, the matrix tablets having a HPMC particle size of more than 113 μm showed rapid drug release behaviour and the release mechanism was considered to be more erosion based. Furthermore, Miranda *et al.* (2007) reported on the relationship between particle size of

matrix components and their percolation threshold. It was concluded that the larger polymer particle sizes were less effective in the formation of a homogeneous gel layer.

4.5.3- Effect of Methocel[®] substitution

Different polymer properties have been reported to be responsible for the rate of polymer hydration, including substitution type. It was initially proposed that cellulose ethers of different substitution levels hydrate at different rates and this factor may be used to optimise the formulation of sustained release matrices (Alderman, 1984). However, Mitchell *et al.* (1993), using a combination of differential scanning calorimetry (DSC) and dissolution studies, showed that the differences in release rates for HPMCs with different substitution levels are not due to differences in hydration rate. Further studies using thermo-mechanical analysis (Mitchell *et al.*, 1993) indicated that the gel layer thickness (which will affect the diffusional path length) is similar in HPMCs of different substitution type. The type of the substituent determines the hydration rate of the polymer and can significantly affect the hydration rate and drug release. The drug release is dependent on the substitution type if the polymer level is kept low, so that the polymer concentration is not the overriding factor in controlling the swelling, erosion and drug release behaviour of hydrophilic matrices (Malamataris and Karidas, 1994). The change in the substitution levels impacts the polymer relaxation in tablet matrices; it was confirmed that different substitution levels gave rise to different water mobility, leading to differing drug-release characteristics (Rajabi-Siahboomi *et al.* 1996). Furthermore, McCrystal *et al.* (1999) confirmed that the amount of water that attaches to the polymer and the amount of tightly bound water significantly depend on the degree of substitution.

The substituents of a polymer side chain alter its polarity and melting point. For example, substitutions of the side-chain groups by more polar groups result in a reduction in the

crystallinity of the polymer, which is reflected in a decrease in its melting point. This affects the solubility of the polymer in water. In general, the water solubility of a polymer can be said to be related to its ability to establish hydrogen bridges between the hydrogen atoms of the water and those of the oxygen present in the side chain and the substituents of the polymer (Sarkar and Walker, 1995). In the particular case of matrix systems, the type of substitution does not only influence the solubility of the polymer in water, but also the gel strength, and the swelling and erosion of the polymer. In the case of HPMC, the rate of swelling depends on the side-chain substituents, such that the higher the number of hydroxyl groups, the faster the hydration (Asare-Addo *et al.*, 2013b; Escudero *et al.*, 2012; Viridén *et al.*, 2009; Viridén *et al.*, 2010; Tiwari *et al.*, 2003). Moreover, Escudero *et al.* (2010) studied the influence of replacement of the HPMC chain on the release of THP contained in mixtures of a swelling polymer with an inert one. Three different types of substitution based on methoxyl and hydroxyl groups were tested; E4M, K4M and F4M, and the HPMC F4M resulted in slower drug release rates because it had the largest number of hydrophobic substituents (methoxyl). For the ratio, inert polymer/swelling polymer 75:25, where the characteristics of viscosity and substitution of the HPMC were less important than the properties of the inert polymer, the mixtures made with HPMC F4M and E4M allowed a more homogeneous gel structure and easier modulation of THP release rate (Escudero *et al.*, 2010).

4.5.4- Effect of Methocel[®] viscosity (molecular size)

The viscosity of MC/ HPMC is considered to be another important parameter that controls and determines the mechanism of release. The viscosity of a polymer in solution very much depends on the chemical structure of the polymer, its molecular weight and its interaction with the solvent. Various authors have studied the impact of MC/HPMC viscosity on drug

release from hydrophilic matrices. It can be concluded from these studies that the higher the viscosity of a polymer, the faster the swelling of its side chains, forming a very strong gel, which decreases the drug release rate. Moreover, studies carried out by Daly *et al.* (1984); Nakano *et al.* (1983) and Salomon *et al.* (1979) reported a decline in the rate of drug release with increase in the polymer viscosity.

A study carried out by Wan *et al.* (1991) proposed that the increase in the viscosity of HPMC tends to increase the swelling and drug release rates. It can be attributed to the fact that the pores of high-viscosity hypromellose block up quickly and inhibit further liquid uptake. This in turn leads to the formation of a turbid gel, which resists dilution and erosion, subsequently resulting in slower drug diffusion and release rates (Gao *et al.* 1996; Talukdar *et al.* 1996; Wan *et al.* 1991).

Furthermore, it has been demonstrated by Campos-Aldrete and Villafuerte-Robles (1997) that in the case of HPMC, increases in the viscosity of the polymer lead to slower drug release rates as long as the percentages of polymer do not surpass 20%. Studies addressing swelling and erosion carried out by Ravi *et al.* (2008) have shown that the percentages of swelling and erosion are completely dependent on the viscosity of the polymer and the percentage of swelling increases as the viscosity of HPMC increases, however, the percentage of erosion decreases when the viscosity of the polymer increases.

4.5.5- Effect of drug solubility

Drug solubility is a very important factor as high or low solubility can significantly affect the gel characteristics and drug release (Conte and Maggi, 1996; Gao *et al.*, 1996; Kim, 1999; Reynolds *et al.*, 2002). Ford *et al.* (1985a, 1985b and 1985c) studied the release of both water soluble (promethazine hydrochloride, aminophylline and propranolol hydrochloride) and poorly soluble (indomethacin) drugs from HPMC matrix systems. For indomethacin, both the

viscosity grade of HPMC and the particle size of the drug were reported to contribute more to controlling the drug release than was the case for water soluble drugs. This was primarily due to the erosion mechanism of drug release dominating in the case of poorly soluble drugs. High concentrations of insoluble drugs and excipients may cause non-uniform swelling of the hydrophilic matrix tablet. However, careful tailoring of the concentrations of insoluble drug and polymer in a system can be used to slow the dissolution rate of the insoluble drug (Ford *et al.*, 1987). It has been suggested that high-solubility drugs can release by diffusing through the gel matrices and this is considered to be the main pathway for their release. However, the drug release also occurs through erosion of the gel matrix. It is said that highly soluble drugs can also act as pore formers with the formation of micro-cavities, rendering the gel structure more porous and weaker, hence leading to increased drug release rates (Yang and Fassihi, 1997). However, poorly soluble drugs are released predominantly by erosion of the gel matrix, as the drug particles translocate and their presence compromises the structural integrity of the gel layer present on the surface of the matrix tablet, leading to drug release through matrix erosion (Bettini *et al.*, 2001). Several authors have studied whether the incorporation of highly water-soluble drugs into matrix systems with hydrophilic or hydrophobic polymers affects the drug release rate. Tramadol was formulated with HPMC or hydrogenated castor oil (HCO) and it was easier to modulate the release rate of the highly water-soluble drug from HPMC matrices than in those made of HCO (Tiwari *et al.*, 2003). Recently, Ghori *et al.* (2014) reported the same findings that the poorly soluble drug released predominately through erosion while the water soluble drug released through diffusion mechanism. Furthermore, Ghori *et al.* (2014) demonstrated that the values of the drug diffusion co-efficient of the Korsmeyer and Peppas model (n) is linearly related to erosion rate of FBP-based matrices, endorsing the view that poorly water soluble drugs are released mainly through an erosion mechanism.

Table 4.1, Summary of factors affecting drug release from Methocel[®] based hydrophilic matrices.

| Factor | Effect | Reference |
|--------------------------------|--|---|
| Effect of concentration | As the concentration of the Methocel [®] polymer increases, or the concentration of drug decreases, the drug release rate from tablet matrices decreases. | Campos-Aldrete and Villafuerte-Robles, 1997; Dabbagh <i>et al.</i> , 1996; Ebube <i>et al.</i> , 1997; Ford <i>et al.</i> , 1985b; Ghori <i>et al.</i> , 2014b; Jain <i>et al.</i> , 2014; Kim and Fassihi, 1997; Nellore <i>et al.</i> , 1998; Mitchell <i>et al.</i> , 1993; Reza <i>et al.</i> , 2003; Xu and Sunada, 1995. |
| Effect of particle size | The greater the particle size of the Methocel [®] powder, the faster the drug release rate from Methocel [®] tablet matrices. | Asare-Addo <i>et al.</i> , 2013b; Campos-Aldrete and Villafuerte-Robles, 1997; Caraballo, 2010; Dabbagh <i>et al.</i> , 1996; Dow, 2006, Escudero <i>et al.</i> , 2012; Heng <i>et al.</i> , 2001; Reza <i>et al.</i> , 2003; Mitchell <i>et al.</i> , 1993, Velasco <i>et al.</i> , 1999; Viridén <i>et al.</i> , 2009; Viridén <i>et al.</i> , 2010; Zuleger and Lippold, 2001. |
| Effect of substitution | Higher levels of the hydrophilic substitution group (Hpo) lead to decreased drug release from Methocel [®] tablet matrices. | Alderman, 1984; Doelker, 1990; Escudero <i>et al.</i> , 2010; Malamataris and Karidas, 1994; McCrystal <i>et al.</i> , 1999; Mitchell <i>et al.</i> , 1993, Sarkar and Rajabi-Siahboomi <i>et al.</i> , 1996 ; Walker, 1995. |
| Effect of viscosity | As the viscosity grade of the Methocel [®] polymer increases, the drug release rate from the tablet matrices decreases. | Campos-Aldrete and Villafuerte-Robles, 1997; Daly <i>et al.</i> , 1984; Gao <i>et al.</i> , 1996; Hiremath and Saha, 2008; Lee <i>et al.</i> , 1999; Li <i>et al.</i> , 2005; Nakano <i>et al.</i> , 1983; Maderuelo <i>et al.</i> , 2011; Salamone, 1996; Sarkar, 1979; Talukdar <i>et al.</i> , 1996; Ravi <i>et al.</i> , 2008; Wan <i>et al.</i> , 1991. |
| Drug solubility | As the solubility of the drug increases, the release rate from Methocel [®] tablet matrices increases. | Bettini <i>et al.</i> , 2001; Conte and Maggi, 1996; Ford <i>et al.</i> , 1985a; Ford <i>et al.</i> , 1985b; Ford <i>et al.</i> , 1987; Gao <i>et al.</i> , 1996; Ghori <i>et al.</i> , 2014b; Kim, 1999; Reynolds <i>et al.</i> , 2002; Tiwari <i>et al.</i> , 2003; Qiu <i>et al.</i> , 1997; Yang and Fassihi, 1997. |

4.6- Section A, Solubility and dissolution study of model drugs

4.6.1- Introduction

Oral ingestion is the most convenient and commonly employed route of drug delivery due to its ease of administration, high patient compliance, cost effectiveness, least sterility constraints and flexibility in the design of dosage forms (Wen and Park, 2011). As a result, many generic drug companies are inclined to produce oral drug products. However, before the drugs become available to their respective receptors, these need to be dissolved to be absorbed by passive diffusion across GI epithelium. Thus, the solubility and dissolution rate of active ingredients have a major importance in pre-formulation studies of pharmaceutical dosage forms. The solubility and intrinsic dissolution rate (IDR) have been used to characterise solid drugs for many years (Liu, 2008). Moreover, drug solubility has a significant impact on the drug diffusivity from the polymer matrices (see section 4.5.5 for more detail). As, the main focus of this research is to develop hydrophilic matrices using poorly and sparingly soluble model drugs, the aim of this set of experiments was to study the solubility and dissolution properties of model drugs before these were incorporated into hydrophilic matrices.

4.6.2- Experimental

4.6.2.1- Materials

4.6.1.1- Model drugs

Model drugs, FBP and THP were obtained as described in section 2.1.1.

4.6.2.1.2- Buffering agents

To prepare dissolution medium, buffering agents were purchased as described in section 2.1.3.

4.6.2.2- Methods

4.6.2.2.1- Solubility studies of model drugs

The drug (FBP or THP) solubility studies were carried out using the method described in section 2.2.2.

4.6.2.2.2- Tableting of model drugs

The model drugs (FBP or THP) were compacted by adopting the method described in section 2.2.7.1.

4.6.2.2.3- Determination of IDR of model drugs

The IDR of model drugs (FBP or THP) was determined using the method described in section 2.2.7.4.

4.6.3- Results and discussion

An understanding of solubility characteristics of a drug can be regarded as one of the most important aspect of pre-formulation studies involved in the development of hydrophilic matrices. As suggested by many authors, tablet matrices must have adequate solubility and release of incorporated drug candidates to attain suitable bioavailability (Alderman, 1984; Maderuelo *et al.*, 2011).

Figure 4.4 shows a typical plot of dissolution of plain FBP and THP compacts in pH 7.2 phosphate buffer (dissolution media). It is apparent from the results that the plain FBP and theophylline compacts have intrinsic dissolution rates of 0.53 (0.027) and 2.31 (0.075) $\text{mg min}^{-1}\text{cm}^{-2}$, respectively (Table 4.2). Moreover, the solubility of FBP and THP in sodium phosphate buffer (pH 7.2) is listed in Table 4.2. FBP has a solubility of 5.91 (0.22) mg/mL whereas THP has a solubility of 11.33 (0.75) mg/mL . The solubility and dissolution rate of FBP are significantly increased in comparison to the stated solubility (0.034 mg/mL , in water) and dissolution rate (0.330 $\text{mg min}^{-1}\text{cm}^{-2}$) in pH 6.8 buffer (Tavornvipas *et al.*, 2002, Miren, 2010). The mechanism behind the solubility and dissolution enhancement of FBP is thought to be the pH dependant ionisation, as the pH of the solvent (i.e. 7.2) is above its pK_a value, 4.22, (Xu and Madden, 2011) it is mainly ionised, and ionised forms of drugs are considered to have higher solubility and dissolution rate in given liquid media (Vogel, 2006). Like FBP, THP also showed an increased solubility and dissolution rate (Table 4.2) in sodium phosphate buffer (pH 7.2) in comparison to its reported solubility (7.3 mg/mL) and IDR (1.88 $\text{mg min}^{-1}\text{cm}^{-2}$) in water (Lee *et al.*, 2011; Yalkowsky *et al.*, 2010). Although, the pK_a of THP is reported to be 8.60 (acidic) and 0.3 (basic) (Brittain, 2007; Haeckel and Hanecke, 1996), it has been reported by various authors that with an increase in pH, THP showed a monotonically increase in its solubility and dissolution rate (Remington and Allen, 2013; Tiekink *et al.*, 2010). This might be because it behaves physiologically like an acid that might be the reason of solubility and dissolution rate enhancement.

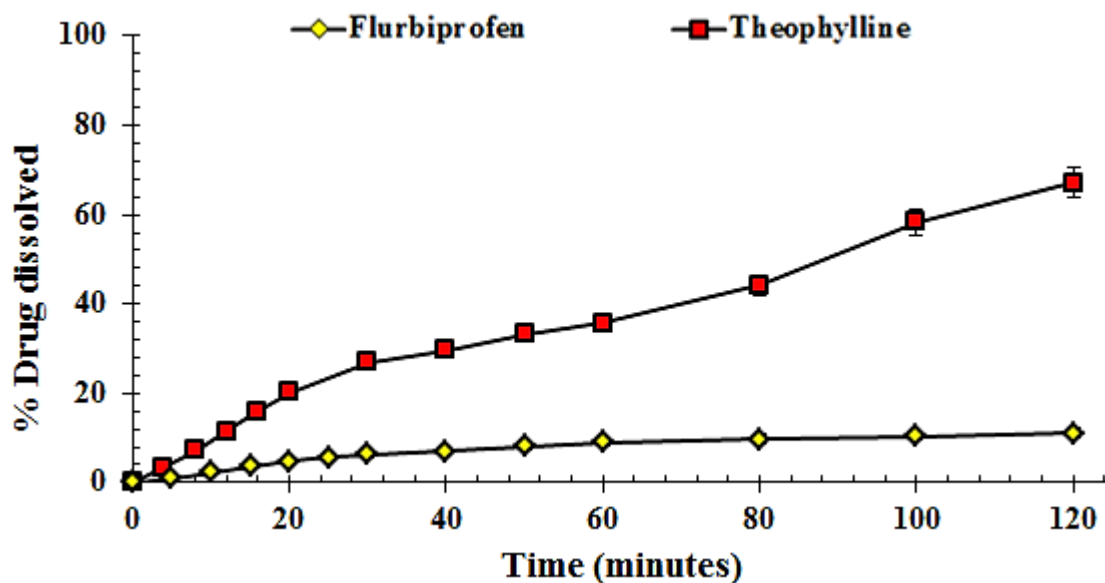


Figure 4.4, Dissolution profiles of FBP and THP compacts (n = 3).

Table 4.2, Solubility and dissolution parameters of FBP and THP (n = 3, standard deviation given in parenthesis)

| Drug | Solubility (mg/ml) | Dissolution rate parameters | | | |
|------------|--------------------|-----------------------------|---------------------------------|----------------|--|
| | | Slope | Surface area (cm ²) | R ² | IDR (mg min ⁻¹ cm ⁻²) |
| FBP | 5.91 (0.22) | 0.705 (0.12) | 1.3227 | 0.993 | 0.53 (0.027) |
| THP | 11.33 (0.75) | 3.050 (0.11) | 1.3227 | 0.998 | 2.31 (0.075) |

4.7- Section B, Swelling, erosion and dissolution properties of hydrophilic matrices.

4.7.1- Introduction

Over the years various types of polymers have been used in developing ER hydrophilic matrices, but the hydrophilic derivatives of cellulose ethers, more specifically methylcellulose (MC) and hypromellose (HPMC) to date are the most frequently employed hydrophilic polymers (Alderman, 1984; Maderuelo *et al.*, 2011), see sections 1.1 - 1.4 and 4.1 - 4.3 for more detail.

Once these hydrophilic matrices are exposed to aqueous media they swell quickly. The penetration of liquid decreases the glass transition temperature (T_g) and the polymer passes from an amorphous glassy to a rubbery state and a thick gelatinous layer develops around the circumference of matrix tablet, commonly known as a gel layer (Colombo *et al.*, 1999; Colombo *et al.*, 2000; Siepmann and Peppas, 2001). The gel layer grows over a period of time as more water penetrates into the matrix network which controls the release of drugs. Instantaneously, this outermost layer becomes fully hydrated and starts to relax, leading to the disentanglement of polymeric chains. Consequently, matrices start to dissolve from the surface, as water continuously permeates towards the core (Tiwari and Rajabi-Siahboomi, 2008), see section 4.4 for more detail.

To develop robust and realistically effective compressed hydrophilic matrices, a good understanding of polymer properties and, how any variation or modification can affect their performance and functionality, is critical. Swelling (liquid uptake), erosion and drug release from these hydrophilic matrices are important parameters. For this purpose, the aims and objectives of present set of experiments were to comparatively evaluate the swelling and

erosion properties of different Methocels[®] (MC and HPMC), with a view to understand how the particle size, substitution ratios and viscosity (molecular size) impact their performance. Moreover, MC and HPMC based matrix tablets, having poorly water soluble drug (FBP, 8.0 mg/L) or water soluble drug (THP, 7.3 g/L) (Yalkowsky *et al.*, 2010) with different polymer to drug ratios (5% – 15 % w/w) were also fabricated in order to study the impact of physico-chemical attributes related to MC and HPMC (particle size, molecular size (viscosity) and Hpo/Meo substitution levels) and drug solubility characteristics on swelling, erosion and drug release kinetics.

4.7.2- Experimental

4.7.2.1- Materials

4.7.2.1.1- Cellulose ethers

Cellulose ethers (MC/HPMC) were obtained as described in the section 2.1.1 and their specifications are enlisted in Table 2.1.

4.7.2.1.2- Model drugs

Model drugs, FBP (FBP) and THP (THP), were obtained as described in section 2.1.1.

4.7.2.1.3- Buffering agents

To prepare dissolution medium, buffering agents were purchased as described in section 2.1.3.

4.7.2.2- Methods

4.7.2.2.1- Preparation of powder mixtures

Binary powder mixtures of Methocel[®] polymers and model drugs were prepared adopting the method described in section 2.2.6.1.

4.7.2.2.2- Preparation of matrix tablets

The plain matrix tablets of Methocel[®] were compacted using the method described in section 2.2.6.2. For drug-containing matrix tablets, all the Methocel[®]: drug powder mixtures were prepared by adopting the method described in section 2.2.6.3.

4.7.2.2.3- Swelling and erosion studies

Swelling and erosion studies of all the matrix tablets were carried out by adopting gravimetric method described in section 2.2.6.4.

4.7.2.2.4- Swelling kinetics

Vergnaud mathematical models were applied to swelling data as described in section 2.2.6.5.

4.7.2.2.5- Drug release studies

The IDR of all the matrix tablets was determined using the method described in section 2.2.7.4.

4.7.2.2.6- Drug release kinetics

To understand the mechanism of drug release from the hydrophilic matrix tablets, zero order, first order, Higuchi and Korsmeyer– Peppas models were applied to drug release data as described in section 2.2.7.5.

4.7.3- Results and discussion

4.7.3.1- Swelling and erosion properties of plain Methocel[®] matrices

Swelling of the polymer matrix is dependent on the rate of liquid penetration. The liquid uptake measurement has been used primarily for evaluating the effect of polymer–liquid interaction. The water uptake (swelling) studies were carried out on all types of Methocels[®] listed in Table 4.3. The matrix tablets, having different particle sizes (90-150 and 150-250 μm) was immersed into the swelling media (pH 7.2 phosphate buffer) and their response is shown in Figure 4.5a and b, in terms of the weight increase (% swelling) due to penetration of liquid *versus* time. On contact with liquid, wetting occurs firstly at the surface and then progressing through the matrix network. The penetration of liquid essentially causes the T_g to fall and, as it becomes equal to the temperature of the system, the polymeric chains begin to relax. The penetrant liquid acted as a plasticizer and the matrices developed a viscous gel across matrix tablet surfaces, regardless of Methocel[®] grade (Colombo *et al.*, 1999; Colombo *et al.*, 2000), as previously explained in the section 4.4. The trend for extent of swelling across different grades of Methocel[®] in the present study was, A4M >F4M >E4M >K4M >K15M >K100M, (Figure 4.5). Moreover, over the period of time studied, the MC/HPMC polymer chains started to erode. The erosion profiles of all the Methocel[®] grades are depicted in Figure 4.6. The results of water uptake data were modelled using a method described by Vergnaud (1993), to determine the rate of water uptake (swelling), section 2.2.6.5. This Vergnaud model has been frequently adopted by different authors to evaluate the swelling mechanism of hydrophilic matrices. The swelling kinetics parameters of the current study have been summarised in Table 4.3.

4.7.3.1.1- Effect of Methocel[®] particle size

It is apparent from the present results that the extent of swelling, swelling kinetics and erosion properties of plain MC/HPMC matrices was markedly affected by the particle size. The MC/HPMC compacts fabricated from particles between 90 - 150 μm tend to have a higher swelling, but low extent of matrix erosion, in comparison to the compacts fabricated from larger polymer particles, 150 - 250 μm (Figure 4.5a and b). Large polymer particles take longer to hydrate and to develop a gel layer compared to smaller particles. The same behaviour has been noticed by various researchers in that fine MC/HPMC powder particles hydrate quickly because of their larger surface area and capability to quickly develop a gel layer around the tablet, which acts as a barrier, controlling the swelling, matrix erosion and drug release (Li *et al.*, 2005; Maderuelo *et al.*, 2011). So, it can be concluded from the present findings that the particle size can potentially affect the erosion properties of polymeric compacts and erosion rate can be modified using MC/HPMC with different particle sizes. It can also be inferred that swelling, or water uptake, by matrix tablets follows a diffusion-controlled mechanism as the swelling exponent (n) values for all the types of Methocel[®] were lower than 0.5. However, with decreasing particle size, the n values decreased, showing an enhancement in the extent of diffusion control on the swelling process. In addition, the higher values of swelling constants, which can be referred to as swelling rate, indicated a burst swelling pattern and rapid water uptake.

4.7.3.1.2- Effect of Methocel[®] substitution

The present results also demonstrate that the different Hpo/Meo substitution ratios in numerous grades of Methocel[®] impact swelling. The extent of swelling, swelling kinetic parameters and matrix erosion tend to decrease with an increase in Hpo/Meo ratios. To investigate the effect of substitution on swelling and erosion, A4M, F4M, E4M and K4M

were selected as these Methocel[®] grades have the same viscosity but different Hpo/Meo substitution ratios, (Table 2.1, Chapter 2). The A4M based matrices have the lowest swelling rate (36.69 and 41.01 % min⁻¹, Table 4.3) and it might be due to its relatively hydrophobic nature, as hydrophilic, hydroxypropyl groups are absent from their structure (Dow, 2006). The HPMC grades F4M and E4M show a slight difference, but swelling rate of K4M was significantly faster (62.09 and 48.03 % min⁻¹, Table 4.3). Furthermore, swelling kinetic parameters indicate a diffusion controlled mechanism, with faster swelling rates as compared to other polymers used in pharmaceutical formulations (Sinha Roy and Rohera, 2002). This disparity in swelling and erosion properties may be due to the variation in the levels (%) of Hpo groups. The increased degree of substitution of Hpo/Meo render Methocel[®] more hydrophilic and, it is evident from the previous studies, that the presence of higher levels (%) of Hpo groups leads to higher swelling and, in turn, a reduction in matrix erosion (Maderuelo *et al.*, 2011).

4.7.3.1.3- Effect of Methocel[®] viscosity (molecular size)

In the present study, MC/HPMC with different viscosities was investigated: K4M, K15M and K100M (see chapter 2, table 2.1 for detailed specifications). The swelling and erosion of plain MC/HPMC matrices decreased with increasing polymer viscosity/molecular weight. It was observed that the higher viscosity grade of HPMC (K100M) has fastest highest swelling rate but lowest extent of erosion (Table 4.3). This can be attributed to its ability to develop a thick gel layer which is resistant to erosion (Lee *et al.*, 1999). For high viscosity grades, their polymer chains tend to disentangle and increase the hydrodynamic volume within a matrix tablet, leading to increased swelling but a lower extent of erosion (Miller-Chou and Koenig, 2003). Moreover, the swelling kinetics parameters indicate that with the increased viscosity,

the swelling rate increased but n values decreased, indicating more diffusion-oriented swelling.

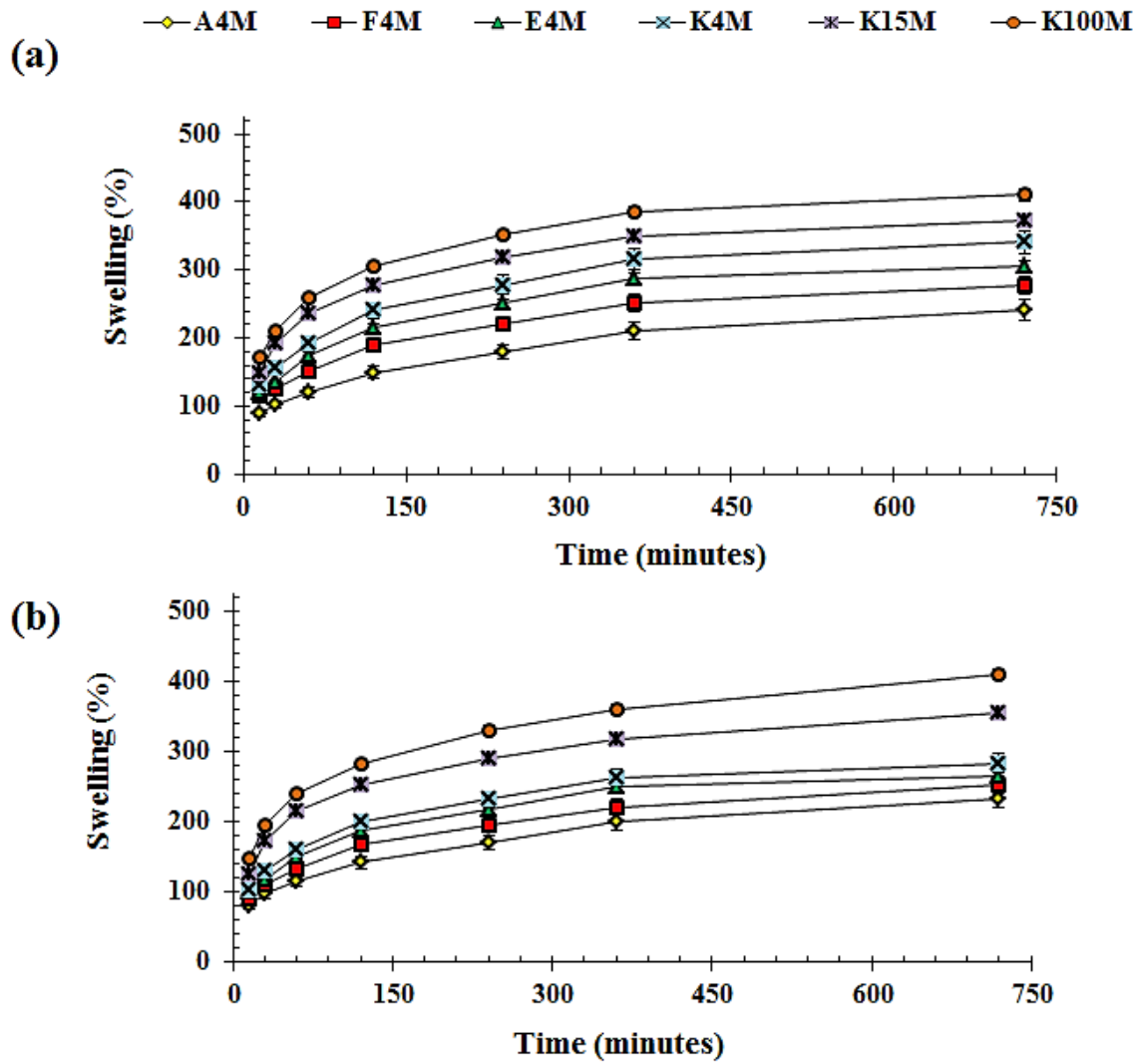


Figure 4.5, Swelling profiles of cellulose ethers based matrix tablets of particle size (a) 90-150 (b) 150-250 μm ($n = 3$).

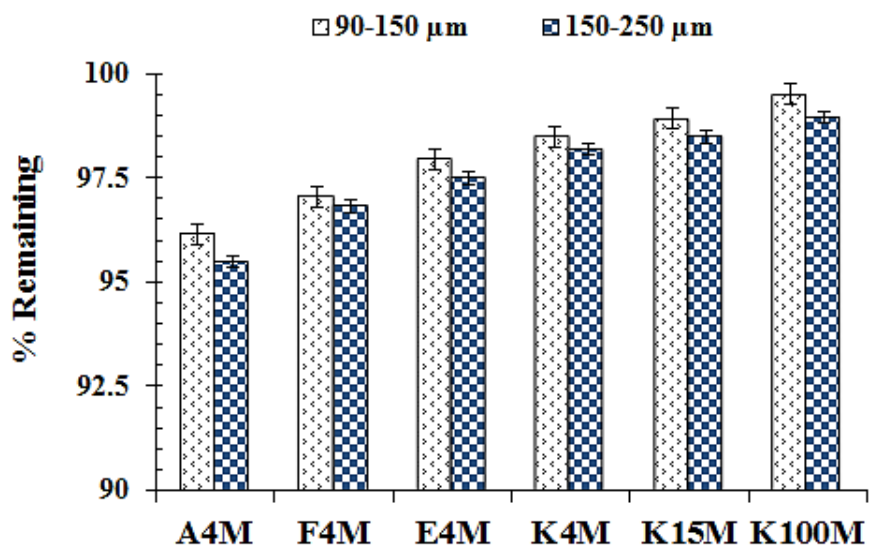


Figure 4.6, Comparative erosion of plain MC/HPMC compacts (n = 3).

Table 4.3, Swelling kinetics and erosion parameters of plain Methocel[®] compacts (n = 3, standard deviation given in parenthesis).

| Methocel [®] | Particle size (μm) | Swelling kinetics parameters | | | Erosion (%) |
|-----------------------|--------------------|------------------------------|----------------|----------------|-------------|
| | | K _w ^a | n ^b | R ² | |
| A4M | 90-150 | 41.01 | 0.269 | 0.995 | 3.85 (0.22) |
| | 150-250 | 36.69 | 0.281 | 0.997 | 4.52 (0.25) |
| F4M | 90-150 | 54.49 | 0.247 | 0.988 | 2.96 (0.39) |
| | 150-250 | 42.85 | 0.270 | 0.996 | 3.18 (0.11) |
| E4M | 90-150 | 55.33 | 0.259 | 0.982 | 2.05 (0.12) |
| | 150-250 | 45.23 | 0.269 | 0.982 | 2.51 (0.19) |
| K4M | 90-150 | 62.09 | 0.258 | 0.988 | 1.51 (0.09) |
| | 150-250 | 48.03 | 0.270 | 0.984 | 1.81(0.12) |
| K15M | 90-150 | 77.76 | 0.238 | 0.972 | 1.08 (0.05) |
| | 150-250 | 63.98 | 0.260 | 0.966 | 1.52 (0.03) |
| K100M | 90-150 | 89.74 | 0.231 | 0.978 | 0.51(0.01) |
| | 150-250 | 78.62 | 0.251 | 0.983 | 1.04 (0.02) |

Swelling constant = k (% min⁻¹), (b) Swelling exponent = n

4.7.3.2- Mixing efficiency for Methocel[®] : FBP/THP powders

A uniform drug distribution in a powder mixture is desirable during tablet preparation. The FBP/THP content uniformity results (n = 3) of powder mixtures are shown in Table 4.4, an acceptance limit of 95-105 % was set (see section 2.2.5.1, chapter 2). All powder blends used in subsequent studies fell between these limits.

Table 4.4, Content uniformity of powder mixture containing FBP and THP (n=3)

| Methocel [®] | Particle Size (μm) | Drug content (%) | | | | | |
|-----------------------|------------------------------------|---------------------------|-------------|-------------|-------------|-------------|-------------|
| | | Polymer concentration (%) | | | | | |
| | | FBP | | | THP | | |
| | | 5 | 10 | 15 | 5 | 10 | 15 |
| A4M | 90 – 150 | 98.2 (1.8) | 99.6 (2.5) | 98.6 (2.3) | 101.2(2.8) | 99.6 (3.1) | 100.5 (2.4) |
| | 150 – 250 | 96.3 (1.2) | 98.5 (2.1) | 99.2 (1.8) | 97.3 (0.5) | 99.3 (2.1) | 98.6 (1.6) |
| F4M | 90 – 150 | 98.5 (2.1) | 98.9 (1.0) | 101.3 (2.1) | 99.3 (1.9) | 98.3 (1.0) | 101.1 (2.1) |
| | 150 – 250 | 99.4 (1.3) | 98.3 (2.3) | 99.6 (1.5) | 100.5 (0.9) | 100.2 (2.2) | 96.3 (1.1) |
| E4M | 90 – 150 | 97.6 (1.4) | 100.5 (2.1) | 99.6 (2.5) | 98.3 (1.2) | 98.8 (2.5) | 99.3 (1.5) |
| | 150 – 250 | 97.4 (2.1) | 98.2 (1.5) | 98.2 (1.1) | 99.6 (1.5) | 100.8 (0.9) | 97.1 (1.3) |
| K4M | 90 – 150 | 99.32 (1.8) | 98.3 (2.5) | 96.3 (1.0) | 97.8 (2.0) | 101.0 (1.5) | 99.8 (2.5) |
| | 150 – 250 | 99.87 (1.3) | 102.5 (1.3) | 98.3 (2.0) | 101.5 (2.8) | 100.5 (2.3) | 99.2 (1.8) |
| K15M | 90 – 150 | 100.5 (1.7) | 99.3 (2.8) | 99.3 (1.8) | 100.5 (1.9) | 97.3 (0.2) | 98.3 (1.7) |
| | 150 – 250 | 98.63 (2.0) | 100.5 (1.9) | 98.3 (2.1) | 99.3 (1.3) | 99.8 (1.8) | 97.6 (0.7) |
| K100M | 90 – 150 | 99.57 (2.8) | 97.3 (1.8) | 100.5 (1.3) | 97.5 (2.4) | 97.5 (2.2) | 99.7 (1.5) |
| | 150 – 250 | 97.82 (1.0) | 98.3 (2.5) | 101.9 (2.8) | 98.6 (1.5) | 100.1 (1.3) | 97.8 (2.3) |

4.7.3.3- Swelling, erosion and dissolution studies of FBP/THP matrices

In the present experiments, swelling, erosion and dissolution properties of FBP-and THP-containing hydrophilic matrices were studied. The main problem in the formulation of these systems lies in achieving a suitable rate of drug release for intended application. However, the physico-chemical attributes of hydrophilic polymers and model drugs significantly affect the performance of these polymeric devices. In the following sections, swelling, erosion and dissolution data are presented with an in-depth mechanistic approach and discussion.

4.7.3.3.1- Effect of Methocel[®] concentration

The swelling, erosion and dissolution behaviours of Methocel[®] (MC/HPMC) are significantly affected by the component ratios, explained in section 4.5.1 (Alderman, 1984; Maderuelo *et al.*, 2011). Swelling, erosion and dissolution were studied for MC/HPMC:FBP and MC/HPMC:FBP hydrophilic matrices, with fixed MC/HPMC to drug (FBP/THP) loading ratios of 5, 10 and 15 w/w %.

The swelling results are depicted in Figures 4.7 (A4M), 4.11 (F4M), 4.15 (E4M), 4.19 (K4M), 4.23 (K15M) and 4.27 (K100M) as liquid uptake (% swelling) due to penetration of liquid *versus* time. The results showed that the extent of swelling (%) increased as the level of MC/HPMC was increased from 5% to 15% in matrices. The erosion of all the FBP and THP matrices was reduced with an increase in MC/HPMC concentration, Figures 4.8 (A4M), 4.12 (F4M), 4.16 (E4M), 4.20 (K4M), 4.24 (K15M) and 4.28 (K100M). The Vergnaud mathematical model was applied to determine the swelling rate (k) and swelling exponent (n) of all the drug based matrices, apart from A4M/FBP (5% and 10%), A4M/THP (5% and 10%), F4M/FBP (5%), F4M/THP (5%), E4M/FBP (5%), E4M/THP (5%) and K4M/FBP (5%), the extent of erosion precluded the application of kinetic swelling analysis. The kinetic swelling parameters for FBP and THP hydrophilic matrices for which the Vergnaud mathematical model was applicable, are summarised in Tables 4.5 (A4M), 4.8 (F4M), 4.11

(E4M), 4.14 (K4M), 4.18 (K15M) and 4.22 (K100M). The swelling exponents for FBP matrices were in the range of 0.5334 – 0.8302. However, n values of THP based matrices were in the range of 0.5120 – 0.7875. Swelling rates ranged between 5.90 – 45.72 (% min⁻¹) and 7.26 – 62.96 (% min⁻¹) for FBP and THP based matrices, respectively. Referring to the criteria of the Vergnaud mathematical model (section 2.2.6.5), the swelling behaviour of FBP and THP hydrophilic matrices is anomalous, with a n value between $0.45 < n < 1$, thus the diffusion of liquid and polymer chain relaxation are of similar magnitude. A reduction in n value with increasing MC/HPMC concentration, from 5% to 15%, can be attributed to diffusion-oriented swelling. However, an increase in the swelling rate suggested an enhanced liquid capturing and holding capacity, as it elicits a greater degree of physical cross-linking of MC/HPMC side chains (Mitchell *et al.*, 1993). These results demonstrated that the initial 5 min are an important period for all the drug -containing matrices to develop a gel layer. It was noticed that the matrices having 5% polymer content develop a very weak gel layer, having lower swelling but higher erosion compared to matrices with a higher polymeric content. From these findings, it can be inferred that at a 5% content, the polymers failed to develop a stable matrix network resulting in a weaker surface gel layer barrier.

Figures 4.9 (A4M/FBP), 4.10 (A4M/THP), 4.13 (F4M/FBP), 4.14 (F4M/THP), 4.17 (E4M/FBP), 4.18 (E4M/THP), 4.21 (K4M/FBP), 4.22 (K4M/THP), 4.25 (K15M/FBP), 4.26 (K15M/THP), 4.29 (K100M/FBP) and 4.30 (K100M/THP) depict the dissolution profiles of combination matrices. The dissolution data were presented as percentage drug release with respect to time. The intrinsic dissolution rates (IDR) of FBP matrices were in the range of 1.57 – 7.65 (mg min⁻¹ cm⁻²) and IDR of THP based matrices were between 2.12 – 12.76 (mg min⁻¹ cm⁻²), (Tables 4.6 (A4M), 4.9 (F4M), 4.12 (E4M), 4.15 (K4M), 4.18 (K15M) and 4.21 (K100M)). Both overall percentage and dissolution rates of FBP/THP reduced as the concentration of MC/HPMC was increased. The higher concentration of MC/HPMC have

resulted in a physical crosslinking, due to which the polymer chains are entangled leading to increased tortuosity and viscosity of the surface gel layer (Li et al., 2005; Maderuelo et al., 2011; Mitchell et al., 1993). Consequently, effective diffusion co-efficient of the drugs was reduced and a decline in the extent and rate of drug release is evident.

To further explore the mechanism of drug release from these matrix devices, zero-order, first-order, Korsmeyer- Peppas and Higuchi mathematical drug release models were applied to the drug release data (see section 2.2.7.5 for more detail). All the drug release kinetics parameters are summarised in Tables 4.7 (A4M), 4.10 (F4M), 4.13 (E4M), 4.16 (K4M), 4.19 (K15M) and 4.22 (K100M). The dissolution data follow first order and Korsmeyer- Peppas drug models most closely, indicating a combination of both erosion and diffusion as the controlling factors for drug release from the resultant matrix. According to the Korsmeyer - Peppas drug model, all the FBP and THP matrices showed anomalous drug release mechanisms (see section 2.2.7.5 for more detail). However, it can be noticed that with an increase in MC/HPMC concentration, the n value falls showing a more diffusion-oriented drug release from matrices.

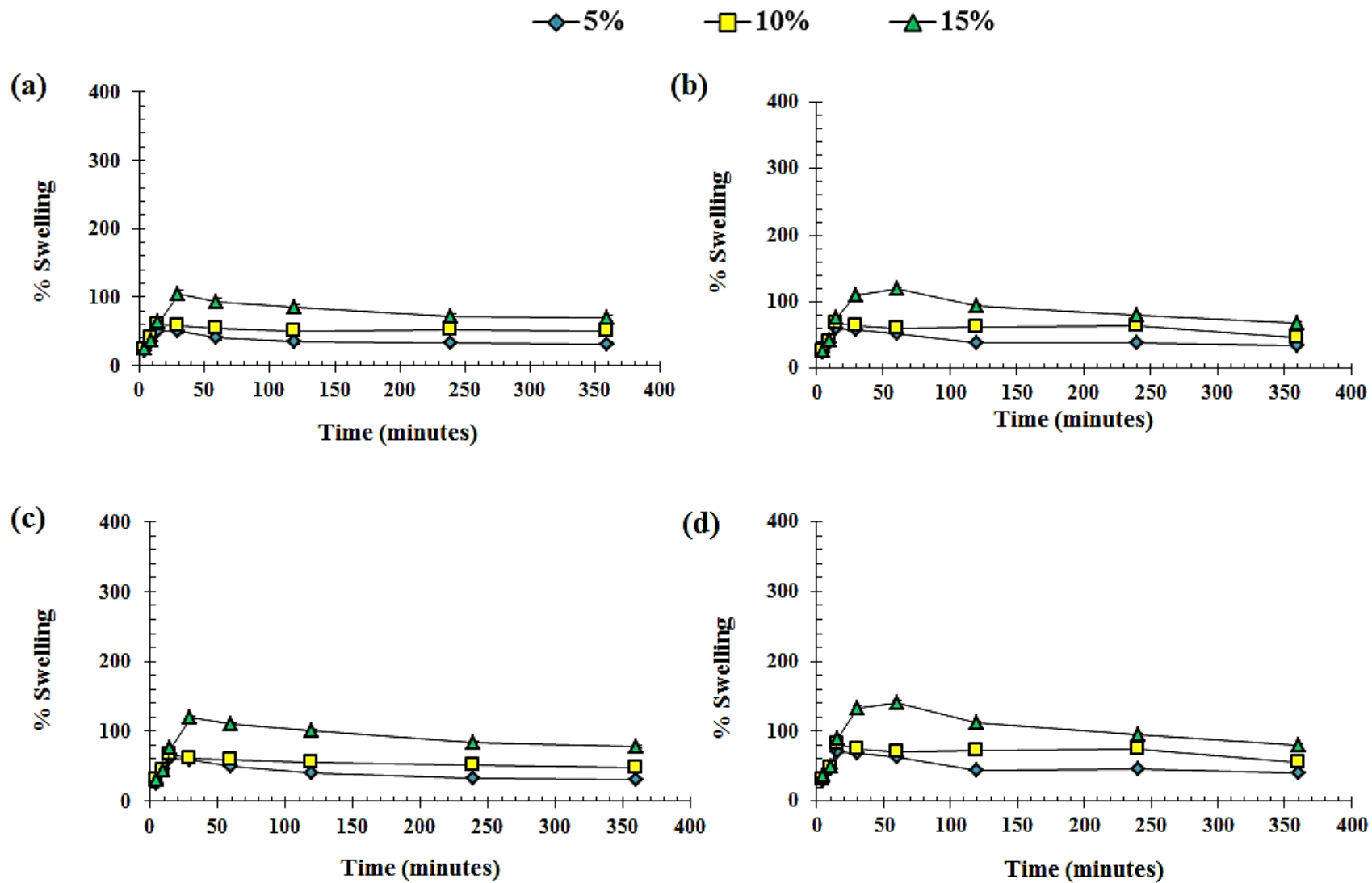


Figure 4.7, Swelling profiles of A4M/FBP, (a) 90-150 μm and (b) 150-250 μm and A4M/THP (c) 90-150 μm and (d) 150-250 μm hydrophilic matrices (n=3)

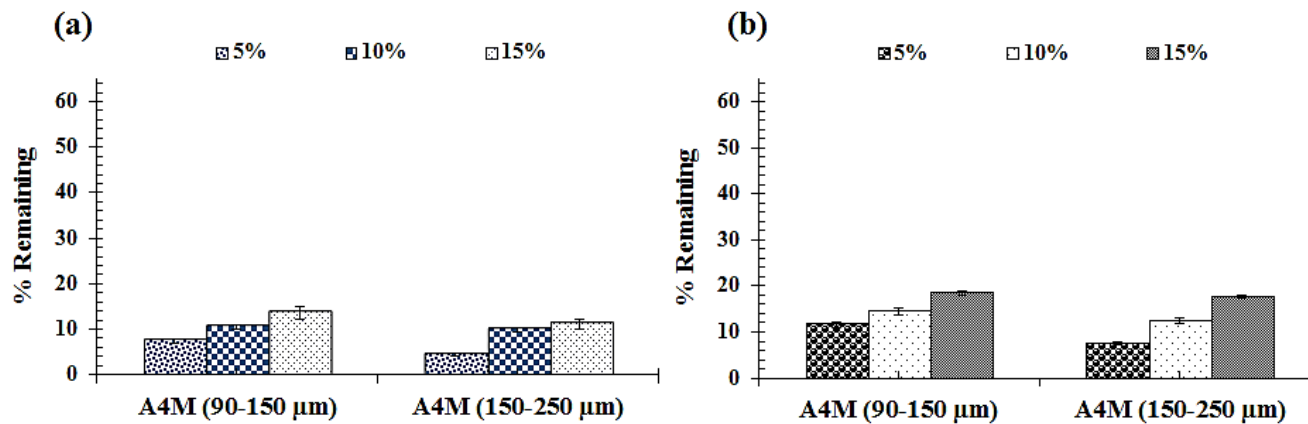


Figure 4.8, Comparative erosion of (a) A4M/FBP and (b) A4M/THP hydrophilic matrices (n=3)

Table 4.5, Swelling kinetics and matrix erosion of A4M based hydrophilic matrices (n = 3, standard deviation given in parenthesis)

| A4M (% w/w) | Particle size (μm) | Swelling kinetics parameters | | | | | | Erosion (%) | |
|----------------|-----------------------|------------------------------|------|--------|--------|-------|-------|--------------|--------------|
| | | k^a | | n^b | | R^2 | | FBP | THP |
| | | FBP | THP | FBP | THP | FBP | THP | | |
| 5 | 90-150 | ---- | ---- | ---- | ---- | ---- | ---- | 92.58 (2.22) | 88.35 (1.79) |
| | 150-250 | ---- | ---- | ---- | ---- | ---- | ---- | 95.64 (1.25) | 92.54 (2.21) |
| 10 | 90-150 | ---- | ---- | ---- | ---- | ---- | ---- | 89.58 (2.32) | 85.58 (2.33) |
| | 150-250 | ---- | ---- | ---- | ---- | ---- | ---- | 90.25 (1.89) | 87.69 (2.51) |
| 15 | 90-150 | 6.48 | 7.51 | 0.8117 | 0.7614 | 0.974 | 0.962 | 86.38 (1.09) | 81.55 (1.55) |
| | 150-250 | 5.90 | 7.26 | 0.8302 | 0.7875 | 0.981 | 0.975 | 88.99 (3.21) | 82.33 (2.89) |

(----, indicates Vergnaud model is not applicable because of matrix erosion)

(a) Swelling constant = k (% min⁻¹), (b) Swelling exponent = n

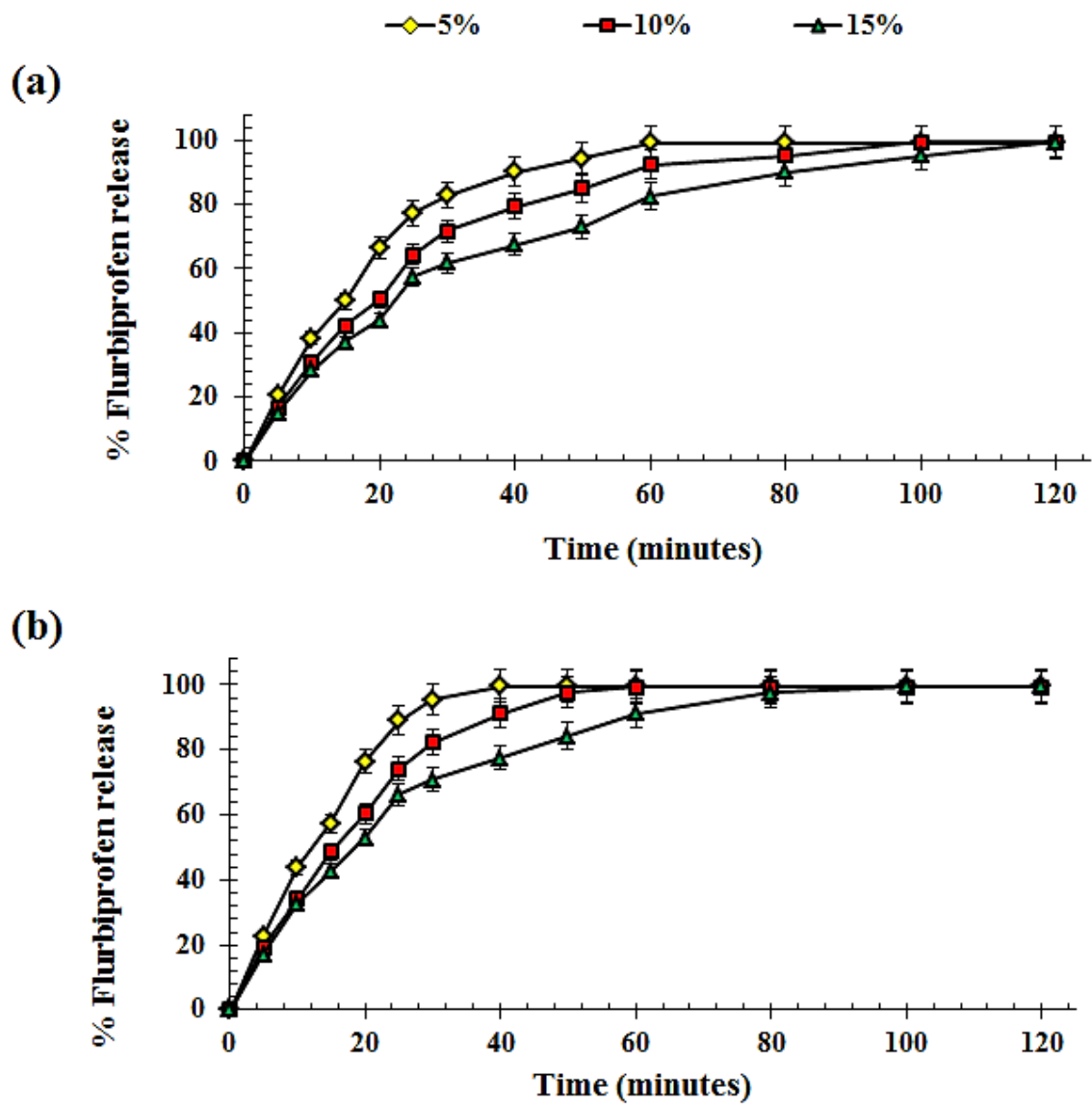


Figure 4.9, Dissolution profiles of A4M/FBP hydrophilic matrices having A4M particle size (a) 90-150 μm and (b) 150-250 μm (n=3).

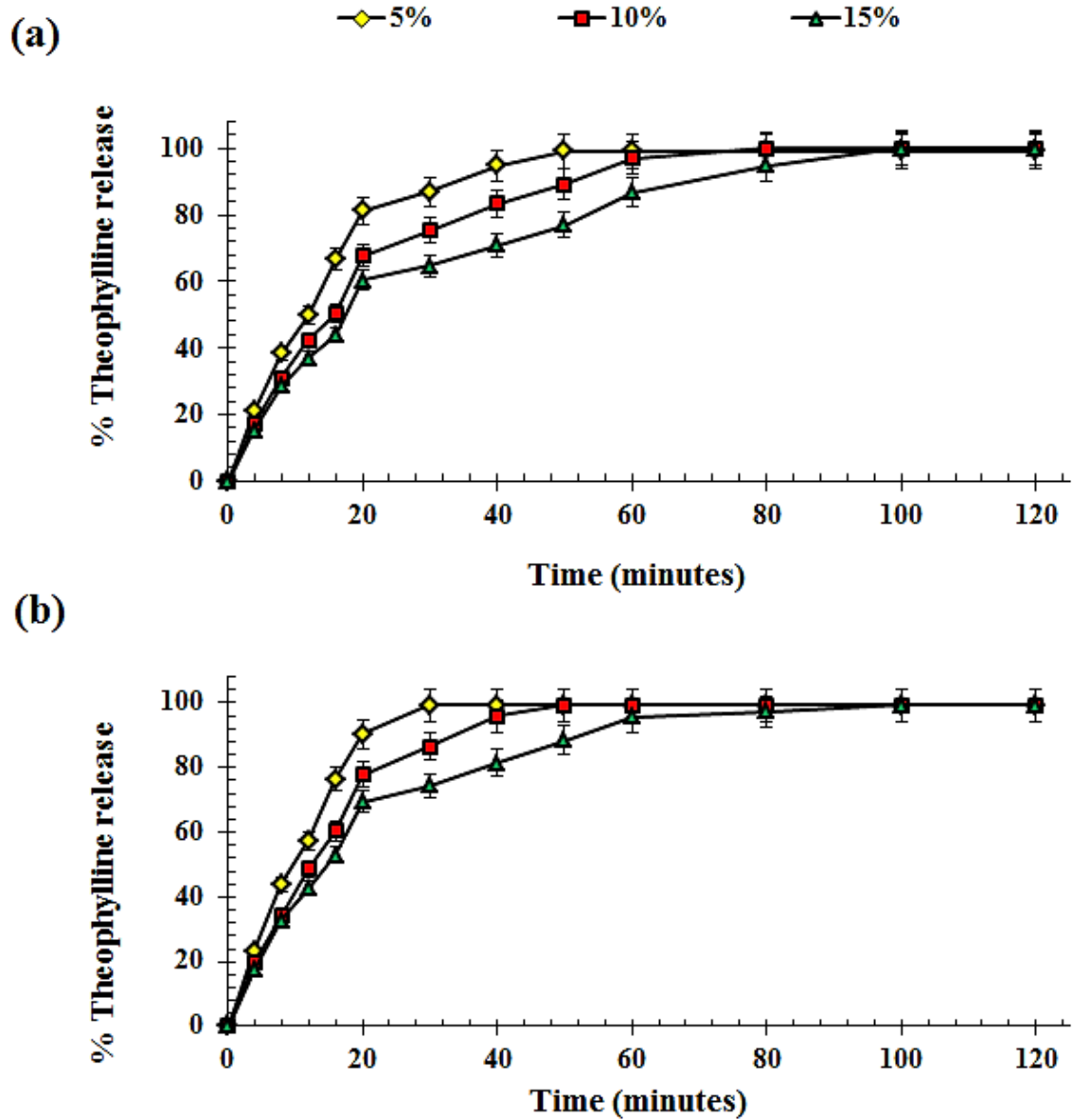


Figure 4.10, Dissolution profiles of A4M/THP hydrophilic matrices having A4M particle size (a) 90-150 μm and (b) 150-250 μm (n=3).

Table 4.6, Summary of dissolution parameters of A4M based hydrophilic matrices (n = 3, standard deviation given in parenthesis)

| A4M (% w/w) | Particle size (μm) | Dissolution rate parameters | | | | | |
|----------------|------------------------------------|-----------------------------|----------------|------------------|--------------|----------------|------------------|
| | | FBP | | | THP | | |
| | | Slope | R ² | IDR ^a | Slope | R ² | IDR ^a |
| 5 | 90-150 | 8.74 (0.33) | 0.988 | 6.61 (0.33) | 11.29 (0.51) | 0.984 | 8.54 (0.43) |
| | 150-250 | 10.12 (0.44) | 0.971 | 7.65 (0.38) | 12.76 (0.38) | 0.975 | 9.65 (0.48) |
| 10 | 90-150 | 6.70 (0.28) | 0.981 | 5.07 (0.25) | 8.66 (0.25) | 0.988 | 6.55 (0.33) |
| | 150-250 | 7.85 (0.51) | 0.989 | 5.93 (0.30) | 10.14 (0.67) | 0.991 | 7.67 (0.38) |
| 15 | 90-150 | 5.58 (0.37) | 0.982 | 4.22 (0.21) | 7.21 (0.29) | 0.985 | 5.45 (0.27) |
| | 150-250 | 6.53 (0.42) | 0.988 | 4.94 (0.25) | 8.44 (0.36) | 0.987 | 6.38 (0.32) |

(a) Intrinsic dissolution rate = IDR ($\text{mg min}^{-1} \text{cm}^{-2}$)

Table 4.7, Summary of drug release kinetics parameters from A4M based hydrophilic matrices (n=3).

| A4M (%, w/w) | Particle size (μm) | Zero order model | | | | First order model | | | | Korsmeyer- Peppas model | | | | | Higuchi model | | | | |
|-----------------|------------------------------------|-----------------------------|----------------|-----------------------------|----------------|-----------------------------|----------------|-----------------------------|----------------|-----------------------------|----------------|----------------|-----------------------------|----------------|----------------|-----------------------------|----------------|-----------------------------|----------------|
| | | FBP | | THP | | FBP | | THP | | FBP | | | THP | | FBP | | THP | | |
| | | K ₀ ^a | R ² | K ₀ ^a | R ² | K ₁ ^b | R ² | K ₁ ^b | R ² | K _p ^c | n ^d | R ² | K _p ^c | n ^d | R ² | K _h ^e | R ² | K _h ^e | R ² |
| 5 | 90-150 | 3.41 | 0.987 | 5.70 | 0.981 | 0.049 | 0.983 | 0.083 | 0.985 | 5.39 | 0.83 | 0.996 | 8.47 | 0.82 | 0.996 | 13.14 | 0.942 | 16.99 | 0.945 |
| | 150-250 | 3.92 | 0.989 | 6.55 | 0.978 | 0.061 | 0.991 | 0.102 | 0.989 | 5.96 | 0.86 | 0.994 | 9.48 | 0.84 | 0.996 | 15.08 | 0.938 | 19.51 | 0.942 |
| 10 | 90-150 | 2.71 | 0.973 | 4.52 | 0.971 | 0.036 | 0.997 | 0.060 | 0.998 | 5.28 | 0.80 | 0.995 | 7.98 | 0.78 | 0.997 | 10.49 | 0.960 | 13.57 | 0.964 |
| | 150-250 | 3.17 | 0.987 | 5.29 | 0.986 | 0.044 | 0.994 | 0.074 | 0.991 | 5.18 | 0.82 | 0.999 | 8.07 | 0.81 | 0.999 | 12.21 | 0.947 | 15.79 | 0.950 |
| 15 | 90-150 | 2.39 | 0.961 | 3.99 | 0.955 | 0.031 | 0.998 | 0.051 | 0.999 | 5.14 | 0.78 | 0.989 | 7.62 | 0.76 | 0.991 | 9.26 | 0.966 | 11.98 | 0.970 |
| | 150-250 | 2.81 | 0.975 | 4.70 | 0.984 | 0.038 | 0.992 | 0.063 | 0.992 | 5.34 | 0.80 | 0.994 | 8.06 | 0.79 | 0.995 | 10.88 | 0.958 | 14.07 | 0.961 |

(a) Zero order constant = K₀ (% min⁻¹), (b) First order constant = K₁ (% min⁻¹), (c) Korsmeyer- Peppas constant = K_p (% min⁻¹), (d) Diffusional exponent = n, (e) Higuchi constant = K_h (% min^{-1/2})

4.7.3.3.2- Effect of Methocel[®] particle size

The effect of Methocel[®] (MC/HPMC) particle size on the swelling, erosion and drug release behaviour of tablet matrices has been studied by various authors and it is generally concluded that an adequate particle size of MC/HPMC in a matrix tablet is necessary to attain specific extended drug release objectives (see section 4.5.2 for more detail).

In the course of current investigations, swelling of all the drug (FBP/THP) containing hydrophilic matrices, having MC/HPMC of different particle sizes (90 -150 μm and 150-250 μm), was studied. It is evident from the results that particle size had an impact on the swelling profiles of matrices. As the particle size of MC/HPMC is increased from 90-150 μm to 150-250 μm , the swelling (%) tends to decrease, regardless of drug solubility and levels (% w/w) of MC/HPMC (Figures 4.7 (A4M), 4.11 (F4M), 4.15 (E4M), 4.19 (K4M), 4.23 (K15M) and 4.27 (K100M)). The erosion profiles of FBP and THP based matrices are shown in Figures 4.8 (A4M), 4.12 (F4M), 4.16 (E4M), 4.20 (K4M), 4.24 (K15M) and 4.28 (K100M) and results are reported as % remaining of tablet matrices after the swelling phenomena. It can be inferred from the erosion results that the reduction of particle size reduces erosion of the matrix. So, it can be assumed from these findings that reducing particle size may be helpful in preventing pre-mature tablet disintegration by developing a more stable gel layer on the surface of the tablet. This trend of swelling and erosion can be explained using the theory postulated by Mitchell *et al.* (1993), that a larger particle size of MC/HPMC promotes disintegration, as they need a longer time for hydration and the larger the polymer particle can leave pores on the surface of matrices, which have a tendency to impair the integrity of the gel layer present on the tablet surface. Instead, matrices constructed using a smaller size tends to hydrate quickly and this behaviour can be attributed to the larger surface area presented in the matrices.

The swelling kinetic parameters of FBP and THP hydrophilic matrices indicated an anomalous mechanism, (Tables 4.5 (A4M), 4.8 (F4M), 4.11 (E4M), 4.14 (K4M), 4.18 (K15M) and 4.22 (K100M)). Reducing particle size results in the decline of n value, showing the dominance of diffusion controlled swelling processes. On the other hand the swelling rates increased with a reduction of HPMC/MC particle size, regardless of drug and level of MC/HPMC (% w/w).

The extent of drug release (%) profiles of all the matrices exhibited a reduction as the MC/HPMC particle size was reduced from 150 - 250 μm to 90-150 μm , (Figures 4.9 (A4M/FBP), 4.10 (A4M/THP), 4.13 (F4M/FBP), 4.14 (F4M/THP), 4.17 (E4M/FBP), 4.18 (E4M/THP), 4.21 (K4M/FBP), 4.22 (K4M/THP), 4.25 (K15M/FBP), 4.26 (K15M/THP), 4.29 (K100M/FBP) and 4.30 (K100M/THP)). Moreover, the IDRs from all the matrices having smaller particle size MC/HPMC were slower, (Tables 4.6 (A4M), 4.9 (F4M), 4.12 (E4M), 4.15 (K4M), 4.16 (K15M) and 4.21 (K100M)). This behaviour can be explained assuming that larger MC/HPMC particles require more time to swell prior to the polymer chains becoming mobile and binding together to the gel layer, which can eventually dictate the drug release. Additionally, zero-order, first-order, Korsmeyer- Peppas and Higuchi mathematical drug release models were applied to the drug release data (see section 2.2.7.5 for more detail). The drug release kinetic parameters indicated a combination of both erosion and diffusion (anomalous) as the controlling factors, Tables 4.7 (A4M), 4.10 (F4M), 4.13 (E4M), 4.16 (K4M), 4.19 (K15M) and 4.22 (K100M)). Moreover, with the reduction of MC/HPMC particle size, the n value fell showing a more diffusion oriented drug release from the tablet matrix. This response may be because of faster swelling of smaller MC/HPMC particles (as explained earlier) that allow the rapid gel layer formation on the surface of matrix tablet.

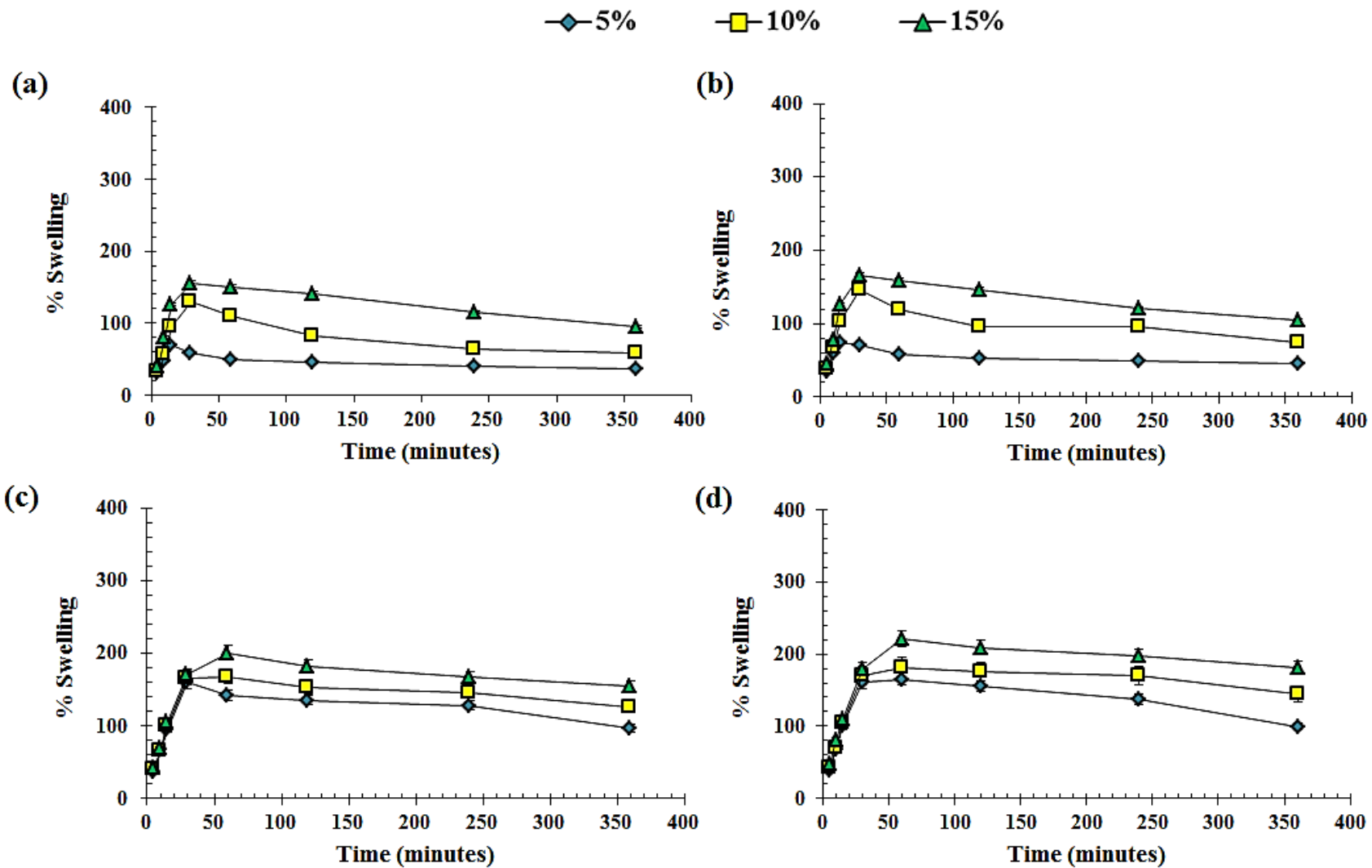


Figure 4.11, Swelling profiles of F4M/FBP, (a) 90-150 μm and (b) 150-250 μm and F4M/THP (c) 90-150 μm and (d) 150-250 hydrophilic matrices (n=3).

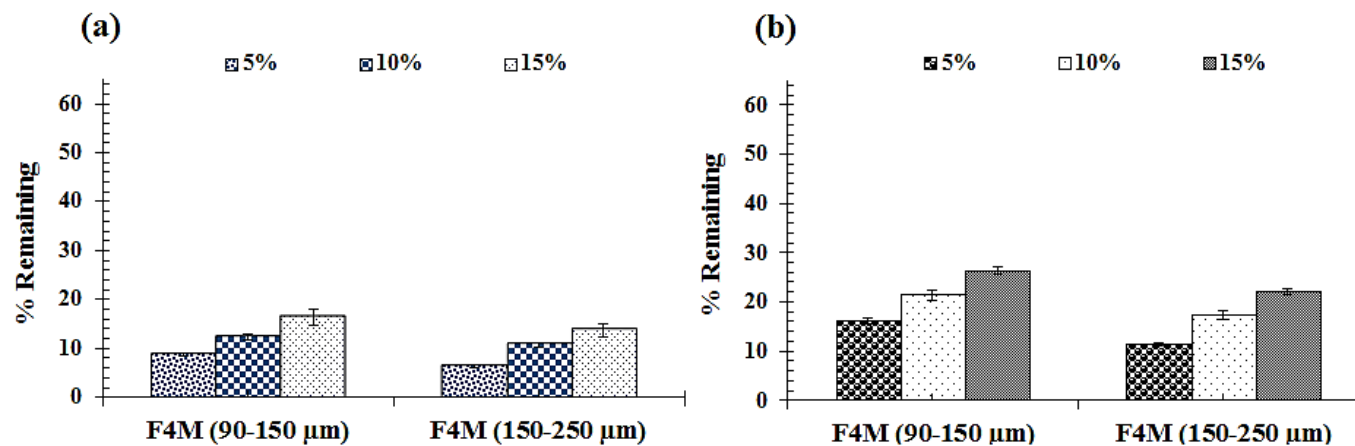


Figure 4.12, Comparative erosion of (a) F4M/FBP and (b) F4M/THP hydrophilic matrices (n=3).

Table 4.8, Swelling kinetics and matrix erosion of F4M based hydrophilic matrices (n = 3, standard deviation given in parenthesis)

| F4M (%, w/w) | Particle size (μm) | Swelling kinetics parameters | | | | | | Erosion (%) | |
|-----------------|-----------------------|------------------------------|-------|--------|--------|-------|-------|--------------|--------------|
| | | k^a | | n^b | | R^2 | | FBP | THP |
| | | FBP | THP | FBP | THP | FBP | THP | | |
| 5 | 90-150 | ---- | 10.75 | ---- | 0.7944 | ---- | 0.996 | 91.25 (1.86) | 83.87 (0.55) |
| | 150-250 | ---- | 9.56 | ---- | 0.8271 | ---- | 0.997 | 93.65 (2.29) | 88.69 (2.20) |
| 10 | 90-150 | 11.02 | 12.02 | 0.7604 | 0.7801 | 0.982 | 0.997 | 87.66 (2.14) | 78.68 (1.89) |
| | 150-250 | 8.51 | 10.82 | 0.8029 | 0.8002 | 0.969 | 0.994 | 89.36 (2.33) | 82.58 (1.77) |
| 15 | 90-150 | 13.74 | 14.47 | 0.7387 | 0.7389 | 0.967 | 0.999 | 83.69 (2.51) | 73.65 (2.02) |
| | 150-250 | 11.17 | 11.72 | 0.7741 | 0.7869 | 0.933 | 0.995 | 86.32 (1.05) | 77.88 (2.09) |

(----, indicates Vergnaud model is not applicable because of early matrix erosion)

(a) Swelling constant = k (% min^{-1}), (b) Swelling exponent = n

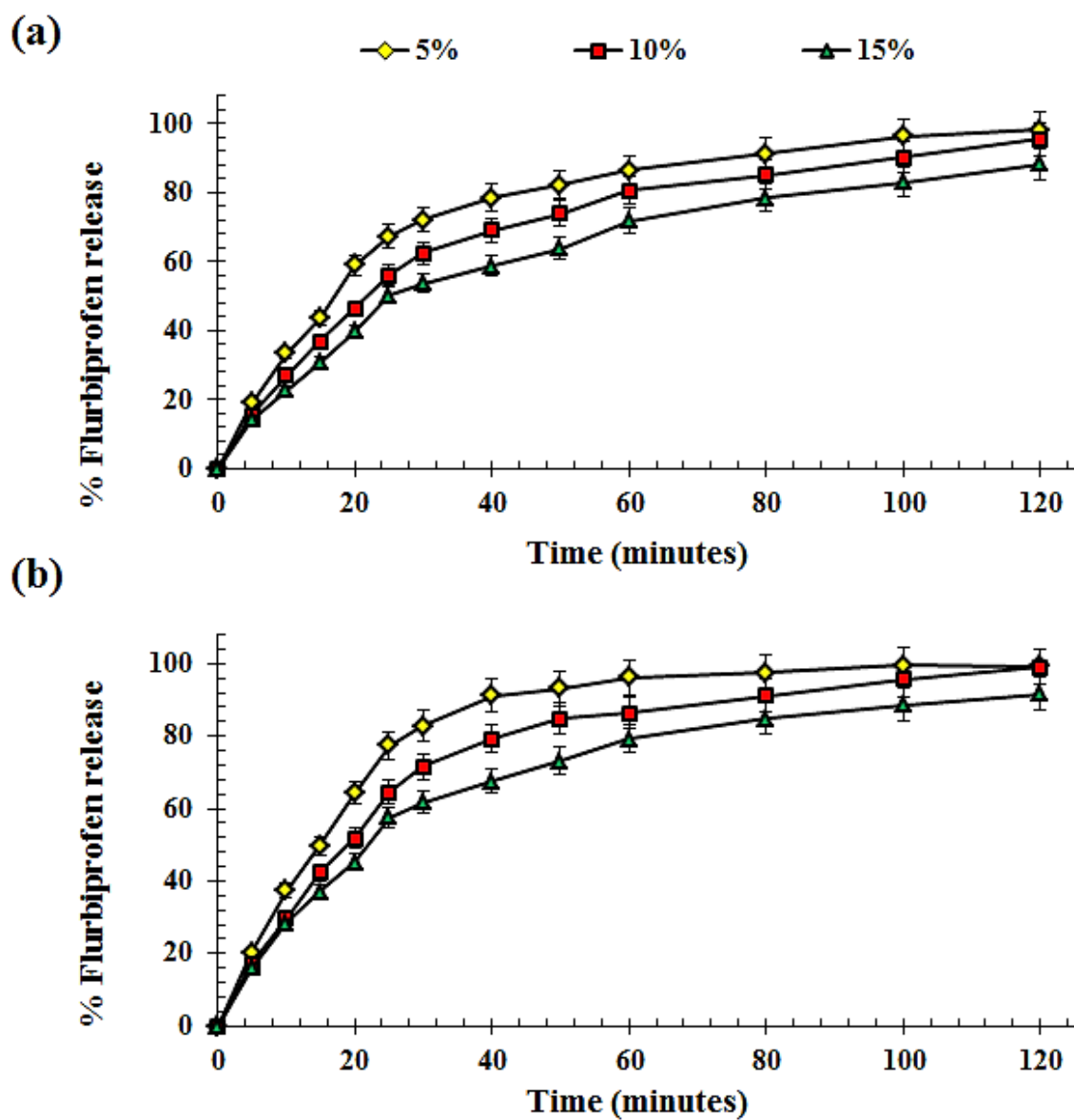


Figure 4.13, Dissolution profiles of F4M/FBP hydrophilic matrices having F4M particle size (a) 90-150 μm and (b) 150-250 μm (n=3).

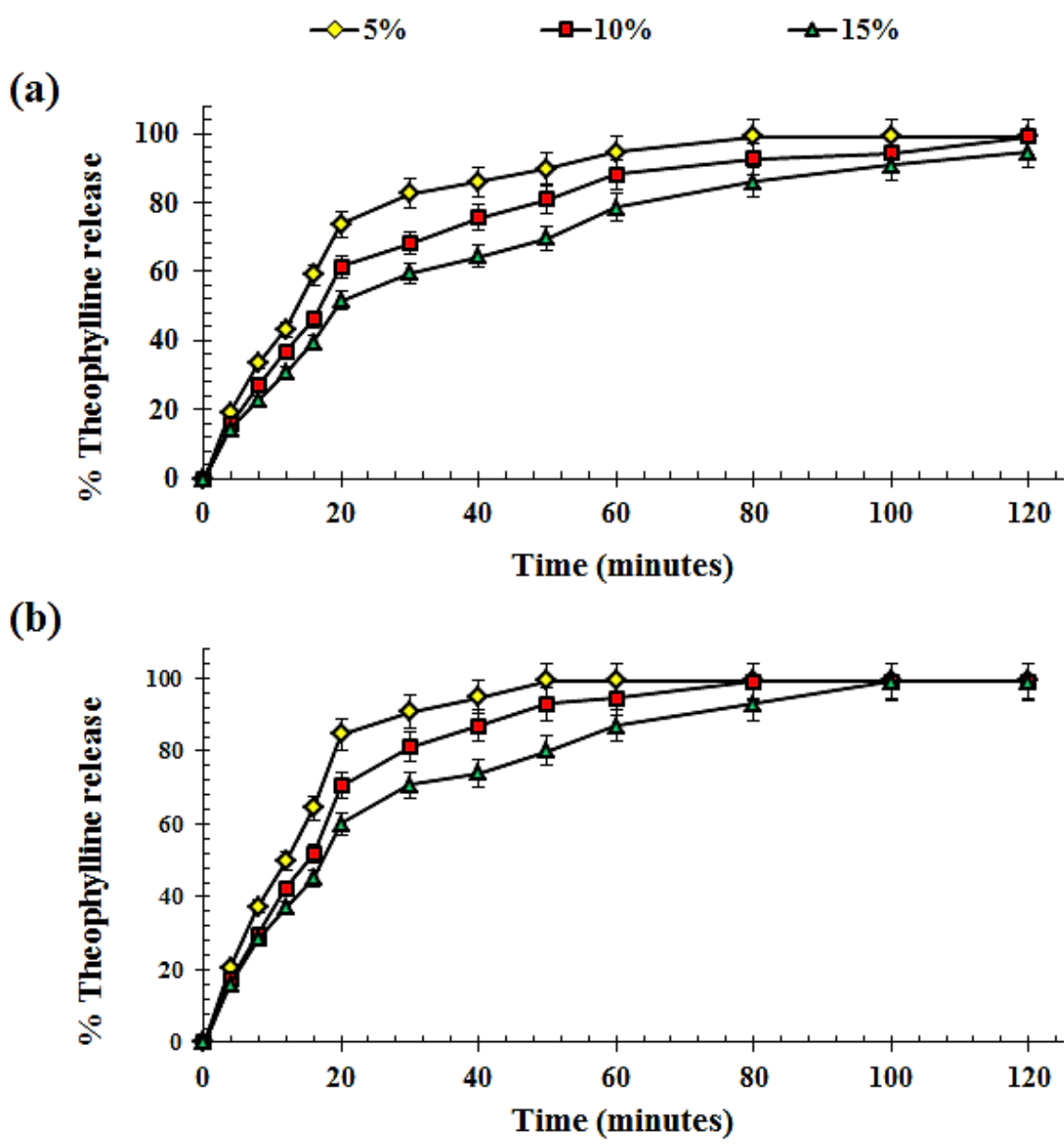


Figure 4.14, Dissolution profiles of F4M/THP hydrophilic matrices having F4M particle size (a) 90-150 µm and (b) 150-250 µm (n = 3).

Table 4.9, Summary of dissolution parameters of F4M based hydrophilic matrices (n = 3, standard deviation given in parenthesis)

| F4M (%, w/w) | Particle size (μm) | Dissolution rate parameters | | | | | |
|-----------------|------------------------------------|-----------------------------|----------------|------------------|--------------|----------------|------------------|
| | | FBP | | | THP | | |
| | | Slope | R ² | IDR ^a | Slope | R ² | IDR ^a |
| 5 | 90-150 | 7.60 (0.25) | 0.992 | 5.75 (0.29) | 10.13 (0.51) | 0.987 | 8.54 (0.43) |
| | 150-250 | 8.68 (0.18) | 0.993 | 6.57 (0.33) | 11.59 (0.38) | 0.992 | 9.65 (0.48) |
| 10 | 90-150 | 5.90 (0.27) | 0.986 | 4.46 (0.22) | 7.86 (0.25) | 0.990 | 6.55 (0.33) |
| | 150-250 | 6.77 (0.59) | 0.987 | 5.12 (0.26) | 9.04 (0.67) | 0.993 | 7.67 (0.38) |
| 15 | 90-150 | 4.87 (0.79) | 0.991 | 3.68 (0.18) | 6.22 (0.29) | 0.992 | 5.45 (0.27) |
| | 150-250 | 5.60 (0.42) | 0.992 | 4.23 (0.21) | 7.22 (0.36) | 0.980 | 6.38 (0.32) |

(a) *Intrinsic dissolution rate = IDR (mg min⁻¹ cm⁻²)*

Table 4.10, Summary of drug release kinetics parameters of F4M based hydrophilic matrices (n = 3).

| F4M (%, w/w) | Particle size (μm) | Zero order model | | | | First order model | | | | Korsmeyer- Peppas model | | | | | Higuchi model | | | | |
|-----------------|------------------------------------|-----------------------------|----------------|-----------------------------|----------------|-----------------------------|----------------|-----------------------------|----------------|-----------------------------|----------------|----------------|-----------------------------|----------------|----------------|-----------------------------|----------------|-----------------------------|----------------|
| | | FBP | | THP | | FBP | | THP | | FBP | | THP | | | FBP | | THP | | |
| | | K ₀ ^a | R ² | K ₀ ^a | R ² | K ₁ ^b | R ² | K ₁ ^b | R ² | K _p ^c | n ^d | R ² | K _p ^c | n ^d | R ² | K _h ^e | R ² | K _h ^e | R ² |
| 5 | 90-150 | 3.01 | 0.984 | 4.18 | 0.982 | 0.041 | 0.992 | 0.052 | 0.995 | 4.86 | 0.80 | 0.995 | 5.98 | 0.78 | 0.994 | 11.58 | 0.944 | 12.97 | 0.946 |
| | 150-250 | 3.34 | 0.985 | 3.76 | 0.985 | 0.048 | 0.995 | 0.060 | 0.996 | 5.56 | 0.82 | 0.998 | 6.81 | 0.81 | 0.999 | 12.88 | 0.948 | 14.42 | 0.950 |
| 10 | 90-150 | 2.43 | 0.981 | 3.42 | 0.980 | 0.031 | 0.999 | 0.039 | 0.998 | 4.36 | 0.79 | 0.998 | 5.37 | 0.77 | 0.999 | 9.37 | 0.956 | 10.50 | 0.959 |
| | 150-250 | 2.74 | 0.983 | 3.04 | 0.981 | 0.036 | 0.998 | 0.046 | 0.995 | 4.79 | 0.80 | 0.999 | 5.81 | 0.79 | 0.999 | 10.56 | 0.953 | 11.82 | 0.955 |
| 15 | 90-150 | 2.06 | 0.971 | 3.04 | 0.975 | 0.025 | 0.993 | 0.032 | 0.991 | 3.96 | 0.73 | 0.997 | 4.80 | 0.71 | 0.995 | 7.98 | 0.961 | 8.93 | 0.963 |
| | 150-250 | 2.44 | 0.965 | 2.58 | 0.963 | 0.031 | 0.995 | 0.039 | 0.995 | 5.20 | 0.75 | 0.996 | 6.22 | 0.74 | 0.993 | 9.43 | 0.969 | 10.55 | 0.971 |

(a) *Zero order constant = K₀(% min⁻¹), (b) First order constant = K₁(% min⁻¹), (c) Korsmeyer- Peppas constant = K_p (% min⁻¹), (d) Diffusional exponent = n, (e) Higuchi constant = K_h (% min^{-1/2})*

4.7.3.3- Effect of Methocel[®] substitution

The type and levels of substituents which are integrated on polymer chains of Methocel[®] have the potential to significantly impact the swelling, erosion and drug characteristics of matrices (Alderman, 1984). In the present study experiments were conducted to investigate the influence of substitution ratios (Hpo/Meo) on swelling, erosion and dissolution properties. For comparative purposes, A4M, F4M, E4M and K4M were selected because these Methocel[®] grades essentially have almost similar viscosity ranges but different Hpo/Meo substitution ratios, A4M = 0.238, F4M = 0.286, E4 = 0.381 and K4M = 0.403, Table 2.1 (Chapter 2).

The present results revealed the impact of Hpo/Meo ratios on the swelling profiles of matrices. As the Hpo/Meo ratios increased from 0.238 to 0.403, the swelling (%) tended to decrease, regardless of drug solubility and levels (% w/w) of MC/HPMC, (Figures 4.7 (A4M), 4.11 (F4M), 4.15 (E4M) and 4.19 (K4M)). Furthermore, it is evident that increasing Hpo/Meo ratios reduced matrix erosion, (Figures 4.8 (A4M), 4.12 (F4M), 4.16 (E4M) and 4.20 (K4M)). The swelling kinetic parameters of FBP and THP hydrophilic matrices showed an anomalous mechanism, (Tables 4.5 (A4M), 4.8 (F4M), 4.11 (E4M) and 4.14 (K4M)). Increasing Hpo/Meo substitution ratios caused n values to decrease, demonstrating a diffusion controlled swelling process. On the other hand, the swelling rates increased with a reduction in Hpo/Meo substitution ratios, regardless of drug and levels of MC/HPMC (% w/w). These swelling and erosion findings may be due to the solubility of the substitution groups, as Hpo are hydrophilic substituents groups, however, Meo groups are hydrophobic. Moreover, the higher levels (%) of Hpo in comparison to Meo may have increased the water holding capacity of macromolecular chains of MC/HPMC (Dow, 2006).

Drug release (%) and IDRs of all the matrices exhibited a reduction as the Hpo/Meo substitution ratios were increased, (Figures 4.9 (A4M/FBP), 4.10 (A4M/THP), 4.13 (F4M/FBP), 4.14 (F4M/THP), 4.17 (E4M/FBP), 4.18 (E4M/THP), 4.21 (K4M/FBP) 4.22 (K4M/THP) and Tables 4.7 (A4M), 4.10 (F4M), 4.13 (E4M) and 4.16 (K4M)). Additionally, zero-order, first-order, Korsmeyer- Peppas and Higuchi mathematical drug release models indicted an anomalous drug release mechanism, (Tables 4.7 (A4M), 4.10 (F4M), 4.13 (E4M) and 4.16 (K4M)). However, it was noticed that as the Hpo/Meo substitution ratios increased, the n value fell, showing a more diffusion dominant drug release behaviour. This is likely due to faster swelling at higher Hpo/Meo substitution ratios, which facilitates rapid gel layer formation on the surface of matrix tablet. The substituents of a MC/HPMC side chain alter its polarity, melting point and crystallinity. This affects the solubility of the MC/HPMC in water. In general, the aqueous solubility of any polymer can be related to its ability to establish hydrogen bonds between the hydrogen atoms of the water and those of the oxygen present in the side chain and the substituents of the polymer (Sarkar and Walker, 1995). In this particular case, the type of substitution does not only influence the solubility of the polymer in water, but also the gel strength, the swelling and erosion of the polymer. These aforesaid factors had a noticeable influence on the drug release properties and it can be concluded that the higher levels of hydroxyl groups have led to higher degree of swelling and lower erosion, thus showing a more diffusion oriented drug release characteristics.

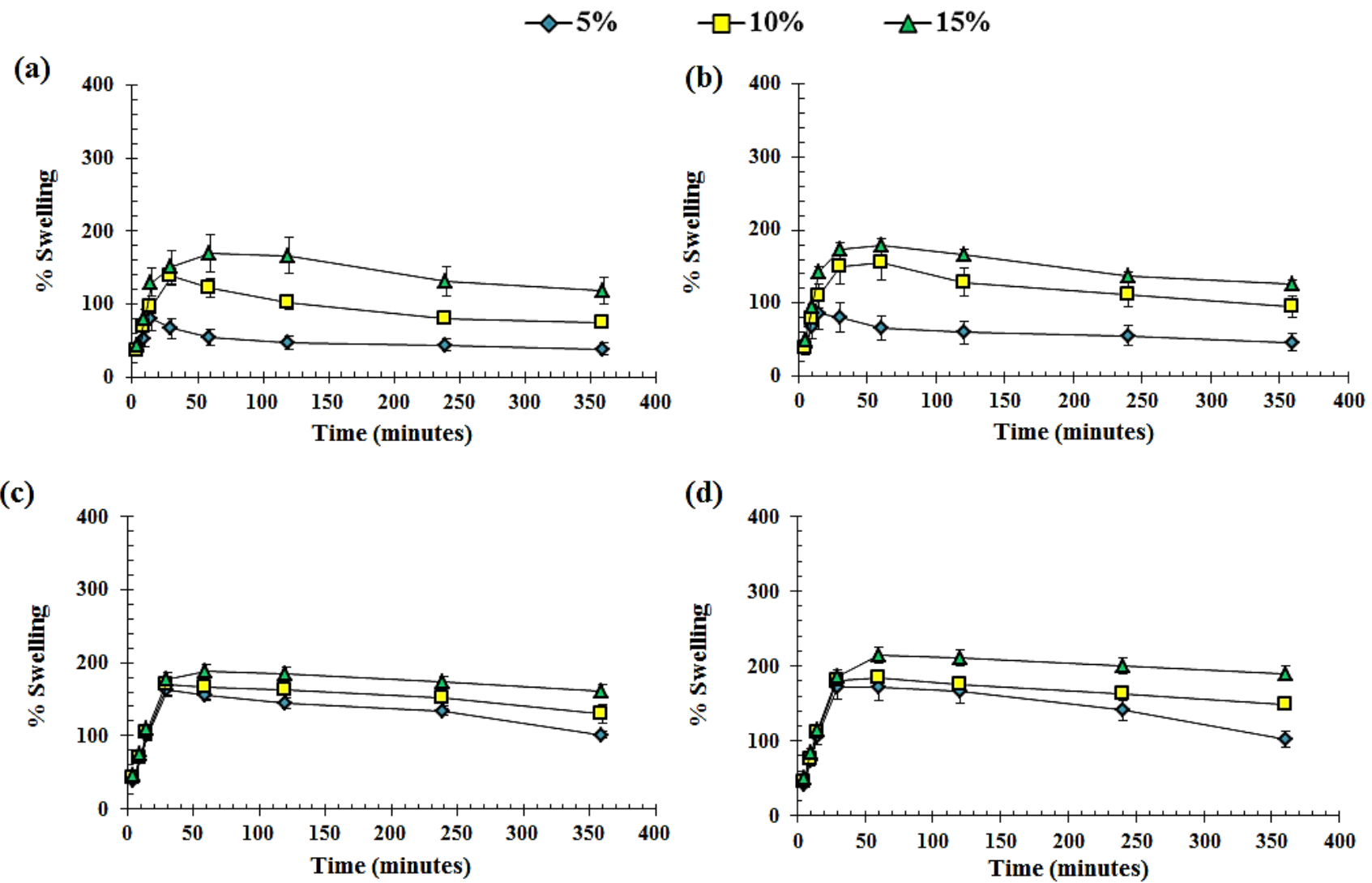


Figure 4.15, Swelling profiles of E4M/FBP, (a) 90-150 μm and (b) 150-250 μm and E4M/THP (c) 90-150 μm and (d) 150-250 μm hydrophilic matrices (n = 3).

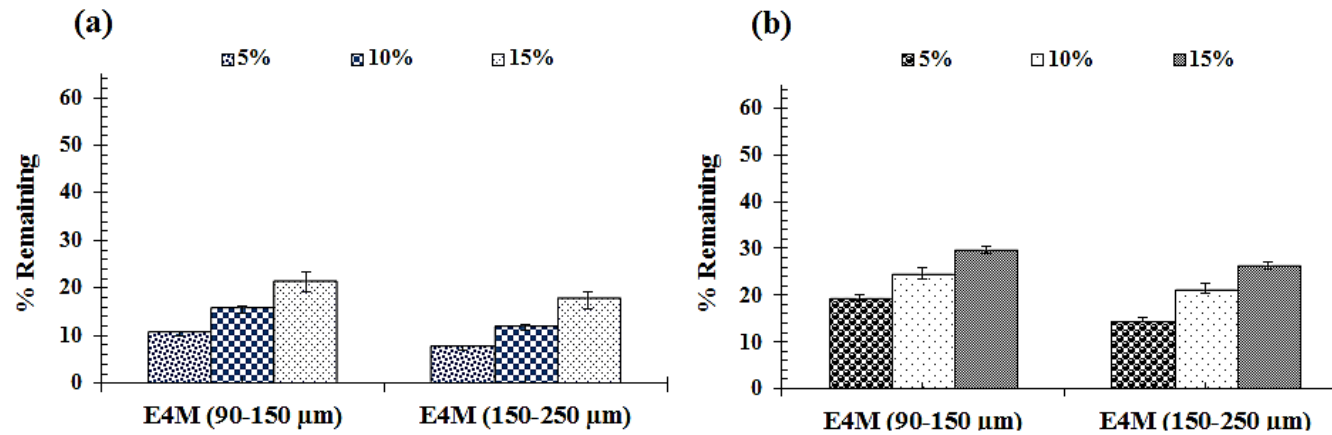


Figure 4.16, Comparative erosion of (a) E4M/FBP and (b) E4M/THP hydrophilic matrices (n = 3).

Table 4.11, Swelling kinetics and matrix erosion of E4M based hydrophilic matrices (n = 3, standard deviation given in parenthesis).

| E4M (% w/w) | Particle size (μm) | Swelling kinetics parameters | | | | | | Erosion (%) | |
|----------------|-----------------------|------------------------------|-------|--------|--------|-------|-------|--------------|--------------|
| | | k^a | | n^b | | R^2 | | FBP | THP |
| | | FBP | THP | FBP | THP | FBP | THP | | |
| 5 | 90-150 | ---- | 11.71 | ---- | 0.7908 | ---- | 0.998 | 85.32 (1.22) | 89.68 (1.77) |
| | 150-250 | ---- | 10.73 | ---- | 0.8006 | ---- | 0.997 | 80.58 (1.73) | 92.58 (1.85) |
| 10 | 90-150 | 11.58 | 12.33 | 0.7515 | 0.7886 | 0.963 | 0.999 | 78.66 (2.09) | 84.55 (1.45) |
| | 150-250 | 10.88 | 11.56 | 0.7484 | 0.7909 | 0.979 | 0.996 | 75.39 (2.31) | 88.39 (1.41) |
| 15 | 90-150 | 14.73 | 15.99 | 0.7260 | 0.7218 | 0.935 | 0.991 | 73.65 (3.02) | 78.69 (1.69) |
| | 150-250 | 12.69 | 12.86 | 0.7273 | 0.7717 | 0.920 | 0.997 | 70.29 (2.89) | 82.55 (2.01) |

(----, indicates Verghnaud model is not applicable because of early matrix erosion)

(a) Swelling constant = k (% min^{-1}), (b) Swelling exponent = n

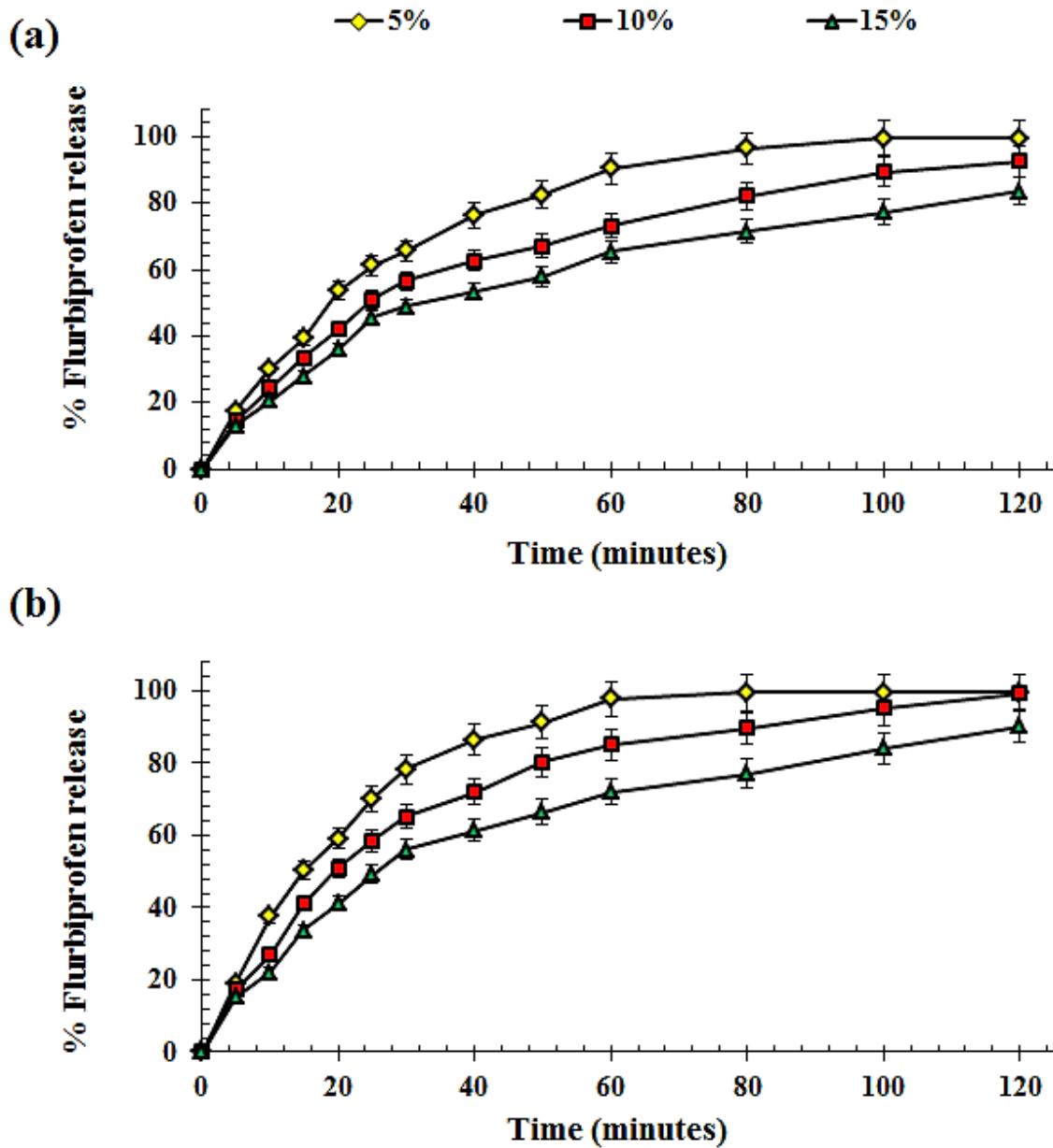


Figure 4.17, Dissolution profiles of E4M/FBP hydrophilic matrices having E4M particle size (a) 90-150 μm and (b) 150-250 μm (n = 3).

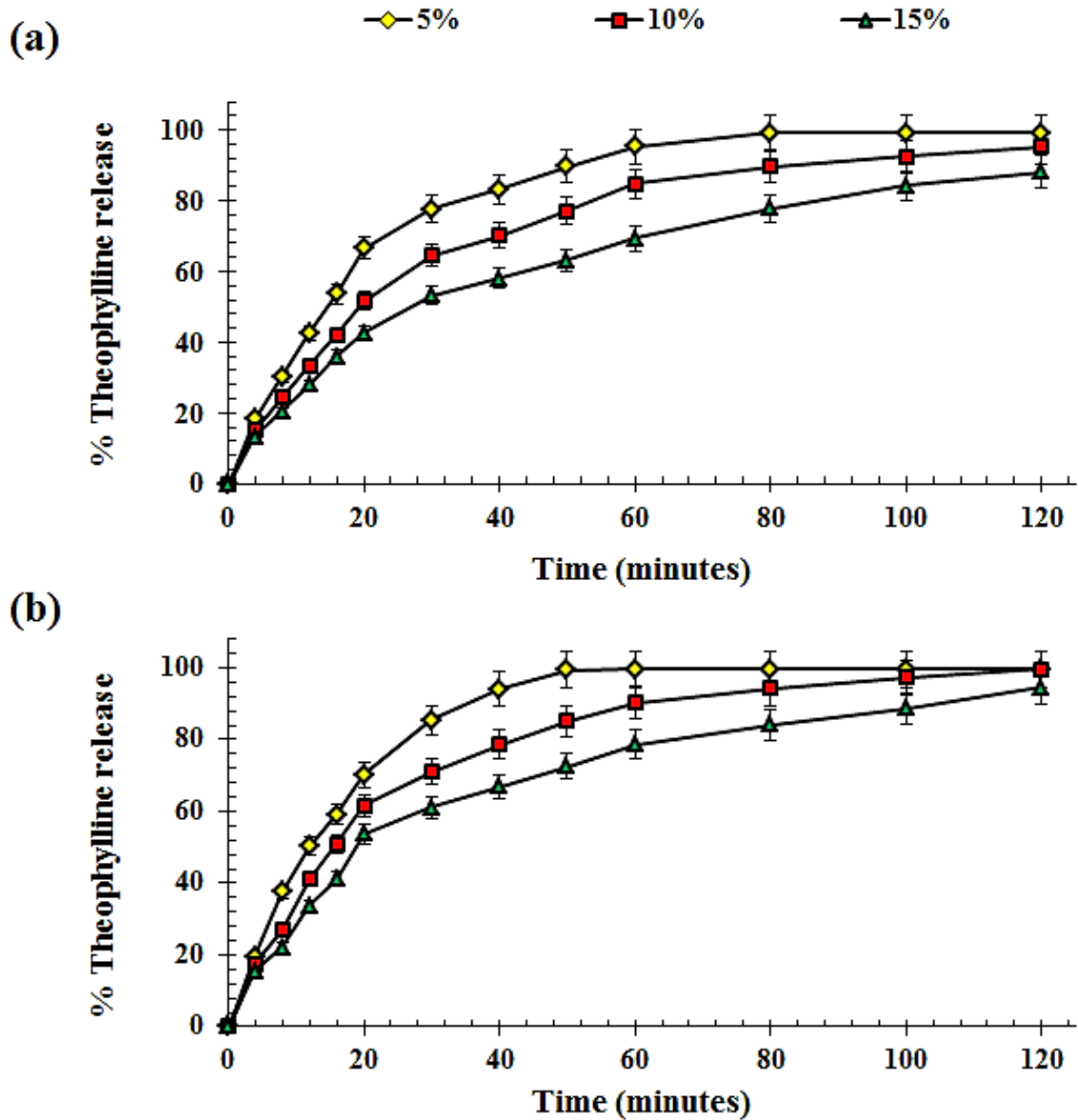


Figure 4.18, Dissolution profiles of E4M/THP hydrophilic matrices having E4M particle size (a) 90-150 μm and (b) 150-250 μm (n = 3).

Table 4.12, Summary of dissolution rate parameters of E4M based hydrophilic matrices (n = 3, standard deviation given in parenthesis)

| E4M (%) | Particle size (µm) | Dissolution rate parameters | | | | | |
|---------|--------------------|-----------------------------|----------------|------------------|-------------|----------------|------------------|
| | | FBP | | | THP | | |
| | | Slope | R ² | IDR ^a | Slope | R ² | IDR ^a |
| 5 | 90-150 | 6.89 (0.35) | 0.988 | 5.21 (0.30) | 9.19 (0.51) | 0.984 | 6.95 (0.43) |
| | 150-250 | 7.92 (0.28) | 0.971 | 5.99 (0.35) | 9.85 (0.38) | 0.971 | 7.45 (0.48) |
| 10 | 90-150 | 5.34 (0.17) | 0.981 | 4.04 (0.27) | 6.71 (0.25) | 0.980 | 5.07 (0.33) |
| | 150-250 | 6.29 (0.49) | 0.989 | 4.76 (0.29) | 8.13 (0.67) | 0.984 | 6.15 (0.38) |
| 15 | 90-150 | 4.41 (0.43) | 0.982 | 3.34 (0.14) | 5.25 (0.29) | 0.975 | 3.97 (0.27) |
| | 150-250 | 4.88 (0.22) | 0.988 | 3.69 (0.27) | 6.49 (0.36) | 0.981 | 4.91 (0.32) |

(a) Intrinsic dissolution rate = IDR (mg min⁻¹ cm⁻²)

Table 4.13, Summary of drug release kinetics parameters of E4M based hydrophilic matrices (n = 3).

| E4M (% w/w) | Particle size (µm) | Zero order model | | | | First order model | | | | Korsmeyer- Peppas model | | | | | Higuchi model | | | | |
|-------------|--------------------|-----------------------------|----------------|-----------------------------|----------------|-----------------------------|----------------|-----------------------------|----------------|-----------------------------|----------------|----------------|-----------------------------|----------------|----------------|-----------------------------|----------------|-----------------------------|----------------|
| | | FBP | | THP | | FBP | | THP | | FBP | | | THP | | FBP | | THP | | |
| | | K ₀ ^a | R ² | K ₀ ^a | R ² | K ₁ ^b | R ² | K ₁ ^b | R ² | K _p ^c | n ^d | R ² | K _p ^c | n ^d | R ² | K _h ^e | R ² | K _h ^e | R ² |
| 5 | 90-150 | 2.73 | 0.984 | 3.50 | 0.968 | 0.036 | 0.993 | 0.057 | 0.998 | 4.55 | 0.78 | 0.994 | 5.90 | 0.77 | 0.989 | 10.54 | 0.946 | 13.90 | 0.954 |
| | 150-250 | 3.21 | 0.970 | 4.01 | 0.984 | 0.046 | 0.998 | 0.047 | 0.998 | 6.27 | 0.82 | 0.989 | 7.52 | 0.81 | 0.999 | 12.41 | 0.958 | 12.10 | 0.960 |
| 10 | 90-150 | 2.21 | 0.978 | 2.77 | 0.983 | 0.028 | 0.998 | 0.044 | 0.995 | 4.17 | 0.76 | 0.999 | 5.20 | 0.73 | 0.998 | 8.54 | 0.961 | 11.46 | 0.965 |
| | 150-250 | 2.66 | 0.985 | 3.32 | 0.975 | 0.035 | 0.994 | 0.035 | 0.994 | 4.31 | 0.78 | 0.988 | 5.29 | 0.77 | 0.999 | 10.24 | 0.950 | 9.58 | 0.946 |
| 15 | 90-150 | 1.87 | 0.973 | 2.35 | 0.972 | 0.023 | 0.990 | 0.034 | 0.989 | 3.73 | 0.71 | 0.994 | 4.45 | 0.70 | 0.995 | 7.27 | 0.964 | 9.37 | 0.964 |
| | 150-250 | 2.16 | 0.975 | 2.71 | 0.971 | 0.027 | 0.991 | 0.028 | 0.989 | 4.04 | 0.73 | 0.981 | 4.92 | 0.71 | 0.994 | 8.37 | 0.955 | 8.13 | 0.957 |

(a) Zero order constant = K₀ (% min⁻¹), (b) First order constant = K₁ (% min⁻¹), (c) Korsmeyer- Peppas constant = K_p (% min⁻¹), (d) Diffusional exponent = n, (e) Higuchi constant = K_h (% min^{-1/2})

4.7.3.3.4- Effect of Methocel[®] viscosity (molecular size)

The viscosity (molecular size) of Methocel[®] (MC/HPMC) in solution depends on the chemical structure of the polymer, its molecular weight and interactions with the solvent. It is obvious from the previous studies that viscosity can significantly impact the swelling, erosion and drug release properties of hydrophilic matrices, (Campos-Aldrete and Villafuerte-Robles, 1997; Maderuelo *et al.*, 2011). The K4M, K15M and K100M, having different viscosity but almost similar range of Hpo/Meo substitution ratios, K4M = 4351, K15M = 17129 and K100M = 79279, Table 2.1 (Chapter 2), were selected.

The results confirmed that the swelling, erosion and dissolution properties are affected by viscosity of MC/HPMC. The swelling (%) tends to decrease as the viscosity of MC/HPMC increases, regardless of drug solubility and levels (% w/w), (Figures (K4M), 4.23 (K15M) and 4.27 (K100M)). The erosion profiles of FBP and THP based matrices are shown in Figures (K4M), 4.24 (K15M) and 4.28 (K100M) and demonstrated a noticeable reduction in the matrix erosion with an increase in the viscosity of MC/HPMC. So, it can be assumed from these findings that the higher viscosity based MC/HPMC matrices develop a more stable and durable gel layer on the surface of the tablet because of the ability of longer polymer chains to capture more water as higher viscosity polymers tend to disentangle on exposure to liquids (Miller-Chou and Koenig, 2003).

Furthermore, increased viscosity results in the decline of the n value, showing a diffusion dominant swelling. However, the overall swelling mechanism was considered to be anomalous, (Figures 4.14 (K4M), 4.18 (K15M) and 4.22 (K100M)). On the other hand the swelling rates were increased with the reduction of HPMC/MC particle size regardless of drug and level of MC/HPMC (% w/w). Moreover, the swelling rate was also higher with increasing MC/HPMC viscosity.

The extent of drug release (%) from all the matrices reduced as the MC/HPMC viscosity increased from 4351 cps to 79279 cps, (Figures (K4M/FBP), 4.22 (K4M/THP), 4.25 (K15M/FBP), 4.26 (K15M/THP), 4.29 (K100M/FBP) and 4.30 (K100M/THP)). Moreover, the IDRs exhibited the similar trend, (Tables 4.15 (K4M), 4.18 (K15M) and 4.21 (K100M)). It can be assumed that the higher viscosity led to the development of more stable gel layer on the surface of matrices which actually controlled drug release. The penetration of liquid into the matrix tablets breaks the hydrogen bonds between the polymer chains and develops interstitial spaces which promote a rapid entry of water into the matrix network. Over time, the imbibition of water actually increases the viscous drag and, as a result, HPMC polymer chains swell faster and further result in the blockage of surface pores of matrix tablets (Wan *et al.*, 1991). This in turn leads to the formation of a turbid gel, which has a capacity to resist matrix erosion. So, as a consequence slower drug diffusion and drug release rates were apparent (Gao *et al.*, 1996; Talukdar *et al.*, 1996; Wan *et al.*, 1991).

The drug release kinetic parameters indicated a combination of both erosion and diffusion (anomalous) as the controlling factors for drug release from the resulting matrix, (4.16 (K4M), 4.19 (K15M) and 4.22 (K100M)). Moreover, a reduction in MC/HPMC particle size caused a decrease in the n value, indicating a more diffusion oriented drug release from the tablet matrix. This response may be because of faster swelling of smaller MC/HPMC particles (as explained earlier) and rapid gel layer formation.

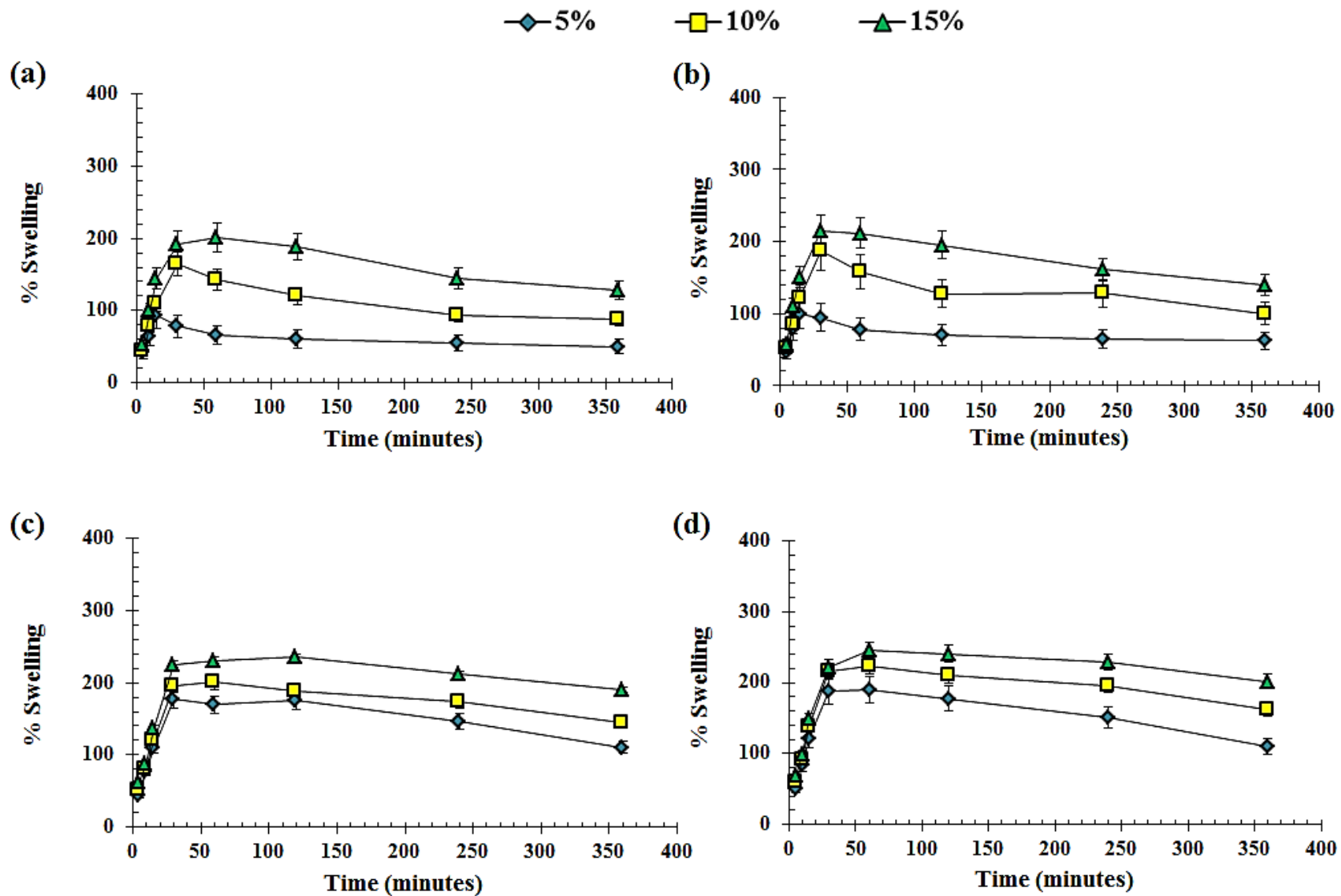


Figure 4.19, Swelling profiles of K4M/FBP, (a) 90-150 μm and (b) 150-250 μm and K4M/THP (c) 90-150 μm and (d) 150-250 μm hydrophilic matrices (n = 3).

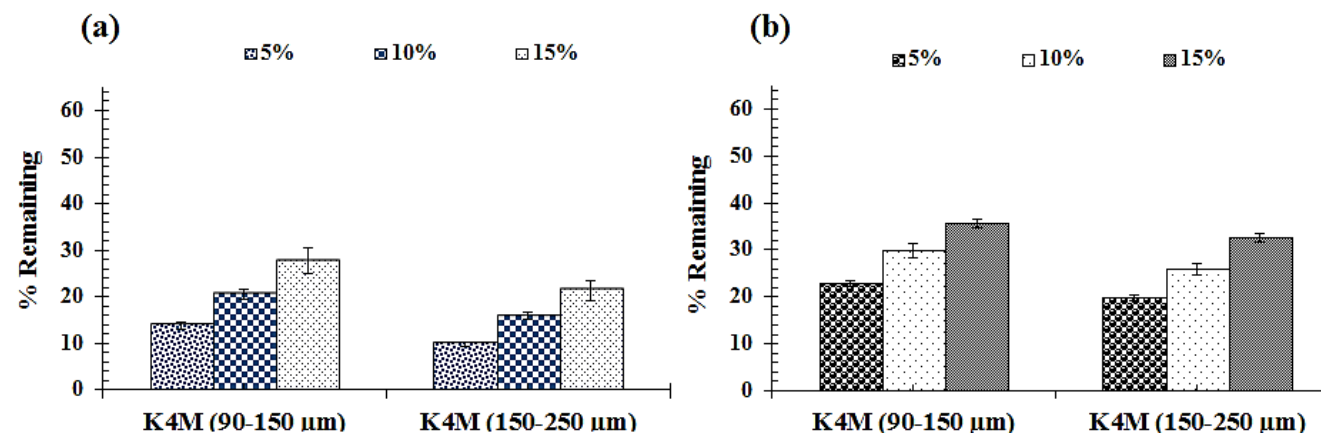


Figure 4.20, Comparative erosion profiles of (a) K4M/FBP and (b) K4M/THP hydrophilic matrices (n = 3).

Table 4.14, Swelling kinetics and matrix erosion of K4M based hydrophilic matrices (n = 3, standard deviation given in parenthesis)

| K4M (%) | Particle size (μm) | Swelling kinetics parameters | | | | | | Erosion (%) | |
|---------|--------------------|------------------------------|-------|--------|--------|-------|-------|--------------|--------------|
| | | k^a | | n^b | | R^2 | | FBP | THP |
| | | FBP | THP | FBP | THP | FBP | THP | | |
| 5 | 90-150 | | 14.93 | | 0.7457 | | 0.997 | 77.25 (2.55) | 86.32 (1.56) |
| | 150-250 | | 12.56 | | 0.7782 | | 0.998 | 80.29 (1.05) | 90.24 (2.21) |
| 10 | 90-150 | 16.09 | 17.83 | 0.7216 | 0.7326 | 0.996 | 0.991 | 70.25 (1.01) | 79.55 (1.89) |
| | 150-250 | 13.51 | 14.68 | 0.7361 | 0.7625 | 0.992 | 0.993 | 74.21 (0.91) | 84.25 (2.51) |
| 15 | 90-150 | 18.05 | 22.45 | 0.7278 | 0.6732 | 0.977 | 0.987 | 64.38 (1.07) | 72.36 (2.52) |
| | 150-250 | 15.19 | 18.76 | 0.7290 | 0.7307 | 0.961 | 0.981 | 67.39 (1.33) | 78.65 (1.87) |

(....., indicates Vergnaud model is not applicable because of early matrix erosion)

(a) Swelling constant = k (% min⁻¹), (b) Swelling exponent = n

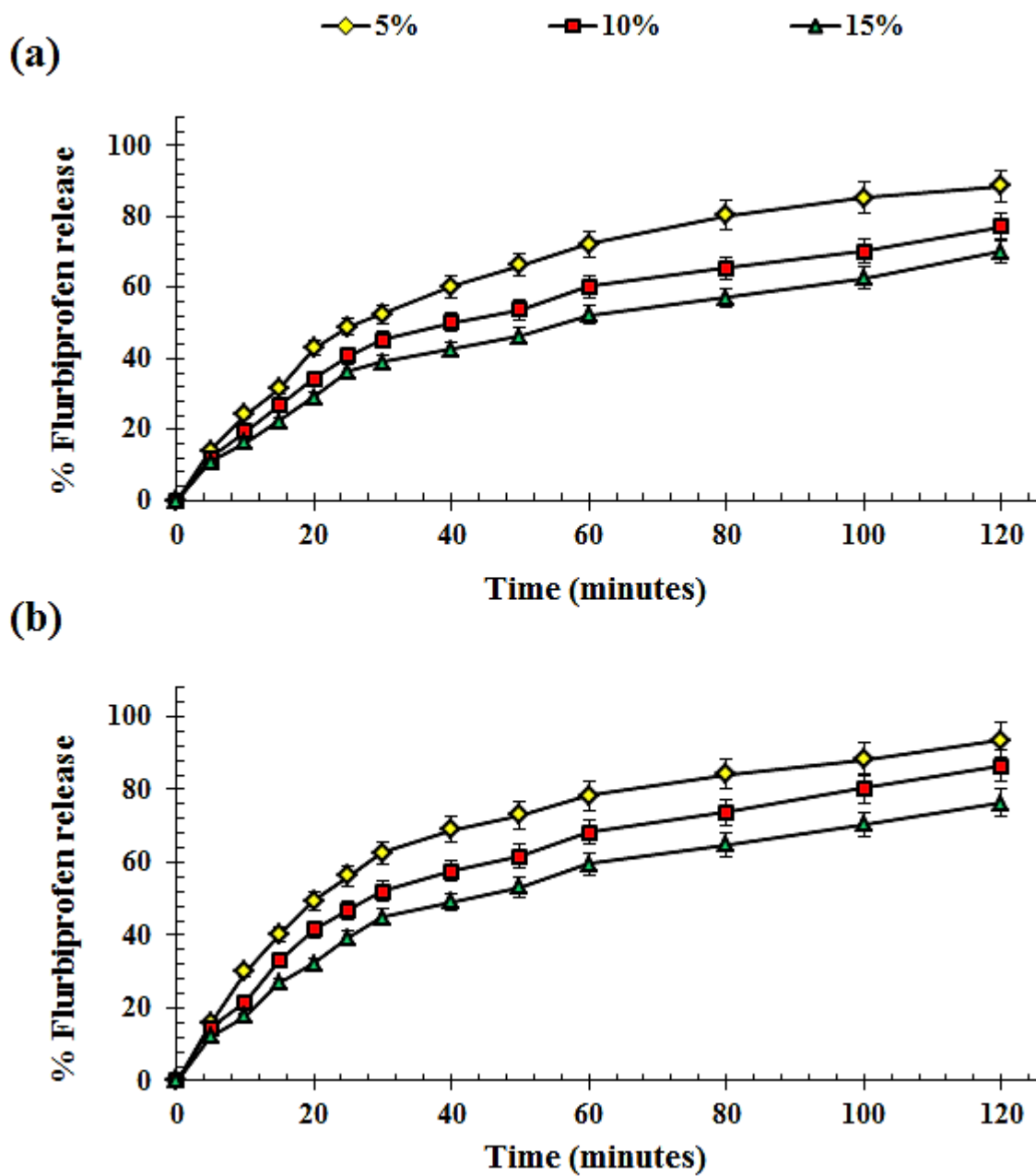


Figure 4.21, Dissolution profiles of K4M/FBP hydrophilic matrices having K4M particle size (a) 90-150 μm and (b) 150-250 μm (n = 3).

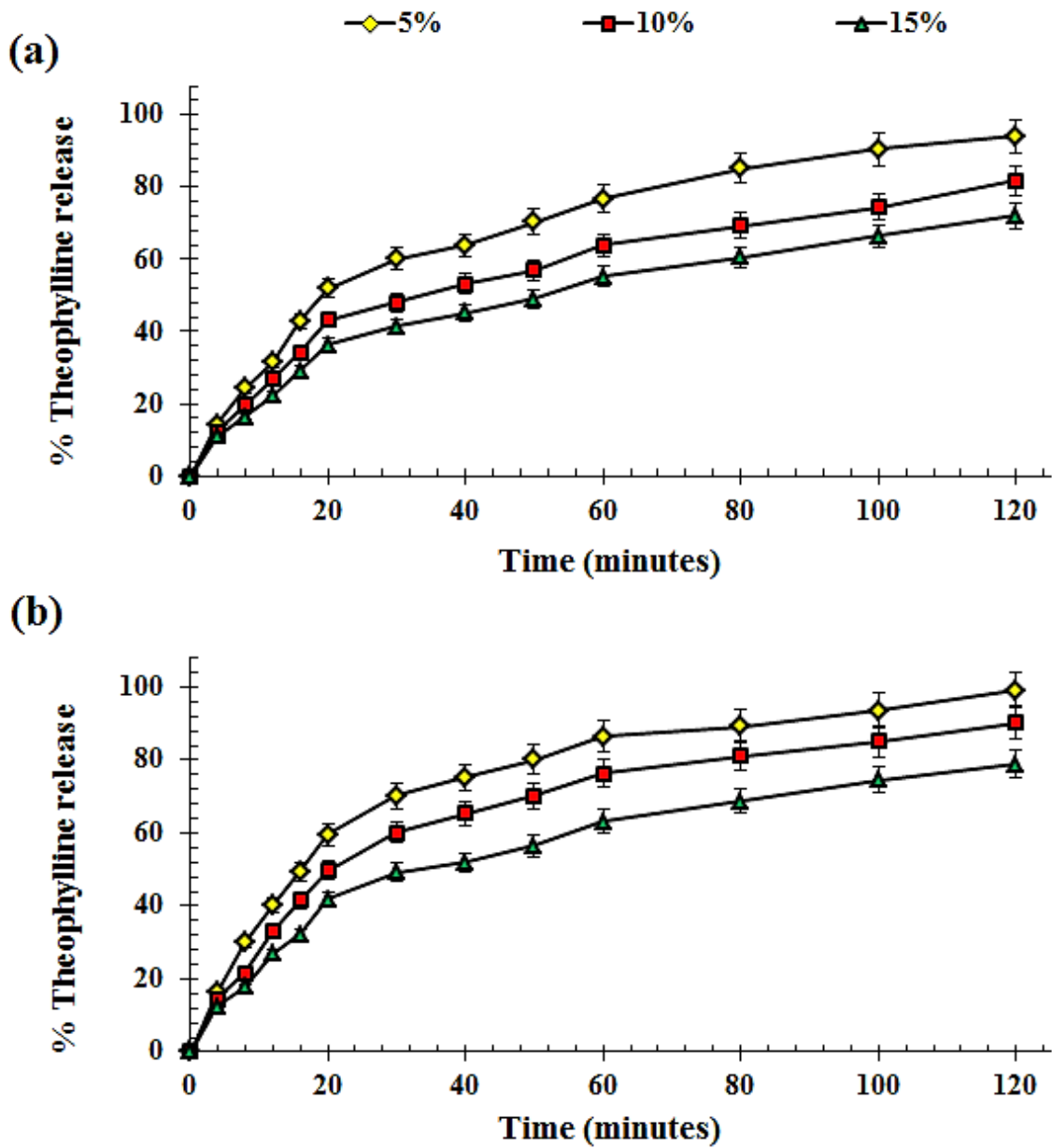


Figure 4.22, Dissolution profiles of K4M/THP hydrophilic matrices having K4M particle size (a) 90-150 μm and (b) 150-250 μm (n = 3).

Table 4.15, Summary of dissolution parameters of K4M based hydrophilic matrices (n = 3, standard deviation given in parenthesis)

| K4M (%) | Particle size (µm) | Dissolution rate parameters | | | | | |
|---------|--------------------|-----------------------------|----------------|------------------|-------------|----------------|------------------|
| | | FBP | | | THP | | |
| | | Slope | R ² | IDR ^a | Slope | R ² | IDR ^a |
| 5 | 90-150 | 5.52 (0.25) | 0.981 | 4.18 (0.21) | 7.17 (0.57) | 0.988 | 5.42 (0.41) |
| | 150-250 | 6.41 (0.38) | 0.971 | 4.85 (0.35) | 8.33 (0.55) | 0.971 | 6.30 (0.40) |
| 10 | 90-150 | 4.28 (0.47) | 0.988 | 3.24 (0.16) | 5.58 (0.35) | 0.981 | 4.22 (0.53) |
| | 150-250 | 5.04 (0.39) | 0.989 | 3.81(0.19) | 6.56 (0.47) | 0.989 | 4.96 (0.28) |
| 15 | 90-150 | 3.53 (0.40) | 0.982 | 2.67 (0.16) | 4.38 (0.19) | 0.982 | 3.31 (0.17) |
| | 150-250 | 3.88 (0.26) | 0.988 | 2.93 (0.17) | 5.05 (0.25) | 0.988 | 3.82 (0.12) |

(a) *Intrinsic dissolution rate = IDR (mg min⁻¹ cm⁻²)*

Table 4.16, Summary of drug release kinetic parameters of K4M based hydrophilic matrices (n = 3).

| K4M (% w/w) | Particle size (µm) | Zero order model | | First order model | | | | Korsmeyer- Peppas model | | | | | Higuchi model | | | | | | |
|-------------|--------------------|-----------------------------|----------------|-----------------------------|----------------|-----------------------------|----------------|-----------------------------|----------------|-----------------------------|----------------|----------------|-----------------------------|----------------|----------------|-----------------------------|----------------|-----------------------------|----------------|
| | | FBP | | THP | | FBP | | THP | | FBP | | | THP | | FBP | | THP | | |
| | | K ₀ ^a | R ² | K ₀ ^a | R ² | K ₁ ^b | R ² | K ₁ ^b | R ² | K _p ^c | n ^d | R ² | K _p ^c | n ^d | R ² | K _h ^e | R ² | K _h ^e | R ² |
| 5 | 90-150 | 2.19 | 0.983 | 2.74 | 0.982 | 0.027 | 0.993 | 0.034 | 0.993 | 3.63 | 0.78 | 0.995 | 4.43 | 0.77 | 0.996 | 8.43 | 0.956 | 9.44 | 0.953 |
| | 150-250 | 2.63 | 0.979 | 3.29 | 0.978 | 0.035 | 0.996 | 0.043 | 0.999 | 4.78 | 0.82 | 0.995 | 5.84 | 0.80 | 0.994 | 10.15 | 0.946 | 11.36 | 0.958 |
| 10 | 90-150 | 1.79 | 0.978 | 2.23 | 0.977 | 0.021 | 0.997 | 0.027 | 0.992 | 3.34 | 0.75 | 0.992 | 4.05 | 0.73 | 0.991 | 6.91 | 0.944 | 7.73 | 0.948 |
| | 150-250 | 2.15 | 0.983 | 2.69 | 0.982 | 0.027 | 0.990 | 0.033 | 0.992 | 3.52 | 0.76 | 0.998 | 4.27 | 0.75 | 0.998 | 8.29 | 0.960 | 9.27 | 0.945 |
| 15 | 90-150 | 1.51 | 0.971 | 1.89 | 0.968 | 0.017 | 0.985 | 0.022 | 0.983 | 3.03 | 0.70 | 0.991 | 3.66 | 0.68 | 0.997 | 5.84 | 0.961 | 6.54 | 0.967 |
| | 150-250 | 1.71 | 0.970 | 1.89 | 0.967 | 0.020 | 0.986 | 0.025 | 0.985 | 3.38 | 0.71 | 0.992 | 4.11 | 0.70 | 0.991 | 6.63 | 0.970 | 7.43 | 0.961 |

(a) *Zero order constant = K₀(% min⁻¹)*, (b) *First order constant = K₁(% min⁻¹)*, (c) *Korsmeyer- Peppas constant = K_p (% min⁻¹)*, (d) *Diffusional exponent = n*, (e) *Higuchi constant = K_h (% min^{-1/2})*

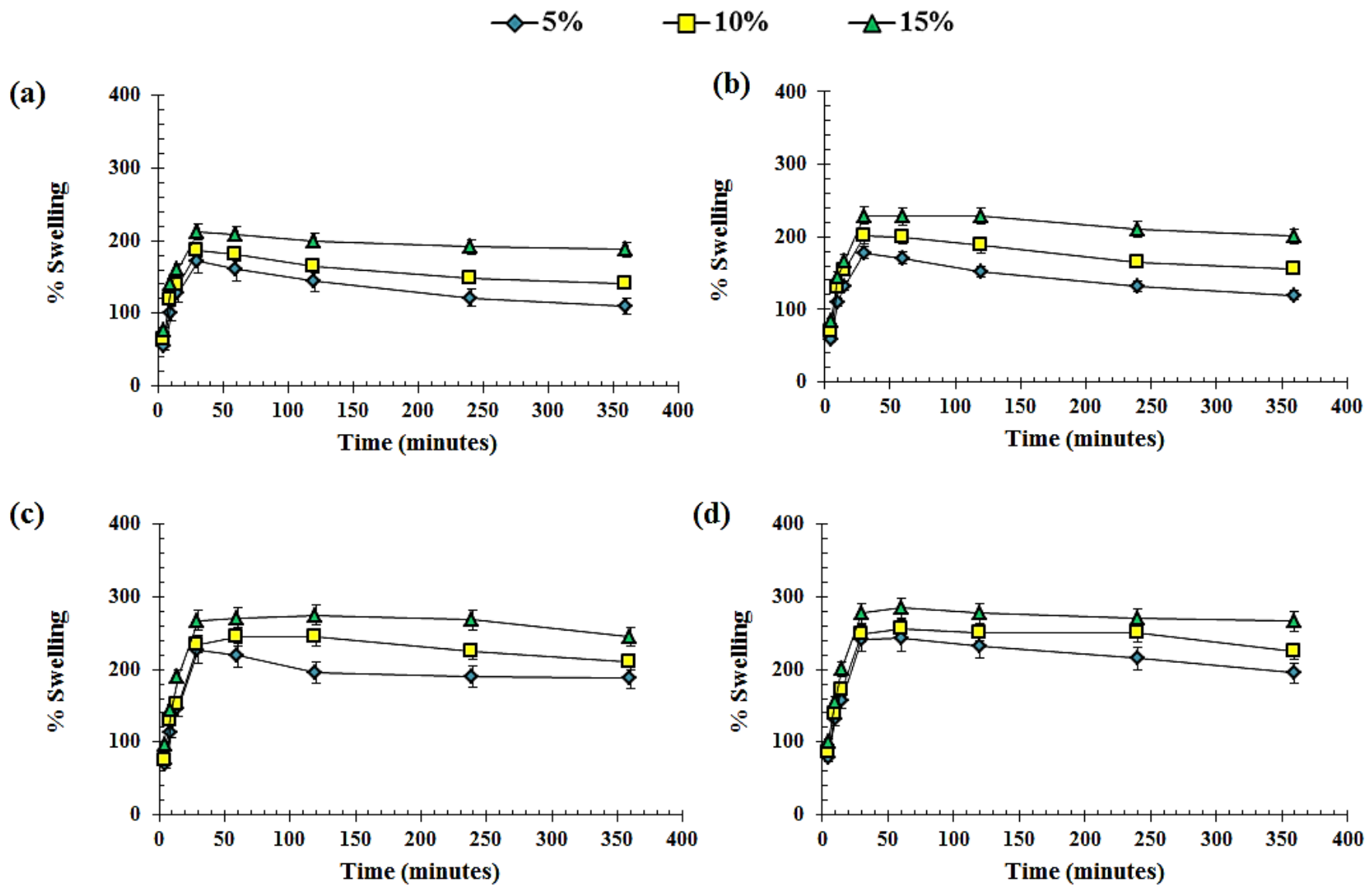


Figure 4.23, Swelling profiles of K15M/FBP, (a) 90-150 μm and (b) 150-250 μm and K15M/THP (c) 90-150 μm and (d) 150-250 μm hydrophilic matrices (n = 3).

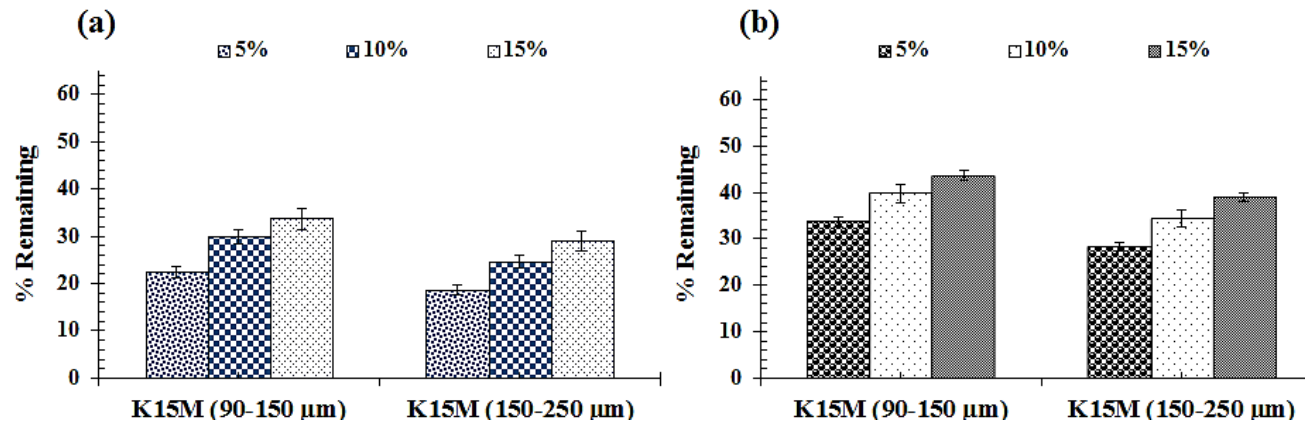


Figure 4.24, Comparative erosion of (a) K15M/FBP and (b) K15M/THP hydrophilic matrices (n = 3).

Table 4.17, Swelling kinetics and matrix erosion of K15M based hydrophilic matrices (n = 3, standard deviation given in parenthesis).

| K15M (% w/w) | Particle size (μm) | Swelling kinetics parameters | | | | | | Erosion (%) | |
|-----------------|-----------------------|------------------------------|-------|--------|--------|-------|-------|--------------|--------------|
| | | k^a | | n^b | | R^2 | | FBP | THP |
| | | FBP | THP | FBP | THP | FBP | THP | | |
| 5 | 90-150 | 22.18 | 29.90 | 0.6409 | 0.6139 | 0.956 | 0.994 | 66.35 (1.39) | 77.55 (1.33) |
| | 150-250 | 19.44 | 24.64 | 0.6129 | 0.6515 | 0.964 | 0.998 | 71.68 (0.88) | 81.37 (0.52) |
| 10 | 90-150 | 28.15 | 33.01 | 0.5829 | 0.5945 | 0.944 | 0.993 | 60.25 (0.59) | 70.25 (1.12) |
| | 150-250 | 25.70 | 27.82 | 0.5774 | 0.6271 | 0.951 | 0.988 | 65.58 (1.61) | 75.38 (1.39) |
| 15 | 90-150 | 35.74 | 39.79 | 0.5581 | 0.5709 | 0.969 | 0.994 | 56.38 (2.02) | 66.39 (0.99) |
| | 150-250 | 35.74 | 37.84 | 0.5466 | 0.5749 | 0.943 | 0.996 | 60.97 (1.11) | 71.05 (1.15) |

(a) Swelling constant = k (% min⁻¹), (b) Swelling exponent = n

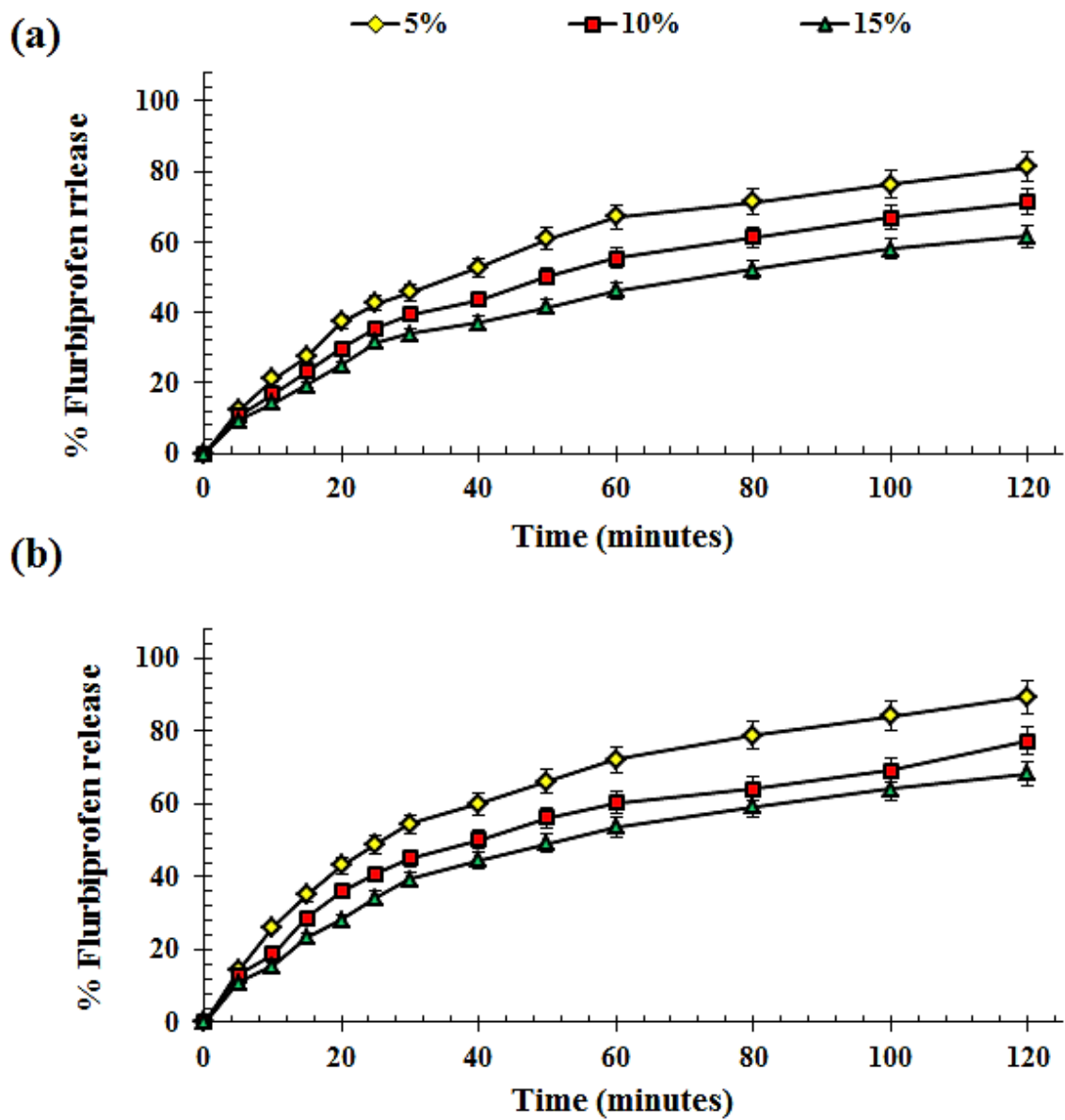


Figure 4.25, Dissolution profiles of K15M/FBP hydrophilic matrices having K15M particle size (a) 90-150 μm and (b) 150-250 μm (n = 3).

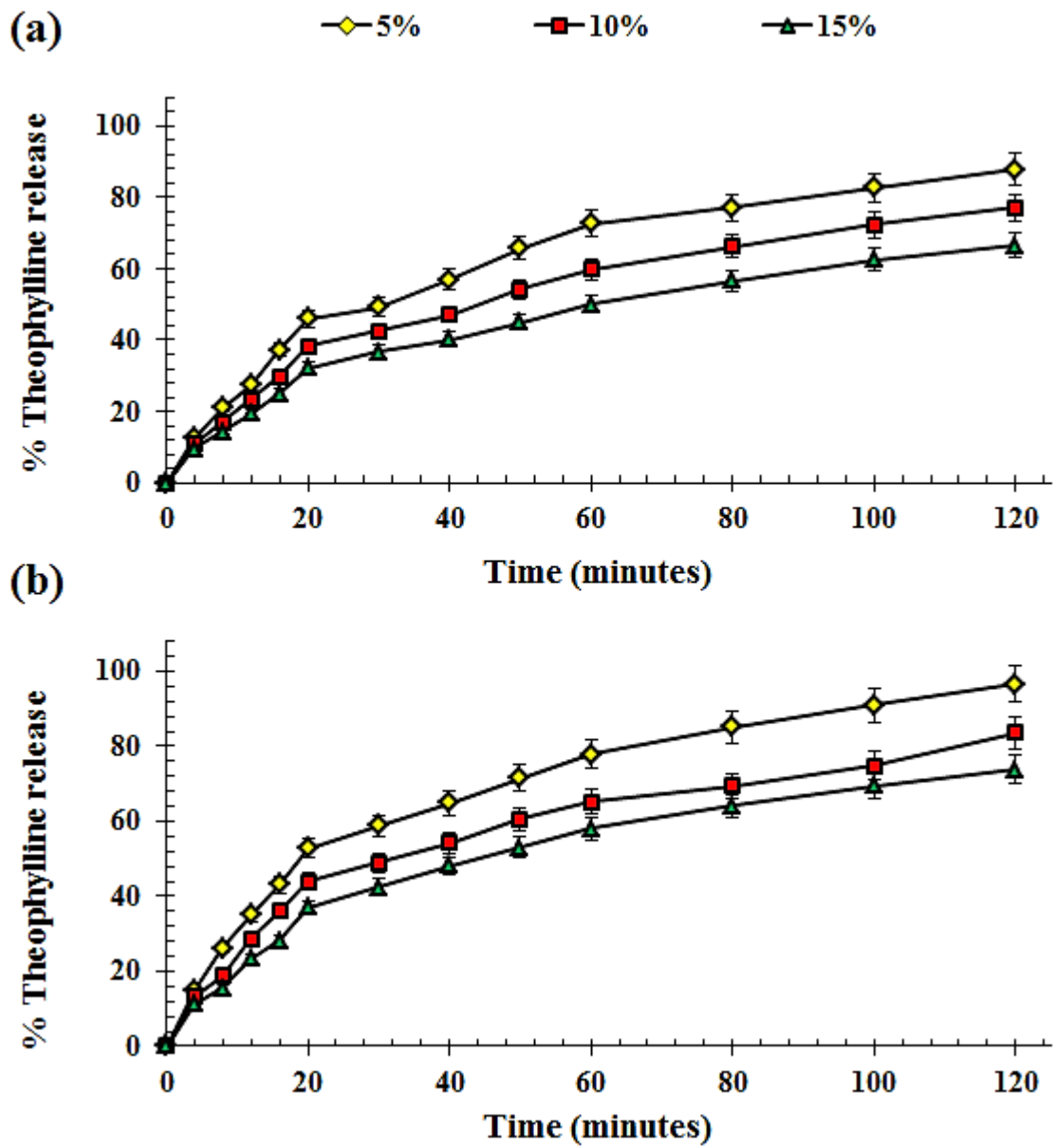


Figure 4.26, Dissolution profiles of K15M/THP hydrophilic matrices having K15M particle size (a) 90-150 μm and (b) 150-250 μm (n = 3).

Table 4.18, Summary of dissolution parameters of K15M based hydrophilic matrices (n = 3, standard deviation given in parenthesis)

| K15M (%) | Particle size (µm) | Dissolution rate parameters | | | | | |
|----------|--------------------|-----------------------------|----------------|------------------|-------------|----------------|------------------|
| | | FBP | | | THP | | |
| | | Slope | R ² | IDR ^a | Slope | R ² | IDR ^a |
| 5 | 90-150 | 4.78 (0.15) | 0.989 | 3.61 (0.18) | 6.32 (0.27) | 0.988 | 4.78 (0.21) |
| | 150-250 | 5.54 (0.25) | 0.978 | 4.19 (0.21) | 7.31 (0.35) | 0.971 | 5.53 (0.20) |
| 10 | 90-150 | 3.72 (0.14) | 0.981 | 2.81 (0.14) | 4.90 (0.39) | 0.988 | 3.70 (0.22) |
| | 150-250 | 4.36 (0.34) | 0.965 | 3.30 (0.16) | 5.75 (0.40) | 0.981 | 4.35 (0.24) |
| 15 | 90-150 | 3.05 (0.45) | 0.975 | 2.31 (0.12) | 3.87 (0.25) | 0.975 | 2.93 (0.19) |
| | 150-250 | 3.37 (0.28) | 0.956 | 2.55 (0.13) | 4.45 (0.35) | 0.982 | 3.36 (0.15) |

(a) Intrinsic dissolution rate = IDR (mg min⁻¹ cm⁻²)

Table 4.19, Summary of drug release kinetic parameters of K15M based hydrophilic matrices (n = 3).

| K15M (%) | Particle size (µm) | Zero order model | | First order model | | | | Korsmeyer- Peppas model | | | | | Higuchi model | | | | | | |
|----------|--------------------|-----------------------------|----------------|-----------------------------|----------------|-----------------------------|----------------|-----------------------------|----------------|-----------------------------|----------------|----------------|-----------------------------|----------------|----------------|-----------------------------|----------------|-----------------------------|----------------|
| | | FBP | | THP | | FBP | | THP | | FBP | | THP | | | FBP | | THP | | |
| | | K ₀ ^a | R ² | K ₀ ^a | R ² | K ₁ ^b | R ² | K ₁ ^b | R ² | K _p ^c | n ^d | R ² | K _p ^c | n ^d | R ² | K _h ^e | R ² | K _h ^e | R ² |
| 5 | 90-150 | 1.90 | 0.982 | 2.38 | 0.981 | 0.023 | 0.992 | 0.029 | 0.992 | 3.21 | 0.78 | 0.994 | 3.91 | 0.76 | 0.993 | 7.34 | 0.959 | 8.21 | 0.949 |
| | 150-250 | 2.29 | 0.977 | 2.86 | 0.978 | 0.029 | 0.997 | 0.036 | 0.997 | 4.32 | 0.79 | 0.998 | 5.32 | 0.77 | 0.998 | 8.84 | 0.948 | 9.91 | 0.963 |
| 10 | 90-150 | 1.55 | 0.976 | 1.94 | 0.974 | 0.018 | 0.998 | 0.023 | 0.989 | 2.99 | 0.73 | 0.997 | 3.63 | 0.72 | 0.996 | 6.02 | 0.944 | 6.74 | 0.964 |
| | 150-250 | 1.87 | 0.980 | 2.34 | 0.977 | 0.022 | 0.990 | 0.028 | 0.988 | 3.18 | 0.74 | 0.987 | 3.92 | 0.72 | 0.995 | 7.22 | 0.962 | 8.09 | 0.953 |
| 15 | 90-150 | 1.30 | 0.969 | 1.63 | 0.969 | 0.015 | 0.982 | 0.018 | 0.982 | 2.71 | 0.69 | 0.992 | 3.19 | 0.69 | 0.992 | 5.06 | 0.960 | 5.65 | 0.967 |
| | 150-250 | 1.50 | 0.968 | 1.88 | 0.963 | 0.017 | 0.985 | 0.022 | 0.979 | 2.99 | 0.70 | 0.991 | 3.68 | 0.68 | 0.993 | 5.81 | 0.967 | 6.51 | 0.952 |

(a) Zero order constant = K₀(% min⁻¹), (b) First order constant = K₁(% min⁻¹), (c) Korsmeyer- Peppas constant = K_p (% min⁻¹), (d) Diffusional exponent = n, (e) Higuchi constant = K_h (% min^{-1/2})

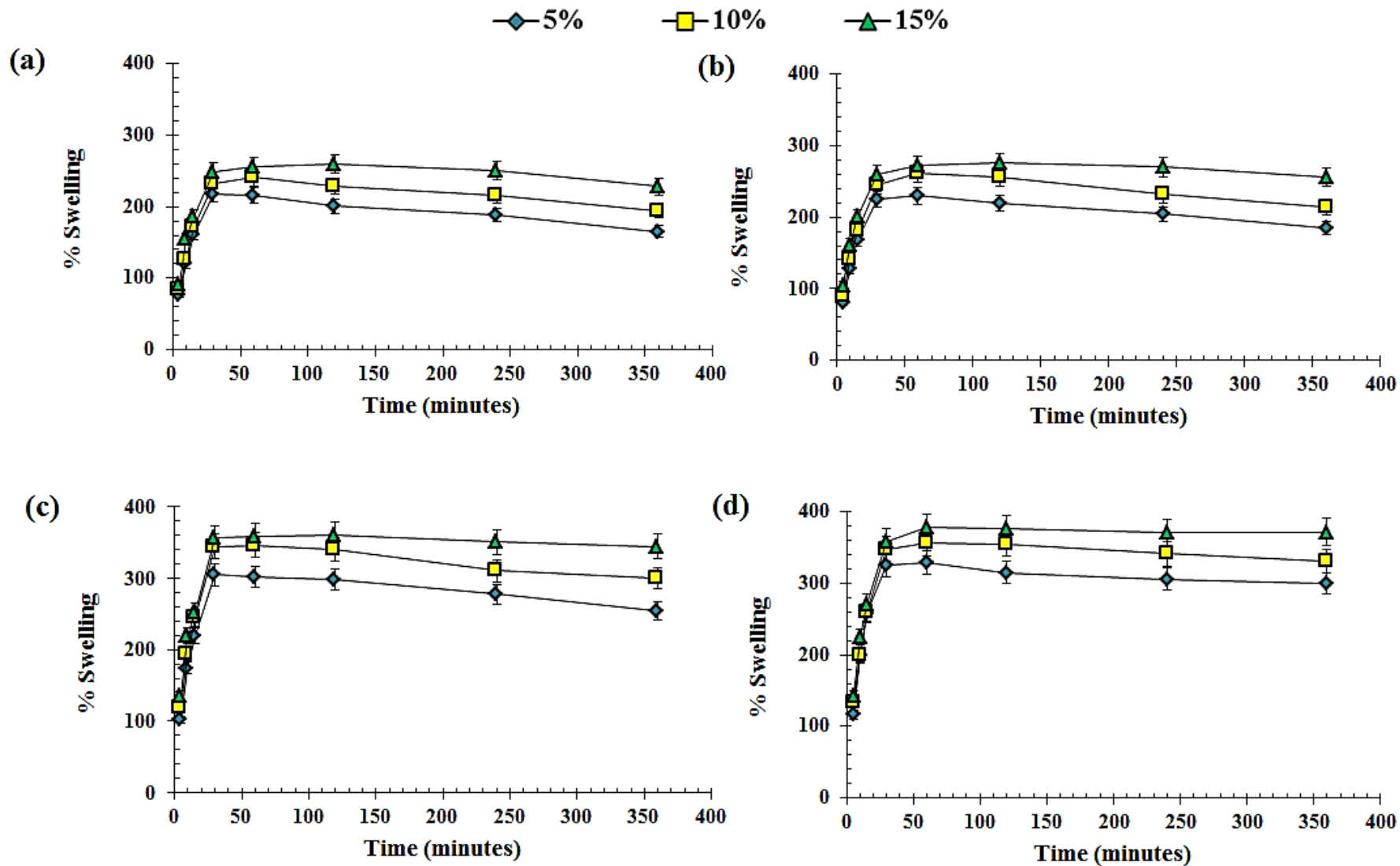


Figure 4.27, Swelling profiles of K100M/FBP, (a) 90-150 μm and (b) 150-250 μm and E4M/THP (c) 90-150 μm and (d) 150-250 μm hydrophilic matrices (n = 3).

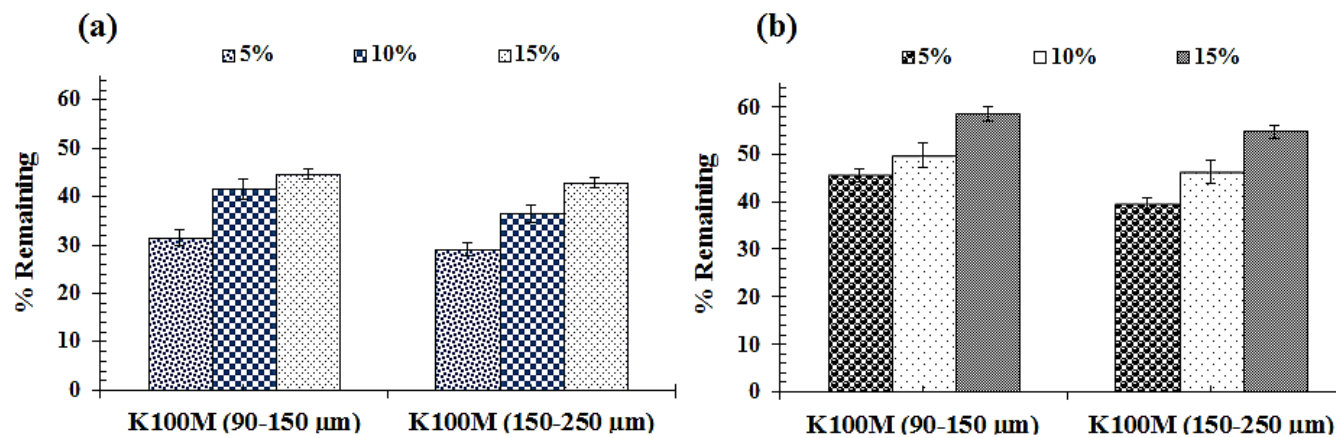


Figure 4.28, Comparative erosion of (a) K100M/FBP and (b) K100M/THP hydrophilic matrices (n = 3).

Table 4.20, Swelling kinetics and matrix erosion of K100M based hydrophilic matrices (n = 3).

| K100M (%) | Particle size (μm) | Swelling kinetics parameters | | | | | | Erosion (%) | |
|-----------|--------------------|------------------------------|-------|--------|--------|-------|-------|-------------|-------|
| | | k^a | | n^b | | R^2 | | FBP | THP |
| | | FBP | THP | FBP | THP | FBP | THP | | |
| 5 | 90-150 | 32.05 | 45.72 | 0.5721 | 0.5763 | 0.987 | 0.960 | 68.55 | 54.33 |
| | 150-250 | 29.06 | 38.12 | 0.5929 | 0.611 | 0.985 | 0.981 | 70.91 | 60.39 |
| 10 | 90-150 | 36.77 | 55.65 | 0.5568 | 0.5392 | 0.989 | 0.991 | 58.55 | 50.25 |
| | 150-250 | 32.76 | 46.51 | 0.575 | 0.5886 | 0.988 | 0.991 | 63.61 | 53.69 |
| 15 | 90-150 | 45.72 | 62.96 | 0.5114 | 0.5120 | 0.982 | 0.982 | 55.35 | 41.58 |
| | 150-250 | 38.47 | 58.79 | 0.5495 | 0.5292 | 0.973 | 0.982 | 57.22 | 42.28 |

(a) Swelling constant = k (% min⁻¹), (b) Swelling exponent = n

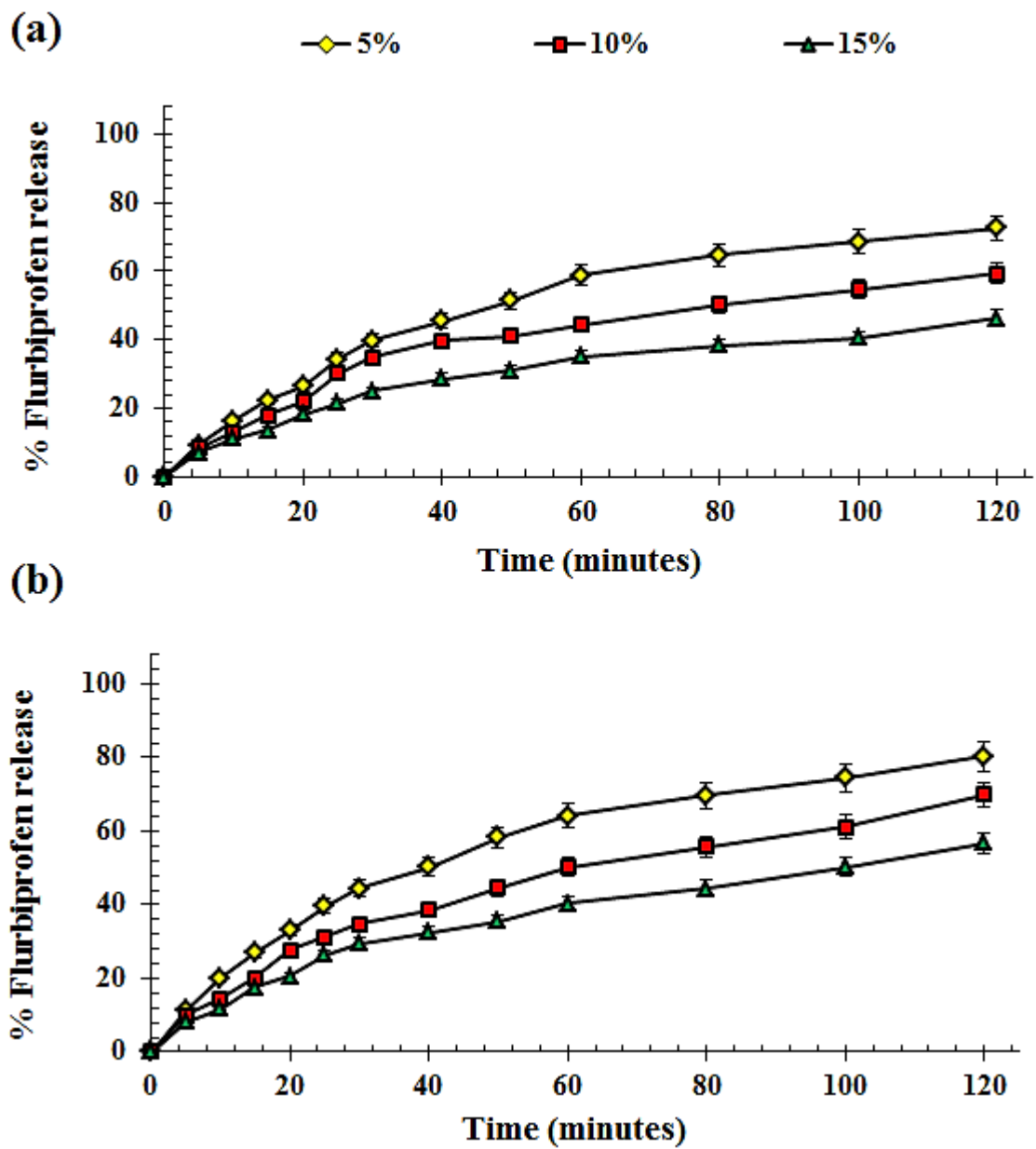


Figure 4.29, Dissolution profiles of K100M/FBP hydrophilic matrices having K100M particle size (a) 90-150 μm and (b) 150-250 μm (n = 3).

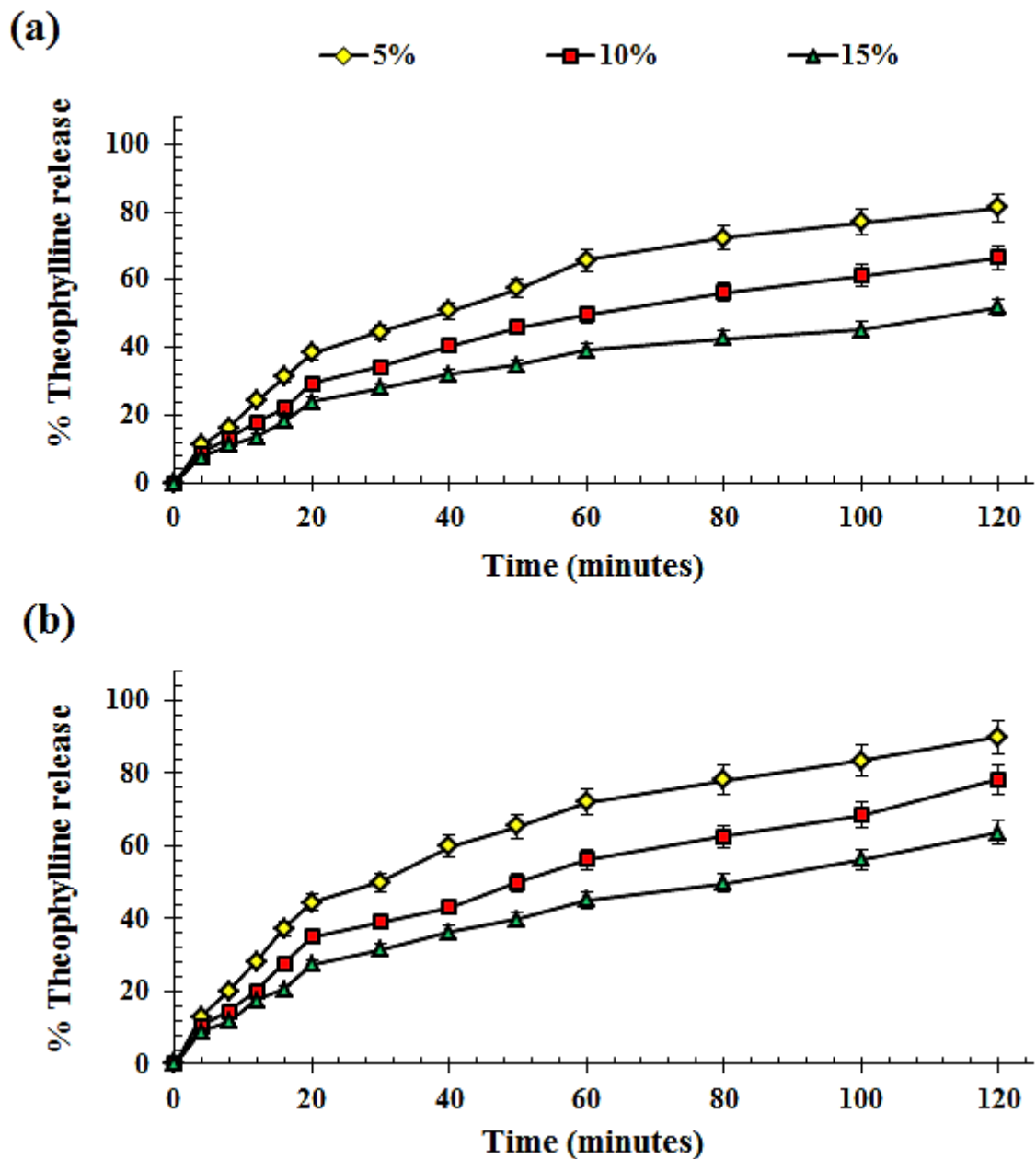


Figure 4.30, Dissolution profiles of K100M/THP hydrophilic matrices having K100M particle size (a) 90-150 μm and (b) 150-250 μm (n = 3).

Table 4.21, Summary of dissolution parameters of K100M based hydrophilic matrices (n = 3, standard deviation given in parenthesis)

| K100M (%) | Particle size (µm) | Dissolution rate parameters | | | | | |
|-----------|--------------------|-----------------------------|----------------|------------------|-------------|----------------|------------------|
| | | FBP | | | THP | | |
| | | Slope | R ² | IDR ^a | Slope | R ² | IDR ^a |
| 5 | 90-150 | 3.72 (0.10) | 0.989 | 2.81 (0.12) | 5.29 (0.21) | 0.981 | 4.00 (0.11) |
| | 150-250 | 4.40 (0.22) | 0.977 | 3.33 (0.20) | 6.19 (0.36) | 0.975 | 4.68 (0.25) |
| 10 | 90-150 | 3.03(0.17) | 0.975 | 2.29 (0.11) | 3.67 (0.37) | 0.962 | 2.77 (0.32) |
| | 150-250 | 3.33 (0.31) | 0.984 | 2.52 (0.13) | 4.49 (0.42) | 0.988 | 3.39 (0.21) |
| 15 | 90-150 | 2.08 (0.43) | 0.963 | 1.57 (0.15) | 2.80 (0.26) | 0.986 | 2.12 (0.05) |
| | 150-250 | 2.54 (0.29) | 0.986 | 1.92 (0.12) | 3.23 (0.31) | 0.977 | 2.44 (0.16) |

(a) Intrinsic dissolution rate = IDR (mg min⁻¹ cm⁻²)

Table 4.22, Summary of drug release kinetics parameters of K100 based hydrophilic matrices (n = 3).

| K100M (%) | Particle size (µm) | Zero order model | | First order model | | | | Korsmeyer- Peppas model | | | | | Higuchi model | | | | | | |
|-----------|--------------------|-----------------------------|----------------|-----------------------------|----------------|-----------------------------|----------------|-----------------------------|----------------|-----------------------------|----------------|----------------|-----------------------------|----------------|----------------|-----------------------------|----------------|-----------------------------|----------------|
| | | FBP | | THP | | FBP | | THP | | FBP | | THP | | | FBP | | THP | | |
| | | K ₀ ^a | R ² | K ₀ ^a | R ² | K ₁ ^b | R ² | K ₁ ^b | R ² | K _p ^c | n ^d | R ² | K _p ^c | n ^d | R ² | K _h ^e | R ² | K _h ^e | R ² |
| 5 | 90-150 | 1.42 | 0.968 | 2.00 | 0.969 | 0.016 | 0.992 | 0.023 | 0.995 | 2.92 | 0.76 | 0.996 | 3.21 | 0.74 | 0.995 | 5.50 | 0.965 | 6.92 | 0.977 |
| | 150-250 | 1.76 | 0.977 | 2.39 | 0.692 | 0.021 | 0.984 | 0.029 | 0.975 | 3.52 | 0.77 | 0.998 | 3.87 | 0.75 | 0.992 | 6.82 | 0.963 | 8.23 | 0.961 |
| 10 | 90-150 | 1.17 | 0.952 | 1.46 | 0.956 | 0.013 | 0.986 | 0.016 | 0.986 | 2.35 | 0.70 | 0.998 | 3.20 | 0.67 | 0.993 | 4.54 | 0.948 | 5.09 | 0.946 |
| | 150-250 | 1.40 | 0.963 | 1.76 | 0.948 | 0.016 | 0.987 | 0.020 | 0.982 | 2.60 | 0.72 | 0.997 | 3.29 | 0.68 | 0.999 | 5.41 | 0.956 | 6.08 | 0.965 |
| 15 | 90-150 | 0.95 | 0.952 | 1.19 | 0.971 | 0.010 | 0.963 | 0.013 | 0.994 | 2.18 | 0.66 | 0.998 | 2.86 | 0.60 | 0.994 | 3.69 | 0.951 | 4.15 | 0.971 |
| | 150-250 | 1.11 | 0.956 | 1.39 | 0.966 | 0.012 | 0.971 | 0.016 | 0.983 | 2.48 | 0.68 | 0.995 | 3.06 | 0.62 | 0.997 | 4.31 | 0.964 | 4.85 | 0.974 |

(a) Zero order constant = K₀(% min⁻¹), (b) First order constant = K₁(% min⁻¹), (c) Korsmeyer- Peppas constant = K_p (% min⁻¹), (d) Diffusional exponent = n, (e) Higuchi constant = K_h (% min^{-1/2})

4.7.3.3.5- Effect of drug solubility

Drug solubility is an important factor and needs careful consideration as drugs having high or low solubility can affect swelling, erosion and drug release (Conte and Maggi 1996, Gao *et al* 1996; Kim 1999, Reynolds *et al* 2002). Highly water soluble drugs are considered to be released by diffusion through the gel matrices, however, poorly soluble drugs are released predominantly by erosion of the gel matrix (Bettini *et al* 2001).

Swelling results are depicted in Figures 4.7 (A4M), 4.11 (F4M), 4.15 (E4M), 4.19 (K4M), 4.23 (K15M) and 4.27 (K100M). Additionally, erosion results are presented in Figures 4.8 (A4M), 4.12 (F4M), 4.16 (E4M), 4.20 (K4M), 4.24 (K15M) and 4.28 (K100M). It is evident that the swelling of FBP matrices was lower than THP matrices. However, due to higher extent of swelling, matrix erosion was lower for THP matrices than FBP matrices. The swelling data were analysed using the Vergnaud mathematical model to determine the swelling rate (k) and swelling exponent (n) of all the drug based matrices. The swelling kinetic parameters of FBP and THP hydrophilic matrices, where Vergnaud mathematical model was applicable, are summarised in Tables 4.5 (A4M), 4.8 (F4M), 4.11 (E4M), 4.14 (K4M), 4.18 (K15M) and 4.22 (K100M). The n values were affected by the solubility of incorporated drugs. Both the drug based matrices had an anomalous swelling mechanism, however, with a more soluble drug there was a higher tendency towards diffusion controlled swelling. Moreover the swelling rate (k) of FBP matrices ($k = 5.90 - 45.72, \% \text{ min}^{-1}$) was slower than THP matrices ($k = 7.26 - 62.96, \% \text{ min}^{-1}$). The present results demonstrate that the solubility of the incorporated drugs have significantly influenced the swelling and erosion properties of matrices. This higher swelling, but decreased erosion, of THP matrices can be attributed to the theory that soluble drugs help MC/HPMC based matrices to develop a more stable gel layer.

Figures 4.9 (A4M/FBP), 4.10 (A4M/THP), 4.13 (F4M/FBP), 4.14 (F4M/THP), 4.17 (E4M/FBP), 4.18 (E4M/THP), 4.21 (K4M/FBP), 4.22 (K4M/THP), 4.25 (K15M/FBP), 4.26 (K15M/THP), 4.29 (K100M/FBP) and 4.30 (K100M/THP) depict the dissolution profiles of matrices as percentage drug release with respect to time. The overall percentage of FBP released was low compared to THP matrices. Moreover, the IDRs of FBP matrices ($1.57 - 7.65 \text{ mg min}^{-1} \text{ cm}^{-2}$) were lower than corresponding THP matrices ($2.12 - 12.76 \text{ mg min}^{-1} \text{ cm}^{-2}$), (Tables 4.6 (A4M), 4.9 (F4M), 4.12 (E4M), 4.15 (K4M), 4.16 (K15M) and 4.21 (K100M)). In respect of the drugs themselves, THP has a faster IDR than pure FBP; moreover, the pK_a of FBP and THP is 4.2 and 8.6, respectively. As 7.2 pH phosphate buffer was used as dissolution media, and both the drugs at this particular pH are mainly present in their ionised form (see section 4.6.3. for more detail). Furthermore, matrices containing 5% MC/HPMC did not have sufficient polymer to develop a stable gel layer, instead these matrices disintegrated, thus, liberating free drug faster than the relatively stronger pure drug based compacts throughout the dissolution experiments. Furthermore, the lower IDRs of FBP matrices may be due to its low swelling and higher erosion. It is evident from the release kinetic data that solubility of drugs affects the drug release parameters. The n value of FBP is higher than THP matrices in all cases, regardless of type and concentration of MC/HPMC, indicating a higher degree of diffusion controlled drug release. As THP matrices have a tendency to form micro-cavities on the surface of gel layer, this essentially helps the gel layer resist the hydrodynamic challenges for extended durations. Moreover, it provides a pathway for drug diffusion without disturbing the surface gel layer of matrices. However, the presence of FBP actually elicits a displacement of solid drug particles of drug in the gel layer. The presence of such FBP particles in the gel layer hinders its further expansion (Bettini *et al.*, 2001; Li *et al.*, 2005; Maderuelo *et al.*, 2011). Therefore, it is more susceptible to matrix erosion which leads to low IDR but higher n values.

4.7.3.4- Inter-relationship between swelling and dissolution rates

Figures 4.31 (FBP : MC/HPMC) and 4.32 (FBP : MC/HPMC) show the correlation between matrix swelling rate (k) and IDR , which indicates that swelling and drug release occur simultaneously but the rate at which these occur is different for each matrix tablet.

The Vergnaud equation could not be applied to A4M/FBP (5% and 10%), A4M/THP (5% and 10 %), F4M/FBP (5%), F4M/THP (5%), E4M/FBP (5%), E4M/THP (5%) and K4M/FBP (5%) matrices and these were not included in the analysis. For the other matrices, swelling had a direct relationship with IDR (and a direct relationship with k , as with the higher values of k the IDR is reduced). Correlation coefficients (R^2) were in the range of 0.894 – 0.967 and 0.73 – 0.992 for FBP and THP matrices, respectively.

This relationship is a likely consequence of the diffusional path length of matrix network within a matrix tablet. As the MC/HPMC chains swell at a faster rate, the diffusional path length increased because of increased tortuosity. However, with a slow swelling rate, the matrices are more prone to matrix erosion, which is likely to shorten the diffusion path-length. So in the latter case, drug molecules had to travel a shorter distance thus leading to a higher IDR.

Table 4.23, Correlation co-efficients of swelling and IDR inter-relationship (n = 3).

| Type of matrix tablet | Correlation co-efficient (R ²) | |
|-----------------------|--|-------------------------------|
| | Particle size (90-150 µm) | Particle size (150-250 µm) |
| A4M/FBP | ----- | ----- |
| F4M/FBP | ----- | ----- |
| E4M/FBP | ----- | ----- |
| K4M/FBP | ----- | ----- |
| K15M/FBP | 0.960 | 0.967 |
| K100MFBP | 0.894 | 0.957 |
| A4M/THP | ----- | ----- |
| F4M/THP | ----- | ----- |
| E4M/THP | 0.736 | 0.980 |
| K4M/THP | 0.956 | 0.949 |
| K15M/THP | 0.908 | 0.888 |
| K100M/THP | 0.992 | 0.962 |

(-----,correlation is not possible because of early erosion of the matrix tablets).

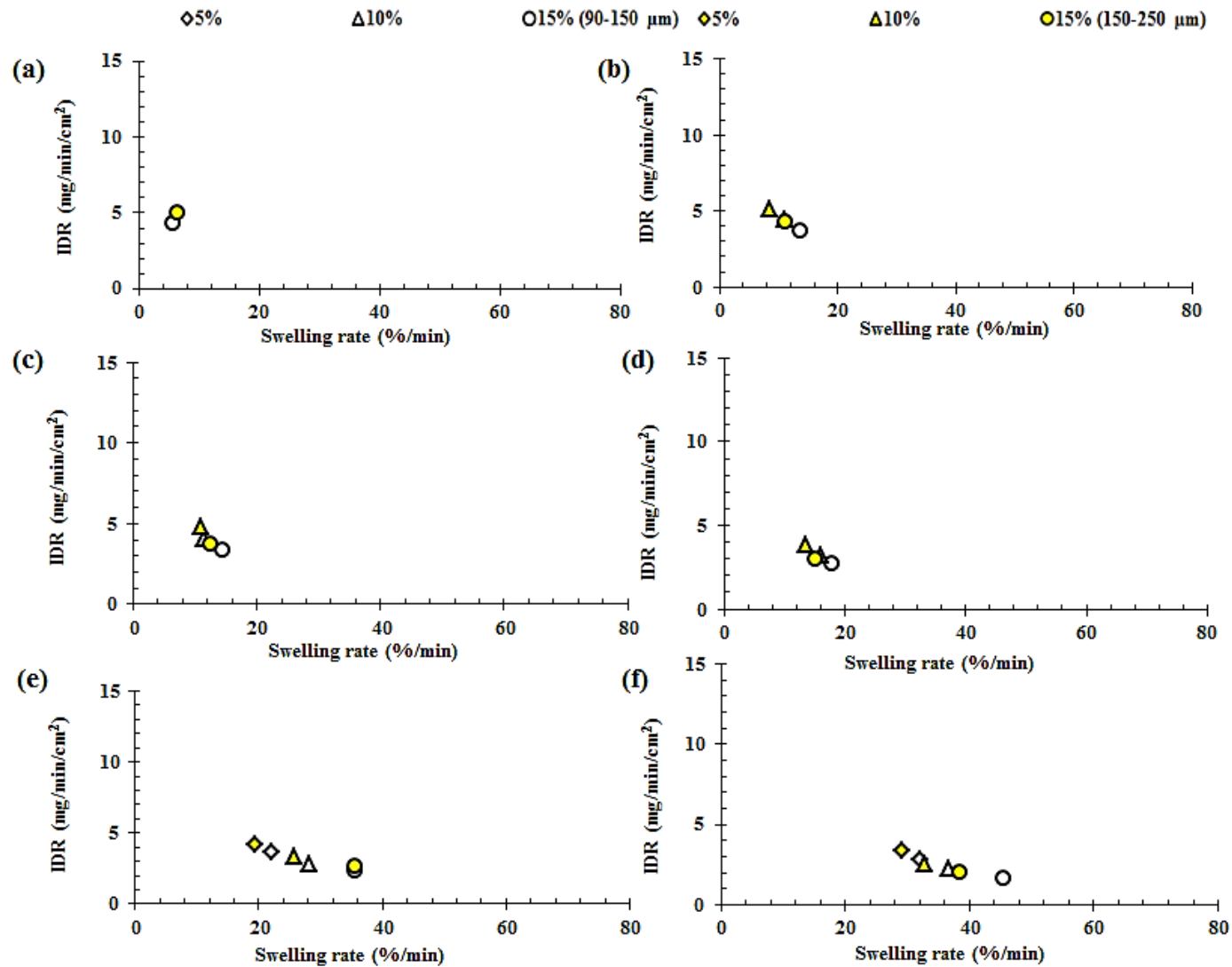


Figure 4.31, Effect of swelling on IDR of FBP based matrix tablets, (a) A4M (b) F4M (c) E4M (d) K4M (e) K15M (f) K100M having polymer particle size 90-150 μm and 150-250 μm (n = 3).

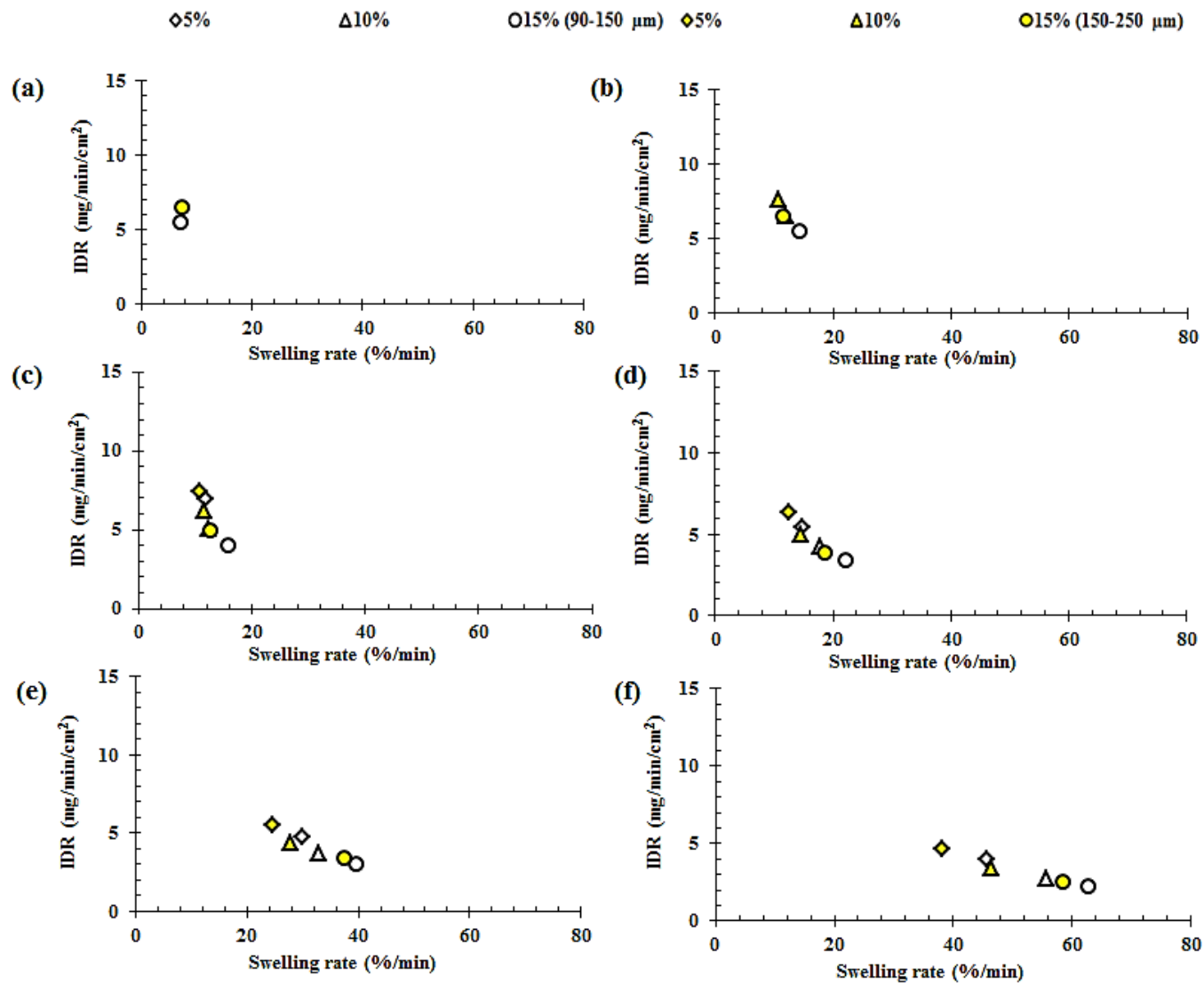


Figure 4.32, Effect of swelling on IDR of THP based matrix tablets, (a) A4M (b) F4M (c) E4M (d) K4M (e) K15M (f) K100M having polymer particle size 90-150 μm and 150-250 μm (n = 3).

4.8- Summary

In summary, the present study confirmed that the particle size, substitution ratios and viscosity of Methocel[®] affect the swelling and erosion of plain MC/HPMC matrices. It can also be concluded that the swelling mechanism was diffusion controlled. Moreover, the present study also confirms that the physico-chemical attribute (concentration, particle size, substitution and viscosity) of MC/HPMC and drug solubility have significant impact on extent of swelling, erosion, mechanism of erosion, dissolution rate and drug release kinetics.

The swelling results confirm that the extent of swelling, swelling rate and swelling exponent were affected by physico-chemical attributes (concentration, particle size, substitution and viscosity) of MC/HPMC and drug solubility. The mechanism of swelling is largely considered to be anomalous. However, it inclined towards more diffusion-oriented swelling with higher MC/HPMC levels, viscosity, Hpo/Meo substitution ratios, drug solubility but lower MC/MC particle size. Moreover, the erosion properties of matrices were also affected by physico-chemical attributes (concentration, particle size, substitution and viscosity) of MC/HPMC and drug solubility.

Regarding FBP and THP release from these matrices, the results presently obtained showed that 5 % MC/HPMC: levels were unsuitable in the case of A4M (MC) and F4M (HPMC). It can be confirmed from the results that IDR of all the matrices was significantly affected by physical-chemical attributes (concentration, particle size, substitution and viscosity) of MC/HPMC and drug solubility. Only first order and Korsmeyer-Peppas models fitted release data well and the release mechanism was considered anomalous for both drugs. However, increased MC/HPMC levels, viscosity, Hpo/Meo substitution ratios, drug solubility and a smaller MC/HPMC particle size, shifted drug release towards a more diffusion controlled mechanism.

5- Development and validation of PSA assay for erosion studies

5- Development and validation of PSA assay for erosion analysis

5.1- Introduction

Extended release (ER) tablets are frequently fabricated to minimise the overall frequency of dosage form administration, thus improving bio-pharmaceutics and more importantly, patient compliance. The hydrophilic matrix system is commonly employed in the pharmaceutical industry to develop ER tablet formulations (Alderman, 1984). Among other hydrophilic polymer-based matrices, HPMC has been extensively used in oral dosage forms (Maderuelo *et al.*, 2011).

Upon contact with liquids (dissolution testing media or biological fluids), these hydrophilic matrices swell and polymer chains eventually disentangle. As a result, a gel layer is developed across the matrix tablet as HPMC changes from a glassy state to a rubbery state (Colombo *et al.*, 1999; Colombo *et al.*, 2000; Jiasheng *et al.*, 2010; Mitchell *et al.*, 1993). HPMC has the potential to hydrate quickly enough to form a gel layer before the drug entrapped in the tablet matrix can dissolve. Highly water soluble drugs can diffuse through the gel layer before the matrix erodes, but it is suggested that the presence of poorly soluble drugs can increase matrix erosion by detrimentally affecting integrity of the gel layer (Bettini *et al.*, 2001; Yang and Fassihi, 1997). Mechanistically both drug diffusion and matrix erosion are contributing factors in controlling drug release from these formulations, however, in practical terms, one process will often play a dominant role over the other, depending on the HPMC level and solubility of other matrix tablet contents (Sinha Roy and Rohera, 2002). The mechanism of drug release from hydrophilic matrices has been previously discussed in detail, see section 4.4.

Owing to the importance of polymer erosion process in controlling the drug release mechanism, the gravimetric method (GM) is commonly used to determine the extent of polymer erosion from hydrophilic matrices (Chaibva *et al.*, 2010; Dhopeswarker and Zatz, 1993; Ebube *et al.*, 1997; Khamanga and Walker, 2006; Ranga Rao *et al.*, 1988; , Sinha Roy and Rohera, 2002) despite it being time consuming and laborious, requiring a significant amount of API and excipients. A

number of analytical techniques can be used to measure carbohydrate concentration including size exclusion chromatography (Viridén *et al.*, 2009) capillary electrophoresis (Cortacero-Ramírez *et al.*, 2004), infrared (IR) spectroscopy (Cadet, 1999), nuclear magnetic resonance (NMR) micro-imaging (Tajarobi *et al.*, 2009) and light scattering detection (Zhang *et al.*, 2008). Recently Viridén *et al.* (2009) successfully employed size exclusion chromatography to study HPMC tablet dissolution to determine the impact of HPMC heterogeneity on drug release. The PSA assay is a classical method which is routinely used in carbohydrate analysis. This is a colorimetric method based on the condensation of furan derivatives which can be produced by treating the carbohydrate with strong sulphuric acid (Harborne and Dey, 2012). Moreover, phenol is employed in PSA assay to produce coloured compounds. This PSA assay is a simple, accurate and specific chemical test for the quantification of carbohydrates. This PSA assay virtually has the ability of detecting all classes of carbohydrates, therefore, it is applicable to quantify total sugar concentration in oligosaccharides, polysaccharides, proteoglycans, glycoproteins and can be scaled down to a microplate retaining sensitivity, with potential for high throughput screening, down to 1 nmol for some sugars (Masuko *et al.*, 2005). The PSA assay is commonly employed for analysing sugars in foods, including mono-, di- and polysaccharides and could potentially provide a simple method to study matrix erosion, negating requirements for separate analytical equipment and associated costs and time (Albalasmeh *et al.*, 2013; Brummer and Cui, 2005; Masuko *et al.*, 2005). Therefore, the present set of experiments has multiple aims: firstly, the quantification of HPMC in dissolution media by using a PSA assay alongside drug release studies. The Korsmeyer and Peppas drug release model was applied to drug release profiles to attain a mechanistic insight into the process. Secondly, the amount of dissolved HPMC and the drug was combined to calculate the degree and rate of erosion. Additionally, matrix erosion was also determined by using a gravimetric method for validation purposes; with an assumption that PSA assay would be an alternative option. Thirdly, the inter-relationship of the HPMC erosion rate and drug release was studied. Fourthly, the effect of HPMC concentration and the solubility of model drugs on polymer dissolution, drug release kinetics and

matrix erosion were also studied. THP (water soluble, 8.3 g/L) and FBP (poorly soluble, 8.0mg/L) were used as a model drugs (Yalkowsky *et al.*, 2010).

5.2- Experimental

5.2.1- Materials

5.2.1.1- Cellulose ethers

Cellulose ethers (MC/HPMC) were obtained as described in the section 2.1.1 and their specifications are enlisted in Table 2.1.

5.2.1.2- Model drugs

Model drugs, FBP (FBP) and THP (THP) were obtained as described in the section 2.1.1

5.2.1.3- Buffering agents

To prepare dissolution medium, buffering agents were purchased as described in the section 2.1.3.

5.2.2- Methods

5.2.2.1- Preparation of powder mixtures

Binary powder mixtures containing HPMC (K4M) and drugs were prepared, moreover their content uniformity was tested as a detail method is described in section 2.2.8.1.

5.2.2.2- Preparation of matrix tablets

Matrix tablets were prepared by using plain MC/HPMC powders and powder mixtures prepared according to section 5.2.2.1 and a method was adopted which has been described in section 2.2.8.2.

5.2.2.3- Drug release studies

The drug (FBP or THP) release studies were carried out using the method described in section 2.2.8.3.1.

5.2.2.4- MC/HPMC release studies

The MC/HPMC release studies were carried out using the method described in section 2.2.8.3.2.

5.2.2.5- Matrix erosion studies

Matrix erosion studies were carried out by adopting gravimetric and combined dissolution methods described in section 2.2.8.4.1 and 2.2.8.4.2, respectively.

5.2.2.6- Drug release kinetics

The Korsmeyer– Peppas mathematical model was applied to drug release data as described in section 2.2.4.5.2 and 2.2.8.4.3.

5.3- Results and discussion

5.3.1- Erosion study of plain MC/HPMC compacts

In hydrophilic polymeric matrix systems, the polymeric carrier present on the surface of the matrix tablet is primarily responsible for the development of the outer viscous gel layer and this layer can control the overall matrix erosion rate (Sinha Roy and Rohera, 2002). The dissolution of MC/HPMC from matrix tablets has been studied throughout the years by using different techniques (Tajarobi *et al.*, 2009; Viridén *et al.*, 2009). In this study, its release from a plain polymeric matrix tablet was quantified using the PSA assay. As MC/HPMC has a glucose monomer backbone with different levels of methoxyl (%) and hydroxypropoxyl (%) substitution groups incorporated to form various grades depending on the need of the industry it was proposed that the phenol-sulphuric acid assay, which is classically used to measure carbohydrate content in foods and beverages (Brummer and Cui, 2005), could be applied to quantify MC/HPMC released from matrix tablets. The degree of matrix erosion as a function of time is depicted in Figure 5.1 (a and b) and is reported as % erosion and a summary of erosion kinetics parameters are enlisted in Table 5.1.

5.3.1.1- Effect of MC/HPMC particle size

In the present study, the matrix erosion rate of MC/HPMC was affected by the particle size. The MC/HPMC compacts fabricated from particles between 90 - 150 μm tend to have a slow erosion rate in comparison to the compacts made from larger particles, (150 - 250 μm) (Figure 5.1a and b). However, the K100M based polymeric compacts shows only a slight difference when particle size was reduced from 150 - 250 μm to 90 - 150 μm (Table 5.1). In general, smaller particle size shows a decrease in the erosion rate and the behaviour can be explained by considering hydration kinetics. Large polymer particles take longer to hydrate and to develop a gel layer across the matrix tablet in comparison to smaller particles. It was noticed by various researchers that the fine MC/HPMC powder particles hydrate quickly because of the larger surface area and develop a gel layer around the tablet faster, which act as a barrier controlling the swelling, matrix erosion and drug release (Campos-Aldrete and Villafuerte-Robles, 1997). Moreover, on hydration, the hypromellose based compacts, having larger HPMC particles left larger pores on the tablet surface which potentially deteriorate the stability of gel layer and can lead to premature matrix erosion. So, it can be concluded from the present findings that the particle size can potentially affect the erosion properties of polymeric compacts and erosion rate can be modified using MC/HPMC with different particle sizes.

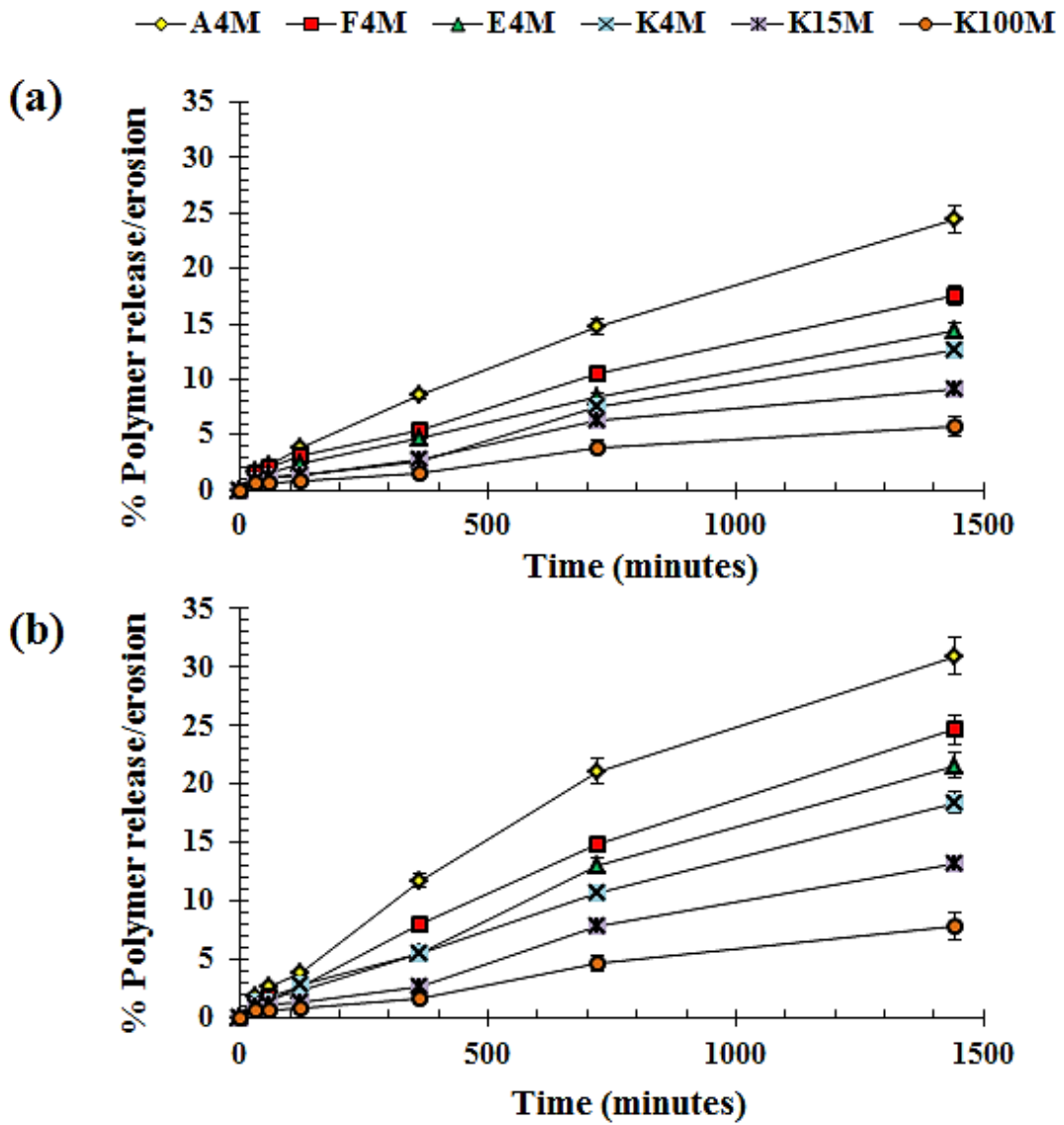


Figure 5.1, Dissolution/erosion profiles of cellulose ethers based matrix tablets of particle size (a) 90-150 (b) 150-250 μm (n = 3).

Table 5.1, Summary of MC/HPMC erosion kinetics parameters (n = 3).

| Methocel [®] | Particle size (µm) | Matrix erosion parameters | |
|-----------------------|--------------------|---------------------------|-------|
| | | K_E | R^2 |
| A4M | 90-150 | 0.020 | 0.989 |
| | 150-250 | 0.022 | 0.968 |
| F4M | 90-150 | 0.013 | 0.979 |
| | 150-250 | 0.017 | 0.989 |
| E4M | 90-150 | 0.011 | 0.985 |
| | 150-250 | 0.015 | 0.99 |
| K4M | 90-150 | 0.010 | 0.953 |
| | 150-250 | 0.011 | 0.989 |
| K15M | 90-150 | 0.008 | 0.953 |
| | 150-250 | 0.009 | 0.985 |
| K100M | 90-150 | 0.005 | 0.964 |
| | 150-250 | 0.005 | 0.985 |

$K_E = \text{Erosion constant/rate } (\% \text{ min}^{-1})$

5.3.1.2- Effect of Methocel[®] substitution ratio

The substitution pattern on the parent glucose ring of MC/HPMC plays a vital role in determining the matrix erosion rate. In the current study, the erosion rates of MC/HPMC having different Hpo/Meo substitution ratios were tested: A4M, F4M, E4M and K4M (see chapter 2, table 2.1 for detailed specifications). The A4M has the highest erosion rate (0.020 and 0.022 % min⁻¹) in comparison to F4M (0.013 and 0.017 % min⁻¹), E4M (0.011 and 0.015 % min⁻¹) and K4M (0.010 and 0.011 % min⁻¹). The comparatively fast erosion of A4M can be attributed to the presence of the higher percentage of hydrophobic substituent (methoxyl, Meo) and absence of the hydrophilic, Hpo, groups, Table 5.1 and 2.1 (chapter 2). As the percentage of Hpo/Meo increases (F4M >E4M >K4M), the erosion rate decreases. The faster swelling rate with increasing Hpo/Meo ratio (see section, 4.6.3.1) lead to rapid formation of the gel layer on the matrix tablet surface and a reduction in erosion rates, Table 5.1 and 2.1 (chapter 2). Previously, it was confirmed with NMR imaging that different substitution levels in cellulose ethers can give rise to different water mobilities (Rajabi-

Siahboomi *et al.*, 1996). It can be further stated that the amount of water that attaches to the polymer and the amount of tightly bound water depends on the degree of substitution which in turn significantly influence erosion (McCrystal *et al.*, 1997). So, from the present findings it can be concluded that the incorporation of Meo and Hpo groups on the parent glucose ring of MC/HPMC can significantly affect the erosion rate.

5.3.1.3- Effect of MC/HPMC viscosity

The erosion or dissolution of polymeric contents decreased with increasing polymer molecular weight. In the present study, the erosion rates of MC/HPMC having different viscosities were tested: K4M, K15M and K100M (see chapter 2, table 2.1 for detailed specifications). It was observed that the higher molecular weight grade of HPMC (K100M) has a lowest erosion rate (0.005 % min⁻¹), Table 5.1. This can be ascribed to its ability to develop a thick gel layer which is resistant to erosion and more durable (Lee *et al.*, 1999). Moreover, MC/HPMC polymeric chains swell faster with an increase in polymer viscosity or molecular weight. The polymer chains of MC/HPMC with higher viscosities tend to entangle and enhance the hydrodynamic volume within a matrix tablet, leading to higher degree of swelling and as a result the pores of high viscosity MC/HPMC inhibit further liquid uptake. This in turn leads to the formation of a turbid gel, which is resistant to dilution or erosion, subsequently resulting in slower matrix erosion and prolonged drug release. The trend of erosion rate with increasing viscosity (molecular weight) was K4M >K15M >K100M (Table 5.1). So, it can be concluded from the present results that the viscosity of MC/HPMC can significantly influence the erosion properties of polymeric compacts.

5.3.2- Drug release studies from K4M : FBP/THP matrices

The *in vitro* drug release profiles where HPMC is primarily used as a matrix forming polymer are depicted in Figure 5.2 (a and b). HPMC on the surface of matrix tablets initially hydrates during the dissolution process and helps to form an outer gel layer around the matrix tablet. The continued contact of the tablet with the dissolution medium leads to subsequent bulk hydration of the matrix. Essentially, this leads to HPMC chain relaxation, followed by erosion of the matrix. The drug release rate and mechanism are controlled by the matrix swelling, diffusion of drug through the gel layer and/or matrix erosion.

It was noticed that the HPMC concentration in a matrix tablet played an important role in regulating the release of THP and FBP from the hydrophilic matrix tablets. FBP and THP release profiles are shown in Figure 5.2 (a and b), and for both drugs, the HPMC ratio significantly affected the release rates, both decreasing with increasing HPMC content as the higher concentrations of HPMC reduced the polymeric chain disentanglement (Li *et al.*, 2005; Maderuelo *et al.*, 2011). At higher ratios of HPMC the increased levels lead to physical cross linking which increases the tortuosity of matrix tablets (Chaibva *et al.*, 2010; Mitchell *et al.*, 1993). This can be considered an important feature impeding the diffusion of drugs from the matrix gel layer during dissolution. The porosity of matrix tablet can be an additional factor, as the matrix tablet exhibits a low porosity at higher levels which may tend to slow down the liquid mobility across the surface of matrix tablet and leads to slower drug release rates (Reza *et al.*, 2003).

A substantially faster drug release was observed for hydrophilic matrices containing 20% HPMC, and the release rates from matrices containing FBP were slower than those with THP. The t_{60} and t_{120} of FBP-containing matrices were lower than those of THP (Table 5.3). The rapid gel layer formation around the matrix tablet is a fundamental feature that can dictate the drug release regardless of its solubility. Higher amounts of HPMC tend to form a quicker, but stronger, gel layer which is more resistant to diffusion and/or erosion. (Mitchell *et al.*, 1993).

The mechanism by which drugs are released from hydrophilic systems can possibly be; (a) (diffusion- Fickian release), (b) non- Fickian or anomalous transport (c) zero-order release or case II mechanism. Water soluble drugs (THP) can act as pore formers in matrix tablets and have the tendency to create micro-cavities on the surface of matrix tablet, thus making the gel layer more porous, increasing liberation into the bulk dissolution media through diffusion (Yang and Fassihi, 1997). Moreover, poorly water soluble drug (FBP) particles can be translocate through the gel layer with a spring-like action caused by the transition of the polymer chains from a glassy to a rubbery state, which disrupts the gel layer structure (Bettini *et al.*, 2001) and can result in exposure of drug particles to water. The mechanism of drug release was determined by applying the Korsmeyer-Peppas model (see chapter 2 and section 2.2.7.5.4 for further detail) to drug release profiles. Attributing to the release kinetics criteria for swellable cylindrical systems (Siepmann and Peppas, 2001), all tablet matrices, regardless of the drug, resulted in non-Fickian release (anomalous transport mechanism) (Table 5.3). The HPMC concentration and drug in the matrices affect the diffusional exponent (n). As the HPMC level increases in the matrix tablet, the n values decreased from 0.88 to 0.60 and 0.75 to 0.50, respectively for FBP- and THP- containing matrices. This implies that the release behaviour of matrix tablets fabricated in the present study is a mixture of diffusion and erosion, however according to the n values, it can be determined that erosion was the dominating mechanism for FBP matrices whilst diffusion dominated for THP matrices.

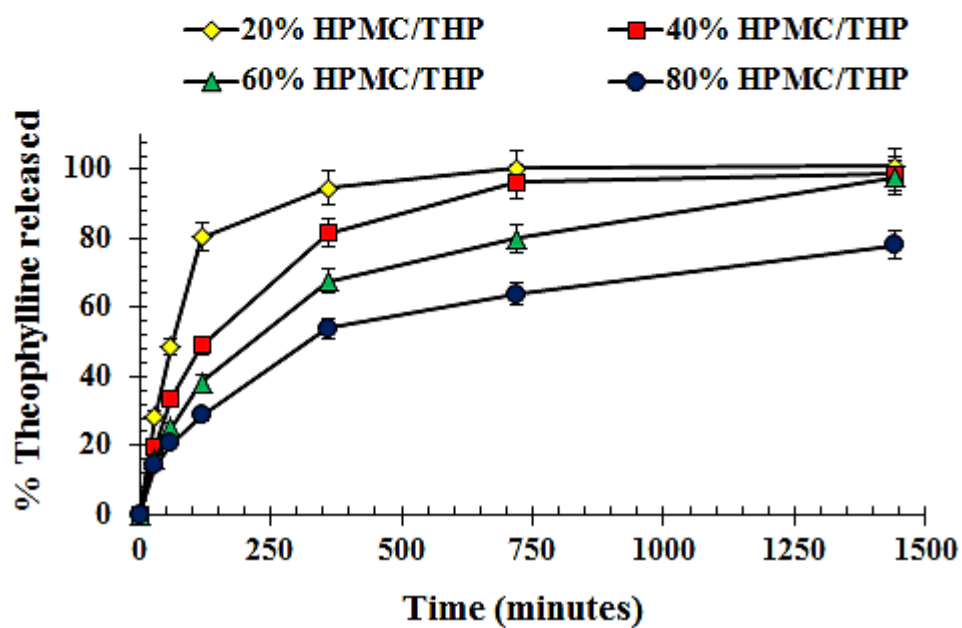
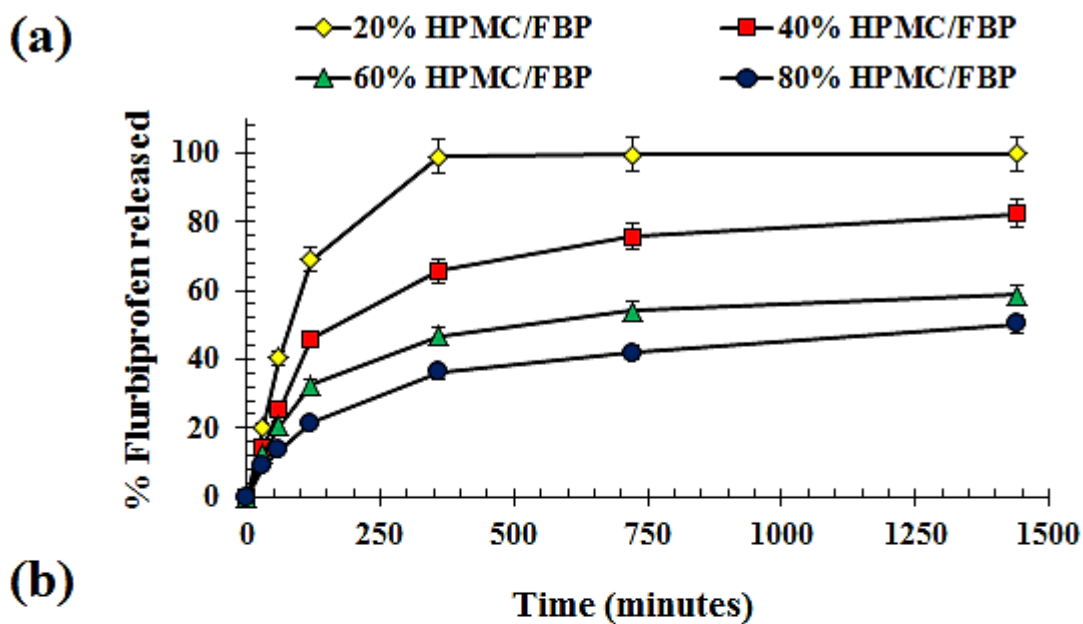


Figure 5.2, Effect of HPMC (K4M) concentration on the (a) FBP and (b) THP release from matrix tablets (n = 3).

5.3.3- HPMC dissolution studies

In this study, HPMC dissolution (using K4M) from matrix tablets containing varying concentrations of drug (THP or FBP), ranging from 0% to 80 %, was quantified using the PSA assay. UV-Vis spectra scanning for both THP and FBP showed that there was no interference with the assay at the wavelength of interest ($\lambda_{\text{max}} = 490 \text{ nm}$).

It can be seen in Figure 5.3 (a and b), that the rate and extent of HPMC dissolution decreased with increasing HPMC concentration. This can be attributed to a thicker, more durable, gel layer formed on the matrix surface at higher concentrations. The HPMC release rates were concentration dependant and a similar trend was seen for both the formulations containing FBP and THP (Table 5.3), i.e. $20 > 40 > 60 > 80 > 100\%$. However, HPMC is relatively soluble at pH 7.2 but the mobility of the macromolecule is decreased with increasing HPMC content in the matrix tablet with chain self-entanglement occurring once hydrated. Moreover, Methocel® K4M has is relatively resistant to polymer erosion compared to lower molecular weight and viscosity grades. The concentration of HPMC necessary to develop a rapid and strong gel layer around the matrix tablet is termed as critical concentration and indicates an ability to withstand the influence of different factors during dissolution or hydration. This is a desirable property of a polymer in controlled drug delivery system and the critical concentration is related to the thickness of the gel layer that forms and specific to each polymer (Maderuelo *et al.*, 2011). It is obvious from Figure 5.3 (a and b) and Table 5.3 (t_{60} and t_{120}), that HPMC dissolution from FBP-containing matrices was higher than THP formulations. This is due to the poor solubility of FBP as it can jeopardise the integrity of gel layer, which can lead to faster HPMC release. The presence of poorly soluble particles in the gel layer hinders the expansion of the polymer and decreases the resistance of the system to erosion, which increases the rate of release of the drug via erosion mechanisms (Table 1). Therefore, THP matrices have slower HPMC dissolution rates in comparison to FBP matrices (Table 5.3).

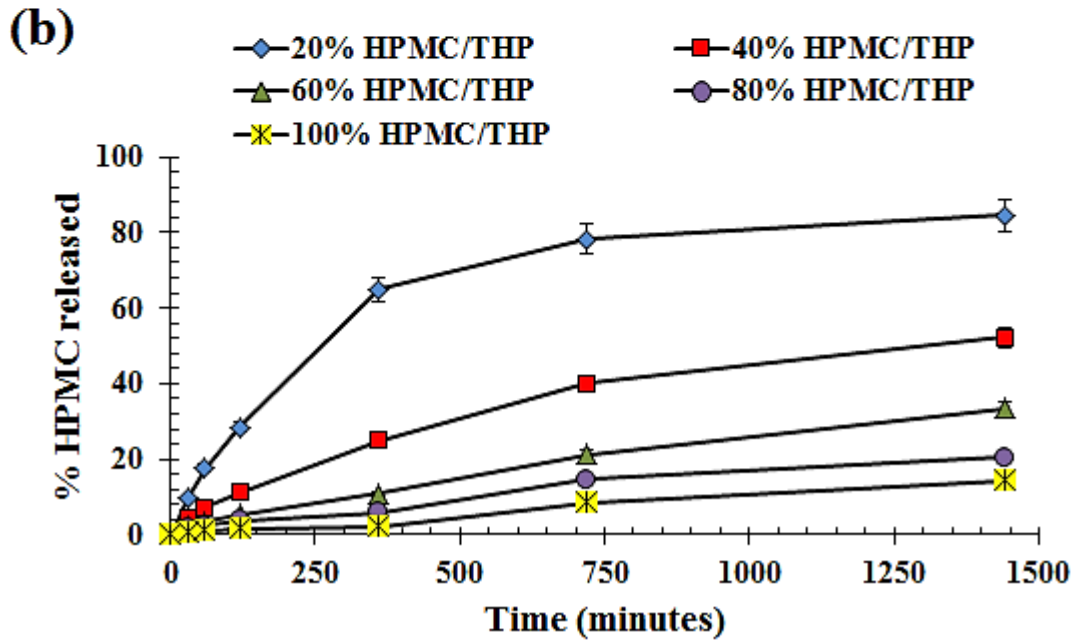
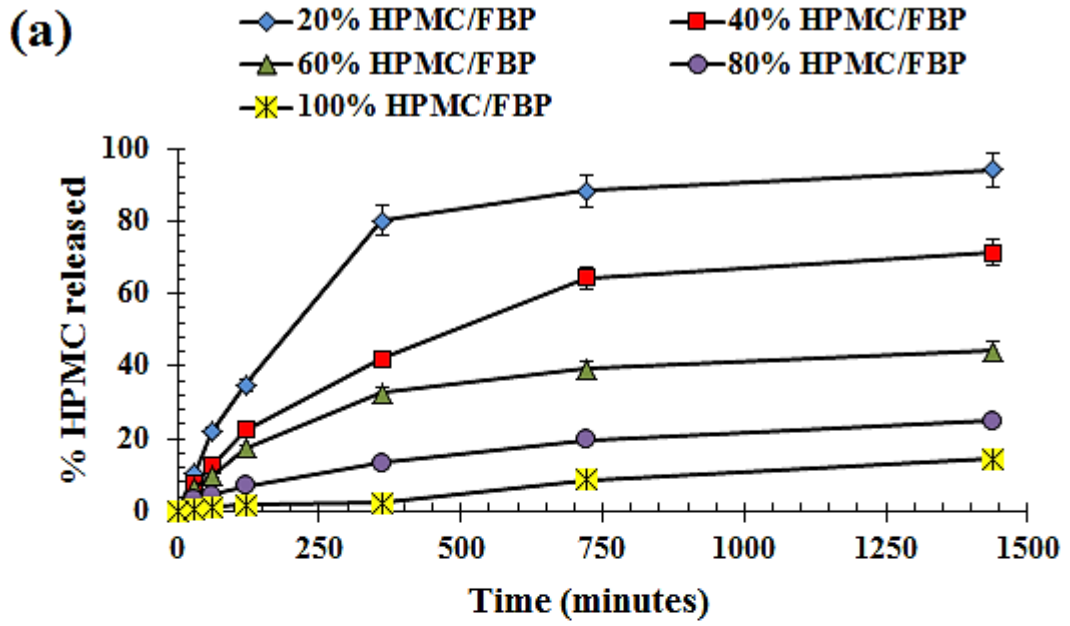


Figure 5.3, Effect of HPMC concentration on the HPMC release from (a) FBP and (b) THP containing matrix tablets (n = 3).

Table 5.2, HPMC (K4M) and drug release kinetics parameters of THP and FBP matrix tablets (n = 3, standard deviation are in parenthesis)

| HPMC:THP | HPMC:FBP | Drug release kinetics parameters | | t_{60} (%) | | t_{120} (%) | |
|--------------|--------------|----------------------------------|-------|--------------|--------------|---------------|--------------|
| | | <i>n</i> | R^2 | Drug | HPMC | Drug | HPMC |
| 100:0 | 100:0 | - | - | - | 1.05 | - | 1.56 |
| 80:20 | - | 0.50 | 0.999 | 20.57 (1.02) | 2.50 (0.12) | 28.64 (1.43) | 3.85 (0.19) |
| 60:40 | - | 0.61 | 0.990 | 25.38 (1.26) | 3.58 (0.17) | 38.31 (1.91) | 5.50 (0.27) |
| 40:60 | - | 0.66 | 0.997 | 33.58 (2.43) | 7.30 (0.36) | 48.95 (2.44) | 11.20 (0.56) |
| 20:80 | - | 0.75 | 0.999 | 48.69 (1.67) | 17.67 (0.88) | 80.32 (4.01) | 28.52 (1.42) |
| - | 80:20 | 0.62 | 0.997 | 13.65 (0.68) | 4.33 (0.21) | 21.37 (1.06) | 6.98 (0.34) |
| - | 60:40 | 0.64 | 0.994 | 20.64 (1.03) | 9.65 (0.48) | 32.68 (1.63) | 17.32 (0.86) |
| - | 40:60 | 0.83 | 0.999 | 25.36 (1.26) | 12.36 (0.61) | 45.87 (2.29) | 22.36 (1.11) |
| - | 20:80 | 0.88 | 0.995 | 40.31 (2.01) | 21.98 (1.09) | 68.96 (3.44) | 34.89 (1.74) |

t_{60} / t_{120} = Percent drug/HPMC release after 60/120 minutes

5.3.4- Matrix tablet erosion studies

The water in the hydrated gel layers of matrix tablet exists in three different states; type I (freezable free or bulk water), type II (freezable bound water) and type III (bound water) (Asare-Addo *et al.*, 2013a; Jhon and Andrade, 1973). Moreover, there is a moisture gradient which is present between the outer surface which is in contact with liquid and the inner dry polymeric matrix core (McCrystal *et al.*, 1997). Over time, the outer surface of the hydrated matrix tablet tends to dissolve and this leads to matrix erosion.

The extent of matrix erosion is shown in Figure 5.4 and 5.5, reported as % matrix erosion (E) and shows the cumulative amount of both dissolved drug and HPMC. In this study, the mass loss from the matrices increased gradually over time. The matrices fabricated from 100 % HPMC eroded slowly compared to those containing drugs (FBP or THP). Both methods for determining erosion, GM and PSA, gave similar results, with the erosion rate of 100% HPMC matrices being $0.011 \text{ \% min}^{-1}$ (Table 5.4). The erosion rate of 80:20, HPMC:FBP was slower (GM = $0.027 \text{ \% min}^{-1}$ PSA = $0.028 \text{ \% min}^{-1}$) increasing to 0.104 and $0.100 \text{ \% min}^{-1}$ respectively for both PSA and GM methods as the HPMC levels declined in the matrix tablets, suggesting that these matrices have reduced resistance to erosion. Similarly, the matrices prepared with 80:20 HPMC: THP have the slowest erosion rate (GM = 0.033 and PSA = $0.028 \text{ \% min}^{-1}$) and the rate tends to decrease as HPMC content increases. The erosion rates of matrices containing 20:80, HPMC: THP were 0.089 and $0.088 \text{ \% min}^{-1}$ respectively with PSA and GM methods. Moreover, it can be concluded that erosion increased as the drugs were incorporated in the matrices (Table 5.4), with erosion rates being higher for the poorly water soluble drug, FBP, as described before.

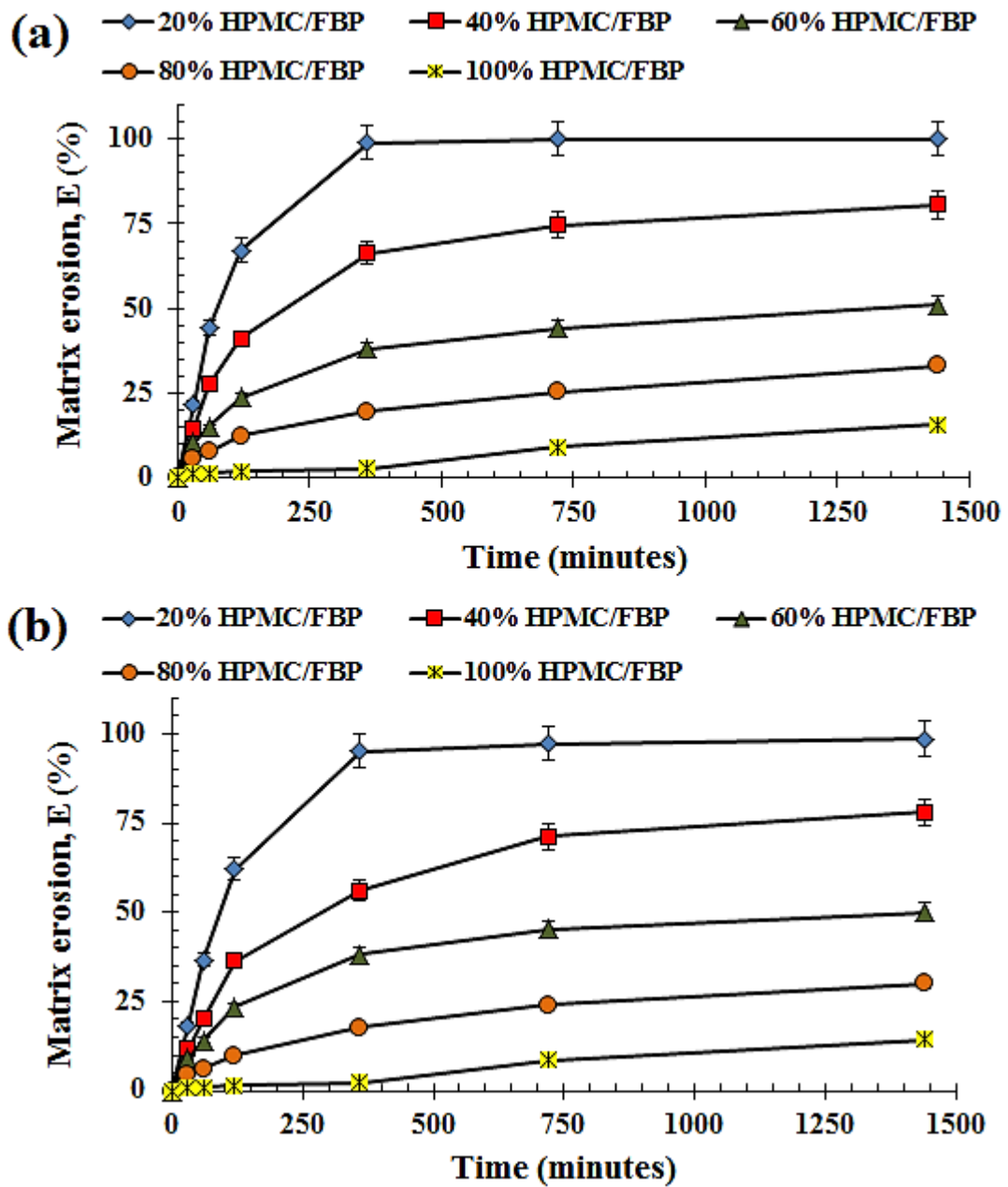


Figure 5.4, Erosion profiles of HPMC/FBP matrix tablets, (a) gravimetric technique and (b) phenol-sulphuric acid assay method (n = 3).

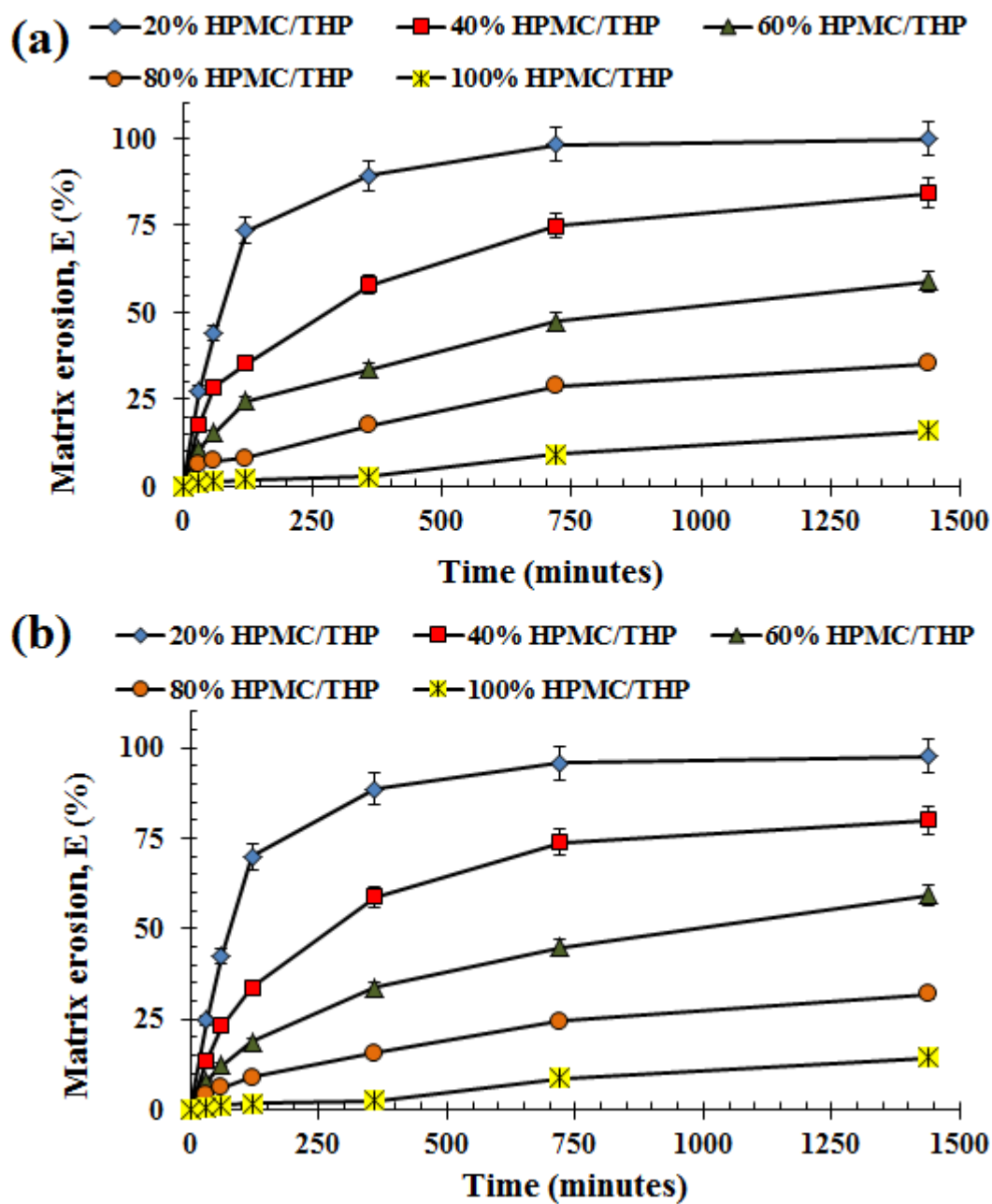


Figure 5.5, Erosion profiles of HPMC/THP matrix tablets, (a) gravimetric technique and (b) phenol-sulphuric acid assay method (n = 3).

Table 5.3, Erosion kinetic parameters for THP and FBP matrix tablets (n = 3).

| HPMC:THP | HPMC:FBP | Erosion rates (k, %min ⁻¹) | | | | | |
|----------|----------|---|----------------|-------|----------------|--------------------|----------------|
| | | PSA* | R ² | GM** | R ² | H _e *** | R ² |
| 100:0 | 100:0 | 0.011 | 0.918 | 0.011 | 0.915 | 0.011 | 0.918 |
| 80:20 | - | 0.028 | 0.989 | 0.033 | 0.996 | 0.018 | 0.970 |
| 60:40 | - | 0.052 | 0.946 | 0.049 | 0.937 | 0.027 | 0.997 |
| 40:60 | - | 0.083 | 0.917 | 0.078 | 0.939 | 0.051 | 0.990 |
| 20:80 | - | 0.089 | 0.716 | 0.088 | 0.716 | 0.099 | 0.903 |
| - | 80:20 | 0.028 | 0.952 | 0.027 | 0.931 | 0.024 | 0.979 |
| - | 60:40 | 0.050 | 0.874 | 0.047 | 0.874 | 0.047 | 0.899 |
| - | 40:60 | 0.081 | 0.890 | 0.080 | 0.833 | 0.080 | 0.976 |
| - | 20:80 | 0.104 | 0.734 | 0.100 | 0.710 | 0.112 | 0.853 |

*PSA = Phenol sulphuric acid assay technique, **GM = Gravimetric method, ***H_e = HPMC erosion rate

5.3.5- Quantitative relationship between GM and PSA

Application of the PSA assay technique to study matrix erosion during tablet dissolution processes was validated by comparing the findings of PSA assays with the more established and conventional gravimetric method. A mass balance was achieved in all cases and the matrix erosion rates and degree of matrix erosion (%) calculated using both techniques are reported in Table 5.4 and Figures 5.4 and 5.5, respectively.

The erosion data obtained from both techniques was used to construct residual plots where the bisector of first quadrant line is $y = x$. The residual plot, comparing the matrix erosion rates of both techniques, is depicted in figure 5.8. The extent of matrix erosion (E, %) of both the techniques with respect to time was also used to generate residual plots and these are depicted in Figure 5.9a and b. Analysis of residuals showed random distribution about the horizontal axis and there was a strong correlation between the results from both techniques (Figure 5.6), with adjusted R^2 of 0.998 and 0.988 (Table 5.5) for FBP and THP, respectively. Additionally, matrix erosion (%) with respect to time showed a higher degree of correlation when both methods were compared (Fig. 5.7a and b), with residual R^2 ranging between 0.986–0.998 (Table 5.6).

The assay can provide a simple, cheap, robust and rapid analysis, and has been successfully applied in this study to determine dissolved HPMC and to characterise matrix erosion of hydrophilic matrices in *in vitro* dissolution studies.

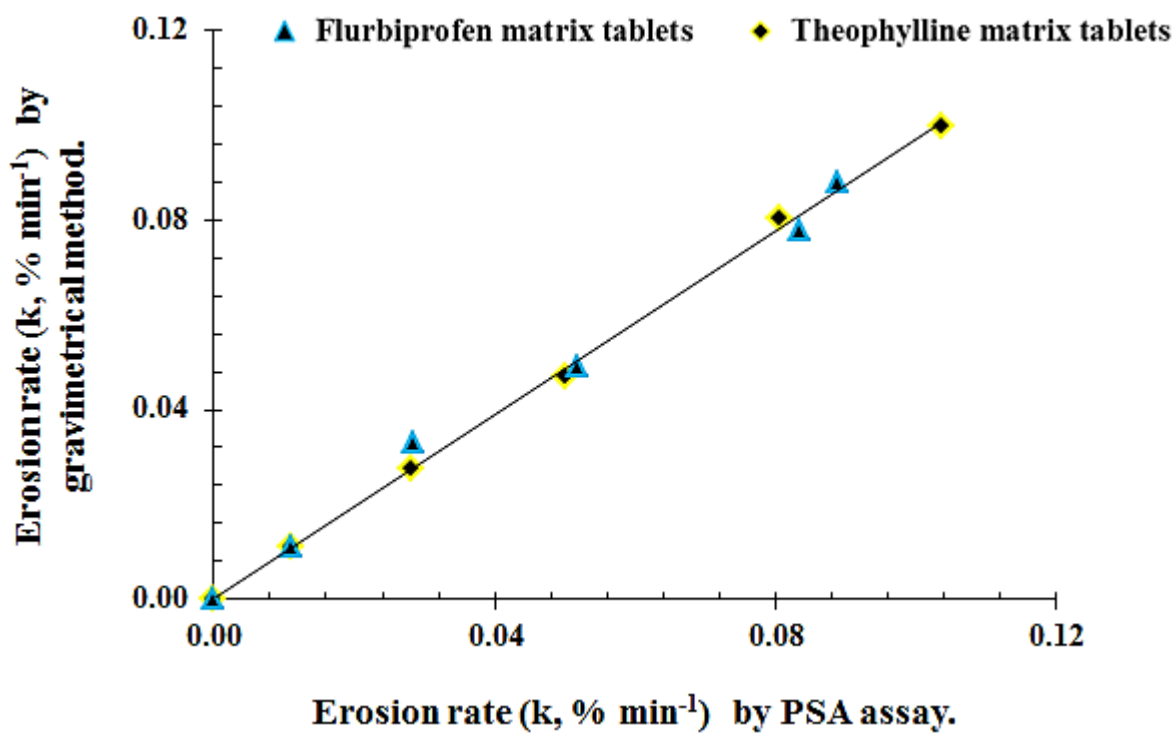


Figure 5.6, Comparative analysis of erosion rates calculated from both techniques.

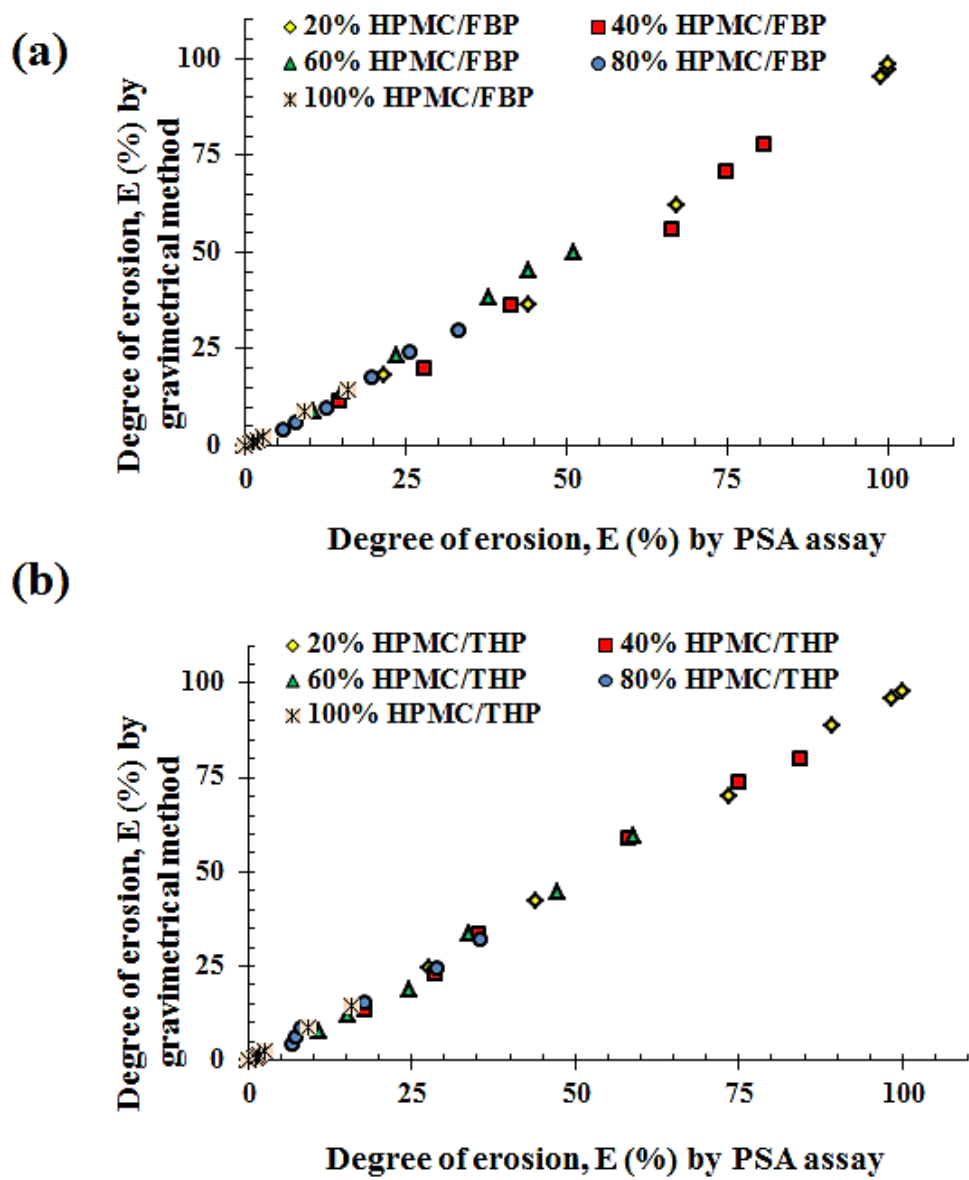


Figure 5.7, Comparative analysis of degree of erosion calculated from both techniques, (a) FBP and (b) THP based hydrophilic matrices.

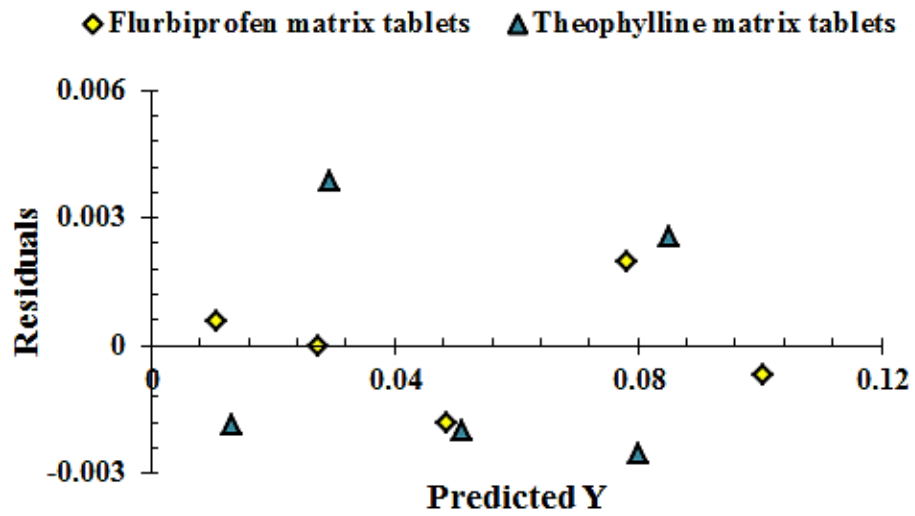


Figure 5.8, Residual plot of erosion rate, a comparison between GM and PSA techniques

Table 5.4, Comparison of erosion rates of matrix tablets from gravimetric and PSA assay from residual plots.

| Type of matrices | Adjusted R ² | Standard error |
|------------------|-------------------------|----------------|
| FBP matrices | 0.998 | 0.0016 |
| THP matrices | 0.988 | 0.0034 |

Table 5.5, Comparison of degree of erosion (%) of matrix tablets from gravimetical and PSA assay from residual plots (n = 3, standard error is in parenthesis).

| HPMC:THP | HPMC:FBP | Correlation co-efficient |
|--------------|--------------|--------------------------|
| | | R² |
| 100:0 | 100:0 | 0.998 (0.18) |
| 80:20 | - | 0.986 (1.45) |
| 60:40 | - | 0.988 (1.99) |
| 40:60 | - | 0.991 (2.53) |
| 20:80 | - | 0.998 (1.17) |
| - | 80:20 | 0.994 (0.86) |
| - | 60:40 | 0.997 (0.87) |
| - | 40:60 | 0.986 (3.57) |
| - | 20:80 | 0.995 (2.68) |

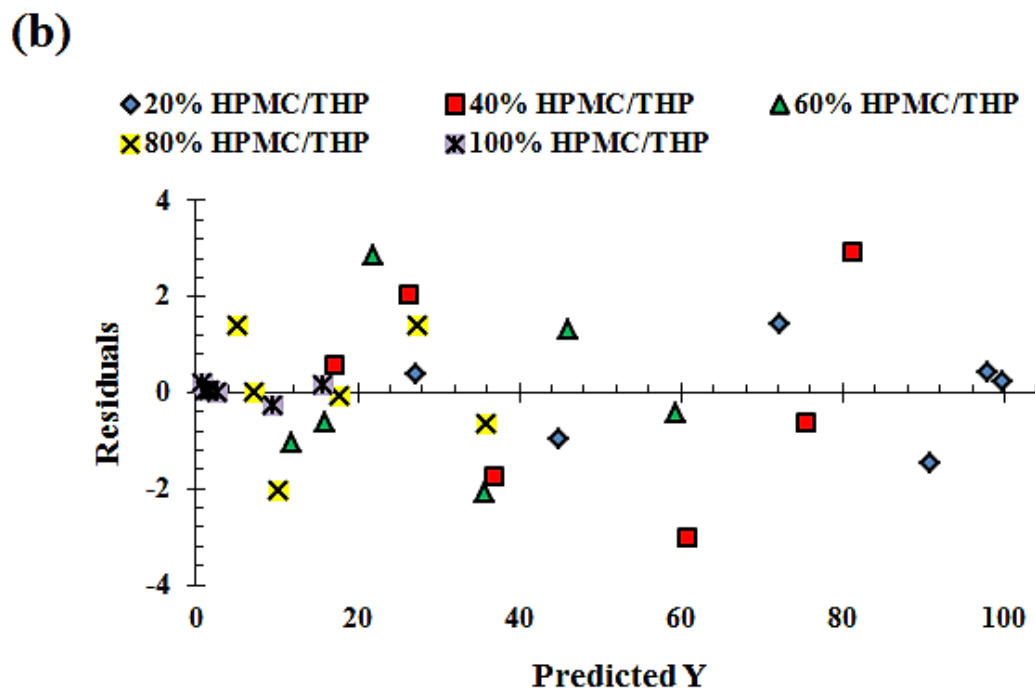
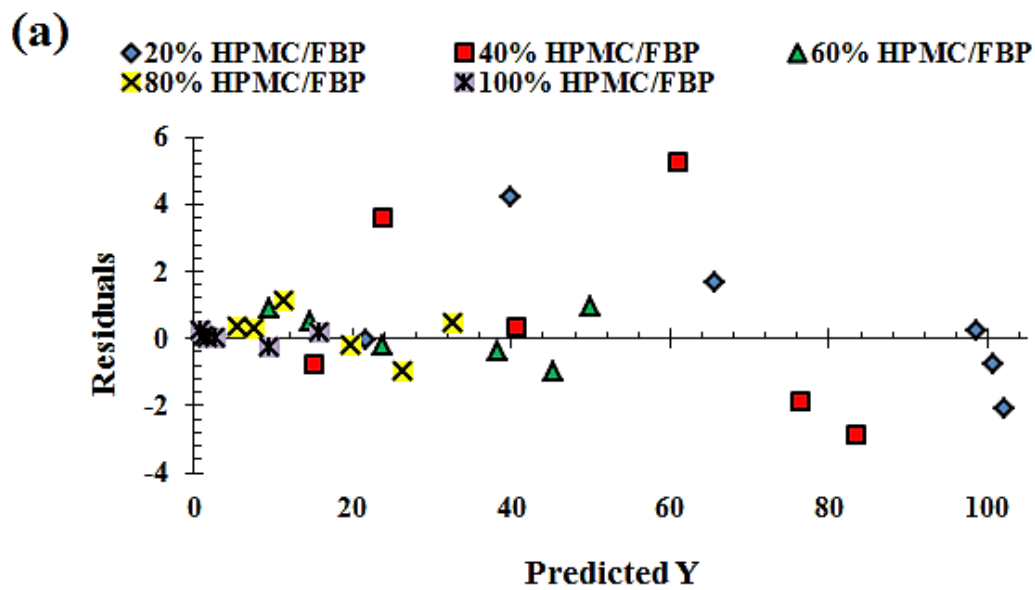


Figure 5.9, Residual plot of comparative degree of erosion between GM and PSA assay, (a) FBP and (b) THP matrices.

5.3.6- Inter-relationship between HPMC erosion and drug release kinetics

It is evident from the drug release kinetics shown in Table 5.2 that HPMC concentration has a significant impact on the drug release diffusional coefficient (n). It can be anticipated from the n values (Table 5.2) that all the matrix tablets have an anomalous drug release mechanism. Thus, both diffusion and erosion are involved during drug release. It has been reported in the past that poorly soluble drugs were released dominantly by erosion of the matrix tablet; however, water soluble drugs were released dominantly by diffusion through the gelatinous layer (Bettini *et al.*, 2001; Yang and Fassihi, 1997). This is confirmed in this study where erosion dominated when FBP was released and diffusion in the case of THP release. Figure 5.10 shows the relationship between the n values of drugs and HPMC erosion rate (k). A simple regression analysis was applied to model their relationship and the values of R^2 were 0.9275 and 0.8549 for FBP and THP matrices, respectively.

Moreover, it is possible to conclude that there is a linear relationship between the n values and HPMC erosion rate (k); the diffusional exponents (n) values are lower for the less water soluble drug, FBP, at all HPMC: drug levels. So, it can be concluded that the hydrophilic matrices containing FBP are less dependent on diffusional drug release and thus a better correlation was apparent between n and polymer erosion rate.

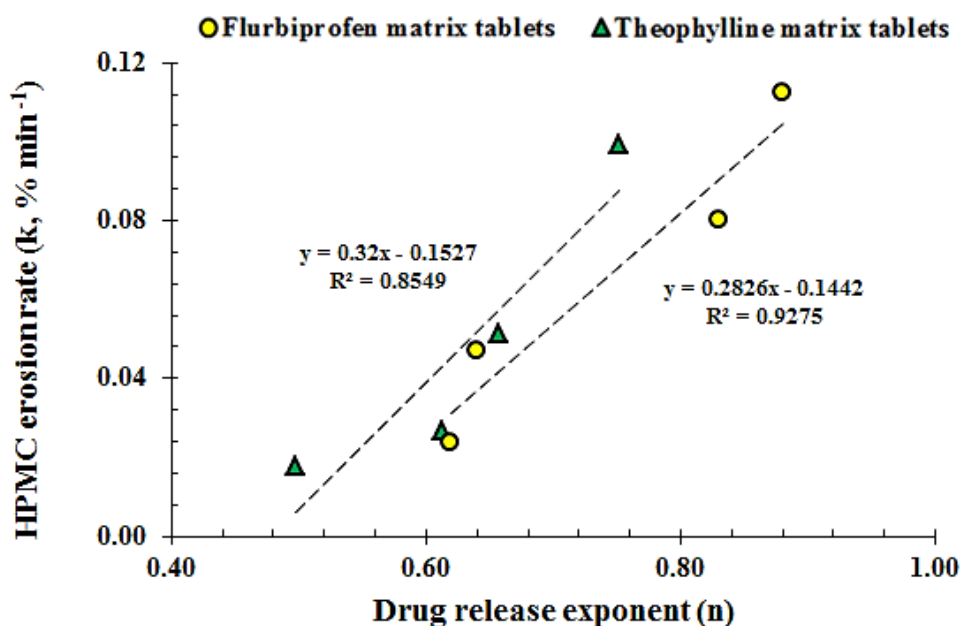


Figure 5.10, Comparative analysis between HPMC erosion rate (k) and drug release diffusional exponent (n).

5.4- Summary

A PSA assay was successfully applied to study polymer erosion kinetics from MC/HPMC compacts with varied physicochemical properties. It can be concluded that particle size, substitution ratios and viscosity (molecular size) of MC and HPMC significantly influence erosion kinetics parameters.

Hydrophilic matrices, containing HPMC K4M as the polymer, and different drugs, FBP and THP, were evaluated for drug content, degree of matrix erosion, HPMC and drug release properties. The phenol-sulphuric acid assay was again successfully adopted for the quantification of dissolved HPMC in the dissolution media. The HPMC dissolution rate increased as the level of HPMC decreased in the matrix tablets. Thus it leads to a conclusion that HPMC levels and solubility of drugs are important factors to consider during the designing of hydrophilic matrix tablet formulations.

The release of FBP and THP was an anomalous transport mechanism, however, Fickian diffusion and erosion dominated for THP and FBP matrices, respectively. The PSA assay also identified an inter-relationship between HPMC erosion rates (k) and Korsmeyer–Peppas parameter, n ,

The matrix erosion results obtained from newly adopted PSA method confirm that the solubility of the drug, and levels of HPMC in a particular matrix tablet, significantly affect the matrix erosion rate and the results were similar to those determined using the much more labour-intensive gravimetric method. Moreover, the combination of conventional UV drug analysis technique and PSA assay can be used to simultaneously quantify the matrix erosion, polymer dissolution and drug release kinetics in a single set of experiments avoiding the need for separate studies.

6- Compaction studies of hydrophilic matrices

6- Compaction studies of hydrophilic matrices

6.1- Introduction

The use of pills and powders to administer drugs was reported as early as 1550 BC in Papyrus Ebers. The pill continued to be one of the most common dosage forms until the middle of the 20th century, when mass-production of tablets was introduced following the invention of the tableting machine, patented in 1843 by William Brockedon (Swarbrick, 2007). Pharmaceutical products have historically been administered to the body using a relatively basic drug and excipient combination in suitable dosage form, usually resulting in rapid release and systemic absorption of the drugs. Different drug delivery technologies and routes of administration have been used to ensure optimal administration of therapeutic agents (Yihong 2009). All through the history of pharmacy, the oral route has been the most preferred way of drug administration and tablets are regarded as most commonly used pharmaceutical dosage form. The advantages of this dosage form are manifold: convenient to dispense and store, and easy administration, and they provide a versatile means of delivering the drug. Release of drug from the tablet can be controlled by altering the design and content of the formulation. Also, since this is a dry dosage form, tablets provide a supportive environment for maintaining drug stability and generally have a relatively long shelf life (Remington and Allen, 2013).

The characteristics of the tablet (mechanical strength, disintegration time and drug release) are affected by both the properties of the constituent materials and the manufacturing process. For instance, tablets must be sufficiently strong to withstand handling during manufacturing and usage, but should also disintegrate and release the drug in a predictable and reproducible manner (Sandell, 1992). All the aforesaid features of tablets are essentially dependant on the properties of the powder particles usually used as raw materials. A powder is a heterogeneous

system of solid dry particles and the air can be present both between, and inside, the particles (Riepma *et al.*, 1993; Sandell, 1992). According to British Standard (BS2955, 1958) the maximum dimension of a particle in a material to be called as powder, is less than 1000 μm (York, 1980). Moreover, powder mixtures intended to fabricate tablets comprise several component materials with different properties and functions. In most cases these can be divided in active pharmaceutical ingredients (APIs) and excipients. The powders can be granulated to improve manufacturability, however direct compression is preferred and more economical method for tablet manufacturing (Masuda *et al.*, 2006).

6.2- Powder compaction

Compaction can be defined as the compression and consolidation of a particulate solid–gas system as a result of an applied pressure and compression involves a reduction in bulk volume as a result of reduced gaseous phase. (Patel *et al.*, 2006). Compaction is a mechanical process in which the state of the material is changed from powder into a compact of desired porosity. Compaction is one of the most important step in tablet production as the physical properties of the compacts, as well as the pressing forces, are determined not only by the properties of the powders constituting the powder mixture (such as particle size distribution, shape, morphology, lubrication conditions) but also by the processing conditions (Alderborn and Nystrom, 1995).

Over the years, there has been considerable confusion in literature around tableting terminology. Different terms like compressibility, compactibility, and tableability, have been used by authors to describe the same type of relationship. The root cause of this confusion is that three variables, pressure, tablet tensile strength and porosity, are not always studied simultaneously (Alderborn and Nystrom, 1995; Nyström *et al.*, 1993). Compressibility is the ability of a material to undergo a reduction in volume as a result of an applied pressure and is

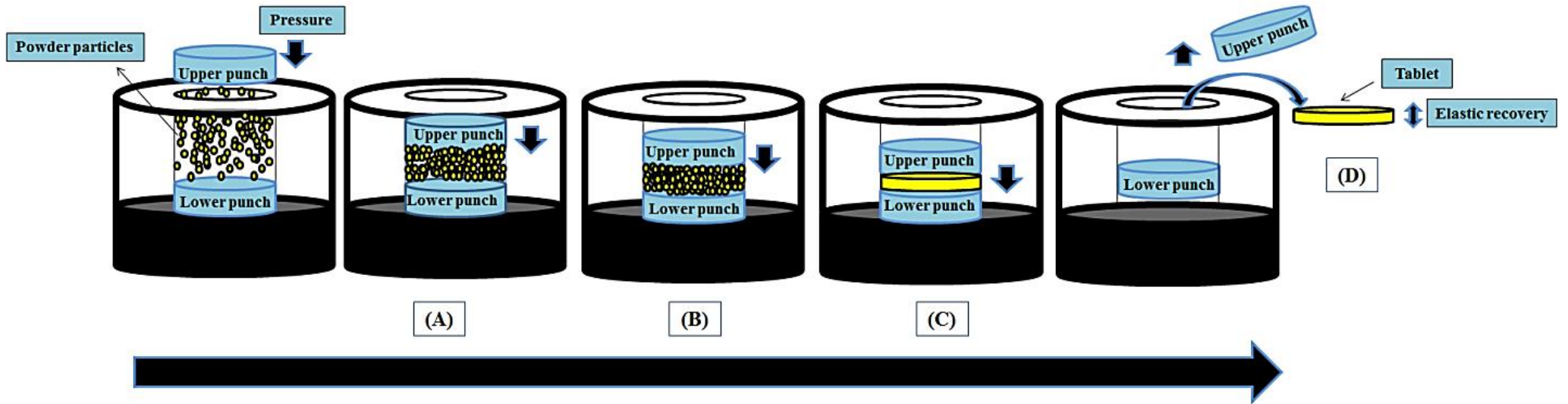
represented by a plot of tablet porosity against compression pressure; compactibility is the ability of a material to produce tablets with sufficient strength under the effect of densification and is represented by a plot of tablet tensile strength against tablet porosity; and finally, tableability is the capacity of a powder to be transformed into a tablet of specified strength under the effect of pressure and is represented by a plot of tablet tensile strength against compression pressure (Patel *et al.*, 2006; Swarbrick, 2007).

6.3- Mechanism of powder compaction

When pressure is applied to a powder bed, the bulk volume of the powder is reduced and the amount of air is decreased; this is an endothermic process as energy is consumed during this initial volume reduction of powder bed. Under compression, the particles are moved into closer proximity to each other and inter-particulate bonds may be established between the powder particles. The formation of bonds is associated with a reduction in the energy of the system as energy is released (exothermic process) (Coffin-Beach and Hollenbeck, 1983). In the literature, the term compression is often used to describe the process of volume reduction and the term compaction is used to describe the whole process, including the subsequent establishment of inter-particulate bonds (Alderborn and Nystrom, 1995; Sandell, 1992). The strength of a tablet composed of a certain material can be used as a measure of the compactibility of that material and volume reduction takes place by various mechanisms and different types of bonds may be established between the particles depending on the pressure applied and the properties of the powder. The process of powder compression into a tablet (compaction) can be generally divided into four predominant stages, which although sequential, in reality can occur simultaneously. These are; rearrangement of powder particles, elastic deformation of powder particles, plastic deformation and/or fragmentation of powder particles, and elastic recovery/relaxation after unloading and tablet ejection (Figure 6.1).

When powder is filled into the tablet die, it is loosely packed. The powder particles are able to translate and rotate with respect to one another to reach a state of dense packing. Soon thereafter, the system reaches a state where its capacity to rearrange itself is exhausted as the powder particles are constrained or locked into position by more structurally stable contact with their neighbours. This junction can be referred to as a constrained state, however there is also a degree of fragmentation that can occur during this initial stage of powder compression (Alderborn and Nystrom, 1995; Frenning *et al.*, 2009). Upon reaching the constrained state, any further reduction in the porosity of the powder bed can only occur as a result of a mechanical change in the structure of each of its composing particles. Simply put, there are two major routes of accommodation: deformation and fragmentation/breakage (Alderborn and Nystrom, 1995; Çelik, 2011; Frenning *et al.*, 2009; Leuenberger, 1982, , Roberts *et al.*, 1989). If the particles are elastic or plastic, they will deform to accommodate the increasing applied compression pressure. However, if a particle is brittle in nature, it will break into smaller pieces and, as the compression pressure increases, the surface inter-particulate voids which were formed during the initial consolidation of powder particles, will displace. Assuming the applied compression pressure is large enough, the powder particles may go through one or all of these structural changes. It is during this transitional phase that bonding occurs between the contacting surfaces of the powder particles, either as in the case of deformation, by an increased area of contact between particles, or by an increase in the number of bonding sites as in the case of breakage (Duberg and Nyström, 1981). Finally, at the maximum compression pressure, porosity is reduced to a minimum (Sonnergaard, 2000). Consequently, when the pressure is removed (unloading), the solid (tablet) begins to relax into its final dimensions, a process referred to as elastic recovery (Leuenberger, 1982). Elastic recovery/relaxation is a reversible part of deformation and higher values of elastic recovery are indicative of poor inter-particulate bonding between powder particles. The last stage in

compression cycle is ejection from die. The ejection phase also requires force to overcome adhesion between the die wall and compact surface and other forces are needed to complete ejection of tablet (Çelik, 2011).



- (A) Powder particle rearrangement
- (B) Elastic deformation of powder particles
- (C) Plastic deformation of powder particles
- (D) Elastic recovery / relaxation

Figure 6.1, Schematic illustration of different phases of powder compaction.

6.4- Bonding during powder compaction

Powder particles move during the compression process and come in close proximity to each other. This provides ample opportunities for inter-particulate bonding, yet, the mechanism of consolidation phenomena by which inter-particulate bonding happens is still elusive. However Rumpf (1958) and Turba and Rumpf (1964) proposed five possible bonding mechanisms discussed in the following sub-sections.

6.4.1- Distance attraction forces

It has been reported by various authors that mainly three different types of attraction forces are responsible for inter-particulate bonding during the compression process. However, the intensity of these forces is affected by the type of material but more importantly the distance between the powder particles in a compression die (Alderborn and Nystrom, 1995; Çelik, 2011; Leuenberger, 1982; Nyström and Karehill, 1996; Sandell, 1992) . Van der Waals forces are considered to be the most important attraction forces holding particles together (Leuenberger *et al.*, 1989). These can operate in vacuum, gas and liquid and act at a distance of 100 – 1000 Å. The second most important bonding forces are those generated because of hydrogen bonding, considered important for certain pharmaceutical materials. Moreover, various authors have proposed that electrostatic forces have a role during compaction (Patel *et al.*, 2006) but Nyström and Karehill (1996) argued that these forces may not have a significant role in tablet formation. The electrostatic forces are generally developed from tribo-electric charging during mixing and compaction. However, electrostatic forces can be neutralised relatively quickly and are not often considered to be of significance in tablets of pharmaceutical materials.

6.4.2- Solid bridges

The formation of solid bridges, also referred to as the diffusion theory of bonding, occurs when two solids are mixed and form a continuous solid phase at their interface (Israelachvili, 2011). Such a mixing process requires that molecules in the solid state are movable, at least temporarily, during compression. An increased molecular mobility can occur due to melting or as a result of a glass-rubber transition of an amorphous solid phase (Adolfsson *et al.*, 1998; Führer, 1977).

6.4.3- Non- freely movable bridges

The powders normally absorb water from the moist air. The thickness of sorbed water layers depends on the polarity of powder surface and the humidity of the atmosphere. In a fairly dry environment, the water will be tightly bound as a non-freely movable layer of water, which is denoted monolayer-absorbed moisture (Sandell, 1992) or water vapour adsorption (Ahlneck and Alderborn, 1989). If two powder particles of this kind are brought in contact, the water sorption layers can interact (Van Campen *et al.*, 1980). This results in a strong inter-particulate attraction and a joint water sorption layer (Zografis, 1988).

6.4.4- Bonding due to movable bridges

At high relative humidity, the amount of water in the powder can increase so much that, in addition to the sorption of water, there will be a separate movable water phase, which is denoted as condensed water (Çelik, 2011). Molecules of the solids can dissolve in this water which can lead to deliquescence of the solid. The critical humidity at which this takes place is characteristic of the solid and is the point above which the absorbed water assumes the character of the bulk solution or condensate (Lordi and Shiromani, 1984). Because of the high surface tension of pure water, there will be a strong attraction between powder particles.

6.4.5- Mechanical interlocking

Mechanical interlocking describes the hooking and twisting of powder particles together in a tablet. This is possible because of particle irregularities and roughness on the surface of the powder particles (Führer, 1977).

6.5- Compaction properties of Methocel[®]

Methocel[®] grades, especially MC/HPMC, are commonly used as a carrier polymer for extended drug release applications. However, various authors have reported their use as a binder in direct compression because they have good compaction properties. The high compactability of MC/HPMC has been attributed to a relatively high propensity for plastic deformation, which enables large surfaces to come close to each other and a large number of bonds, mainly intermolecular forces, to be established between the particles (Karehill *et al.*, 1990; Nyström *et al.*, 1993). Mechanical interlocking may also contribute to the mechanical strength (Karehill and Nyström, 1990). Other commonly used binders in direct compression processes include microcrystalline cellulose, starches and their derivatives, such as pre-gelatinised and granulated starches. A common feature of many such filler-binders is that they undergo plastic deformation during compaction. However, dibasic calcium phosphate dihydrate deforms via fragmentation which might be due to its brittle nature. Lactose is also used in direct compression but, compared to other filler-binders, lactose exhibits relatively poor bonding properties. By modifying lactose, for example by spray drying, a material with enhanced bonding properties can be obtained (Adolfsson and Nyström, 1996; Bolhuis and Chowhan, 1996).

6.5- Factors affecting compaction properties of Methocel®

The compaction of Methocel® (MC/HPMC) is a complex processes affected by different factors. In this section, the principal factors that can affect the compaction properties of MC/HPMC are discussed; and are summarised in Table 6.2.

6.5.1- Effect of particle size

The particle size of Methocel® (MC/HPMC) powders may determine the deformation mechanism and therefore have the tendency to dictate the consolidation phenomena (Malamataris *et al.*, 1994; Nokhodchi and Rubinstein, 2001; Rajabi-Siahboomi *et al.*, 1998). Malamataris and Karidas (1994) showed that when the particle size of Methocel® (K4M and F4M) was reduced from <320 µm to <120 µm, the tensile strength of tablets was increased. Nokhodchi *et al.* (1995) investigated the effect of particle size on the compaction properties of Methocel® (K100, K4M, K15M and K100M) and it was reported that the particle size has a noticeable impact on the tensile strength of HPMC compacts with smaller particle sizes leading to compacts with higher tensile strength. This is consistent with the theory that a smaller particle size allows greater packing density and a larger number of contact points between the powder particles for inter-particulate bonding. Moreover, the compressibility index (CI, %) of HPMC decreased with increasing particle size, as CI is frequently used to assess the powder compressibility and it gives information regarding the flowability of powders. However, the yield pressure (P_y) values of different HPMC grades were reported to be independent of particle size. Additionally, it was reported by Nokhodchi *et al.* (1995) in the same study that the elastic recovery increased as the particle size increased, indicating the greater inter-particulate bonding between the finer powder particles.

6.5.2- Effect of substitution

The levels of Hpo and Meo substitution of HPMC grades (%) (i.e. F4M, E4M and K4M) showed a marked effect on the compaction properties of matrices (Rajabi-Siahboomi *et al.*, 1998; Nokhodchi and Rubinstein, 2001). It was noticed that K4M exhibited greater packing ability than F4M and E4M. However, F4M produced compacts with higher strength than K4M at the same compression pressure. Moreover, it was also reported that the increase in Meo/Hpo substitution ratios leads to an increase in P_y (Malamataris and Karidas, 1994; Malamataris *et al.*, 1994). It is further reported by Rajabi-Siahboomi and Nokhodchi (1999) that A4M (MC) has the ability to produce tablets with higher tensile strength in comparison to F4M, E4M and K4M. Gustafsson *et al.* (1999) studied the effects of substitution on the particle characteristics and compaction behaviour of HPMC obtained from two different suppliers. Low, medium and high substitution ratios were studied using Methocel[®] K4M, E4M and F4M and compared with Metolose[®] 90 SH 4000, 60 SH 4000 and 65 SH 4000, respectively. Differences in drug release from Methocel[®] E4M matrices compared with the other two Methocel[®] products were related to a reduced powder surface area, differing particle morphology and lower fragmentation propensity (Gustafsson *et al.*, 1999). Additionally, its compacts were weaker and had different porosity and elastic recovery properties. There were no differences between the polymers in degree of disorder, as evaluated by solid-state NMR spectroscopy (Gustafsson *et al.*, 1999). The different behaviour of Methocel[®] E4M may be related to the overall higher total degree of substitution of this polymer and, in particular, the high content of hydrophobic methoxy groups, which may change the particulate and mechanical properties of the powder. Presence of methoxy groups might also decrease the development of inter-particulate hydrogen bonds during compaction. After a series of studies, Escudero *et al.* (2008, 2010 and 2012) concluded that A4M (MC) has best compaction properties, which might be due to the absence of hydrophilic Hpo

groups. It was reported that the A4M has a plasticity index (PI) of 99.0 %, which is higher than F4M (96.8 %), E4M (95.2 %) and K4M (97.0 %). Moreover, it was also reported that the substitution levels influenced pores on the surface of tablets as the K4M compacts have macroscopic pores (601 Å) whereas A4M, F4M and E4M have microscopic surface pores (Escudero *et al.*, 2008; Escudero *et al.*, 2012).

6.5.3- Effect of molecular size (viscosity)

The compression and compaction properties of HPMC are affected by viscosity grade (Nokhodchi and Rubinstein 2001). It was reported by Nokhodchi *et al.* (1996) that as the viscosity of HPMC decreases, the ability of powder particles to deform plastically increases and the tensile strength of HPMC K100 is much higher than other HPMC grades as a consequence of its viscosity. However, Malamataris *et al.* (1994) found that the P_y of HPMC tablets was not affected by polymer viscosity grade. The average surface pore size of K100M based compacts was 434.5 Å and considered to be microscopic in magnitude, compared to a pore size in K4M compacts (601.0 Å) of macroscopic dimensions but the molecular size have no effect of the PI (Escudero *et al.*, 2008).

6.5.4- Effect of humidity

Increased moisture uptake causes a decrease in tensile strength of tablets due to weak inter-particulate bonding caused by softening of the HPMC (Malamataris and Karidas 1994). The thickness of Methocel® K4M compacts fell as the moisture content increased from 0 to 14.9% w/w (Nokhodchi *et al.*, 1996b), which also resulted in a marked increase in the tensile strength of the tablets. The increase in moisture content also reduced the elastic recovery of the compacts because of greater tablet consolidation. The influence of moisture content on Heckel analysis, energy analysis and strain-rate sensitivity of HPMC 2208 has also been reported. An increase in moisture content from 0 to 14.9 % w/w decreased the mean yield

pressure, probably because of a plasticising effect of moisture that reduced the resistance of particles to deformation (Nokhodchi *et al.*, 1996a). The strain-rate sensitivity, which is the ability of the material to resist necking, increased from 21.6 to 50.7 % as the moisture content increased from 0 to 14.9% w/w, indicating that the plasticity of HPMC increased with an increase in moisture content (Nokhodchi *et al.*, 1996a).

Table 6.1, Summary of factors affecting compaction properties of Methocel® matrices

| Factor | Effect | References |
|--------------------------------|--|---|
| Effect of particle size | A reduction in particle size leads to higher tensile strength of matrix tablets | Malamataris and Karidas, 1994, Malamataris <i>et al.</i> , 1994, Nokhodchi <i>et al.</i> , 1995, Rajabi-Siahboomi <i>et al.</i> , 1998, Nokhodchi and Rubinstein, 2001 |
| Effect of substitution | Tensile strength of tablets increases with increased presence of the hydrophobic group (Meo). However, the P_y values decrease | Malamataris and Karidas, 1994, Malamataris <i>et al.</i> , 1994, Rajabi-Siahboomi <i>et al.</i> , 1998, Rajabi-Siahboomi and Nokhodchi, 1999, Nokhodchi and Rubinstein, 2001, Escudero <i>et al.</i> , 2008, Escudero <i>et al.</i> , 2010, Escudero <i>et al.</i> , 2012 |
| Effect of viscosity | Higher viscosity grades have a tendency to produce low tensile strength tablets and have higher P_y values. | Malamataris <i>et al.</i> , 1994, Nokhodchi <i>et al.</i> , 1996b, Nokhodchi and Rubinstein, 2001, Escudero <i>et al.</i> , 2008 |
| Effect of humidity | Higher moisture content leads to increased tensile strength of tablets. | Malamataris and Karidas, 1994, Nokhodchi <i>et al.</i> , 1996a, Nokhodchi <i>et al.</i> , 1996c, Rajabi-Siahboomi <i>et al.</i> , 1998, Nokhodchi and Rubinstein, 2001 |

6.6- Mathematical models of powder compression

6.6.1- The Heckel mathematical equation

The natural logarithm of the tablet porosity as a function of the applied pressure can be used to describe the compression process (Alderborn and Nystrom, 1995; Çelik, 2011). However, the Heckel equation has become the most well-known and most commonly used (Heckel, 1961b; Heckel, 1961a) relationship. The equation is based on the assumption that compression of powders is analogous to a first-order chemical reaction, the pores being the reactant and densification of the bulk being the product. The equation was first developed and applied to compression of metals, materials known to predominately deform plastically. A Heckel profile is normally distinguished by three different regions, an initial non-linear portion (Region I), followed by a linear part where the data obey the expression (Region II), and finally a non-linear region (Region III) (Figure 6.2). The existence of these three different regions is normally explained using the underlying rate controlling compression mechanisms that dominate the respective regions. For region I, there are two main explanations proposed: firstly that the curvature is regarded to be dependent on particle rearrangement during compression (Heckel, 1961b), and secondly that the curvature is due to particle fragmentation (Israelachvili, 2011). Regarding the second region, it is generally widely accepted that particle deformation, either elastic or plastic, is controlling the mechanism of powder compression. Finally for region III, it is proposed that elastic deformation of the compact controls the process (Sun and Grant, 2001). The parameter, A , in the Heckel equation (equation 2.16) is said to reflect low pressure densification by inter-particulate motion. The inverse of the slope (parameter K) can be calculated using the linear region. This is referred to as the Heckel parameter or the yield pressure, P_y , and is commonly used as an indicator of the relative plasticity or hardness of a particle (see section 2.2.9.2). Differences between reported values for the Heckel parameters exist in the literature and

may arise due to differences in determination of the linear region, deviations in the measured true densities or in the accuracy of the data acquisition. Negative porosities in the upper pressure part of the profile have also been reported, which could lead to substantially lower retrieved yield pressures, and might contradict the assumption that the particle density is constant during compression (Adolfsson *et al.*, 1999; Adolfsson and Nyström, 1996). Finally, and most importantly, experimental conditions affect the result of the Heckel parameter, such as maximum applied pressure, punch velocity or punch diameter (Kiekens *et al.*, 2004; Patel *et al.*, 2010).

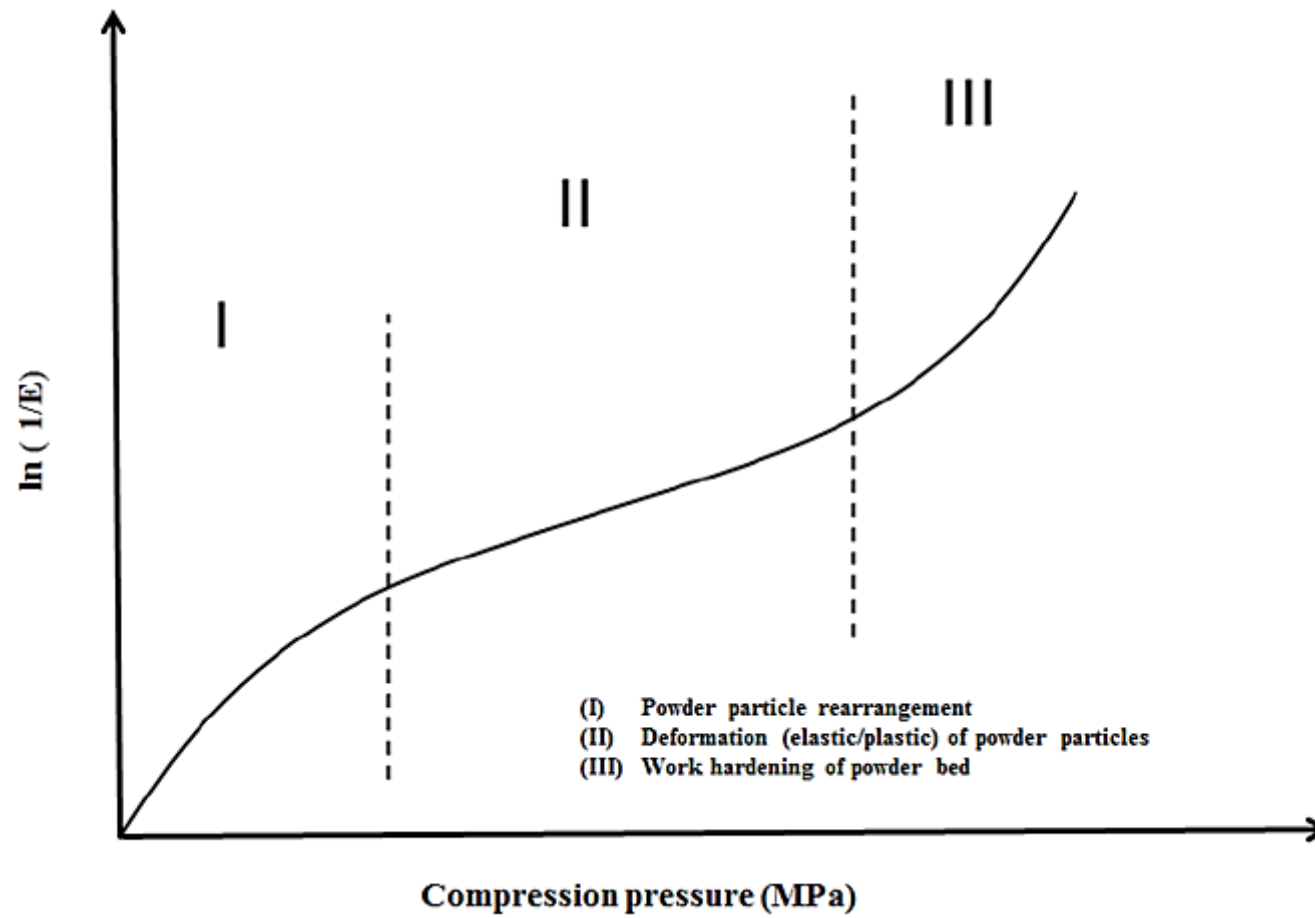


Figure 6.2, Schematic illustration of a typical Heckel plot, representing three different powder compression regions

6.6.2- The Kawakita mathematical equation

The basis for the Kawakita equation for powder compression is that powder particles are subjected to a compressive load in equilibrium at all stages of compression, so that the product of pressure and volume is constant. The Kawakita equation, compression data subjected to Equation (See chapter 2, section 2.2.9.) and engineering strain (C) of a powder bed with respect to the applied pressure (P) is calculated, which relates the strain in a powder bed to the applied compression pressure (Kawakita and Lüdde, 1971).

The linear relationship between P and C makes it possible to derive values for the parameters, a and b . The parameter ' a ' represents the maximal engineering strain, C_{\max} , of the powder bed, and mathematically the parameter ' b ' is equal to the reciprocal of the pressure when the value, C , reaches one-half of the limiting value ($C = C_{\max}/2$), as illustrated in Figure 6.3. The Kawakita equation is often considered to be best suited for analysis of soft, fluffy powders compressed under low pressures. However, setting the start volume for the calculation is a critical point that should be carefully considered; as this has a major influence on the parameters retrieved (Kawakita and Lüdde, 1971). Physical interpretation of the Kawakita parameters has been discussed in the literature, and the inverted b -parameter (b^{-1}) is claimed to reflect the agglomerate strength (Adams *et al.*, 1994), fracture strength of single particles or the plasticity of a granule (Nordström *et al.*, 2008)

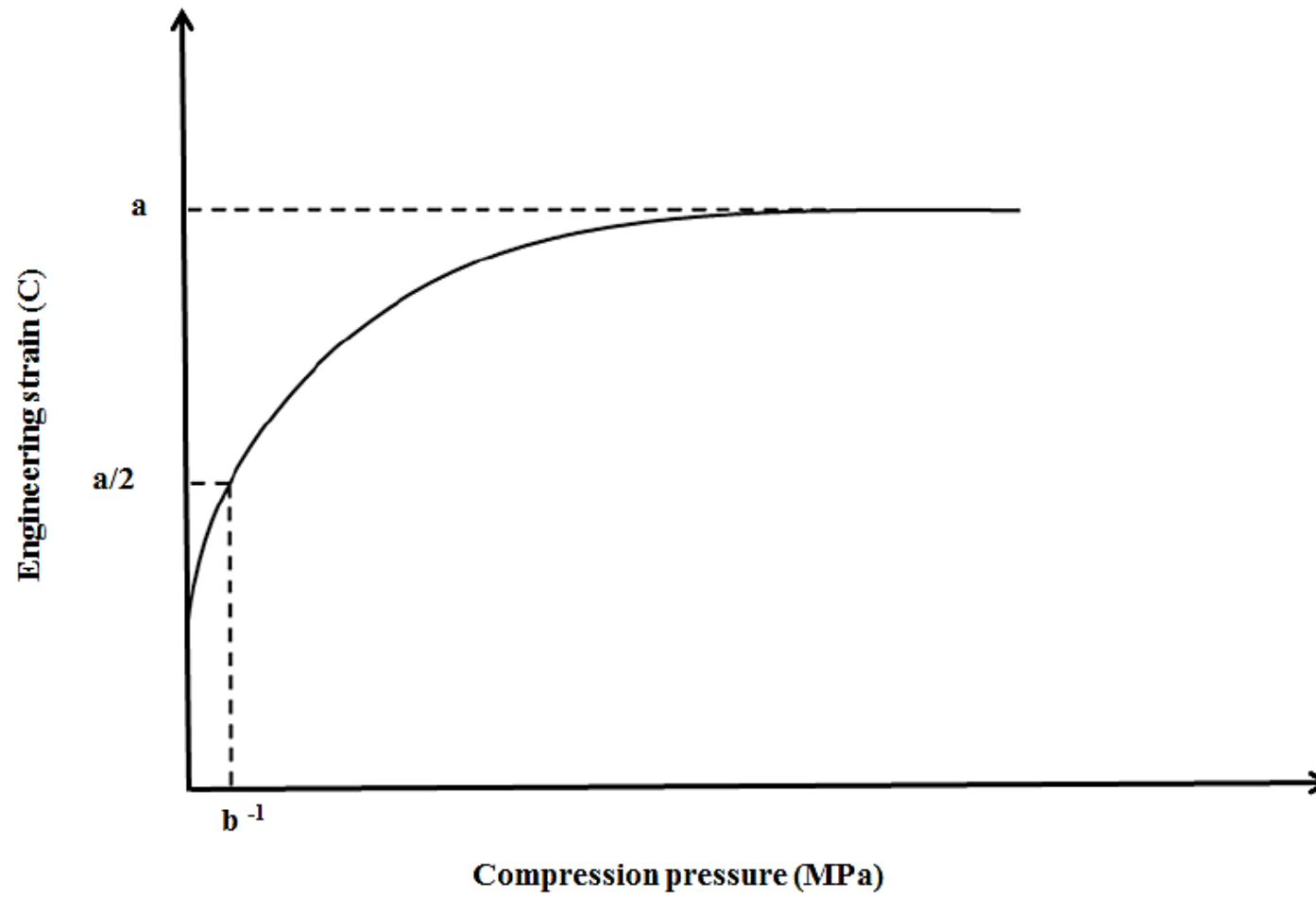


Figure 6.3, Schematic illustration of a typical engineering strain (C) and compressional pressure (MPa) and interpretation of Kawakita parameters

6.7- Section A, Compaction of model drugs

6.7.1- Introduction

The successful development of tablet matrices requires an understanding of the fundamental properties of both the drugs and hydrophilic carrier polymers. It has been estimated that less than 20 % of APIs can be processed by direct compression as the majority of the APIs lack the flow, cohesion and mechanical properties required (McCormick, 2005). Therefore, it is important to study the compaction properties of model drugs (FBP/THP) with an objective to understand the mechanism of compression and elastic relaxation.

6.7.2- Experimental

6.7.2.1- Materials

6.7.2.1.1- Model drugs

Model drugs, FBP (FBP) and THP (THP) were obtained as described in section 2.1.1.

6.7.2.2- Methods

SEM analysis was carried out as described in section 2.2.4.1 and all other methods are described in sections 2.2.9.1-2.2.9.3.

6.7.3- Results and discussion

The model drugs (FBP and THP) like many other APIs possess a high degree of crystallinity (Florence and Attwood, 2011). FBP powder particles are rectangular shaped with a density of 1.279 g cm^{-3} , whereas THP comprises elongated crystals with a columnar habit and a particle density value of 1.466 g cm^{-3} (Figure 3.5 and Table 6.2). Additionally, it can also be noticed that the THP particles have a rougher surface than FBP (section 3.6.4.1 and Figure

3.5). The compaction behaviour of the model drugs was studied using both in-die and out of die parameters as illustrated in Figure 6.4.

When powder samples of model drugs (FBP/THP) were introduced into the die, the in-die relative densities (solid fractions) of the powder bed increased with increasing pressure (Figure 6.5), however, the increasing pressure reduced the porosity of the powder bed (Figure 6.6). The initial in-die relative densities of FBP and THP compacts were 0.443 and 0.520, respectively. The relative densities of FBP and THP compact were increased to 0.798 and 0.938, respectively, at the highest compression pressure (150.77 MPa), Table 6.2. Moreover, it can be determined from the findings that an increase in the solid fraction of a powder bed inside the die reduces its porosity. At zero pressure the in-die porosity of FBP and THP was 55.70 % and 48.00 %, respectively, however the porosity of powder bed was reduced to 20.20 % (FBP) and 7.60 % (THP) (Table 6.2). The in-die relative density and porosity data at maximum pressure (150.77 MPa) correlates well with the out-of-die data (0 h) (Table, 6.2). It can also be noticed that the THP compacts have higher relative density than FBP compacts. As the relative density has a direct relationship with the porosity (%) of compacts, thus THP compacts have a lower porosity (%) than FBP compacts. This trend was maintained even after 24 hours, however, due to elastic relaxation over this period of time, the relative densities decreased with a consequent increase in porosity. The better densification properties of THP can be attributed to its good flow and adhesion compared to FBP (Crouter and Briens, 2014). Moreover, FBP particles have the tendency to generate more adhesion forces which may be the cause of their low densification with respect to pressure (Šupuk *et al.*, 2013; Wang *et al.*, 2004). Previously, it has been reported that powders which have a tendency to generate higher adhesion forces undergo reduced particle densification when pressure is applied, as a significant proportion of the powder particles stick to the die wall (Wang *et al.*, 2004).

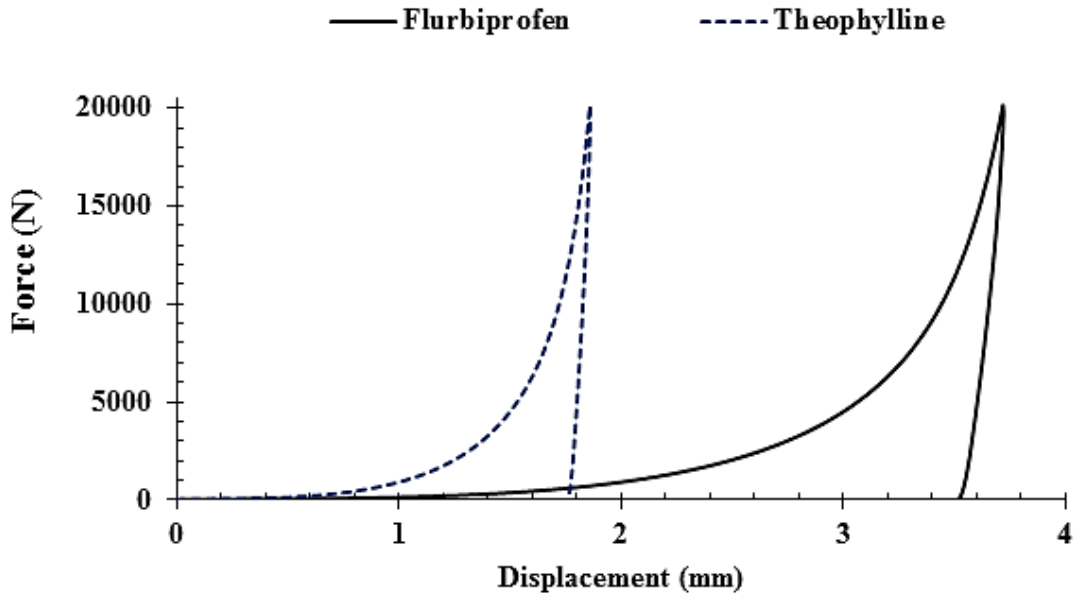


Figure 6.4, A typical force-displacement curve for FBP and THP (n = 3).

The force-displacement data were then further subjected to Heckel and Kawakita compressional equations in order to analyse compressional behaviour of FBP and THP compacts. The Heckel parameters A , K and P_y were calculated by using linear regression method on the straight line portions of the Heckel plots (Figure 6.7). The co-efficient of linearity (R^2) was > 0.99 in all cases. The Kawakita compressional parameters a , b^{-1} and ab^{-1} were calculated using Kawakita compression profiles (Figure 6.8) by applying linear regression over a wide range of pressure ranges with high correlation co-efficients ($R^2 > 0.99$). The parameters obtained from both Heckel and Kawakita analysis are summarised in Table 6.3 and show that the yield pressure (P_y) and b^{-1} are higher for FBP compacts at an applied pressure of 150.77 MPa. It can be inferred from that FBP powder particles need a higher degree of compression pressure to deform, as both the parameters are related to the plasticity of the powder bed during compaction. The initial bends in the Heckel and Kawakita compression profiles (Figures 6.7 and 6.8) were proposed to be linked with the

initial particle rearrangement during compression which can be explained by Heckel parameter A and Kawakita ab^{-1} . The A values for FBP and THP compacts were 0.960 and 1.080, respectively, however FBP and THP have ab^{-1} values of 0.0316 and 0.0418, respectively. A value of $ab^{-1} > 0.1$ is indicative of significant particle rearrangement during powder compression (Nordström *et al.*, 2009) so neither API showed significant rearrangement. However, the parameters were higher for THP than FBP, potentially due to its elongated crystal shape. When elongated crystals are filled into a compaction die, there may be more inter-particulate voids which might lead to more particle rearrangement than FBP powder compacts. Moreover fragmentation of THP particles may also contribute. The tensile strength (T) of THP compacts (2.11 MPa) was high whilst it was low for FBP (0.54 MPa). The elastic recovery (ER, %) of the FBP compacts (16.24 %) was significantly higher than THP compacts (9.51 %). The low T, but higher ER, of FBP can be attributed to its poor inter-particulate bonding. A schematic illustration of FBP and THP powder compaction is represented in Figure 6.9.

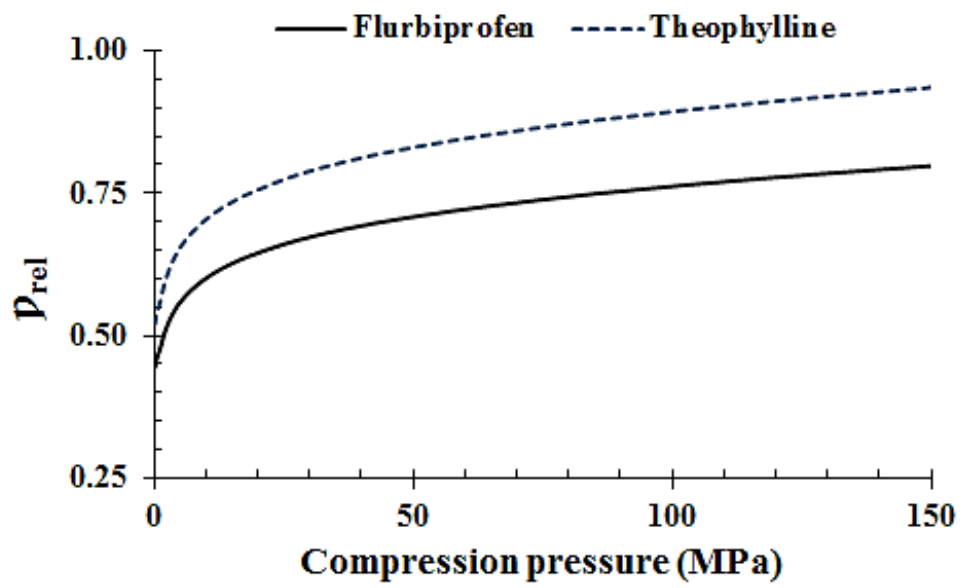


Figure 6.5, In-die relative density profile of FBP and THP (n = 3).

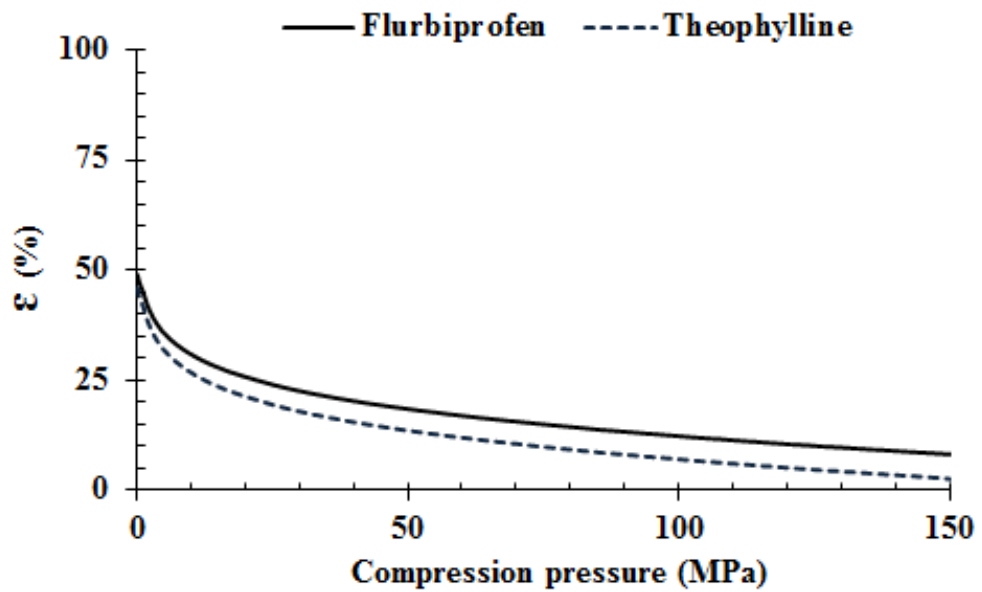


Figure 6.6, In-die porosity profile of FBP and THP.

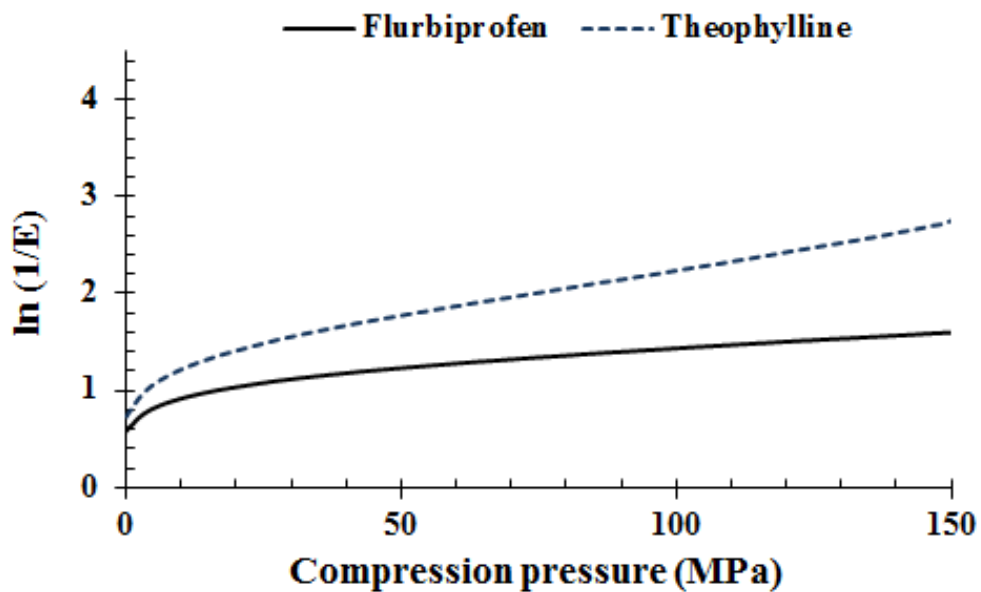


Figure 6.7, Heckel plots of FBP and THP with respect to pressure.

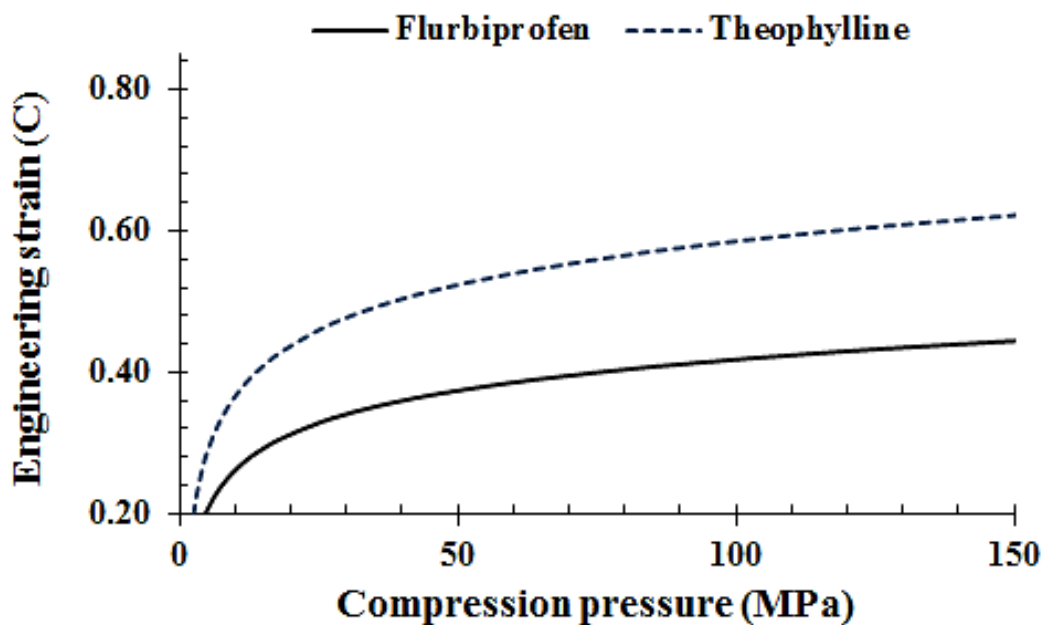


Figure 6.8, Kawakita plots of FBP and THP with respect to pressure.

Table 6.2, Relative density, porosity (in-die and out-of-die), tensile strength and elastic recovery of FBP and THP compacts (n = 3, standard deviation given in parenthesis)

| Drug | True density (ρ_t , g cm ⁻³) | Relative density (ρ_{rel}) | | | | Porosity (ϵ , %) | | | | T (MPa) | ER (%) |
|------|---|-----------------------------------|--------|----------------|-------|----------------------------|--------|----------------|-------|-------------|--------------|
| | | In-die | | After ejection | | In-die | | After ejection | | | |
| | | zero P | Max. P | 0 hr | 24 hr | zero P | Max. P | 0 hr | 24 hr | | |
| FBP | 1.279 | 0.443 | 0.798 | 0.789 | 0.768 | 55.70 | 20.20 | 21.10 | 23.20 | 0.54 (0.12) | 18.14 (3.15) |
| THP | 1.466 | 0.520 | 0.938 | 0.924 | 0.887 | 48.00 | 6.20 | 7.60 | 11.30 | 2.11 (0.09) | 9.51 (2.15) |

T = Tensile strength (MPa), ER = Elastic recovery (%)

Table 6.3, Heckel and Kawakita compression parameters for FBP and THP compacts (n = 3).

| Drug | Heckel parameters | | | Kawakita parameters | | |
|------|-------------------|----------|----------------------|---------------------|-----------------------|-----------|
| | <i>A</i> | <i>K</i> | <i>P_y</i> | <i>a</i> | <i>b⁻¹</i> | <i>ab</i> |
| FBP | 0.960 | 0.0101 | 99.00 | 0.445 | 14.05 | 0.0316 |
| THP | 1.080 | 0.0114 | 87.71 | 0.622 | 14.88 | 0.0418 |

A and K = Heckel constants, P_y (MPa) = Yield pressure, a, b⁻¹ (MPa) and ab = Kawakita constants

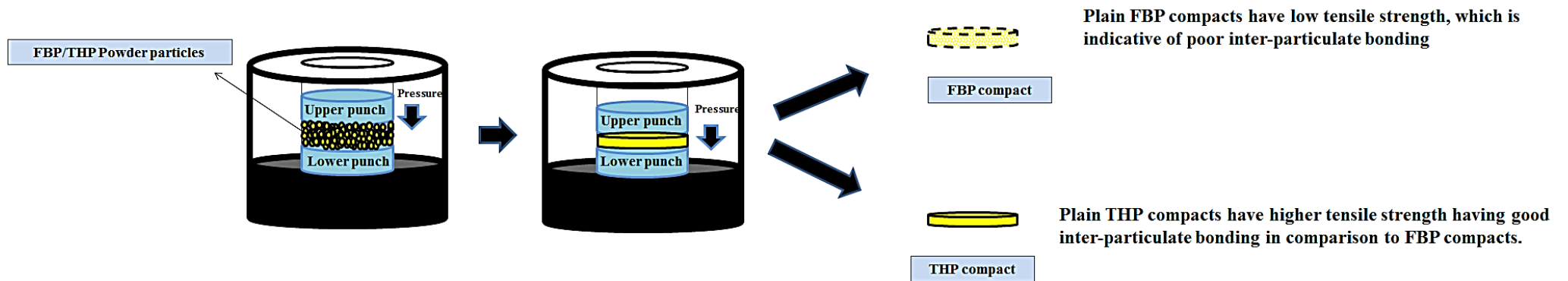


Figure 6.9, Schematic illustrating the compaction mechanisms of FBP and THP.

6.9- Section B, Compaction properties of hydrophilic matrices.

6.9.1- Introduction

Poor compaction properties can lead to large variations in tablet weight, poor content uniformity and inconsistent tablet properties including hardness, disintegration and drug release (Masuda *et al.*, 2006). Hydrophilic tablet matrices are commonly manufactured by using DC. During DC, powder particles consolidate into tablets, reducing pores in a powder bed while creating inter-particulate bonds (Sandell, 1992). Under compression, pharmaceutical materials experience multifaceted stresses which engender powder particle rearrangement, deformation (elastic or plastic) and fragmentation, and these processes are considered to be the events that brought structural changes to the in-die powder bed. Moreover, brittle materials consolidate predominantly by fragmentation whereas plastic materials deform plastically (Nyström *et al.*, 1993). However, compaction of brittle materials is less speed dependent because fragmentation is rapidly achieved and prolonged exposure to the force has a more limited effect on tablet properties (Alderborn and Nystrom, 1995).

Cellulose ethers, more specifically MC and HPMC, are the most frequently employed hydrophilic polymers for the development of compressed hydrophilic matrices (see section 4.1 for more detail). The mechanical properties of MC and HPMC are important as most of matrix tablets are manufactured through DC. The physico-chemical attributes of MC and HPMC (particle size, substitution levels and molecular size) can significantly affect mechanical behaviour. A sound understanding of material properties either polymers (MC/HPMC) or model drugs (FBP/THP) is very important. It is critical and very important to investigate how any change in their physico-chemical properties can affect their performance. Physical characterization of powder compaction of MC/HPMC and their

respective powder mixtures is an attractive area of research from both performance and material consumption prospective.

The deformation and consolidation characteristics of MC and HPMC based matrices have been studied in the past (Maderuelo *et al.*, 2011; Rajabi-Siahboomi *et al.*, 1998) but there is limited information available regarding in-depth mechanics behind these processes and how these variations can affect their functionality. Furthermore, there is a lack of literature on inter-relationship between the various compressional mathematical models and the influence of MC and HPMC inherent deformation and consolidation properties on the derived constants. For this purpose, the present work was designed to focus on comparative evaluation of different cellulose ethers (MC/HPMC) and their respective powder mixtures with model drugs (FBP/THP) of varying polymer ratios, with a view to understand their compression, compaction and relaxation properties. Heckel and Kawakita mathematical compression models (Heckel, 1961a; Heckel, 1961b; Kawakita and Lüdde, 1971,) were applied to study the deformation properties of matrices. Moreover, the impact of physico-chemical attributes related to MC and HPMC (concentration, particle size, molecular size (viscosity) and Hpo/Meo substitution levels) on the compaction and compression parameters was also studied.

6.9.2- Experimental

6.9.2.1- Materials

6.9.2.1.1- Cellulose ethers

Cellulose ethers (MC/HPMC) were obtained as described in the section 2.1.1 and their specifications are enlisted in Table 2.1.

6.9.2.1.2- Model drugs

Model drugs, FBP (FBP) and THP (THP), were obtained as described in section 2.1.1.

6.9.2.2- Methods

SEM analysis was carried out as described in section 2.2.4.1 and all other methods are described in sections 2.2.9.1-2.2.9.3.

6.9.3- Results and discussion

6.9.3.1- Compaction properties of plain Methocel[®] compacts

All the polymer grades contained mixtures of irregular-shaped flat and fibrous particles (Figure 3.8, chapter 3). Generally the proportion of fibrous particles is higher for MC than HPMC. The K-chemistry grades of HPMC, and specifically K100M, contain more irregularly shaped particles with rough surfaces than all other grades of cellulose ethers. This might be due to the higher Hpo/Meo substitution ratio and molecular weight, which result in the particles having a complex surface (see section 3.7.4.1, chapter 3 for more detail). The physical responses of polymeric powders, especially relative density and porosity of matrix tablets in a compression process play an important role in determining their quality (Bonferoni *et al.*, 1996; Gustafsson *et al.*, 1999). The true densities of MC and HPMC powders, which were determined by using helium pycnometer, were in the range of 1.288 - 1.373 g/cm³ (Table 6.4). The initial in-die relative density and porosity (ϵ , %) of the powder bed at zero and maximum pressure were determined using the force-displacement profiles for each polymer grade, as exemplified in Figure 6.4. Moreover, both parameters were calculated promptly after ejection (out-of-die) at zero and 24 h. When MC and HPMC were introduced into the die, the in-die relative densities (solid fractions) of the powder bed increased with increasing pressure (Figure 6.10). Moreover, the increasing pressure brings

the powder particles closer and the porosity of the powder bed starts to decrease with the increasing pressure (Figure 6.11). The rate of densification was rapid in the initial phase, but it became slower at higher pressures which causes packing of powder particles and results in an increased relative density and decreased porosity. Both of these factors are exceptionally important in the development of coherent matrix tablets. The in-die relative density and porosity data at maximum pressure (150.77 MPa) show a good correlation with the out of die data (0 h) (Table, 6.4). It can also be deduced from Figure 6.11 and Table 6.4 that the A4M (MC) had a higher relative density while K100M (HPMC) had the lowest relative density with respect to increasing pressure. As relative density is directly related to porosity, A4M and K100M are the grades of Methocel[®], with lowest and highest porosity, respectively. The same trend persisted even after 24 hours; however, due to elastic relaxation over the period of time, the relative densities decreased which consequently enhances the porosity of the matrix tablets.

Mechanistically, when the powder particles were filled in a tablet die and pressure is applied, powder particles rearrange themselves and undergo deformation and possibly fragmentation during compaction. These events appear sequentially or in parallel, but the physico-chemical properties of materials play an important role. Therefore, the present set of experiments was designed to investigate the effect of particle size, Hpo/Meo substitution and molecular size (viscosity) of cellulose ethers on parameters derived from Heckel and Kawakita mathematical models. An attempt was made to compare Heckel and Kawakita parameters, although, these models are based on different assumptions (Figures 6.12 and 6.13). The Heckel model provides a method for transforming a parametric view of the force and displacement data to a linear relationship for materials undergoing compaction. The equation is based on the assumption that the dependence of densification on pressure is of first-order kinetics. For studying the compression behaviour of MC and HPMC based matrix tablets on

the basis of derived Heckel parameters, linear regression was carried out on straight line portions of the Heckel plots (Figure 6.12a and b). The co-efficient of linearity (R^2) was > 0.99 in all cases. The Kawakita compressional parameters a , b^{-1} and ab were calculated using Kawakita compression profiles (Figure 6.13a and b) by applying linear regression over a wide range of pressure ranges with high correlation co-efficients ($R^2 > 0.99$). The parameters obtained from Heckel and Kawakita mathematical analysis for all the matrices having different particle size fractions (90-150 and 150-250 μm) are summarised in Table 6.5.

The initial bends in the Heckle and Kawakita compression profiles (Figures 6.12 and 6.13) were proposed to be linked with the initial particle rearrangement during compression which can be explained by Heckel parameter, A , and Kawakita, ab . The Heckel parameter A ranged between 0.900 – 0.543, with E4M showing more particle rearrangement during compression while K100M showing the lowest. The ab values for all the grades of MC and HPMC were in the range of 0.086 - 0.025 (Table 6.5), therefore these grades expressed non-significant particle rearrangement (see section 6.7.3). However F4M and K100M show highest and lowest extent of particle rearrangement during the compression cycle, respectively. The particle size also affects the particle rearrangement being higher for reduced particle size fractions.

6.9.3.1.1- Effect of Methocel[®] particle size

It can be also inferred from Table 6.4 that, as the particle size is reduced from 150-250 to 90-150 μm , the relative densities start to increase, which actually decreases the porosity of the matrix tablets; a similar trend has been noticed for all the grades of MC and HPMC used in the current study. This behaviour can be attributed to the fact that fine powder particles have more contact points and generate more intense compression forces during compression (Rajabi-Siahboomi *et al.*, 1998). Therefore, the finer particles have a higher degree of

densification than coarser particles. Heckel and Kawakita analysis revealed that the values of yield pressure (P_y) and b^{-1} were higher for larger sized fractions (150-250 μm) at maximum applied pressure for all the matrices (Table 6.5) thus requiring higher compression pressure to deform. Hence, mechanistically the increase in both parameters might be attributed to larger surface area and smaller particle to particle gaps increasing contact points for inter-particulate bonding. Furthermore, a higher degree of densification was exhibited by the smaller particle fractions. The tensile strength of the resultant matrices increased but there was a decrease in elastic recovery of matrices, regardless of grade. The increase in strength and decrease in elastic recovery with particle size reduction can be attributed to the theory that particle size reduction allows a high degree of packing and densification (Table 6.4). Owing to this, a greater number of contact points were generated as powder particles are confined to close proximity, hence the chances of inter-particulate bonding increases. MC and HPMC matrices showed a dependence on particle size which indicates the absence of extensive fragmentation. These findings were in complete accordance with the previous studies (Gustafsson *et al.*, 1999; Nokhodchi *et al.*, 1995; Rajabi-Siahboomi *et al.*, 1998; Rajabi-Siahboomi and Nokhodchi, 1999).

6.9.3.1.2- Effect of Methocel[®] substitution

The total substitution levels also seem to play an important role during the compression process, as the E4M based matrix tablets (with highest level of collective Hpo and Meo groups, Table 2.1, see chapter 2) have the lowest relative densities and highest porosities, regardless if it is in-die or out of die (zero h) for a given particle size fraction (Table 6.4). However, after 24 h the trend is lost, which might be due to the variation in the inter-particulate bonding and elastic relaxation of the compressed matrices. For a given particle size fraction, the variation in Hpo and Meo levels affect the apparent mean yield pressure. A4M (MC) which has only Meo substitution groups has the lowest P_y value compared with

other grades. Moreover, E4M has the highest P_y values, which might be due the presence of the high content of Meo, a hydrophobic group expected to prevent hydrogen bonding during the compression process. K4M shows higher P_y values than F4M and the trend can be described as E4M >K4M >F4M >A4M (Table 6.5). From the present finding, it can be assumed that the total substitution levels seem to be directly related to the deformation behaviour of matrix tablets. However, K4M has lower total substitution than F4M but it has a rougher particle surface (Figure 3) which is hypothesized to affect the development of bonds during tableting. The Kawakita parameter of plasticity (b^{-1}) was also affected when cellulose ethers having the same viscosity but varying substitutions were compared. The A4M has lower values than F4M but K4M has slightly lower values than E4M. However the trend of plastic deformation remains the same as per the findings of Heckel analysis.

A4M, F4M, E4M and K4M were compared with the intention to study the effect of substitution levels as these grades have same molecular size but different chemistries as described before. The effect of substitution levels seems to be complex as A4M compacts, which have only Meo (~30%) substitution groups, produced tablets with a high tensile strength. E4M based matrices had the lowest tensile strength and elastic recovery. Furthermore, as various Hpo levels were introduced (F4M and K4M), the tensile strength begins to decrease but elastic recovery is enhanced. On the other hand, when both the Meo and Hpo levels were at their maximum (E4M), the strength of the tablets was perceptibly decreased. The low tensile strength of E4M based matrix tablets was previously reported by Gustafsson *et al.* (1999). It was assumed in that particular study that hydrophobic Meo groups hinder hydrogen bonding during compaction, which leads to the development of matrices having low tensile strength, but A4M was not included in the study. Rajabi-Siahboomi and Nokhodchi, 1999 previously reported that A4M has the ability to produce matrices with high tensile strength which is in agreement with the present findings, however,

they compacted the powders at a lower compression pressure than the current study. Considering all these elements, it can be concluded that the effect of total substitution appeared to be more prominent than the individual levels of singular substitution groups.

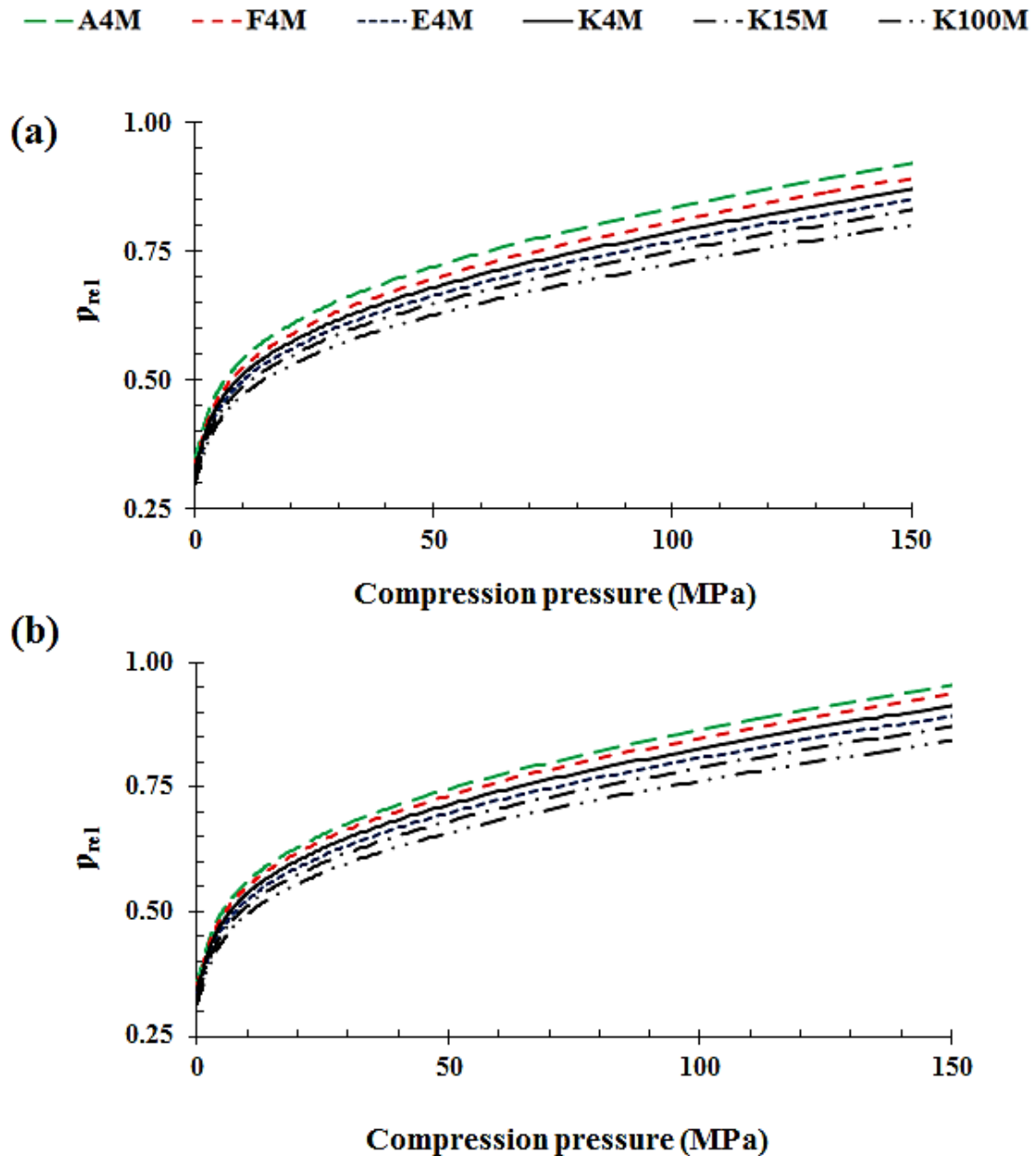


Figure 6.10, In-die relative density profiles of Methocel[®] with respect to compression pressure (a) 90-150 μm and (b) 150-250 μm ($n = 3$).

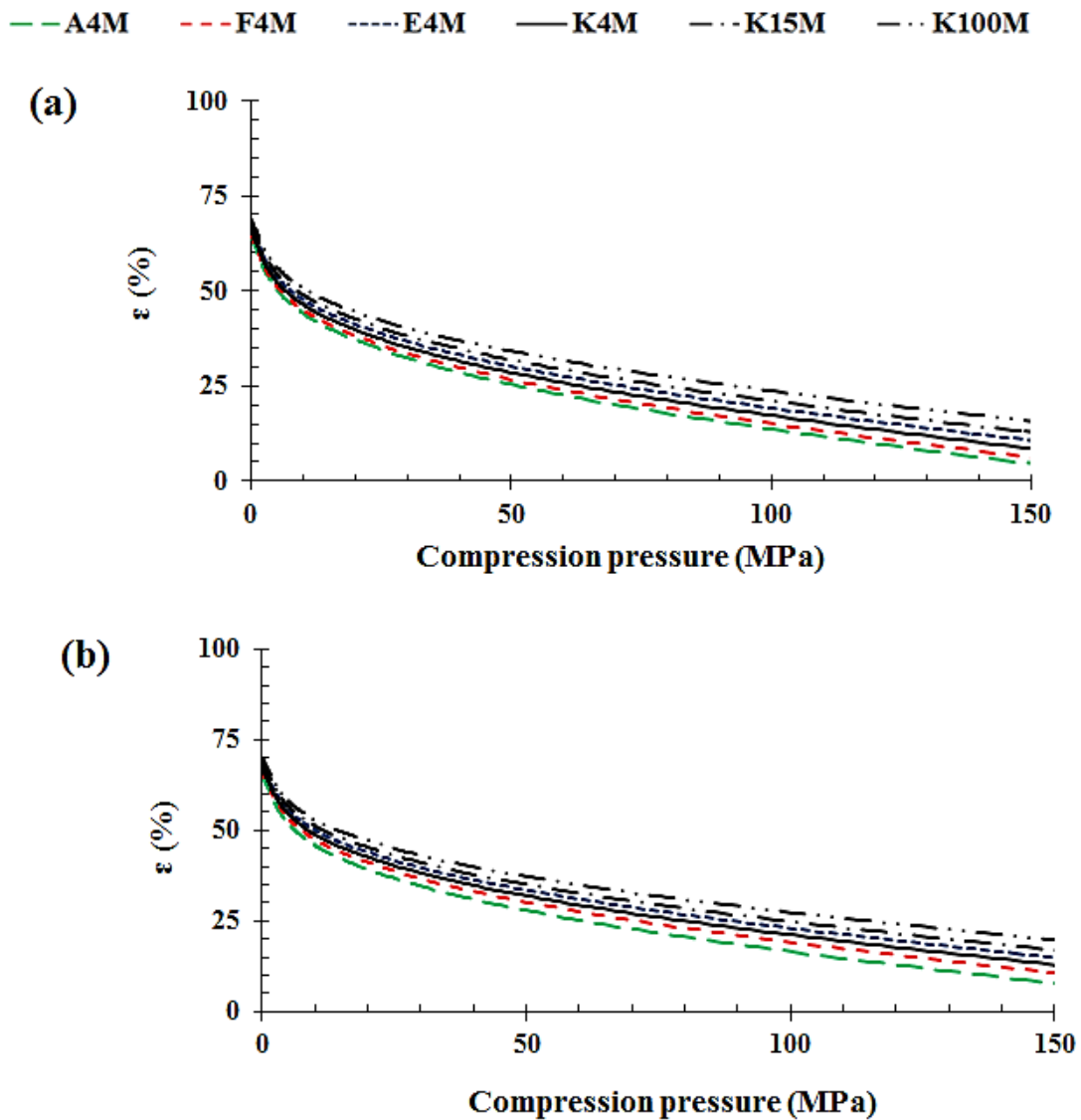


Figure 6.11, In-die porosity profiles of Methocel[®] with respect to compression pressure (a) 90-150 μm and (b) 150-250 μm ($n = 3$).

Table 6.4, Relative density, porosity (in-die and out-of-die), tensile strength and elastic recovery of Methocel[®] compacts (n = 3, standard deviation given in parenthesis)

| Methocel [®] | Particle size (μm) | ρ_t (gcm^{-3}) | Relative density (ρ_{rel}) | | | | Porosity (ϵ , %) | | | | T (MPa) | ER (%) |
|-----------------------|------------------------------------|-----------------------------------|--|--------|----------------|---------|----------------------------|--------|----------------|---------|-------------|--------------|
| | | | In die | | After ejection | | In die | | After ejection | | | |
| | | | zero P | Max. P | 0 hour | 24 hour | zero P | Max. P | 0 hour | 24 hour | | |
| A4M | 90-150 | 1.338 | 0.3575 | 0.9560 | 0.9552 | 0.783 | 64.25 | 4.4 | 4.48 | 21.7 | 5.28 (0.22) | 14.13 (1.33) |
| | 150-250 | | 0.3453 | 0.9236 | 0.9170 | 0.741 | 65.46 | 7.63 | 8.3 | 25.9 | 4.96 (0.11) | 20.65 (1.15) |
| F4M | 90-150 | 1.309 | 0.3512 | 0.9393 | 0.9294 | 0.782 | 64.88 | 6.07 | 7.06 | 21.8 | 4.87 (0.07) | 12.57 (2.03) |
| | 150-250 | | 0.3344 | 0.8945 | 0.8862 | 0.737 | 66.55 | 10.54 | 11.38 | 26.3 | 4.45 (0.21) | 19.37 (2.33) |
| E4M | 90-150 | 1.288 | 0.3345 | 0.8946 | 0.8901 | 0.834 | 66.55 | 10.54 | 10.99 | 16.1 | 3.15 (0.10) | 8.04 (1.15) |
| | 150-250 | | 0.3185 | 0.8519 | 0.8443 | 0.828 | 68.14 | 14.8 | 15.57 | 17.2 | 2.88 (0.09) | 10.55 (1.11) |
| K4M | 90-150 | 1.327 | 0.3424 | 0.9158 | 0.9051 | 0.807 | 65.76 | 8.42 | 10.49 | 19.3 | 4.30 (0.21) | 15.05 (2.34) |
| | 150-250 | | 0.3261 | 0.8722 | 0.8711 | 0.785 | 67.39 | 12.8 | 12.89 | 21.5 | 3.98 (0.22) | 18.28 (1.50) |
| K15M | 90-150 | 1.324 | 0.3265 | 0.8732 | 0.873 | 0.834 | 67.35 | 12.68 | 12.70 | 16.6 | 3.61 (0.30) | 9.47 (1.29) |
| | 150-250 | | 0.3109 | 0.8315 | 0.8294 | 0.792 | 68.91 | 16.84 | 17.06 | 20.8 | 3.15 (0.10) | 15.26 (2.51) |
| K100M | 90-150 | 1.373 | 0.3156 | 0.8439 | 0.8429 | 0.823 | 68.44 | 15.61 | 15.71 | 17.7 | 2.98 (0.08) | 7.85 (1.33) |
| | 150-250 | | 0.3005 | 0.8037 | 0.8011 | 0.788 | 69.95 | 19.63 | 19.89 | 21.2 | 2.65 (0.11) | 12.57 (1.12) |

ρ_t = True density

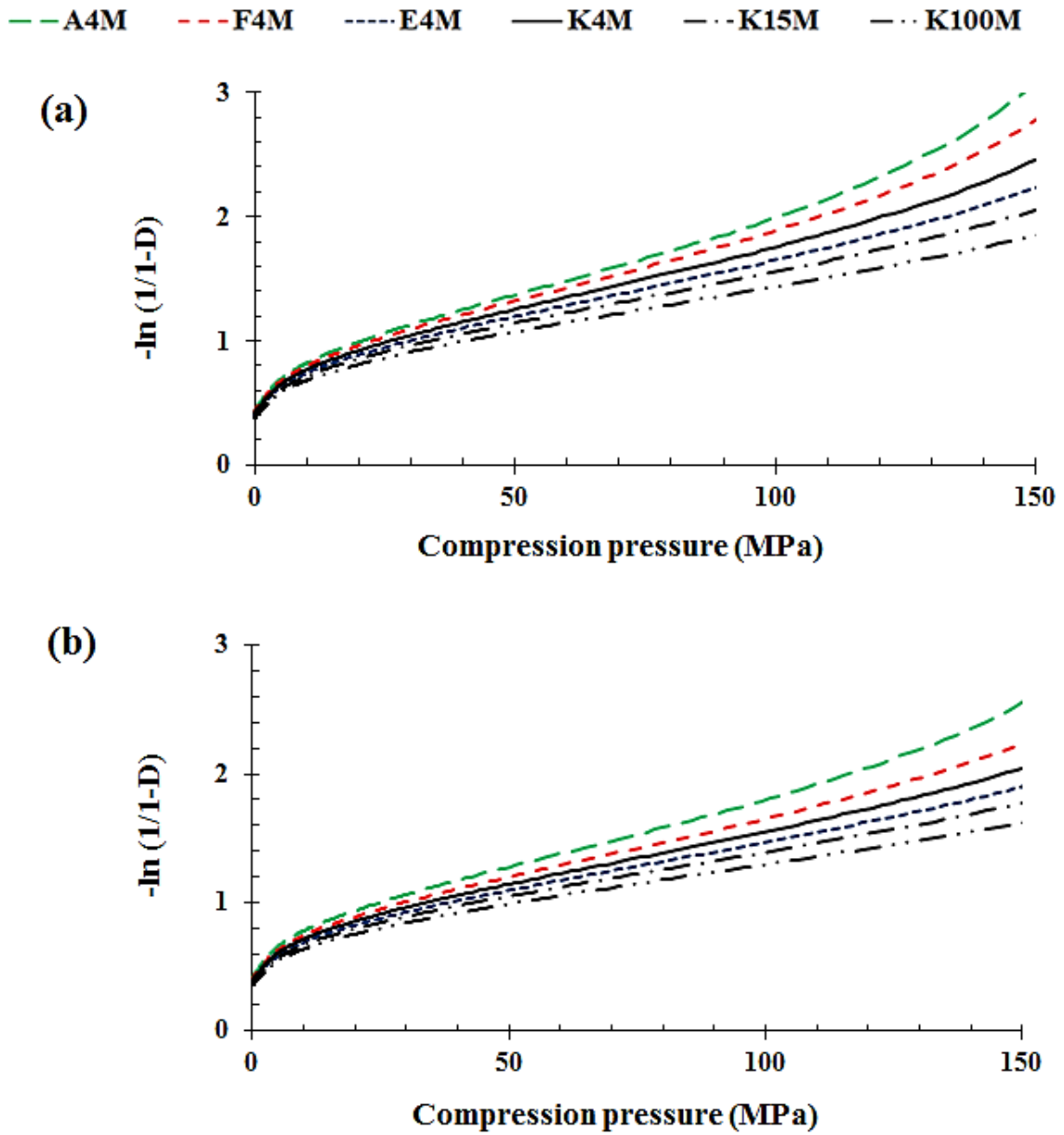


Figure 6.12, Heckel plots of Methocel[®] with respect to compression pressure (a) 90-150 μm and (b) 150-250 μm ($n = 3$).

-- A4M
 -- F4M
 - - - E4M
 — K4M
 - · - K15M
 - · · K100M

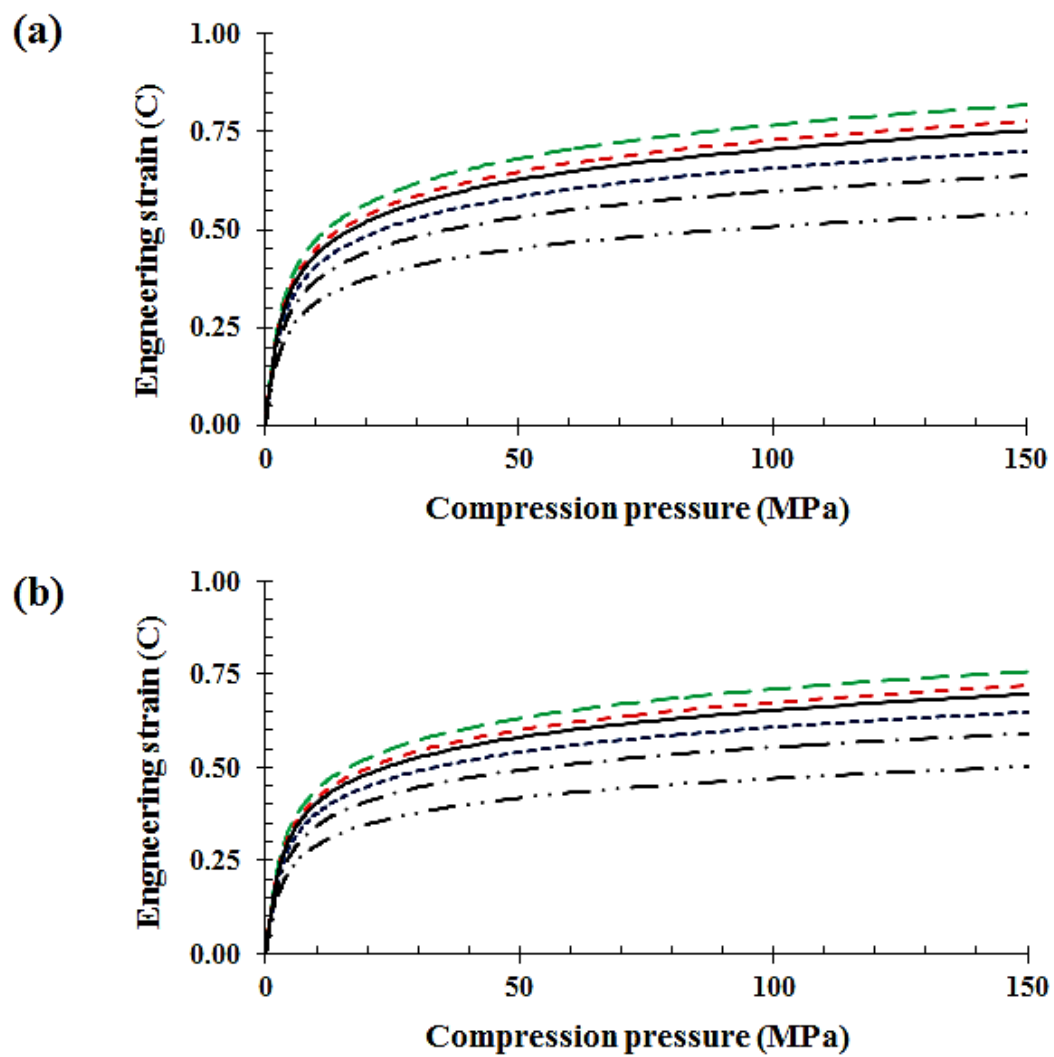


Figure 6.13, Kawakita plots of Methocel[®] with respect to compression pressure (a) 90-150 μm and (b) 150-250 μm (n = 3).

Table 6.5, Heckel and Kawakita compression parameters of Methocel® compacts (n = 3).

| Methocel® | Particle size (μm) | Heckel parameters | | | Kawakita parameters | | |
|-----------|------------------------------------|-------------------|----------|----------------------|---------------------|-----------------------|-----------|
| | | <i>A</i> | <i>K</i> | <i>P_y</i> | <i>a</i> | <i>b⁻¹</i> | <i>ab</i> |
| A4M | 90-150 | 0.815 | 0.0126 | 79.37 | 0.721 | 8.97 | 0.080 |
| | 150-250 | 0.839 | 0.0115 | 86.96 | 0.690 | 9.60 | 0.072 |
| F4M | 90-150 | 0.800 | 0.0118 | 84.75 | 0.782 | 9.14 | 0.086 |
| | 150-250 | 0.780 | 0.0097 | 103.09 | 0.701 | 9.97 | 0.070 |
| E4M | 90-150 | 0.715 | 0.0096 | 104.17 | 0.556 | 10.78 | 0.052 |
| | 150-250 | 0.900 | 0.0083 | 120.48 | 0.515 | 11.64 | 0.044 |
| K4M | 90-150 | 0.785 | 0.0107 | 93.46 | 0.528 | 10.36 | 0.051 |
| | 150-250 | 0.727 | 0.0090 | 111.11 | 0.516 | 11.04 | 0.047 |
| K15M | 90-150 | 0.714 | 0.0086 | 116.28 | 0.562 | 11.50 | 0.049 |
| | 150-250 | 0.590 | 0.0079 | 126.58 | 0.548 | 12.25 | 0.045 |
| K100M | 90-150 | 0.636 | 0.0081 | 123.46 | 0.495 | 13.42 | 0.037 |
| | 150-250 | 0.543 | 0.0072 | 138.89 | 0.379 | 15.28 | 0.025 |

A and K = Heckel constants, P_y (MPa) = Yield pressure, a, b⁻¹ (MPa) and ab = Kawakita constants

6.9.3.1.3- Effect of Methocel[®] molecular size (viscosity)

As the molecular size (viscosity) of the polymers increased, both the relative density and porosity of matrix tablet decreased (Figures 6.10 and 6.11) and the trend on the basis of molecular size was, K4M < K15M < K100M (Table 6.4). This phenomenon might be due to the rapid deformation of low molecular size HPMC powder particles under pressure during compression. To analyse the effect of the molecular size of HPMC on the compression features, K4M, K15M and K100M were selected. These HPMC grades essentially have the same chemistry but different chain lengths. The P_y and b^{-1} both were increased with increase in chain length of HPMC for a specific particle size fraction (Table 6.5). K100M has longer chains compared with K15M and K4M with polymeric chain length being directly linked to molecular weight and size. The increase in molecular weight affects the material's ability to deform as the higher molecular weight HPMC (K100M) needs higher compression pressures to deform in comparison to other grades. The trend of plasticity was K4M > K15M > K100M. This might be due to low viscosity HPMC having shorter polymeric chains and these can deform readily to fill inter-particulate gaps (Nokhodchi *et al.*, 1995). The matrices made of K4M were stronger than the matrices composed of either K15M or K100M (Table 6.4). This behaviour might be attributed to the prompt deformation of the shorter chain lengths as described earlier. However, once these higher molecular size HPMC grades were compacted, they had low elastic recovery, which may be linked to their surface roughness (Table 6.4).

6.9.3.2- Mixing efficiency for Methocel[®] : FBP/THP powders

A uniform drug distribution in a powder mixture is desirable during tablet preparation. The FBP/THP content uniformity results ($n = 3$) of powder mixtures are shown in Table 4.4 (see chapter 4) and an acceptance limit of 95 - 105 % was set (see section 2.2.5.1, chapter 2). All powder blends used in subsequent studies fell between these limits.

6.9.3.3- Compaction properties of FBP/THP matrices

The complexity of the compaction process has led to the majority of fundamental studies carried out on single pharmaceutical materials (Alderborn and Nystrom, 1995). As hydrophilic matrices consist of more than one material, so the prediction of compaction properties of powder mixtures from those of singular component materials is of obvious interest. However, the physico-chemical characteristics of model drugs and hydrophilic polymers can significantly affect the quality and functionality of these matrices (Ghori *et al.*, 2014b; Li *et al.*, 2005; Maderuelo *et al.*, 2011; Wen and Park, 2011). Thus, the present experiments were designed to study the compaction, compression and elastic relaxation properties of FBP-and THP-containing hydrophilic matrices. The true density of all the powder mixtures was determined using helium pycnometry. The true densities of mixtures containing 5 % to 15 % of MC/HPMC were in the range of 1.279 -1.293 g/cm³ and 1.439 -1.461 g/cm³ for FBP and THP respectively (Tables 6.6, 6.10, 6.14, 6.18, 6.22 and 6.26). The initial in-die relative density and porosity (ϵ , %) of the powder bed at zero and maximum pressure was determined by using the force-displacement profiles for each Methocel[®]: FBP/THP based powder mixtures, as exemplified in Figure 6.4. Moreover, both parameters were calculated promptly after ejection (out-of-die) at zero and 24 h. Additionally, to study, the compression features of FBP/THP hydrophilic matrices on the basis of derived Heckel parameters, linear regression was carried out on the straight line portions of the Heckel plots (Figures 6.17, 6.21, 6.25, 6.29, 6.33 and

6.37). The co-efficient of linearity (R^2) was > 0.99 in all cases. The Kawakita compression parameters a , b^{-1} and ab were calculated by using Kawakita compression profiles (Figures 6.18, 6.22, 6.26, 6.30, 6.34 and 6.38) by applying linear regression over a wide range of pressure ranges with high correlation co-efficient ($R^2 > 0.99$). The parameters obtained from Heckel and Kawakita mathematical analysis of all the matrices having different particle size fractions (90-150 and 150-250 μm) are summarised in Tables 6.9, 6.13, 6.17, 6.21, 6.25 and 6.29. In the following sections, compaction, compression and elastic relaxation data are presented with an in-depth mechanistic approach and discussion.

6.9.3.3.1- Effect of Methocel[®] concentration

The presence of polymer can modulate the characteristics of hydrophilic matrices. In the current set of experiments the effect of Methocel[®] concentration (5, 10 and 15 w/w %) on the compaction properties of FBP and THP-based matrices was studied. The relative density profiles are depicted in Figures 6.15, 6.19, 6.23, 6.27, 6.31 and 6.35 with respect to increasing compression pressure. The in-die and out-of-die relative density values are summarised in Tables 6.6, 6.10, 6.14, 6.18, 6.22 and 6.26. It can be inferred from the results that with an increase in the concentration of MC or HPMC, the relative density tends to increase. The relative densities of A4M: FBP tablet matrices were increased from 0.810 to 0.894 and A4M: THP from 0.853 – 0.910 as the A4M concentration was increased from 5 % to 15 % w/w. All other MC/HPMC based matrices showed a similar trend (Table 6.6, 6.10, 6.14, 6.18, 6.22 and 6.26). Moreover, the porosity profiles with increasing compression pressure for the FBP/THP matrices are shown in Figures 6.16, 6.20, 6.24, 6.28, 6.32 and 6.36. The increasing relative density affects the porosity (%) of matrices. The in-die and out-of-die porosity (%) values were decreased as the MC/HPMC concentration was increased from 5 % to 15 % w/w (A4M: FBP from 19.03 to 10.61 %, A4M: THP from 15.29 to 8.42 %, F4M: FBP from 19.13 to 10.98 %, F4M: THP from 15.38 to 8.87 %, E4M: FBP from 19.50 to 14.04 %, E4M: THP from 15.84 to

10.16 %, K4M: FBP from 21.51 to 14.13 %, K4M: THP from 17.19 to 11.16 %, K15M: FBP from 19.68 to 13.76 %, K15M: THP from 14.44 to 9.02 %, K100M: FBP from 21.72 to 14.13 % and K100M: THP from 14.72 to 9.00 %), (Tables 6.7, 6.11, 6.15, 6.19, 6.23 and 6.27). This trend was consistent during the course of this study, regardless of MC/HPMC grade or drug used.

Furthermore, the incorporation of MC/HPMC increased the tensile strength of the FBP and THP matrices. The tensile strength was increased as the concentration of MC/HPMC was increased from 5 % to 15 % w/w. The tensile strength ranges were A4M: FBP 1.11 – 1.68 MPa, A4M: THP 2.74 – 3.55 MPa, F4M: FBP 1.08 – 1.63 MPa, F4M: THP 2.54 – 3.29 MPa, E4M: FBP 1.06 – 1.60 MPa, E4M: THP 2.56 – 3.32 MPa, K4M: FBP 0.99 – 1.50 MPa, K4M: THP 2.42 – 3.13 MPa, K15M: FBP 0.95 – 1.44 MPa, K15M: THP 2.35 – 3.04 MPa, K100M: FBP 0.88 – 1.33 MPa, and K100M: THP 2.21 – 2.87 MPa. However, the elastic recovery of matrices decreased as the MC/HPMC concentration was increased from 5 % to 15 % w/w, (Tables 6.8, 6.12, 6.16, 6.20, 6.24 and 6.28).

To study the in-depth compression features of matrices, the Heckel and Kawakita compression models were applied. It was noticed that the P_y (yield pressure, Heckel parameter of particle plasticity) and b^{-1} (Kawakita parameter of particle plasticity) started to fall as the concentration of MC/HPMC increased from 5 % to 15 % w/w (Tables 6.9, 6.13, 6.17, 6.21, 6.25 and 6.29). The P_y values of A4M: FBP matrices decreased from 77.52 to 66.23 MPa, similarly all other matrices showed the same behaviour as A4M: THP decreased from 87.72 to 76.19 MPa, F4M: FBP from 78.29 to 66.89 MPa, F4M: THP from 89.47 to 77.71 MPa, E4M: FBP from 78.15 to 67.56 MPa, E4M: THP from 89.16 to 78.49 MPa, K4M: FBP from 81.40 to 69.54 MPa, K4M: THP from 92.17 to 80.06 MPa, K15M: FBP from 82.95 to 70.55 MPa, K15M: THP from 93.22 to 80.86 MPa, K100M: FBP from 84.25 to 72.28 MPa and K100M: THP from 94.03 to 81.67 MPa. The b^{-1} values also decreased as the MC/HPMC concentration was

increased from 5 % to 15 % w/w (A4M: FBP 11.20 – 8.32 MPa, A4M: THP 7.84 – 6.12 MPa, F4M: FBP 11.31 – 8.40 MPa, F4M: THP 8.00 – 6.24 MPa, E4M: FBP 11.42 – 8.49 MPa, E4M: THP 7.92 – 6.18 MPa, K4M: FBP 12.54 – 9.32 MPa, K4M: THP 8.00 – 6.24 MPa, K15M: FBP 13.05 – 9.69 MPa, K15M: THP 8.16 – 6.37 MPa, K100M: FBP 13.57 – 10.08 MPa and K100M: THP 8.40 – 6.56 MPa). As both the compression parameters are inversely related to particle deformation, it can be inferred from the present findings that the deformation of powder mixtures, regardless of drug type and MC/HPMC grade, starts at low compression pressures. It can be noticed from the results that the concentration of MC/HPMC significantly affects the relative density, porosity, deformation, tensile strength and elastic relaxation of the FBP/THP matrices. In current scenario, the binary powder mixtures contain two component mixtures of drugs (FBP/THP) and Methocel[®] (MC/HPMC). It can be assumed that three types of bonds (drug – drug, drug - Methocel[®] and Methocel[®] - Methocel[®]) can be developed when these powder mixtures are subjected to compression pressure. Ghori *et al.* (2014) recently reported that FBP and THP attain negative tribo-electric charge during mixing, whereas the MC/HPMC has the tendency to gain positive charge (see sections 3.7.4.1 and 3.8.4.2, chapter 3 for more detail). We postulate that as the tribo-electric charging of drugs and Methocel[®] grades are opposite, so the negatively charged drug particles can be attached on the surface of MC/HPMC particles (see section 3.9.3.1, chapter 3 for more detail). Moreover, it was observed, from the SEM images of powder mixtures (Figures 3.10 and 3.11), that the negatively charged drug particles have a tendency to attach to the polymer surface (Figure 6.14). So, it can be assumed that the propensity of particulate bonding between the drug - Methocel[®] will be higher which can lead to a higher degree of densification and, as a result, reduced porosity and a decline in P_y and b^{-1} is evident.

Moreover, the mechanism of FBP/THP : MC/HPMC can be further explained using the qualitative tablet model described by Nyström *et al.* (1993). This model is considers the tablet

as powder particles dispersed in a gas. According to this model, three types of particulate fracture might be possible, (A) fracture through the drug particles only, (B) fracture through Methocel[®] particles only and (C) fracture between the Methocel[®] and drug particles. According the current results, it can be hypothesized that the fracture is more likely to be between the Methocel[®] and drug particles, as the drug particles are attached on the carrier polymer surface (Ghori *et al.*, 2014d) (Figure 6.14), thus enhancing the tensile strength of matrices (Alderborn, 1995; Adolfsson and Nyström, 1996). However, the occurrence of other types of fracture pattern cannot be completely ruled out.

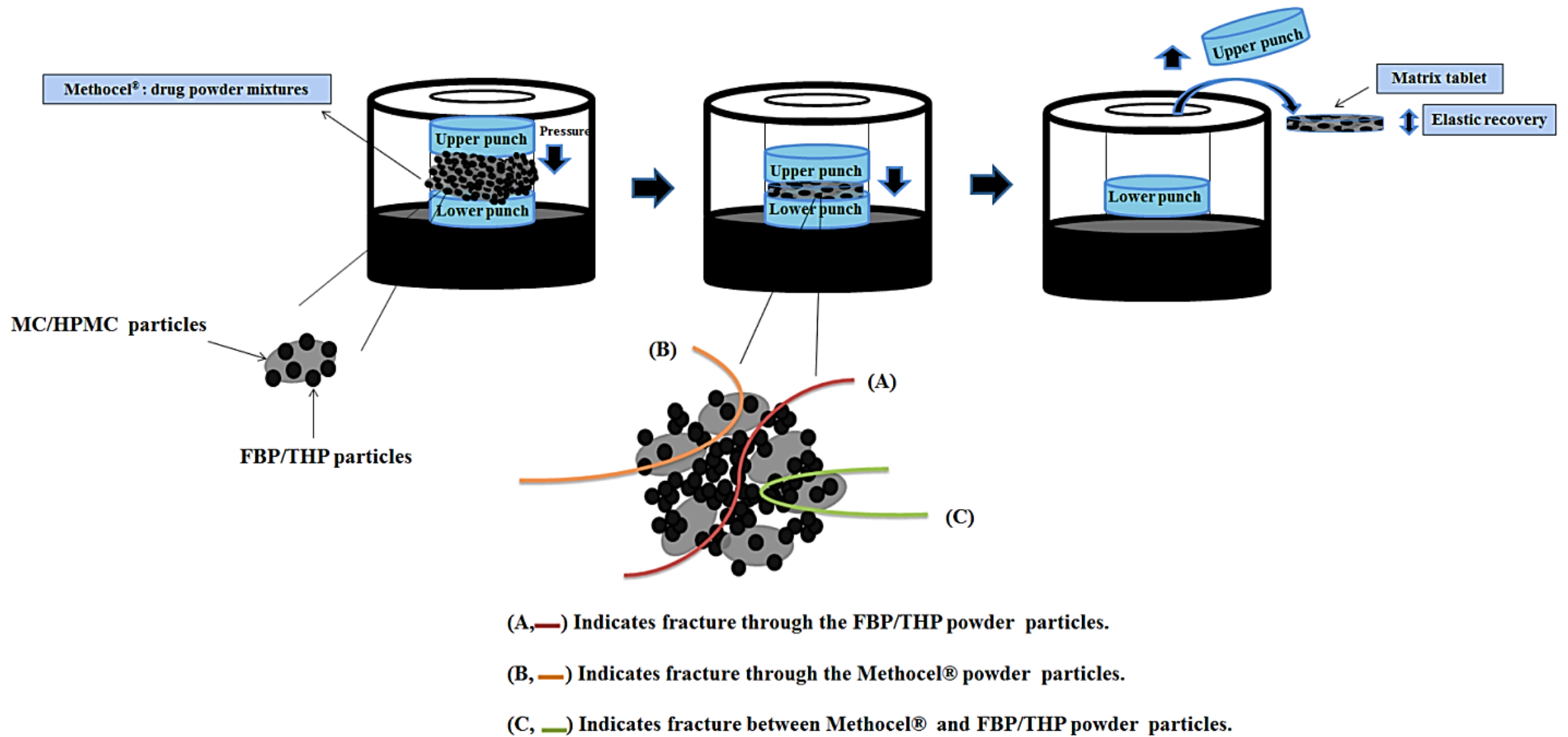


Figure 6.14, Compaction mechanism of MC/HPMC : FBP/THP matrices.

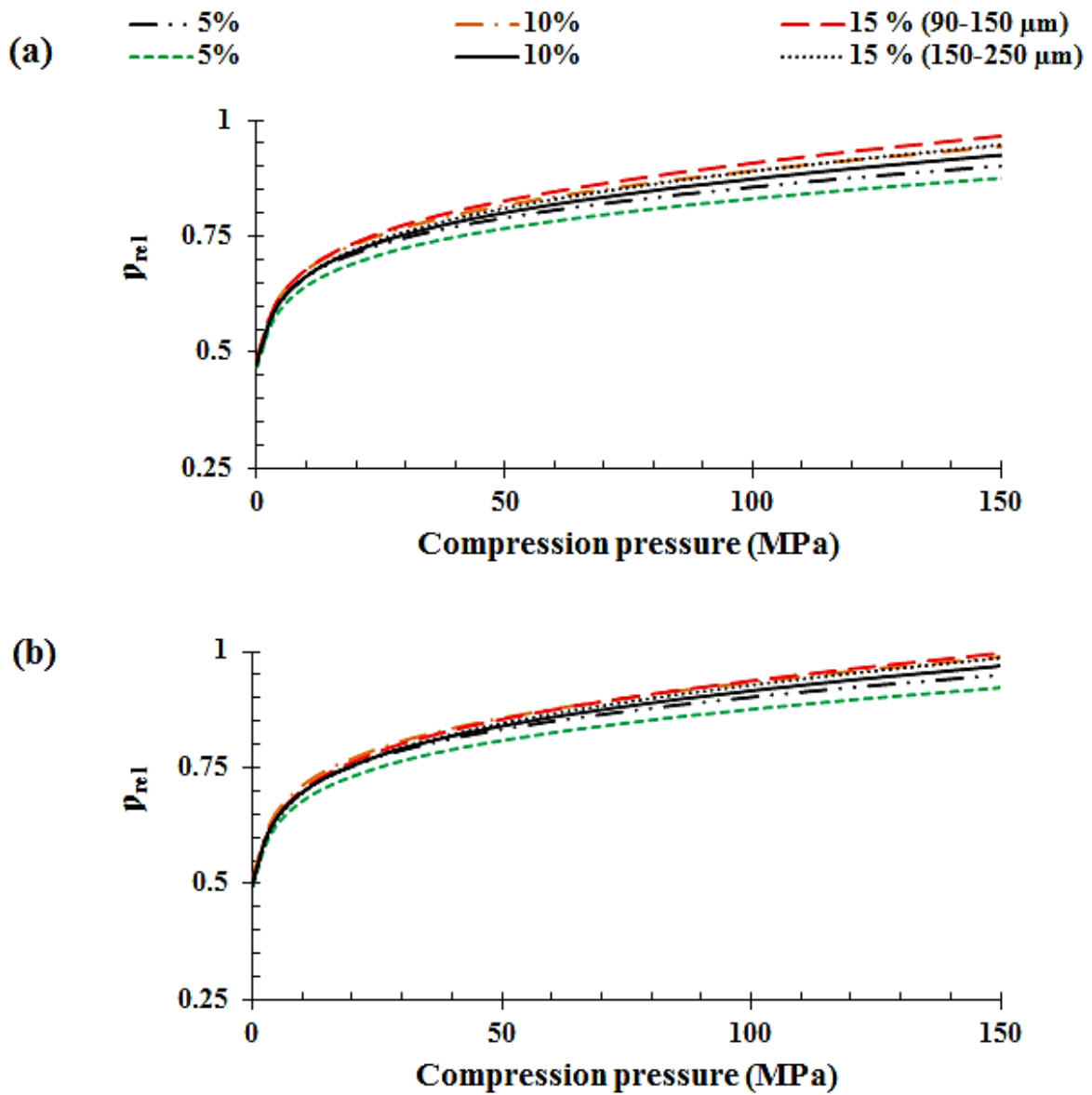


Figure 6.15, In-die relative density profiles of matrices with respect to compression pressure (a) A4M: FBP and (b) A4M : THP (n = 3).

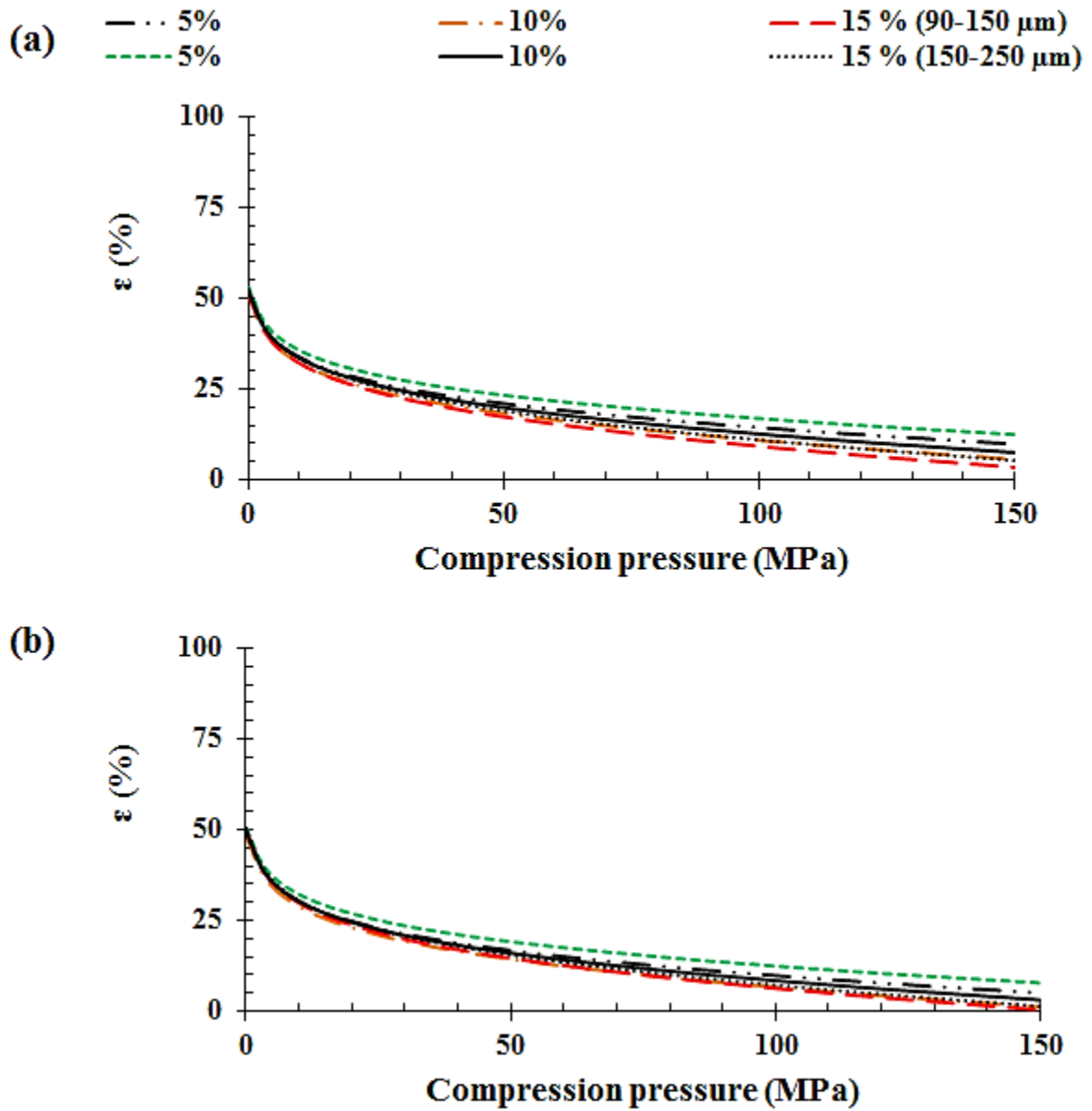


Figure 6.16, In-die porosity profiles of matrices with respect to compression pressure

(a) A4M : FBP and (b) A4M : THP (n = 3).

Table 6.6, Summary of in-die and out-of-die relative density values of A4M : FBP/THP matrices (n = 3).

| A4M (%) | Particle size (µm) | True density (ρ _t , g cm ⁻³) | | Relative density (ρ _{rel}) | | | | Relative density (ρ _{rel}) | | | |
|---------|--------------------|---|-------|--------------------------------------|--------|----------------|-------|--------------------------------------|--------|----------------|-------|
| | | | | FBP | | | | THP | | | |
| | | | | In-die | | After ejection | | In-die | | After ejection | |
| | | | | Zero P | Max. P | 0 h | 24 h | Zero P | Max. P | 0 h | 24 h |
| 5 | 90-150 | 1.281 | 1.459 | 0.483 | 0.902 | 0.893 | 0.835 | 0.510 | 0.952 | 0.943 | 0.873 |
| | 150-250 | | | 0.469 | 0.875 | 0.866 | 0.810 | 0.495 | 0.924 | 0.915 | 0.847 |
| 10 | 90-150 | 1.284 | 1.450 | 0.489 | 0.944 | 0.935 | 0.874 | 0.514 | 0.991 | 0.981 | 0.909 |
| | 150-250 | | | 0.479 | 0.925 | 0.916 | 0.856 | 0.504 | 0.971 | 0.961 | 0.890 |
| 15 | 90-150 | 1.287 | 1.447 | 0.483 | 0.966 | 0.956 | 0.894 | 0.501 | 0.999 | 0.989 | 0.916 |
| | 150-250 | | | 0.474 | 0.947 | 0.938 | 0.876 | 0.496 | 0.989 | 0.979 | 0.907 |

Table 6.7, Summary of in-die and out-of-die porosity values of A4M : FBP/THP matrices (n = 3).

| A4M (%) | Particle size (µm) | Porosity (ε, %) | | | | Porosity (ε, %) | | | |
|---------|--------------------|-----------------|--------|----------------|-------|-----------------|--------|----------------|-------|
| | | FBP | | | | THP | | | |
| | | In-die | | After ejection | | In-die | | After ejection | |
| | | Zero P | Max. P | 0 h | 24 h | Zero P | Max. P | 0 h | 24 h |
| 5 | 90-150 | 51.68 | 9.79 | 10.69 | 16.54 | 48.99 | 4.79 | 5.74 | 12.72 |
| | 150-250 | 53.09 | 12.41 | 13.37 | 19.03 | 50.48 | 7.56 | 8.51 | 15.29 |
| 10 | 90-150 | 51.10 | 5.59 | 6.53 | 12.65 | 48.60 | 0.93 | 1.88 | 9.15 |
| | 150-250 | 52.06 | 7.44 | 8.42 | 14.41 | 49.61 | 2.88 | 3.86 | 10.98 |
| 15 | 90-150 | 51.62 | 3.33 | 4.36 | 10.61 | 49.86 | 0.13 | 1.09 | 8.42 |
| | 150-250 | 52.57 | 5.23 | 6.24 | 12.37 | 50.36 | 1.12 | 2.08 | 9.33 |

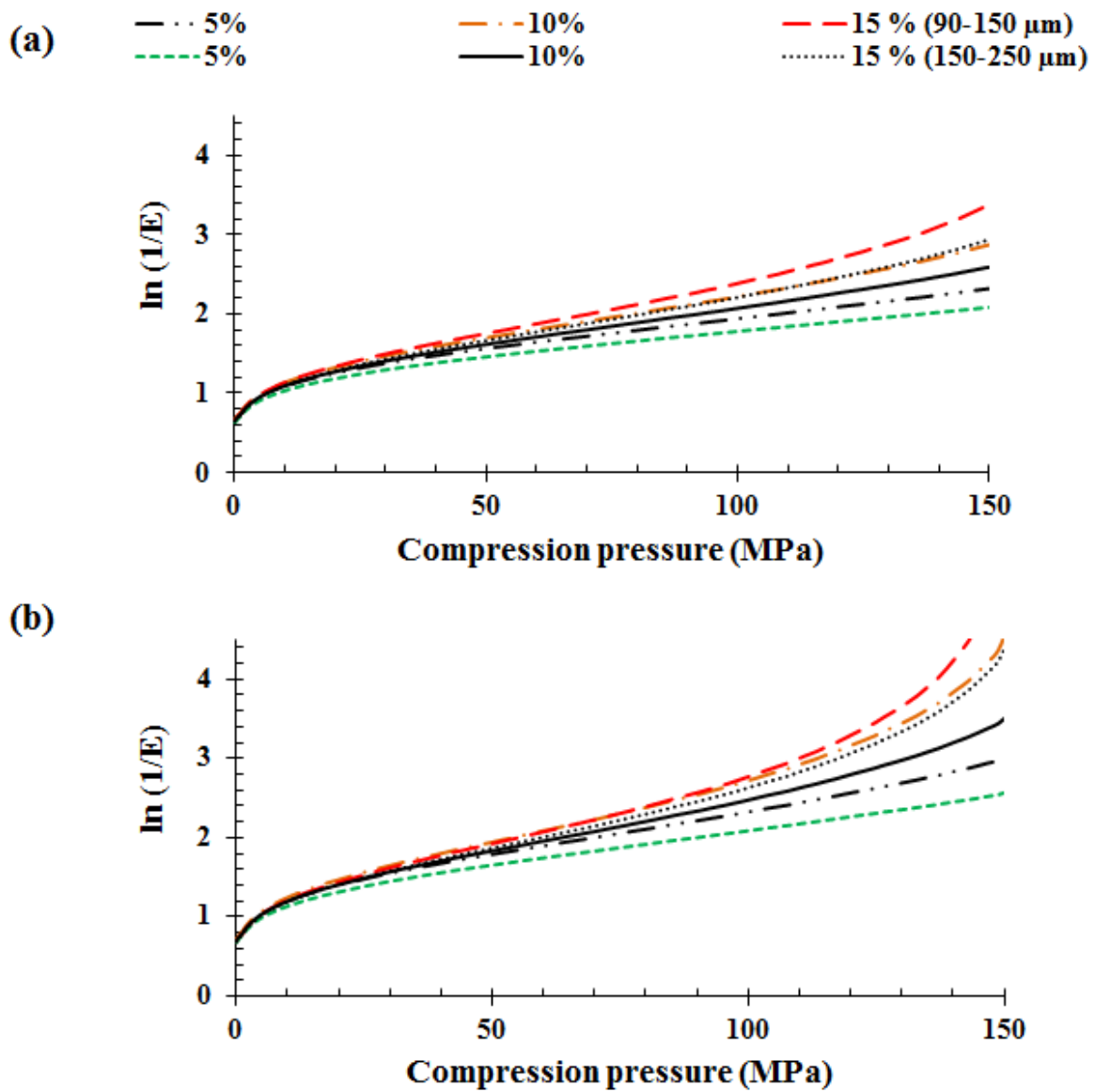


Figure 6.17, Heckel plots of matrices with respect to compression pressure (a) A4M : FBP and (b) A4M : THP (n = 3).

--- A4M - - - F4M - - - - E4M — K4M - - - K15M - · · K100M

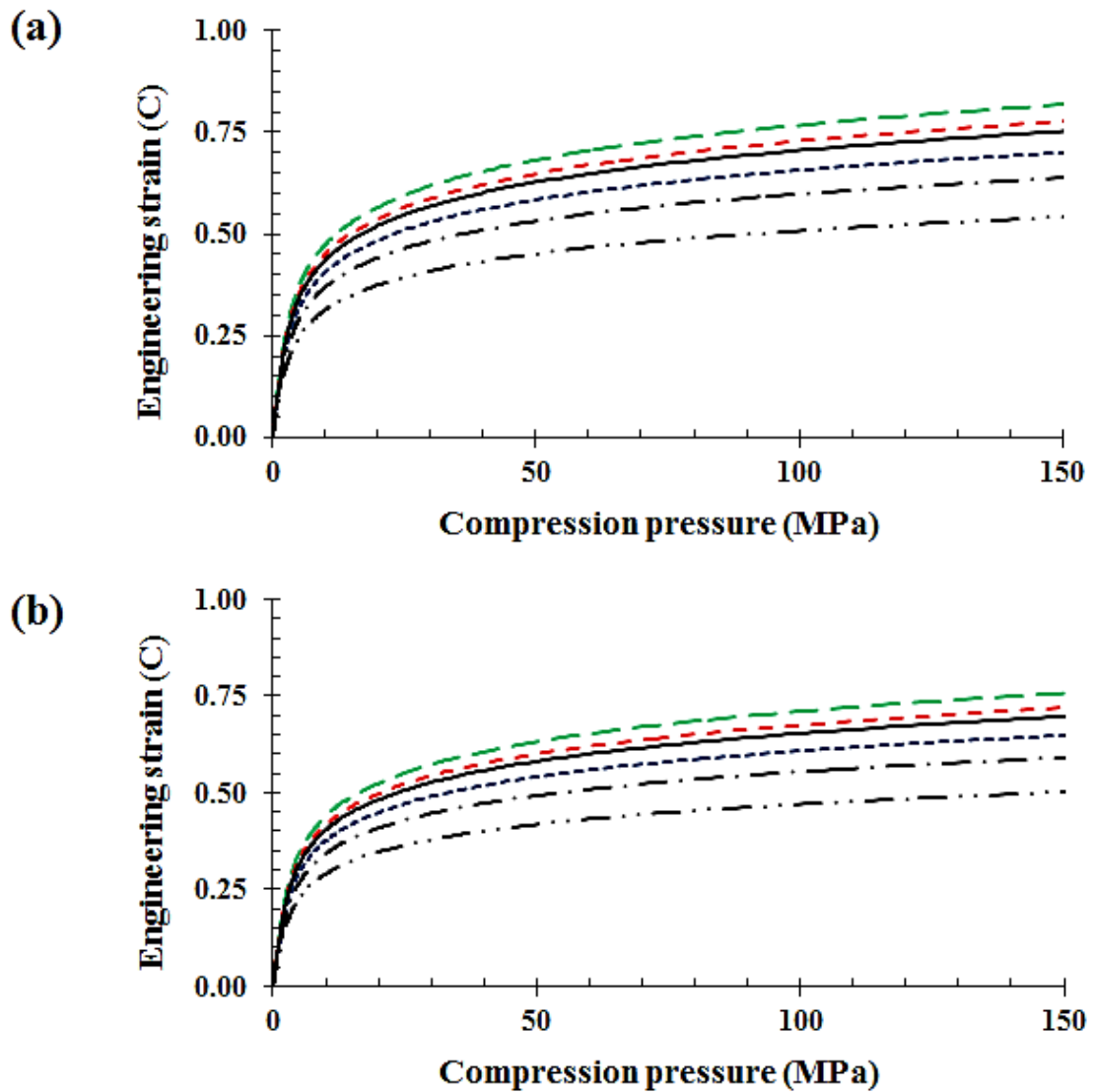


Figure 6.18, Kawakita plots of matrices with respect to compression pressure (a) A4M : FBP and (b) A4M : THP (n = 3).

Table 6.8, Summary of tensile strength and elastic recovery of A4M : FBP/THP matrices (n = 3, standard deviation given in parenthesis)

| A4M (%) | Particle size (μm) | Tensile strength (T, MPa) | | Elastic recovery (ER, %) | |
|---------|---------------------------------|---------------------------|-------------|--------------------------|-------------|
| | | FBP | THP | FBP | THP |
| 5 | 90-150 | 1.26 (0.01) | 2.88 (0.05) | 13.12 (0.83) | 7.50 (0.89) |
| | 150-250 | 1.11 (0.10) | 2.74 (0.01) | 14.25 (1.23) | 8.60 (0.31) |
| 10 | 90-150 | 1.31 (0.11) | 3.19 (0.11) | 12.15 (1.14) | 7.10 (0.72) |
| | 150-250 | 1.23 (0.09) | 3.08 (0.05) | 13.33 (0.94) | 7.80 (1.11) |
| 15 | 90-150 | 1.68 (0.07) | 3.55 (0.10) | 10.78 (0.21) | 5.90 (0.38) |
| | 150-250 | 1.43 (0.08) | 3.32 (0.11) | 11.50 (1.50) | 6.90 (0.62) |

Table 6.9, Summary of Heckel and Kawakita compressional parameters of A4M : FBP/THP matrices (n = 3).

| A4M (%) | Particle size (μm) | Heckel parameters | | | | | | Kawakita parameters | | | | | |
|---------|---------------------------------|-------------------|----------|----------------------|----------|----------|----------------------|---------------------|-----------------------|-----------|----------|-----------------------|-----------|
| | | FBP | | | THP | | | FBP | | | THP | | |
| | | <i>A</i> | <i>K</i> | <i>P_y</i> | <i>A</i> | <i>K</i> | <i>P_y</i> | <i>a</i> | <i>b⁻¹</i> | <i>ab</i> | <i>a</i> | <i>b⁻¹</i> | <i>ab</i> |
| 5 | 90-150 | 0.81 | 0.0129 | 77.52 | 0.94 | 0.0119 | 84.03 | 0.539 | 10.15 | 0.053 | 0.754 | 7.55 | 0.100 |
| | 150-250 | 0.70 | 0.0133 | 75.19 | 0.90 | 0.0114 | 87.72 | 0.523 | 11.20 | 0.047 | 0.732 | 7.84 | 0.093 |
| 10 | 90-150 | 0.80 | 0.0136 | 73.53 | 0.86 | 0.0125 | 80.00 | 0.573 | 9.11 | 0.063 | 0.803 | 7.1 | 0.113 |
| | 150-250 | 0.66 | 0.0139 | 71.94 | 0.80 | 0.0122 | 81.97 | 0.560 | 10.21 | 0.055 | 0.785 | 7.45 | 0.105 |
| 15 | 90-150 | 0.79 | 0.0144 | 69.44 | 0.82 | 0.0128 | 78.13 | 0.630 | 8.32 | 0.076 | 0.891 | 6.12 | 0.146 |
| | 150-250 | 0.65 | 0.0151 | 66.23 | 0.78 | 0.0131 | 76.19 | 0.612 | 9.33 | 0.066 | 0.856 | 6.89 | 0.124 |

A and *K* = Heckel constants, *P_y* (MPa) = Yield pressure, *a*, *b⁻¹* (MPa) and *ab* = Kawakita constants

6.9.3.3.2- Effect of Methocel[®] particle size

The Methocel[®] (MC/HPMC) particle size has the potential to affect the compaction properties of hydrophilic matrices and thus their performance (see section 6.5.1 for more detail). Therefore, the present study was designed to investigate the impact of MC/HPMC particle size on the compaction, compression and elastic relaxation properties of FBP/THP: MC/HPMC matrices.

In the present study, the reduction in MC/HPMC particle size fraction from 150 – 250 μm to 90 – 150 μm , showed that the relative density profiles of FBP/THP matrices start to increase (Figures 6.15, 6.19, 6.23, 6.27, 6.31 and 6.35). The *in-die* and *out of die* relative density values also showed a similar trend. This increase in relative density of tablet matrices was attributed to a greater degree of powder densification, which in turn reduces the overall porosity of matrix tablets (Figures 6.16, 6.20, 6.24, 6.28, 6.32 and 6.36). Moreover the *in-die* and *out of die* relative density and porosity values showed a good correlation (Tables 6.6, 6.7, 6.10, 6.11, 6.14, 6.15, 6.18, 6.19, 6.22, 6.23, 6.26 and 6.27). This behaviour can be attributed to the fact that fine powder particles have more contact points and generate more intense compressional forces during compression (Sandell, 1992, Dabbagh *et al.*, 1996). Therefore, the smaller particle size fraction has a higher degree of densification than the larger size fraction. The FBP/THP matrices fabricated from MC/HPMC with particle sizes between 90 – 150 μm , has a higher tensile strength (MPa) but a reduced elastic recovery (%) of matrices regardless of Methocel[®] grade.

To further analyse the *in-die* compression behaviour of these binary mixtures having different polymer size fractions, Heckel and Kawakita models were used (Figures 6.17, 6.18, 6.21, 6.22, 6.25, 6.26, 6.29, 6.30, 6.33, 6.34, 6.37 and 6.38). The findings of compressional mathematical modelling revealed that the values of yield pressure (P_y) were higher for small

particle size based binary mixtures (with the exception of 5 and 10 % MC/HPMC : THP matrices where the P_y values fell with the reduction in particle size) (Tables 6.9, 6.13, 6.17, 6.21, 6.25 and 6.29). However, the values of the Kawakita plasticity constant decreased as the particle size of MC/HPMC was reduced to 90-150 μm and these Kawakita findings were consistent regardless of drug and MC/HPMC grade. Furthermore, the P_y and b^{-1} values show an explainable direct relationship with the abovementioned relative density and porosity data, where a reduction in particle size increases relative density but decreases the overall porosity of the matrix tablet. This increase in tensile strength, reduction in the elastic recovery and variations in the compression parameters can be explained in the light of the theory that particle size reduction allows a high degree of packing and densification. Owing to this, a greater number of contact points were generated as powder particles are confined within close proximity, hence the chances of inter-particulate bonding increases (Alderborn and Nystrom, 1995; Malamataris *et al.*, 1994; , Rajabi-Siahboomi *et al.*, 1998). All the matrices showed a dependence on particle size which indicates the absence of extensive fragmentation (Adolfsson *et al.*, 1997).

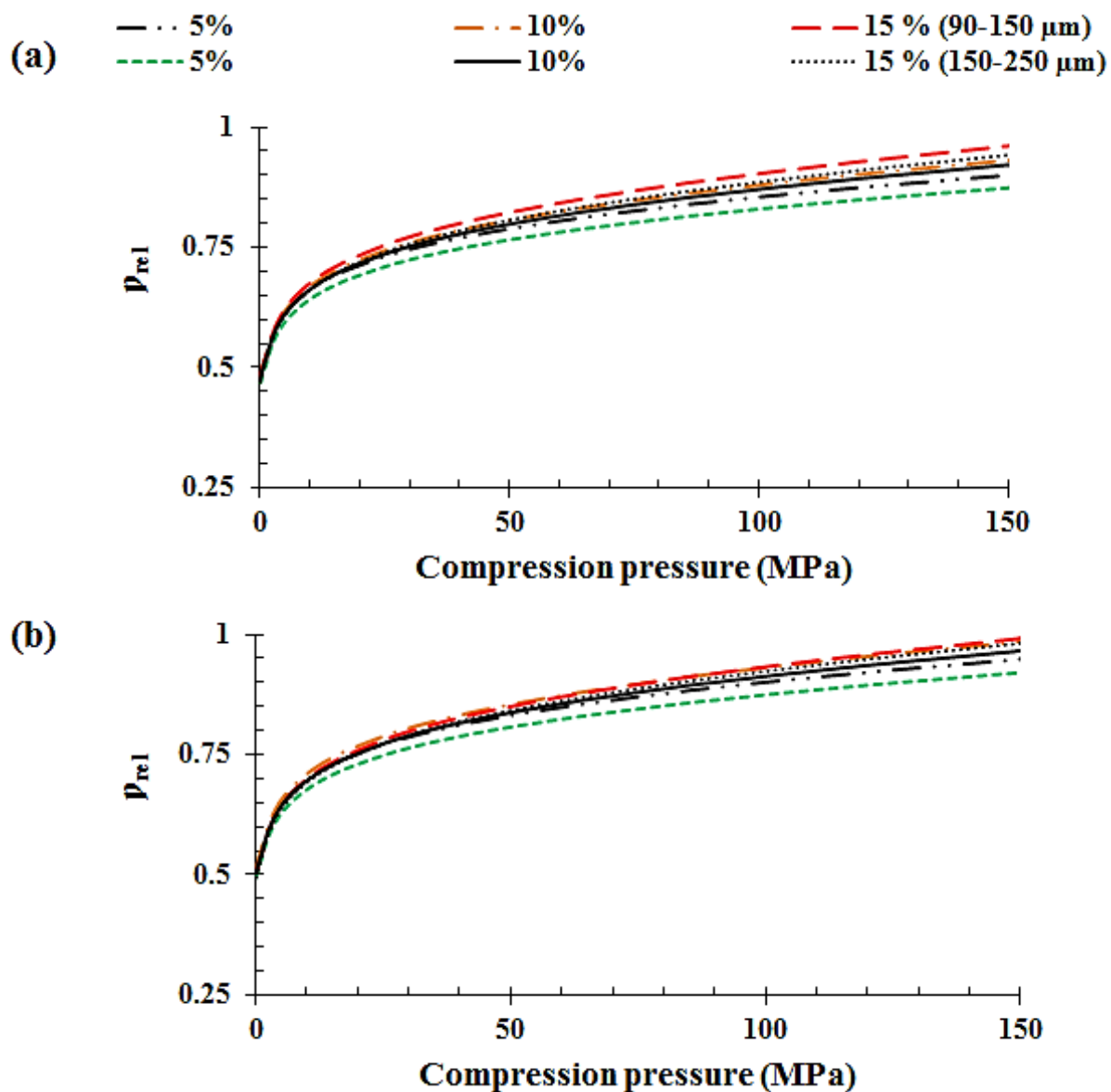


Figure 6.19, In-die relative density profiles of matrices with respect to compression pressure (a) F4M : FBP and (b) F4M : THP ($n = 3$).

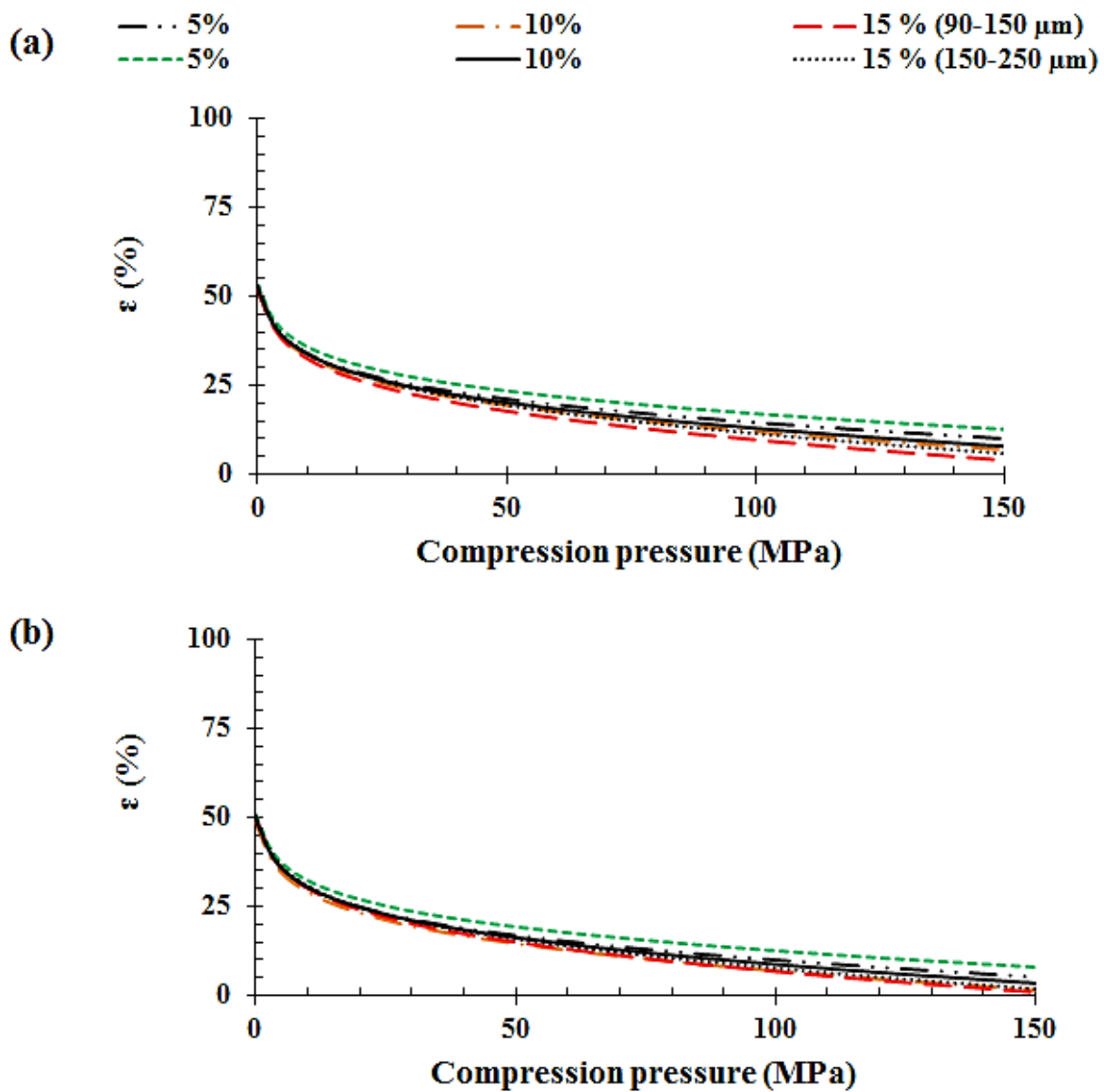


Figure 6.20, In-die porosity profiles of matrices with respect to compression pressure
 (a) F4M : FBP and (b) F4M : THP (n = 3).

Table 6.10, Summary of in-die and out-of-die relative density values of F4M : FBP/THP matrices (n = 3).

| F4M (%) | Particle size (µm) | True density (ρ _t , g cm ⁻³) | | Relative density (ρ _{rel}) | | | | Relative density (ρ _{rel}) | | | |
|---------|--------------------|---|-------|--------------------------------------|--------|----------------|-------|--------------------------------------|--------|----------------|-------|
| | | | | FBP | | | | THP | | | |
| | | | | In-die | | After ejection | | In-die | | After ejection | |
| | | | | Zero P | Max. P | 0 h | 24 h | Zero P | Max. P | 0 h | 24 h |
| 5 | 90-150 | 1.280 | 1.458 | 0.487 | 0.900 | 0.891 | 0.833 | 0.509 | 0.950 | 0.941 | 0.871 |
| | 150-250 | | | 0.469 | 0.874 | 0.865 | 0.809 | 0.495 | 0.923 | 0.914 | 0.846 |
| 10 | 90-150 | 1.282 | 1.450 | 0.476 | 0.931 | 0.922 | 0.861 | 0.513 | 0.987 | 0.977 | 0.905 |
| | 150-250 | | | 0.471 | 0.922 | 0.913 | 0.853 | 0.503 | 0.968 | 0.958 | 0.887 |
| 15 | 90-150 | 1.283 | 1.442 | 0.482 | 0.962 | 0.952 | 0.890 | 0.499 | 0.994 | 0.984 | 0.911 |
| | 150-250 | | | 0.472 | 0.943 | 0.934 | 0.873 | 0.495 | 0.984 | 0.974 | 0.902 |

Table 6.11, Summary of in-die and out-of-die porosity values of F4M : FBP/THP matrices (n = 3).

| F4M (%) | Particle size (µm) | Porosity (ε, %) | | | | Porosity (ε, %) | | | |
|---------|--------------------|-----------------|--------|----------------|-------|-----------------|--------|----------------|-------|
| | | FBP | | | | THP | | | |
| | | In-die | | After ejection | | In-die | | After ejection | |
| | | Zero P | Max. P | 0 h. | 24 h | Zero P | Max. P | 0 h | 24 h |
| 5 | 90-150 | 51.27 | 9.95 | 10.89 | 16.72 | 49.06 | 4.96 | 5.94 | 12.91 |
| | 150-250 | 53.15 | 12.58 | 13.47 | 19.13 | 50.55 | 7.73 | 8.61 | 15.38 |
| 10 | 90-150 | 52.41 | 6.85 | 7.82 | 13.85 | 48.73 | 1.28 | 2.28 | 9.52 |
| | 150-250 | 52.89 | 7.77 | 8.71 | 14.68 | 49.74 | 3.21 | 4.16 | 11.26 |
| 15 | 90-150 | 51.81 | 3.84 | 4.75 | 10.98 | 50.05 | 0.64 | 1.58 | 8.87 |
| | 150-250 | 52.75 | 5.72 | 6.63 | 12.74 | 50.55 | 1.62 | 2.57 | 9.79 |

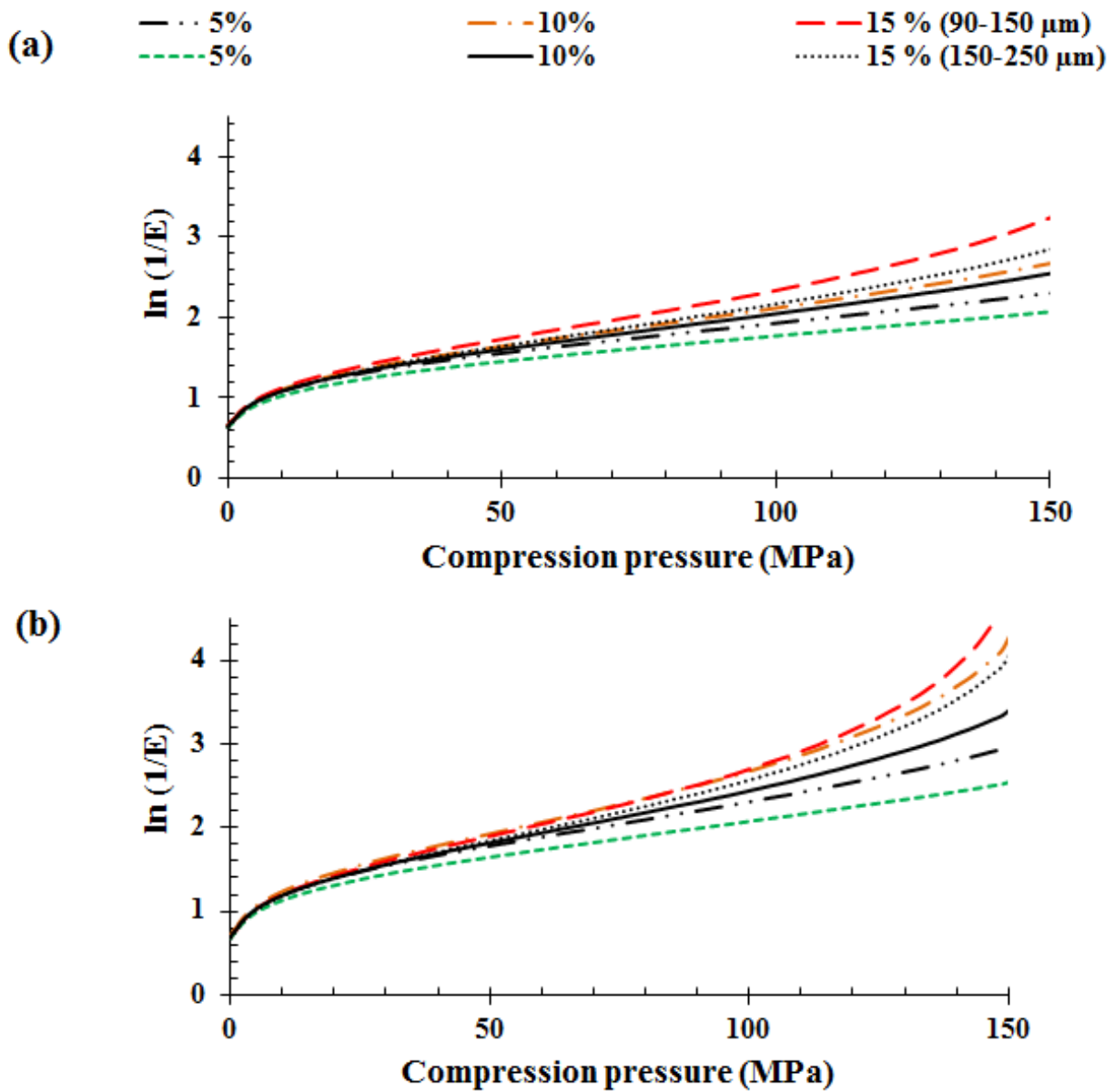


Figure 6.21, Heckel plots of matrices with respect to compression pressure (a) F4M : FBP and (b) F4M : THP (n = 3).

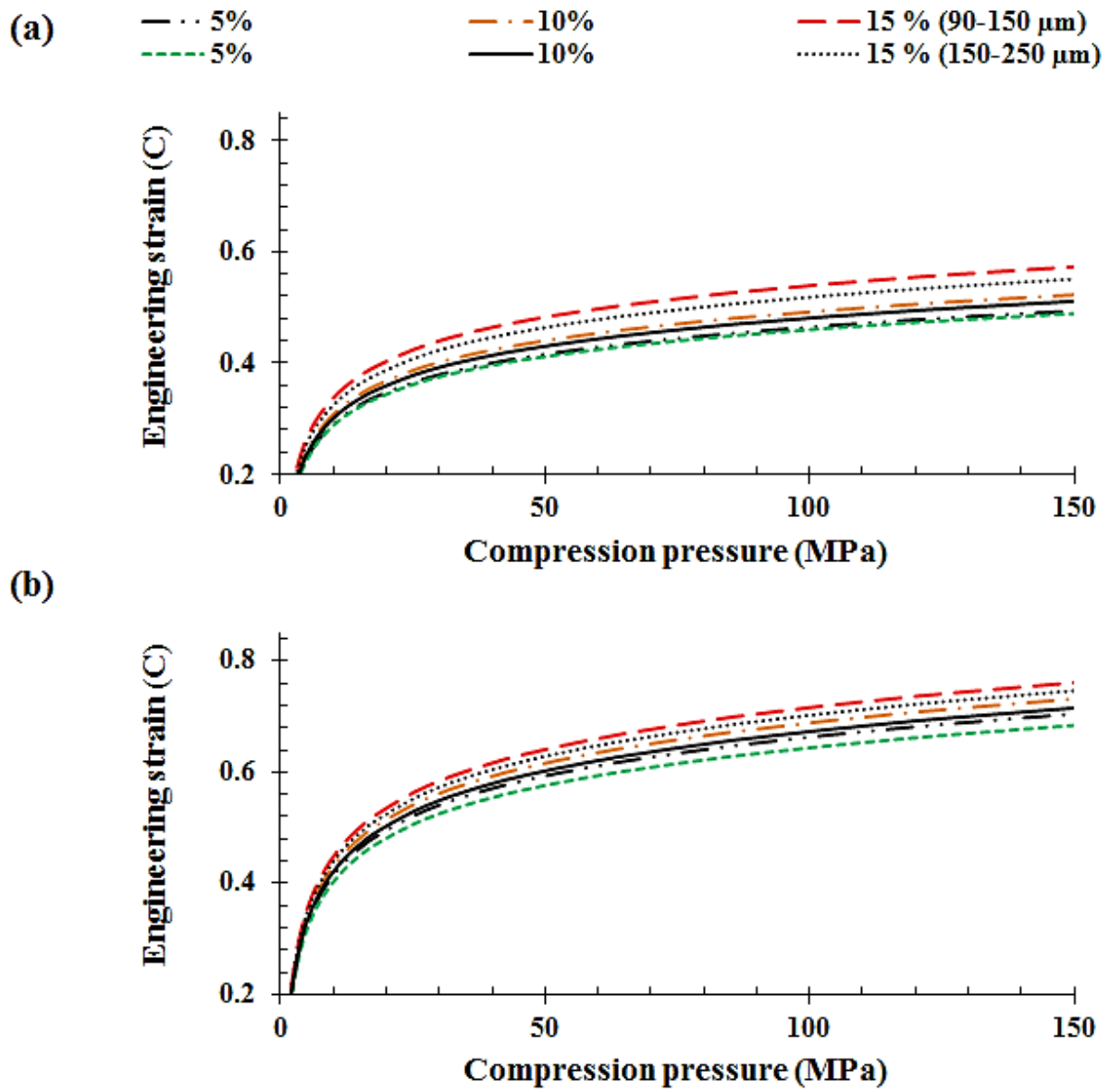


Figure 6.22, Kawakita plots of matrices with respect to compression pressure (a) F4M : FBP and (b) F4M : THP (n = 3).

Table 6.12, Summary of tensile strength and elastic recovery of F4M : FBP/THP matrices (n = 3).

| F4M (%) | Particle size (µm) | Tensile strength (T, MPa) | | Elastic recovery (ER, %) | |
|---------|--------------------|---------------------------|-------------|--------------------------|-------------|
| | | FBP | THP | FBP | THP |
| 5 | 90-150 | 1.22 (0.05) | 2.67 (0.10) | 12.74 (1.52) | 6.94 (1.14) |
| | 150-250 | 1.08 (0.06) | 2.54 (0.08) | 13.83 (1.11) | 7.96 (0.31) |
| 10 | 90-150 | 1.27 (0.01) | 2.93 (0.02) | 11.80 (0.29) | 6.57 (0.55) |
| | 150-250 | 1.21 (0.10) | 2.85 (0.08) | 12.94 (0.89) | 7.22 (0.89) |
| 15 | 90-150 | 1.63 (0.04) | 3.29 (0.04) | 10.47 (1.19) | 5.46 (0.34) |
| | 150-250 | 1.39 (0.07) | 3.07 (0.01) | 11.50 (0.39) | 6.39 (0.33) |

Table 6.13, Summary of Heckel and Kawakita compressional parameters of F4M : FBP/THP matrices (n = 3).

| F4M (%) | Particle size (µm) | Heckel parameters | | | | | | Kawakita parameters | | | | | |
|---------|--------------------|-------------------|---------|-------|------|--------|-------|---------------------|----------|-------|-------|----------|-------|
| | | FBP | | | THP | | | FBP | | | THP | | |
| | | A | K | P_y | A | K | P_y | a | b^{-1} | ab | a | b^{-1} | ab |
| 5 | 90-150 | 0.79 | 0.01277 | 78.29 | 0.87 | 0.0117 | 85.71 | 0.519 | 10.25 | 0.051 | 0.741 | 7.70 | 0.096 |
| | 150-250 | 0.68 | 0.01317 | 75.94 | 0.83 | 0.0112 | 89.47 | 0.514 | 11.31 | 0.045 | 0.719 | 8.00 | 0.090 |
| 10 | 90-150 | 0.78 | 0.01347 | 74.26 | 0.80 | 0.0123 | 81.60 | 0.549 | 9.20 | 0.060 | 0.769 | 7.24 | 0.106 |
| | 150-250 | 0.64 | 0.01376 | 72.66 | 0.74 | 0.0120 | 83.61 | 0.537 | 10.31 | 0.052 | 0.752 | 7.60 | 0.099 |
| 15 | 90-150 | 0.76 | 0.01426 | 70.14 | 0.76 | 0.0125 | 79.69 | 0.602 | 8.40 | 0.072 | 0.800 | 6.24 | 0.128 |
| | 150-250 | 0.63 | 0.01495 | 66.89 | 0.73 | 0.0129 | 77.71 | 0.579 | 9.42 | 0.061 | 0.785 | 7.03 | 0.112 |

A and K = Heckel constants, P_y (MPa) = Yield pressure, a, b^{-1} (MPa) and ab = Kawakita constants

6.9.3.3.3- Effect of Methocel[®] substitution

The level of different substitution groups has the potential to affect the compaction properties of MC/HPMC matrices (Rajabi-Siahboomi *et al.*, 1998). In the present study the influence of substitution ratios (Hpo/Meo) on compaction, compression and relaxation properties of matrices were studied. For this purpose, A4M, F4M, E4M and K4M were selected because these Methocel[®] grades have similar viscosity ranges but have varying levels of Hpo/Meo substitution ratios, A4M = 0.238, F4M = 0.286, E4 = 0.381 and K4M = 0.403, (Table 2.1, see Chapter 2 for more detail).

The present results showed that the A4M: FBP/THP matrices have a higher relative density, but lower porosity than F4M, E4M and K4M based matrices (Figures 6.15,6.16, 6.19, 6.20, 6.23, 6.24, 6.27 and 6.28). After 24 h following ejection, the out-of-die relative density of A4M: FBP matrices were in the range of 0.810 – 0.894, however the A4M: THP matrices were in the range of 0.873 – 0.916. The A4M is a MC grade of Methocel[®] having only Meo hydrophobic substitution groups. When hydrophilic substitution groups were introduced the relative density decreased with those of K4M: FBP (0.808 – 0.859) and K4M: THP (0.828 – 0.888) being the lowest in the series. Moreover, the porosity decreased with an increase in the relative density of tablet matrices, attributed to increased densification of powder particles inside the die. There was a strong correlation between in-die and out-of-die values of relative density and porosity (Tables 6.6,6.7, 6.10, 6.11, 6.14, 6.15, 6.18 and 6.19).

The substitution ratio had a marked impact on the tensile strength and elastic relaxation of matrices. A4M matrices, regardless of the drug, produced tablets of highest tensile strength in the series. With the introduction of Hpo levels (F4M, E4M and K4M) the tensile strength decreases but elastic recovery is enhanced. K4M based matrices had the lowest tensile strength, but highest elastic recovery (%) (Tables 6.8, 6.12, 6.16 and 6.20). The inclusion of

Hpo groups in the various Methocel[®] grades makes their particle surface rougher and the greater strength of A4M based matrices may be because it possesses a higher percentage of fibrous polymer particles compared to F4M, E4M and K4M (Ghori *et al.*, 2014d; Gustafsson *et al.*, 1999).

To further analyse the mechanism of compression, the Heckel and Kawakita mathematical models were applied (Figures 6.17, 6.18, 6.21, 6.22, 6.25, 6.26, 6.29 and 6.30). The findings of these models revealed that A4M (MC) based matrices have lowest P_y values b^{-1} values. However, the K4M based matrices (regardless of type of drug), have the highest P_y and b^{-1} values. Differences for F4M and E4M based matrices were less pronounced, however these were higher than A4M (Tables 6.9, 6.13, 6.17 and 6.21). The increase in both P_y and b^{-1} values may be linked to the incorporation of hydroxyl groups on the parent glucose ring of the polymer. As it is a hydrophilic substitution group and has a tendency to change the surface morphology of polymer particles (Gustafsson *et al.*, 1999), so it can be assumed that due to surface irregularities it may need a higher compression pressure to deform, however, the more fibrous A4M based matrices deform plastically at low compression pressure (Rajabi-Siahboomi *et al.*, 1998).

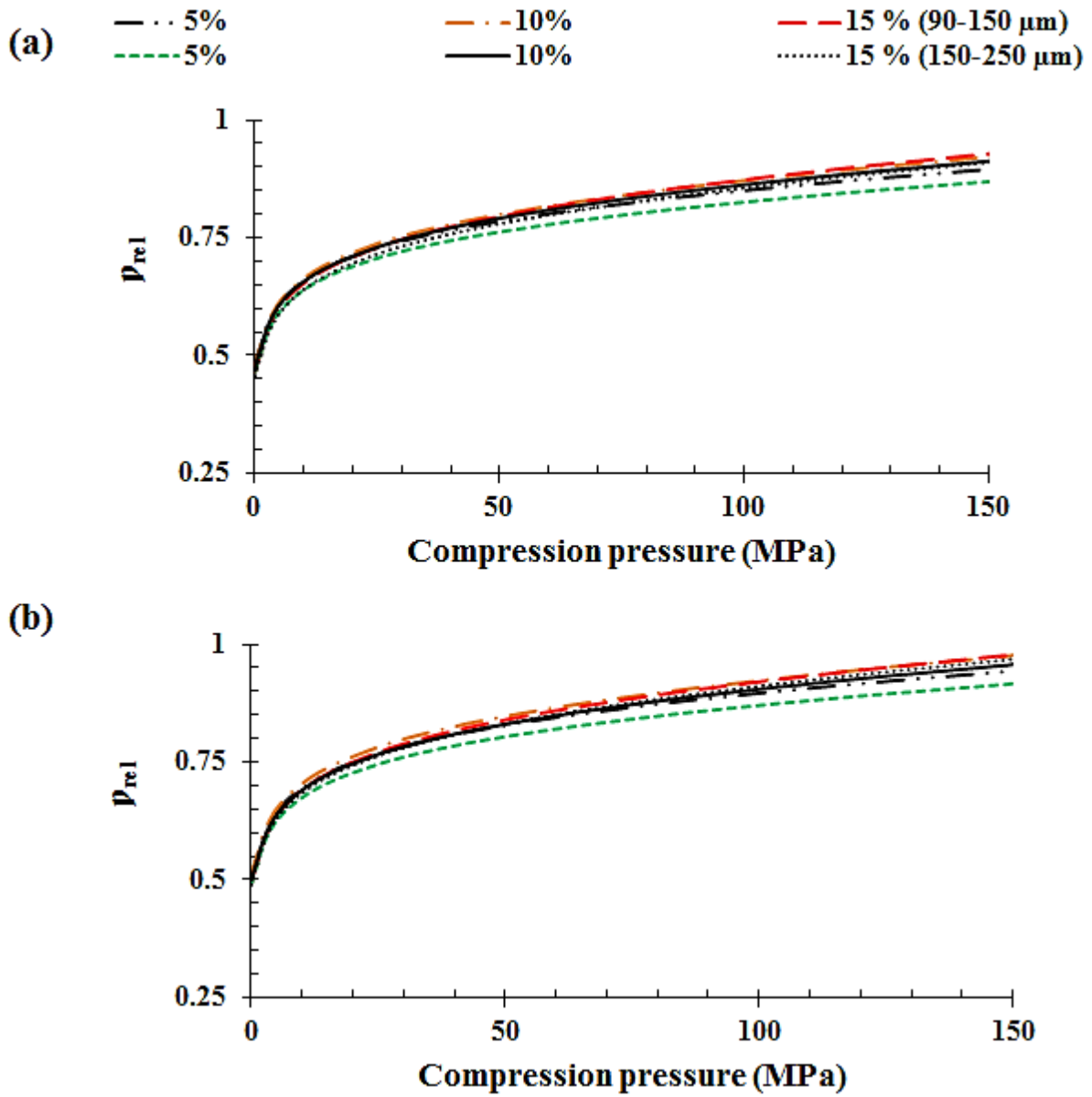


Figure 6.23, In-die relative density profiles of matrices with respect to compression pressure (a) E4M : FBP and (b) E4M : THP ($n = 3$).

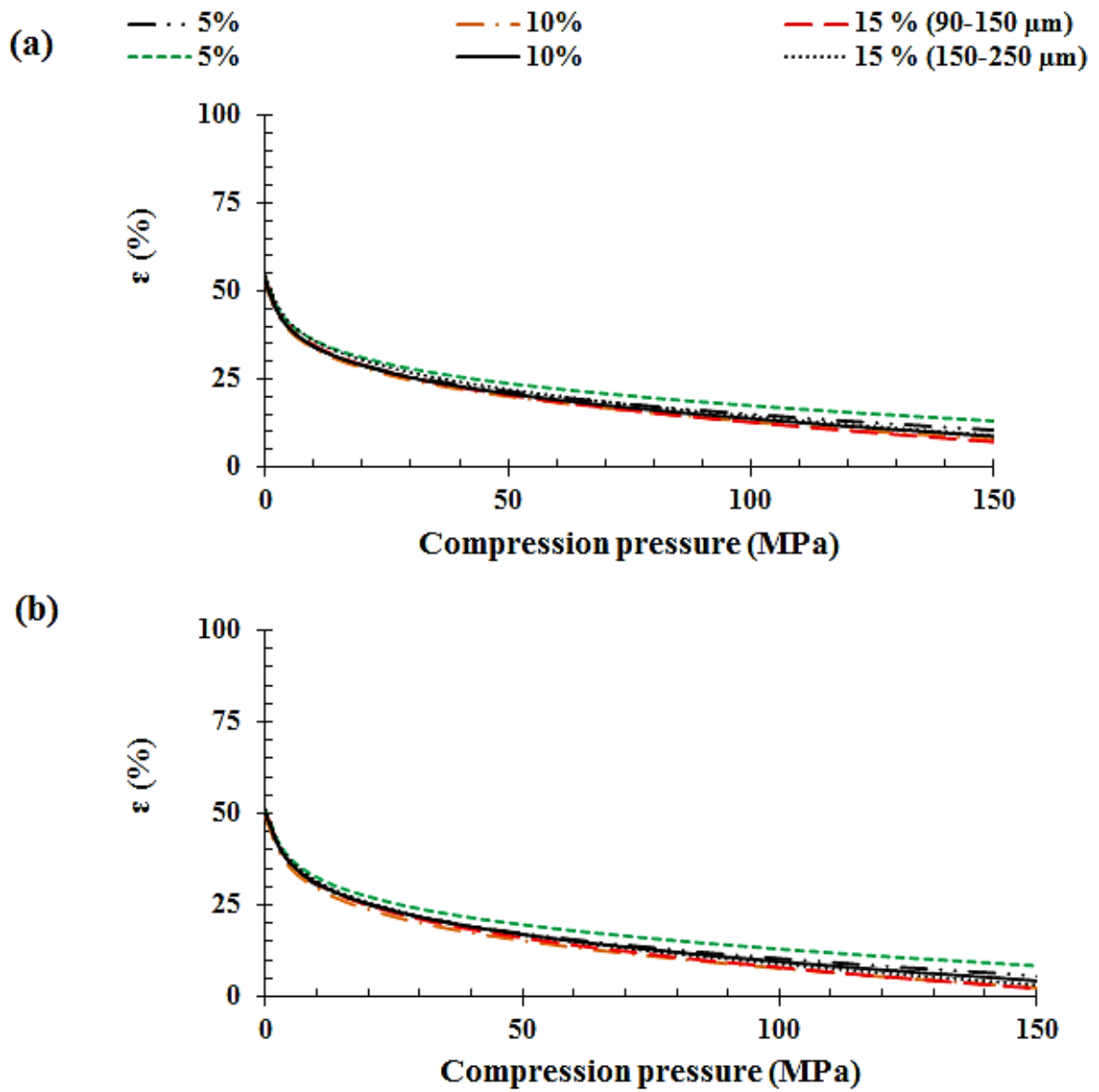


Figure 6.24, In-die porosity profiles of matrices with respect to compression pressure
 (a) E4M : FBP and (b) E4M : THP (n = 3).

Table 6.14, Summary of in-die and out-of-die relative density values of E4M : FBP/THP matrices (n = 3).

| E4M (%) | Particle size (μm) | True density (ρ _t , g cm ⁻³) | | Relative density (ρ _{rel}) | | | | Relative density (ρ _{rel}) | | | |
|---------|--------------------|---|-------|--------------------------------------|--------|----------------|-------|--------------------------------------|--------|----------------|-------|
| | | | | FBP | | THP | | FBP | | THP | |
| | | | | In-die | | After ejection | | In-die | | After ejection | |
| | | FBP | THP | Zero P | Max. P | 0 h | 24 h | Zero P | Max. P | 0 h | 24 h |
| 5 | 90-150 | 1.279 | 1.457 | 0.486 | 0.896 | 0.887 | 0.829 | 0.493 | 0.918 | 0.909 | 0.842 |
| | 150-250 | | | 0.467 | 0.870 | 0.861 | 0.805 | 0.508 | 0.946 | 0.937 | 0.867 |
| 10 | 90-150 | 1.279 | 1.448 | 0.473 | 0.922 | 0.913 | 0.853 | 0.499 | 0.959 | 0.950 | 0.879 |
| | 150-250 | | | 0.468 | 0.913 | 0.904 | 0.845 | 0.509 | 0.978 | 0.968 | 0.897 |
| 15 | 90-150 | 1.280 | 1.439 | 0.466 | 0.929 | 0.920 | 0.860 | 0.490 | 0.970 | 0.960 | 0.889 |
| | 150-250 | | | 0.457 | 0.911 | 0.902 | 0.843 | 0.494 | 0.980 | 0.970 | 0.898 |

Table 6.15, Summary of in-die and out-of-die porosity values of E4M : FBP/THP matrices (n = 3).

| E4M (%) | Particle size (μm) | Porosity (ε, %) | | | | Porosity (ε, %) | | | |
|---------|--------------------|-----------------|--------|----------------|-------|-----------------|--------|----------------|-------|
| | | FBP | | THP | | FBP | | THP | |
| | | In-die | | After ejection | | In-die | | After ejection | |
| | | Zero P | Max. P | 0 h | 24 h | Zero P | Max. P | 0 h | 24 h |
| 5 | 90-150 | 51.45 | 10.42 | 11.29 | 17.09 | 50.71 | 8.18 | 9.11 | 15.84 |
| | 150-250 | 53.31 | 13.02 | 13.86 | 19.50 | 49.23 | 5.42 | 6.34 | 13.27 |
| 10 | 90-150 | 52.72 | 7.76 | 8.71 | 14.68 | 50.07 | 4.11 | 5.05 | 12.08 |
| | 150-250 | 53.19 | 8.67 | 9.60 | 15.52 | 49.07 | 2.19 | 3.17 | 10.34 |
| 15 | 90-150 | 53.36 | 7.08 | 8.02 | 14.04 | 51.05 | 2.96 | 3.96 | 11.07 |
| | 150-250 | 54.27 | 8.90 | 9.80 | 15.70 | 50.56 | 1.99 | 2.97 | 10.16 |

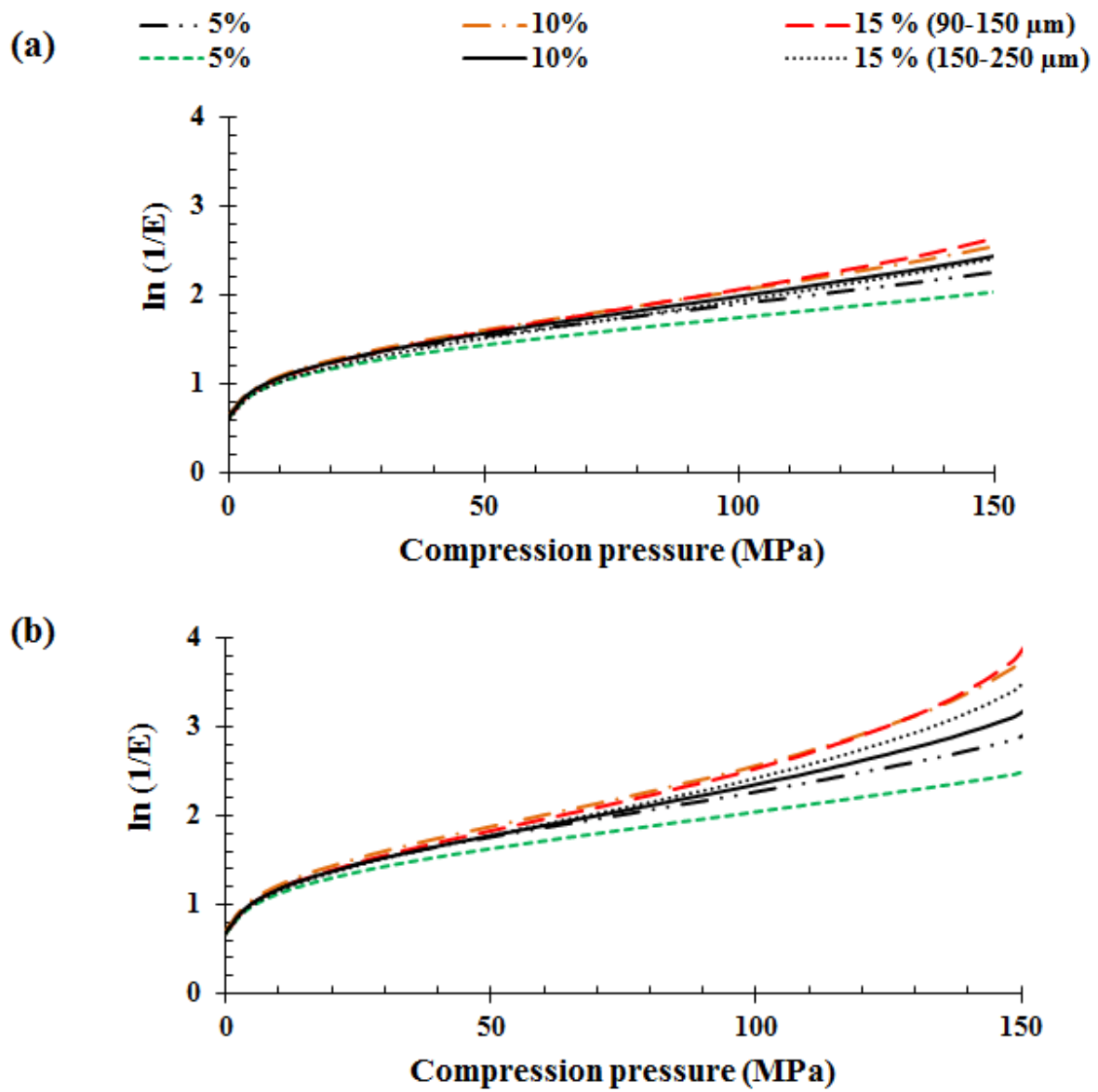


Figure 6.25, Heckel plots of matrices with respect to compression pressure (a) E4M : FBP and (b) E4M : THP (n = 3).

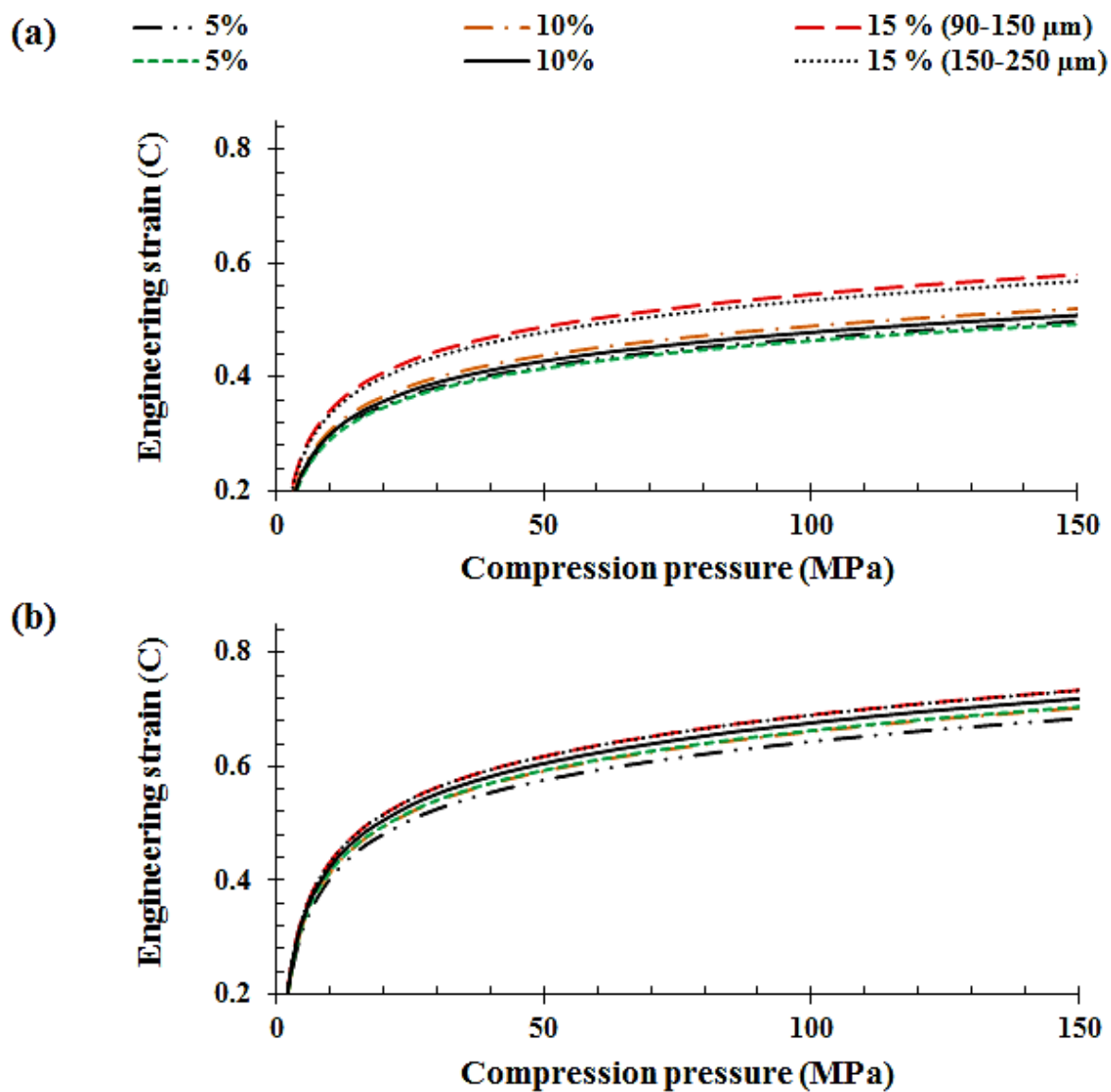


Figure 6.26, Kawakita plots of matrices with respect to compression pressure (a) E4M : FBP and (b) E4M : THP (n = 3).

Table 6.16, Summary of tensile strength and elastic recovery of E4M : FBP/THP matrices (n = 3, standard deviation given in parenthesis)

| E4M (%) | Particle size (µm) | Tensile strength (T, MPa) | | Elastic recovery (ER, %) | |
|---------|--------------------|---------------------------|-------------|--------------------------|-------------|
| | | FBP | THP | FBP | THP |
| 5 | 90-150 | 1.20 (0.07) | 2.69 (0.08) | 12.50 (1.23) | 7.01 (0.59) |
| | 150-250 | 1.06 (0.02) | 2.56 (0.12) | 13.57 (0.56) | 8.04 (0.81) |
| 10 | 90-150 | 1.25 (0.09) | 2.95 (0.05) | 11.57 (1.20) | 6.64 (0.23) |
| | 150-250 | 1.17 (0.03) | 2.88 (0.09) | 12.70 (1.33) | 7.29 (1.09) |
| 15 | 90-150 | 1.60 (0.01) | 3.32 (0.03) | 9.95 (0.68) | 5.51 (0.23) |
| | 150-250 | 1.37 (0.05) | 3.10 (0.01) | 10.95 (0.89) | 6.45 (1.06) |

Table 6.17, Summary of Heckel and Kawakita compressional parameters of E4M : FBP/THP matrices (n = 3).

| E4M (%) | Particle size (µm) | Heckel parameters | | | | | | Kawakita parameters | | | | | |
|---------|--------------------|-------------------|--------|-------|------|--------|-------|---------------------|----------|-------|-------|----------|-------|
| | | FBP | | | THP | | | FBP | | | THP | | |
| | | A | K | P_y | A | K | P_y | a | b^{-1} | ab | a | b^{-1} | ab |
| 5 | 90-150 | 0.78 | 0.0126 | 78.15 | 0.88 | 0.0116 | 86.57 | 0.524 | 10.35 | 0.051 | 0.684 | 7.63 | 0.089 |
| | 150-250 | 0.67 | 0.0130 | 76.70 | 0.84 | 0.0111 | 89.16 | 0.518 | 11.42 | 0.045 | 0.705 | 7.92 | 0.089 |
| 10 | 90-150 | 0.76 | 0.0133 | 75.01 | 0.81 | 0.0121 | 82.41 | 0.547 | 9.29 | 0.059 | 0.703 | 7.17 | 0.098 |
| | 150-250 | 0.63 | 0.0136 | 74.26 | 0.75 | 0.0118 | 84.44 | 0.535 | 10.41 | 0.051 | 0.719 | 7.52 | 0.095 |
| 15 | 90-150 | 0.75 | 0.0141 | 70.84 | 0.77 | 0.0124 | 79.95 | 0.610 | 8.49 | 0.072 | 0.734 | 6.18 | 0.118 |
| | 150-250 | 0.62 | 0.0148 | 67.56 | 0.73 | 0.0127 | 78.49 | 0.598 | 9.52 | 0.063 | 0.734 | 6.96 | 0.105 |

A and K = Heckel constants, P_y (MPa) = Yield pressure, a, b^{-1} (MPa) and ab = Kawakita constants

6.9.3.3.4- Effect of Methocel[®] molecular size (viscosity)

The previous studies showed that the molecular size of Methocel[®] (MC/HPMC) can influence the compaction, compression and elastic relaxation properties of hydrophilic matrices (Nokhodchi and Rubinstein, 2001). To study the impact of MC/HPMC molecular size in binary mixtures, K4M, K15M and K100M grades were used, having different viscosity but a similar range of Hpo/Meo substitution ratios, K4M = 4351 cps, K15M = 17129 cps and K100M = 79279 cps, Table 2.1 (see chapter 2 for more detail), were selected.

The results confirmed that the relative density and porosity of the matrix tablet decreased as the molecular size of HPMC increased. The present results showed that the K4M: FBP/THP matrices have higher relative density but lower porosity than K15M and K100M based matrices (Figures 6.27, 6.28, 6.31, 6.32, 6.35 and 6.36). Twenty-four hours following ejection, the out-of-die relative density of K4M: FBP matrices ranged from 0.808 – 0.859, however the K4M: THP matrices were in the range of 0.828 – 0.888. Moreover, the porosity values were increased with increasing HPMC chain length, which might be attributed to poor densification of the powder particles inside the die. Moreover, the in-die and out-of-die values of relative density and porosity showed a good correlation (Tables 6.18, 6.19, 6.22, 6.23, 6.26 and 6.27). Additionally, the molecular size of HPMC impacted the tensile strength and relaxation properties of matrices. K4M matrices, regardless of drug, had the highest tensile strength in the series; the tensile strength begins to decrease with increasing polymer particle size but elastic recovery was enhanced. K100M based matrices had the lowest tensile strength but highest elastic recovery (%), (Tables 6.20, 6.24 and 6.28).

To further analyse the mechanism of compression, the Heckel and Kawakita mathematical models were applied (Figures 6.29, 6.30, 6.33, 6.34, 6.37 and 6.38). The findings of these models revealed that K4M based matrices have lowest P_y values b^{-1} values. However, the

K100M based matrices (regardless of type of drug) have highest P_y and b^{-1} values (Tables 6.21, 6.25 and 6.29). The increase in the P_y values b^{-1} may be linked to the rapid deformation of shorter chain lengths under pressure during compression. The increase in molecular weight affects the materials' ability to deform, as the higher molecular weight HPMC (K100M) needs a higher pressure to deform in comparison with other grades. Thus HPMC with shorter polymeric chains may deform more readily to fill inter-particulate gaps (Nokhodchi *et al.*, 1995).

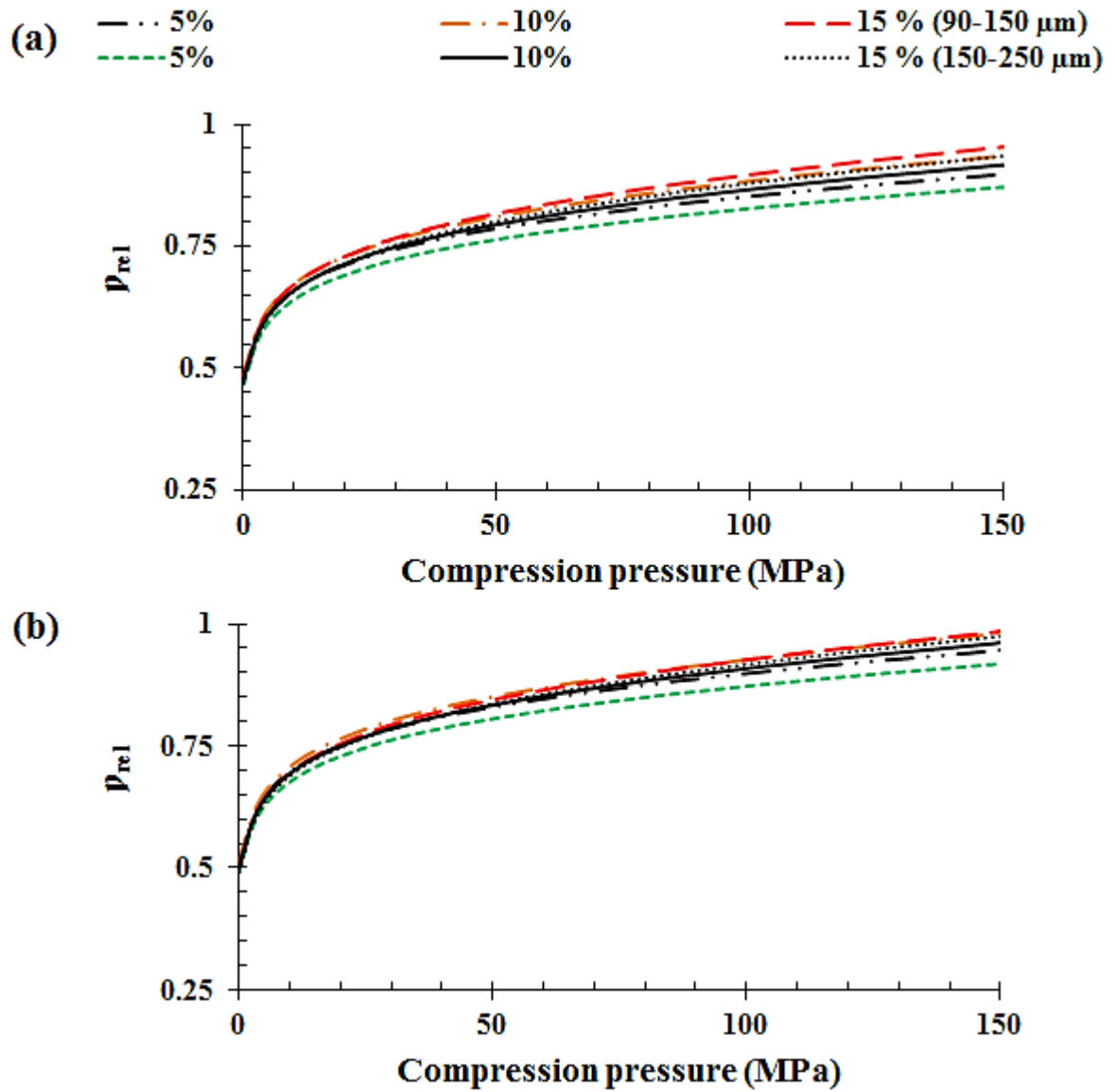


Figure 6.27, In-die relative density profiles of matrices with respect to compression pressure (a) K4M : FBP and (b) K4M : THP (n = 3).

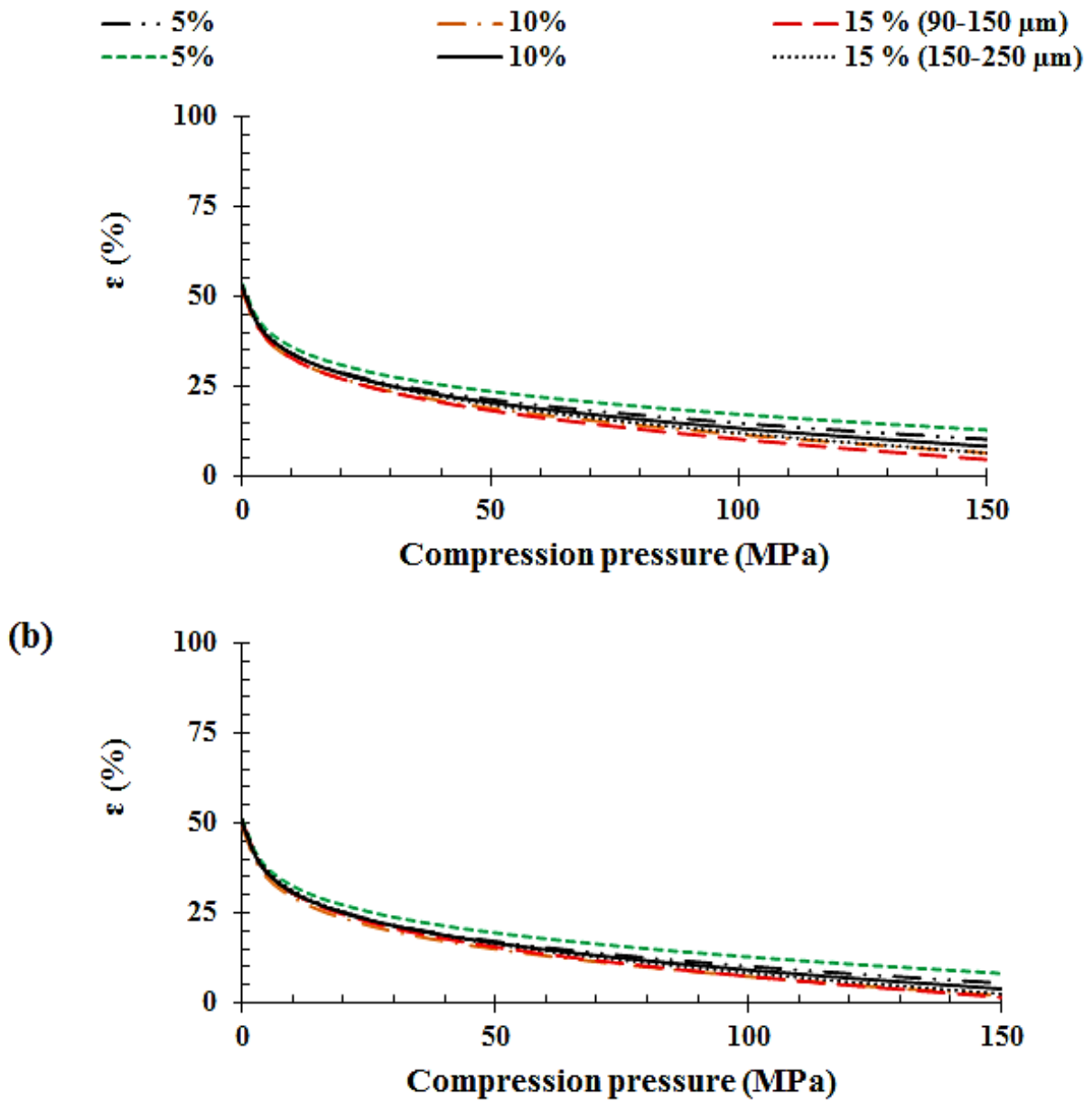


Figure 6.28, In-die porosity profiles of matrices with respect to compression pressure (a) K4M : FBP and (b) K4M : THP (n = 3).

Table 6.18, Summary of in-die and out-of-die relative density values of K4M : FBP/THP matrices (n = 3).

| K4M (%) | Particle size (µm) | True density (ρ _t , g cm ⁻³) | | Relative density (ρ _{rel}) | | | | Relative density (ρ _{rel}) | | | |
|---------|--------------------|---|-------|--------------------------------------|--------|----------------|-------|--------------------------------------|--------|----------------|-------|
| | | | | FBP | | | | THP | | | |
| | | | | In-die | | After ejection | | In-die | | After ejection | |
| | | | | Zero P | Max. P | 0 h | 24 h | Zero P | Max. P | 0 h | 24 h |
| 5 | 90-150 | 1.281 | 1.459 | 0.482 | 0.898 | 0.889 | 0.808 | 0.508 | 0.948 | 0.939 | 0.853 |
| | 150-250 | | | 0.468 | 0.872 | 0.863 | 0.785 | 0.494 | 0.920 | 0.911 | 0.828 |
| 10 | 90-150 | 1.283 | 1.452 | 0.486 | 0.936 | 0.927 | 0.842 | 0.511 | 0.982 | 0.972 | 0.884 |
| | 150-250 | | | 0.476 | 0.918 | 0.909 | 0.826 | 0.501 | 0.963 | 0.953 | 0.867 |
| 15 | 90-150 | 1.286 | 1.445 | 0.479 | 0.954 | 0.945 | 0.859 | 0.497 | 0.987 | 0.977 | 0.888 |
| | 150-250 | | | 0.470 | 0.936 | 0.927 | 0.842 | 0.492 | 0.977 | 0.967 | 0.879 |

Table 6.19, Summary of in-die and out-of-die porosity values of K4M : FBP/THP matrices (n = 3).

| K4M (%) | Particle size (µm) | Porosity (ε, %) | | | | Porosity (ε, %) | | | |
|---------|--------------------|-----------------|--------|----------------|-------|-----------------|--------|----------------|-------|
| | | FBP | | | | THP | | | |
| | | In-die | | After ejection | | In-die | | After ejection | |
| | | Zero P | Max. P | 0 h | 24 h | Zero P | Max. P | 0 h | 24 h |
| 5 | 90-150 | 51.83 | 10.20 | 11.09 | 19.17 | 49.15 | 5.21 | 6.14 | 14.67 |
| | 150-250 | 53.23 | 12.81 | 13.66 | 21.51 | 50.63 | 7.97 | 8.91 | 17.19 |
| 10 | 90-150 | 51.41 | 6.41 | 7.33 | 15.75 | 48.91 | 1.76 | 2.77 | 11.61 |
| | 150-250 | 52.36 | 8.24 | 9.11 | 17.37 | 49.91 | 3.68 | 4.65 | 13.32 |
| 15 | 90-150 | 52.07 | 4.56 | 5.54 | 14.13 | 50.32 | 1.35 | 2.28 | 11.16 |
| | 150-250 | 53.01 | 6.43 | 7.33 | 15.75 | 50.81 | 2.33 | 3.27 | 12.06 |

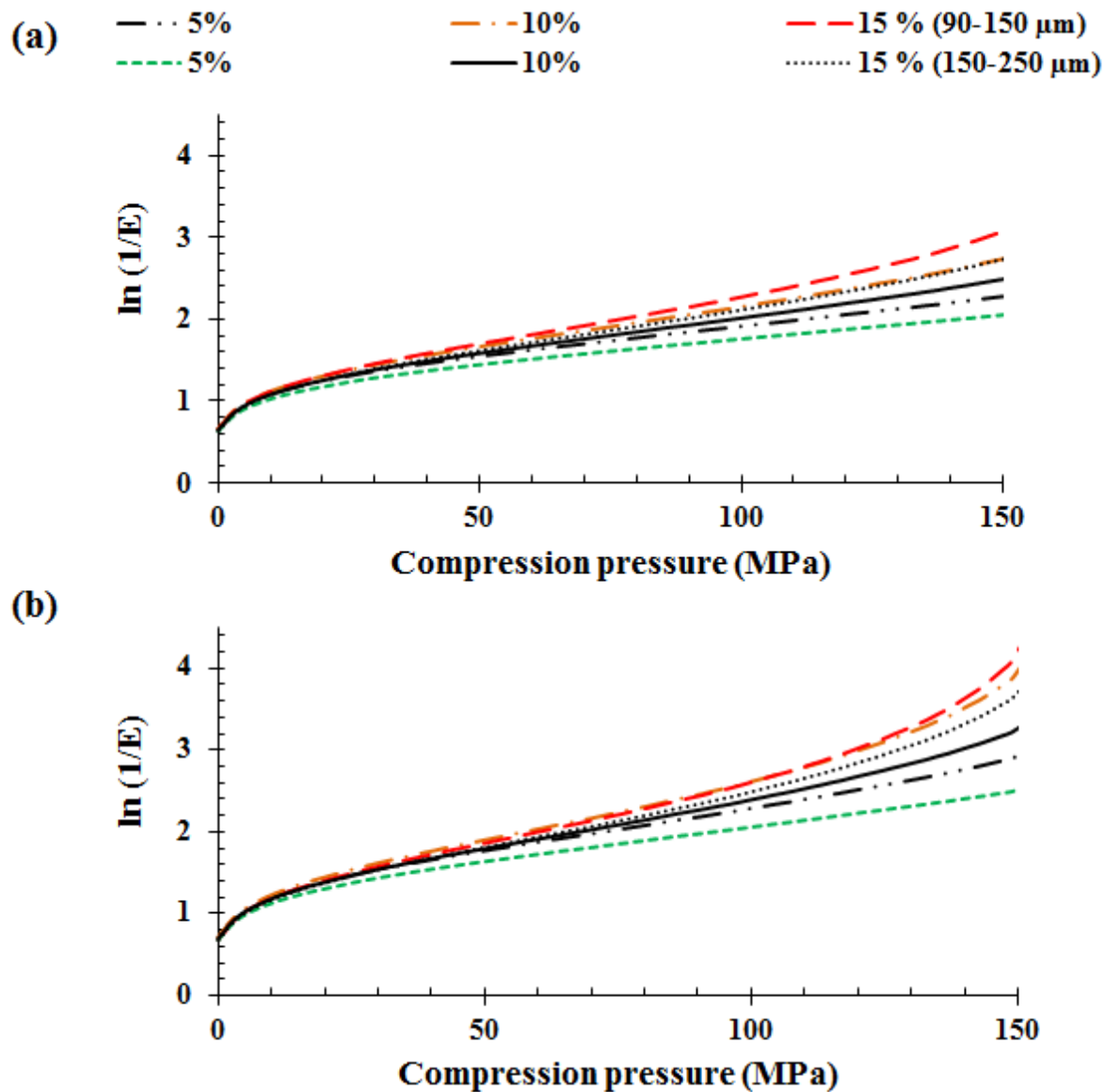


Figure 6.29, Heckel plots of matrices with respect to compression pressure (a) K4M : FBP and (b) K4M : THP (n = 3).

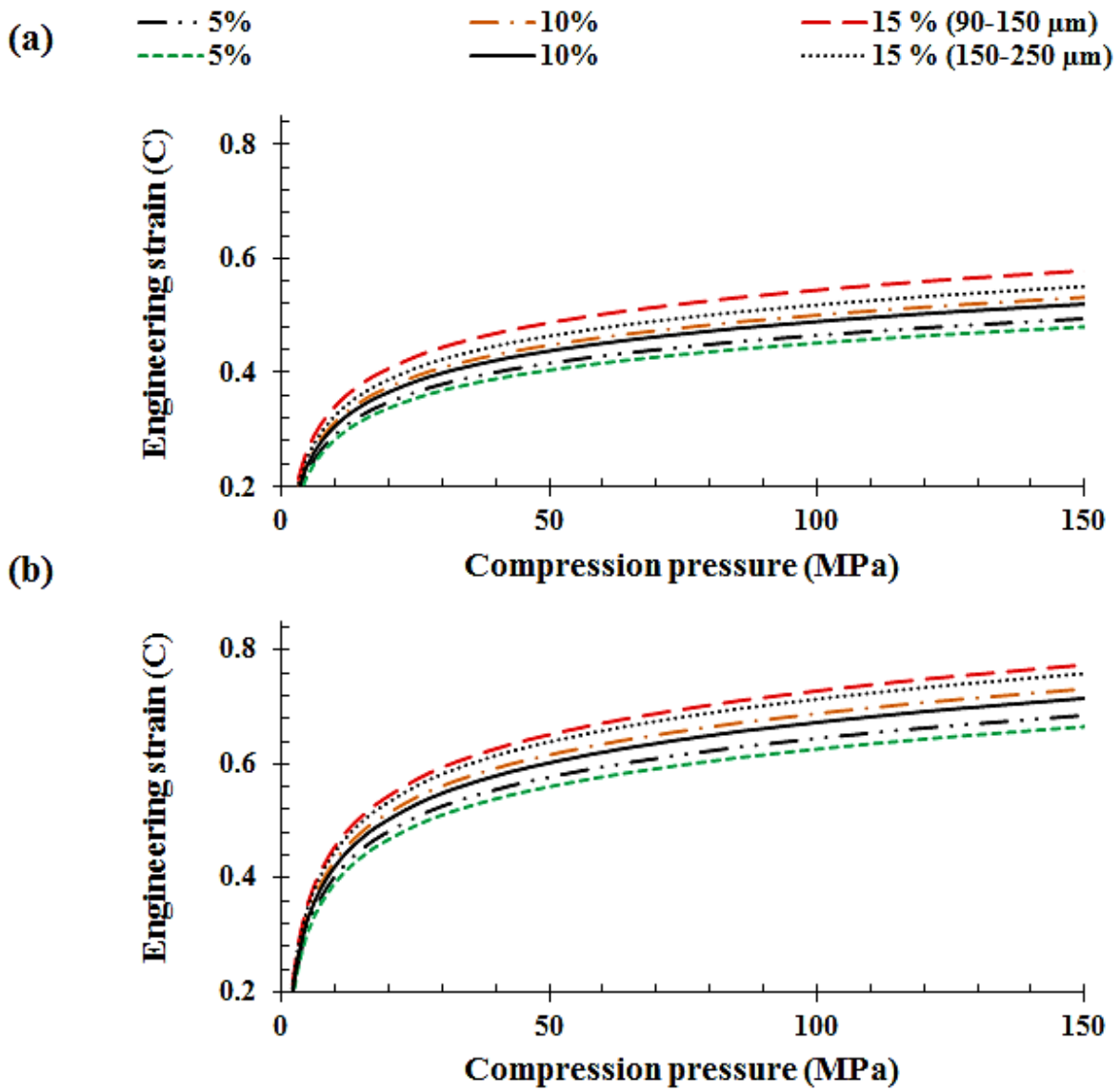


Figure 6.30, Kawakita plots of matrices with respect to compression pressure (a) K4M : FBP and (b) K4M : THP (n = 3).

Table 6.20, Summary of tensile strength and elastic recovery of K4M : FBP/THP matrices (n = 3, standard deviation given in parenthesis)

| K4M (%) | Particle size (μm) | Tensile strength (T, MPa) | | Elastic recovery (ER, %) | |
|---------|---------------------------------|---------------------------|-------------|--------------------------|-------------|
| | | FBP | THP | FBP | THP |
| 5 | 90-150 | 1.13 (0.06) | 2.54 (0.05) | 13.78 (0.21) | 7.43 (1.02) |
| | 150-250 | 0.99 (0.02) | 2.42 (0.02) | 14.96 (1.35) | 8.52 (1.55) |
| 10 | 90-150 | 1.17 (0.05) | 2.79 (0.01) | 12.76 (1.05) | 7.03 (0.66) |
| | 150-250 | 1.09 (0.09) | 2.72 (0.04) | 14.00 (0.33) | 7.73 (0.23) |
| 15 | 90-150 | 1.50 (0.03) | 3.13 (0.06) | 11.32 (1.55) | 5.84 (1.02) |
| | 150-250 | 1.28 (0.01) | 2.93 (0.07) | 12.08 (1.03) | 6.84 (0.39) |

Table 6.21, Summary of Heckel and Kawakita compressional parameters of K4M : FBP/THP matrices (n = 3).

| K4M (%) | Particle size (μm) | Heckel parameters | | | | | | Kawakita parameters | | | | | |
|---------|---------------------------------|-------------------|--------|-------|------|--------|-------|---------------------|----------|-------|-------|----------|-------|
| | | FBP | | | THP | | | FBP | | | THP | | |
| | | A | K | P_y | A | K | P_y | a | b^{-1} | ab | a | b^{-1} | ab |
| 5 | 90-150 | 0.73 | 0.0123 | 81.40 | 0.83 | 0.0113 | 88.30 | 0.495 | 11.37 | 0.044 | 0.686 | 7.70 | 0.089 |
| | 150-250 | 0.63 | 0.0127 | 78.95 | 0.79 | 0.0108 | 92.17 | 0.480 | 12.54 | 0.038 | 0.666 | 8.00 | 0.083 |
| 10 | 90-150 | 0.72 | 0.0130 | 75.62 | 0.76 | 0.0119 | 84.06 | 0.532 | 10.20 | 0.052 | 0.732 | 7.24 | 0.101 |
| | 150-250 | 0.59 | 0.0132 | 76.33 | 0.71 | 0.0116 | 86.13 | 0.520 | 11.44 | 0.046 | 0.716 | 7.60 | 0.094 |
| 15 | 90-150 | 0.70 | 0.0137 | 72.92 | 0.72 | 0.0122 | 82.44 | 0.579 | 9.32 | 0.062 | 0.775 | 6.24 | 0.124 |
| | 150-250 | 0.58 | 0.0144 | 69.54 | 0.69 | 0.0125 | 80.06 | 0.551 | 10.45 | 0.053 | 0.760 | 7.03 | 0.108 |

A and K = Heckel constants, P_y (MPa) = Yield pressure, a, b^{-1} (MPa) and ab = Kawakita constants

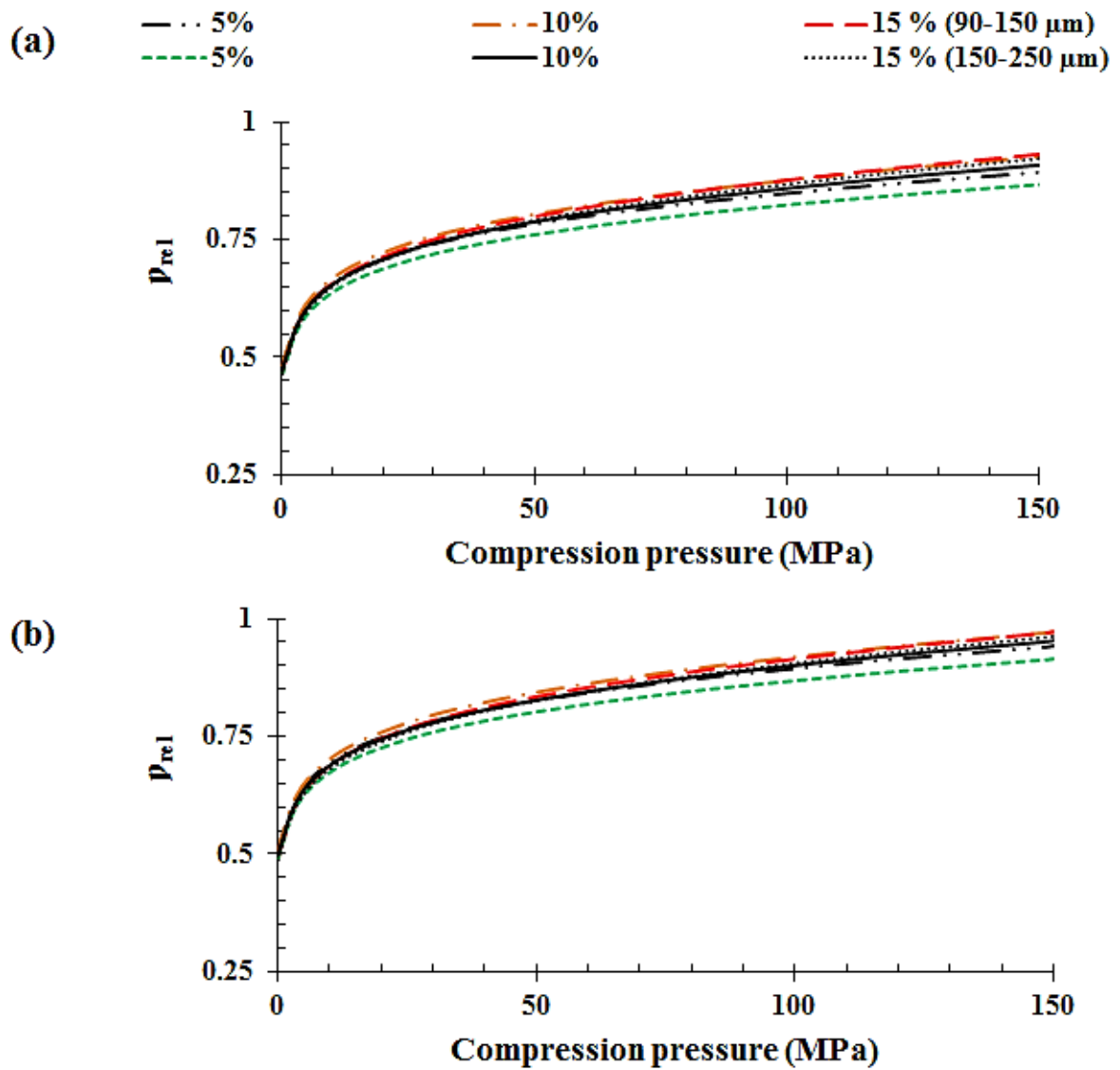


Figure 6.31, In-die relative density profiles of matrices with respect to compression pressure (a) K15M : FBP and (b) K15M : THP (n = 3).

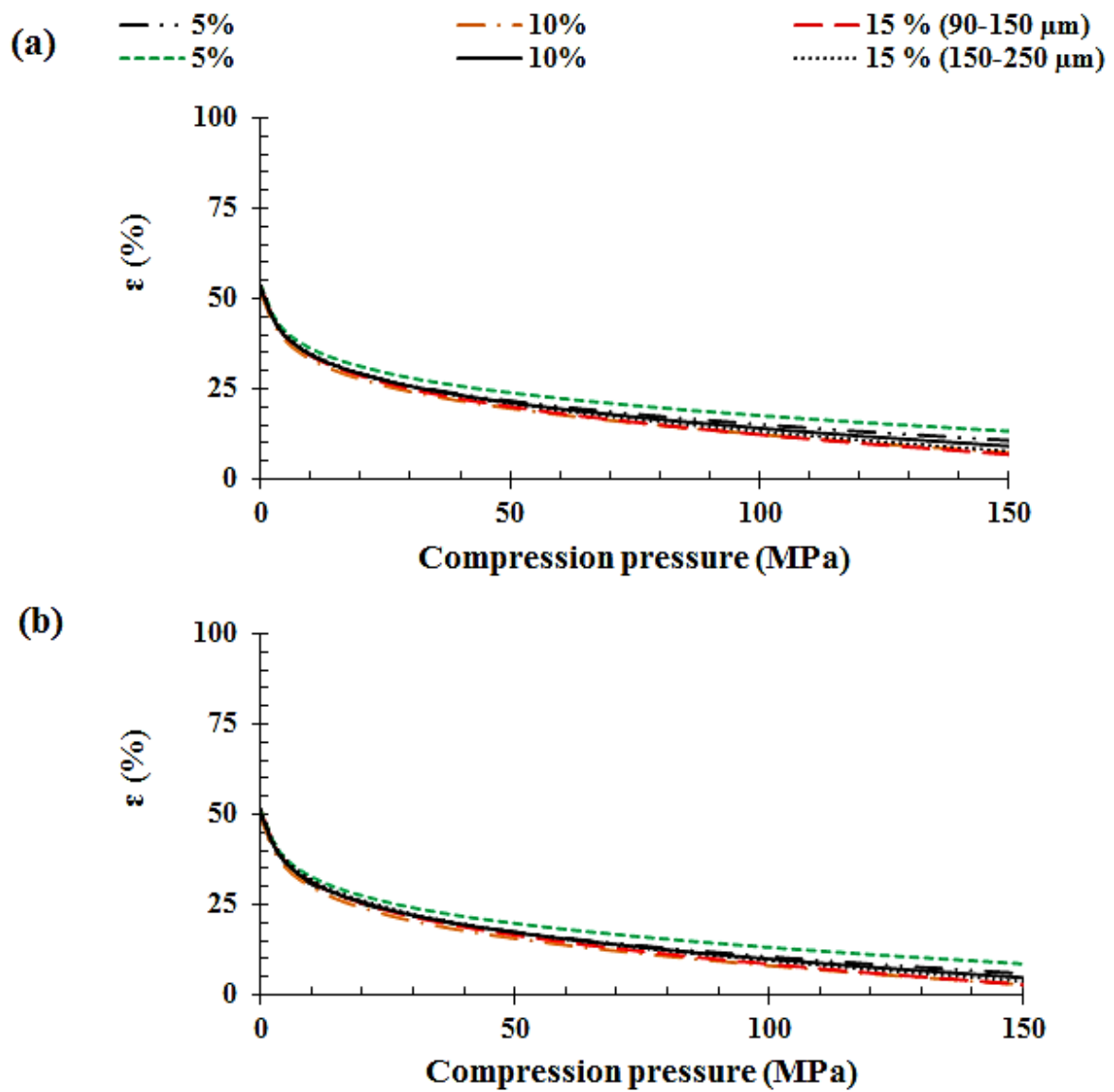


Figure 6.32, In-die porosity profiles of matrices with respect to compression pressure
 (a) K15M : FBP and (b) K15M : THP (n = 3).

Table 6.22, Summary of in-die and out-of -die relative density values of K15M : FBP/THP matrices (n = 3).

| K15M (%) | Particle size (µm) | True density (ρ _t , g cm ⁻³) | | Relative density (ρ _{rel}) | | | | Relative density (ρ _{rel}) | | | |
|----------|--------------------|---|-------|--------------------------------------|--------|----------------|-------|--------------------------------------|--------|----------------|-------|
| | | | | FBP | | | | THP | | | |
| | | | | In-die | | After ejection | | In-die | | After ejection | |
| | | | | Zero P | Max. P | 0 h | 24 h | Zero P | Max. P | 0 h | 24 h |
| 5 | 90-150 | 1.281 | 1.459 | 0.480 | 0.894 | 0.885 | 0.827 | 0.507 | 0.944 | 0.935 | 0.882 |
| | 150-250 | | | 0.466 | 0.868 | 0.859 | 0.803 | 0.492 | 0.916 | 0.907 | 0.856 |
| 10 | 90-150 | 1.283 | 1.452 | 0.483 | 0.927 | 0.918 | 0.858 | 0.508 | 0.974 | 0.964 | 0.910 |
| | 150-250 | | | 0.473 | 0.909 | 0.900 | 0.841 | 0.498 | 0.955 | 0.946 | 0.892 |
| 15 | 90-150 | 1.285 | 1.445 | 0.470 | 0.932 | 0.923 | 0.862 | 0.492 | 0.974 | 0.964 | 0.910 |
| | 150-250 | | | 0.465 | 0.923 | 0.914 | 0.854 | 0.487 | 0.964 | 0.954 | 0.900 |

Table 6.23, Summary of in-die and out-of -die porosity (%) values of K15M : FBP/THP matrices (n = 3).

| K15M (%) | Particle size (µm) | Porosity (ε, %) | | | | Porosity (ε, %) | | | |
|----------|--------------------|-----------------|--------|----------------|-------|-----------------|--------|----------------|-------|
| | | FBP | | | | THP | | | |
| | | In-die | | After ejection | | In-die | | After ejection | |
| | | Zero P | Max. P | 0 h | 24 h | Zero P | Max. P | 0 h | 24 h |
| 5 | 90-150 | 51.99 | 10.64 | 11.49 | 17.28 | 49.32 | 5.65 | 6.53 | 11.83 |
| | 150-250 | 53.39 | 13.24 | 14.06 | 19.68 | 50.79 | 8.39 | 9.31 | 14.44 |
| 10 | 90-150 | 51.73 | 7.28 | 8.22 | 14.22 | 49.23 | 2.63 | 3.56 | 9.02 |
| | 150-250 | 52.68 | 9.10 | 10.00 | 15.89 | 50.23 | 4.54 | 5.45 | 10.80 |
| 15 | 90-150 | 53.03 | 6.79 | 7.72 | 13.76 | 50.80 | 2.64 | 3.56 | 9.02 |
| | 150-250 | 53.49 | 7.71 | 8.61 | 14.59 | 51.29 | 3.61 | 4.55 | 9.96 |

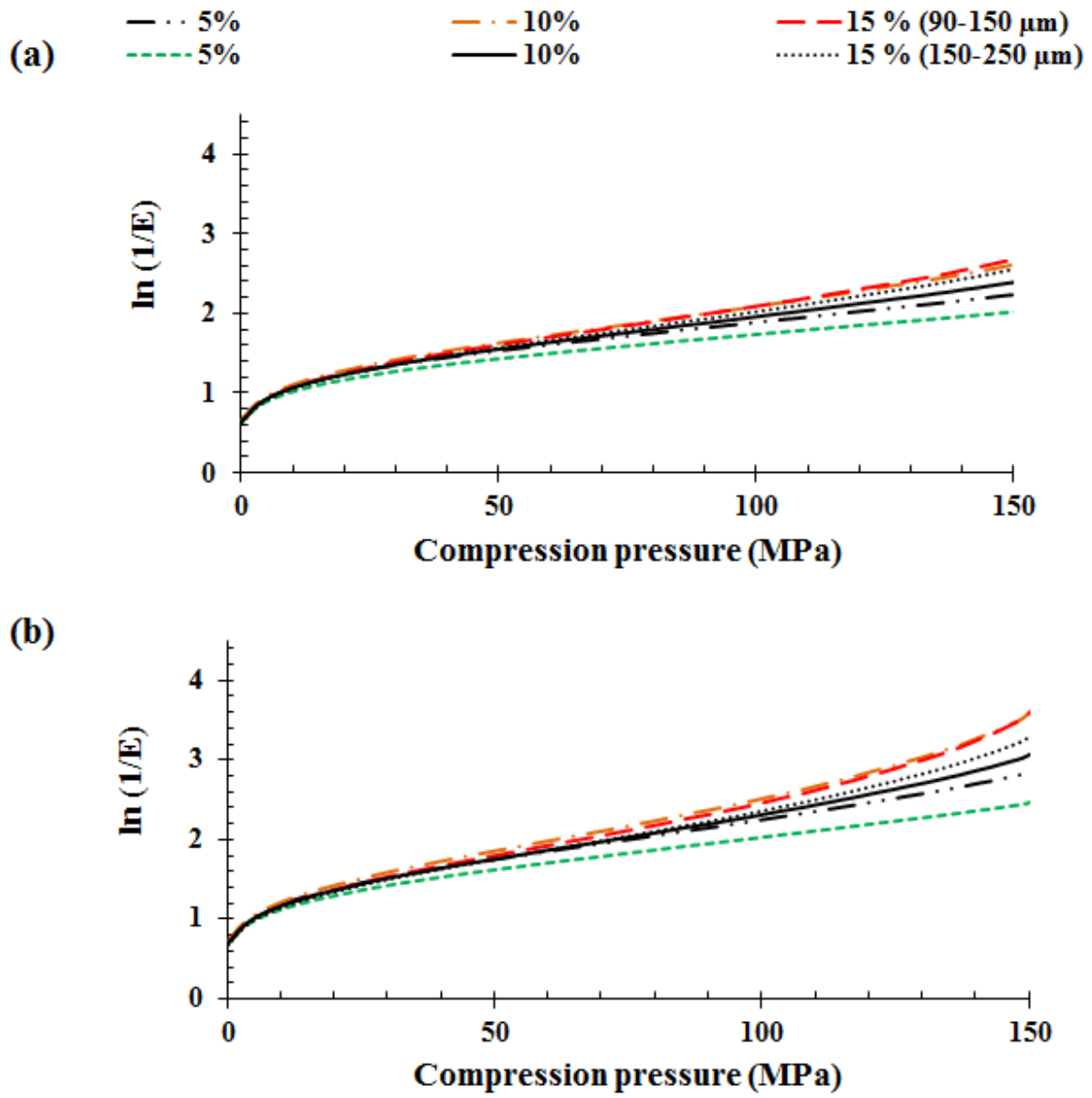


Figure 6.33, Heckel plots of matrices with respect to compression pressure (a) K15M : FBP and (b) K15M : THP (n = 3).

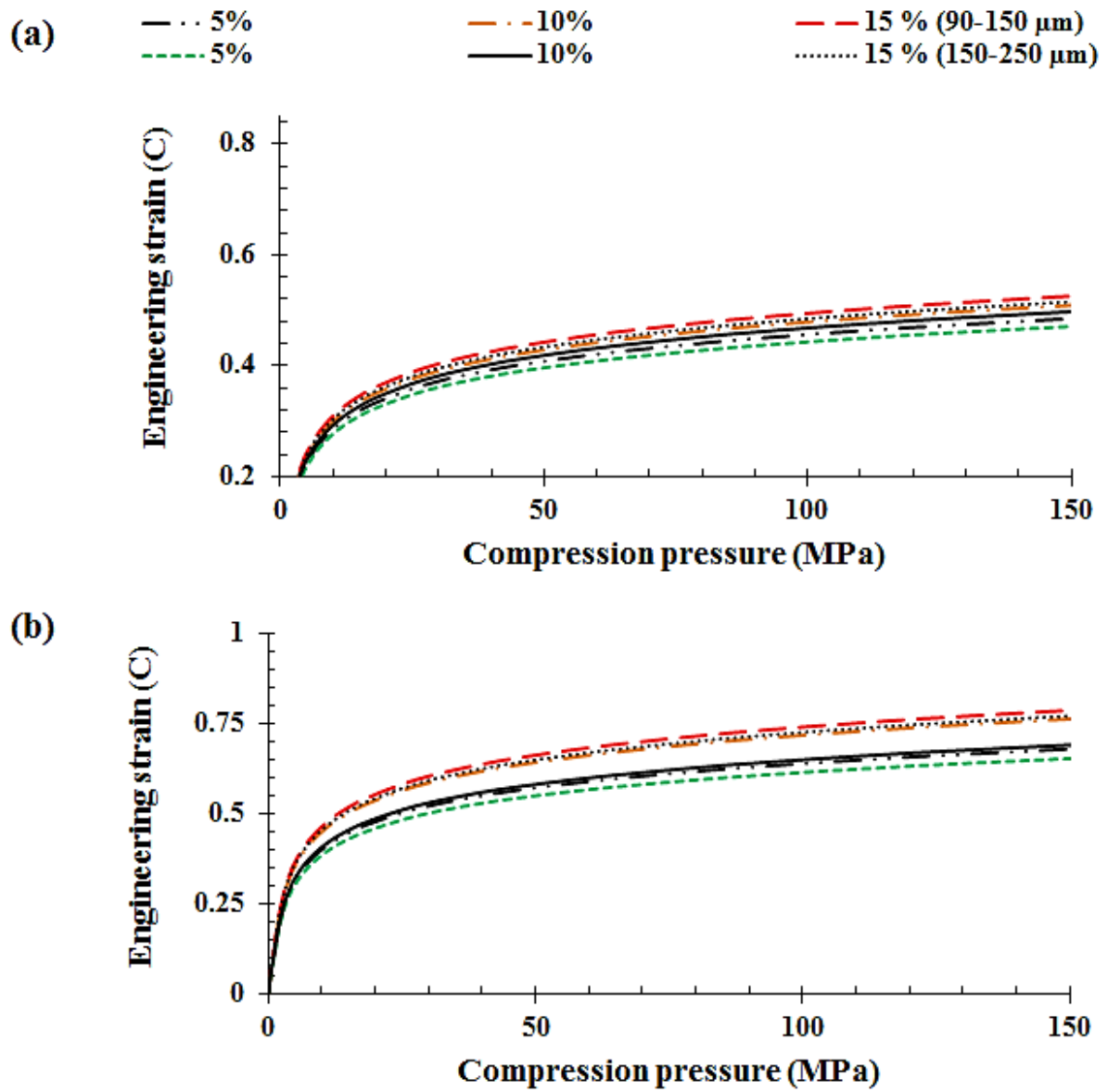


Figure 6.34, Kawakita plots of matrices with respect to compression pressure (a) K15M: FBP and (b) K15M : THP (n = 3).

Table 6.24, Summary of tensile strength and elastic recovery of K15M : FBP/THP matrices (n = 3, standard deviation given in parenthesis)

| K15M (%) | Particle size (μm) | Tensile strength (T, MPa) | | Elastic recovery (ER, %) | |
|----------|---------------------------------|---------------------------|-------------|--------------------------|-------------|
| | | FBP | THP | FBP | THP |
| 5 | 90-150 | 1.08 (0.05) | 2.47 (0.01) | 14.33 (0.94) | 7.65 (0.88) |
| | 150-250 | 0.95 (0.03) | 2.35 (0.06) | 15.56 (1.33) | 8.78 (0.52) |
| 10 | 90-150 | 1.13 (0.01) | 2.70 (0.04) | 13.27 (0.49) | 7.24 (1.10) |
| | 150-250 | 1.05 (0.06) | 2.64 (0.02) | 14.56 (1.55) | 7.96 (0.56) |
| 15 | 90-150 | 1.44 (0.09) | 3.04 (0.09) | 11.66 (2.12) | 6.02 (1.01) |
| | 150-250 | 1.23 (0.03) | 2.84 (0.08) | 12.56 (1.32) | 7.04 (0.55) |

Table 6.25, Summary of Heckel and Kawakita compressional parameters of K15M : FBP/THP matrices (n = 3).

| K15M (%) | Particle size (μm) | Heckel parameters | | | | | | Kawakita parameters | | | | | |
|----------|---------------------------------|-------------------|--------|-------|------|--------|-------|---------------------|----------|-------|-------|----------|-------|
| | | FBP | | | THP | | | FBP | | | THP | | |
| | | A | K | P_y | A | K | P_y | a | b^{-1} | ab | a | b^{-1} | ab |
| 5 | 90-150 | 0.70 | 0.0121 | 82.95 | 0.81 | 0.0112 | 89.18 | 0.486 | 11.82 | 0.041 | 0.680 | 7.86 | 0.087 |
| | 150-250 | 0.60 | 0.0124 | 80.45 | 0.77 | 0.0107 | 93.22 | 0.471 | 13.05 | 0.036 | 0.654 | 8.16 | 0.080 |
| 10 | 90-150 | 0.69 | 0.0127 | 78.68 | 0.74 | 0.0118 | 84.90 | 0.510 | 10.61 | 0.048 | 0.764 | 7.39 | 0.103 |
| | 150-250 | 0.57 | 0.0130 | 76.98 | 0.69 | 0.0115 | 86.99 | 0.498 | 11.89 | 0.042 | 0.691 | 7.75 | 0.089 |
| 15 | 90-150 | 0.67 | 0.0135 | 74.02 | 0.70 | 0.0121 | 82.91 | 0.526 | 9.69 | 0.054 | 0.788 | 6.37 | 0.124 |
| | 150-250 | 0.56 | 0.0141 | 70.55 | 0.67 | 0.0124 | 80.86 | 0.516 | 10.87 | 0.047 | 0.772 | 7.17 | 0.108 |

A and K = Heckel constants , P_y (MPa) = Yield pressure, a, b^{-1} (MPa) and ab = Kawakita constants

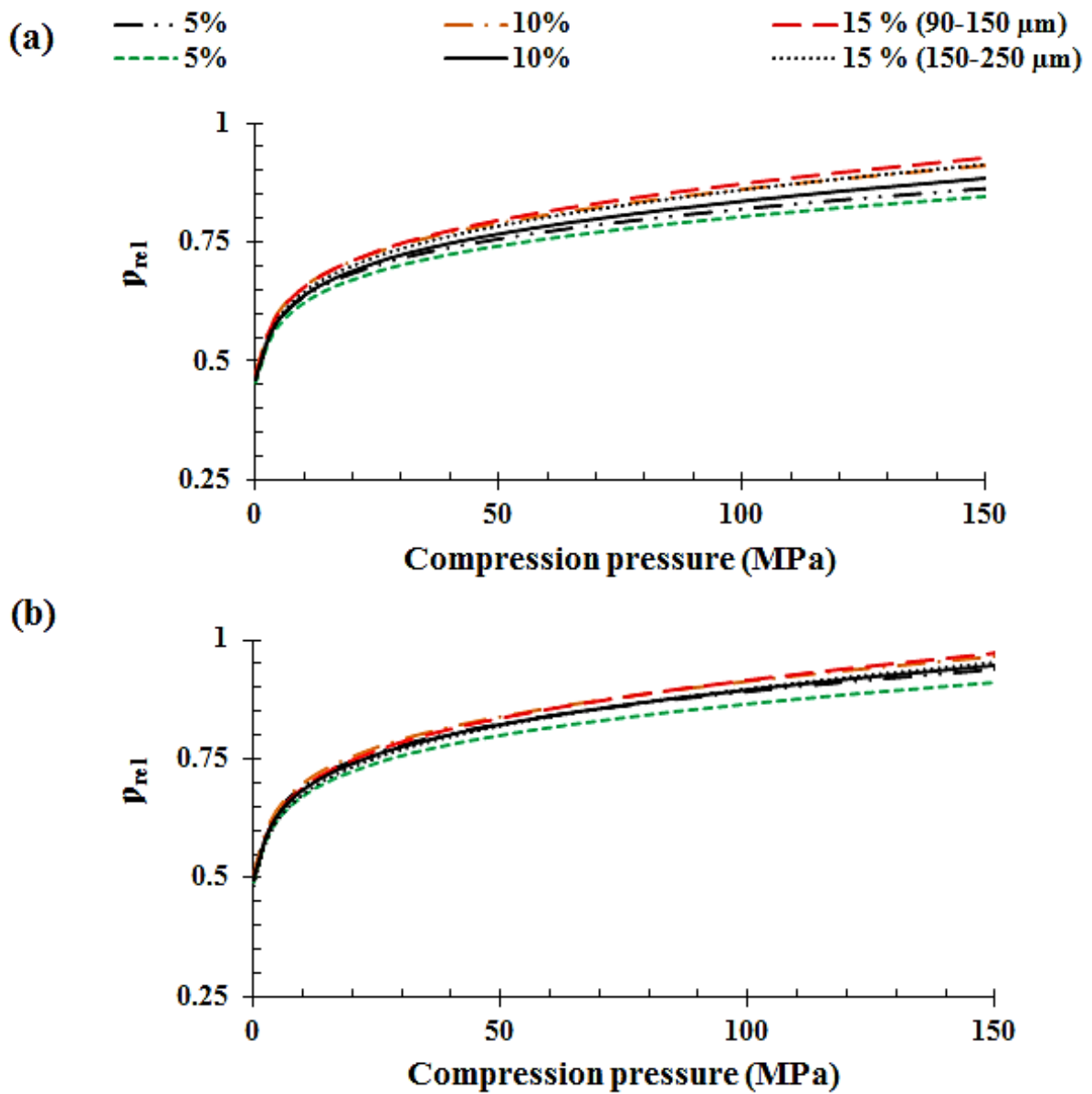


Figure 6.35, In-die relative density plots of matrices with respect to compression pressure (a) K100M : FBP and (b) K100M : THP (n = 3).

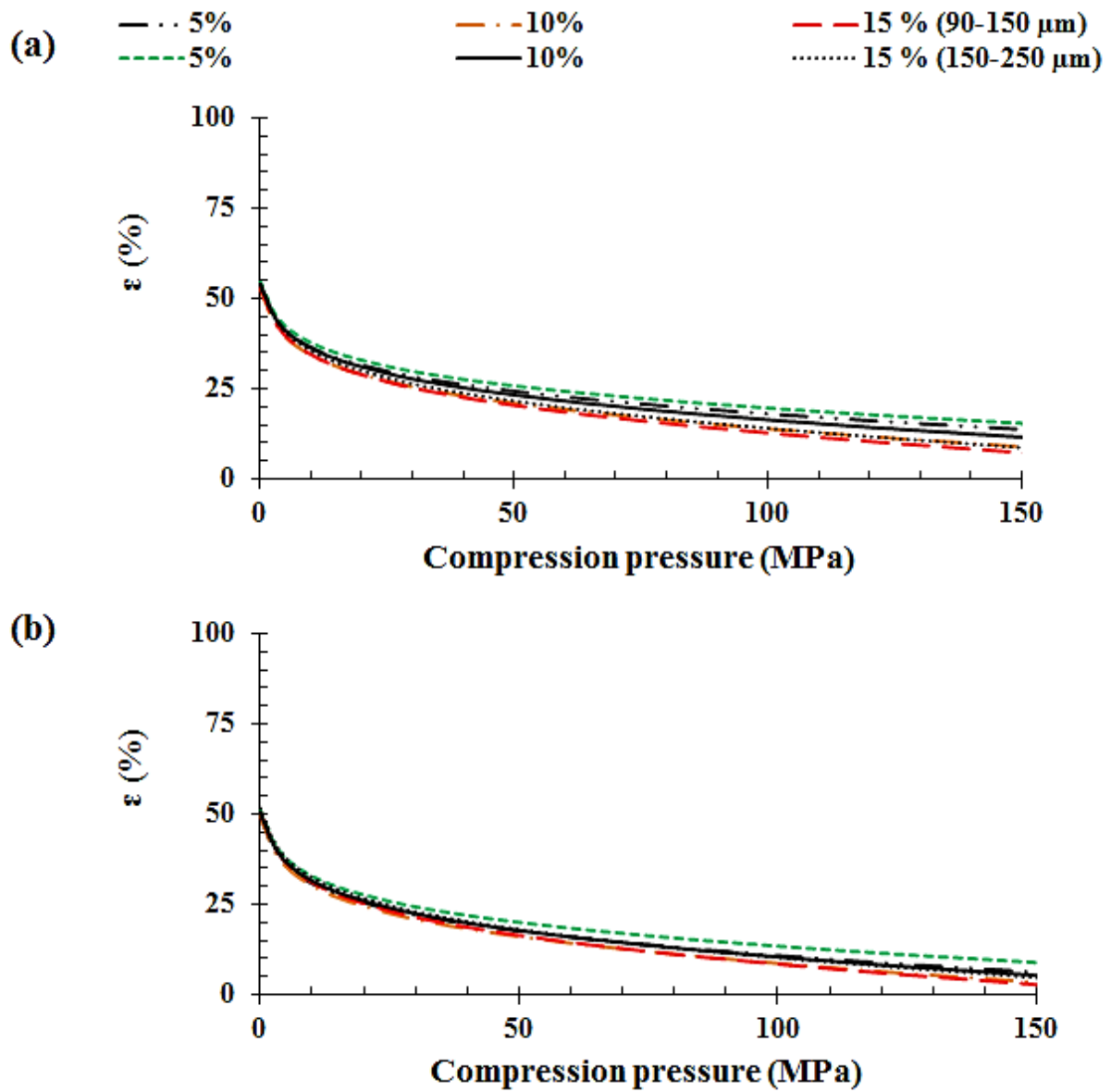


Figure 6.36, In-die porosity plots of matrices with respect to compression pressure (a) K100M : FBP and (b) K100M : THP (n = 3).

Table 6.26, Summary of in-die and out-of -die relative density values of K100M : FBP/THP matrices (n = 3).

| K100M (%) | Particle size (μm) | True density (ρ _t , g cm ⁻³) | | Relative density (ρ _{rel}) | | | | Relative density (ρ _{rel}) | | | |
|-----------|--------------------|---|-------|--------------------------------------|--------|----------------|-------|--------------------------------------|--------|----------------|-------|
| | | | | FBP | | | | THP | | | |
| | | | | In-die | | After ejection | | In-die | | After ejection | |
| | | | | Zero P | Max. P | 0 h | 24 h | Zero P | Max. P | 0 h | 24 h |
| 5 | 90-150 | 1.283 | 1.461 | 0.464 | 0.863 | 0.854 | 0.799 | 0.506 | 0.941 | 0.932 | 0.879 |
| | 150-250 | | | 0.455 | 0.846 | 0.838 | 0.783 | 0.491 | 0.913 | 0.904 | 0.853 |
| 10 | 90-150 | 1.288 | 1.457 | 0.475 | 0.911 | 0.902 | 0.843 | 0.505 | 0.968 | 0.958 | 0.904 |
| | 150-250 | | | 0.461 | 0.885 | 0.876 | 0.819 | 0.496 | 0.949 | 0.940 | 0.886 |
| 15 | 90-150 | 1.293 | 1.452 | 0.469 | 0.928 | 0.919 | 0.859 | 0.494 | 0.974 | 0.964 | 0.910 |
| | 150-250 | | | 0.462 | 0.914 | 0.905 | 0.846 | 0.484 | 0.955 | 0.946 | 0.892 |

Table 6.27, Summary of in-die and out-of -die porosity (%) values of K100M : FBP/THP matrices (n = 3).

| K100M (%) | Particle size (μm) | Porosity (ε, %) | | | | Porosity (ε, %) | | | |
|-----------|--------------------|-----------------|--------|----------------|--------|-----------------|--------|----------------|--------|
| | | FBP | | | | THP | | | |
| | | In-die | | After ejection | | In-die | | After ejection | |
| | | Zero P | Max. P | 0 hr. | 24 hr. | Zero P | Max. P | 0 hr. | 24 hr. |
| 5 | 90-150 | 53.61 | 13.67 | 14.55 | 20.14 | 49.43 | 5.95 | 6.83 | 12.11 |
| | 150-250 | 54.52 | 15.37 | 16.24 | 21.72 | 50.90 | 8.69 | 9.60 | 14.72 |
| 10 | 90-150 | 52.53 | 8.86 | 9.80 | 15.70 | 49.46 | 3.22 | 4.16 | 9.58 |
| | 150-250 | 53.92 | 11.52 | 12.38 | 18.11 | 50.45 | 5.12 | 6.04 | 11.36 |
| 15 | 90-150 | 53.13 | 7.21 | 8.12 | 14.13 | 50.64 | 2.56 | 3.56 | 9.02 |
| | 150-250 | 53.82 | 8.59 | 9.50 | 15.43 | 51.61 | 4.47 | 5.45 | 10.80 |

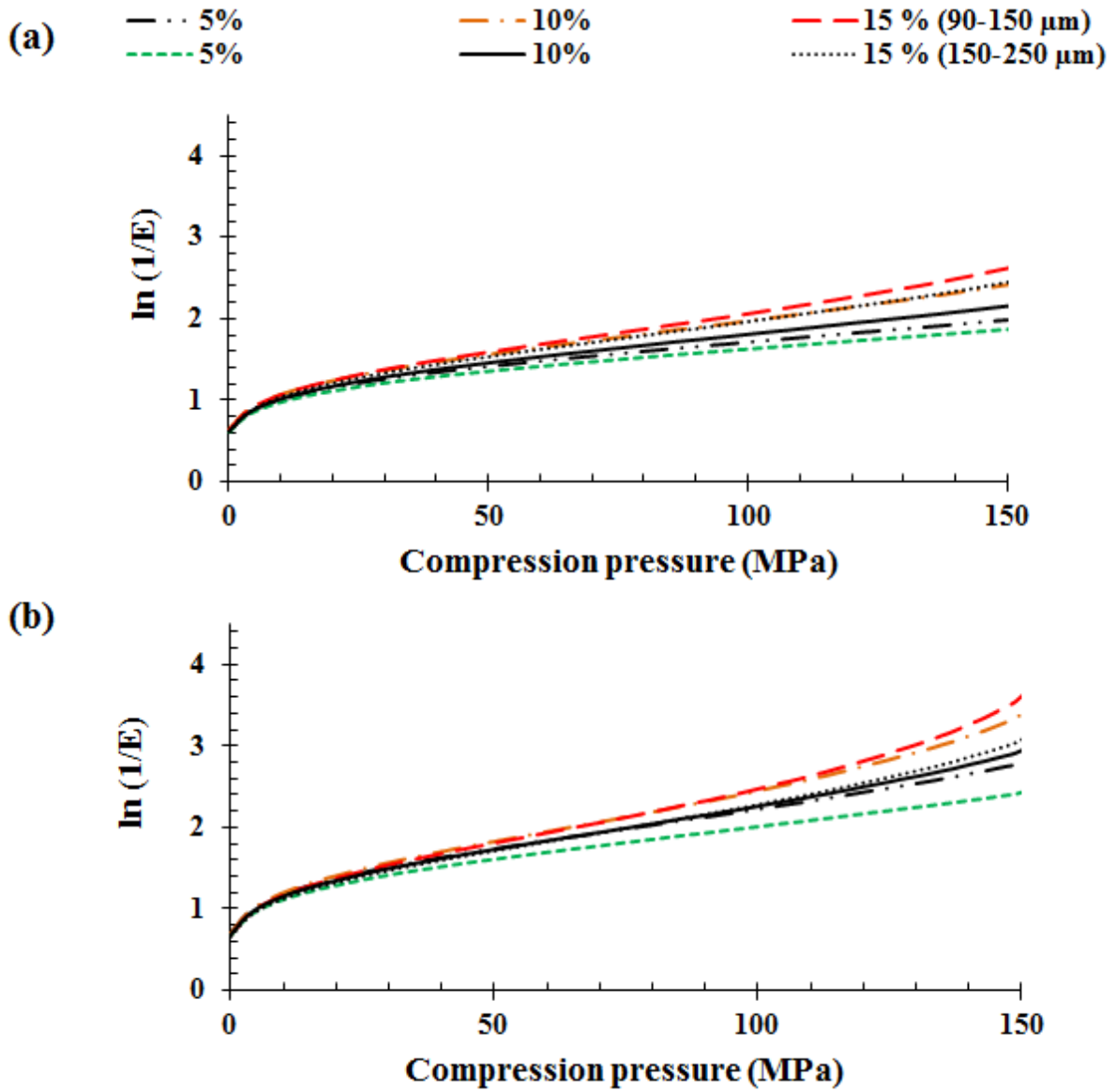


Figure 6.37, Heckel plots of matrices with respect to compression pressure (a) K100M : FBP and (b) K100M : THP (n = 3).

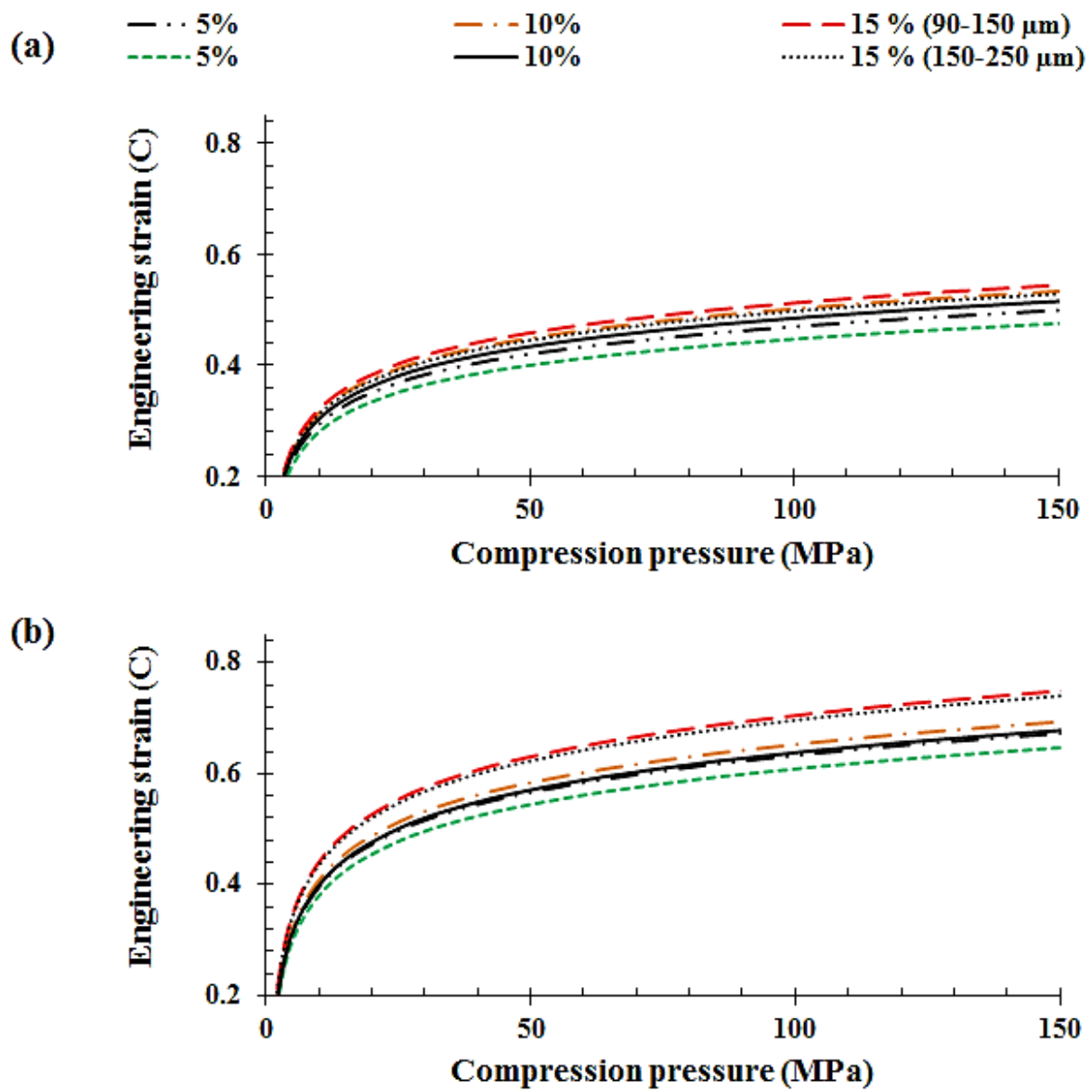


Figure 6.38, Kawakita plots of matrices with respect to compression pressure (a) K100M : FBP and (b) K100M : THP (n = 3).

Table 6.28, Summary of tensile strength and elastic recovery of K100M : FBP/THP matrices (n = 3, standard deviation given in parenthesis)

| K100M (%) | Particle size (µm) | Tensile strength (T, MPa) | | Elastic recovery (ER, %) | |
|-----------|--------------------|---------------------------|-------------|--------------------------|-------------|
| | | FBP | THP | FBP | THP |
| 5 | 90-150 | 1.01 (0.01) | 2.33 (0.02) | 14.61 (1.12) | 8.11(1.07) |
| | 150-250 | 0.88 (0.03) | 2.21 (0.09) | 15.87 (1.30) | 9.30 (1.21) |
| 10 | 90-150 | 1.09 (0.01) | 2.55 (0.02) | 13.53 (0.56) | 7.68 (1.06) |
| | 150-250 | 0.97 (0.06) | 2.49 (0.05) | 14.85 (2.15) | 8.44 (1.12) |
| 15 | 90-150 | 1.33 (0.02) | 2.87 (0.03) | 11.68 (1.06) | 6.38 (0.55) |
| | 150-250 | 1.18 (0.01) | 2.68 (0.07) | 12.82 (0.91) | 7.46 (0.67) |

Table 6.29, Summary of Heckel and Kawakita compressional parameters K100M : FBP/THP matrices (n = 3).

| K100M (%) | Particle size (µm) | Heckel parameters | | | | | | Kawakita parameters | | | | | |
|-----------|--------------------|-------------------|--------|-------|------|--------|-------|---------------------|----------|-------|-------|----------|-------|
| | | FBP | | | THP | | | FBP | | | THP | | |
| | | A | K | P_y | A | K | P_y | a | b^{-1} | ab | a | b^{-1} | ab |
| 5 | 90-150 | 0.65 | 0.0118 | 84.25 | 0.76 | 0.0111 | 90.08 | 0.500 | 12.30 | 0.041 | 0.673 | 8.09 | 0.083 |
| | 150-250 | 0.56 | 0.0122 | 82.51 | 0.73 | 0.0106 | 94.03 | 0.476 | 13.57 | 0.035 | 0.648 | 8.40 | 0.077 |
| 10 | 90-150 | 0.64 | 0.0125 | 80.25 | 0.70 | 0.0117 | 85.75 | 0.534 | 11.04 | 0.048 | 0.694 | 7.61 | 0.091 |
| | 150-250 | 0.53 | 0.0127 | 78.52 | 0.65 | 0.0114 | 87.86 | 0.516 | 12.37 | 0.042 | 0.679 | 7.98 | 0.085 |
| 15 | 90-150 | 0.62 | 0.0132 | 75.79 | 0.66 | 0.0119 | 83.74 | 0.545 | 10.08 | 0.054 | 0.750 | 6.56 | 0.114 |
| | 150-250 | 0.52 | 0.0138 | 72.28 | 0.63 | 0.0122 | 81.67 | 0.529 | 11.30 | 0.047 | 0.741 | 7.38 | 0.100 |

A and K = Heckel constants, P_y (MPa) = Yield pressure, a, b^{-1} (MPa) and ab = Kawakita constants

6.9.3.4- Inter-relationship between P_y and b^{-1}

Figures 4.39 (FBP : MC/HPMC) and 4.40 (THP : MC/HPMC) show the correlation between the derived plasticity parameters of Heckel and Kawakita compression models. There is a reasonable correlation between the parameters, as predicted, as both are inversely related to the propensity of powder particle deformation during compression pressure. The correlation coefficient (R^2) values of FBP based matrices were in the range of 0.912 – 0.992 (90 - 150 μm) and 0.913 – 0.974 (150 – 250 μm). However, the R^2 of THP based matrices was in the range of 0.721 – 0.879 (90 - 150 μm) and 0.974 – 0.999 (150 – 250 μm), Table 6.30.

There is unanimous agreement in literature that the Heckel and Kawakita models are the compression equations considered most important (Çelik, 2011; Denny, 2002). It can be inferred from the present finding that, if pressure dependant parameters are derived from Heckel equation, the results are very similar to the generalised Kawakita equation.

Table 6.30, Correlation co-efficients of P_y and b^{-1} inter-relationship (n = 3).

| Type of matrix tablet | Correlation co-efficient (R^2) | |
|-----------------------|---------------------------------------|--|
| | Particle size (90-150 μm) | Particle size (150-250 μm) |
| A4M/FBP | 0.912 | 0.963 |
| F4M/FBP | 0.992 | 0.964 |
| E4M/FBP | 0.974 | 0.913 |
| K4M/FBP | 0.984 | 0.923 |
| K15M/FBP | 0.989 | 0.957 |
| K100MFBP | 0.988 | 0.974 |
| A4M/THP | 0.834 | 0.989 |
| F4M/THP | 0.835 | 0.990 |
| E4M/THP | 0.879 | 0.999 |
| K4M/THP | 0.800 | 0.974 |
| K15M/THP | 0.721 | 0.988 |
| K100M/THP | 0.833 | 0.989 |

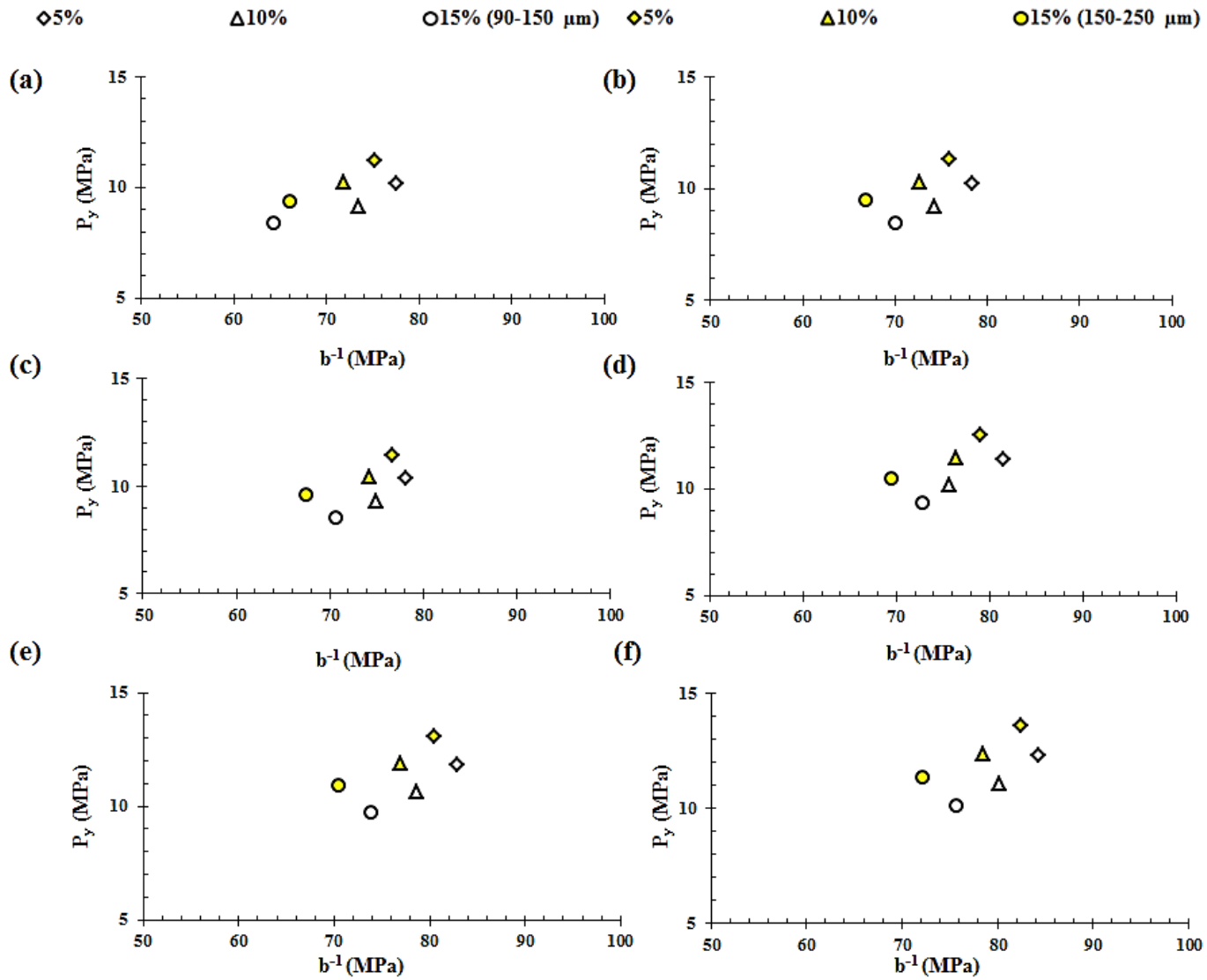


Figure 6.39, Relationship between P_y and b^{-1} of FBP based matrices, (a) A4M, (b) F4M, (c) E4M, (d) K4M, (e) K15M AND (f) K100M.

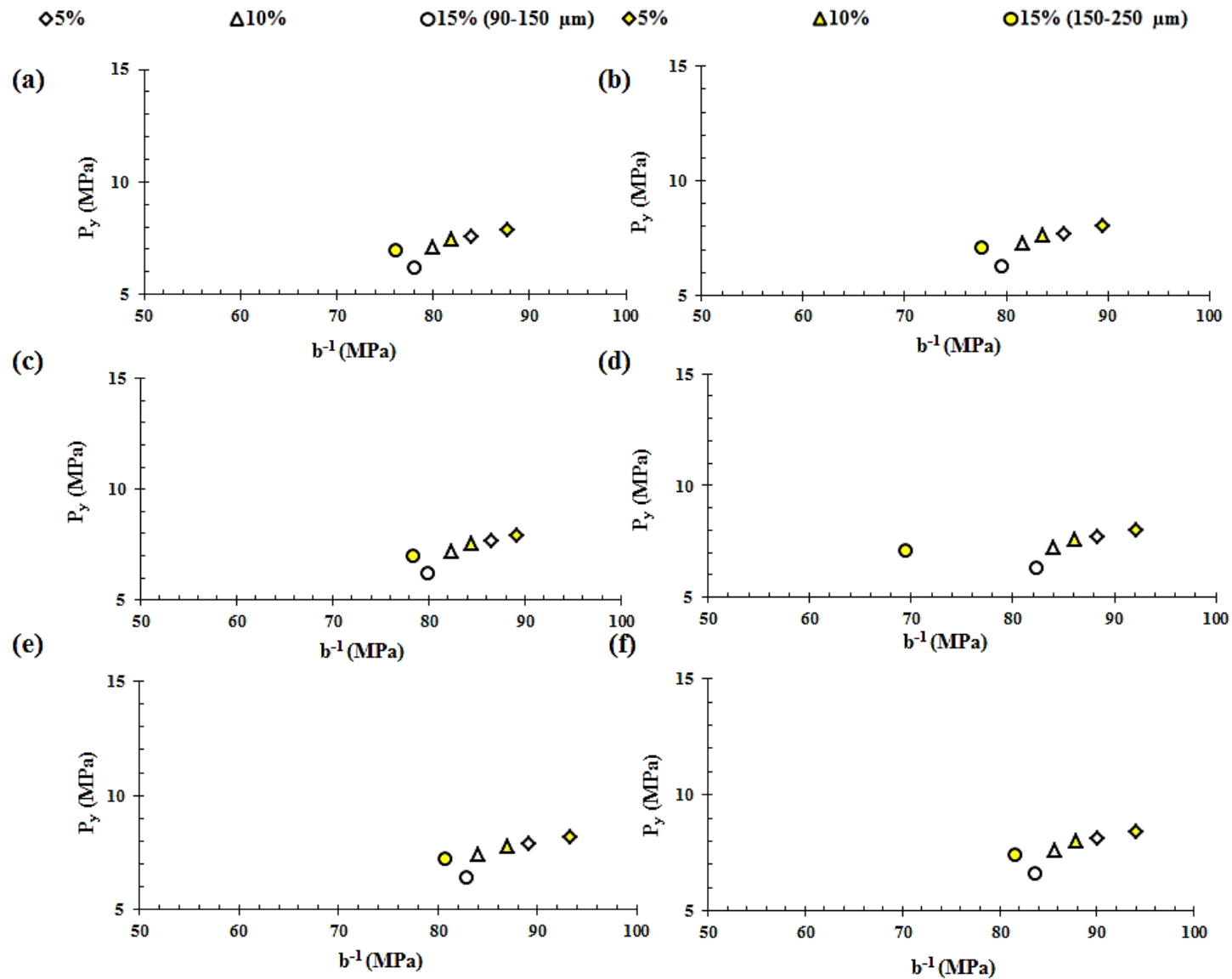


Figure 6.40, Relationship between P_y and b^{-1} of THP based matrices, (a) A4M, (b) F4M, (c) E4M, (d) K4M, (e) K15M AND (f) K100M.

6.9- Summary

In summary, the current study confirmed that the FBP has poor compaction properties, with a low ability to develop inter-particulate bonding during the compression process. However, THP had relatively good compaction properties.

The particle size, substitution ratios and viscosity (molecular size) of Methocel[®] affect the compaction and consolidation behaviour of plain MC/HPMC compacts. It can also be concluded all the MC/HPMC powders deform plastically and have non-significant particle rearrangement during compression phases.

Regarding FBP and THP based matrices, it can be concluded that the concentration of MC/HPMC (5 – 15 % w/w) has a noticeable positive effect on the compaction properties of FBP and THP. Moreover, it can be concluded that the physico-chemical attributes like particle size, chemistry and molecular size, of MC and HPMC significantly influence the densification and consolidation process of hydrophilic matrices. The fine particle size fractions and increase in total substitution levels tends to increase matrix relative density, but a causes a reduction in the porosity, P_y , b^{-1} and elastic relaxation. Furthermore, these properties have the potential to modify relative density, porosity and tortuosity of the matrix network within a tablet which can further impact the drug release mechanism. The information extracted from the current study can be used in the future to develop and adopt strategies for development and further optimization of compressed hydrophilic matrices.

Chapter 7

Conclusions and future work

7- Conclusions and future work

7.1- Conclusions

The main goals of this thesis were to contribute to the field of electrostatics, powder compaction and drug release kinetics from hydrophilic matrices. To understand the governing mechanisms various physical parameters were determined which can be utilised to improve the functionality and performance of pharmaceutical formulation development. Moreover, the objectives of this thesis, as stated in chapter 1 (section 1.6) were successfully achieved and summarised in the following sub-sections.

7.1.1- Electrostatic and adhesion studies of powder mixtures

Chapter 3 discussed the tribo-electrification and adhesion studies of model drugs, MC/HPMC and their binary mixtures. It can be confirmed that both drugs charged negatively, with the electrostatic behaviour of FBP and THP categorised as highly charging and low charging materials, respectively, when compared to other APIs and pharmaceutical excipients. It can be inferred that the MC and HPMC powder particles charged positively, moreover, the physico-chemical properties associated with MC and HPMC, such as particle size, chemical heterogeneity and molecular size of cellulose ethers all have a significant impact on charging and adhesion behaviour. It can also be concluded that the concentration, particle size, chemical heterogeneity and molecular size of MC/HPMC all significantly impact the charging and SA propensity of FBP and THP. The decrease in SA and charge dissipation for FBP and THP powder mixtures is intuitively expected to improve flowability and compaction, which is expected to have a positive effect on the finished pharmaceutical dosage forms.

7.1.2- Swelling, erosion and dissolution studies

Chapter 4 explored the swelling, erosion and dissolution properties of FBP and THP hydrophilic matrices. The present study confirmed that the particle size, substitution ratios

and viscosity of Methocel[®] affect the swelling and erosion of plain MC/HPMC matrices. Moreover, results also confirmed that the physico-chemical attributes (concentration, particle size, substitution and viscosity) of MC/HPMC and drug solubility have a significant impact on the extent of swelling, erosion, mechanism of erosion, dissolution rate and drug release kinetics.

The swelling and dissolution results confirm that the extent of swelling, swelling rate, swelling exponent, dissolution rate and drug release kinetic parameters were affected by physico-chemical attributes (concentration, particle size, substitution and viscosity) of MC/HPMC and drug solubility. The mechanism of swelling and drug release is largely considered to be anomalous. However, it inclined towards more diffusion-oriented swelling/drug release with higher MC/HPMC levels, viscosity, Hpo/Meo substitution ratios, drug solubility but smaller MC/MC particle size.

7.1.3- Development and validation of PSA assay for erosion analysis

In Chapter 5, a Phenol-sulphuric acid (PSA) assay was applied to study polymer erosion. The assay was successfully applied to study polymer erosion kinetics from MC/HPMC compacts with varied physico-chemical properties. It can be concluded that particle size, substitution ratios and viscosity (molecular size) of MC and HPMC significantly influence erosion kinetics parameters.

The matrix erosion results obtained from newly adopted PSA method confirmed that the solubility of the drug, and levels of HPMC in a particular matrix tablet, significantly affect the matrix erosion rate and the results were similar to those determined using the much more labour-intensive gravimetric method. Moreover, the combination of conventional UV drug analysis technique and PSA assay can be used to simultaneously quantify the matrix

erosion, polymer dissolution and drug release kinetics in a single set of experiments avoiding the need for separate studies.

7.1.4- Compaction studies

Chapter 6 discussed the compaction properties of model drugs, plain MC/HPMC and their respective powder mixtures. It can be confirmed that the FBP has poor compaction properties and with a low propensity to develop inter-particulate bonding during the compression process. However, THP had relatively good compaction properties. The particle size, substitution ratios and viscosity (molecular size) of Methocel[®] affect the compaction and consolidation behaviour of plain MC/HPMC compacts. Furthermore, it can be concluded that the concentration and physico-chemical attributes (particle size, chemistry and molecular size) of MC/HPMC have a significant influence on the densification and consolidation process of hydrophilic matrices. The information extracted from the current study can be used in the future to develop and adopt strategies for development and further optimization of compressed hydrophilic matrices.

7.2- Future work

There are many areas of potential opportunities to expand this work, including;

7.2.1- Tribo-electrification

Tribo-electrification is an area of research which is still considered elusive. To better understand the electrostatic behaviour of powders during processing, a dynamic tribo-electric charging apparatus attached to UV-photoelectron spectroscopy, having the power to quantify the propensity of work function alongside the electrostatic charging, can be developed. Moreover, the present work has confirmed that the physico-chemical attributes of pharmaceutical materials have significant impact on the electrostatic and adhesion behaviour of final powder mixtures. Therefore, the present studies can be further expand to investigate how the experimental factors (mixing speed, type of mixer, type of contacting surface, the charging induction techniques, humidity and temperature) on the electrostatic and adhesion properties of pharmaceutical powder.

7.2.2- Swelling, erosion and drug release kinetics

The present work has open up potential options to explore the mechanism of swelling, matrix erosion and drug release by using different imaging techniques, especially atomic force microscopy (AFM) and X-ray micro-tomography (X- μ T).

7.2.2- Applications of PSA assay

The PSA assay technique gives a unique opportunity to study drug release alongside polymer erosion. In the future, potential studies can be carried out to investigate its validity of more complex formulation systems.

7.2.2- Powder compaction studies

This study has demonstrated the option to simultaneously study various compaction parameters in a single study with the utilisation of a minimum amount of powder. In future, a potential opportunity can be carried out to determine Youngs' modulus, alongside these derived physical parameters of compaction. It has been noticed that deformation and fragmentation have a marked effect on the tablet characteristics. Potentially AFM and X- μ T may be utilised in future to quantify any change in the surface morphology of powder particles. Moreover, there is a continuous debate regarding the validity of the compaction modelling equation, so considering these; attempts can be made to modify the Heckel and Kawakita equations.

In summary, the information given in this thesis can be used to improve different processing stages of pharmaceutical product development. However, there is far more that could be conducted to fully explore the areas of electrostatics, drug release kinetics and powder compaction.

8- References

References

- ADAMS, M., MULLIER, M. & SEVILLE, J. 1994. Agglomerate strength measurement using a uniaxial confined compression test. *Powder Technology*, 78, 5-13.
- ADOLFSSON, Å., CARAMELLA, C. & NYSTRÖM, C. 1998. The effect of milling and addition of dry binder on the interparticulate bonding mechanisms in sodium chloride tablets. *International Journal of Pharmaceutics*, 160, 187-195.
- ADOLFSSON, Å., GUSTAFSSON, C. & NYSTRÖM, C. 1999. Use of tablet tensile strength adjusted for surface area and mean interparticulate distance to evaluate dominating bonding mechanisms. *Drug Development and Industrial Pharmacy*, 25, 753-764.
- ADOLFSSON, Å. & NYSTRÖM, C. 1996. Tablet strength, porosity, elasticity and solid state structure of tablets compressed at high loads. *International Journal of Pharmaceutics*, 132, 95-106.
- ADOLFSSON, Å., OLSSON, H. & NYSTRÖM, C. 1997. Effect of particle size and compaction load on interparticulate bonding structure for some pharmaceutical materials studied by compaction and strength characterisation in butanol. *European Journal of Pharmaceutics and Biopharmaceutics*, 44, 243-251.
- AHLNECK, C. & ALDERBORN, G. 1989. Moisture adsorption and tableting. II. The effect on tensile strength and air permeability of the relative humidity during storage of tablets of 3 crystalline materials. *International Journal of Pharmaceutics*, 56, 143-150.
- AKANDE, A. & ADEDOYIN, J. 2001. Correlation of charge transfer in metal/polymer contact with contact potential. *Journal of Electrostatics*, 51, 105-110.
- ALBALASMEH, A. A., BERHE, A. A. & GHEZZEHEI, T. A. 2013. A new method for rapid determination of carbohydrate and total carbon concentrations using UV spectrophotometry. *Carbohydrate Polymers*, 97, 253-261.
- ALDERBORN, G. & NYSTROM, C. 1995. *Pharmaceutical Powder Compaction Technology*, Taylor & Francis.
- ALDERMAN, D. A. 1984. A review of cellulose ethers in hydrophilic matrices for oral controlled-release dosage forms. *International Journal of Pharmaceutical Technology and Product Manufacture*, 5, 1-9.
- ARFKEN, G. B. 1984. *University Physics*, Academic Press.
- ARMSTRONG, N. A. & HAINES-NUTT, R. F. 1972. Elastic recovery and surface area changes in compacted powder systems. *Journal of Pharmacy and Pharmacology*, 24, Suppl:135P-136.

- ASARE-ADDO, K., CONWAY, B. R., LARHRIB, H., LEVINA, M., RAJABI-SIAHBOOMI, A. R., TETTEH, J., BOATENG, J. & NOKHODCHI, A. 2013a. The effect of pH and ionic strength of dissolution media on in-vitro release of two model drugs of different solubilities from HPMC matrices. *Colloids and Surfaces B: Biointerfaces*, 111, 384-391.
- ASARE-ADDO, K., KAIALY, W., LEVINA, M., RAJABI-SIAHBOOMI, A., GHORI, M. U., SUPUK, E., LAITY, P. R., CONWAY, B. R. & NOKHODCHI, A. 2013b. The influence of agitation sequence and ionic strength on in vitro drug release from hypromellose (E4M and K4M) ER matrices-The use of the USP III apparatus. *Colloids and Surfaces B: Biointerfaces*, 104, 54-60.
- ATKINSON, A. J., HUANG, S. M., LERTORA, J. J. L. & MARKEY, S. P. 2012. *Principles of Clinical Pharmacology*, Elsevier Science.
- AUGUST, J. T., ANDERS, W., MURAD, F. & COYLE, J. T. 1996. *Advances in Pharmacology*, Elsevier Science.
- BAILEY, A. 1984. Electrostatic phenomena during powder handling. *Powder Technology*, 37, 71-85.
- BAILEY, A. 1993. Charging of solids and powders. *Journal of Electrostatics*, 30, 167-180.
- BAILEY, A. G. & SMEDLEY, C. J. A. 1991. The impact charging of polymer particles. *Advanced Powder Technology*, 2, 277-284.
- BANKER, G., PECK, G., JA, S., PIRAKITIKULR, P. & TAYLOR, D. 1981. Evaluation of hydroxypropyl cellulose and hydroxypropyl methyl cellulose as aqueous based film coatings. *Drug Development and Industrial Pharmacy*, 7, 693-716.
- BAVEJA, S., RANGA RAO, K. & PADMALATHA DEVI, K. 1987. Zero-order release hydrophilic matrix tablets of β -adrenergic blockers. *International Journal of Pharmaceutics*, 39, 39-45.
- BAYTEKIN, H. T., BAYTEKIN, B., HERMANS, T. M., KOWALCZYK, B. & GRZYBOWSKI, B. A. 2013. Control of Surface Charges by Radicals as a Principle of Antistatic Polymers Protecting Electronic Circuitry. *Science*, 341, 1368-1371.
- BENNETT, F. 1998. Electrostatic charge phenomena in powder processes for dry powder inhalers. *Ph.D. Thesis, University of Sunderland*
- BENNETT, F. S., CARTER, P. A., ROWLEY, G. & DANDIKER, Y. 1999. Modification of electrostatic charge on inhaled carrier lactose particles by addition of fine particles. *Drug Development and Industrial Pharmacy*, 25, 99-103.
- BENNETT, P. N., BROWN, M. J. & SHARMA, P. 2012. *Clinical Pharmacology*, Elsevier Health Sciences UK.
- BETTINI, R., CATELLANI, P. L., SANTI, P., MASSIMO, G., PEPPAS, N. A. & COLOMBO, P. 2001. Translocation of drug particles in HPMC matrix gel layer:

- Effect of drug solubility and influence on release rate. *Journal of Controlled Release*, 70, 383-391.
- BNF 2014. *British National Formulary (BNF) 67*, Pharmaceutical Press.
- BOLHUIS, G. & CHOWHAN, Z. 1996. v knize: *Pharmaceutical Powder Compaction Technology* (Alderborn G., Nyström Ch., ed.), kap. 14. *Marcel Dekker Inc., New York*, 20-40.
- BOSCHUNG, P. & GLOR, M. 1980. Methods for investigating the electrostatic behaviour of powders. *Journal of Electrostatics*, 8, 205-219.
- BP 2012. *British Pharmacopoeia Commission.*, London, England, Stationery Office.
- BRITAIN, H. G. 2007. *Profiles of Drug Substances, Excipients and Related Methodology: Critical Compilation of pKa Values for Pharmaceutical Substances*, Elsevier Science.
- CADET, F. 1999. Measurement of sugar content by multidimensional analysis and mid-infrared spectroscopy. *Talanta*, 48, 867-875.
- CAMPOS-ALDRETE, M. E. & VILLAFUERTE-ROBLES, L. 1997. Influence of the viscosity grade and the particle size of HPMC on metronidazole release from matrix tablets. *European Journal of Pharmaceutics and Biopharmaceutics*, 43, 173-178.
- CARABALLO, I. 2010. Factors affecting drug release from hydroxypropyl methylcellulose matrix systems in the light of classical and percolation theories. *Expert Opinion on Drug Delivery*, 7, 1291-1301.
- CARTER, P., ROWLEY, G., FLETCHER, E. & HILL, E. 1992. An experimental investigation of triboelectrification in cohesive and non-cohesive pharmaceutical powders. *Drug Development and Industrial Pharmacy*, 18, 1505-1526.
- CARTER, P. A., CASSIDY, O. E., ROWLEY, G. & MERRIFIELD, D. R. 1998a. Triboelectrification of fractionated crystalline and spray-dried lactose. *Pharmacy and Pharmacology Communications*, 4, 111-115.
- CARTER, P. A., ROWLEY, G., ROUGHLEY, N. & SUGGETT, J. 1998b. Electrostatic charge accumulation and decay in pharmaceutical polymer materials used in metered dose inhalers. *Journal of Pharmacy and Pharmacology*, 50, 55.
- CASSIDY, O. E., CARTER, P. A., ROWLEY, G. & MERRIFIELD, D. R. 2000. Triboelectrification of Spray-dried Lactose Prepared from Different Feedstock Concentrations. *Journal of Pharmacy and Pharmacology*, 52, 13-17.
- CASTLE, G. 1997. Contact charging between insulators. *Journal of Electrostatics*, 40, 13-20.
- ÇELİK, M. 2011. *Pharmaceutical Powder Compaction Technology, Second Edition*, Taylor & Francis.
- CHAIBVA, F. A., KHAMANGA, S. M. M. & WALKER, R. B. 2010. Swelling, erosion and drug release characteristics of salbutamol sulfate from hydroxypropyl

- methylcellulose-based matrix tablets. *Drug Development and Industrial Pharmacy*, 36, 1497-1510.
- CHANG, J. S., KELLY, A. J. & CROWLEY, J. M. 1995. *Handbook of Electrostatic Processes*, Taylor & Francis.
- CHOWHAN, Z. T. 1980. Role of binders in moisture-induced hardness increase in compressed tablets and its effect on in vitro disintegration and dissolution. *Journal of Pharmaceutical Sciences*, 69, 1.
- COFFIN-BEACH, D. P. & GARY HOLLENBECK, R. 1983. Determination of the energy of tablet formation during compression of selected pharmaceutical powders. *International Journal of Pharmaceutics*, 17, 313-324.
- COLOMBO, P., BETTINI, R. & PEPPAS, N. A. 1999. Observation of swelling process and diffusion front position during swelling in hydroxypropyl methyl cellulose (HPMC) matrices containing a soluble drug. *Journal of Controlled Release*, 61, 83-91.
- COLOMBO, P., BETTINI, R., SANTI, P. & PEPPAS, N. A. 2000. Swellable matrices for controlled drug delivery: gel-layer behaviour, mechanisms and optimal performance. *Pharmaceutical Science & Technology Today*, 3, 198-204.
- CONTE, U. & MAGGI, L. 1996. Modulation of the dissolution profiles from Geomatrix sup® multi-layer matrix tablets containing drugs of different solubility. *Biomaterials*, 17, 889-896.
- CONTI, S., MAGGI, L., SEGALE, L., OCHOA MACHISTE, E., CONTE, U., GRENIER, P. & VERGNAULT, G. 2007. Matrices containing NaCMC and HPMC. 2. Swelling and release mechanism study. *International Journal of Pharmaceutics*, 333, 143-151.
- CORTACERO-RAMÍREZ, S., SEGURA-CARRETERO, A., CRUCES-BLANCO, C., HERNÁNDEZ-BERMÚDEZ DE CASTRO, M. & FERNÁNDEZ-GUTIÉRREZ, A. 2004. Analysis of carbohydrates in beverages by capillary electrophoresis with precolumn derivatization and UV detection. *Food Chemistry*, 87, 471-476.
- COSTA, P. & SOUSA LOBO, J. M. 2001. Modeling and comparison of dissolution profiles. *European Journal of Pharmaceutical Sciences*, 13, 123-133.
- COSTE, J. & PECHERY, P. 1981. Influence of surface profile in polymer-metal contact charging. *Journal of Electrostatics*, 10, 129-136.
- CRAIG, C. R. & STITZEL, R. E. 2004. *Modern Pharmacology with Clinical Applications*, Lippincott Williams & Wilkins.
- CRAVER, C. & CARRAHER, C. 2000. *Applied Polymer Science: 21st Century: 21st Century*, Elsevier Science.
- CROSS, J. 1987a. *Electrostatics: Principles, Problems and Applications*, Adam Hilger.

- CROSS, J. A. 1987b. *Electrostatics: Principles, Problems and Applications*. IOP Publishing Limited.
- CROSS, J. A., MUMFORD-VAN URK, H. & SINGH, S. 1981. Some experiments in powder charging and its significance to industrial processes. *Journal of Electrostatics*, 10, 235.
- CROUTER, A. & BRIENS, L. 2014. The Effect of Moisture on the Flowability of Pharmaceutical Excipients. *AAPS PharmSciTech*, 15, 65-74.
- CUNNINGHAM, S. & GOODINGS, A. 1986. Plastic deformation and the transfer of electrostatic charge between metals and polymers during repeated-contact experiments. *Journal of Electrostatics*, 18, 103-108.
- DABBAGH, M. A., FORD, J. L., RUBINSTEIN, M. H. & HOGAN, J. E. 1996. Effects of polymer particle size, compaction pressure and hydrophilic polymers on drug release from matrices containing ethylcellulose. *International Journal of Pharmaceutics*, 140, 85-95.
- DALY, P., DAVIS, S. & KEIMERLEY, J. 1984. The effect of anionic surfactants on the release of chlorpheniramine from a polymer matrix tablet. *International Journal of Pharmaceutics*, 18, 201-205.
- DASH, A., SINGH, S. & TOLMAN, J. 2013. *Pharmaceutics: Basic Principles and Application to Pharmacy Practice*, Elsevier Science.
- DAVIES, D. 1969. Charge generation on dielectric surfaces. *Journal of Physics D: Applied Physics*, 2, 1533.
- DENNY, P. 2002. Compaction equations: a comparison of the Heckel and Kawakita equations. *Powder Technology*, 127, 162-172.
- DHOPESHWARKER, V. & ZATZ, J. L. 1993. Evaluation of xanthan gum in the preparation of sustained release matrix tablets. *Drug Development and Industrial Pharmacy*, 19, 999-1017.
- DOELKER, E. 1990. Swelling behavior of water-soluble cellulose derivatives. *Absorbent Polymer Technology, Amsterdam*, 125-146.
- DOW 2006. *The dow chemical company, Using Dow Excipients for Controlled Release of Drugs in Hydrophilic Matrix Systems, 2006*.
- DUBERG, M. & NYSTRÖM, C. 1981. Studies on direct compression of tablets. VI. Evaluation of methods for the estimation of particle fragmentation during compaction. *Acta Pharmaceutica Suecica*, 19, 421-436.
- DUBOIS, M., GILLES, K. A., HAMILTON, J. K., REBERS, P. A. & SMITH, F. 1956. Colorimetric method for determination of sugars and related substances. *Analytical Chemistry*, 28, 350-356.

- DUFF, N. & LACKS, D. J. 2008. Particle dynamics simulations of triboelectric charging in granular insulator systems. *Journal of Electrostatics*, 66, 51-57.
- EBUBE, N. K., HIKAL, A. H., WYANDT, C. M., BEER, D. C., MILLER, L. G. & JONES, A. B. 1997. Sustained release of acetaminophen from heterogeneous matrix tablets: Influence of polymer ratio, polymer loading, and co-active on drug release. *Pharmaceutical Development and Technology*, 2, 161-170.
- EHRHARDT, C. & KIM, K. J. 2007. *Drug Absorption Studies: In Situ, In Vitro and In Silico Models*, Springer.
- EILBECK, J., ROWLEY, G., CARTER, P. & FLETCHER, E. 1999a. Effect of Materials of Construction of Pharmaceutical Processing Equipment and Drug Delivery Devices on the Triboelectrification of Size-fractionated Lactose. *Pharmacy and Pharmacology Communications*, 5, 429-433.
- EILBECK, J., ROWLEY, G., CARTER, P. & FLETCHER, E. 2000. Effect of contamination of pharmaceutical equipment on powder triboelectrification. *International Journal of Pharmaceutics*, 195, 7-11.
- EILBECK, J., ROWLEY, G., CARTER, P. A. & FLETCHER, E. J. 1999b. Effect of materials of construction of pharmaceutical processing equipment and drug delivery devices on the triboelectrification of size-fractionated lactose. *Pharmacy and Pharmacology Communications*, 5, 429-433.
- ELAJNAF, A., CARTER, P. & ROWLEY, G. 2006. Electrostatic characterisation of inhaled powders: Effect of contact surface and relative humidity. *European Journal of Pharmaceutical Sciences*, 29, 375-384.
- ELAJNAF, A., CARTER, P. & ROWLEY, G. 2007. The effect of relative humidity on electrostatic charge decay of drugs and excipient used in dry powder inhaler formulation. *Drug Development and Industrial Pharmacy*, 33, 967-974.
- ELSDON, R. & MITCHELL, F. 1976. Contact electrification of polymers. *Journal of Physics D: Applied Physics*, 9, 1445.
- EMBUSCADO, M. E. 2014. *Functionalizing Carbohydrates for Food Applications: Texturizing and Bioactive/Flavor Delivery Systems*, DEStech Publications, Incorporated.
- ENGERS, D. A., FRICKE, M. N., STOREY, R. P., NEWMAN, A. W. & MORRIS, K. R. 2006. Triboelectrification of pharmaceutically relevant powders during low-shear tumble blending. *Journal of Electrostatics*, 64, 826-835.
- ENTWISTLE, C. & ROWE, R. 1979. Plasticization of cellulose ethers used in the film coating of tablets. *Journal of Pharmacy and Pharmacology*, 31, 269-272.
- ESCUDERO, J., FERRERO, C. & JIMÉNEZ-CASTELLANOS, M. 2010. Compaction properties, drug release kinetics and fronts movement studies from matrices combining mixtures of swellable and inert polymers. II. Effect of HPMC with

- different degrees of methoxy/hydroxypropyl substitution. *International Journal of Pharmaceutics*, 387, 56-64.
- ESCUADERO, J. J., FERRERO, C., CASAS, M. & JIMÉNEZ-CASTELLANOS, M. R. 2012. Compaction properties, drug release kinetics and fronts movement studies of matrices combining mixtures of swellable and inert polymers. III: Effect of polymer substitution type. *International Journal of Pharmaceutics*, 434, 215-223.
- ESCUADERO, J. J., FERRERO, C. & JIMÉNEZ-CASTELLANOS, M. R. 2008. Compaction properties, drug release kinetics and fronts movement studies from matrices combining mixtures of swellable and inert polymers: Effect of HPMC of different viscosity grades. *International Journal of Pharmaceutics*, 351, 61-73.
- ESEZOBO, S. 1989. Disintegrants: effects of interacting variables on the tensile strengths and dissolution times of sulfaguanidine tablets. *International Journal of Pharmaceutics*, 56, 207.
- FASSO, L., CHAO, B. T. & SOO, S. 1982. Measurement of electrostatic charges and concentration of particles in the freeboard of a fluidized bed. *Powder Technology*, 33, 211-221.
- FELL, J. T. & NEWTON, J. M. 1970. Determination of tablet strength by the diametral-compression test. *Journal of Pharmaceutical Sciences*, 59, 688-691.
- FELLER, R. L. & WILT, M. H. 1991. *Evaluation of Cellulose Ethers for Conservation*, Getty Conservation Institute.
- FERRERO, C., MASSUELLE, D. & DOELKER, E. 2010. Towards elucidation of the drug release mechanism from compressed hydrophilic matrices made of cellulose ethers. II. Evaluation of a possible swelling-controlled drug release mechanism using dimensionless analysis. *Journal of Controlled Release*, 141, 223-233.
- FLORENCE, A. T. & ATTWOOD, D. 2011. *Physicochemical Principles of Pharmacy*, Pharmaceutical Press.
- FORD, J. L., RUBINSTEIN, M. H., CHANGELA, A. & HOGAN, J. E. 1985a. Influence of pH on the dissolution of promethazine hydrochloride from hydroxypropylmethylcellulose controlled release tablets. *Journal of Pharmacy and Pharmacology*, 37, 115P-115P.
- FORD, J. L., RUBINSTEIN, M. H. & HOGAN, J. E. 1985b. Formulation of sustained release promethazine hydrochloride tablets using hydroxypropyl-methylcellulose matrices. *International Journal of Pharmaceutics*, 24, 327-338.
- FORD, J. L., RUBINSTEIN, M. H., MCCAUL, F., HOGAN, J. E. & EDGAR, P. J. 1987. Importance of drug type, tablet shape and added diluents on drug release kinetics from hydroxypropylmethylcellulose matrix tablets. *International Journal of Pharmaceutics*, 40, 223-234.

- FRENNING, G., MAHMOODI, F., NORDSTRÖM, J. & ALDERBORN, G. 2009. An effective-medium analysis of confined compression of granular materials. *Powder Technology*, 194, 228-232.
- FÜHRER, C. 1977. Substance behaviour in direct compression. *Labo-Pharma Probi. Techn*, 25, 759-762.
- FUKUI, E., MIYAMURA, N., UEMURA, K. & KOBAYASHI, M. 2000. Preparation of enteric coated timed-release press-coated tablets and evaluation of their function by in vitro and in vivo tests for colon targeting. *International Journal of Pharmaceutics*, 204, 7-15.
- GAISFORD, S. & SAUNDERS, M. 2012. *Essentials of Pharmaceutical Preformulation*, Wiley.
- GALLO, C. & LAMA, W. 1976. Some charge exchange phenomena explained by a classical model of the work function. *Journal of Electrostatics*, 2, 145-150.
- GAO, P., SKOUG, J. W., NIXON, P. R., ROBERT JU, T., STEMM, N. L. & SUNG, K.-C. 1996. Swelling of hydroxypropyl methylcellulose matrix tablets. 2. Mechanistic study of the influence of formulation variables on matrix performance and drug release. *Journal of Pharmaceutical Sciences*, 85, 732-740.
- GHORI, M. U., ALBA, K., SMITH, A. M., CONWAY, B. R. & KONTOGIORGOS, V. 2014a. Okra extracts in pharmaceutical and food applications. *Food Hydrocolloids*.
- GHORI, M. U., GINTING, G., SMITH, A. M. & CONWAY, B. R. 2014b. Simultaneous quantification of drug release and erosion from hypromellose hydrophilic matrices. *International Journal of Pharmaceutics*, 465, 406-412.
- GHORI, M. U., ŠUPUK, E. & CONWAY, B. R. 2014c. Tribo-electric charging and adhesion of cellulose ethers and their mixtures with FBP. *European Journal of Pharmaceutical Sciences*, 65, 1-8.
- GLOR, M. 1985. Hazards due to electrostatic charging of powders. *Journal of Electrostatics*, 16, 175-191.
- GLOR, M. 2003. Ignition hazard due to static electricity in particulate processes. *Powder Technology*, 135-136, 223-233.
- GLOR, M. 2005. Electrostatic ignition hazards in the process industry. *Journal of Electrostatics*, 63, 447-453.
- GREASON, W. D. 2000. Investigation of a test methodology for triboelectrification. *Journal of Electrostatics*, 49, 245-256.
- GUSTAFSSON, C., BONFERONI, M. C., CARAMELLA, C., LENNHOLM, H. & NYSTRÖM, C. 1999. Characterisation of particle properties and compaction behaviour of hydroxypropyl methylcellulose with different degrees of

- methoxy/hydroxypropyl substitution. *European Journal of Pharmaceutical Sciences*, 9, 171-184.
- HAECKEL, R. & HANECKE, P. 1996. Application of saliva for drug monitoring an in vivo model for transmembrane transport. *European Journal of Clinical Chemistry and Clinical Biochemistry*, 34, 171-192.
- HARBORNE, J. B. & DEY, P. M. 2012. *Carbohydrates*, Elsevier Science.
- HARPER, W. 1953. Surfaces showing no electrification after light contact with metals. *Proceedings of the Royal Society of London. Series A. Mathematical and Physical Sciences*, 218, 111-121.
- HARPER, W. R. 1967. *Contact and Frictional Electrification*, Clarendon Press.
- HECKEL, R. 1961a. An analysis of powder compaction phenomena. *Transactions of the Metallurgical Society of AIME*, 221, 1001-1008.
- HECKEL, R. 1961b. Density-pressure relationships in powder compaction. *Trans Metall Soc AIME*, 221, 671-675.
- HENG, P. W. S., CHAN, L. W., EASTERBROOK, M. G. & LI, X. 2001. Investigation of the influence of mean HPMC particle size and number of polymer particles on the release of aspirin from swellable hydrophilic matrix tablets. *Journal of Controlled Release*, 76, 39-49.
- HERSEY, J. A. 1975. Ordered mixing: a new concept in powder mixing practice. *Powder Technology*, 11, 41-44.
- HIGUCHI, T. 1961. Rate of release of medicaments from ointment bases containing drugs in suspension. *Journal of Pharmaceutical Sciences*, 50, 874-875.
- HIGUCHI, T. 1963. Mechanism of sustained-action medication. Theoretical analysis of rate of release of solid drugs dispersed in solid matrices. *Journal of Pharmaceutical Sciences*, 52, 1145-1149.
- HIREMATH, P. & SAHA, R. 2008. Oral controlled release formulations of rifampicin. Part II: Effect of formulation variables and process parameters on in vitro release. *Drug Delivery*, 15, 159-168.
- HOFMANN, N. & STEINER, R. 1980. Interference with Spermatozoal Motility. *Regulation of Male Fertility*. Springer.
- HOGUE, M., BUHLER, C., CALLE, C., MATSUYAMA, T., LUO, W. & GROOP, E. 2004. Insulator-insulator contact charging and its relationship to atmospheric pressure. *Journal of Electrostatics*, 61, 259-268.
- HUSSAIN, T., KAIALY, W., DENG, T., BRADLEY, M. S. A., NOKHODCHI, A. & ARMOUR-CHÉLU, D. 2013. A novel sensing technique for measurement of

- magnitude and polarity of electrostatic charge distribution across individual particles. *International Journal of Pharmaceutics*, 441, 781-789.
- ISRAELACHVILI, J. N. 2011. *Intermolecular and Surface Forces: Revised Third Edition*, Elsevier Science.
- ITIOLA, O. A. 1991. Formulation effects on the mechanical properties of metronidazole tablets. *Journal of Pharmacy and Pharmacology*, 43, 145.
- JAIN, A. K., SÖDERLIND, E., VIRIDÉN, A., SCHUG, B., ABRAHAMSSON, B., KNOPKE, C., TAJARABI, F., BLUME, H., ANSCHÜTZ, M. & WELINDER, A. 2014. The influence of hydroxypropyl methylcellulose (HPMC) molecular weight, concentration and effect of food on in vivo erosion behavior of HPMC matrix tablets. *Journal of Controlled Release*, 187, 50-58.
- JAIN, V. & BAHADUR, S. 1978. Material transfer in polymer-polymer sliding. *Wear*, 46, 177-188.
- JANSOOK, P., MUANKAEW, C., STEFÁNSSON, E. & LOFTSSON, T. 2014. Development of eye drops containing antihypertensive drugs: formulation of aqueous irbesartan/ γ CD eye drops. *Pharmaceutical Development and Technology*, 1-7.
- JHON, M. S. & ANDRADE, J. D. 1973. Water and hydrogels. *Journal of Biomedical Materials Research*, 7, 509-522.
- JIASHENG, T., SHEN, Y., RAVICHANDRAN, M., BHASKARA, J. & XIAOLING, L. 2010. Polymers in oral modified release systems. In: WEN, H. & PARK, K. (eds.) *Oral Controlled Release Formulation Design and Drug Delivery: Theory to Practice*. John Wiley & Sons.
- JIVRAJ, M., MARTINI, L. G. & THOMSON, C. M. 2000. An overview of the different excipients useful for the direct compression of tablets. *Pharmaceutical Science & Technology Today*, 3, 58-63.
- KAMIYAMA, M., MAEDA, M., OKUTANI, H., KOYAMA, K., MATSUDA, H. & SANO, Y. 1994. Effect of functional groups on the triboelectric charging property of polymer particles. *Journal of Applied Polymer Science*, 51, 1667-1671.
- KAREHILL, P., GLAZER, M. & NYSTRÖM, C. 1990. Studies on direct compression of tablets. XXIII. The importance of surface roughness for the compactability of some directly compressible materials with different bonding and volume reduction properties. *International Journal of Pharmaceutics*, 64, 35-43.
- KARNER, S. & ANNE URBANETZ, N. 2011. The impact of electrostatic charge in pharmaceutical powders with specific focus on inhalation-powders. *Journal of Aerosol Science*, 42, 428-445.
- KARNER, S. & URBANETZ, N. A. 2012. Arising of electrostatic charge in the mixing process and its influencing factors. *Powder Technology*, 226, 261-268.

- KARNER, S. & URBANETZ, N. A. 2013. Triboelectric characteristics of mannitol based formulations for the application in dry powder inhalers. *Powder Technology*, 235, 349-358.
- KATZUNG, B. G. 2007. *Basic & Clinical Pharmacology*, McGraw-Hill Medical.
- KAUR, I. P., SINGH, M. & KANWAR, M. 2000. Formulation and evaluation of ophthalmic preparations of acetazolamide. *International Journal of Pharmaceutics*, 199, 119-127.
- KAWAKITA, K. & LÜDDE, K. H. 1971. Some considerations on powder compression equations. *Powder Technology*, 4, 61-68.
- KEARY, C. M. 2001. Characterization of METHOCEL cellulose ethers by aqueous SEC with multiple detectors. *Carbohydrate Polymers*, 45, 293-303.
- KHAMANGA, S. M. & WALKER, R. B. 2006. Evaluation of rate of swelling and erosion of verapamil (VRP) sustained-release matrix tablets. *Drug Development and Industrial Pharmacy*, 32, 1139-1148.
- KIEKENS, F., DEBUNNE, A., VERVAET, C., BAERT, L., VANHOUTTE, F., VAN ASSCHE, I., MENARD, F. & REMON, J. P. 2004. Influence of the punch diameter and curvature on the yield pressure of MCC-compacts during Heckel analysis. *European Journal of Pharmaceutical Sciences*, 22, 117-126.
- KIM, C.-J. 1999. Release kinetics of coated, donut-shaped tablets for water soluble drugs. *European Journal of Pharmaceutical Sciences*, 7, 237-242.
- KIM, H. & FASSIHI, R. 1997. Application of a binary polymer system in drug release rate modulation. 1. Characterization of release mechanism. *Journal of Pharmaceutical Sciences*, 86, 316-322.
- KONG, D. 2006. Analysis of a dust explosion caused by several design errors. *Process Safety Progress*, 25, 58-63.
- KORNFELD, M. 1976. Frictional electrification. *Journal of Physics D: Applied Physics*, 9, 1183.
- KORSMEYER, R. W., GURNY, R., DOELKER, E., BURI, P. & PEPPAS, N. A. 1983. Mechanisms of solute release from porous hydrophilic polymers. *International Journal of Pharmaceutics*, 15, 25-35.
- KROSCWITZ, J. I. & SEIDEL, A. 2007. *Kirk-Othmer Encyclopedia of Chemical Technology*, Wiley-Interscience.
- KWEK, J., HENG, D., LEE, S., NG, W., CHAN, H.-K., ADI, S., HENG, J. & TAN, R. B. 2013. High speed imaging with electrostatic charge monitoring to track powder deagglomeration upon impact. *Journal of Aerosol Science*, 65, 77-87.
- KWOK, P. C. L. & CHAN, H. K. 2009. Electrostatics of pharmaceutical inhalation aerosols. *Journal of Pharmacy and Pharmacology*, 61, 1587-1599.

- LACKS, D. J., DUFF, N. & KUMAR, S. K. 2008. Nonequilibrium accumulation of surface species and triboelectric charging in single component particulate systems. *Physical Review Letters*, 100, 188305.
- LACKS, D. J. & LEVANDOVSKY, A. 2007. Effect of particle size distribution on the polarity of triboelectric charging in granular insulator systems. *Journal of Electrostatics*, 65, 107-112.
- LACKS, D. J. & SANKARAN, R. M. 2011. Contact electrification of insulating materials. *Journal of Physics D: Applied Physics*, 44, 453001.
- LAM, K. & NEWTON, J. 1991. Investigation of applied compression on the adhesion of powders to a substrate surface. *Powder Technology*, 65, 167-175.
- LANG, N. & KOHN, W. 1971. Theory of metal surfaces: work function. *Physical Review B*, 3, 1215.
- LEE, B. J., RYU, S. G. & CUI, J. H. 1999. Formulation and release characteristics of hydroxypropyl methylcellulose matrix tablet containing melatonin. *Drug Development and Industrial Pharmacy*, 25, 493-501.
- LEE, H. G., ZHANG, G. G. & FLANAGAN, D. R. 2011. Cocrystal intrinsic dissolution behavior using a rotating disk. *Journal of Pharmaceutical Sciences*, 100, 1736-1744.
- LEMKE, T. L. & WILLIAMS, D. A. 2012. *Foye's Principles of Medicinal Chemistry*, Wolters Kluwer Health.
- LEUENBERGER, H. 1982. The compressibility and compactibility of powder systems. *International Journal of Pharmaceutics*, 12, 41-55.
- LEUENBERGER, H., HOLMAN, L., USTERI, M. & WINZAP, S. 1989. Percolation theory, fractal geometry, and dosage form design. *Pharmaceutica Acta Helveticae*, 64, 34-39.
- LI, C. L., MARTINI, L. G., FORD, J. L. & ROBERTS, M. 2005. The use of hypromellose in oral drug delivery. *Journal of Pharmacy and Pharmacology*, 57, 533-546.
- LI, T., BAN, H., HOWER, J., STENCEL, J. & SAITO, K. 1999. Dry triboelectrostatic separation of mineral particles: a potential application in space exploration. *Journal of Electrostatics*, 47, 133-142.
- LIU, R. 2008. *Water-Insoluble Drug Formulation, Second Edition*, Taylor & Francis.
- LIU, Z., LI, J., NIE, S., LIU, H., DING, P. & PAN, W. 2006. Study of an alginate/HPMC-based in situ gelling ophthalmic delivery system for gatifloxacin. *International Journal of Pharmaceutics*, 315, 12-17.
- LOEWIT, K. 1977. In vitro immobilization of human spermatozoa with hydroxypropylmethylcellulose. *Contraception*, 15, 233-237.

- LORDI, N. & SHIROMANI, P. 1984. Mechanism of hardness of aged compacts. *Drug Development and Industrial Pharmacy*, 10, 729-752.
- LOWELL, J. 1976. The electrification of polymers by metals. *Journal of Physics D: Applied Physics*, 9, 1571.
- LOWELL, J. 1979. Tunnelling between metals and insulators and its role in contact electrification. *Journal of Physics D: Applied Physics*, 12, 1541.
- LOWELL, J. & AKANDE, A. 1988. Contact electrification-why is it variable? *Journal of Physics D: Applied Physics*, 21, 125.
- LOWELL, J. & ROSE-INNES, A. 1980. Contact electrification. *Advances in Physics*, 29, 947-1023.
- MACLEOD, G. S., FELL, J. T., COLLETT, J. H., SHARMA, H. L. & SMITH, A.-M. 1999. Selective drug delivery to the colon using pectin: chitosan: hydroxypropyl methylcellulose film coated tablets. *International Journal of Pharmaceutics*, 187, 251-257.
- MADERUELO, C., ZARZUELO, A. & LANAO, J. M. 2011. Critical factors in the release of drugs from sustained release hydrophilic matrices. *Journal of Controlled Release*, 154, 2-19.
- MAITRE, M. M., LONGHI, M. R. & GRANERO, G. G. 2007. Ternary complexes of FBP with HP- β -CD and ethanolamines characterization and transdermal delivery. *Drug Development and Industrial Pharmacy*, 33, 311-326.
- MALAMATARIS, S. & KARIDAS, T. 1994. Effect of particle size and sorbed moisture on the tensile strength of some tableted hydroxypropyl methylcellulose (HPMC) polymers. *International Journal of Pharmaceutics*, 104, 115-123.
- MALAMATARIS, S., KARIDAS, T. & GOIDAS, P. 1994. Effect of particle size and sorbed moisture on the compression behaviour of some hydroxypropyl methylcellulose (HPMC) polymers. *International Journal of Pharmaceutics*, 103, 205-215.
- MARK, H. F. 2014. *Encyclopedia of Polymer Science and Technology, 15 Volume Set*, Wiley.
- MASUDA, H., HIGASHITANI, K. & YOSHIDA, H. 2006. *Powder Technology Handbook, Third Edition*, Taylor & Francis.
- MASUKO, T., MINAMI, A., IWASAKI, N., MAJIMA, T., NISHIMURA, S.-I. & LEE, Y. C. 2005. Carbohydrate analysis by a phenol-sulfuric acid method in microplate format. *Analytical Biochemistry*, 339, 69-72.
- MATSUSAKA, S., GHADIRI, M. & MASUDA, H. 2000. Electrification of an elastic sphere by repeated impacts on a metal plate. *Journal of Physics D: Applied Physics*, 33, 2311.

- MATSUSAKA, S., MARUYAMA, H., MATSUYAMA, T. & GHADIRI, M. 2010. Triboelectric charging of powders: A review. *Chemical Engineering Science*, 65, 5781-5807.
- MATSUSAKA, S. & MASUDA, H. 2003. Electrostatics of particles. *Advanced Powder Technology*, 14, 143-166.
- MATSUSAKA, S., UMEMOTO, H., NISHITANI, M. & MASUDA, H. 2002. Electrostatic charge distribution of particles in gas–solids pipe flow. *Journal of Electrostatics*, 55, 81-96.
- MAZUMDER, M., SIMS, R., BIRIS, A., SRIRAMA, P., SAINI, D., YURTERI, C., TRIGWELL, S., DE, S. & SHARMA, R. 2006a. Twenty-first century research needs in electrostatic processes applied to industry and medicine. *Chemical Engineering Science*, 61, 2192-2211.
- MAZUMDER, M. K., SIMS, R. A., BIRIS, A. S., SRIRAMA, P. K., SAINI, D., YURTERI, C. U., TRIGWELL, S., DE, S. & SHARMA, R. 2006b. Twenty-first century research needs in electrostatic processes applied to industry and medicine. *Chemical Engineering Science*, 61, 2192-2211.
- MCCORMICK, D. 2005. Evolutions in direct compression. *Pharmaceutical Technology*, 17, 52-62.
- MCCRISTAL, C. B., FORD, J. L. & RAJABI-SIAHBOOMI, A. R. 1997. A study on the interaction of water and cellulose ethers using differential scanning calorimetry. *Thermochimica Acta*, 294, 91-98.
- MCCRISTAL, C. B., FORD, J. L. & RAJABI-SIAHBOOMI, A. R. 1999. Water distribution studies within cellulose ethers using differential scanning calorimetry. 2. Effect of polymer substitution type and drug addition. *Journal of Pharmaceutical Sciences*, 88, 797-801.
- MILLER-CHOU, B. A. & KOENIG, J. L. 2003. A review of polymer dissolution. *Progress in Polymer Science*, 28, 1223-1270.
- MITCHELL, K., FORD, J. L., ARMSTRONG, D. J., ELLIOTT, P. N. C., ROSTRON, C. & HOGAN, J. E. 1993. The influence of concentration on the release of drugs from gels and matrices containing Methocel[®]. *International Journal of Pharmaceutics*, 100, 155-163.
- MURATA, Y., HODOSHIMA, T. & KITAKA, S. 1979. Evidence for electron transfer as the mechanism of contact charging of polyethylene with metals. *Japanese Journal of Applied Physics*, 18, 2215.
- MURTOMAA, M., HARJUNEN, P., MELLIN, V., LEHTO, V.-P. & LAINE, E. 2002. Effect of amorphicity on the triboelectrification of lactose powder. *Journal of Electrostatics*, 56, 103-110.

- MURTOMAA, M. & LAINE, E. 2000. Electrostatic measurements on lactose–glucose mixtures. *Journal of Electrostatics*, 48, 155-162.
- MURTOMAA, M., MELLIN, V., HARJUNEN, P., LANKINEN, T., LAINE, E. & LEHTO, V.-P. 2004. Effect of particle morphology on the triboelectrification in dry powder inhalers. *International Journal of Pharmaceutics*, 282, 107-114.
- MURTOMAA, M., OJANEN, K. & LAINE, E. 2002b. Effect of surface coverage of a glass pipe by small particles on the triboelectrification of glucose powder. *Journal of Electrostatics*, 54, 311-320.
- NAKANO, M., OHMORI, N., OGATA, A., SUGIMOTO, K., TOBINO, Y., IWAOKU, R. & JUNI, K. 1983. Sustained release of THP from hydroxypropylcellulose tablets. *Journal of Pharmaceutical Sciences*, 72, 378-380.
- NELLORE, R. V., SINGH REKHI, G., HUSSAIN, A. S., TILLMAN, L. G. & AUGSBURGER, L. L. 1998. Development of metoprolol tartrate extended-release matrix tablet formulations for regulatory policy consideration. *Journal of Controlled Release*, 50, 247-256.
- NFPA 1986. *National Fire Codes: A Compilation of NFPA Codes, Standards, Recommended Practices, Manuals and Guides*, National Fire Protection Association.
- NGUYEN, T. & NIEH, S. 1989. The role of water vapor in the charge elimination process for flowing powders. *Journal of Electrostatics*, 22, 213-227.
- NIEH, S. & NGUYEN, T. 1988. Effects of humidity, conveying velocity, and particle size on electrostatic charges of glass beads in a gaseous suspension flow. *Journal of Electrostatics*, 21, 99-114.
- NOKHODCHI, A., FORD, J. L., ROWE, P. H. & RUBINSTEIN, M. H. 1996a. The Effect of Moisture on the Heckel and Energy Analysis of Hydroxypropylmethylcellulose 2208 (HPMC K4M). *Journal of Pharmacy and Pharmacology*, 48, 1122-1127.
- NOKHODCHI, A., FORD, J. L., ROWE, P. H. & RUBINSTEIN, M. H. 1996b. The effects of compression rate and force on the compaction properties of different viscosity grades of hydroxypropylmethylcellulose 2208. *International Journal of Pharmaceutics*, 129, 21-31.
- NOKHODCHI, A., FORD, J. L., ROWE, P. H. & RUBINSTEIN, M. H. 1996c. The Influence of Moisture Content on the Consolidation Properties of Hydroxypropylmethylcellulose K4M (HPMC 2208). *Journal of Pharmacy and Pharmacology*, 48, 1116-1121.
- NOKHODCHI, A. & RUBINSTEIN, M. H. 2001. An overview of the effects of material and process variables on the compaction and compression properties of hydroxypropyl methylcellulose and ethylcellulose. *S.T.P. Pharma Sciences*, 11, 195-202.

- NOKHODCHI, A., RUBINSTEIN, M. H. & FORD, J. L. 1995. The effect of particle size and viscosity grade on the compaction properties of hydroxypropylmethylcellulose 2208. *International Journal of Pharmaceutics*, 126, 189-197.
- NOMURA, T., SATOH, T. & MASUDA, H. 2003. The environment humidity effect on the tribo-charge of powder. *Powder Technology*, 135, 43-49.
- NORDSTRÖM, J., KLEVAN, I. & ALDERBORN, G. 2009. A particle rearrangement index based on the kawakita powder compression equation. *Journal of Pharmaceutical Sciences*, 98, 1053-1063.
- NORDSTRÖM, J., WELCH, K., FRENNING, G. & ALDERBORN, G. 2008. On the physical interpretation of the Kawakita and Adams parameters derived from confined compression of granular solids. *Powder Technology*, 182, 424-435.
- NYSTRÖM, C., ALDERBORN, G., DUBERG, M. & KAREHILL, P.-G. 1993. Bonding Surface area and Bonding Mechanism-Two Important Factors fir the Understanding of Powder Comparability. *Drug Development and Industrial Pharmacy*, 19, 2143-2196.
- NYSTRÖM, C. & KAREHILL, P.-G. 1996. The importance of intermolecular bonding forces and the concept of bonding surface area. *Drugs & the Pharmaceutical Sciences*, 71, 17-54.
- OHSAWA, A. 2011. Statistical analysis of fires and explosions attributed to static electricity over the last 50 years in Japanese industry. *Journal of Physics: Conference Series*, 301, 012033.
- OKIMOTO, K., MIYAKE, M., IBUKI, R., YASUMURA, M., OHNISHI, N. & NAKAI, T. 1997. Dissolution mechanism and rate of solid dispersion particles of nilvadipine with hydroxypropylmethylcellulose. *International Journal of Pharmaceutics*, 159, 85-93.
- OYELOLA, O., AYANGADE, S. & AMOLE, F. 1987. In vitro inhibition of sperm motility by some local mineral water drinks. *Contraception*, 36, 435-440.
- PATEL, S., KAUSHAL, A. M. & BANSAL, A. K. 2006. Compression physics in the formulation development of tablets. *Critical Reviews in Therapeutic Drug Carrier Systems*, 23.
- PATEL, S., KAUSHAL, A. M. & BANSAL, A. K. 2010. Mechanistic investigation on pressure dependency of Heckel parameter. *International journal of pharmaceutics*, 389, 66-73.
- PINGALI, K. C., SHINBROT, T., HAMMOND, S. V. & MUZZIO, F. J. 2009. An observed correlation between flow and electrical properties of pharmaceutical blends. *Powder Technology*, 192, 157-165.
- PIPERNO, S., COHEN, H., BENDIKOV, T., LAHAV, M. & LUBOMIRSKY, I. 2011. The absence of redox reactions for palladium (II) and copper (II) on electrostatically

charged teflon: Relevance to the concept of “cryptoelectrons”. *Angewandte Chemie International Edition*, 50, 5654-5657.

- PODCZECK, F. 1998. *Particle-particle adhesion in pharmaceutical powder handling*, World Scientific.
- PRADHAN, R., KIM, Y.-I., CHANG, S. W. & KIM, J. O. 2014. Preparation and evaluation of once-daily sustained-release coated tablets of tolterodine-L-tartrate. *International Journal of Pharmaceutics*, 460, 205-211.
- PU, Y., MAZUMDER, M. & COONEY, C. 2009. Effects of electrostatic charging on pharmaceutical powder blending homogeneity. *Journal of Pharmaceutical Sciences*, 98, 2412-2421.
- QIU, Y., FLOOD, K., MARSH, K., CARROLL, S., TRIVEDI, J., ARNERIC, S. P. & KRILL, S. L. 1997. Design of sustained-release matrix systems for a highly water-soluble compound, ABT-089. *International Journal of Pharmaceutics*, 157, 43-52.
- RAGHAVAN, S., SCHUESSEL, K., DAVIS, A. & HADGRAFT, J. 2003. Formation and stabilisation of triclosan colloidal suspensions using supersaturated systems. *International Journal of Pharmaceutics*, 261, 153-158.
- RAJABI-SIAHBOOMI, A. R., BOWTELL, R. W., MANSFIELD, P., DAVIES, M. C. & MELIA, C. D. 1996. Structure and behavior in hydrophilic matrix sustained release dosage forms: 4. Studies of water mobility and diffusion coefficients in the gel layer of HPMC tablets using NMR imaging. *Pharmaceutical Research*, 13, 376-380.
- RAJABI-SIAHBOOMI, A. R. & NOKHODCHI, A. 1999. Compression properties of methylcellulose and hydroxypropylmethylcellulose polymers. *Pharmacy and Pharmacology Communications*, 5, 67-71.
- RAJABI-SIAHBOOMI, A. R., NOKHODCHI, A. & RUBINSTEIN, M. H. 1998. Compaction behaviour of hydrophilic cellulose ether polymers. *Pharmaceutical Technology*, 22.
- RAMIREZ M. 2010. Molecular architecture influences on material properties of pharmaceutical compounds. *PhD thesis, Aston University*.
- RANGA RAO, K. V., PADMALATHA DEVI, K. & BURI, P. 1988. Cellulose matrices for zero-order release of soluble drugs. *Drug Development and Industrial Pharmacy*, 14, 2299-2320.
- RAVI, P. R., GANGA, S. & SAHA, R. N. 2008. Design and in vitro evaluation of zidovudine oral controlled release tablets prepared using hydroxypropyl methylcellulose. *Chemical and Pharmaceutical Bulletin*, 56, 518-524.
- ROWE, R. C., SHESKEY, P. J., WALTER G. COOK, P. D. & FENTON, M. E. 2012. *Handbook of Pharmaceutical Excipients*, Pharmaceutical Press.

- REMINGTON, J. P. & ALLEN, L. V. 2013. *Remington: The Science and Practice of Pharmacy*, Pharmaceutical Press.
- REYNOLDS, T. D., MITCHELL, S. A. & BALWINSKI, K. M. 2002. Investigation of the effect of tablet surface area/volume on drug release from hydroxypropylmethylcellulose controlled-release matrix tablets. *Drug Development and Industrial Pharmacy*, 28, 457-466.
- REZA, M. S., QUADIR, M. A. & HAIDER, S. S. 2003. Comparative evaluation of plastic, hydrophobic and hydrophilic polymers as matrices for controlled-release drug delivery. *Journal of Pharmacy and Pharmaceutical Sciences*, 6, 282-291.
- RIEPMA, K., VROMANS, H., ZUURMAN, K. & LERK, C. 1993. The effect of dry granulation on the consolidation and compaction of crystalline lactose. *International Journal of Pharmaceutics*, 97, 29-38.
- RITGER, P. L. & PEPPAS, N. A. 1987a. A simple equation for description of solute release I. Fickian and non-Fickian release from non-swellable devices in the form of slabs, spheres, cylinders or discs. *Journal of Controlled Release*, 5, 23-36.
- RITGER, P. L. & PEPPAS, N. A. 1987b. A simple equation for description of solute release II. Fickian and anomalous release from swellable devices. *Journal of Controlled Release*, 5, 37-42.
- ROBERTS, R., ROWE, R. & KENDALL, K. 1989. Brittle—ductile transitions in die compaction of sodium chloride. *Chemical Engineering Science*, 44, 1647-1651.
- ROBINS, E., LOWELL, J. & ROSE-INNES, A. 1980. The role of surface ions in the contact electrification of insulators. *Journal of Electrostatics*, 8, 153-160.
- ROMÂNIA, A. R. S. 1995. *Cellulose Chemistry and Technology*.
- ROWLEY, G. 2001. Quantifying electrostatic interactions in pharmaceutical solid systems. *International Journal of Pharmaceutics*, 227, 47-55.
- ROWLEY, G. & MACKIN, L. 2003. The effect of moisture sorption on electrostatic charging of selected pharmaceutical excipient powders. *Powder Technology*, 135, 50-58.
- RUMPF, H. 1958. Grundlagen und methoden des granulierens. *Chemie Ingenieur Technik*, 30, 144-158.
- SALAMONE, J. C. 1996. *Polymeric Materials Encyclopedia, Twelve Volume Set*, Taylor & Francis.
- SANDELL, E. 1992. *Industrial Aspects of Pharmecuticals*, Taylor & Francis.
- SARKAR, N. 1979. Thermal gelation properties of methyl and hydroxypropyl methylcellulose. *Journal of Applied Polymer Science*, 24, 1073-1087.

- SARKAR, N. & WALKER, L. 1995. Hydration—dehydration properties of methylcellulose and hydroxypropylmethylcellulose. *Carbohydrate Polymers*, 27, 177-185.
- SCHULZ, M. B. & DANIELS, R. 2000. Hydroxypropylmethylcellulose (HPMC) as emulsifier for submicron emulsions: influence of molecular weight and substitution type on the droplet size after high-pressure homogenization. *European Journal of Pharmaceutics and Biopharmaceutics*, 49, 231-236.
- SHARMA, R. 2004. Modification of electrostatic properties of polymer powders using atmospheric plasma reactor. *Polymer Surface Modification: Relevance to Adhesion*, 3, 25.
- SHARMA, R., HOLCOMB, E., TRIGWELL, S. & MAZUMDER, M. 2007. Stability of atmospheric-pressure plasma induced changes on polycarbonate surfaces. *Journal of Electrostatics*, 65, 269-273.
- SHARMA, R., TRIGWELL, S., BIRIS, A. S., SIMS, R. A. & MAZUMDER, M. K. 2003. Effect of ambient relative humidity and surface modification on the charge decay properties of polymer powders in powder coating. *Industry Applications, IEEE Transactions on*, 39, 87-95.
- SHAW, L. R., IRWIN, W. J., GRATTAN, T. J. & CONWAY, B. R. 2005. The effect of selected water-soluble excipients on the dissolution of paracetamol and ibuprofen. *Drug Development and Industrial Pharmacy*, 31, 515-525.
- SHEKUNOV, B. Y., FEELEY, J. C., CHOW, A. H., TONG, H. H. & YORK, P. 2002. Physical properties of supercritically-processed and micronised powders for respiratory drug delivery. *KONA Powder and Particle Journal*, 20, 178-187.
- SHINOHARA, I., YAMAMOTO, F., ANZAI, H. & ENDO, S. 1976. Chemical structure and electrostatic properties of polymers. *Journal of Electrostatics*, 2, 99-110.
- SHOKRI, J. & ADIBKIA, K. 2013. Application of Cellulose and Cellulose Derivatives in Pharmaceutical Industries.
- SIEPMANN, J. & PEPPAS, N. A. 2001. Modeling of drug release from delivery systems based on hydroxypropyl methylcellulose (HPMC). *Advanced Drug Delivery Reviews*, 48, 139-157.
- SIEPMANN, J., SIEGEL, R. A. & RATHBONE, M. J. 2011. *Fundamentals and Applications of Controlled Release Drug Delivery*, Springer.
- SINHA ROY, D. & ROHERA, B. D. 2002. Comparative evaluation of rate of hydration and matrix erosion of HEC and HPC and study of drug release from their matrices. *European Journal of Pharmaceutical Sciences*, 16, 193-199.
- SMELTZER, E., WEAVER, M. & KLINZING, G. E. 1982. Individual electrostatic particle interaction in pneumatic transport. *Powder Technology*, 33, 31-42.

- SMITH, H. A., BLECHA, M. K. & STERNIG, J. 1966. *Science*, Laidlaw.
- SONNERGAARD, J. 2000. Impact of particle density and initial volume on mathematical compression models. *European journal of pharmaceutical sciences*, 11, 307-315.
- SRI 2013. *Chemical Economic Handbook*, SRI International, Maleno Park, USA.
- STANIFORTH, J. & REES, J. 1982a. Electrostatic charge interactions in ordered powder mixes. *Journal of Pharmacy and Pharmacology*, 34, 69-76.
- STANIFORTH, J. N. & REES, J. E. 1981. Powder mixing by triboelectrification. *Powder Technology*, 30, 255-256.
- STANIFORTH, J. N. & REES, J. E. 1982b. Electrostatic charge interactions in ordered powder mixes. *Journal of Pharmacy and Pharmacology*, 34, 69-76.
- SUN, C. & GRANT, D. J. 2001. Influence of elastic deformation of particles on Heckel analysis. *Pharmaceutical Development and Technology*, 6, 193-200.
- ŠUPUK, E., GHORI, M. U., ASARE-ADDO, K., LAITY, P. R., PANCHMATIA, P. M. & CONWAY, B. R. 2013. The influence of salt formation on electrostatic and compression properties of FBP salts. *International Journal of Pharmaceutics*, 458, 118-127.
- ŠUPUK, E., HASSANPOUR, A., AHMADIAN, H., GHADIRI, M. & MATSUYAMA, T. 2011. Tribo-electrification and associated segregation of pharmaceutical bulk powders. *KONA Powder and Particle Journal*, 29, 208-223.
- ŠUPUK, E., SEILER, C. & GHADIRI, M. 2009. Analysis of a simple test device for tribo-electric charging of bulk powders. *Particle and Particle Systems Characterization*, 26, 7-16.
- ŠUPUK, E., ZARREBINI, A., REDDY, J. P., HUGHES, H., LEANE, M. M., TOBYN, M. J., TIMMINS, P. & GHADIRI, M. 2012. Tribo-electrification of active pharmaceutical ingredients and excipients. *Powder Technology*, 217, 427-434.
- SWARBRICK, J. 2007. *Encyclopedia of Pharmaceutical Technology: Comp-Dry* (p. 671 - 1434), Informa Healthcare.
- SWEETMAN, S. C. 2009. *Martindale: The Complete Drug Reference*, Pharmaceutical Press.
- TAJAROBI, F., ABRAHMSÉN-ALAMI, S., CARLSSON, A. S. & LARSSON, A. 2009. Simultaneous probing of swelling, erosion and dissolution by NMR-microimaging-Effect of solubility of additives on HPMC matrix tablets. *European Journal of Pharmaceutical Sciences*, 37, 89-97.
- TALUKDAR, M. M., MICHOEL, A., ROMBAUT, P. & KINGET, R. 1996. Comparative study on xanthan gum and hydroxypropylmethyl cellulose as matrices for controlled-

- release drug delivery I. Compaction and in vitro drug release behaviour. *International Journal of Pharmaceutics*, 129, 233-241.
- TANOUE, K.-I., EMA, A. & MASUDA, H. 1999. Effect of Material Transfer and Work Hardening of Metal Surface on the Current Generated by Impact of Particles. *Journal of Chemical Engineering of Japan*, 32, 544-548.
- TAVORNVIPAS, S., HIRAYAMA, F., ARIMA, H., UEKAMA, K., ISHIGURO, T., OKA, M., HAMAYASU, K. & HASHIMOTO, H. 2002. 6-O- α -(4-O- α -d-glucuronyl)-d-glucosyl- β -cyclodextrin: solubilizing ability and some cellular effects. *International Journal of Pharmaceutics*, 249, 199-209.
- TIEKINK, E. R. T., VITTAL, J. & ZAWOROTKO, M. 2010. *Organic Crystal Engineering: Frontiers in Crystal Engineering*, Wiley.
- TIWARI, S. B., MURTHY, T. K., PAI, M. R., MEHTA, P. R. & CHOWDARY, P. B. 2003. Controlled release formulation of tramadol hydrochloride using hydrophilic and hydrophobic matrix system. *AAPS Pharmscitech*, 4, 18-23.
- TRAINI, D., SCALIA, S., ADI, H., MARANGONI, E. & YOUNG, P. M. 2012. Polymer coating of carrier excipients modify aerosol performance of adhered drugs used in dry powder inhalation therapy. *International Journal of Pharmaceutics*, 438, 150-159.
- TRIGWELL, S., BIRIS, A., SIMS, R. A. & MAZUMDER, M. K. 2008. Effects of powder velocity and contact materials on tribocharging of polymer powders for powder coating applications. *Particulate Science and Technology*, 26, 145-157.
- TRIGWELL, S., GRABLE, N., YURTERI, C. U., SHARMA, R. & MAZUMDER, M. K. 2003a. Effects of surface properties on the tribocharging characteristics of polymer powder as applied to industrial processes. *Industry Applications, IEEE Transactions on*, 39, 79-86.
- TRIMM, H. H. 2011. *Organic Chemistry: Structure and Mechanisms*, Apple Academic Press.
- TURBA, E. & RUMPF, H. 1964. Zugfestigkeit von Preßlingen mit vorwiegender Bindung durch van der Waals-Kräfte und ihre Beeinflussung durch Adsorptionsschichten. *Chemie Ingenieur Technik*, 36, 230-240.
- TURNER, G. & BALASUBRAMANIAN, M. 1976. The frequency distributions of electrical charges on glass beads. *Journal of Electrostatics*, 2, 85-89.
- VAN CAMPEN, L., ZOGRIFI, G. & CARSTENSEN, J. 1980. An approach to the evaluation of hygroscopicity for pharmaceutical solids. *International Journal of Pharmaceutics*, 5, 1-18.
- VELASCO, M., FORD, J. L., ROWE, P. & RAJABI-SIAHBOOMI, A. R. 1999. Influence of drug: hydroxypropylmethylcellulose ratio, drug and polymer particle size and compression force on the release of diclofenac sodium from HPMC tablets. *Journal of Controlled Release*, 57, 75-85.

- VERGNAUD, J. M. 1993. Liquid transport controlled release processes in polymeric materials: Applications to oral dosage forms. *International Journal of Pharmaceutics*, 90, 89-94.
- VIRIDÉN, A., LARSSON, A. & WITTGREN, B. 2010. The effect of substitution pattern of HPMC on polymer release from matrix tablets. *International Journal of Pharmaceutics*, 389, 147-156.
- VIRIDÉN, A., WITTGREN, B., ANDERSSON, T. & LARSSON, A. 2009. The effect of chemical heterogeneity of HPMC on polymer release from matrix tablets. *European Journal of Pharmaceutical Sciences*, 36, 392-400.
- VOGEL, H. G. 2006. *Drug Discovery and Evaluation: Safety and Pharmacokinetic Assays ; with 125 Tables*, Springer.
- VUEBA, M. L., BATISTA DE CARVALHO, L. A. E., VEIGA, F., SOUSA, J. J. & PINA, M. E. 2005. Role of cellulose ether polymers on ibuprofen release from matrix tablets. *Drug Development and Industrial Pharmacy*, 31, 653-665.
- WAN, L. S. C., HENG, P. W. S. & WONG, L. F. 1991. The effect of hydroxypropylmethylcellulose on water penetration into a matrix system. *International Journal of Pharmaceutics*, 73, 111-116.
- WANG, J. J., GUILLOT, M. A., BATEMAN, S. D. & MORRIS, K. R. 2004. Modeling of Adhesion in Tablet Compression. II. Compaction Studies Using a Compaction Simulator and an Instrumented Tablet Press. *Journal of Pharmaceutical Sciences*, 93, 407-417.
- WATANABE, H., GHADIRI, M., MATSUYAMA, T., DING, Y. L., PITT, K. G., MARUYAMA, H., MATSUSAKA, S. & MASUDA, H. 2007. Triboelectrification of pharmaceutical powders by particle impact. *International Journal of Pharmaceutics*, 334, 149-155.
- WEN, H. & PARK, K. 2011. *Oral Controlled Release Formulation Design and Drug Delivery: Theory to Practice*, Wiley.
- WEN, X., ALI, N. & ALI, R.-S. 2010. Oral extended release hydrophilic matrices: formulation and design. In: WEN, H. & PARK, K. (eds.) *Oral Controlled Release Formulation Design and Drug Delivery: Theory to Practice*. John Wiley & Sons.
- WERTZ, J. L., BÉDUÉ, O. & MERCIER, J. P. 2010. *Cellulose Science and Technology*, EFPL Press.
- WILES, J. A., FIALKOWSKI, M., RADOWSKI, M. R., WHITESIDES, G. M. & GRZYBOWSKI, B. A. 2004. Effects of surface modification and moisture on the rates of charge transfer between metals and organic materials. *The Journal of Physical Chemistry B*, 108, 20296-20302.

- WISE, D. L. 2000. *Handbook of Pharmaceutical Controlled Release Technology*, Taylor & Francis.
- WOLLENWEBER, C., MAKIEVSKI, A., MILLER, R. & DANIELS, R. 2000. Adsorption of hydroxypropyl methylcellulose at the liquid/liquid interface and the effect on emulsion stability. *Colloids and Surfaces A: Physicochemical and Engineering Aspects*, 172, 91-101.
- WONG, J., KWOK, P. C. L. & CHAN, H.-K. 2014a. Electrostatics in pharmaceutical solids. *Chemical Engineering Science*, DOI: 10.1016/j.ces.2014.05.037 (*In press*).
- WONG, J., KWOK, P. C. L., NOAKES, T., FATHI, A., DEHGHANI, F. & CHAN, H.-K. 2014b. Effect of Crystallinity on Electrostatic Charging in Dry Powder Inhaler Formulations. *Pharmaceutical Research*, 1-9.
- WORDEN, E. C. 2011. *Technology of Cellulose Ethers*, BiblioBazaar.
- XU, G. & SUNADA, H. 1995. Influence of formulation change on drug release kinetics from hydroxypropylmethylcellulose matrix tablets. *Chemical & Pharmaceutical Bulletin*, 43, 483-487.
- XU, Q. A. & MADDEN, T. L. 2011. *Analytical Methods for Therapeutic Drug Monitoring and Toxicology*, Wiley.
- YALKOWSKY, S. H., HE, Y. & JAIN, P. 2010. *Handbook of Aqueous Solubility Data, Second Edition*, Taylor & Francis.
- YANG, L. & FASSIHI, R. 1997. Examination of drug solubility, polymer types, hydrodynamics and loading dose on drug release behavior from a triple-layer asymmetric configuration delivery system. *International Journal of Pharmaceutics*, 155, 219-229.
- YIHONG, Q. 2009. Development of modified release oral solid dosage forms. In: Q. YIHONG, C. Y., G. Z. ZHANG (ed.) *Developing Solid Oral Dosage Forms : Pharmaceutical Theory and Practice* Elsevier.
- YOKOTA, H. 1985. The mechanism of cellulose alkalization in the isopropyl alcohol–water–sodium hydroxide–cellulose system. *Journal of Applied Polymer Science*, 30, 263-277.
- BRUMMER, Y. & CUI, S. W. 2005. Understanding carbohydrate analysis. In: CUI, S. W. (ed.) *Food carbohydrates : chemistry, physical properties, and applications*. Boca Ranton FL (USA): Taylor & Francis Group
- YORK, P. 1980. Powder failure testing—pharmaceutical applications. *International Journal of Pharmaceutics*, 6, 89-117.
- YOSHIDA, M., II, N., SHIMOSAKA, A., SHIRAKAWA, Y. & HIDAKA, J. 2006. Experimental and theoretical approaches to charging behavior of polymer particles. *Chemical Engineering Science*, 61, 2239-2248.

- YOSHIDA, M., SHIMOSAKA, A., SHIRAKAWA, Y., HIDAKA, J., MATSUYAMA, T. & YAMAMOTO, H. 2003. Estimation of electrostatic charge distribution of flowing toner particles in contact with metals. *Powder Technology*, 135, 23-34.
- ZHANG, M. L., SHENG, G. P. & YU, H. Q. 2008. Determination of proteins and carbohydrates in the effluents from wastewater treatment bioreactors using resonance light-scattering method. *Water Research*, 42, 3464-3472.
- ZHAO, H., CASTLE, G. P., INCULET, I. I. & BAILEY, A. G. 2003. Bipolar charging of poly-disperse polymer powders in fluidized beds. *Industry Applications, IEEE Transactions on*, 39, 612-618.
- ZHU, K., NG, W. K., SHEN, S., TAN, R. B. H. & HENG, P. W. S. 2008. Design of a device for simultaneous particle size and electrostatic charge measurement of inhalation drugs. *Pharmaceutical Research*, 25, 2488-2496.
- ZHU, K., TAN, R. B., CHEN, F., ONG, K. H. & HENG, P. W. 2007. Influence of particle wall adhesion on particle electrification in mixers. *International Journal of Pharmaceutics*, 328, 22-34.
- ZOGRAFI, G. 1988. States of water associated with solids. *Drug Development and Industrial Pharmacy*, 14, 1905-1926.
- ZULEGER, S. & LIPPOLD, B. C. 2001. Polymer particle erosion controlling drug release. I. Factors influencing drug release and characterization of the release mechanism. *International Journal of Pharmaceutics*, 217, 139-152.

Appendix- A

Journal Articles

- 1- * **The Influence of Agitation Sequence and Ionic Strength on In-Vitro Drug Release from Hypromellose (E4M and K4M) ER Matrices – The use of USP III Apparatus.**

Kofi Asare-Addo, Marina Levina, Ali Rajabi-Siahboomi, **Muhammad U. Ghori**, Enes Supuk, Peter R Laity, , Barbara R. Conway, Ali Nokhodchi (2013)
Colloids and surfaces B: Biointerfaces , 104, 54-60

- 2- ** **The Influence of Salt Formation on Electrostatic and Compression Properties of FBP Salts.**

Enes Supuk, **Muhammad U. Ghori**, Kofi Asare-Addo, Peter R Laity, Pooja M. Panchmatia, Barbara R. Conway, (2013) **International Journal of Pharmaceutics**, 458 (1), 118-127.

- 3- **Simultaneous Quantification of Drug Release Kinetics and Erosion from Hydrophilic Matrix Tablets.**

Muhammad U. Ghori, Gidion Ginting, Alan M Smith, BR Conway, (2014)
International Journal of Pharmaceutics, 465 (1-2), 405-412.

- 4- **Tribo-electric Charging and Adhesion Properties of Cellulose Ethers and their Powder Mixtures with FBP.**

Muhammad U. Ghori, Enes Supuk, Barbara R Conway (2014)
European Journal of Pharmaceutical Sciences DOI: 10.1016/j.ejps.2014.08.010

- 5- **Swelling, Erosion and Compaction Properties of Cellulose Ethers.**

Muhammad U. Ghori, Alan M. Smith, Barbara R Conway (In-manuscript)

* *Only tribo-electrification data of THP and plain polymers were used from this thesis*

** *Only tribo-electrification data of FBP was used from this thesis.*

6- Probing the Influence of Viscosity, Particle size and Concentration of Hypromellose on Liquid Uptake, Intrinsic Dissolution Rate and Mechanical Properties of Hydrophilic Matrices.

Muhammad U. Ghori, Barbara R Conway (In-manuscript)

7- Swelling rate, Release Kinetics and Compaction Properties of Cellulose Ether Based hydrophilic Matrices: Influence of Substitution, Particle size and Concentration.

Muhammad U. Ghori, Barbara R Conway (In-manuscript)

8- The Influence of Concentration, Particle size, Substitution Ratios and Molecular Weight of Cellulose Ethers on Tribo-electric Charging and Adhesion Properties of THP.

Muhammad U. Ghori, Enes Supuk, Barbara R Conway (In-manuscript)

Conference proceedings

- 1- Tribo-electrification Properties of Cellulose Ethers. (ACCEPTED)**
MU Ghori, Enes Supuk, BR Conway, AAPS Annual Meeting and Exposition
San Diego. November 2-6, 2014.
- 2- Swelling and Erosion Properties of Cellulose Ethers. (ACCEPTED)**
MU Ghori, AM Smith, BR Conway, AAPS Annual Meeting and Exposition
San Diego. November 2-6, 2014.
- 3- Swelling and Erosion Kinetics of Hypromellose Hydrophilic Matrices.**
MU Ghori, BR Conway, UkPharmSci, Hertforshire, UK. September 2014.
- 4- Novel Method to Study Matrix Erosion of HPMC Based Hydrophilic Matrices.**
MU Ghori, AM Smith, BR Conway. Annual Research Conference, University of
Huddersfield, UK. September 2013.
- 5- Novel Application of Phenol Sulphuric Acid Assay.**
MU Ghori, AM Smith, BR Conway.
In proceedings of 1st UK Hydrocolloids Symposium. September 2013.
- 6- Tribo-electrification, Swelling and dissolution properties of hydrophilic matrices.**
MU Ghori, Enes Supuk, BR Conway.
Annual Research Conference, University of Huddersfield, UK. September 2012.
- 7- The impact of hypromellose substitution levels on tribo-electrification, swelling and dissolution properties of FBP matrices.**
MU Ghori, Enes Supuk, BR Conway
In proceedings of UkPharmSci, Nottingham, UK. September 2012
- 8- Impact of hypromellose substitution levels on swelling & dissolution rate of FBP matrices.**
MU Ghori, PR Laity, BR Conway.
In proceedings of UK Control Release Society, Birmingham, UK. May 2012
- 9- Swelling and dissolution properties of FBP hydrophilic matrices.**
MU Ghori, BR Conway.
Annual Research Conference, University of Huddersfield, UK. September 2011.

10- Dissolution & Swelling properties of hydrophilic matrices.

MU Ghori, BR Conway.

In proceedings of UkPharmSci, Nottingham, UK. September 2011.



The influence of agitation sequence and ionic strength on *in vitro* drug release from hypromellose (E4M and K4M) ER matrices—The use of the USP III apparatus

Kofi Asare-Addo^a, Waseem Kaialy^b, Marina Levina^c, Ali Rajabi-Siahboomi^c, Mohammed U. Ghori^a, Enes Supuk^a, Peter R. Laity^a, Barbara R. Conway^a, Ali Nokhodchi^{b,d,*}

^a Pharmacy and Pharmaceutical Sciences, University of Huddersfield, Huddersfield HD1 3DH, UK

^b Medway School of Pharmacy, University of Kent, Chatham, Kent ME4 4TB, UK

^c Colorcon Ltd., Flagship House, Victory Way, Crossways, Dartford, Kent DA2 6QD, UK

^d Drug Applied Research Center and Faculty of Pharmacy, Tabriz University of Medical Sciences, Tabriz, Iran

ARTICLE INFO

Article history:

Received 6 October 2012

Received in revised form

19 November 2012

Accepted 22 November 2012

Available online 14 December 2012

Keywords:

Agitation

Ionic concentration strength

HPMC

Similarity factor

Kinetics of drug release

DSC

Particle size

Triboelectrification

Theophylline

USP III

ABSTRACT

Theophylline extended release (ER) matrices containing hypromellose (hydroxypropyl methylcellulose (HPMC) E4M and K4M were evaluated in media with a pH range of 1.2–7.5, using an automated USP type III, Bio-Dis dissolution apparatus. The objectives of this study were to evaluate the effects of systematic agitation, ionic strength and pH on the release of theophylline from the gel forming hydrophilic polymeric matrices with different methoxyl substitution levels. Tribo-electric charging of hypromellose, theophylline and their formulated blends containing E4M and K4M grades has been characterised, along with quantitative observations of flow, compression behaviour and particle morphology. Agitations were studied at 5, 10, 15, 20, 25, 30 dips per minute (dpm) and also in the ascending and descending order in the dissolution vials. The ionic concentration strength of the media was also varied over a range of 0–0.4M to simulate the gastrointestinal fed and fasted states and various physiological pH conditions. To study the effect of ionic strength on the hydrophilic matrices, agitation was set at 20 dpm. The charge results on individual components imply that the positively charged particles have coupled with the negatively charged particles to form a stable ordered mixture which is believed to result in a more homogeneous and stable system. The particle shape analysis showed the HPMC K4M polymer to have a more irregular morphology and a rougher surface texture in comparison to the HPMC E4M polymer, possibly a contributory factor to the gelation process. The results showed gelation occurred quicker for the K4M tablet matrices. Drug release increased with increased agitation. This was more pronounced for the E4M tablet matrices. The ionic strength also had more of an effect on the drug release from the E4M matrices. The experiments highlighted the resilience of the K4M matrices in comparison with the E4M matrices. The results thus show that despite similar viscosities of E4M and K4M, the methoxyl substitution makes a difference to their control of drug release and as such care and consideration should be given to the choice of polymer used for extended release. The use of systematic change of agitation method and ionic strength may indicate potential fed and fasted effects on drug release from hydrophilic matrices.

© 2012 Elsevier B.V. All rights reserved.

1. Introduction

Tablets made with HPMC swell in contact with water forming a gel layer around the matrix. The release of the drug from the matrix thus depends on the possible interactions between aqueous medium, polymer, drug and other tablet ingredients [1]. It is well known that food administration can affect the bioavailability of oral dosage forms as a result of interactions which may occur between the formulation and the food [2,3]. Researchers have demonstrated that the gel layer formed around hydrophilic matrices, upon its

contact with gastro-intestinal (GI) fluids, is eroded allowing drug release. This erosion is the dominant release mechanism for poorly soluble drugs [2–6]. The other mechanistic approach is that the soluble portion of drug is released by diffusion through the gel layer [4–6]. The non-ionic nature of HPMC means that when drug solubility is pH-independent, the matrices also exhibit pH-independent drug release profiles. Generally, the higher the solubility of the drug, the faster its release; this is due to a higher diffusional driving force.

Two major characteristics of the GI fluids are pH and ionic strength. They vary greatly along the GI tract under both fasting and fed conditions [7,8] and can affect the rate at which a drug is released from hydrophilic ER matrices [9–11]. The ionic strength of the fluids of the GI tract in man under both fasted and fed states

* Corresponding author. Tel.: +44 1634 202947; fax: +44 1634 883927.
E-mail address: a.nokhodchi@kent.ac.uk (A. Nokhodchi).



The influence of salt formation on electrostatic and compression properties of flurbiprofen salts



Enes Šupuk^{a,*}, Muhammad U. Ghorī^a, Kofi Asare-Addo^a, Peter R. Laity^a, Pooja M. Panchmatia^b, Barbara R. Conway^a

^a Pharmacy and Pharmaceutical Sciences, School of Applied Sciences, University of Huddersfield, Huddersfield HD1 3DH, UK

^b Chemical and Biological Sciences, School of Applied Sciences, University of Huddersfield, Huddersfield HD1 3DH, UK

ARTICLE INFO

Article history:

Received 29 July 2013

Received in revised form

29 September 2013

Accepted 2 October 2013

Available online 17 October 2013

Keywords:

Triboelectrification

Electrostatic

Salt formation

Crystal structure

Compaction

ABSTRACT

Salt formation is an effective method of improving physicochemical properties of acidic and basic drugs. The selection of a salt form most suitable for drug development requires a well-designed screening strategy to ensure various issues are addressed in the early development stages. Triboelectrification of pharmaceutical powders may cause problems during processing such as segregation of components due to the effects of particle adhesion. However, very little work has been done on the effect of salt formation on triboelectrification properties. In this paper, salts of flurbiprofen were prepared by combining the drug with a selection of closely related amine counter ions. The aim of the work was to investigate the impact of the counter ion on electrostatic charge of the resultant salts to inform the salt selection process. The experimental results show the magnitude of charge and polarity of the flurbiprofen salts to be highly dependent on the type of counter ion selected for the salt formation. Furthermore, particle adhesion to the stainless steel surface of the shaking container and the salts' compression properties were measured. The formed salts had lower electrostatic charges, improved tabletability, and resulted in reduced adhesion of these powders compared with the parent drug.

© 2013 Elsevier B.V. All rights reserved.

1. Introduction

In many instances, physical properties of pharmaceutical powders need to be modified to attain optimal processing characteristics suitable for formulation design (Wouters and Quérel, 2012). Various strategies for modifying the physical properties of pharmaceutical materials have been attempted to address specific drug formulation problems. Crystallising acidic or basic drugs into salts is a method routinely used in the pharmaceutical industry to enhance the solubility or stability of drugs and can overcome some undesirable characteristic which exist in the parent drug. Salt formation can increase the solubility by several orders of magnitude, which has a significant effect on the dissolution rate of pharmaceutical compounds (Serajuddin, 2007). The increase in solubility and dissolution rate effectively translates into an increased rate and extent of absorption for the drug (Elder et al., 2013). An estimated half of all drug molecules used in medicinal therapy are administered as salts (Stahl and Wermuth, 2002). The charged groups of the parent drug and the counter ion are attracted by intermolecular coulombic force. The salt form is

then precipitated and recrystallised at set conditions to minimise impurities which otherwise may have a significant effect on the strength of the resulting intermolecular bonds leading to changes in crystal habit. Consequently, salt formation is often the final stage that determines the physical properties of primary materials for formulation development. The basis for salt formation generally begins with the selection of small, compact counter ions to enhance solubility (Elder et al., 2013). Additions of hydrophilic groups to the counter ion can improve solubility, but the additional H-bonding capability can result in undesirable properties, e.g. polymorphism or hydrate formation (David et al., 2012), which may result in differences in physicochemical properties of the material (Vranić, 2003).

However, there is often a compromise to be made between solubility and other physicochemical properties. Selection of the appropriate solid form is critical both for chemical and pharmaceutical processing (Kumar et al., 2008) and therefore significant efforts are typically expended into selecting the optimum salt form for ionisable compounds. The selection process requires a well-designed screening strategy to ensure various development issues are addressed as early as possible. The selection process must therefore be rational and streamlined to aid the selection of a suitable salt as numerous salt forms are available. Alternatively, several salt forms of the drug candidate may be synthesised for

* Corresponding author. Tel.: +44 1484 472 813; fax: +44 1484 472 182.
E-mail addresses: e.supuk@hud.ac.uk, esupuk@gmail.com (E. Šupuk).



Contents lists available at ScienceDirect

International Journal of Pharmaceutics

journal homepage: www.elsevier.com/locate/ijpharm

Simultaneous quantification of drug release and erosion from hypromellose hydrophilic matrices



Muhammad U. Ghor, Gidion Ginting, Alan M. Smith, Barbara R. Conway*

Pharmacy and Pharmaceutical Sciences, University of Huddersfield, Queensgate, Huddersfield HD1 3DH, United Kingdom

ARTICLE INFO

Article history:

Received 17 February 2014

Received in revised form 17 February 2014

Accepted 17 February 2014

Available online 19 February 2014

Keywords:

Hydroxypropyl methylcellulose

Hydrophilic matrix

Drug release

Matrix erosion

Phenol-sulphuric acid assay

ABSTRACT

Hypromellose, HPMC, is frequently used to control drug release from matrix tablet formulations. Drug is released by a combination of diffusion through and erosion of, the matrix and is usually measured *in vitro* by separate dissolution and swelling/erosion studies. The present study was designed to measure matrix erosion, polymer dissolution and drug release kinetics and their inter-relationship in a single experiment using a phenol-sulphuric acid assay to quantify dissolved HPMC alongside spectrophotometrical analysis of drug release. HPMC-based matrix tablets were manufactured containing two drugs at various drug: HPMC ratios. Drug release was determined and the degree of erosion was calculated by gravimetry. Results showed the matrix erosion rate and drug release were dependent on HPMC content and drug solubility, as expected. It was also apparent that the erosion rate was directly related to the drug release kinetics and comparative analysis of both matrix erosion techniques showed a high level of correlation. The findings show that a simple and inexpensive assay can be utilised not only to quantify HPMC but can also be used to calculate the degree of erosion of tablet matrices, negating the need for a separate study and providing a simplified practical approach that may be of use during product optimization.

© 2014 Elsevier B.V. All rights reserved.

1. Introduction

The use of hydrophilic matrices to develop extended release (ER) formulations has become progressively widespread because of their potential to control the release of wide range of active pharmaceutical ingredients (APIs) and to produce robust tablet formulations (Alderman, 1984). Hydrophilic matrices containing hypromellose, HPMC (hydroxypropyl methylcellulose), as the polymeric carrier have been extensively used in oral dosage forms (Maderuelo et al., 2011). The popularity of HPMC can be attributed to its non-toxic nature, availability in different grades, good compression properties, ability to give pH independent drug release profiles, good regulatory acceptance and amenability to high levels of drug loading (Li et al., 2005). On incorporation of HPMC into the tablet formulation, the tortuosity and porosity of matrix tablets can be altered and are intuitively expected to influence the rate and mechanism of drug release from monolithic HPMC-based devices (Reza et al., 2003).

Upon submersion in liquids, such as dissolution testing media or biological fluids, these hydrophilic matrices swell and polymer chains eventually disentangle which leads to the breakage of

hydrogen bonds formed during tablet compaction. However, persistent liquid ingress and interaction between HPMC polymeric chains and the ingressing liquid can cause hydrogen bond formation accommodating water molecules (Gao et al., 1996). This leads to the formation of gel layer across the matrix tablet as HPMC passes from an amorphous to rubbery state. (Colombo et al., 1999; Colombo et al., 2000; Jiasheng et al., 2010). The polymeric chains present on the surface of matrix tablet hydrate quickly compared to those located inside the core and contact with liquid causes chain relaxation (swelling) which initiates erosion of the matrix. The relative rates of liquid uptake and erosion of a polymer matrix play a critical role in controlling the rate of drug release. The swelling, matrix erosion, drug release mechanism and rate are dependent on the concentration and viscosity of HPMC being used in the hydrophilic matrices (Mitchell et al., 1993; Wan et al., 1991). HPMC has the potential to hydrate quickly enough to form a gel layer before the drug entrapped in the tablet matrix can dissolve. Moreover, the higher the viscosity and density of the gel layer, the more resistant the gel is to dissolution and/or erosion as it can retain integrity, thus increasing drug diffusion path length (Khamanga and Walker, 2006). Highly water soluble drugs diffuse through the gel layer before the matrix erodes but it is suggested that the presence of poorly soluble drugs can increase matrix erosion by imperilling the integrity of the gel layer (Bettini et al., 2001; Yang and Fassihi, 1997). So, the solubility of entrapped drugs is another key factor in determining the drug

* Corresponding author. Tel.: +44 1484 472347; fax: +44 1484 472182.

E-mail address: b.r.conway@hud.ac.uk (B. R. Conway).



Tribo-electric charging and adhesion of cellulose ethers and their mixtures with flurbiprofen



Muhammad U. Ghor, Enes Šupuk, Barbara R. Conway*

Department of Pharmacy, University of Huddersfield, Queensgate, Huddersfield HD1 3DH, United Kingdom

ARTICLE INFO

Article history:

Received 13 March 2014

Received in revised form 25 July 2014

Accepted 24 August 2014

Available online 1 September 2014

Keywords:

Tribo-electricity

Surface adhesion

Electrostatic charging

Hydroxypropyl methylcellulose

Methylcellulose

Flurbiprofen

ABSTRACT

The pervasiveness of tribo-electric charge during pharmaceutical processing can lead to the exacerbation of a range of problems including segregation, content heterogeneity and particle surface adhesion. The excipients, hydroxypropyl methylcellulose (HPMC) and methylcellulose (MC), are often used in drug delivery systems and so it is important to understand the impact of associated factors on their charging and adhesion mechanisms, however, little work has been reported in this area. Such phenomena become more prominent when excipients are introduced to a powder mixture alongside the active pharmaceutical ingredient(s) (APIs) with inter- and intra-particulate interactions giving rise to electrification and surface adhesion of powder particles. The aim of this study was to understand the impact of material attributes (particle size, hydroxypropyl (Hpo) to methoxyl (Meo) ratio and molecular size) on the charging and adhesion characteristics of cellulose ethers. Furthermore, a poorly compactible and highly electrostatically charged drug, flurbiprofen, was used to develop binary powder mixtures having different polymer to drug ratios and the relationship between tribo-electric charging and surface adhesion was studied. Charge was induced on powder particles and measured using a custom built device based on a shaking concept, consisting of a Faraday cup connected to an electrometer. The diversity in physico-chemical properties has shown a significant impact on the tribo-electric charging and adhesion behaviour of MC and HPMC. Moreover, the adhesion and electrostatic charge of the API was significantly reduced when MC and HPMC were incorporated and tribo-electric charging showed a linear relationship ($R^2 = 0.81–0.98$) with particle surface adhesion, however, other factors were also involved. It is anticipated that such a reduction in charge and particle surface adhesion would improve flow and compaction properties during processing.

© 2014 Elsevier B.V. All rights reserved.

1. Introduction

Tribo-electricity is intrinsically a dynamic, strenuous and dissipative phenomenon, which is generated due to the difference in electrical potential when two materials come into contact with each other (either by impact, friction or shear) and then separated (Harper, 1967). The charge duration on a surface depends on relaxation time, which is the product of permittivity and surface resistivity of materials. As the majority of pharmaceutical materials are insulators, this process is extended, perhaps over minutes to hours, in comparison to conductive materials (Bailey, 1984; Rowley, 2001). A fundamental understanding of the phenomenon is still elusive (Soh et al., 2012), however, on the basis of existing theories, the mechanism of charge generation can be due to electron transfer, (charge is produced due to the flow of electrons

between particles); ion transfer (diffusion of ions between the surface of particles); or due to material transfer (some material is rubbed off from one contacting body and attached onto the surface of another particle). Commonly, the tribo-electric charging process is a combination of these processes, although the charging behaviour of pharmaceutical materials is usually ascribed to the electron transfer theory because it provides a relatively understandable description of the charging process (Matsusaka et al., 2010). During the contact charging process, the valence electron energy state of powder particles on an atomic scale is designated as the fermi level whilst the vacuum energy level is a thermodynamic state of electrons far from the atom and can be considered as a reference point. The difference between the fermi level and vacuum energy level equates to the work function (ϕ), which is a unique surface property of materials and refers to the minimum energy difference required for the liberation of loosely bonded electrons present in the outer electron shells of an atom (Lowell, 1979). When inter or intra-particulate contacts of powder particles are established,

* Corresponding author. Tel.: +44 (0)1484 472347; fax: +44 (0)1484 472182.
E-mail address: b.r.conway@hud.ac.uk (B.R. Conway).